TTI: 0-6784

Texas A&M Transportation Institute

Creep Behavior of Soil Nail Walls in High Plasticity Index (PI) Soils: Technical Report

Technical Report 0-6784-1

Cooperative Research Program

TEXAS A&M TRANSPORTATION INSTITUTE
COLLEGE STATION, TEXAS

in cooperation with the
Federal Highway Administration and the
Texas Department of Transportation
http://tti.tamu.edu/documents/0-6784-1.pdf

Technical Report Documentation Page

1. Report No.	2. Government Accession No.	3. Recipient's Catalog No.
FHWA/TX-15/0-6784-1		

4. Title and Subtitle	5. Report Date
CREEP BEHAVIOR OF SOIL NAIL WALLS IN HIGH PLASTICITY INDEX (PI) SOILS: TECHNICAL REPORT	Published: April 2017
	6. Performing Organization Code
7. Author(s)	8. Performing Organization Report No.
Marcelo Sanchez, Jean-Louis Briaud, Stefan Hurlebaus, Mohsen Mahdavi Kharanaghi, and Gang Bi	Report 0-6784-1
9. Performing Organization Name and Address	10. Work Unit No. (TRAIS)
Texas A&M Transportation Institute College Station, Texas 77843-3135	11. Contract or Grant No. Project 0-6784
12. Sponsoring Agency Name and Address	13. Type of Report and Period Covered
Texas Department of Transportation Research and Technology Implementation Office 125 E. 11th Street Austin, Texas 78701-2483	Technical Report: September 2012–August 2015
	14. Sponsoring Agency Code

15. Supplementary Notes

Project performed in cooperation with the Texas Department of Transportation and the Federal Highway Administration.
Project Title: Creep Behavior of Soil Nail Walls in High Plasticity Index (PI) Soils
URL: http://tti.tamu.edu/documents/0-6784-1.pdf

16. Abstract

An aspect of particular concern in the *Geotechnical Engineering Circular No. 7: Soil Nail Walls* (i.e., the soil nail wall manual and construction guidelines) is the creep behavior of soil nail systems in high-plasticity clays. This research project was aimed at gaining a better understanding of the long-term behavior of the soil nail walls in fine-grained soil with plasticity index higher than 20. The project was composed of field, laboratory, and numerical modeling investigations. Pullout tests were performed at the National Geotechnical Experimental Site at Texas A&M University (NGES-TAMU) and at the actual soil nail wall project site selected by the Texas Department of Transportation (TxDOT). The TxDOT site was also instrumented and monitored for more than one year. The tests at the NGES-TAMU were focused on the effect of the load level on creep behavior of soil nails in a natural clay deposit of high plasticity. The tests were conducted on 10 existing anchors (installed in 1991), 16 vertical soil nails installed in this research, and 6 sacrificial soil nails installed during the construction of a TxDOT soil nail wall. This wall corresponds to a new excavation project in an embankment fill, in which nine permanent soils nails were instrumented with the aim of monitoring the long-term behavior and performance of the wall in a high-plasticity clay. Complementary laboratory tests to learn about the creep behavior of the clays involved in this research project were performed at Texas A&M University using samples gathered from the two investigated sites. The numerical modeling had three goals: 1) to calibrate the constitutive models using the information gathered from the laboratory and the pullout tests; 2) to simulate the long-term behavior of the actual soil nail wall and to compare the model and monitoring results; and 3) to perform a parametric analysis to study the effect of different factors (among others, wall geometry and soil parameters). Based on the information obtained from the project activities, a tentative procedure was proposed to take into account the creep effects in the design of soil nail wall in high-plasticity soils.

17. Key Words	18. Distribution Statement
Soil Nail Wall, High Plasticity Clay, Creep, Time Dependent Behavior, Pullout Test, Monitoring, Numerical Modeling	No restrictions. This document is available to the public through NTIS: National Technical Information Service Alexandria, Virginia. http://www.ntis.gov

19. Security Classif.(of this report)	20. Security Classif.(of this page)	21. No. of Pages	22. Price
Unclassified	Unclassified	440	

Form DOT F 1700.7 (8-72) Reproduction of completed page authorized

CREEP BEHAVIOR OF SOIL NAIL WALLS IN HIGH PLASTICITY INDEX (PI) SOILS: TECHNICAL REPORT

by

Marcelo Sanchez
Research Engineer
Texas A&M Transportation Institute

Jean-Louis Briaud
Research Engineer
Texas A&M Transportation Institute

Stefan Hurlebaus
Research Engineer
Texas A&M Transportation Institute

Mohsen Mahdavi Kharanaghi
Graduate Student
Texas A&M Transportation Institute

and

Gang Bi
Graduate Student
Texas A&M Transportation Institute

Report 0-6784-1
Project 0-6784
Project Title: Creep Behavior of Soil Nail Walls in High Plasticity Index (PI) Soils

Performed in cooperation with the
Texas Department of Transportation
and the
Federal Highway Administration

Published: April 2017

TEXAS A&M TRANSPORTATION INSTITUTE
College Station, Texas 77843-3135

DISCLAIMER

This research was performed in cooperation with the Texas Department of Transportation (TxDOT) and the Federal Highway Administration (FHWA). The contents of this report reflect the views of the authors, who are responsible for the facts and the accuracy of the data presented herein. The contents do not necessarily reflect the official view or policies of the FHWA or TxDOT. This report does not constitute a standard, specification, or regulation. The engineer in charge of this part of the project was Dr. Marcelo Sanchez.

ACKNOWLEDGMENTS

This project was conducted in cooperation with TxDOT and FHWA. The director of the project was Wade Odell. Other members of the project monitoring committee from TxDOT were Marcus Galvan, Sean Yoon, John Delphia, Bryan Esmaili-Doki, Dina Dewane, and Taya Retterer. The authors are grateful for their support during this project.

TABLE OF CONTENTS

LIST OF FIGURES

Page

LIST OF TABLES

Page

CHAPTER 1:
INTRODUCTION

BACKGROUND

Soil nailing is a convenient and economic stabilization method for the reinforcement of existing soil or excavation by installing threaded steel bars into cuts or slopes as the wall construction progresses from the top down. In this technique, the first step to create a stable soil mass is to install grouted bars into the soil. The nailing process creates a single block of earth able to hold back its overburden during the excavation. Afterward, a layer of shotcrete (i.e., concrete/mortar conveyed through a hose and pneumatically projected at high velocity onto a surface) is applied and bearing plates are installed at the end of the nails before a final facing is put in place to complete the soil nail wall (FHWA, 1998a).

Soil nail walls are becoming very popular in the United States because this method has been shown to be a technically feasible, flexible, easy-to-modify, rapid, and cost-effective alternative to conventional retaining walls used in top-to-bottom excavations in temporary and permanent applications (FHWA, 2003). Soil nail walls have been generally used for temporary retaining structures. However, the use of soil nail walls as a permanent structure has increased substantially in the last few years (FHWA, 2003).

The objective of this research project is to investigate the creep behavior of the soil nail walls in high-plasticity (HP) clays (i.e., according to GEC#7, those clays with plasticity index [PI] higher than 15 [FHWA, 2003]). One of the first precedents in this subject is the French research project named Clouterre (i.e., clou=nail, terre=soil), carried out in 1985 and devised to construct full-scale soil nail walls and bring them to failure. Clouterre consisted of three fully instrumented experiments involving soil nail walls that were built and monitored from construction to failure. The main objective of the Clouterre project was to better understand the behavior of soil nail walls, explore the limitations of this technique, and recommend design guidelines (Plumelle et al., 1990). After five years of research, a French specification entitled "Recommendations Clouterre 1991" was published. In 1993, the U.S. Federal Highway Administration (FHWA) sponsored an English version of this recommendation. In 1996, FHWA published a design manual of soil nail walls, intended for the design, construction, and monitoring of soil nail walls. This manual was then revised in 1998. In November 2003, the FHWA published an updated version of the manual published in 1998, which is known as

Geotechnical Engineering Circular No. 7: Soil Nail Walls, also identified as "GEC#7" (FHWA, 2003). This guideline was recently updated (i.e., in February 2015) under the name of *Geotechnical Engineering Circular No. 7—Soil Nail Walls Reference Manual, 2015* (FHWA, 2015).

MOTIVATION

An aspect of particular concern in the GEC#7 is the creep behavior of soil nail systems in HP clays. Since there was limited information about the creep behavior of soil nail walls in HP clays, the GEC#7 followed some general guidelines about possible creep issues in fine-grained soils with PI > 20 and the construction of soil nails walls in such soil was not recommended. In several sections, the GEC#7 establishes serious limitations and warnings about the construction of soil nail walls in soils with PI > 20. However, soil nail walls have been constructed with success in HP soils (particularly in Texas) and no issues associated with creep behavior have been observed so far, including walls that were built more than 20 years ago. The motivation of this research project is to gain a better understanding of the behavior of soil nail walls in fine-grained soils and to suggest possible modifications to the current guideline.

OBJECTIVES

Creep behavior in soils is closely related to the stress level. However, the GEC#7 associates creep behavior with the presence of HP clays solely, regardless of the load level. The Texas Department of Transportation (TxDOT) has been using soil nail walls in projects involving HP clays without observing major problems associated with creep. It is known that in those applications, the service load is relatively low compared to the maximum load that the nail can sustain. In this project, researchers studied the effect of the load level on the creep behavior of soil nails in HP clays. A good understanding of the creep behavior of soil nail wall in HP clay would allow a safe use of the soil nail walls in a large variety of applications involving fine-grained soils with HP.

When dealing with soil nail walls in HP clays, two distinct issues can be associated with creep effects:

- Problems associated with local effects related to creep behavior of nails and the surrounding soils. These issues are mostly related to the effect of creep on the bonding strength between the grouted nails and the clay.
- Problems associated with the long-term behavior of the creeping soil mass. The direct consequence of this phenomenon is that the lateral movements induced by the creep of the soil mass are reflected in an increase in the nail's load.

ACTIVITIES

To address the problems associated with local (internal) effects related to creep behavior of nails and the surrounding soil, researchers performed pullout tests in different clays to gain a better understanding of creep behavior of soil nails in HP soils. The aim was to study the effect of load level on creep behavior in these types of soils. Pullout experiments under different conditions included: 1) pullout tests on existing anchors at the National Geotechnical Experimentation Site at Texas A&M University (NGES-TAMU) clay site, 2) pullout tests on new nails installed at the NGES-TAMU clay site, and 3) pullout tests carried put on new nails installed in an actual soil nail wall selected by TxDOT. For condition 1, the research team retested anchors installed at the NGES-TAMU clay site in 1991 and explored any effect related to long-term installation. To create condition 2, 16 new vertical soil nails were installed in this research project at the NGES-TAMU clay site, and researchers conducted pullout tests with different load protocols and creep tests at different load levels. For condition 3, six sacrificial nails were installed at different heights of an actual soil nail wall selected by TxDOT in its Beaumont District. These onsite pullout tests were aimed at understanding the effect of different confining stresses on the creep behavior for permanent nails under actual field conditions; they are explained in detail in Chapter 5. These pullout studies were complemented with laboratory tests (e.g., triaxial creep and oedometer tests) performed on samples retrieved from the two sites investigated in this project. These activities are related in Chapter 7.

To study the potential effects of the creeping soil mass on the soil nail wall, the research team selected an actual wall project in collaboration with TxDOT. The site under study corresponds to an emergency slope repair project at TxDOT's Beaumont District in Southeast Texas. The soil nail wall was instrumented and monitored under operational conditions for a period of 13 months after construction. One of the aims of this study is to learn about the service

load. The PI of the embankment fill is around 50, which made this site a very attractive option for the field tests and monitoring campaign proposed in this project. Horizontal movements of the wall, load distribution in the nails, service load in the nails, load change in the nails due to the excavations during construction and due to the creep after the construction, nail loads at the wall face, and change in water content of the embankment were obtained from monitoring the wall. These activities are related in Chapter 5.

To thoroughly investigate the creep behavior of soil nail wall in HP clays, this research project combined experimental and numerical studies. Researchers used a number of computational tools to investigate the performance of soil nail walls in HP clay. FLAC3D™ numerical modeling software by Atasca Consulting Group was adopted to simulate the time-dependent (creep) behavior of soil nail walls during and after construction. The advantages of using FLAC3D in this research project include the following: it is a well-known and validated code for geotechnical problems involving excavations, it allows the modeling of soil nails with special elements (i.e., cable elements), and it provides a variety of creep models (e.g., eight creep models).

The numerical codes were used in the following types of analyses:

- Effect of sacrificial nail on the axial load of the production nails around it.
- Wall design and verification.
- Simulation and model calibration against the field data collected from the actual TxDOT project.
- Parametric analysis to study the effect of different factors and soil parameters on the performance of soil nail walls in HP clays.

REPORT ORGANIZATION

This report is organized into nine chapters. Chapter 1 relates the background information and identifies the problem statement, motivations, objectives, and the significance of this research project. Chapter 2 focuses on the literature review and previous works in this field.

Chapter 3 presents the instrumentation design of the pullout tests at the National Geotechnical Experimental Site at Texas A&M University, and also the sensors and devices selected for the long-term monitoring of the TxDOT project. The instrumentation is a crucial component of this research because the data gathered from the experiments are used to gain a

better understanding of the identified problem. It is also critical for calibrating the numerical models.

Chapter 4 discusses the loading tests at the NGES-TAMU site and the related activities. Two different kinds of tests were performed at the NGES-TAMU: experiments on existing anchors installed more than 20 years ago (with a very well-known load history) and tests on newly constructed soil nails. These tests focus on the effect of the load level on the creep behavior of soil nails in HP clays.

Chapter 5 focuses on the instrumentation and long-term monitoring of the TxDOT soil nail wall located in the Beaumont District. The wall monitoring was aimed at gathering the following information: horizontal movements of the wall, load distribution in the nails, service load in the nails, load change in the nails due to the excavations during construction and due to the creep after construction, nail loads at the wall face, and change in water content of the embankment as obtained at the end of monitoring. Creep tests were performed at different load levels on the sacrificial nails to gain a better understanding of the effect of stress level on creep behavior. Since the ultimate pullout capacity and the service load of the permanent nails depend on the nail position, sacrificial nails were installed and tested at different heights of the wall.

Chapter 6 is devoted to the laboratory tests performed at TAMU facilities on samples gathered from the two test sites investigated in this research project.

Chapter 7 examines the numerical modeling. The numerical modeling had three goals: 1) to calibrate the constitutive models using the information gathered from the laboratory and pullout tests; 2) to simulate the long-term behavior of the actual soil nail wall and to compare the model and monitoring results; and 3) to perform a sensitivity analysis to study the effect of different factors (e.g., wall geometry and soil parameters) on soil nail wall behavior.

Chapter 8 focuses on the anticipated design method. The researchers suggest a tentative procedure to include soil creep effects in the design of soil nail walls in HP clays. This possible modification is based on the following studies: pullout tests at the NGES-TAMU clay site, instrumentation and monitoring of the emergency slope repair project at the Beaumont District, laboratory tests, and numerical models, which were calibrated using the laboratory and field data. Chapter 9 presents the summary and the main conclusions of this report.

CHAPTER 2:
LITERATURE REVIEW

INTRODUCTION

The concept of combining passive steel reinforcement and shotcrete started in the early 1960s with the stabilization of rock slopes. The use of passive (i.e., no post-tensioning) steel reinforcement in the rock followed by the application of reinforced shotcrete is also a key component of the well-known and widely used New Austrian Tunneling method. The first application of soil nailing was implemented in 1972 for a railroad widening project near Versailles, France (FHWA, 2003). Soil nails were used to stabilize a 59-ft-high slope consisting of sandy soil. This method proved to be more cost-effective and cut down the construction time when compared to conventional support methods.

One of the first applications of soil nailing in the United States was to support a 45-ft-deep foundation excavation in dense silty sands. The project was part of the expansion of a hospital in Portland, Oregon, in 1976 (FHWA, 1998b). The first nailed walls were built in Texas in the mid to late 1980s (Galvan, 2012). Figure 1 illustrates the usage of retaining walls by TxDOT. The chart is based on statistical data collected from August 2010 through September 2011 (Galvan, 2012). Over the past year, approximately 500,000 linear feet of soil nail was installed on TxDOT projects.

Drilled soil nails are the most popular type in the United States. They consist of a steel bar placed in a predrilled hole and then grouted. Figure 2 presents the basic elements of a soil wall, showing the components for a zone near the nail head (FHWA, 2003).

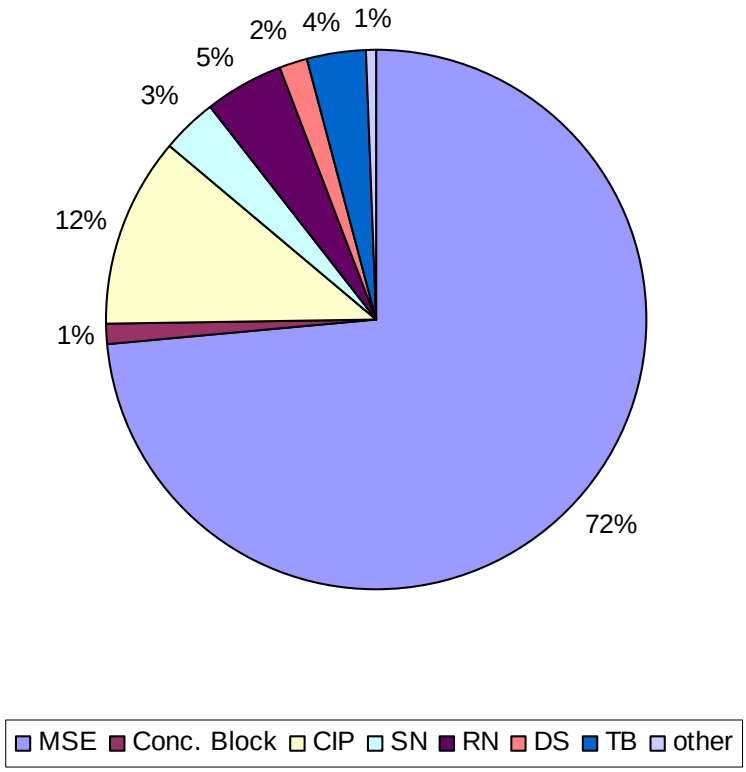

Figure 1. Retaining Walls Used by TxDOT from 08/2010 through 09/2011 (after Galvan, 2012).

Soil nails are passive elements because they are not mechanically pretensioned after installation (Tuozzolo, 2003). This lack of pre-tension is a significant difference with respect to tieback anchors. During the process of excavation, the earth mass supported by the soil nails tends to deform laterally and the nails are loaded (generally) in tension.

a)

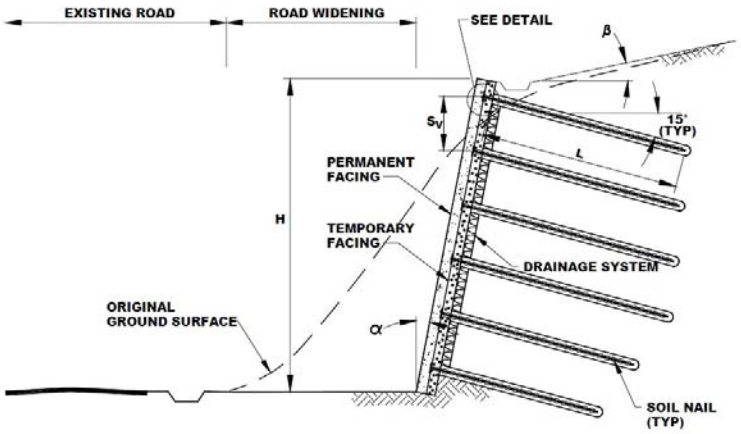

b)

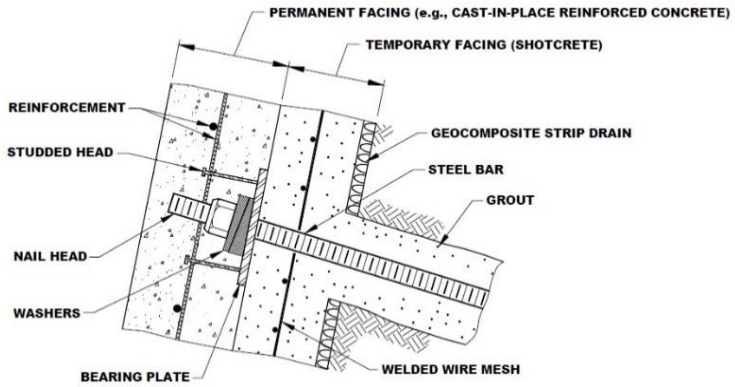

Figure 2. a) Typical Cross Section of a Soil Nail Wall; b) Detail of the Nail Head (after FHWA, 2003).

In this type of problem, two zones can be distinguished: 1) the active zone, and 2) the passive zone (or resistant zone). As illustrated in Figure 3, a potential failure surface separates the active and resistant zones (Geoguide 7, 2008). The active zone is the region in front of the potential failure surface, where there is a tendency to detach from the soil-nailed system. The passive zone is the region behind the potential failure surface, where the soil remains more or less intact. The soil nails act to tie the active zone to the passive zone (Geoguide 7, 2008). The two-zone configuration is a very simplified model generally adopted in limit equilibrium analyses. One limitation of this kind of analysis is that it does not account for the deformation of the soil nail system.

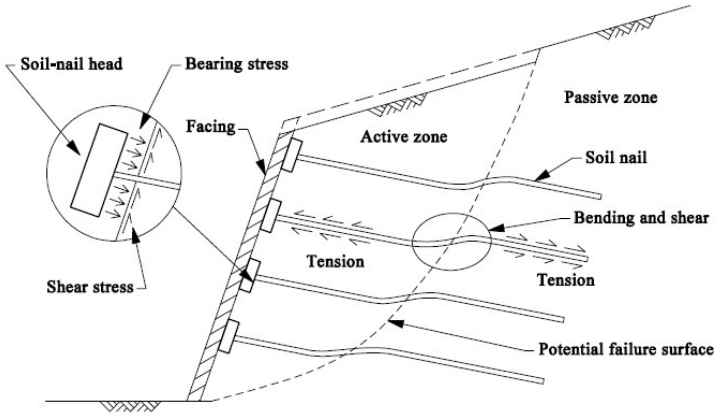

Figure 3. The Two-Zone Model of a Soil-Nailed System (after Geoguide 7, 2008).

The actual nail-ground interactions are much more complex, and the forces developed in the soil nails are influenced by many factors. Those factors include, among others: the mechanical properties of the soil nails (e.g., tensile strength, shear strength, and bending capacity); the inclination and orientation of the soil nails; the shear strength of the ground; the relative stiffness of the soil nails and the ground; the friction between the soil nails and the ground; the size of the soil-nail heads; and the nature of the slope facing (Geoguide 7, 2008). Figure 4 presents schematically the typical sequence of construction for a soil nail wall using solid steel nail bars (FHWA, 2003).

According to GEC#7 (FHWA, 2003), soil nail walls are becoming very popular in the United States because it has been demonstrated that they are technically feasible and, in many cases, are a cost-effective alternative to conventional retaining walls used in top-to-bottom excavations in temporary and permanent applications. Soil nail walls have been generally used for temporary retaining structures. However, the use of soil nail walls as permanent structures has increased substantially in the last few years (FHWA, 2003).

Soil nail walls have some additional advantages:

- They are less disruptive than other means of constructing retaining systems.
- The technique is flexible and easy to modify.
- They require a smaller right-of-way than ground anchor walls.
- Their installation is relatively rapid and typically uses less materials and smaller construction equipment than ground anchor walls.

- They can follow irregular curves.
- They create less noise and traffic obstructions than other solutions.
- The impact on nearby properties is small compared to other alternatives.
- The equipment is portable for tight spaces.

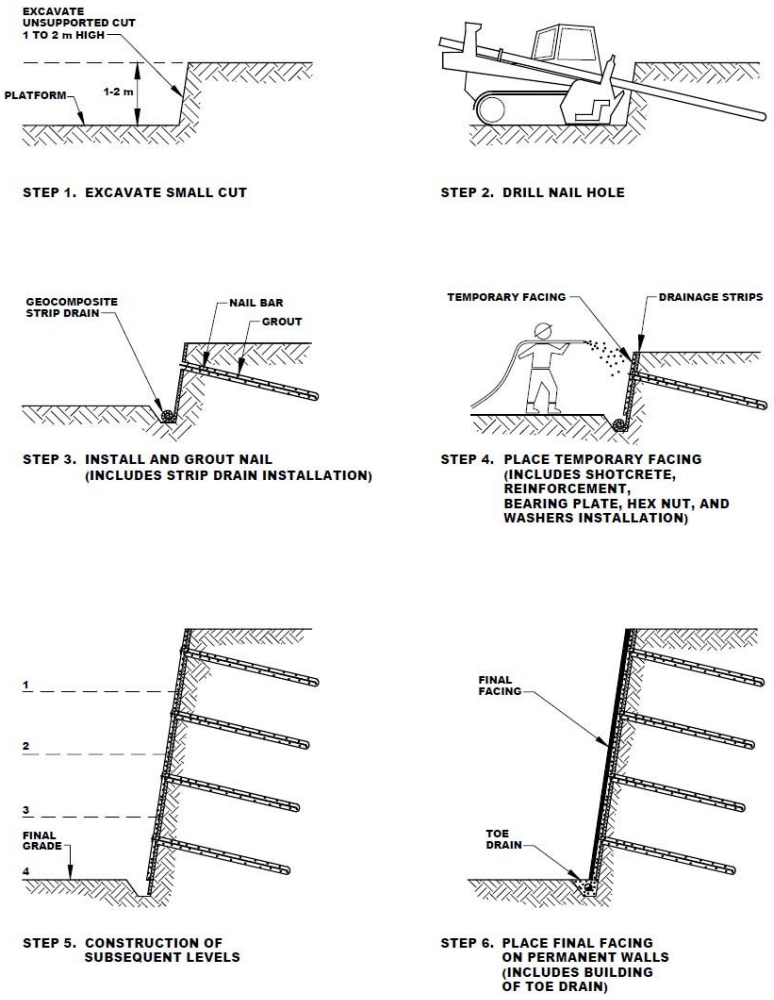

Figure 4. Typical Soil Nail Wall Construction Sequence (after FHWA, 2003).

An aspect of particular concern in the GEC#7 (FHWA, 2003) is the creep behavior of soil nail systems in HP clays (i.e., PI > 15) and the associated long-term deformations. A large number of observations can be found in GEC#7 for projects involving soil nail walls in HP clays. The validation of a design approach for soil nail walls in those types of profiles is necessary because HP clays are very common in Texas. Furthermore, a relatively new application of soil

nailing that is becoming very popular in Texas is related to the construction of the "Texas Turnaround." In this application, soils nails are commonly used in the construction of walls under piled bridge abutments (Figure 5).

TxDOT has made use of this kind of application in projects involving a variety of soil types, including many walls designed and constructed in soil profiles with PIs greater than 20. More details about this application can be found in this chapter.

This chapter is organized as follows. First, a brief summary of the GEC#7 is presented, including: design method for soil nail walls, possible failure modes of this kind of retaining structures, typical nail load tests to be performed in the field, and specific concerns of this guideline associated with the long-term behavior of soil nails walls in HP clays. Afterward, the usage of soil nail walls in Texas is briefly discussed, alongside the TxDOT design method used for soil nail walls. The chapter continues with a short summary of the recent and ongoing projects and activities in this area performed by other departments of transportation in the United States and other countries.

Finally, the literature review is presented in more detail, focusing on contributions related to soil nail walls in HP clays. Special attention is paid to works related to the creep behavior of soils (both experimental and numerical). It includes a brief summary of some contributions associated with the instrumentation and monitoring of retaining walls and slopes involving soil nails, and some relevant works related to the numerical modeling of soil nail systems. The chapter ends with a summary and the conclusions from this review.

Figure 5. Typical Soil Nail Wall Solution in a Texas Turnaround (after Galvan, 2012).

SOIL NAIL WALL DESIGN ACCORDING TO GEC#7 – BRIEF SUMMARY

FHWA published in 1996 the *Manual for Design and Construction Monitoring of Soil Nail Walls*. This manual was then revised in 1998. In November 2003, FHWA published an updated version of the one published in 1998, which is known as the *Geotechnical Engineering Circular No. 7* (GEC#7). This manual is used as the primary reference in the United States for the design of soil nail walls. The main aspects related to the design of soil nail walls and nails testing according to the GEC#7 are briefly outlined below. Some parts of the text have been taken from GEC#7 (FHWA, 2003). The analysis and design of soil nail walls must consider two distinct conditions (FHWA, 2003):

1. **Strength Limit State:** These limit states refer to failure or collapse modes in which the applied loads induce stresses that are greater than the strength of the whole system or individual components, and the structure becomes unstable. As explained in more detail in the following section, three failure modes can be distinguished in this category:
   a. External failure mode.
   b. Internal failure mode.
   c. Facing failure mode.

2. **Service Limit State:** These limit states refer to conditions that do not involve collapse, but rather impair the normal and safe operation of the structure. The more relevant service limit state is related to wall deformation.

External Failure Mode

External failure modes refer to the development of potential failure surfaces passing through or behind the soil nails. Figure 6 depicts the external failure modes, as follows GEC#7 (FHWA, 2003):

- Global stability failure.
- Sliding stability failure.
- Bearing capacity failure.

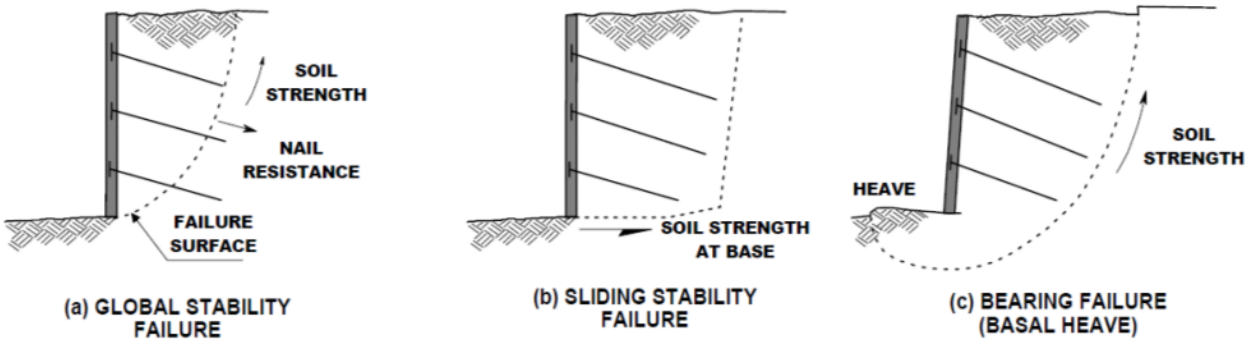

Figure 6. External Failure Modes (after FHWA, 2003).

Global stability analyses are performed using computer programs specifically developed for the design of soil nail walls. SNAILZ and GOLDNAIL are the programs most commonly used in the United States for the analysis and design of soil nail walls. The typical steps involved in this kind of analysis are as follows: 1) estimate the soil nail wall parameters (e.g., nail length, nail length pattern, nail vertical and horizontal spacing, and nail inclination); 2) calculate the global factor of safety (FS) using the selected nail length; 3) compare the calculated global FS to the recommended minimum F; and 4) increase (or decrease) the nail length if the calculated FS is lower (or higher) than the recommended value, and start the process again (FHWA, 2003).

Table 1. Minimum Recommended FS (after FHWA, 2003).

Failure Mode	Resisting Component	Symbol	Minimum Recommended Factors of Safety		
			Static Loads[1]		Seismic Loads[2] (Temporary and Permanent Structures)
			Temporary Structure	Permanent Structure	
External Stability	Global Stability (long-term)	FS_G	1.35	1.5[1]	1.1
	Global Stability (excavation)	FS_G	1.2-1.3[2]		NA
	Sliding	FS_{SL}	1.3	1.5	1.1
	Bearing Capacity	FS_H	2.5[3]	3.0[3]	2.3[5]
Internal Stability	Pullout Resistance	FS_P	2.0		1.5
	Nail Bar Tensile Strength	FS_T	1.8		1.35
Facing Strength	Facing Flexure	FS_{FF}	1.35	1.5	1.1
	Facing Punching Shear	FS_{FP}	1.35	1.5	1.1
	H.-Stud Tensile (A307 Bolt)	FS_{HT}	1.8	2.0	1.5
	H.-Stud Tensile (A325 Bolt)	FS_{HT}	1.5	1.7	1.3

Internal Failure Mode

Internal failure mode refers to failure in the load transfer mechanisms between the soil, the nail, and the grout. Figure 7 shows the different internal failure modes.

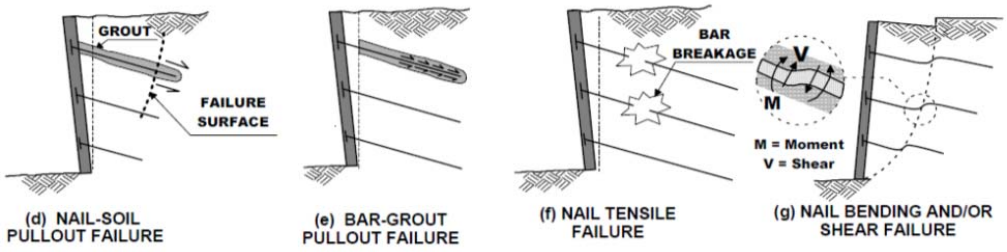

Figure 7. Internal Failure Modes (after FHWA, 2003).

As illustrated in Figure 7, the internal modes recognized in GEC#7 (FHWA, 2003) are as follows:

- **Nail Pullout Failure:** Pullout failure is the primary internal failure mode in a soil nail wall. This failure mode may occur when the pullout capacity per unit length is inadequate and/or the nail length is insufficient. The pullout capacity is mobilized when the ultimate bond strength is achieved and is expressed as:

$$Q_U = \pi q_u D_{DH} \quad (1)$$

where Q_U is the pullout capacity; D_{DH} is the diameter of drilling hole; and q_u is the bond strength (typical q_u values are presented in Table 2).

- **Slippage of the Bar–Grout Interface:** The strength against slippage along the grout and steel bar interface is derived mainly from mechanical interlocking of grout between the protrusions and valleys of the nail bar surface. Mechanical interlocking provides significant resistance when threaded bars are used and is negligible in smooth bars.
- **Bending and Shear of the Nails:** Soil nails work predominantly in tension, but they also mobilize stresses due to shear and bending at the intersection of the slip surface with the soil nail. Shear and bending nail strengths contribute no more than approximately 10 percent of the overall stability of the wall. Due to this relatively modest contribution, the shear and bending strengths of the soil nails are conservatively disregarded in the FHWA guideline.
- **Tensile Failure of the Nail:** The tensile force in the soil nail (T) may vary from the anchoring zone to the facing. A typical distribution of the tensile force is presented in Figure 8, alongside the distribution of $q_{(x)}$. T is equal to zero at the end of the nail and then increases (from the end to the face) up to a maximum value, T_{max}, at an intermediate length, then decreases until reaching the value T_o, known as the tensile force at nail head. The value T_{max} is constrained by three limiting conditions: the pullout capacity (RP), the tensile capacity (RT), and the facing capacity (RF). If $RP < RT$ and RF, pullout failure controls the value of T_{max}. If $RT < RP$ and RF, tensile failure controls T_{max}. Finally, if $RF < RT$ and RP, failure of the facing may control. In soft soil, the pullout capacity controls the T_{max}.

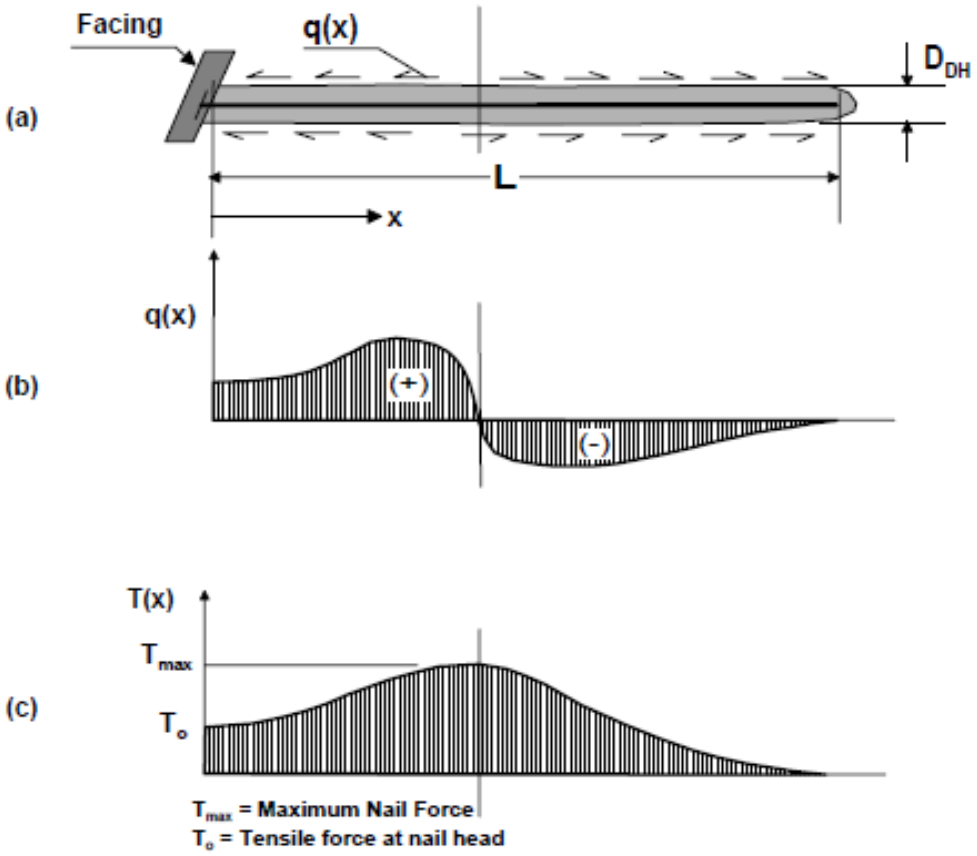

Figure 8. Soil Nail Stress-Transfer Mechanism (after FHWA, 2003).

Table 2. Estimated Bond Strength of Soil Nails in Soiland Rock (after FHWA, 2003).

Material	Construction Method	Soil/Rock Type	Ultimate Bond Strength, q_u (kPa)
Rock	Rotary Drilled	Marl/limestone	300 - 400
		Phyllite	100 - 300
		Chalk	500 - 600
		Soft dolomite	400 - 600
		Fissured dolomite	600 - 1000
		Weathered sandstone	200 - 300
		Weathered shale	100 - 150
		Weathered schist	100 - 175
		Basalt	500 - 600
		Slate/Hard shale	300 - 400
Cohesionless Soils	Rotary Drilled	Sand/gravel	100 - 180
		Silty sand	100 - 150
		Silt	60 - 75
		Piedmont residual	40 - 120
		Fine colluvium	75 - 150
	Driven Casing	Sand/gravel	
		low overburden	190 - 240
		high overburden	280 - 430
		Dense Moraine	380 - 480
		Colluvium	100 - 180
	Augered	Silty sand fill	20 - 40
		Silty fine sand	55 - 90
		Silty clayey sand	60 - 140
	Jet Grouted	Sand	380
		Sand/gravel	700
Fine-Grained Soils	Rotary Drilled	Silty clay	35 - 50
	Driven Casing	Clayey silt	90 - 140
	Augered	Loess	25 - 75
		Soft clay	20 - 30
		Stiff clay	40 - 60
		Stiff clayey silt	40 - 100
		Calcareous sandy clay	90 - 140

Load Testing according to GEC#7

Tests on soil nails are an important part of this research project and are summarized in this section. Soil nails are tested in the field to verify that the nail design loads can be carried without excessive movements and with an adequate FS. Testing is also used to verify the adequacy of the contractor's drilling, installation, and grouting operations prior to and during construction of the soil nail wall. It is important to highlight that if soil nail test results indicate faulty construction practice or soil nail capacities are less than that required, the contractor should be required to change nail installation/construction methods. If excessive creep is measured, it is necessary to modify the design by reducing nail spacing or increasing the nail length.

Testing procedures and nail acceptance criteria must be included in the specifications. Three kinds of load tests are contemplated in GEC#7 (FHWA, 2003), as follows:

1. **Verification or Ultimate Load Tests:** These tests are conducted to verify the compliance with pullout capacity and bond strengths used in design and resulting from the contractor's installation methods. Verification load tests should be conducted to failure or, as a minimum, to a test load that includes the design bond strength and pullout FS. The number of verification load tests will vary depending on the size of the project and the number of ground types in which nails will be installed. As a minimum, two verification tests should be conducted in each soil strata that is encountered. Verification tests are performed on sacrificial test nails, which are not incorporated into the permanent work.
2. **Proof Tests:** These tests are conducted during construction on a specified percentage, typically 5 percent, of the total production nails installed. Proof tests are intended to verify that the contractor's construction procedure has remained constant and that the nails have not been drilled and grouted in a soil zone not tested by the verification stage testing. Soil nails are proof tested to a load typically equal to 150 percent of the design load.
3. **Creep Tests:** These tests are performed as part of ultimate, verification, and proof testing. A creep test consists of measuring the movement of the soil nail at a constant load over a specified period of time. Acceptance criteria typically require that creep movement between the 1- and 10-minute readings, at maximum test load, must be less than 1 mm (0.04 in.), or that creep movement between the 6- and 60-minute readings must be less than 2 mm (0.08 in.) at maximum test load. The creep criterion is based largely on experience and current practice with ground anchors and has been established to ensure that nail design loads can be safely carried throughout the structure's service life.

Figure 9 shows the basic setup for those tests. The setup consists of two major components: loading and displacement reading systems. The loading system encompasses a load transfer frame, hydraulic jack, and hydraulic pump. For displacement reading, two dial gauges that are capable of measuring to the nearest 0.02 mm (0.001 in.) and are able to accommodate a

minimum travel equivalent to the estimated elastic elongation of the test nail at the maximum test load plus 25 mm (1 in.) is recommended (FHWA, 2003).

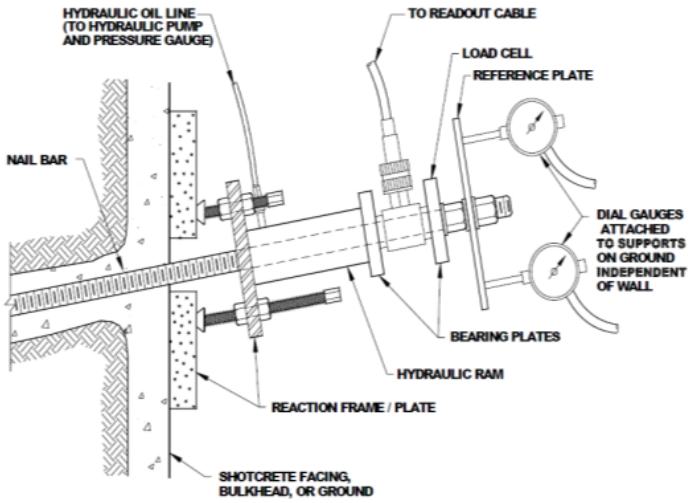

Figure 9. Setup for Loading Tests (after FHWA, 2003).

Table 3 shows the verification test load schedule. The notation follows GEC#7 convention. The design test load (DTL) is determined as the product of the allowable pullout resistance (Q_{All}) times the bonded length L_{BVT}. According to this loading protocol (i.e., Table 3), it is necessary to hold each load increment for at least 10 minutes; monitor the verification test nail for creep at 1.50 DTL load increment; and measure and record nail movements during the creep portion of the test in increments of 1, 2, 3, 5, 6, 10, 20, 30, 50, and 60 minutes. The protocol also requires maintainance of the load during the creep test within 2 percent of the intended load (by using a load cell).

Table 3. Verification Test Load Schedule, Creep Step (after FHWA, 2003).

Load	Hold Time
0.05 DTL max.(AL)	1 minute
0.25 DTL	10 minutes
0.50 DTL	10 minutes
0.75 DTL	10 minutes
1.00 DTL	10 minutes
1.25 DTL	10 minutes
1.50 DTL (Creep Test)	60 minutes
1.75 DTL	10 minutes
2.00 DTL	10 minutes
2.50 DTL	10 minutes max.
3.0 DTL or Failure	10 minutes max.
0.05 DTL max. (AL)	1 minute (record permanent set)

GEC#7 and Soil Nail Walls in HP Soils

Potential issues associated with the construction of soil nail walls in HP clays are mentioned a number of times in the GEC#7. Creep behavior is of special concern in the guidelines. Those issues are the primary motivation for this project. The paragraphs in the GEC#7 (FHWA, 2003) that refer to problems related to soil nail walls involving HP clays and/or creep are cited below:

- **Page 14:** To minimize potential long-term lateral displacements of the soil nail wall, fine-grained soils should be of relatively low plasticity (i.e., in general, **PI < 15**).
- **Page 15:** Soft to very soft fine-grained soils typically have standard penetration test (SPT) N-values less than 4 and are unfavorable for soil nailing because they develop relatively low bond strengths at the nail–grout–soil interface, thereby requiring unreasonably long nail lengths to develop the required resistance. Long-term deformations (creep) of the soils may be a concern for highly plastic clays. Concerns for creep deformations are generally less critical for temporary applications.
- **Page 17:** Soil nails can be installed in engineered fill if it is a mixture of well graded granular material (approximately 90 percent of the mix or more) and fine-grained soil with low plasticity (typically, **PI < 15**).
- **Page 38:** There are no specific criteria that can be used to establish whether a soil exhibits unfavorable creep potential. However, practice has shown that soils with

potential for creep include: 1) fine-grained soils with a liquid limit (LL) > 50, and 2), fine-grained soils with **PI > 20**.

- **Page 38:** Sustained, long-term loading of fine-grained soils surrounding soil nails may cause creep deformation. Creep takes place under constant effective stresses in the soil and may cause deformations that adversely affect the lateral deflection of soil nail walls.
- **Page 39:** Creep rates exceeding 2 mm (0.08 in.) in a time period between 6 and 60 minutes in logarithmic scale indicate substantial creep potential. If excessive creep is calculated, it is necessary to modify the design by reducing nail spacing or increasing the nail length.
- **Page 89:** The tensile forces in the nail develop gradually with time as excavation proceeds from top to bottom in front of the wall. Generally, maximum nail tensile forces in a given row develop when the two subsequent excavation lifts are exposed. Tensile forces may increase moderately (e.g., generally 15 percent) in the time period between the end-of-construction condition and the long-term, steady condition (Plumelle et al., 1990). These post-construction increases occur due to post-construction soil creep and stress relaxation. Although this additional load is not calculated, it is taken into consideration in the design of soil nail walls by means of factors of safety.
- **Page 104:** During construction and after its completion, a soil nail wall and the soil behind it tend to deform outward. The outward movement is initiated by incremental rotation about the toe of the wall, similar to the movement of a cantilever retaining wall. Most of the movement occurs during or shortly after excavation of the soil in front of the wall. Post-construction deformation is related to stress relaxation and creep movement, which are caused by post-construction moderate increases in tensile force in the soil nail.
- **Page 106:** Post-construction monitoring of soil nail wall displacements indicates that movements tend to continue after wall construction, sometimes up to 6 months, depending on ground type. Typically, the post-construction deformation increases up to 15 percent of the deformations observed soon after construction. As a result of this movement, additional tension develops in the nails. In general, fine-grained soils of HP (i.e., approximately PI > 20) and high water contents (such that liquidity index [LI] > 0.2) tend to incur deformation for longer periods of time.

Creep behavior in soils is closely related to the stress level. However, GEC#7 associates creep behavior with the presence of HP clays solely, regardless of the load level. As explained in the next section, TxDOT has been using soil nail walls for an extended time in projects involving HP clays without observing major problems associated with creep. It is known that in those applications the service load is relatively low compared to the maximum load the nail can sustain. This project aims to study the effect of the load level on the creep behavior of soil nails in HP clay and the effect of the creep of the soil mass in the wall movements and additional loads in nails.

USAGE OF SOIL NAIL WALLS IN TEXAS AND TXDOT DESIGN METHOD

As mentioned in previous sections, soil nail walls have been regularly used as possible solutions for the construction of temporary and permanent retaining walls in Texas. Table 4 provides information on the wall usage by TxDOT (Galvan, 2012).

Table 4. Wall Usage by TxDOT, August 2010 through September 2011 (Galvan, 2012).

Wall Type	Area (ft^2)	%
MSE*	3,196,417	72
Concrete Block (no r/f)	47,791	1
Cantilever Drilled Shaft	72,286	2
Soil Nailed	146,793	3
Rock Nailed	197,216	5
Tied-back	161,827	4
Spread Footing	505,019	12
Other	22,389	1

* Mechanically stabilized earth

TxDOT uses this type of wall in projects involving a variety of soil types, including many walls in HP clays. Soil nail walls are used for cuts only, and in projects with restricted areas (both overhead and laterally) and with adequate room for nails (Galvan, 2012). Furthermore, soil nails are generally used in the construction of unimpeded turnaround lanes under bridges where such lanes were not planned in the first place (Briaud and Lim, 1997). This is an innovative way of making the traffic flows easier in large urban areas. This is achieved by moving the

embankment slope in front of the abutment under the bridge and nailing the soil between the piles that support the abutment (Figure 10). The slope is typically 15 ft high with a 2:1 horizontal to vertical slant. The 30-ft width, which is freed by this technique, gives ample room for the turnaround lane.

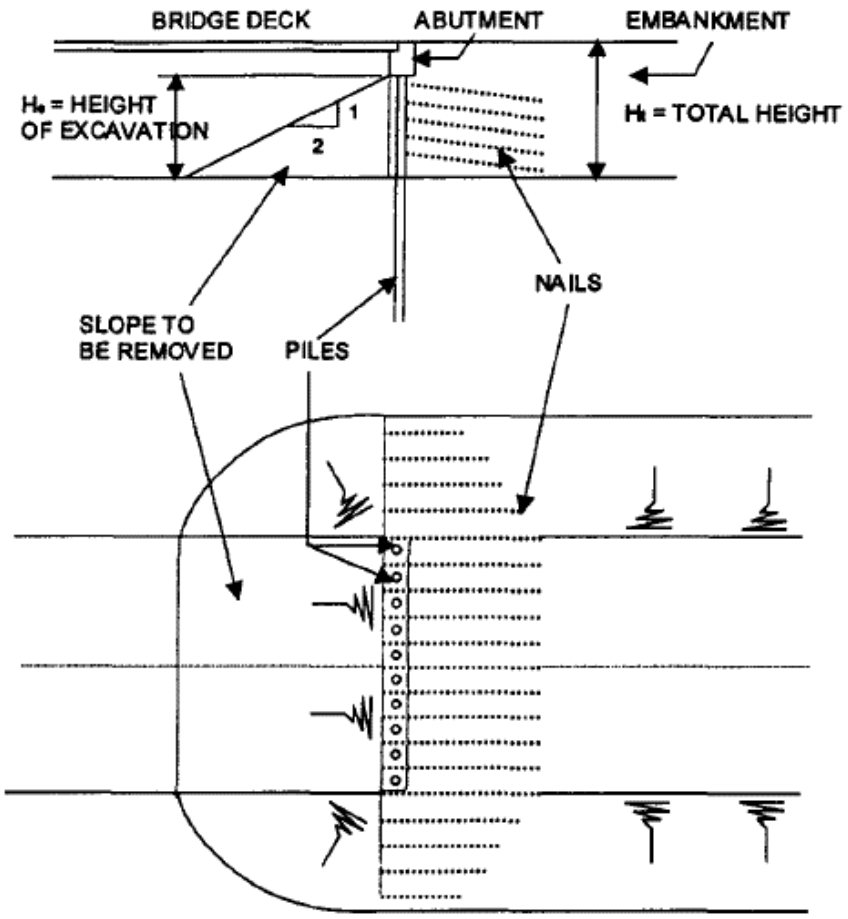

Figure 10. Soil-Nailed Wall under Polled Bridge Abutment (after Briaud and Lim, 1997).

Such a solution based on soil-nailed walls under piled bridge abutments represents a relatively new application of soil nailing that has become quite common in Texas and other states in United States. In Texas, the design of such soil nail walls in existing embankments generally involves the presence of HP clays. Figure 11 presents the cross section of a typical soil nail wall for an existing bridge and a picture of a typical unimpeded turnaround. The basic information required for the design of this kind of project involving a soil nail wall is (Galvan, 2012):

- Soil borings through zone to be nailed.
- Cross sections normal to wall face.
- Existing bridge plans.
- Roadway alignments, including tie-in to existing bridge.

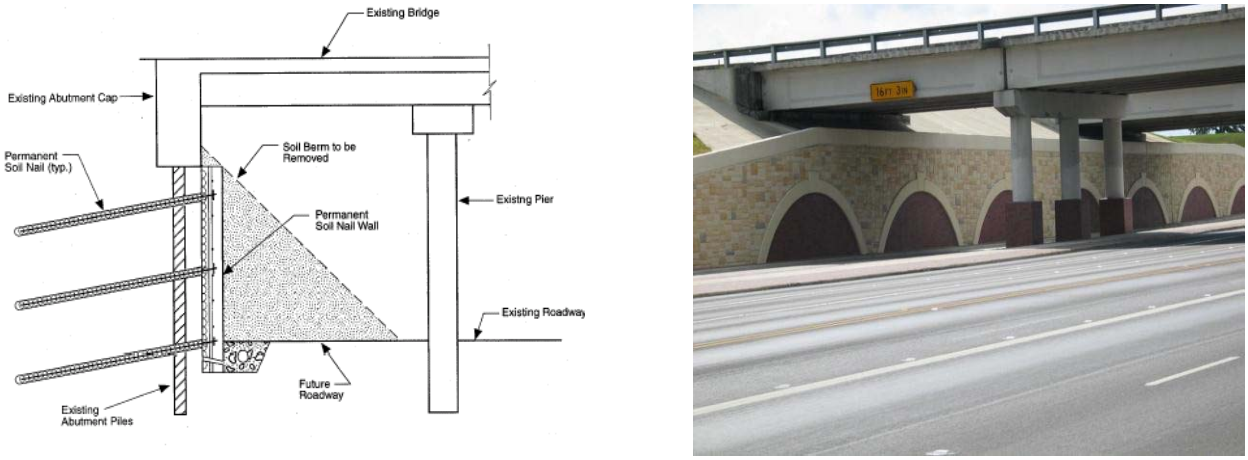

Figure 11. Typical Soil Nail Wall Cross Section for Existing Bridge (after Galvan, 2012).

The method generally adopted by TxDOT for the design of a soil nail wall follows the guidelines established in GEC#7, but includes some additional recommendations from the TxDOT *Geotechnical Manual* (TxDOT, 2006), as explained below. According to Galvan (2012) the principal TxDOT design tools are: 1) GEC#7, 2) GOLDNAIL computer program, 3) SNAILZ software, and 4) TxDOT *Geotechnical Manual*.

As for the soil parameters to be adopted in the design; Galvan (2012) recommends using ultimate cohesion and the friction angle, which should be determined from drained (long-term) strengths. On occasion, it may be difficult to perform drained soil testing, so correlation with PI, or experience can be used in the design. Cohesion (c) should be very low (i.e., between 0 and 100 psf), and the angle of friction (ϕ) is generally adopted between 24° and 34° (Galvan, 2012). Reasonable parameters in an average compacted clay embankment are as follows: $\phi = 30°$, c = 0 psf, and unit weight = 120 pcf. Embankments known to be soft, wet, or with a history of failures should use lower values (Galvan, 2012). It is not recommended to reduce soil strengths because programs have multiple partial factors of safety (Galvan, 2012). Additional TxDOT recommendations for the design of soil nail walls are as follows (Galvan, 2012):

- For nail spacing, it is recommended to use between 3 ft and 4.5 ft for vertical spacing and between 3.5 ft and 5 ft for horizontal spacing.
- The top nail should be within 2 ft of the top of wall and the bottom nail within 3 ft of the base of wall.
- Typically, nail lengths are equivalent to wall height. This ultimately depends on geometry, soil conditions, and loading (i.e., from 0.7 h up to 1.5 h).
- All the nails should have the same length.
- The diameter of the hole in the soil nail wall is typically 6 in., but occasionally 8-in. hole diameter is used on tall walls and/or soft soils.
- Bars sizes #6 or #8 are typically adopted. The grade is generally 60 or 75.
- Typically, two nails per wall are used for testing.
- The ultimate pullout resistance is the anticipated ultimate shear transfer per foot of nail and is determined from the Texas Cone Penetrometer (TCP) tests.

The last item of the list above is perhaps the main difference between TxDOT's design method and GEC#7 guidelines. GEC#7 recommends to do the pullout test to obtain the bond strength. It also provides Table 2, which includes typical values of ultimate bond for drilled and grouted nails installed in various soils and using different drilling methods. Alternatively, TxDOT recommends using the TCP to determine the ultimate pullout resistance. The ultimate pullout resistance is the anticipated ultimate shear transfer per foot of nail. Figure **12** can be used to estimate the allowable skin friction (S). The lines in this plot refer to the different soil types (CH, CL, SC, Other) and N is related to the number of blows obtained from the TCP test. The same method for calculating the skin friction on a drilled shaft or pile can be used here. It is necessary to convert the skin friction from allowable to ultimate, and then to convert it to tons per square foot (tsf) from pounds per square foot (psf) (i.e., 1 tsf = 2000 psf).

The simple example below from Galvan (2012) illustrates how the ultimate pullout resistance can be estimated using the method explained above:

- Sample = 6-in.-diameter nail in 15 blow-per-foot clay (CL) embankment.
- Unit Shear = (15/60) * 2(FS) * 2000 (conversion from tsf to psf) = 1000 psf.
- Nail Circumference = 0.5 ft * 3.14 = 1.57 ft.

- Ultimate Pullout Resistance = 1000 psf * 1.57 ft. = 1570 lb per foot of nail.
- This value also determines the Test Nail Load.

Note that for the design of rock nails the ultimate pullout resistance is limited to 3000 lb per foot. For soils the TxDOT Bridge Division has limited this value to 2000 lb per foot (i.e., max cohesion of 1300 psf).

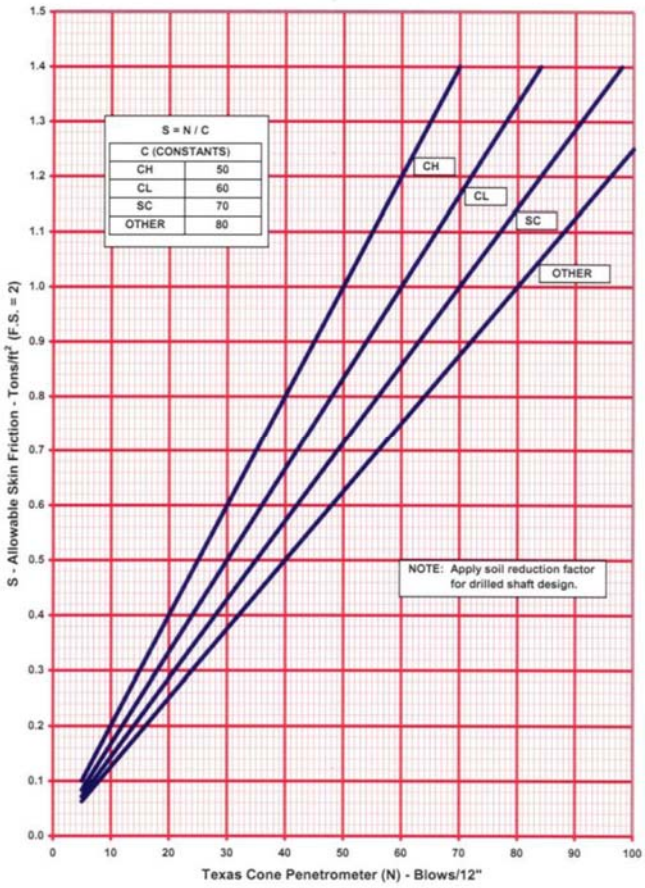

Figure 12. Allowable Skin Friction (after TxDOT, 2012).

CURRENT PRACTICE IN OTHER STATES AND COUNTRIES

In the United States, almost all of the state departments of transportation follow the GEC#7 guidelines for the design of soil nail walls. Therefore, they share the same concern about the design of soil nail walls in HP clays. Guidelines and manuals from other countries have some recommendations and comments when dealing with the design of soil nail walls in HP clays. In

the following sections, some design manuals are briefly discussed with special emphasis on aspects related to soil nail walls in HP clay and creep tests on soil nails.

Design and Construction Guidelines for a Soil Nail Wall System – NYSDOT

Geotechnical Engineering Manual GEM#21, Revision #2 was published by the State of New York, Department of Transportation (NYSDOT, 2008b). This manual mentions that soft clays are susceptible to creep and that permanent wall systems may not be practical in this kind of soil.

The criterion for the soil creep test has been set to ensure that the nail design loads can be safely carried throughout the service life of the structure. The creep movement in the verification test is set such that the total movement is less than 0.08 in. (2 mm) between the 6-minute and 60-minute readings. During a proof test, the creep portion may be terminated if less than 0.04 in. (1 mm) of movement has occurred between the 1-minute and 10-minute readings.

Guide to Soil Nail Design and Construction – Geoguide 7

Geoguide 7 presents the recommended standard of good practice for the design, construction, monitoring, and maintenance of soil-nailed systems in Hong Kong (Geoguide 7, 2008). This Geoguide summarizes the experience gained from use of the soil nailing technique in Hong Kong, including the findings coming from related technical works recently developed. This guideline is concerned with the effect of creeping on the stability and serviceability of the excavation, in particular if the soil nails are designed to carry sustained loads.

For soil nails designed to carry sustained loads and bonded in the soil mass, a creep test should be carried out to determine the susceptibility of the soil nails to long-term creep. Figure 13 illustrates the load-deformation cycle of a creep test as part of a pullout test. The procedure for a creep test is similar to the one for the pullout test except that only one loading cycle is required. T_{DL1} should be the allowable pullout resistance provided by the bond length of the cement grout sleeve of the test soil nail (Figure 13). T_{DL2} is the intermediate test load for a pullout test. T_{DL2} should be T_{DL1} times the FS against pullout failure at the soil–grout interface. The soil nail should be loaded from the initial load (T_a) to the creep test load (T_c). In creep tests, T_c is coincident with T_{DL2}. The creep period should be considered to begin when T_c is applied. The load should be maintained for 60 minutes for deformation measurement.

During the creep period, the measurement should be taken at time intervals of 1, 3, 6, 10, 20, 30, 40, 50, and 60 minutes.

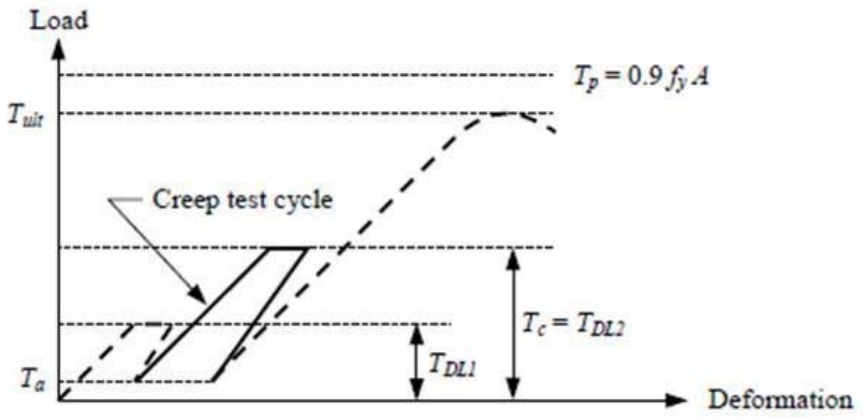

Figure 13. Schematic Diagram of Load-Deformation Cycle of a Creep Test as Part of Pullout Test (after Geoguide 7, 2008).

A soil nail should be considered acceptable when: 1) the difference of soil nail movements at 6 minutes and 60 minutes during the creep period does not exceed 2 mm or 0.1 percent of the bond length of the test soil nail; and 2) the overall trend of creep rate (i.e., soil nail movement/log time) is decreasing throughout the creep period. In the event that the acceptance criteria cannot be met by any of the creep tests, the design bond strength of the soil nails, which the creep test represents, should be reviewed and revised as needed.

Recommendations Clouterre 1991 – France

This recommendation was compiled from studies performed by the French National Project "Clouterre" (Clou=nail, terre=soil) carried out from 1986 to 1990. Details about this work can be found in Recommendations Clouterre (1991) and Plumelle et al. (1990). The originality of the project lies in the fact that three fully instrumented experiments involving soil nail walls were built and monitored from construction to failure. The results of the Clouterre program have been very useful to understand better the behavior of soil nail systems. They have been published and constituted the basis for the soil-nailing design approach adopted in France. It was translated to English and printed by FHWA as report FHWA-SA-93-026.

This recommendation states that the soil nail technique does not generally perform well in very plastic, clayey soils and very sensitive soils, particularly where there is a relatively low unit skin friction value between the soil and the inclusion.

Two different kinds of pullout tests are contemplated: controlled displacement test (constant speed) and controlled force test (creep steps). With the controlled displacement pullout test, it is possible to determine the maximum pullout force (T_L), the residual force, and the value of the initial slope of the force displacement curve. With the controlled force test, the critical creep tension (T_C) and eventually the limit tensile force (T_L) can be measured. Table 5 summarizes results from a wide number of controlled force tests in Clouterre project have allowed the development of correlations between T_L and T_C (i.e., $k = T_L/T_C$) k values.

Table 5. Magnitude of $k = T_L/T_C$ as a Function of the Type of Soil and the Installation Method (Recommendations Clouterre, 1991).

		$K=T_L/T_C$
Gravity Injection	Sands	1.2
	Clays	1.3
	Marls and Chalks	1.3
Driving	Sands	1.4

The controlled force test was used for creep experiments. In this type of test, the nail is gradually subjected to a pullout force, which increases up to the estimated pullout force, T_{LE}. This is the nail's pullout tension estimated on the basis of geotechnical data or based on the contractor's experience. In practice it is usually assessed from the controlled displacement pullout test, which is always carried out first. This force must be lower than 0.6 T_G (i.e., the elastic limit of the reinforcement), so as to limit creep in the steel. The first loading step is applied at 0.2 T_{LE}. The displacement measurements are taken at each loading steps and performed at the following time intervals, t_0: 1, 2, 3, 4, 5, 8, 10, 15, 20, 25, 30, 45, and 60 minutes. Successive loading steps are applied every 0.1 T_{LE} and are maintained for 60 minutes, except for the 0.7 T_{LE} loading step, which is maintained for 3 hours. The creep tests were performed at constant load, and a load cell was used to measure the applied load. The

jack pressure was adjusted to guarantee that force required for a given loading step was actually applied.

The results were plotted in decimal logarithmic scale for the time and arithmetical scale for the displacement. Typical creep curves of the pullout tests performed in this project are shown in Figure 14 (note that in Figure 14 $T_{max} = T_{LE}$). In this plot, the slope α characterizes the creep curve, and it can be calculated for each load step (as shown in Figure 14). For the first loading steps, the creep curves are straight lines and α (and so the creep rate) gradually increases with the load level. At higher loads, the creep curves are no longer straight lines. This experimental evidence confirms the idea that creep rate in nails depends on stress level. Very small creep rates were observed when the load acting on the nail was small.

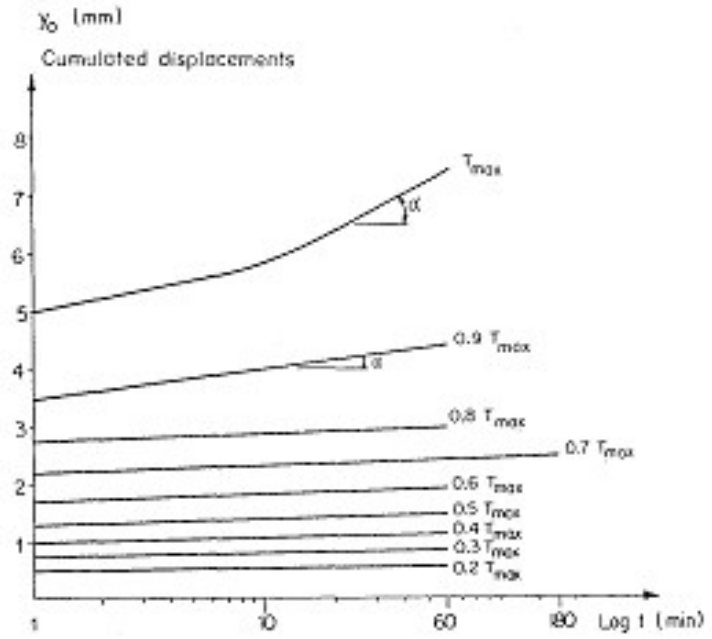

Figure 14. Creep Curves of a Pullout Test (after Recommendations Clouterre, 1991).

Another useful way to present the information from the creep tests is by plotting the results as shown in Figure 15. From this plot, the critical creep tension, T_C, can be obtained. T_C corresponds to the last loading step before the curve bends. T_C' corresponds to the intersection of the two straight lines fitting the experimental data (generally $T_C \cong 0{,}9\ T_c'$).

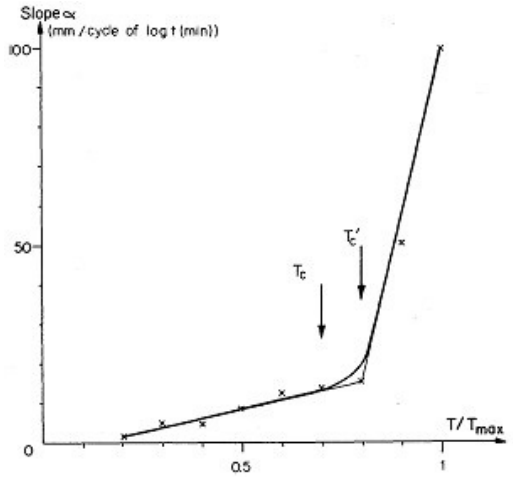

Figure 15. Determination of Critical Creep Tension (after Recommendations Clouterre, 1991).

RESEARCH OUTCOMES IN OTHER STATES RELATED TO SOIL NAILS

In the United States, the majority of the state departments of transportation follow the GEC#7 guidelines for the design of soil nail walls, with practically no additional research in this area. Just a few states have been doing research related to soil nail walls. The more relevant ones are briefly summarized below.

California Department of Transportation – Caltrans

Caltrans has been very active in undertaking research associated with the behavior of soil nail walls. Perhaps the two more relevant contributions are the two pieces of software developed to assist with the design of soil nail walls:

- **CalNail** is a design tool for soil nail projects that compiles field case histories related to soil nail walls. In June 2006, The California Department of Transportation's Division of Research and Innovation released a report that describes CalNail (Turner and Parnell, 2006). CalNail is a web-based centralized repository of information for individuals involved in the research, design, construction, and maintenance of soil nailing infrastructure in California's highways. CalNail currently hosts over 30 documented case histories for soil nail walls in California.
- **SNAILZ** is a computer program developed under DOS. The name of the program comes from "Soil NAIL," and Z identifies this version from previous ones. This program is

intended for the analysis of stability in slope reinforced with soil nail walls. To perform the analysis of stability, the program adopts a bilinear wedge model for failure planes existing at the toe of the walls and a trilinear wedge model for those cases involving planes of failure developed below and beyond the wall toe. The soil interslice forces are based on the mobilized angle of internal friction and cohesion.

Montana Department of Transportation – MDT

MDT has started a new 10-year experimental program on soil nail walls. The research project is entitled, "Experimental Projects Work Plan: Evaluation of Launched Soil Nails for Slope Stabilization." The project started in April 2011 and is expected to continue until around 2022 (tentatively).

New York State Department of Transportation – NYSDOT

The NYSDOT has performed a few studies on soil nail walls, but two reports can be highlighted here:

- ***Design Procedure for Launched Soil Nails Shallow Slough Treatment.*** This report was edited in September 2008. It is a very short document (16 pages) that provides some basic guidelines to treat shallow slough using soil nails (NYSDOT, 2008a). The concepts presented in this report and the technologies used for the treatment are similar to the ones mentioned in GEC#7.
- ***Design and Construction Guidelines for a Soil Nail Wall System.*** This project report, published in November 2008, is a short report (27 pages) that focuses on the construction procedure of a soil nail system (NYSDOT, 2008b). The material reported in this document follows GEC#7 guidelines.

Oregon Department of Transportation – ODOT

The Oregon Department of Transportation (ODOT) has studied the behavior of soil nails walls for a very long time. They performed their first numerical analyses about 20 years ago. The most prominent ODOT reports prepared out of those projects are listed below:

- ***Monitoring of Soil Nailed Walls at the Highway 217 and Highway 26 Interchange, Final Report.*** This document was prepared by Landau Associates Inc. in November

1999. The report presents the results of a soil nail wall research project undertaken by ODOT. The aim of this project was to gain a better understanding of the performance of soil nail walls under different scenarios and a variety of loading and boundary conditions (ODOT, 1999).

- **Part I, *Soil Nailing of a Bridge Fill Embankment* (August 1991), and Part II, *Design and Field Performance Report* (July 1995).** The report associated with this research consists of two parts. It summarizes the results of ODOT's extensive investigation on soil nail technique as an alternative to more conventional bridge embankment retention methods. The soil nailing technique was used for an underpass widening to provide for additional traveling lanes under the existing Oregon Slough Bridge in Portland, Oregon (ODOT, 1991; ODOT, 1995).
- ***A Numerical Investigation into the Performance of the Soil Nail Wall and Pile Foundation at the Swift Delta I-5 Interchange.*** This report was prepared by Dr. Smith, from Portland State University in December 1993. In Smith (1993), numerical codes based on the finite element method (FEM) were used to study the soil nail wall construction process. Two-dimensional (2D) numerical analyses were performed using FENaiL, which is a new FEM code written specifically for this study. A full three-dimensional (3D) FEM analysis was also carried out with Abaqus. Different soil models for the soil were adopted (i.e., linear elastic and anisotropic elastic models, and a single elastic-plastic model) to study the interaction between the different components of the soil nail system (Smith, 1993).

Tennessee Department of Transportation – TDOT

TDOT recently published (in February 2012) a report entitled *Tennessee Department of Transportation Earth Retaining Structures Manual*. This manual encompasses the design of different structures typically used for retaining earth and it includes soil nail walls (TDOT, 2012).

Washington State Department of Transportation – WSDOT

The WSDOT has also studied the behavior of soil nail walls. For example, the report entitled *Evaluation of Design Methodologies for Soil-Nailed Walls, Volume 1* in July 1998 (WSDOT, 1998) focuses on the study of seven computer programs typically used in the design

of soil nail walls: SNAIL, NAIL-SOLVER, STARS, NAILM, GOLDNAIL, TALREN, and COLDUIM. The response of a soil nail system under actual conditions is also addressed in a more recent report, *Geotechnical Engineering Services Wall 18–SR522 at US 2 Overcrossing Monroe, Washington* (WSDOT, 2010).

LITERATURE REVIEW

The underlying aim of this project is to gain a better understanding of the long-term behavior of soil nail walls in HP clays. This is a quite complex problem that encompasses a large number of subjects, which are difficult to cover in full in a single review. In this section, the researchers compile some selected publications related to the objectives of this project.

This section starts with a general introduction about the creep behavior of soils, alongside some typical results of experimental investigations related to the long-term behavior of soils and constitutive models developed to describe the creep behavior of soils. Then, some relevant contributions related to the numerical modeling of soil nail walls are presented. Afterward, a brief summary of works related to the monitoring and behavior of walls in the field is presented. This section closes with a table summarizing the major contributions in this field.

Creep Behavior of Soils

The general case of creep in soils is characterized by the three steps shown in Figure 16 (Vyalov, 1986) and described as follows:

- **Step I** is related to a primary creep (δ^{I}), characterized by an attenuated deformation with a decreasing rate of deformation ($d\delta/dt$). The duration of this stage is generally very short.
- **Step II** is known as secondary creep (δ^{II}) and takes place at a constant deformation rate.
- **Step III** is associated with a tertiary creep (δ^{III}) and is characterized by a non-attenuated deformation, with an increasing rate of deformation.

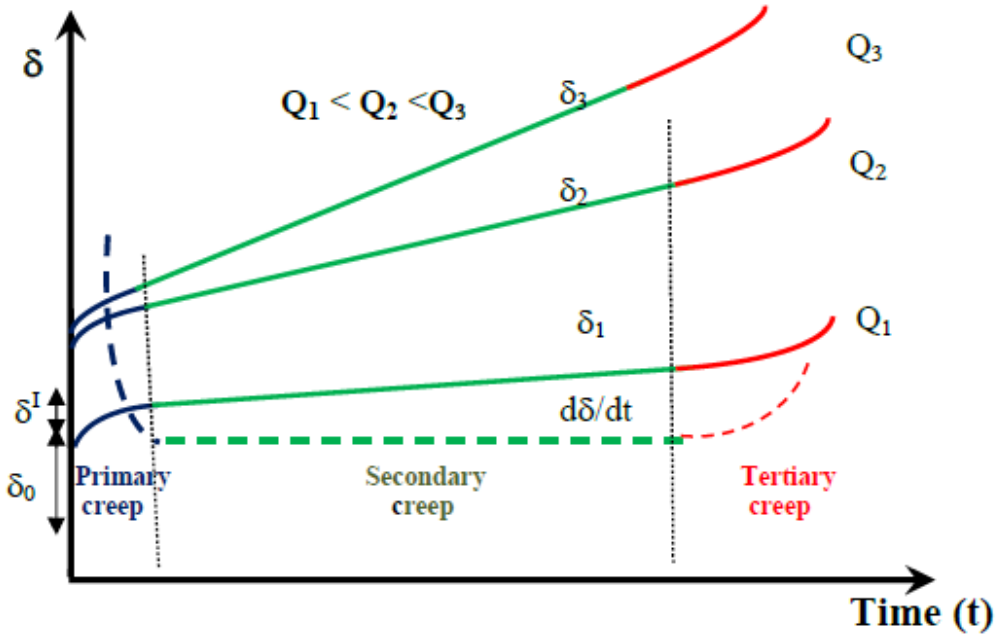

Figure 16. Three Steps Associated with Creep in Soils (after Vyalov, 1986).

The actual configuration of these curves will depend on conditions such as soil type, stress level, water content, and temperature. The load level (Q) has a predominant effect on creep behavior. Figure 16 illustrates the effect of different load levels (Q_1, Q_2, and Q_3) on creep.

As suggested by Vyalov (1986), the three steps are generally associated with changes in the clay fabric that take place during creep (Figure 17). In this conceptual model, it is assumed that the soil fabric is composed of clay particles, aggregates, and pores. Before loading, the orientation of the clay particles and aggregates is random. Once the load is applied, stress concentration occurs near the aggregates (at the contact points), bonds are broken, and the particles tend to be oriented in the direction of the load. At this point the material starts to creep at an increasing rate. Generally, the breaking of the bonds starts at the weakest point of the soil structure. Therefore, after some rearrangements of the soil particles, the soil structure tends to a more stable skeleton. Obviously, this condition will depend on the dry density and strength of the material. If the stress level is low, the new rearrangement of the soil particles is capable of equilibrating the external load, and so the movement is attenuated in time and, under certain circumstances, the creep may eventually stop. This step corresponds to what is known as primary creep.

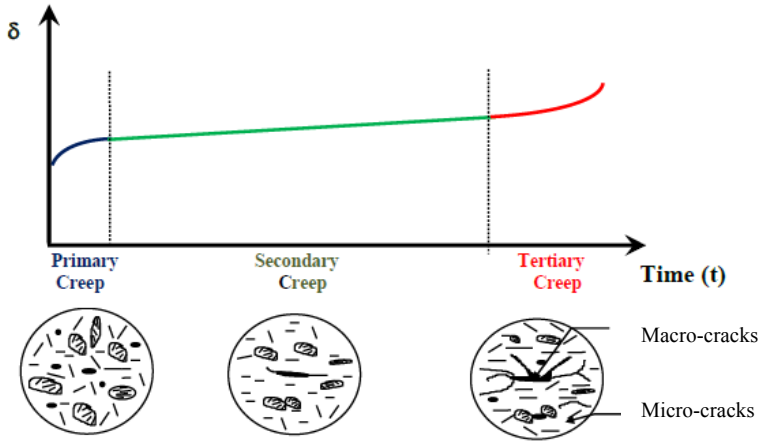

Figure 17. Changes in the Soil Fabric during Creep (after Vyalov, 1986).

However, if the stress level is such that after the initial rearrangement of the soil particles (described above) the modified soil structure cannot equilibrate external stresses, the material will continue creeping. This step corresponds to the secondary creep, where the rearrangement and reorientation of the soil particles take place at a constant creep rate. It could happen that after important deformations some microcracks may develop. Those microcracks affect the strength of the soil, leading to a stage of non-attenuated strain rate with big changes in the soil structure and with the formation of macrocracks.

A proper geotechnical design must prevent tertiary creep to be developed at any time of the earth-structure lifetime. It must assure that the constant creep rate (i.e., Step II) is below the maximum established in the guidelines. The total deformation at a given time can be calculated as the instantaneous deformation ($_0\delta$), plus the one related to Step 1 (δ^I), plus the strain rate associated with Step II ($d^{II}\delta/dt$) times the elapsed time (Δt). This is because the (short) time related to Step I is generally disregarded.

$$\delta = \delta_0 + \delta^I + d\delta^{II}/dt \times \Delta t \qquad (2)$$

Note that the graphs presented in Figure 16 and Figure 17 are very general and aimed at explaining the basic concepts associated with creep in soils and the patterns of behavior typically observed in soils. In practice, it is quite common to plot creep tests in semi-log scale (i.e., displacements versus log time) or log scale (i.e., log displacement versus log time), as explained below.

Similar behavior and stages can be anticipated in the problem studied in this project. The creep movement of the soil nail can be regarded as the sum of different contributions, including the following: creep of the steel nail, the progressive (relative) movement of the grout, and the creep of the soil itself.

The creep behavior of soils has been a matter of special interest in geotechnical engineering, and different models have been proposed in recent years. As an example of a creep law, the model proposed by Pestana and Whittle (1995) is briefly introduced below.

Pestana and Whittle (1995) proposed a nonlinear compression model for freshly deposited cohesionless soils that assumes that specimens loaded from different formation densities approach a unique response at high stresses. This limiting compression curve (*LCC*) is characterized by a linear relationship in log (*e*)–log(σ') space:

$$\log(e) = -\rho_c \log\left(\frac{\sigma'_v}{\sigma'_{vz}}\right) \tag{3}$$

where ρ_c = compressibility index; and σ = reference effective stress at unit void ratio (e = 1.0).

Pestana and Whittle (1998) proposed later on a simple extension of the compression model to account for time-dependent creep deformations. The *LCC* regime is characterized by parallel isochronous compression lines, which are analogous to the secondary compression models for cohesive soils:

$$\log(e) = -\rho_c \log\left[\frac{\sigma'_v}{\sigma'_{vr}(t_{ref})}\right] - \rho_a\left(\frac{t}{t_{ref}}\right) \tag{4}$$

where ρ_a is a creep rate coefficient that characterizes the rate of deformation at constant vertical effective stress in the *LCC* regime; and t_{ref} is a reference time.

Sanzeni et al. (2012) used the Pestana and Whittle (1998) model to study the compression and creep behavior of Venice Lagoon sands. The compression test procedures included: 1) one-dimensional (1D) compression at a strain rate of 1.0 percent per hour to a maximum vertical effective stress of 2.0 MPa, 2) drained creep for a period of 24 hours at the maximum stress, and 3) unloading at a strain rate of −0.5 percent per hour. Figure 18 presents some comparisons in

terms of creep strain between experimental observations and model predictions. In Figure 18, quite good results were obtained with this model.

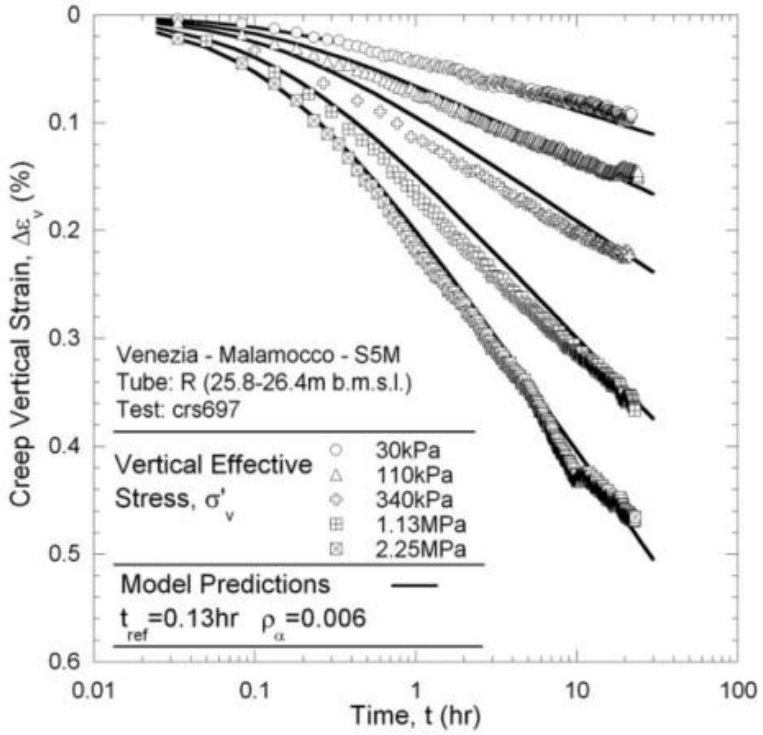

Figure 18. Comparison between Experimental Creep Rate and Model Results (after Sanzeni et al., 2012).

Briaud and Garland (1985) proposed the rate effect model to predict the time-dependent behavior of soils. The model can be expressed as follows:

$$\frac{s}{s_1} = \left(\frac{t}{t_1}\right)^n \tag{5}$$

where the settlement, s_1, is the value of settlement, s, observed at a time t_1 = 1 minute (after the beginning of a load step); and *n* is the creep exponent, which is considered a soil property. Typical *n* values range from 0.005 to 0.03 for sands and 0.02 to 0.08 for clays.

Briaud and Gibbens (1999) used this model to interpret the data from five large spread-footing field tests. The testing procedure consisted of applying the load in increments equal to one-tenth of the estimated footing capacity. Each load step lasted 30 minutes or 24 hours. Figure

19 shows the load settlement curve. Important creep settlements took place during the time that the load was kept constant.

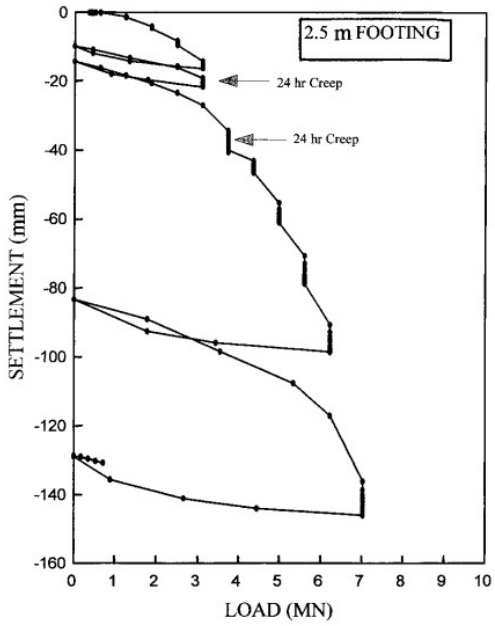

Figure 19. Load-Settlement Curve (after Briaud and Gibbens, 1999).

The creep curves for different load steps and different load levels are shown in Figure 19. Figure 20a shows the creep curve for 30-minute load steps. These results show the strong dependency of the creep rate on the applied load. Figure 20b presents the results of tests obtained for the 24-hour load step.

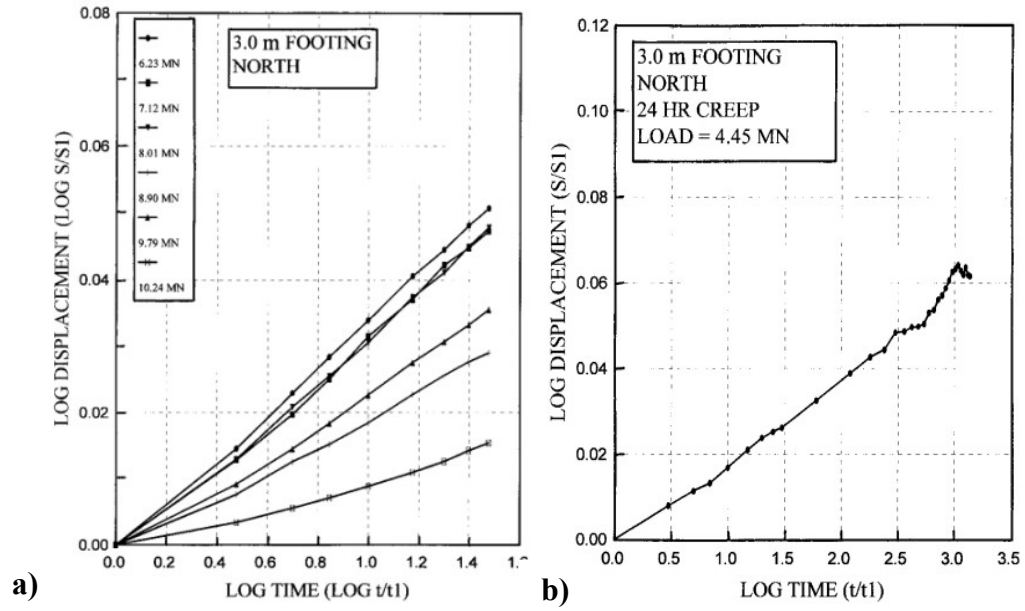

Figure 20. Creep Curves for a) 30-Minute Load Steps, and b) 24-Hour Load Steps (after Briaud and Gibbens, 1999).

As for the creep behavior of soils under deviatoric loads, there is less information compared with the contributions related to creep behavior of soils under volumetric or oedometric conditions. In general terms, the study of the creep behavior in geotechnical engineering has been quite intensive for problems involving rock salt and frozen soils (e.g., Eckardt, 1982).

Perhaps one of the more relevant contributions related to the creep behavior of clays is the work by Briaud et al. (1998a). They were the first ones to mention that creep will cut across the hump of the stress–strain curve. This means that failure may be induced before reaching the peak stress, by creep, if the deviatoric load is held constant at a relatively high stress level. This phenomenon can be explained better with Figure 21, in which when the creep test (represented with the empty triangular symbols) is performed at a high deviatoric stress (but below the peak stress), the stress–strain curve will follow the path of the gradual failure, crossing (nearly horizontally) below the stress–strain curve obtained in the standard test (represented by the dark triangular symbols) and reaching failure at large strains.

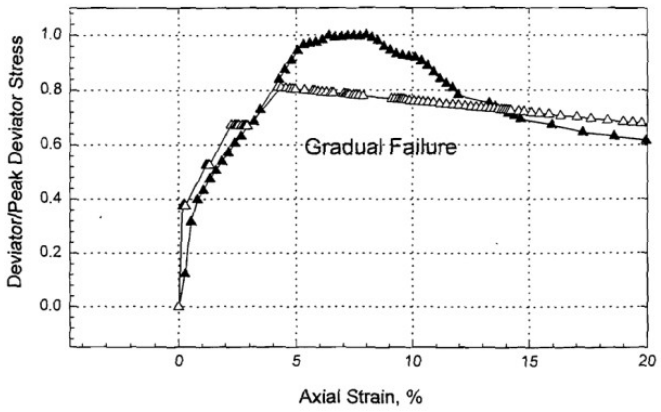

Figure 21. Failure under Constant Load (after Briaud et al., 1998a).

Hunter and Khalili (2000) and Dornfest et al. (2007) both proposed similar models based on the concept of cutting across the hump to explain the creep behavior in over-consolidated clays. The scheme in Figure 22a presents the idealized creep failure model, showing that when the constant stress is higher than the critical state stress, it will start to creep (onset of tertiary creep). The stress–strain curve will cut across the hump, until merging with the stress–strain curve of the standard triaxial test.

Figure 22b presents what could happen in different situations; for example, if the stress is kept constant at a point like A, the creep path will be A to B. In Dornfest et al. (2007), they explain other possible paths when creep tests start at lower stress level, as C and F.

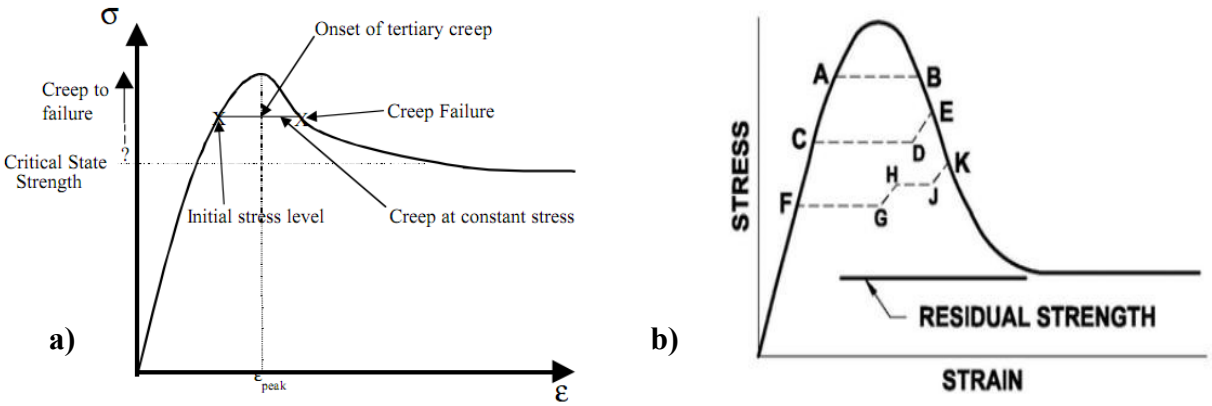

Figure 22. a) Scheme Showing Soil Failure during Creep Tests (after Hunter and Khalili, 2000); b) Idealized Stress–Strain Curve for Over-Consolidated Clay and Creep Test Paths (after Dornfest et al., 2007).

Hunter and Khalili (2000) present results of drained creep tests performed in different clay types. The aim of those tests was to prove the concept of cutting across the hump. For

example, Figure 23 shows some typical results from this paper in terms of the ratio between the axial strain and axial strain at peak stress (in constant strain rate triaxial test) versus axial strain rate. The results are presented for tests performed at different ratios between the stress at which the creep test is performed and the peak stress. In this figure, when the ratio is not that high, the axial strain rate is decreasing, tending to very small values. However, when the stress ratio is high, the axial strain rate is increasing. This means that the displacements are also increasing and the sample will fail.

Most of the laboratory tests that focus on creep behavior of soils under deviatoric load are triaxial consolidated drained (CD) tests (Hunter and Khalili, 2000). Other stress paths have been used, but they are not very popular; for example, typical results from triaxial consolidated undrained (CU) tests performed by Martinez-Vasques and Diaz-Rodriguez (2009) are presented in Figure 24.

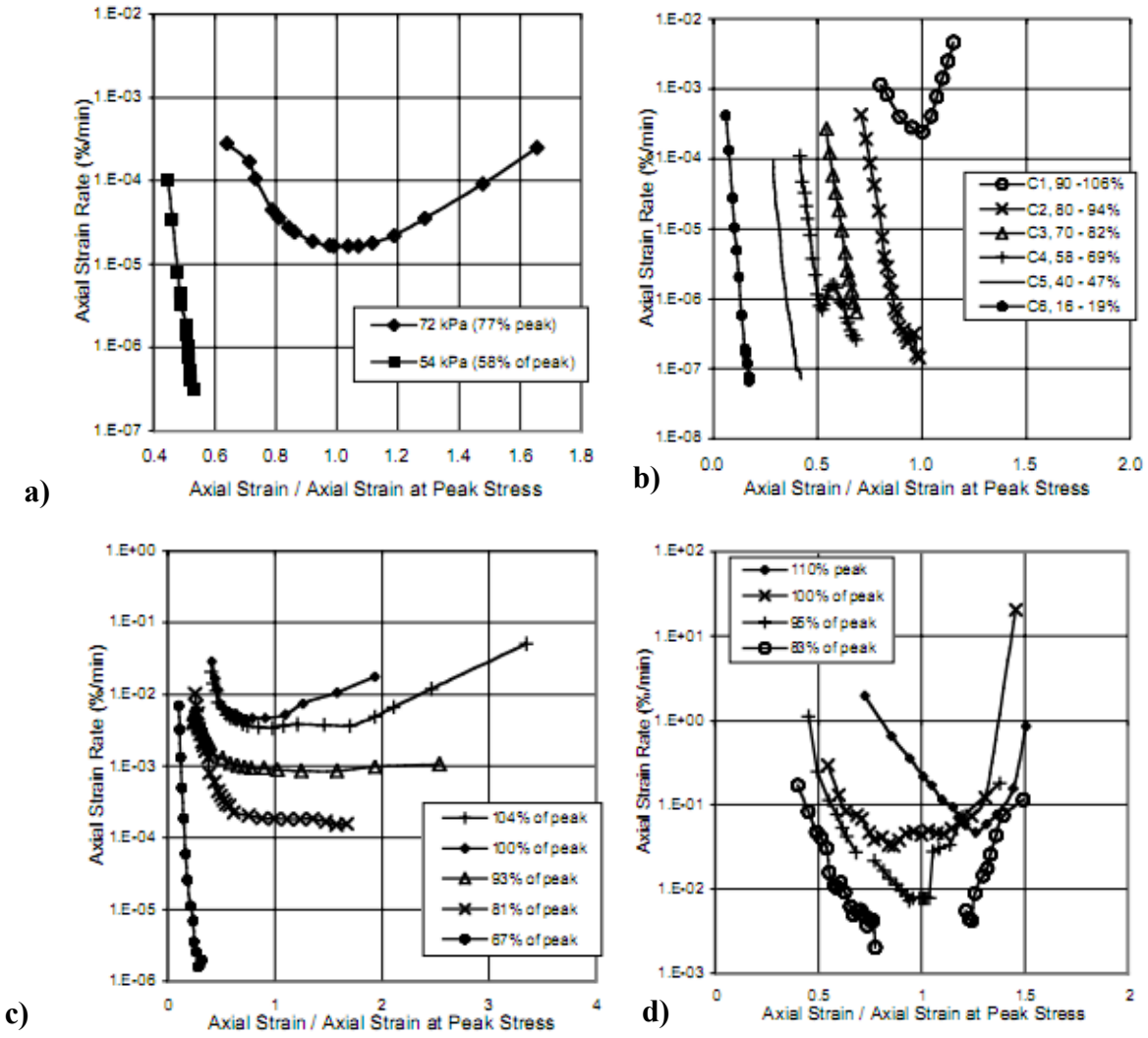

Figure 23. Drained Creep Test Results on Different Clays: a) Nicolet Clay, b) London Clay, c) Saint Alban Clay, and d) Umeda Clay (after Hunter and Khalili, 2000).

In relation to the duration of the creep tests in the laboratory, different strategies have been adopted in the past. For typical laboratory tests, creep stages (i.e., time during which the load is kept constant) of 24 hours have been generally adopted. For example, the creep tests performed on Venice Lagoon sands last 24 hours (Figure 18; Sanzeni et al., 2012). There has been, however, some exemptions. For example, the creep stages of the CU triaxial tests carried out by Martinez-Vasques and Diaz-Rodriguez (2009) lasted over 10,000 minutes (one week). The soil studied in this work was an undisturbed, lightly over-consolidated clay.

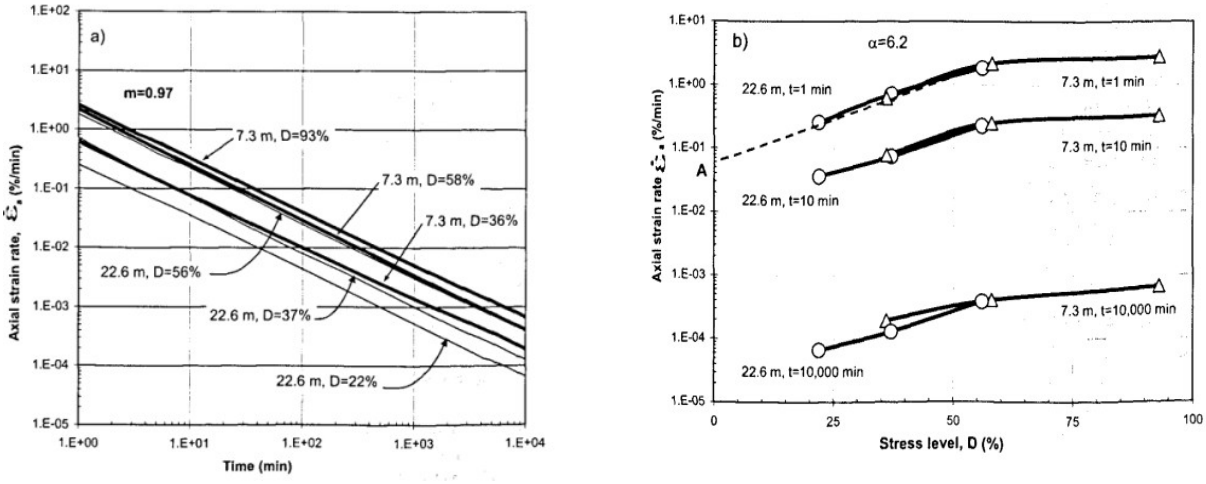

Figure 24. Results of Triaxial CU Test on Mexico City Soils (after Martinez-Vasques and Diaz-Rodriguez, 2009).

Figure 24 shows that for a given stress level, the longer the time, the smaller the axial strain rate is. For a given duration of the creep test (e.g., t = 10,000 minutes), as the stress level increases, the axial strain rate also increases. This observation indirectly shows that creep will be more relevant at high stress level.

As for the field investigations, different timespans for the creep tests have been adopted. For example, Briaud and Gibbens (1999) held the load for 30 minutes (at most) in each load step. From those experiments they proposed the power law model. Figure 25 presents results of creep tests on anchors performed by Ostermayer (1975), in which the load was hold for 100 to 1000 minutes at different load levels. When the load is higher than 515 kN, the displacement versus the time (semi-log) is no longer a line, and the displacement starts to increase more when compared with the behavior at low load level.

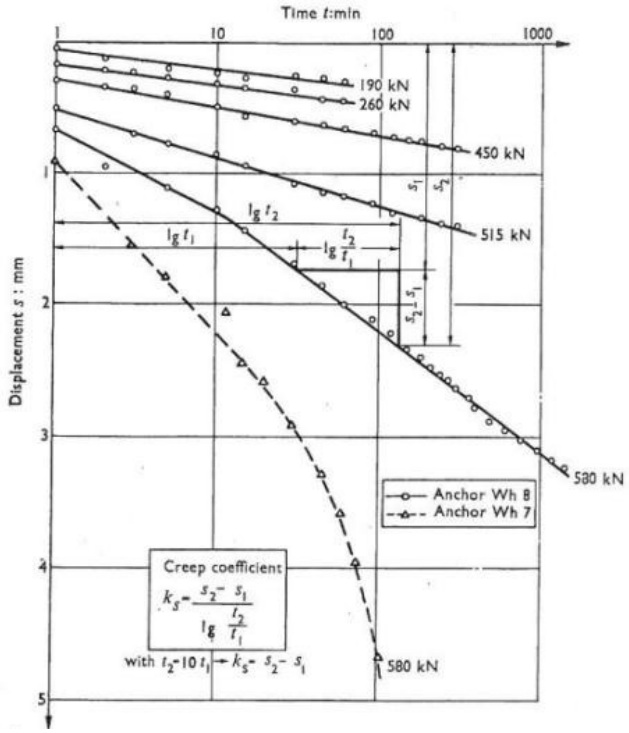

Figure 25. Time–Displacement Curves for Various Loading Steps on Anchors (after Ostermayer, 1975).

An important number of contributions have focused on the creep behavior of anchors (Briaud et al., 1998a; Ludwig, 1984; Ludwig et al., 1985; Ostermayer, 1975; and Weatherby, 1982 and 1998). Weatherby (1998) presents the apparent earth pressure diagrams to design the permanent ground anchor walls based on the research performed on two full-scale wall sections, four model-scale walls, and 10 large-diameter ground anchors installed in a fine-grained soil.

Ludwig (1984) and Ludwig et al. (1985) studied load tests performed on instrumented tiebacks anchored in a variety of cohesive soils. A series of cyclic loads was applied to the tieback. The peak load of each successive load cycle was greater than its predecessor. At the end of each load cycle, the load was released to a nominal alignment load. In the creep tests, the peak load of each load cycle was held constant for periods ranging from 10 minutes to 10,000 minutes. The result of creep tests on anchors is illustrated in Figure 26. These curves show that the creep behavior is dependent on load level. In the low load level, the creep rate is almost zero. As the load level increases, the creep rate increases. Figure 27 shows that for a load higher than 70 to 80 percent of the ultimate load, the residual anchor movement increases rapidly.

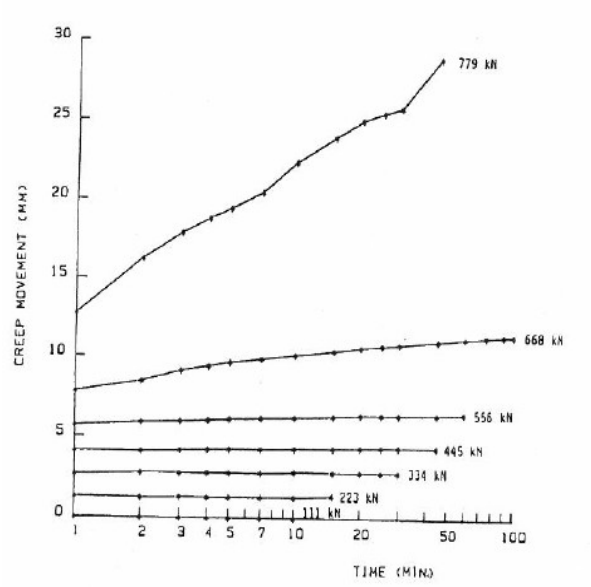

Figure 26. Typical Creep Curves of Straight-Shafted Tiebacks Anchored in Cohesive Soils (after Weatherby, 1982).

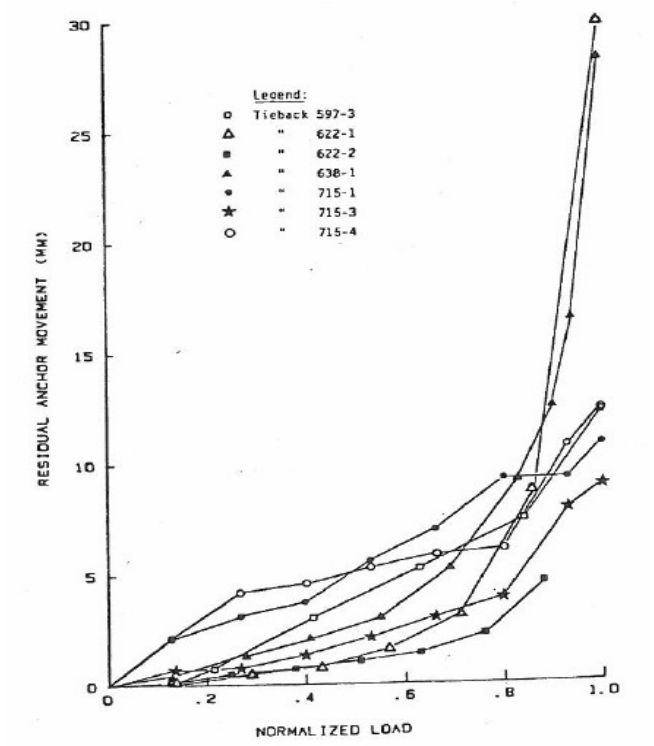

Figure 27. Residual Anchor Movement. Normalized Load Curves of Several Straight-Shafted Tiebacks Anchoredin Different Cohesive Soils (after Weatherby, 1982).

Pullout Tests, Field Experiments, and Monitoring of Soil Nail Walls

Pullout devices to perform tests in the laboratory under controlled conditions have been developed to gain a better understanding of the key processes associated with the transfer of load between the soil and the nail (Chu and Yin, 2005; Yin et al., 2009; and Su et al., 2008). Figure 28 shows a schematic representation of the pullout test device and a picture of the device taken during a test.

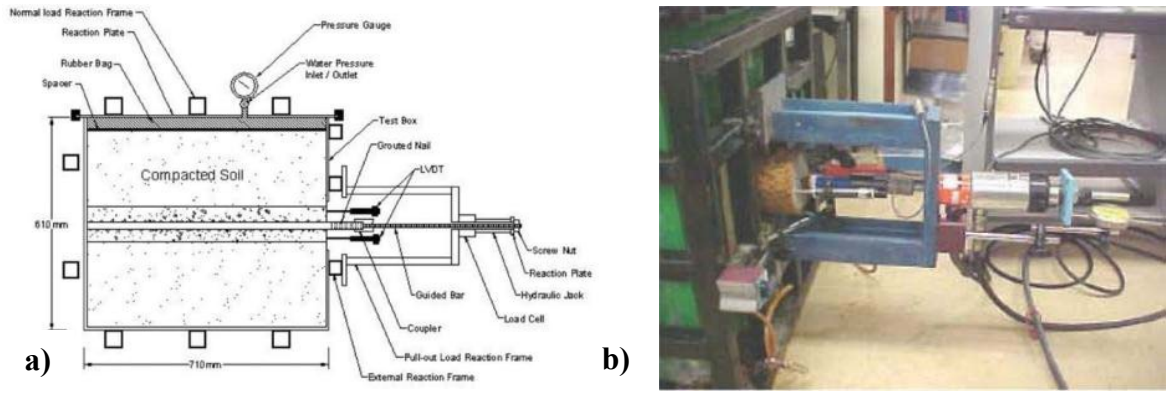

Figure 28. Laboratory Soil Nail Pullout Test Apparatus: a) Schematic Representation, and b) Picture of the Device during Testing (after Chu and Yin, 2005).

This kind of device allows for studying most of the possible factors related to soil nail behavior, for example, degree of saturation, overburden pressure, and grouting pressure. Figure 29 shows that the pullout shear strength decreases as the degree of saturation increases.

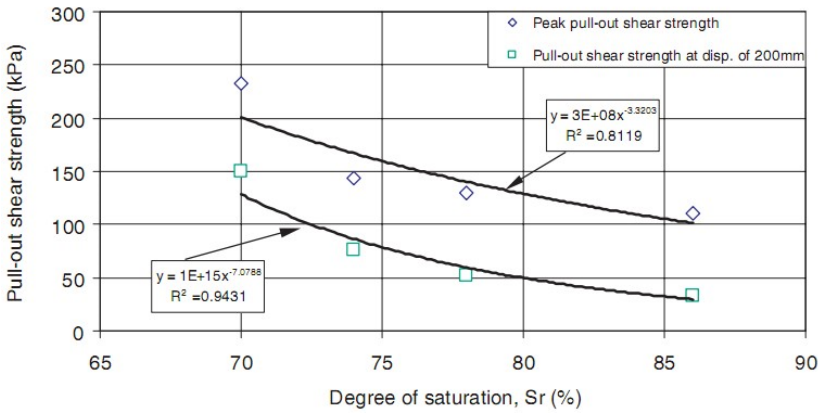

Figure 29. Correlation between Degree of Saturation and Pullout Strength (after Yin and Su, 2006).

Li et al. (2008) presented results obtained from a full-scale test involving soil nails in a loose fill slope. The inclination of the slope was 33° with respect to the horizontal. The slope was 9 m wide and 4.75 m high. The grouted nails were arranged in two rows of five nails per row, following a square grid of 1.5 m × 1.5 m. The nails were installed with an inclination of 20° with respect to the horizontal (Figure 30).

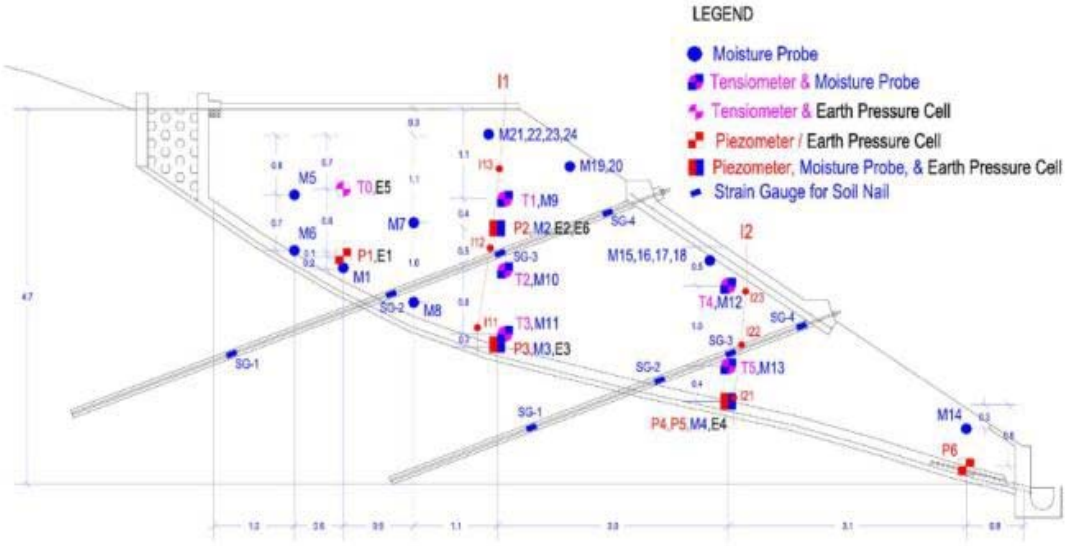

Figure 30. Arrangement of Instruments for a Tested Soil Nail Wall (after Li et al., 2008).

Various instruments were installed to monitor the performance of the soil nail wall. The monitoring was performed for about 6 months, and then the wall was subjected to loading and wetting. Figure 31 shows the surcharge applied and the wetting of the slope, and some typical results gathered from this test related to development of earth pressure during loading. As expected, the earth pressure increases as the slope is loaded.

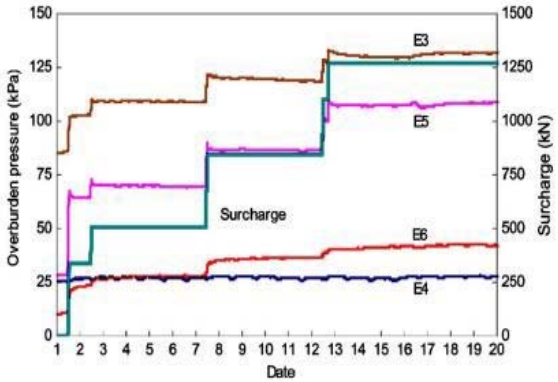

Figure 31. Soil Nail Slope with Surcharge (after Li et al., 2008).

Figure 32 presents the variations of suction, pore pressure, and displacement during wetting. The slope was initially unsaturated and became fully saturated at the end of the wetting stage (wetting II) with the measurements of positive pore pressure. At that time, the more important displacements took place. Figure 32 shows the development of the load taken by the nails in different positions during wetting. The load in the nails increased slightly after the first wetting (wetting I) and considerably during the second wetting (wetting II), when significant displacements were observed. The soil suction plays a crucial role in the creep behavior of the soil nail walls.

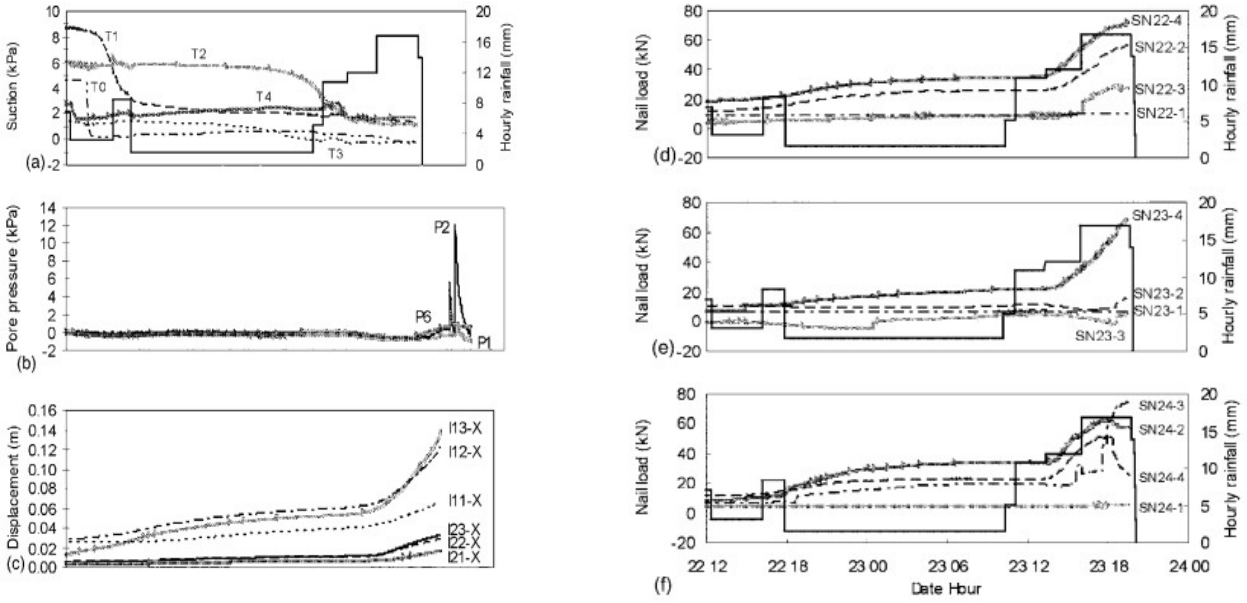

Figure 32. Measured Deformations and Pore Pressure during Wetting and the Associated Response of Nails (after Li et al., 2008).

Turner and Jensen (2005) reported the results of the monitoring campaign of a soil nail system constructed for the stabilization of an active landslide in Wyoming (Figure 33). A data logger was used to gather the information from the strain gauges. A solar panel and a battery were adopted for the power supply. Two slope inclinometer casings were also installed to track the deflections of the slope. The monitoring of this soil nail wall was very useful in assessing the service conditions of the wall and checking the method used in the design. This project allowed a better understanding of how the different components of the soil nail system interact under actual field conditions.

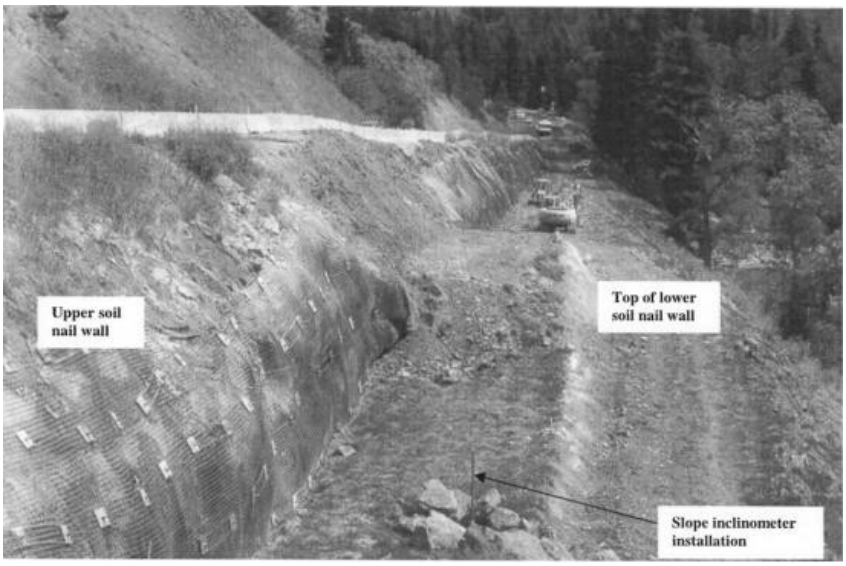

Figure 33. Picture of an Instrumented Soil Nail Wall (Turner and Jensen, 2005).

The Dublin Port Tunnel project is another successful case in which the instrumentation played a crucial role in gaining a better understanding of the behavior of soil nail walls. Full details about this case study can be found in Menkiti and Long (2008). The instrumentation was composed of strain gauges; piezometers (at 4, 8, and 12 m depths); inclinometer; surface-mounted prism for detecting slope face movements; and settlement markers at the slope crest. The strain gauges (installed only in some selected nails) were installed in a way that made it possible to measure the influence of vertical bending. The strain gauges were also equipped with thermistors to measure the temperature at each instrument location. Photos in Figure 34 present different aspects of the instrumentation in this project: photo (a) shows the adopted strain-gauges together with the treated nail; photo (b) is related to the attachment of strain-gauges to the nail; photo (c) shows the adopted protection; and photo (d) shows the nails installed in the wall.

Menkiti and Long (2008) concluded that nails work in tension largely and that the influence of bending is marginal. The instrumentation also assisted researchers in understanding better the loads acting during the installation and excavation. The more significant loads on the nail were related to the drilling and nailing of the lift immediately below and not with the excavation as it is generally assumed in the current design methods. The upper nails were the ones that developed the highest forces, whereas most design methods assume that the maximum bond capacity develops in depth.

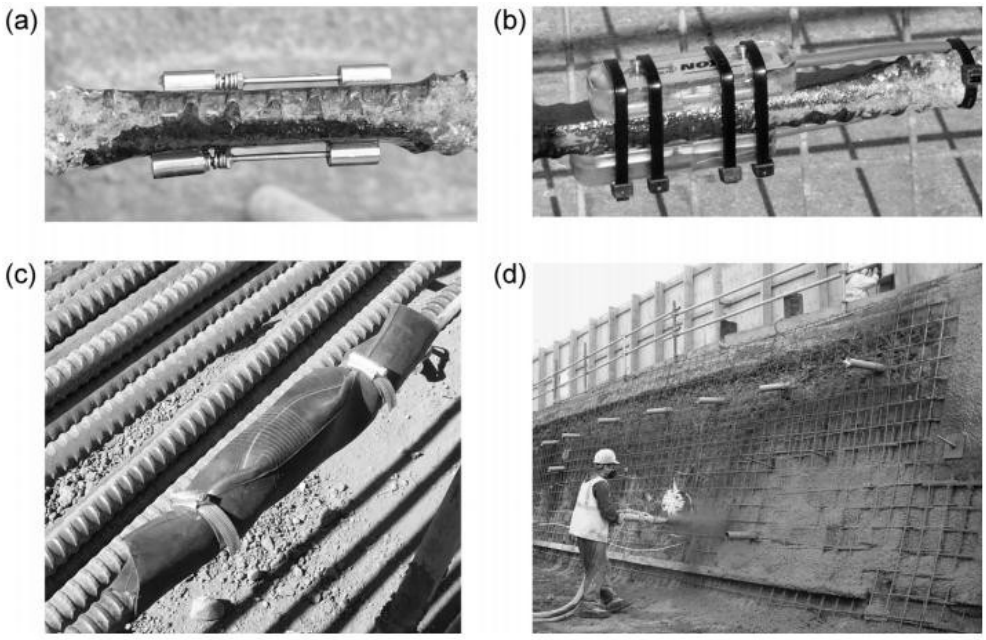

Figure 34. Different Aspects of the Instrumentation with Strain-Gauges (after Menkiti and Long, 2008).

In these two works (Turner and Jensen, 2005; Menkiti and Long, 2008), there are not many details about the long-term or creep behavior of the soil nail systems. Based on the information gathered from the monitoring of the soil nail walls, these two contributions (Turner and Jensen, 2005; Menkiti and Long, 2008) agree that the guidelines used for the design of these two walls resulted in conservative designs.

Modeling of Soil Nail Walls

Numerical modeling of soil nail walls is often carried out to assess the performance and stability of the retaining system. Global stability analyses of soil nail walls are approached by using limit equilibrium software specifically developed for the design of soil nail walls. The two computer programs most commonly used in the United States for the analysis and design of soil nail walls are SNAIL and GOLDNAIL. A limitation of both of these computer codes is that they are not able to analyze composite failure surfaces, which might be applicable when multiple soil layers with dissimilar strengths exist (e.g., FHWA's GEC#7). Another limitation inherent to numerical codes based on the limit equilibrium method is that they cannot assess the performance of soil nail walls in terms of deformations or load distribution in the nails.

A good example of the numerical analysis of a soil-nailed system using different pieces of software corresponds to the study of the soil nail wall constructed and instrumented at the National Geotechnical Experimentation Site at the University of Amherst, Massachusetts. The wall was built in a moderately plastic varved clay. After construction, the wall was over-excavated up to failure. The lateral deformations of the wall were monitored during this process. The data gathered during the test showed that the deformation of the wall occurred mostly at the face of the wall. As one moves away from the face of the wall, the deformations decrease significantly. Furthermore, the more significant lateral deformations of the wall were concentrated above the first row of the nails. Oral and Sheahan (1998) back analyzed the wall by using three software packages to determine the global FS for the soil nail wall. Table 6 shows the results of these analyses.

These three very popular pieces of software computed values for the FS between 1.00 and 1.17. However, the actual wall reached failure. Those analyses have a number of assumptions and important limitations (e.g., 2D conditions, simplified soil-and-nails models, and nails working only in tension), so some discrepancies between the actual observed behavior and the numerical predictions may be expected. For example, the failed wall did experience some 3D effects due to its limited length. Furthermore, the deformation pattern and lack of nail pullout indicated nail bending as one of the reinforcement mechanisms.

Table 6. Results from Stability Analysis of the Wall (after Oral and Sheahan, 1998).

GoldNail	F.S.= 1.148 at 5.6 m (18.4 ft) with a base angle of 29°
Shen	F.S. against sliding through toe: 1.00 F.S. against deep seated rotation: 1.64
Snail	F.S.= 1.172 at 5.5 m (18 ft) Lower failure plane: 39.8° length 5.7 m (18.7 ft)[a] Upper failure plane: 65.8° length 2.7 m (8.8 ft)[a]

[a]Angles of orientation for failure wedge.

Numerical models using FLAC were adopted to assess the lateral movement of a 20 m soil-nailed wall. The soil nail wall was built in a HP clay, with SPT over 20 blow-counts in the city of Zagreb, Croatia (Maric et al., 2001). In order to assess the performance of the soil

nail wall, the deformations of the wall were monitored from May to November 2000. The maximum horizontal displacement was 2 mm, while the numerical modeling prediction for this magnitude was 20 mm. Overall, these results demonstrate that the calculations should account for a wide range of modes of behavior when assessing the loading effects during service. It was also clear that special attention should be given to 3D effects. From October 2000, no extra deformations in this wall were measured (Maric et al., 2001).

The performance of soil nail walls depends on the interaction between the soil, nails, and facing. Many other parameters affect the performance of soil nail walls, for example, nail inclination, method of installing nail, grouting, and construction. Programs based on the FEM programs, such as Plaxis (Singh and Babu, 2010), FLAC (Briaud, 1997; Maric et al., 2001) and Abaqus (Barrows, 1994), have been used to assess the performance of the soil nail walls. These programs can predict horizontal and vertical deformations of the wall and can calculate the load distribution in the nails.

PLAXIS 2D has been found to be an appropriate tool for evaluating the behavior of the soil nail walls, and many researchers have used it (Shiu and Chang, 2006; Fan and Luo, 2008; Singh and Babu, 2010; Akhavan et al., 2011). The Plaxis bulletin published the work by Babu and Singh (2009), which focuses on the impact of different elements on the modeling of soil nail walls. The Mohr–Coulomb (MC) model was used to simulate the soil behavior. In 2010, this study was extended (Singh and Babu, 2010), and three soil models were used to simulate the soil behavior: the MC model, hardening soil (HS) model, and hardening soil with small-strain stiffness (HSsmall) model. In this work, researchers investigated the influence of the different soil models on the predictions of the: 1) base heave of excavation, 2) lateral displacements of the wall, and 3) global stability. In soft soils, the bottom of the excavation is generally at risk of heaving. The MC model predicted approximately twice the base heave in front of the soil nail wall as the HS and HSsmall models.

For up to 60 percent of the construction, the lateral displacement at the top of the wall predicted by the MC model is higher than the displacement predicted by the HS and HSsmall models. However, between the point of 60 percent of construction and the completion of the wall, the MC model predictions are approximately half of the amount predicted by the HS and HSsmall models. These observations may be attributed to the following two reasons: 1) with the progression of the construction stages, cumulative plastic strains in the soil nail system increase

and thereby reduce the stiffness of the retained soil mass significantly, and 2) the assumption of the linear elastic pre-failure behavior of the soil in the MC model. Figure 35 shows the lateral displacements obtained with different soil models.

Another relevant conclusion of this work is that the selection of the soil models does not have a significant effect on the global stability of the soil nail wall. Regardless of the type of the soil model adopted, approximately the same FS was reached for the analyses performed for the period after the end of construction. Furthermore, the three soil models analyzed predicted similar responses in terms of the axial force developed in soil nails during the construction stages. The HS model is suitable for all soils but is not able to account for viscous effects (e.g., creep and stress relaxation). Plaxis has a specific creep model called the Soft Soil Creep model that is certainly not recommended for use in excavation. More info can be found in Plaxis Manual (2014).

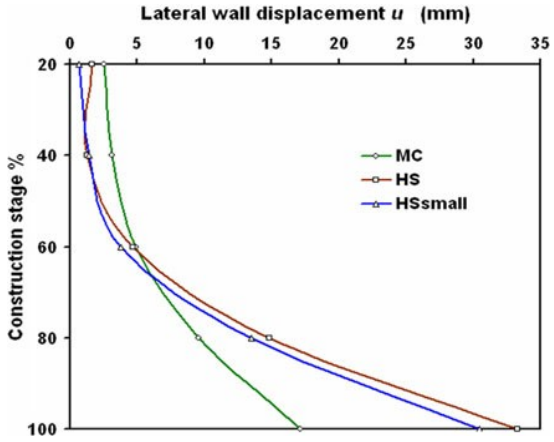

Figure 35. Lateral Displacement of Soil Nail Wall with Construction (after Singh and Babu, 2010).

As mentioned before, finite element analyses allow the calculation of the load taken by the nails. For example, in the Plaxis program, it is possible to use geogrid elements or plate elements. Geogrid elements do not account for the bending stiffness of nails, and the nail elements have axial stiffness only. On the other hand, the plate elements have both axial and bending stiffness. In order to consider the bending stiffness, Singh and Babu (2010) simulated two series of 10 m high soil nail walls using PLAXIS 2D. One series used the plate to simulate nail elements and the other one adopted the geogrid elements. Figure 36 shows the axial load

distribution along the nail length for both plate elements and geogrid elements. This information is very important because it tells about the nail service load.

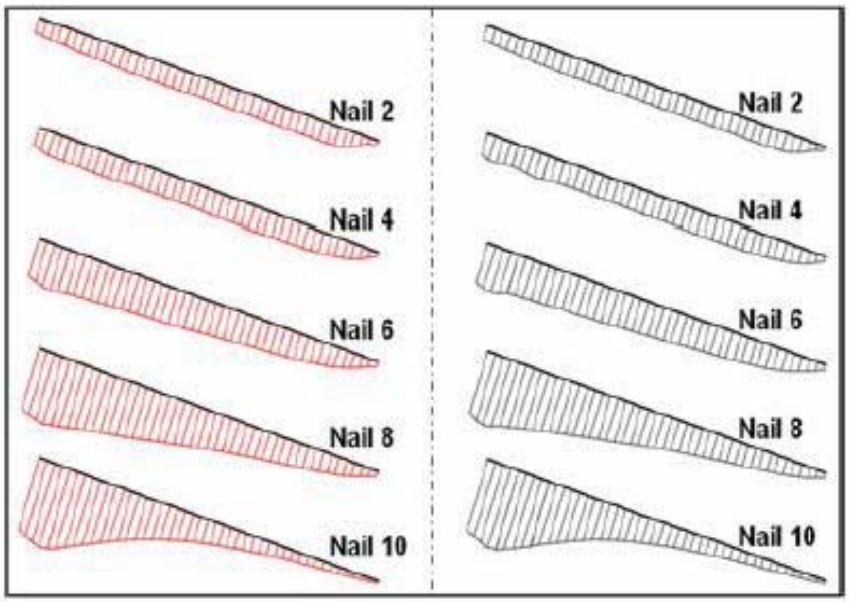

Figure 36. Variation of Axial Force along Nail Length (after Singh and Babu, 2010).

Contributions Related to Soil Nail Walls in HP Clays.

Table 7 compiles some of the most significant contributions related to the behavior of soil nail walls in HP clays, including papers related to experimental behavior of clays subjected to creep, constitutive modeling of creep behavior, soil nail wall performance, instrumentation and monitoring of retaining structures involving anchors and/or nails, and numerical modeling of soil nail walls.

Table 7. Literature on the Behavior of Soil Nail Walls in HP Clays.

Title	Authors	Year	Source	Highlights	Relevance to This Project
Long-term Behavior of Ground Anchors and Tieback Walls	Briaud, Griffin, Yeung, Soto, Suroor, and Park	1998a	TxDOT Report	• For a given anchor length, anchors with a short bond length have higher capacities and lower creep rates than grouted anchors with a long tendon bond length. • The capacity of grouted anchors in the clay was found to increase over 5 years. • For stress level larger than the yield stress, delayed failure occurred in triaxial tests. • A power law model fit the creep data well.	• The anchors are at Riverside Campus (clay site, where soil tests will be performed). • Creep tests on those anchors are 70 days. • Provide useful information about the bond strength. • Cutting across the hump on the stress–strain curve.
Should Grouted Anchors Have Short Tendon Bond Length?	Briaud, Powers, and Weatherby	1998b	Journal of Geotechnical and Geoenvironmental Engineering	• Summary of key information from Briaud et al. (1998a) (above).	• Summary of key information from Briaud et al. (1998a) (above).
Behavior of 10 Full-scale Ground Anchors Installed in Stiff Clay	Powers	1993	Master's Thesis, Texas A&M University	• 70-day load creep tests on 10 full-scale instrumented anchors at Riverside Campus. • These 10 anchors were retested in 1998 (Briaud et al., 1998a) report.	• Give additional data (for longer period) compared with Briaud et al. (1998a) report (see above). • Gauges and strainmeters work extremely well.

Table 7. Literature on the Behavior of Soil Nail Walls in High-Plasticity Clays (Continued).

Title	Authors	Year	Source	Highlights	Relevance to This Project
Behavior of Five Large Spread Footings in Sand	Briaud and Gibbens	1999	Journal of Geotechnical and Geoenvironmental Engineering	• 5 square spread footings ranging in size from 1 to 3 m were load tested up to 150 mm of settlement. • Load-settlement curves + creep curves relating settlement and time under a constant load.	• Validate the power law model to predict the creep. • Provide a range of value for the power 'n'. • 'n' may be dependent of load history.
Research on Tiebacks Anchored in Cohesive Soils	Ludwig, Weatherby, and Schnabel	1985	11th Int. Conf. on Soil Mechanics and Foundation Engineering	• Load creep tests on instrumented tiebacks anchored in a variety of cohesive soils. The peak load of each load cycle was held constant for periods range from 10 to 1000 minutes.	• Testing procedures to verify the short-term, load-carrying capacity of tiebacks anchored in cohesive soils and evaluate long-term, load-carrying capacity.
Short-term and Long-term Behavior of Tiebacks Anchored in Clay	Ludwig	1984	PhD Dissertation, McGill University	• A series of full-scale tests were conducted on instrumented and non-instrumented straight-shafted, post-grouted, and single-underreamed tiebacks anchored in different cohesive soils. • Physical model to describe short-term and long-term tieback behavior in a cohesive soil.	• Excellent experimental data to develop and validate creep models in clays.
Construction, Carrying Behavior and Creep Characteristics of Ground Anchors	Ostermayer	1975	Proceedings of Diaphragm Walls and Anchorages Conference	• Aspects related to the construction and testing of anchors are discussed. Special emphases on creep tests involving anchors. • A number of applications of anchored walls for different uses and dispositions are analyzed.	• Study summarizing the German experience in anchors (more than 300 anchors installed and tested in different projects).

Table 7. Literature on the Behavior of Soil Nail Walls in High-Plasticity Clays (Continued).

Title	Authors	Year	Source	Highlights	Relevance to This Project
Design Manual for Permanent Ground Anchor Walls	Weatherby	1998	Report, U.S. Department of Transportation	• Apparent earth pressure diagrams to design the permanent ground anchor walls. • Study based on 2 full-scale wall sections, 4 model-scale walls, 10 large-diameter ground anchors installed in a fine-grained soil.	• Guideline for designing anchors in fine-grained soils.
Landslide Stabilization Using Soil Nail and MSE Earth Walls: Case Study	Turner and Jensen	2005	Jnl. of Geotech. and Geoenvironmental Eng. (American Society of Civil Engineers [ASCE])	• A feasibility study for slope stabilization using soil nail walls in an active landslide.	• Design, construction of an actual soil nail project. • Instrumentation and monitoring.
Performance of Soil Nails in Dublin Glacial Till	Menkiti and Long	2008	Canadian Geotechnical Journal	• Most of the load in the nail was induced as the result of drilling and nailing the lift immediately below the nail. • The highest forces were developed in the upper nails where the largest ground movements occurred (this is the reverse of what most current design methods state).	• Large-scale soil nailing, instrumentation, and field monitoring in Dublin glacial till clay.
Loose Fill Slope Stabilization with Soil Nails: Full-scale Test	Li, Tham, Junaideen, Yue, and Lee	2008	Jnl. of Geotech. and Geoenvironmental Engineering (ASCE)	• Performance of soil-nailed slope monitored with various instruments for about 6 months. • Slope tested to failure by surcharging and wetting. • Soil nailing organized in a grid is effective to enhance the stability of fill slopes.	• Increase of earth pressure with surcharge. • Influence of moisture on slope movements. Impact of wetting on nail load.
Creep and Failure of Slopes in Clays	Tavenas and Leroueil	1981	Canadian Geotechnical Journal	• Slope stability analysis incorporating time-dependent behavior of natural clays. • Study of both man-made and natural slopes. Study of both soft and stiff clays (intact or fissured).	• Information about the stress level at which the creep rate does not increase or remain constant.

Table 7. Literature on the Behavior of Soil Nail Walls in High-Plasticity Clays (Continued).

Title	Authors	Year	Source	Highlights	Relevance to This Project
The Influence of Grouting Pressure on the Pullout Resistance of Soil Nails in Compacted Completely Decomposed Granite Fill	Yin, Su, Cheung, Shiu, and Tang	2009	Géotechnique	• Fully instrumented pullout box with a special pressure grouting device. • Pullout box test to study in the laboratory the effect of grouting pressure on the pullout pressure.	• Shear stress between nail & soil increased ~linearly with the grouting pressure. • This confirms observations from field pullout tests.
Influence of Overburden Pressure on Soil-nail Pullout Resistance in a Compacted Fill.	Su, Chan, Yin, Shiu, and Chiu	2008	Jnl. of Geotech. and Geoenvironmental Eng. (ASCE)	• A laboratory soil nail pullout box with full instrumentation to study the effect of overburden pressure on the pullout pressure.	• Soil nail pullout shear resistance is independent of the overburden pressure.
A Laboratory Device to Test the Pullout Behavior of Soil Nails	Chu and Yin	2005	Geotechnical Testing Journal	• A laboratory device is built to overcome limitations of field pullout tests of soil nail.	• Lab pullout test for soil nails.
Influence of Degree of Saturation on Soil Nail Pullout Resistance in Compacted Completely Decomposed Granite Fill	Su, Chan, Shiu, Cheung, and Yin	2007	Canadian Geotechnical Journal	• Laboratory pullout box tests to study the impact of moisture on soil nail pullout resistance. • Tests performed at different values of the degree of saturation. • Strong impact of moisture on pullout strength.	• Peak pullout shear strengths of soil nails decreases with the increase of the degree of saturation of the soil.
Compression and Creep of Venice Lagoon Sands	Sanzeni, Whittle, Germaine, and Colleselli	2012	Jnl. of Geotech. and Geoenvironmental Engineering (ASCE)	• 1D compression and creep properties of intact sand samples from a borehole in Venice Lagoon. • Results confirmed a strong correlation between creep rate coefficient and compressibility index. • Compression behavior well described by a nonlinear compression model.	• Experimental data do not fit well (no linear) in the log–log curve. • Creep depends on stress level.

Table 7. Literature on the Behavior of Soil Nail Walls in High-Plasticity Clays (Continued).

Title	Authors	Year	Source	Highlights	Relevance to This Project
Case History and Causes of a Progressive Block Failure in Gently Dipping Bedrock	Dornfest, Nelson, and Overton	2007	1st North American Landslide Conference	• Core samples with a failure plane. • Monitoring with inclinometer slope movements for 2 years.	• Highly plastic clay. • Cutting across the hump in the stress–strain curve.
Creep Behavior of an Undisturbed Lightly Overconsolidated Clay	Martinez-Vasques and Diaz-Rodriguez	2009	17th Int. Conf. on Soil Mechanics and Geotechnical Engineering	• Creep behavior of Mexico City sediments. • Creep influence in the destructured range is not important at low shear stress level. • Creep failure was not observed. • The post-creep strength clearly shows tendency to increase or decrease.	• Creep tests isotropically consolidated up to 80 kPa. • Creep stage lasting over 10,000 minutes. • Small creep at low shear stress level was observed.
A Simple Criterion for Creep Induced Failure of Over-consolidated Clays	Hunter and Khalili	2000	GeoEng 2000 Conference	• Criterion for the prediction of the long-term shear strength based on accumulated strains. • Criterion based on long-term drained creep tests on over-consolidated and structured clays.	• Criterion for creep induced failure for over-consolidated clays under drained loading. • Cutting across the hump on the stress–strain curve.
Creep in Soft Soils	Havel	2004	PhD Thesis, Norwegian Univ. of Sci. and Technology	• Oedometric study of the long-term consolidation of undisturbed and remolded clays. • Study of the undrained and drained deviatoric creep behavior of clays under triaxial compression.	• A larger number of 1D, undrained and drained deviatoric creep tests under different conditions.
Time Dependent Characteristics of Strength and Deformation of a Mudstone	Ohtsuki, Nishi, Okamoto, and Tanaka	1981	Symposium on Weak Rock	• Study of soft sedimentary rocks with strain softening and creep behavior. • Progressive and delayed failure in time. • Focus on over-consolidated states.	• Triaxial compression tests including creep behavior.

Table 7. Literature on the Behavior of Soil Nail Walls in High-Plasticity Clays (Continued).

Title	Authors	Year	Source	Highlights	Relevance to This Project
Modeling Construction and Failure of Soil Nailed Structures in Clay	Taib and Craig	2006	6th International Conference on Physical Modelling in Geotechnics	• Performance of 5 centrifuge tests on instrumented nail clay slopes. • Found 2 main mechanisms of failure: pullout failure and slippage of soil against the nails.	• Good data to understand the short-term behavior of soil nail in clayed slopes. • Physical modeling of a soil nail wall.
The Use of Soil Nails in Soft Clays	Oral and Sheahan	1998	Conference Design and Construction of Earth Retaining Systems	• Instrumented test on a soil nail wall in a moderately plastic clay at the Univ. of Amherst and over-excavated up to failure. • Stability back-analysis performed with: GOLDNAIL, SNAIL, and Shen. • FS > 1 obtained from the 3 analyses (the actual embankment failed). • Need to include 3D effects and nail bending to perform more realistic analysis.	• Relevant information about experimental (field data) and modeling of a real soil nail wall in clay. • Discrepancy between observations and model can be related to limitations of existing software based on 2D limit analysis method.
Soil Nailing: Where, When and Why. A Practical Guide.	Tuozzolo	2003	20th Central Pennsylvania Geot. Conf.	• Compiles very useful information about practical aspects related to the construction and testing of soil nails. It also contains design considerations.	• Useful guide for the design, construction, and testing of soil nails.
Creep Tests with Frozen Soils Under Uniaxial Tension and Uniaxial Compression	Eckardt	1982	4th Canadian Permafrost Conference	• Creep curves obtained from uniaxial test results. • Both granular and a cohesive soil samples showed qualitatively the same creep behavior.	• Creep behavior of (frozen) soils under compression and shear in the laboratory. • Power law validation.

Table 7. Literature on the Behavior of Soil Nail Walls in High-Plasticity Clays (Continued).

Title	Authors	Year	Source	Highlights	Relevance to This Project
Soil-nailed Wall Under Piled Bridge Abutment: Simulation and Guidelines	Briaud and Lim	1997	Jnl. of Geotech. and Geoenvironmental Eng. (ASCE).	• 3D nonlinear FEM analysis to study the behavior of soil-nailed walls under bridge abutments. • Soil model based on a modified hyperbolic model with unloading hysteresis.	• Successful 3D modeling of a soil nail wall. • Useful results to assist design guidelines.
Numerical Investigation of Soil Nail Wall During Construction	Olia and Liu	2011	GEO's 12th Annual International Conference	• 2D FEM of soil nail wall compared to field measurements.	• 2D FEM consistent results of wall lateral movements. • However, conservative in predicting nail load.
2D Numerical Simulations of Soil Nail Walls	Singh and Babu	2010	Jnl. of Geotech. and Geoenvironmental Eng. (ASCE).	• Numerical modeling based on advanced soil models (including hardening, small-strain stiffness behavior) to study numerically the behavior of in situ soils.	• Use of different soil models available in Plaxis to simulate the behavior of soil nail walls.
Numerical Study of Different Creep Models Used for Soft Soils	Tian	2011	Master's Thesis, Chalmers University of Technology	• Validation of 3 models against laboratory tests. • The 3 models simulate well the small-scale laboratory tests and describe the creep effects. • Soft Soil Creep Model (SSC); Anisotropic Creep Model (ACM), and non-associated creep model for Structured Anisotropic Clay (n-SAC).	• Validation of different soil models that account for creep behavior and are implemented in finite element software, Plaxis.
CalNail – A Design Tool for Soil Nail Projects using Field Case Histories	Turner and Parnell	2006	Report, California Department of Transportation	• Web-based database of soil nail wall case histories on California's highways.	• CalNail currently hosts over 30 documented case histories for soil nail walls in California.

Table 7. Literature on the Behavior of Soil Nail Walls in High-Plasticity Clays (Continued).

Title	Authors	Year	Source	Highlights	Relevance to This Project
Design & Construction Guidelines for a Soil Nail Wall System	NYSDOT	2008b	NYSDOT Manual	• Brief manual for soil nail system (27 pages).	• NYSDOT Guideline.
Design Procedure for Launched Soil Nail Shallow Slough Treatment	NYSDOT	2008a	NYSDOT Manual	• Brief manual for soil nail system (16 pages).	• NYSDOT Guideline.
Monitoring of Soil Nailed Walls at the Highway 217 and Highway 26 Interchange	ODOT	1999	Report, Oregon Department of Transportation	• Result of a soil nail wall research project completed. • Report by Oregon Department of Transp.	• Details are given to monitor soil nail walls.
A Numerical Investigation into the Performance of the Soil Nail Wall and Pile Foundation at the Swift Delta I-5 Interchange	Smith	1993	Report, Oregon Department of Transportation	• Five layers of soil nails were installed between existing bridge supporting pipe piles. • Instrumentation: strain gauges in the nails and single pile; load cells in the nail heads; inclinometers in the wall and fill outside the bridge; tiltmeters and extensometer on the pile cap. • FEM analysis (FENail). • Good (overall) modeling results from FENail.	• ODOT Outcome. • FENail code written specifically for this study. • The pile's lateral load stiffness response is improved by nailing of the soil mass.
Soil Nailing of a Bridge Fill Embankment	Sakr and Kimmerling	1995	Report, Oregon Department of Transportation	• Design and performance of the Interstate-5 soil nail wall. • The performance predicted by the original design methodology is compared critically to the measured.	• ODOT Outcome.
Tennessee Department of Transportation Earth Retaining Structures Manual	TDOT	2012	Manual, Tennessee Department of Transportation	• General policy, introduction, design, and construction requirements of earth-retaining systems.	• ODOT Outcome.

Table 7. Literature on the Behavior of Soil Nail Walls in High-Plasticity Clays (Continued).

Title	Authors	Year	Source	Highlights	Relevance to This Project
Geotechnical Engineering Services Wall 18 – SR 522 at US 2 Overcrossing	WSDOT	2010	Report, Washington State Department of Transportation	• Results of geotechnical engineering services conducted by WSDOT related to a soil nail wall, Washington.	• WSDOT Outcome.
Evaluation of Design Methodologies for Soil-Nailed Walls, Volume 1	Banerjee, Finney, Wentworth, and Bahiradhan	1998	Report, Washington State Department of Transportation	• Analyses of soil nails for a number of walls instrumented with strain gauges. • The magnitude and distribution of loads on the nails under working condition.	• WSDOT Outcome.
Guide to Soil Nail Design and Construction (Geoguide 7)	Civil Engineering and Development Department, Hong Kong	2008	Manual, Hong Kong	• This Geoguide presents a recommended standard of good practice for the design, construction, monitoring, and maintenance of soil-nailed systems in Hong Kong.	• Hong Kong Geoguide (similar to GEC#7).
Recommendations Clouterre, 1992	Schlosser, Plumelle, Unterreiner, and Benoît	1992	Report FHWA-SA-93-026	• English Translation of the "French Soil Nailing Recommendation" 1991. For designing, calculating, constructing, and inspecting earth support system using soil nailing.	• The creep test is different from GEC#7. • Strong impact of load level on creep behavior of soil nails.
A Soft Soil Model that Accounts for Creep	Vermeer and Neher	1999	Conf. Beyond 2000 in Computational Geotechnics	• Validation of an advanced creep model against laboratory data. Model captures well such phenomena as undrained creep and soil aging.	• Constitutive model including creep behavior (secondary compression).

SUMMARY AND CONCLUSIONS

This chapter summarizes the main contributions related to behavior of soil nail walls in HP clays. A brief summary of the design guidelines presented in GEC#7 was presented, with special attention to the concerns in that manual about the long-term behavior and creep effects associated with the construction of soil nail retaining system in HP clays. Other guidelines also refer to potential problems associated with soil nail walls in HP clays (e.g., Hong Kong, France guidelines). In general, the Hong Kong manual is quite similar to GEC#7. Results from a wide number of controlled force tests (i.e., creep tests) performed in the context of the Clouterre project (France) show that for the first loading steps there are practically no deformations differed in time; thus, the creep curves are straight lines (i.e., no appreciable creep effects). At higher loads, the creep curves are no longer straight, and the creep effect starts to be more noticeable. In that study, a critical load (tension, Tc) is defined for those cases in which, at a given stress level, a sudden change of the creep curve is detected (which is associated with the tertiary creep).

When dealing with soil nail walls in HP clays two different issues can be associated with creep effects:

- **Problems associated with local (or internal) effects related to creep.** These issues are related to the effect of creep on the bonding strength between the grouted nails and the clay. Any problem or failure related to these problems should be considered *internal failure mode*.
- **Problems associated with the long-term behavior of the creeping earth mass.** The lateral movement of the soil mass that may be induced by the creep of the clay will be reflected in an increase in the load in the nails. Any failure or issue related to this phenomenon should be considered *external failure mode*.

In this work, contributions related to creep in soils have been reviewed and discussed. There are numerous papers and reports dealing with the creep behavior of soils, especially for oedometric conditions. Several constitutive models have been proposed and implemented in FEM codes, but just a few of them have been applied successfully to reproduce the creep behavior in excavations. From the numerical point of view, pieces of software based on limit

analysis are the most common for the study of stability of soil nail walls. However, they are not capable of simulating creep or long-term behavior.

Case studies dealing with instrumentation and monitoring of soil nail walls have also been discussed. No problems associated with creep were reported in these contributions. In fact, there are not evidences, or reported cases, of actual soil nail walls in HP clays that have failed because of creep-related issues. From the literature review, it is also clear that increases in soil moisture (or decrease in soil suction) can trigger creep or viscous effects. From this review, it is clear that creep rate in soils depends on stress level, particularly at high load levels.

CHAPTER 3:
INSTRUMENTATION DESIGN AND INSTALLATION

INTRODUCTION

The instrumentation was a crucial component of this research project because the data gathered from the experiments were used to gain a better understanding of the creep behavior of HP clays. Furthermore, this is the basic information used to calibrate the numerical models in this study and to revisit current design guidelines. The design of the instrumentation is oriented toward two activities: 1) soil nail pullout tests, and 2) long-term monitoring of an actual TxDOT site. These two activities require different kinds of sensors and instruments. The aim of this chapter is to present the devices adopted for this research project.

As for the loading tests, the *Geotechnical Engineering Circular No. 7: Soil Nail Walls* (FHWA, 2003) establishes that soil nails are load tested in the field to verify that the nail design loads can be carried without excessive movements and with an adequate FS. The creep test could be done as part of the ultimate test, or verification test, or proof tests. It is performed by holding the load for a specific period of time while the displacements at the nail head are monitored.

According to the GEC#7, the basic setup for pullout tests consists of the main components illustrated in Figure 37. A center-hole hydraulic jack and a hydraulic pump are used to apply the load to the nail bar. Two dial gauges mounted on a tripod or fixed to a rigid support that is independent of the jacking setup and wall are used to measure the movement of the nail head. The center-hole load cells are used to monitor the applied load during the creep test, while the hydraulic jack pump is incrementally adjusted (FHWA, 2003). This allows for conducting creep tests in which the load is held constant during the steps defined in the load test protocol.

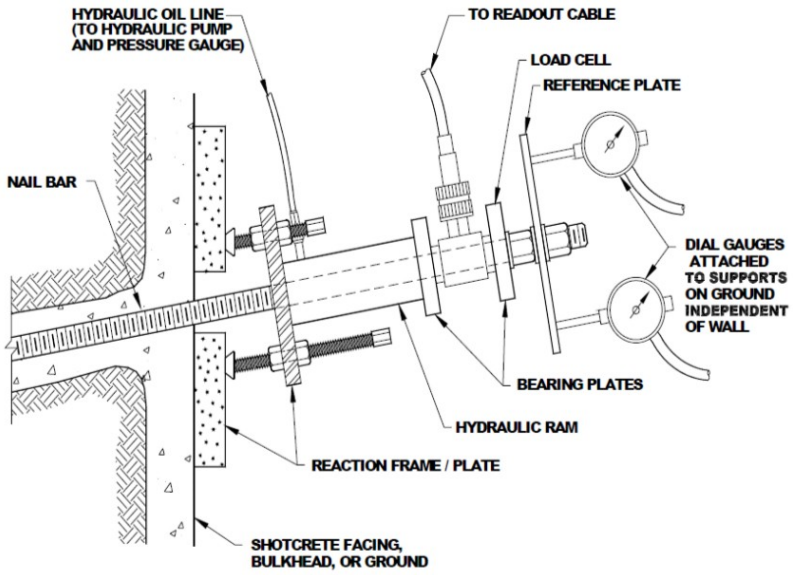

Figure 37. Soil Nail Load Testing Setup (after FHWA, 2003).

In addition to this basic information proposed for the load tests in the GEC#7, this research project is also aimed at learning about the distribution of stresses in the nails. Strain gauges (glued to the steel bar) can be used to measure the stresses in the nail.

For the long-term monitoring of the actual soil nail wall, the basic instrumentation suggested in GEC#7 is presented in Figure 38. The instrumentation for the long-term study of soil nail walls is divided into two components: 1) soil nail wall instrumentation, and 2) nails instrumentation. In the wall instrumentation, the more relevant magnitude to monitor is the wall deflection, together with the horizontal and vertical wall movements. In relation to the nail instrumentation the more relevant parameters to study are: the load in the soil nails (at different positions) and the load in the nail head. An additional aim of this research project is to measure the changes in water content to explore the impact of moisture on creep rate.

Table 8 presents the primary magnitudes to be measured in this research project, the devices that can be used to measure them, and the context in which these magnitudes will be measured and the devices will be used.

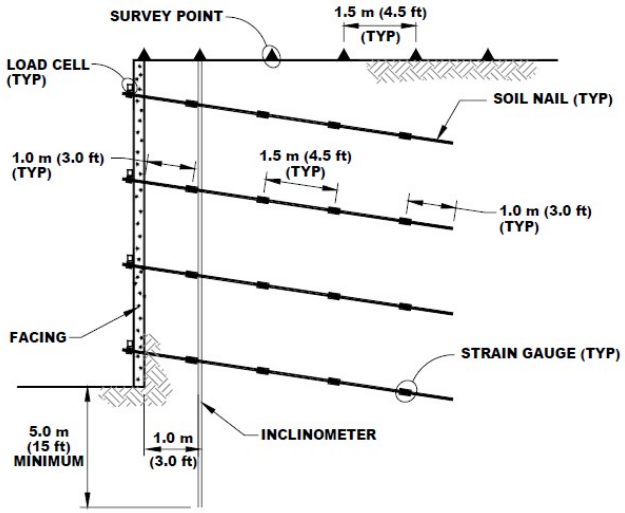

Figure 38. Typical Soil Nail Wall Instrumentation (after FHWA, 2003).

To support the experimental campaign, other devices were necessary for data acquisition and power supply. Two different types of power supply were used: 1) a 5 kW generator used during the load test; and 2) a solar panel to provide power (around 20 W) for long-term monitoring. In the following sections, some general comments about the adopted sensors are briefly presented.

Table 8. Devices and Instruments Selected for the Different Tests.

Magnitude	Instrument	Test
Load	Hydraulic jack	Nail load
	Load cell	Nail load
		Long-term monitoring
Displacement	Dial gauge	Nail load
	LVDT*	
	String potentiometer	Long-term monitoring
	Survey.26	
Deflection	Slope inclinometer	Long-term monitoring
	Tiltmeter	
Soil Moisture	Water content probe	Long-term monitoring
Stress	Strain gauge	Nail load
		Long-term monitoring

*Linear variable differential transducer.

INSTRUMENTS AND TESTING DESIGN

For each of the devices presented in Table 8, there are different options that can be adopted. In general terms, two functional systems can be distinguished: the traditional ones based on voltage measurements, and (relatively) new systems based on the vibrating wire (VW) technology to make the measurements. In voltage measurements systems, the parameter to be measured is transmitted via the gauge base (electrical insulation) to the resistance wire (or foil) in the gauge. As a result, the fine wire experiences a variation in the electrical resistance. The variation of the electrical resistance is proportional to the parameter to be measured. For example, a strain gauge is constructed by bonding a fine electric resistance wire to an electrical insulation base. A crucial component of this system is the perfect bonding between the gauge and the material to be tested.

The VW system is based on the fact that the resonant frequency of vibration of a tensioned steel wire depends on the tension in the wire. This principle is used in a number of configurations for the measurement of load, pressure, force, strains, temperature, and tilt. A characteristic of VW sensors is their long-term stability. The advantage of this kind of sensor over the voltage systems lies primarily in the sensor output, which is a frequency rather than a voltage. Frequencies can be transmitted over long cables (i.e., thousands of meters), without significant degradation of the signal caused by variations in cable resistance. The variation in resistance may arise from water penetration, temperature fluctuations, contact resistance, or leakage to ground. This factor results in sensors that exhibit a good long-term stability and are convenient for long-term measurements in adverse environments.

Hydraulic Jack

As mentioned in previous sections in this chapter, a center-hole hydraulic jack was used for the pullout test of the new nails and existing anchors. The hydraulic jack and the associated pump were used as shown in Figure 37. Figure 39 corresponds to a setup typically used in this kind of test. Due to the different load capacity of the nails and anchors contemplated in this research project, two different hydraulic jacks were used. It was estimated that a 50-ton center-hole hydraulic jack was required for the new nails and a 175-ton jack was necessary for testing the existing anchors.

Figure 39. A Nail Load Test Performed in Inclined Soil Nails.

Load Cell

The load cell is a transducer that consists of a cylinder of high-strength steel with a series of electrical resistance strain gauges connected around the periphery as a Wheatstone bridge, which usually consists of four strain gauges. In this way, the transducer can compensate for unevenly distributed loads. The load cells are also compensated for temperature variations typically found during normal operating conditions. Via a multicore sheathed cable, the load cell can be connected to a direct portable readout, switched terminal units, or a data logging system. They are manufactured with a central hole to accommodate nails and anchors (Figure 40).

In this research project, the load cell was used in two activities: 1) to measure the applied load during the nail and anchor load tests (as illustrated in Figure 37), and 2) to measure the load at the head of the nail during the long-term monitoring (as shown in Figure 38).

Two different load cells were used in this research project: 1) the Geokon Model 3000 (500 kN) for the soil nail load tests (at both NGES and TxDOT sites) and the long-term monitoring of the soil nails, and 2) the Geokon Model 3000 (1500 kN) used in the tests involving the existing anchors. Note that this last cell, able to work at higher loads, is necessary because the maximum load on the anchors is much higher than that on the nails.

Figure 40. Central-hole Load Cell (Geokon).

Dial Gauge

Dial gauges were used to manually record the displacements to be measured during the soil nail test. They can measure the relative displacement of the nail with respect to a fixed reference plate. Figure 37 shows the setup with which relative displacements were measured during the load tests.

A dial gauge (also known as a dial test indicator and/or lever arm test indicator and/or finger indicator) are very popular devices in geotechnical laboratory investigations to measure displacements. In fact, a dial gauge measures angular displacement and not linear displacement. Linear distance can be correlated to the angular displacement based on the correlating variables. If the cause of movements is perpendicular to the finger, the linear displacement error is acceptably small (within the display range of the dial). Contact points of the dial gauges are generally built with a standard spherical tip of 1, 2, or 3 mm diameter.

Slope Inclinometer

Slope inclinometers provide significant quantitative data associated with the deflection or inclination along a borehole. This device is perhaps the more common one used to measure lateral movements of earthworks or structures. It also provides the pattern of deformation and the zone of potential failure. As mentioned before, in this research project, it was used to measure horizontal deflections of the soil nail wall. This technique requires the installation of an

inclinometer casing in a borehole that passes beside the structure to be monitored (in this case the soil nail wall).

The boreholes are typically located approximately 3 ft from the face of the wall and at a minimum depth of around 15 ft below the foundation of the soil nail wall (see Figure 38).

In this research project, the DGSI inclinometer manufactured by Slope Indicator Company was used. The components of this device are presented in Figure 41, as follows:

- **Traversing inclinometer probe** is the standard device for surveying the casing. The traversing probe obtains a complete profile because it is drawn from the bottom to the top of the casing.
- **Portable readout** is used to record the surveys obtained with the portable probe. Advance readouts store readings in solid-state memory, eliminating pencil, paper, and transcription errors, and transfer the data to a computer for processing.

The inclinometer allows recording of the deflection of the entire profile (in depth) at given times. In order to use this technique, it is necessary to drill a vertical borehole and insert the inclinometer casing. The inclinometer probe is then made to pass through the entire length of the hole, taking readings at fixed, predetermined depths from the top surface. During the reading process, two accelerometer probes sense the inclination of the access tube in two planes at right angles to each other.

Figure 41. Portable Inclinometer.

The high level voltage output from the probe is directly proportional to the sine of the angle of inclination of the long axis of the probe from vertical. A set of initial base readings is taken at given depths within the gauge well. This set of readings corresponds to the reference datum. All subsequent readings are taken over a period of time at identical depths, thereby indicating rate, magnitude, and direction of lateral deformation. This inclination is displayed in terms of angular or horizontal displacements (deviation) on the electronic readout equipment at the ground level commanded by the operator. Provided that one end of the access tubing is known to be fixed, it is possible to obtain a complete profile of the gauge well by taking a succession of readings. By comparing these profiles, the horizontal displacements of the gauge well at different depths over a period of time can be determined.

Tiltmeter

The tiltmeter is an instrument that allows for the measurement of the inclination of an object. It responds to the local acceleration of gravity, g. The tiltmeter output is determined by the mass distribution of the earth. This instrument allows tracking of the (continuous) variation of the inclination in time at fixed positions.

The operational principle can be shown with tools commonly used in carpentry. A plumb-bob orients itself along the direction of gravity, and then defines the local vertical. Alternatively, a fluid bubble, contained by a tube, will determine one of the loci of directions, orthogonal to gravity, which constitute the local level. For this kind of instrument there are different options in the market, which depend largely on the chosen manufacturer. The Cline Labs, Inc. 100010-02 tiltmeter was used in this research project (Figure 42).

Figure 42. Tiltmeter.

Water Content Probes

There are different techniques to estimate the amount of water in the soil. The more popular devices are based on the measurement of the dielectric constant. This constant is a measure of the capacity of a non-conducting material, such as soil mixture, to transmit electromagnetic waves, and it is defined as the ratio of the permittivity of a substance to the permittivity of free space. The dielectric constant of water (i.e., around 80 at 20°C) is so much greater than solid particles (between 2 and 6) and air (around 1). This is because the water molecule has a dipole moment, so water can be polarized. Consequently, the contribution of water to the overall soil mixture dominates the soil dielectric constant. This implies that relatively small changes in the quantity of water have important effects on the soil dielectric constant. Using this relationship, the water content can be determined with a calibration model relating soil dielectric constant to the volumetric water content.

Two approaches are typically used to measure the dielectric constant of soil mixture and to estimate the volumetric water content: time domain reflectometry and frequency domain reflectometry.

In this research project, the water content probe was used to learn about the moisture content at different depths. In this way, the distribution of water content was determined at different depths at different times of the year.

Strain Gauges

A strain gauge (or strain gage) is a sensor that measures the strain of an object. The most common type of strain gauge consists of an insulating flexible backing that supports a metallic foil pattern (Figure 43). The gauge is attached to the object by a suitable adhesive. As the object is deformed, the foil is deformed, causing its electrical resistance to change. This resistance change, usually measured using a Wheatstone bridge, is related to the strain by the quantity known as the gauge factor. Basically, this sensor converts force, pressure, tension, weight, etc. into a change in electrical resistance that can then be measured. Strain gauges are widely used for physical force measurement in mechanical, marine, aircraft, and civil engineering.

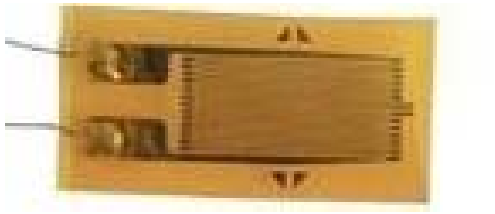

Figure 43. Strain Gauge.

The principles used in construction of the strain gauges can be used as the basis for classifying them into four groups: mechanical, optical, electrical, and acoustical. In this research project, mechanical strain gauges were used, based on a full-bridge configuration with four strain gauges. This disposition guarantees a linear relationship, while the others do not. Quarter-bridge and half-bridge circuits provide an output (imbalance) signal that is only approximately proportional to applied strain gauge force. Linearity, or proportionality, of these bridge circuits is best when the amount of resistance change due to applied force is very small compared to the nominal resistance of the gauge(s). With a full-bridge, however, the output voltage is directly proportional to the applied force, with no approximation (provided that the change in

resistance caused by the applied force is equal for all four strain gauges). Moreover, by using full-bridge strain, it is compensated both for bending (by installing at both sides of the nail) and for temperature (by installing one perpendicular to the main one).

The more common strain gauges used in the literature are Geokon Model VK-4100 VW strain gauges (ODOT, 1999); Geokon Model VCE-4200 VW strain gauges (ODOT, 1999); and Geokon VK-4100/4150 strain gauges (Menkiti and Long, 2008). In this research project, UFCA-5-11 strain gauges from Tokyo Sokki Kenkyujo Co. Ltd. (TML) and Geokon Model VK-4100 VW strain gauges were chosen for the field tests and monitoring.

Data Acquisition System

The data acquisition system is used to read the data from instruments and store it. The following basic components are necessary: data logger, solar panel, and battery. A brief explanation of each is presented as follows.

Data Logger

The data logger used in this research project is the Campbell Scientific CR1000. Figure 44 shows the adopted device. This system has worked very well in previous Texas A&M Transportation Institute (TTI) research, and so the research team adopted it for this research project as well. Some of the positive aspects of this device are as follows:

- Serial communications with serial sensors and devices are supported via I/O port pairs. It supports all of the devices used in this research project.
- Solar panels and batteries can be used as the power supply.
- It offers compatibility with channel expansion peripherals, allowing expansion of the system up to 32 channels if necessary (by default it has 16 channels).

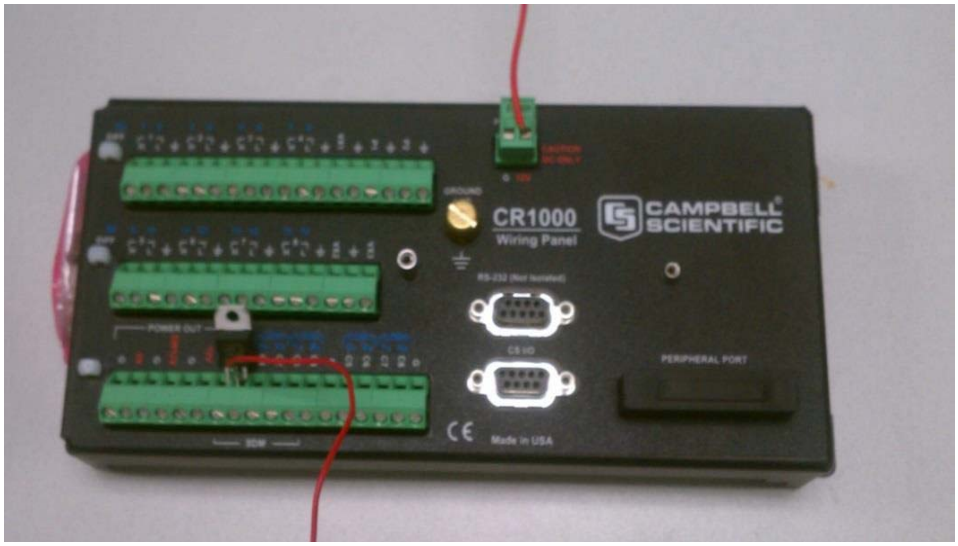

Figure 44. CR1000 Data Logger.

Solar Panel

Researchers adopted the Campbell Scientific SP10 10 W solar panel for the power supply. Figure 45 shows the device used in this research project. It supplies electrical power when working in locations where AC power is unreliable, expensive, or not available.

Figure 45. SP10 10 W Solar Panel.

Battery

Campbell Scientific PS100 rechargeable power supply was also used in this research project. The PS100 provides a 12-Vdc, 7-Ah rechargeable power supply. The rechargeable battery can be trickle-charged from AC or from an external solar panel. Figure 46 shows the device.

Figure 46. PS100 Rechargeable Power Supply.

SUMMARY AND CONCLUSIONS

This chapter presented a brief discussion about the variables and parameters that should be measured in projects involving soils nails walls, together with the devices typically used to that end. It also presented the devices, sensors, and techniques adopted in this research to perform the pullout tests on soil nails and also those adopted for the long-term monitoring of the actual TxDOT project.

CHAPTER 4:
TESTS AT THE NGES-TAMU CLAY SITE

INTRODUCTION

Creep behavior in soils is closely related to the stress level. However, the GEC#7 associates creep behavior directly with the presence of HP clays, regardless of the load level. To determine the effect of load level on creep behavior of soil nails, researchers performed pullout tests at the NGES-TAMU clay site. Two different kinds of tests were performed: 1) tests on existing anchors installed more than 20 years ago (with a very well-known load history), and 2) tests on new soil nails constructed in the context of this research project. These tests focus on studying the effect of the load level on creep behavior of soil nails in HP clays.

All the activities related to the existing anchors installed in 1991, including the background and results of the tests performed in 1991 and 1997, are presented in the following sections. In addition, this chapter covers the load test setup and the results of the pullout tests on the new nails.

NGES-TAMU CLAY SITE CHARACTERISTICS

This section presents the test site characteristics, including the location of the test site and existing anchors, the new soil nails layout, and the soil properties. In the context of this research project, soil samples were collected from different boreholes and laboratory tests were performed. A detailed description of the laboratory tests is included in Chapter 6.

Test Site

The location of the test site for the existing anchors and the new nails is at the NGES-TAMU clay site (Figure 47), which covers about 5500 m^2 at the end of Runway 4 located on the Texas A&M University Riverside Campus (Figure 48).

Figure 47. Location of Test Site on Google Maps™.

Figure 48. Location of Test Site (NGES-TAMU Clay Site) on Riverside Campus.

New nails were installed very close to the existing anchors. Figure 49 shows a detailed layout of the new nails. Seven boreholes were drilled by Terracon Consultants, Inc. The researchers' goal was to sample the soil at the testing location to obtain the basic properties of the soil at this location through laboratory tests. Figure 49 shows the positions of these boreholes (BH1 to BH7). Figure 50 shows the location of the existing anchors.

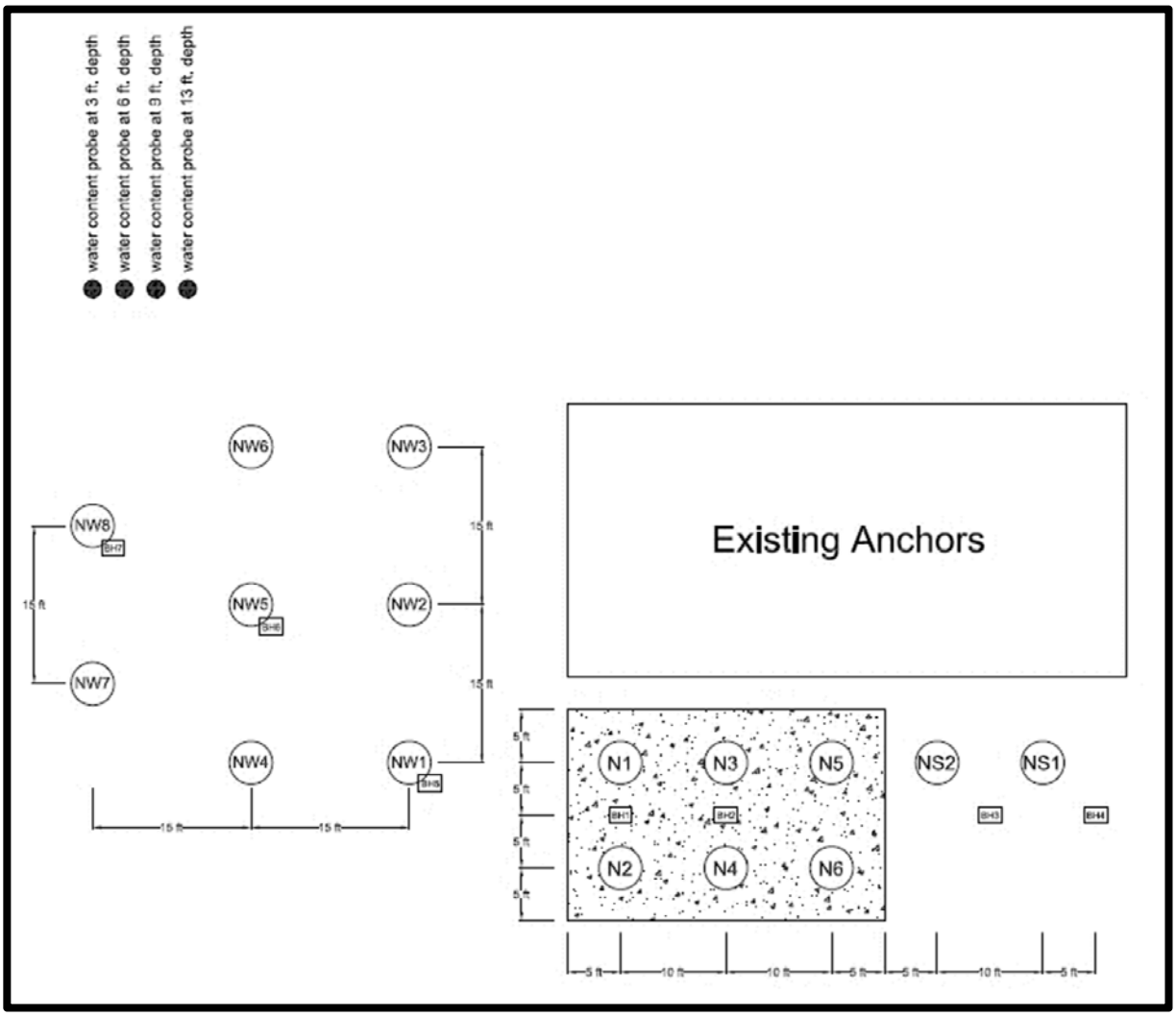

Figure 49. Layout of Nails and Boreholes.

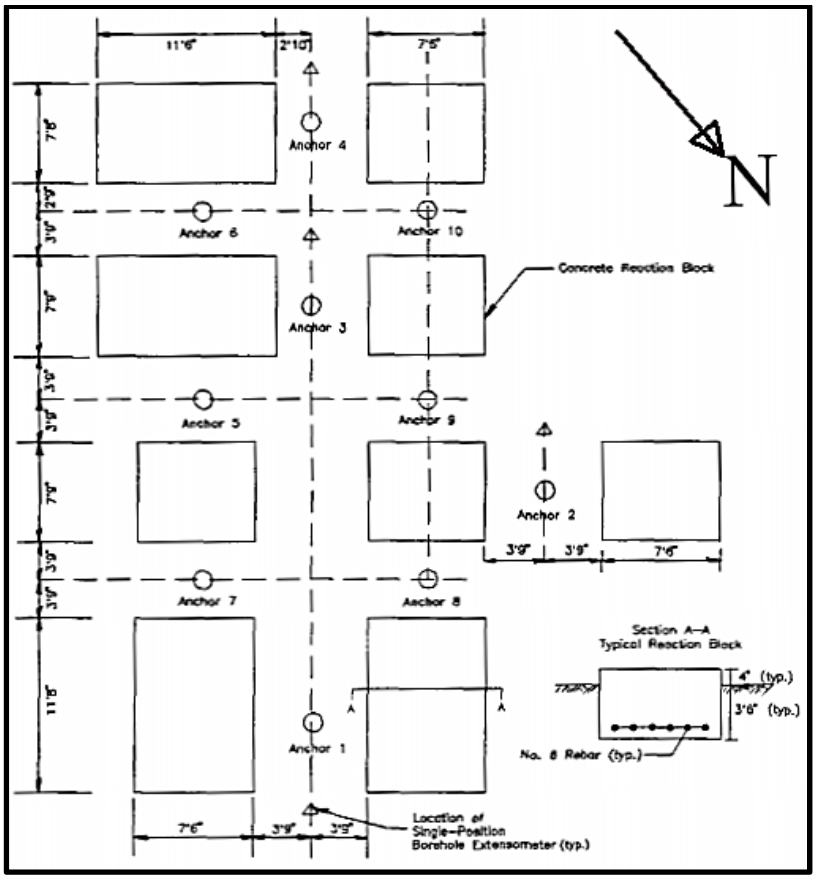

Figure 50. Location of Anchors and Spread Footings (after Powers, 1993).

Soil Properties

A large number of tests have been performed at the NGES-TAMU clay site over the last few decades (Briaud et al., 1998a). Figure 51 shows a wide view of the zone with the location of the more relevant tests performed in the 1990s.

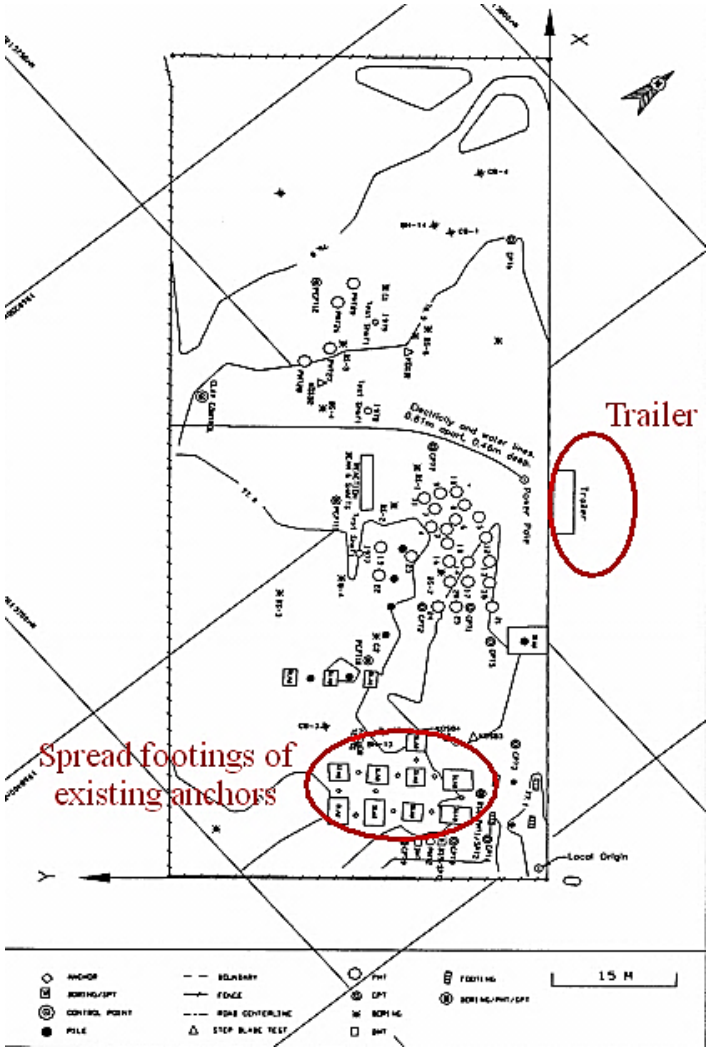

Figure 51. Previous Tests Done at the NGES-TAMU Clay Site (after Briaud et al., 1998a).

Figure 52 illustrates the stratigraphy of the NGES-TAMU clay site, as described by Briaud et al. (1998a): "The clay site is underlain by four distinct layers. The clay unit at the surface is very uniform in thickness down to about 18 ft (5.5 m) in depth below the surface. Below the clay, the sand unit is variable in thickness and averages 3 ft (1 m). The third unit, another clay unit, generally reaches around 21 ft (6.5 m) below the surface and continues to a depth of approximately 42 ft (12.5 m). The fourth unit continues to a depth greater than 165 ft (50 m)."

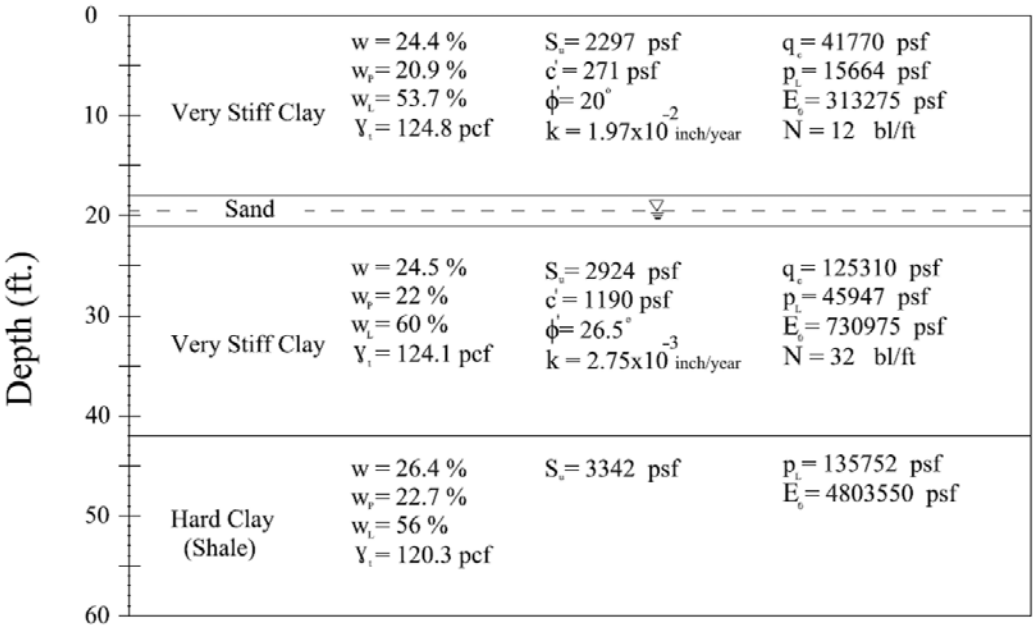

Figure 52. Stratigraphy and Soil Properties of the NGES-TAMU Clay Site (after Briaud et al., 1998a).

The summaries of soil properties from laboratory tests and from field tests are shown in Figure 53 and Figure 54 (Briaud et al., 1998a).

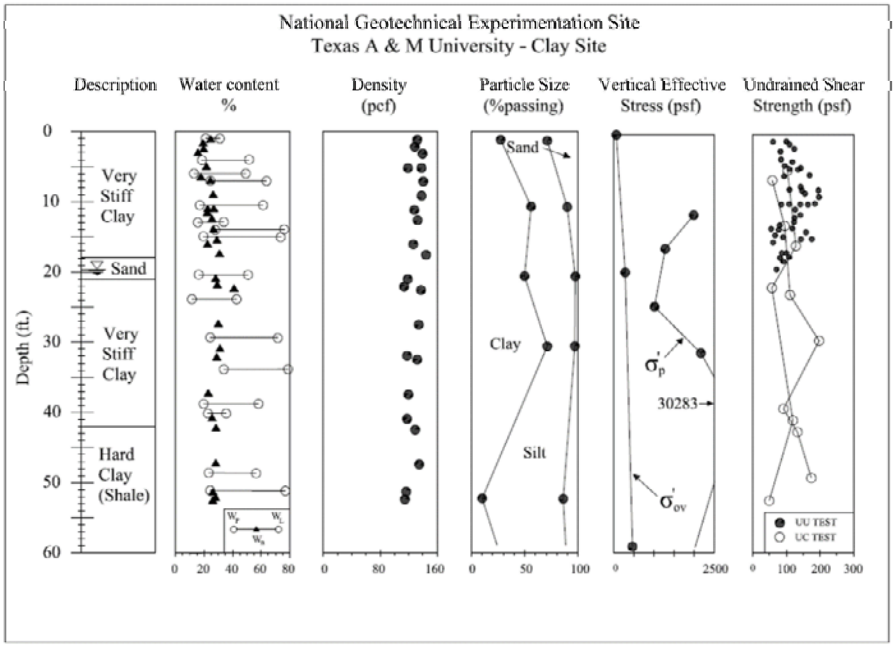

Figure 53. Soil Properties from Laboratory Tests at the NGES-TAMU Clay Site (after Briaud et al., 1998a).

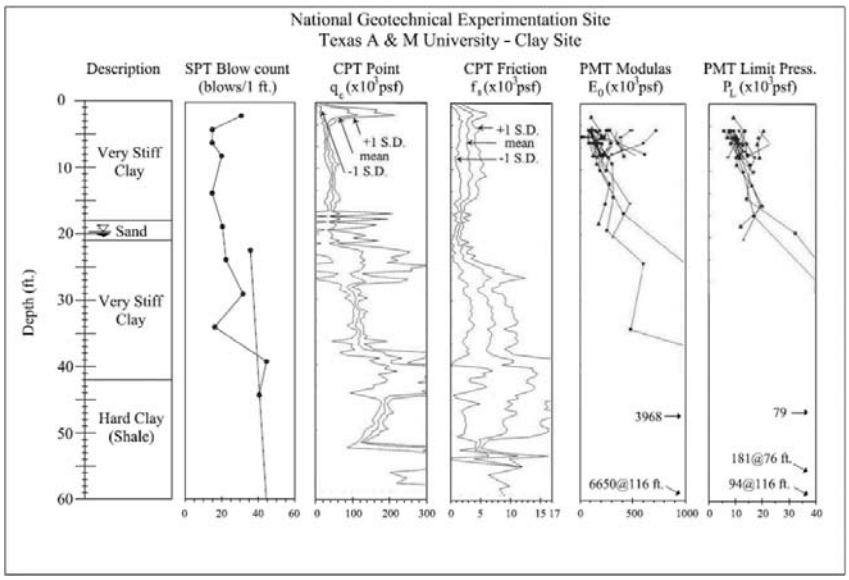

Figure 54. Soil Properties from Field Tests at the NGES-TAMU Clay Site (after Briaud et al., 1998a).

Table 9 (Briaud et al., 1998a) and Table 10 (Powers, 1993) present the soil properties that were used to design the existing anchors. This information was used in this research for the preliminary design of the soil nail length and test load protocol.

Table 9. Soil Properties of Layers (after Briaud et al., 1998a).

Soil Properties	0 to 21 ft Clay	23.8 to 41 ft Clay	Clay Shale
Water content	$w = 24.4\%$	$w = 24.5\%$	
Plastic limit	$w_p = 20.9\%$	$w_p = 22\%$	
LL	$w_l = 53.7\%$	$w_l = 65.5\%$	
Natural unit weight	$\gamma_t = 124.8\,pcf$	$\gamma_t = 124.1 pcf$	
Undrained shear strength	$S_u = 2298 psf$	$S_u = 2924.6 psf$	
Cone penetrometer tip resistance	$q_c = 41780 psf$	$q_c = 125340 psf$	
Pressuremeter limit pressure, p_L	$p_L = 16712 psf$	$p_L = 45958\,psf$	$p_L = 135785 psf$
SPT blow count	$N = 32 blows / 1 ft.$	$N = 32 blows / 1 ft.$	
Ratio of E_o over p_L	$E_0 / p_L = 25$	$E_0 / p_L = 16$	$E_0 / p_L = 230 / 6.5 \approx 35$

A ratio between the modulus E_0 over the limit pressure P_L around 12 (i.e., $E_0/P_L \sim 12$) would be expected for a normally consolidated clay. The clay between ground level and 21 ft is judged to be highly over-consolidated. However, based on the same ratio, it is considered that the clay between 24 and 41 ft is moderately over-consolidated.

Table 10. SPT, CPT, and Laboratory Data to Design Existing Anchors (Powers, 1993).

	Laboratory tests				Atterberg limits			In situ tests						
Depth (ft)	Soil type (USCS)	Unit weight (pcf)	Moisture content (%)	S_u (psi)	Liquid limit (%)	Plastic limit (%)	Plasticity index	SPT (blows/ft)	CPT8			CPT9		
									Q_s (tsf)	Q_c (tsf)	F_r (tsf)	Q_s (tsf)	Q_c (tsf)	F_r (tsf)
5	CH	125	23.9	12.5	51	18	33	9	0.8	10	8	1.5	18	8.3
10		122	23.6	11.5				11	1	18	5.6	0.9	20	8.3
15	CH	129	29.3	18	77	27	49	16	1.1	20	5.5	2	40	4.5
20		129	29.7	12.2				16	1.5	220	4.7	0.5	10	5
25	CL	127	24.2	18.6	43	11	32	27	2	50	4			
30		122	29.5					35	3.5	60	5.8	1.3	63	2.1
35	CH	119	29.6	18.3	84	34	50	31	2.7	61	4.4	1.2	62	1.9
40		122	27.3	19.7				44	3.4	90	3.8	1	82	1.2

In the context of this research, laboratory tests were performed to obtain the soil properties and shear strength of the soil. The water content (Figure 55) is quite constant from ground surface to a depth of 10 ft, then gradually increases by 30 percent at depth 18 ft (which is the bottom of the nails). The unit weight (Figure 56) is around 125 pcf. Soil is considered to be fully saturated ($S_r \geq 85\%$) even if the ground water level is at the depth of 18 ft (Figure 57), and it is high PI clay (Figure 58). Shear strength profile of the soil obtained from triaxial test and direct shear test is shown in Figure 59.

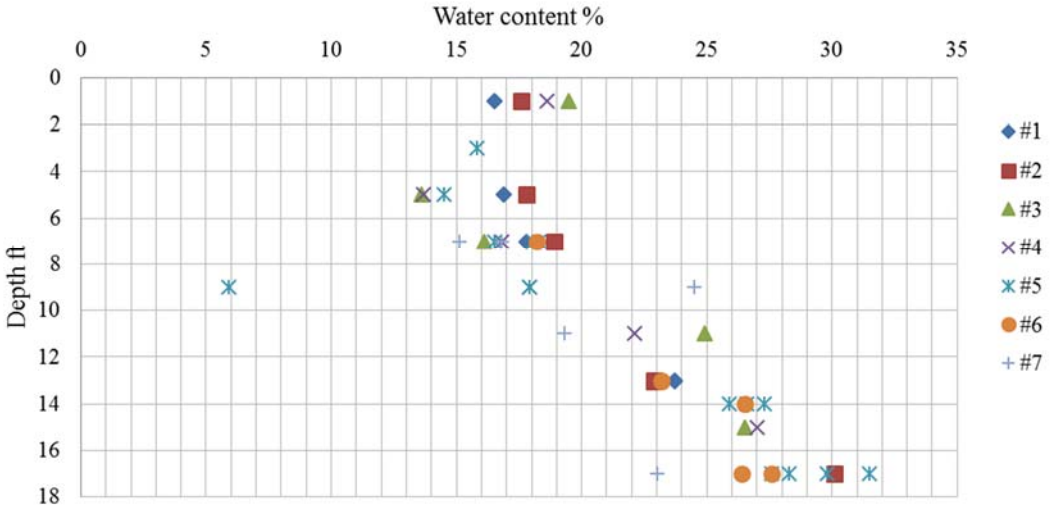

Figure 55. Water Content Profile with Depth.

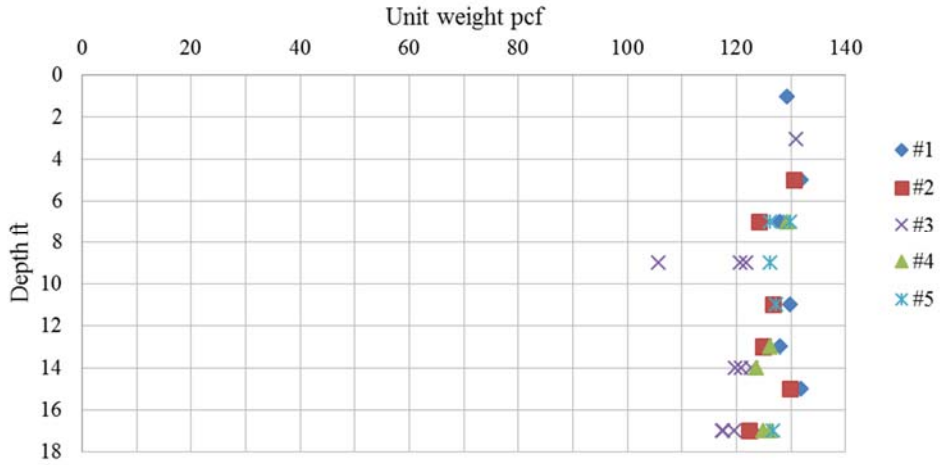

Figure 56. Unit Weight Profile with Depth.

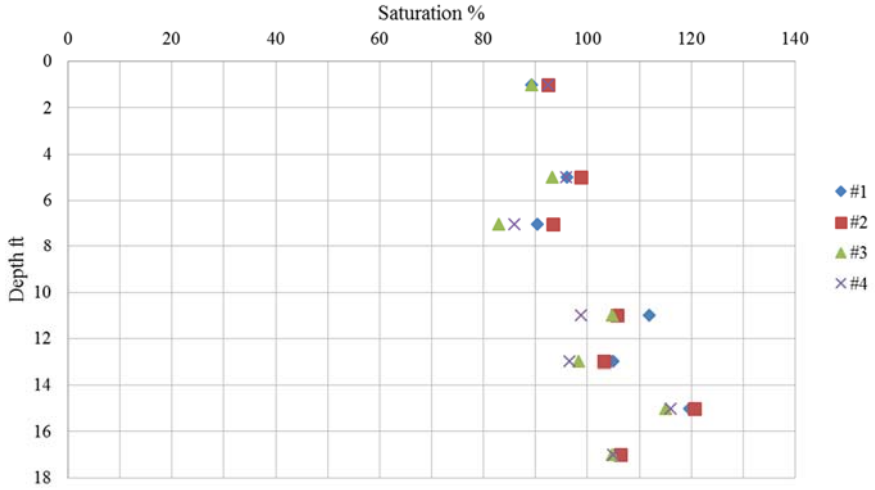

Figure 57. Saturation Profile with Depth.

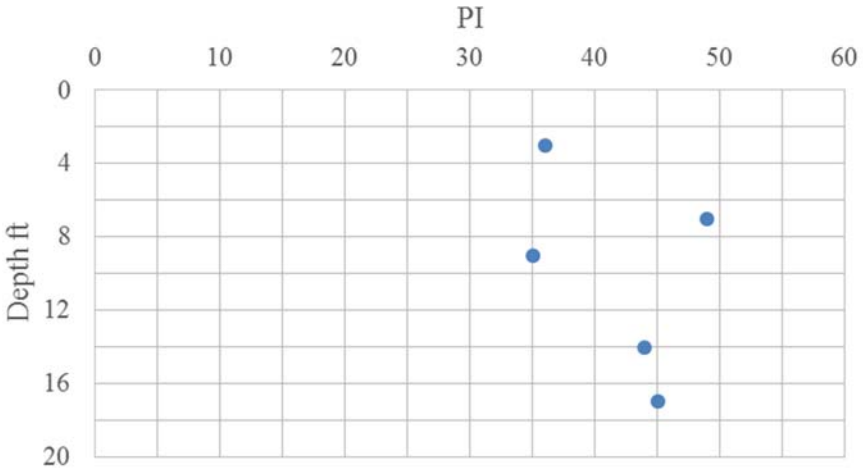

Figure 58. PI Profile with Depth.

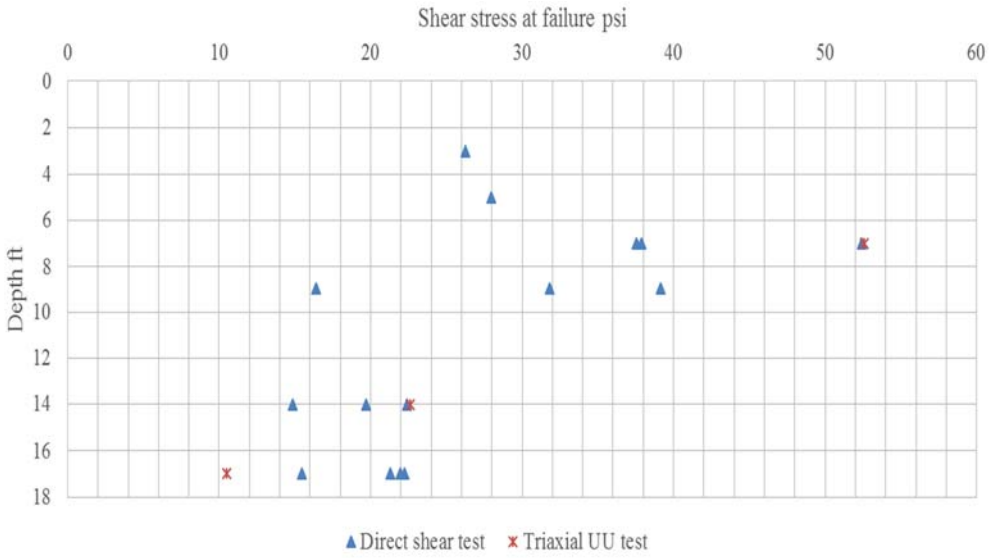

Figure 59. Soil Strength Profile at Different Depths.

TESTS ON EXISTING ANCHORS AT THE NGES-TAMU CLAY SITE

This section addresses the retesting of the existing anchors at the NGES-TAMU clay site. This project provided a unique opportunity to retest the anchors and study their creep behavior 23 years after installation. First, a summary of the previous research on existing anchors at the NGES-TAMU clay site is introduced as background information. Afterward, the test setups, loading protocols, and the results of the load tests performed in July 2013 (during this research) are presented. Results of the new tests are then compared to the results of the tests carried out in 1991 and 1997.

Introduction to Previous Research on Anchors at the NGES-TAMU Clay Site

Ten anchors were constructed at the NGES located on the Texas A&M University Riverside Campus. Those anchors were initially load tested in 1991 and then retested in 1997 (Figure 60).

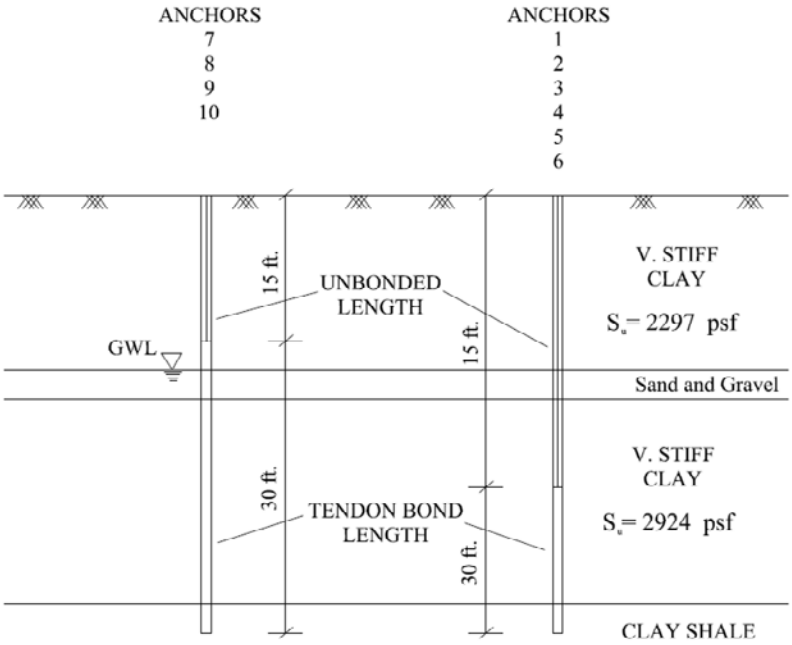

Figure 60. Stratigraphy and Anchor Specifications for Existing Anchors (after Briaud et al., 1998a).

All anchors were embedded 45.2 ft (13.8 m) in the clay deposit, going through the four soil layers as shown in Figure 60. A total of 68 instruments were installed in the bonded lengths and at the beginning of the unbonded lengths of the six anchors. The installation of the 10 anchors and the subsequent load testing took place from November 1990 to July 1991. The load tests were tension or uplift tests performed by pulling on the anchors with a hollow hydraulic jack with a capacity of 385.8 kips (175 tons) (Figure 61).

Test Details of Previous Research on Anchors

There are three important aspects to consider with respect to the previous test results on the anchors:

- The ultimate load on each anchor.
- The difference of ultimate load between tests in 1991 and tests in 1997.
- The creep load threshold of each anchor.

Table 11 shows the ultimate load (or failure load) on each anchor tested in 1991 (Powers, 1993). The failure load is defined as the load at which the residual movement reached 1 in.

(Powers, 1993). In all cases, the residual movement did not reach 1 in. and the failure load was estimated by manual extrapolation (Powers, 1993).

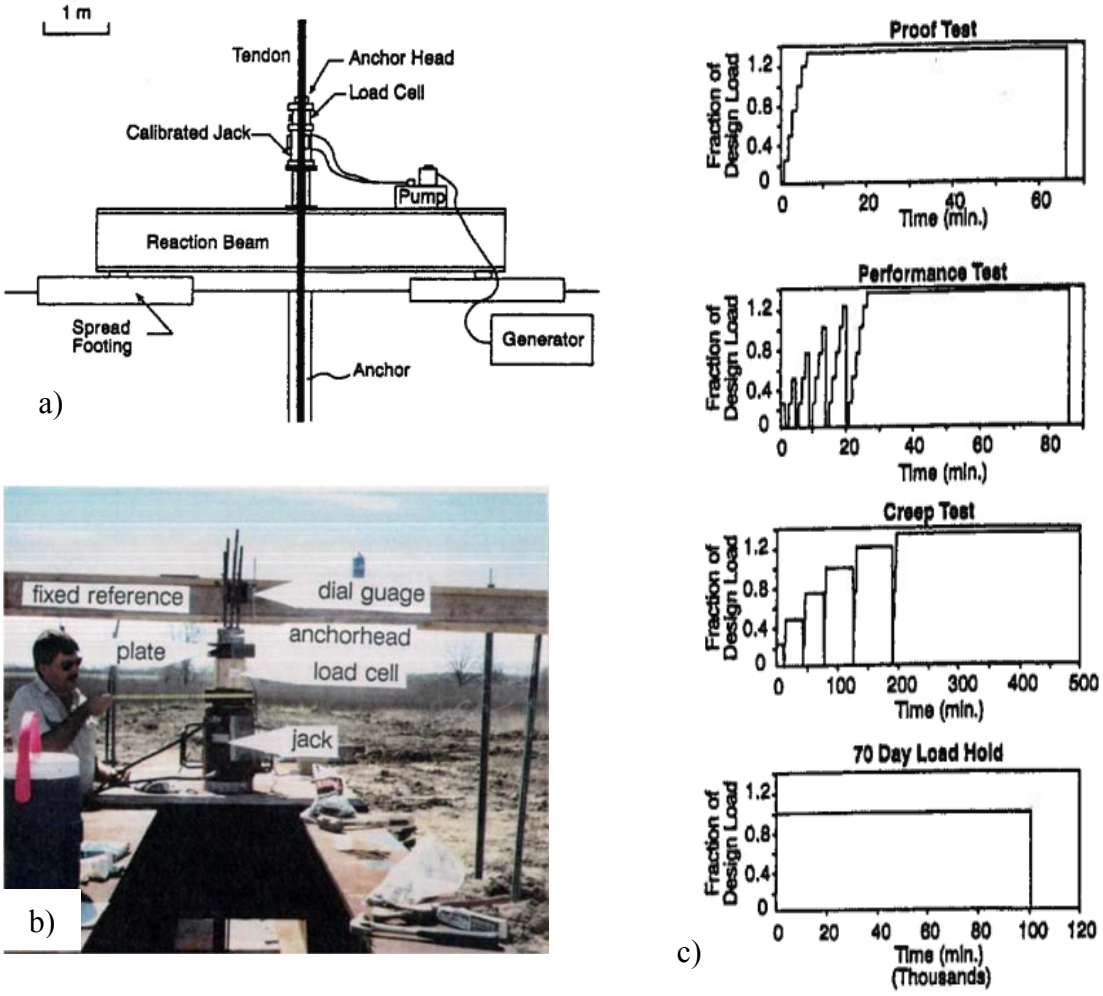

Figure 61. Existing Anchors: a) Load Test Setup (after Briaud et al., 1998a); b) Photo of Pullout Test (after Powers, 1993); and c) Load History for Four Load Test Types (after Briaud et al., 1998a).

The anchors 1, 2, 7, and 8 were retested on August 1997. The results of the 1991 and 1997 ultimate loads are compared in Table 12. The gain on ultimate load was at least 20 percent regardless of a hold load on the anchor (e.g., as for anchor 1 = 117.5 kips [523 kN], or anchor 2 = 136 kips [606 kN]) or not (e.g., as for anchors 7 and 8) (Briaud et al., 1998a).

The ultimate load for each anchor was defined as the load obtained for a residual displacement of one-tenth of the anchor diameter (B/10). Alternatively, the ultimate load was also defined as the load measured for a total displacement of B/10 plus the elastic elongation of

the unbonded length of the anchor (the maximum load applied divided by the extrapolated ultimate load >0.8) (Briaud et al., 1998a).

Table 11. Predicted Ultimate Capacity of Anchors Tested (after Powers, 1993).

Anchor	Type of Test						Date(s) of tests	Maximum Test Load (kips)	Failure Load (kips)	Load @ 0.08 inches/log cycle	Stiffness (kips/in)	Stiffness @ 0.5* (kips/in)	Creep Rate @ Max. Load (inches/log cycle)	Creep Rate @ Fail Load (inches/log cycle)
	Proof		Performance		Creep									
	Initial Loading	Final Loading	Initial Loading	Final Loading	Initial Loading	Final Loading								
1					*	*	4/8/91 - 4/10/91 7/14/91 - 7/16/91	174 177	208 291	– –	549 671	354 416	0.050 0.009	0.146 0.042
2					*	*	4/10/91 - 4/12/91 7/12/91, 7/13/91	197 198	262 352	– –	732 1203	407 473	0.050 0.034	0.162 0.181
3	*	*					4/4/91 7/10/1991	236 249	**** ****	– –	842 1264	**** ****	0.021 0.030	**** ****
4			*	*			4/3/91 7/9/91	179 176	222 376	174 –	657 1237	363 502	0.103 0.029	0.301 0.285
5	*	*					3/26/91 3/26/91	134 226	**** 243	– 206	1034 10346	**** 375	0.009 0.473	**** 0.862
6			*	*			3/20/91 3/20/91	133 132	133 135	– –	526 12300	247 271	0.017 0.025	0.017 0.025
7					*	*	3/8/91, 3/11/91 3/18/91, 3/19/91	163 186	180 188	158 164	623 1144	303 339	0.094 0.231	0.154 0.244
8					*	*	3/6/91, 3/7/91 3/7/91	169 176	147 167	144 167	164 2239	84 312	0.438 0.310	0.128 0.072
9					*	*	3/27/91 3/27/91, 3/28/91	149 149	247 286	– –	853 5605	338 414	0.050 0.044	0.103 0.357
10					*	*	3/21/91 3/22/91	177 176	177 172	161 155	533 9436	326 328	0.300 0.500	0.300 0.409

Table 12. Comparison of 1991 and 1997 Ultimate Loads (after Briaud et al., 1998a).

Anchor Number	Date Installed	Date Tested	Capacity (kN)	Date Tested	Capacity (kN)	Date Tested	Capacity (kN)
1	1-16-91	4-9-91	867	7-15-91*	978(?)	8-30-97	1245
2	1-16-91	4-11-91	1080(?)	7-13-91*	1156(?)	8-30-97	1255
7	12-19-90	3-7-91	801	3-18-91	738	8-30-97	1090
8	12-19-90	3-7-91	747	3-7-91	738	8-30-97	1060

Note: All capacities correspond to a residual movement of 25 mm.
***Denotes capacity after 70-day load-hold test.**
(?) Capacity calculated by extrapolating load-movement curve.

Examining Figure 62 and Figure 63, a creep load threshold exists and below that threshold load the creep rate is very small. On the contrary, for loads above this threshold load the creep rate is much larger (Briaud et al., 1998a).

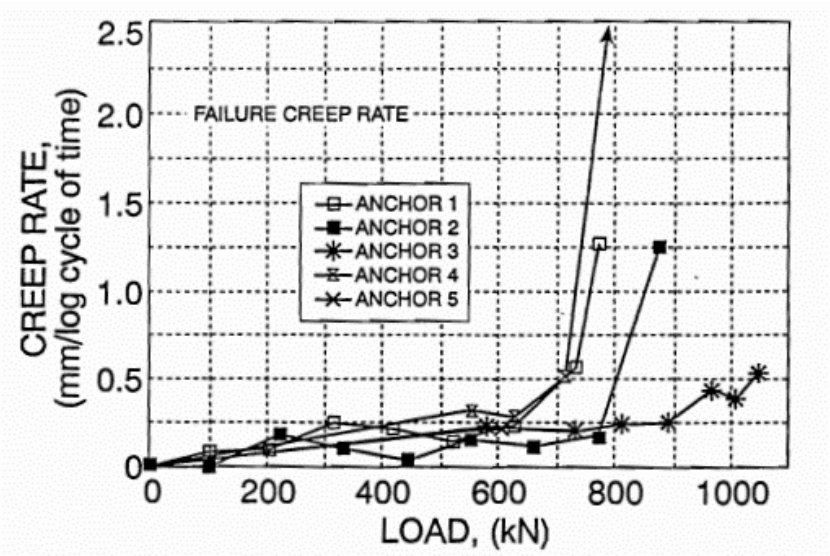

Figure 62. Creep Rate vs. Load Curves for First Loading on 4.6 m Bonded Length Tested in 1991 (after Briaud et al., 1998a).

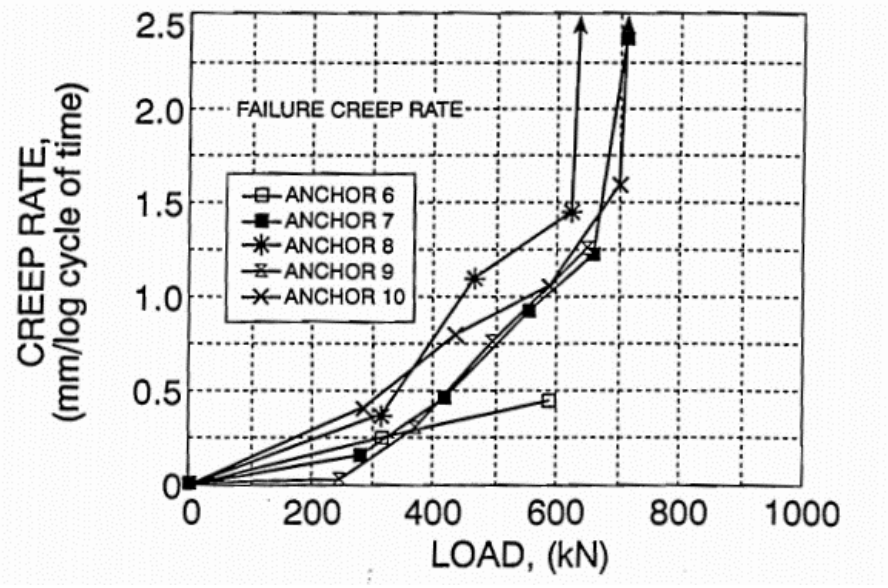

Figure 63. Creep Rate vs. Load Curves for Reload on 9.2 m Bonded Length Tested in 1991 (after Briaud et al., 1998a).

The comparison of the tests results of anchors 1, 2, 7, and 8 tested in 1991 and 1997 shows there is a minimum gain of 20 percent on strength (Briaud et al., 1998a). In the context of

this research, the pullout tests were performed to check the current ultimate load of the anchor (i.e., how much the strength has increased or decreased since 1997).

Details of Tests on Anchors in Context of This Research (July 2013)

The anchors 1, 2, 3, 4, 7, 8, 9, and 10 were retested in July 2013 (i.e., after 23 years of installation). These anchors were constructed and tested at the NGES-TAMU clay site in 1991. During the tests on anchors 3 and 4, tendons of these anchors failed at 238 kips due to corrosion and the tests were stopped. Figure 64 shows the failure of the tendons for these anchors. Figure 65 shows the load test setup adopted to retest the anchors. It consists of a reaction beam, a hollow hydraulic jack, a load cell, an anchor head, and dial gauges. The load protocols and results of the pullout tests are presented as follows.

Figure 64. Failure of Anchor 3 and 4 Tendons during the Test at 238 Kips.

Figure 65. Load Test Setup in July 2013: a) Photo of Pullout Test, b) Placing the Reaction Beam, and c) Load Cell and Dial Gauges.

Load Test Protocol

Verification tests with creep steps were conducted on anchors 1, 2, 3, 4, 7, 8, 9, and 10. In the verification test, load steps with a duration of 10 minutes were applied and the movement of the anchor head was recorded at 1, 2, 3, 5, 6, and 10 minutes after the load application. If the creep movements exceeded 0.04 in. for a 10-minute reading, the load was held for 60 minutes and the movement of the anchor head was recorded at 20, 30, 50, and 60 minutes also. Figure 66 illustrates the load test protocol for the anchors.

The anchors tested in 1991 and 1997 did not fail, and the ultimate pullout capacity of the anchors reported in previous works was estimated by manual extrapolation (Table 12). Therefore, to obtain the ultimate pullout capacity, the loading steps were increased and the anchors were loaded until the failure was reached. The increment for each load step was 26 kips.

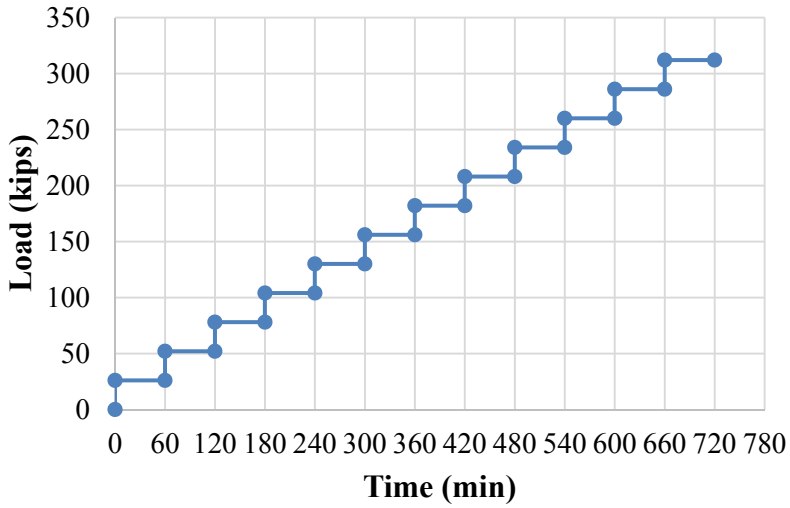

Figure 66. Load Sequence for Pullout Test on Existing Anchors in July 2013.

Total, Elastic, and Residual Movements

During the tests, the anchors were incrementally loaded until failure occurred. The total movement is defined as the measured movement of the anchorhead during the test. The total movement consists of the elastic movement and the residual movement. The elastic movement is the recoverable movement when the anchor is unloaded (i.e., the anchor load is reduced from a test load to an alignment load). The residual movements are the non-recoverable ones measured when the anchor is unloaded (FHWA, 1998b). Figure 67 to Figure 74 show the total, elastic, and residual movements versus the test loads in the different anchors.

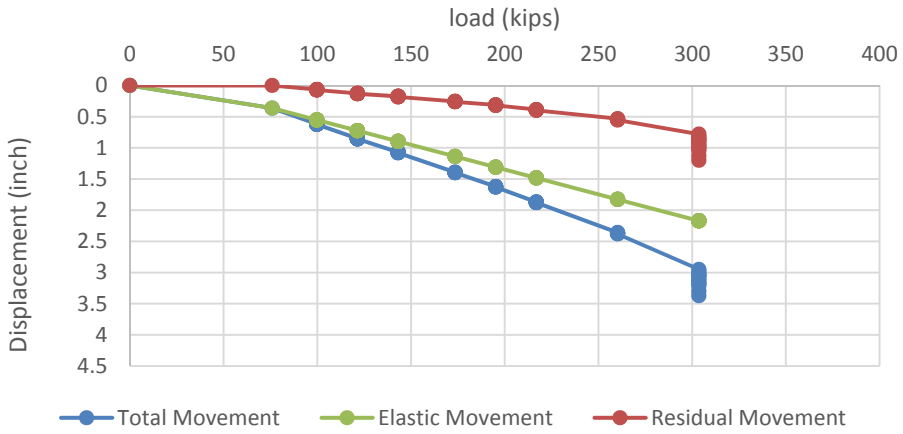

Figure 67. Load–displacement for Anchor 1.

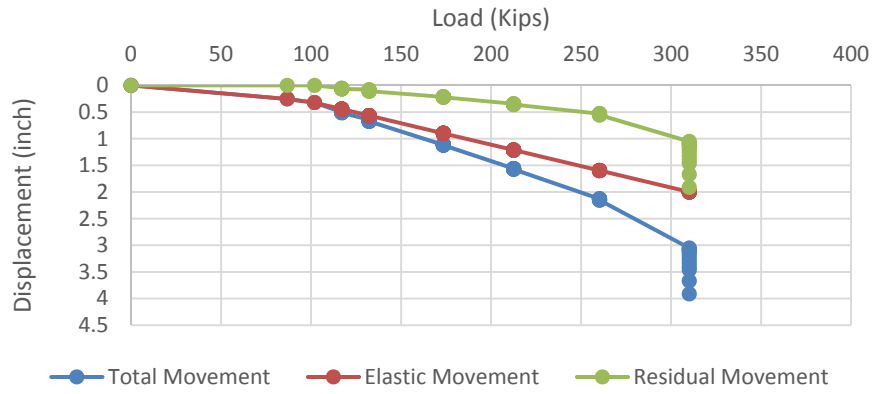

Figure 68. Load–displacement for Anchor 2.

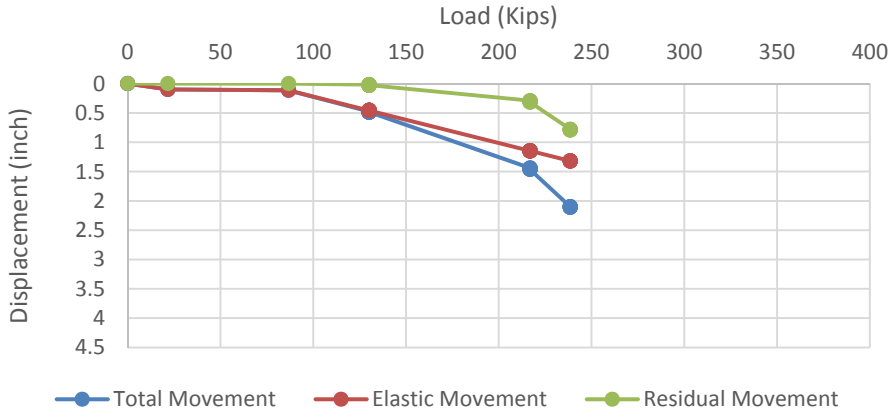

Figure 69. Load–displacement for Anchor 3.

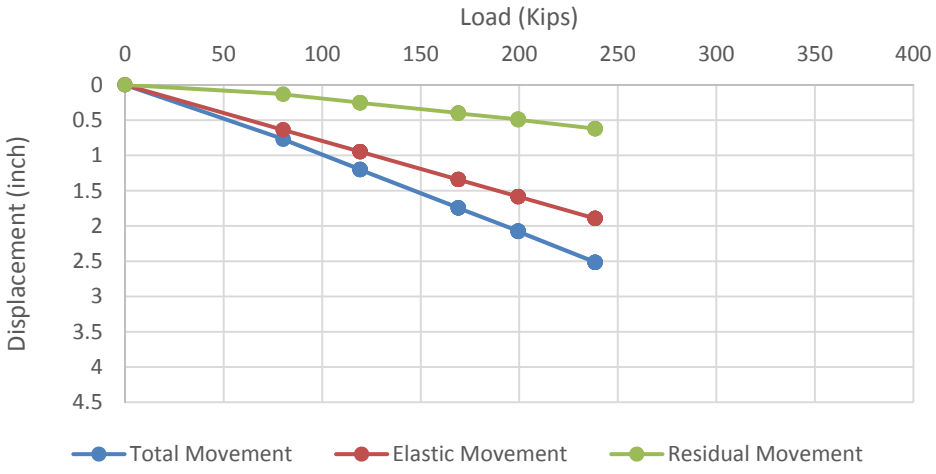

Figure 70. Load–displacement for Anchor 4.

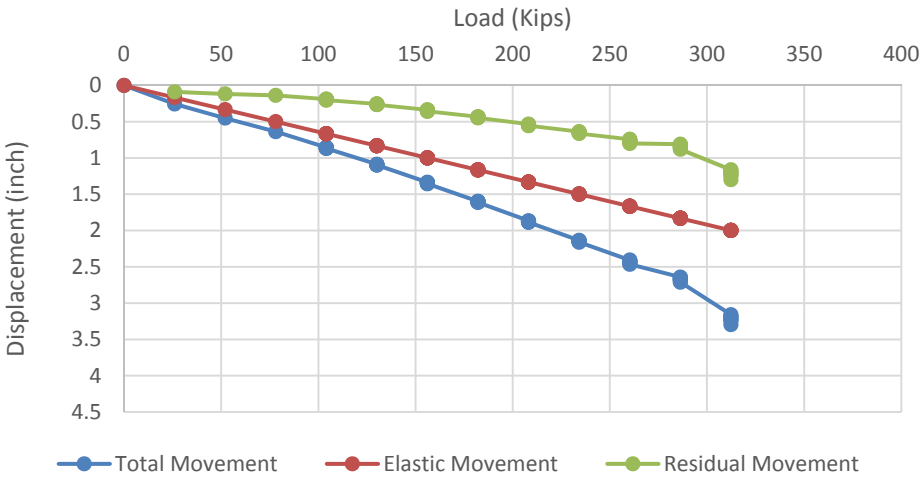

Figure 71. Load–displacement for Anchor 7.

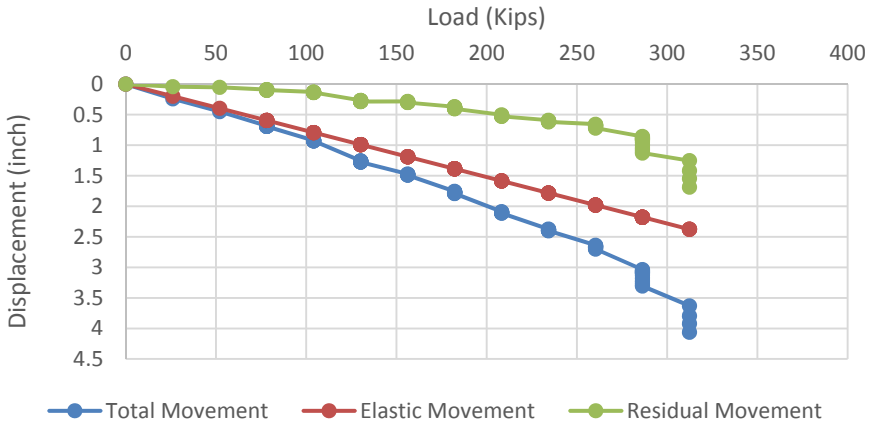

Figure 72. Load–displacement for Anchor 8.

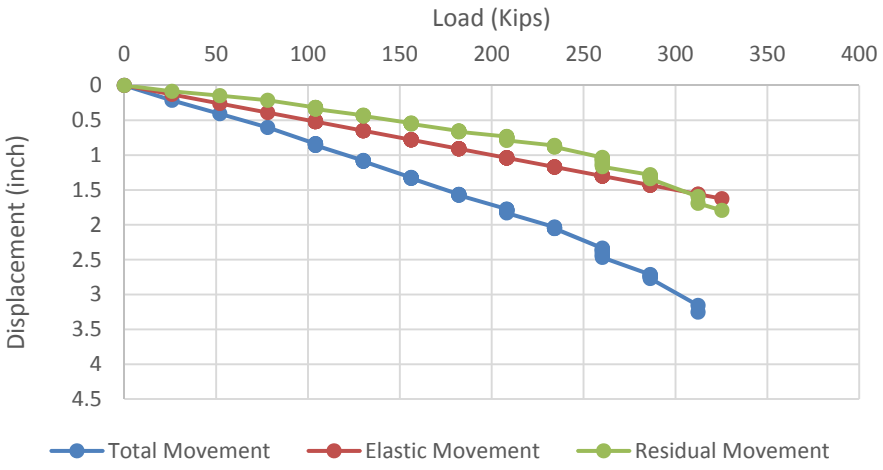

Figure 73. Load–displacement for Anchor 9.

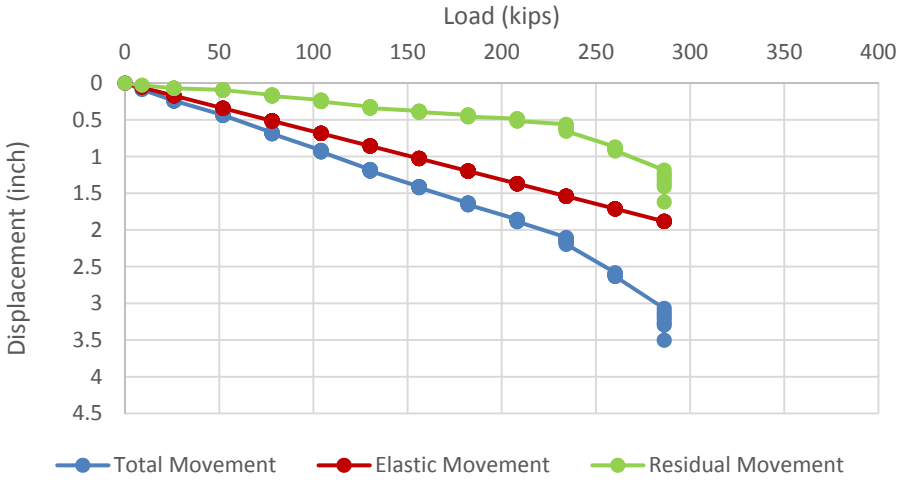

Figure 74. Load–displacement for Anchor 10.

Table 13 presents the lengths of the tested anchors. The drilled depths were 45 ft. The bond length of anchors 1 to 4 is 15 ft, and the unbonded length is 36 ft, while for anchors 7 to 10 the bond length is 30 ft and the unbonded length is 21 ft.

Table 13. Length for Tested Anchors (after FHWA, 1998b).

Anchor No.	Total Tendon Length (ft)	Drilled Length (ft)	Tendon Bond Length (ft)	Unbonded Length (ft)
1–4	51	45	15	36
7–10	51	45	30	21

Figure 75 and Figure 76 show the residual movement for the tested loads for anchors 1 to 4, and 7 to 10, respectively.

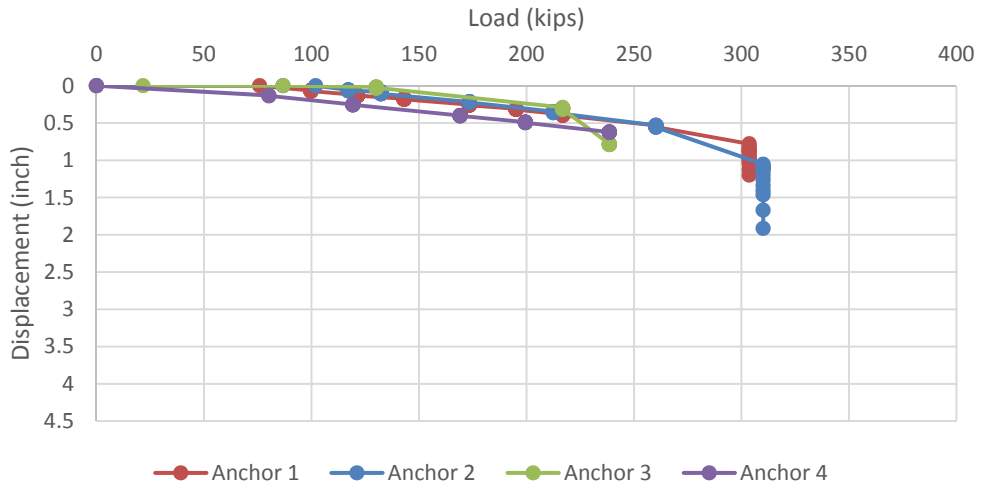

Figure 75. Residual Displacement versus Load for Anchors 1 to 4.

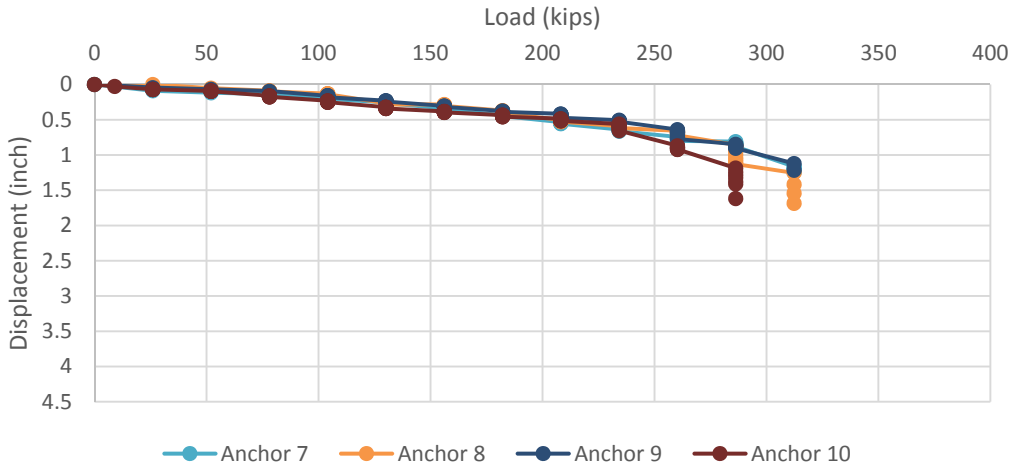

Figure 76. Residual Displacement versus Load for Anchors 7 to 10.

The ultimate load for each anchor was defined as the load obtained for a residual movement equal to one-tenth of the anchor diameter (B/10) or for a total displacement of B/10 plus the elastic elongation of the unbonded length of the anchor (Briaud et al., 1998a):

$$\frac{B}{10} = \frac{12in}{10} = 1.2\ inch \tag{6}$$

Therefore, the ultimate load capacity of the anchors is defined as the load for the residual movement of 1.2 in. The ultimate load capacity is the load that mobilizes the maximum friction between the grout and the soil. The ultimate pullout capacity of the anchors, Q_u, is defined as:

$$Q_u = \pi D L_a f_{max} = F_{max} L_a \text{ (Briaud et al., 1998a)} \quad (7)$$

where F_{max} is the maximum friction load per unit length of anchors; L_a is anchor bond length; D is the diameter of the drilling hole; and f_{max} is the maximum shear strength of the interface between the soil and grout. The parameter f_{max} is correlated to the undrained shear strength (S_u) of the soil and it is defined as:

$$f_{max} = \propto S_u \text{ (Briaud et al., 1998a)} \quad (8)$$

As shown in Figure 77, the α value was measured and recommended by many researchers. The α value measured from the tests in 1991 and 1997 was 0.51. However, the back-calculated α value from the tests in 2013 is 0.80. This increase in the α value is related to the *aging effect* that provides an apparent additional strength at the interface between grout and soil.

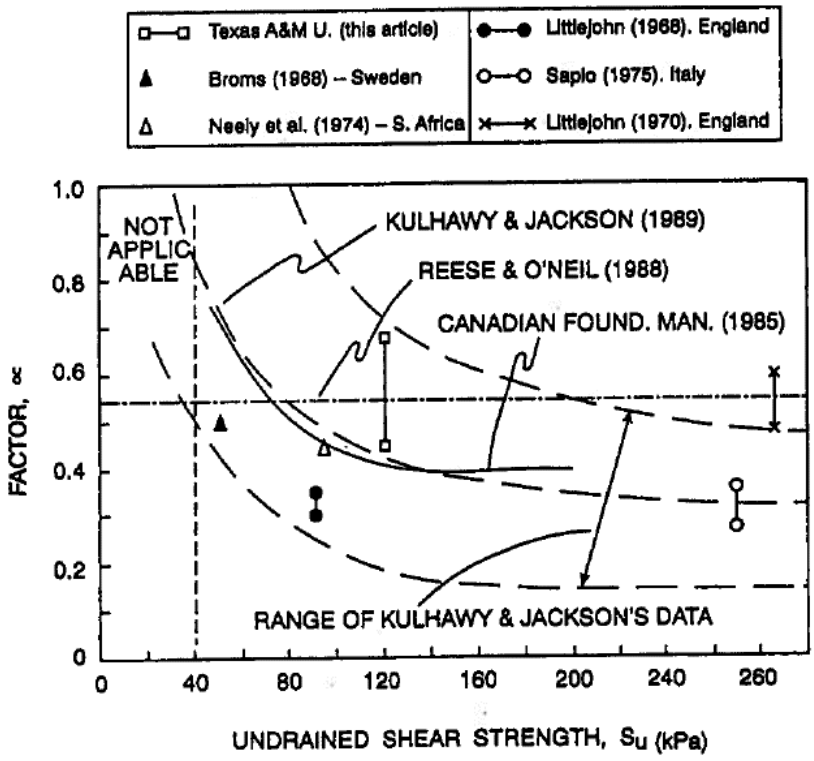

Figure 77. The α Value for Low Pressure Grouted Anchors in Clay (after Briaud et al., 1998a).

Table 14 shows the maximum shear strength at the interface between the soil and grout (f_{max}) obtained from the tests in 1997. The back-calculated f_{max} from the tests in 2013 shows the maximum shear strength at the interface between grout and soil increased between 30 percent and 80 percent since 1997. This means that the ultimate pullout capacity of the anchors in 2013 increased by almost 60 percent compared to the corresponding values measured in 1997. The comparison of test results on anchors in 1991, in 1997 shows that there was a gain of 20 percent in strength (Briaud et al., 1998a), and in 1997 and in 2013, there was gain of 60 percent in strength. This gain in strength could be because of long-term aging effects and past loading history. Table 14 presents the detailed comparison between the tests on anchors in 1997 and 2013.

Table 14. Comparison of the Tests on Anchors in 1997 and 2013.

Anchor No.	Predicted failure load for the anchors in 1997 (kips)	Friction stress at failure (psf)	Average undrained shear strength (psf)	α value (1991)	Actual Failure load in 2013 (kips) (not predicated)	Friction stress at failure (psf)	Average undrained shear strength (psf)	α value (2013)
1	195	1380.04	2700	0.51	303	2144.37	2700	0.79
2	243	1719.75	2700	0.64	310	2193.91	2700	0.81
7	180	1273.89	2700	0.47	325	2300.07	2700	0.85
8	168	1188.96	2700	0.44	286	2024.06	2700	0.75
9	-	-	-	-	312	2208.07	2700	0.82
10	180	1273.89	2700	0.47	286	2024.06	2700	0.75
			Avg	0.51			Avg	0.80

Creep Tests

During the pullout tests, each load increment was held constant for 60 minutes and the creep movements were recorded. Because anchors 3 and 4 failed during the test, no creep data were recorded for those two anchors. Creep movements at different load steps versus time are shown in Figure 78 to Figure 83.

The acceptance criteria typically require that the creep movement be less than 0.04 in. (1 mm) for the readings between 1 to 10 minutes, or it must be less than 0.08 in. (2 mm) for the readings between 6 to 60 minutes (FHWA, 2003).

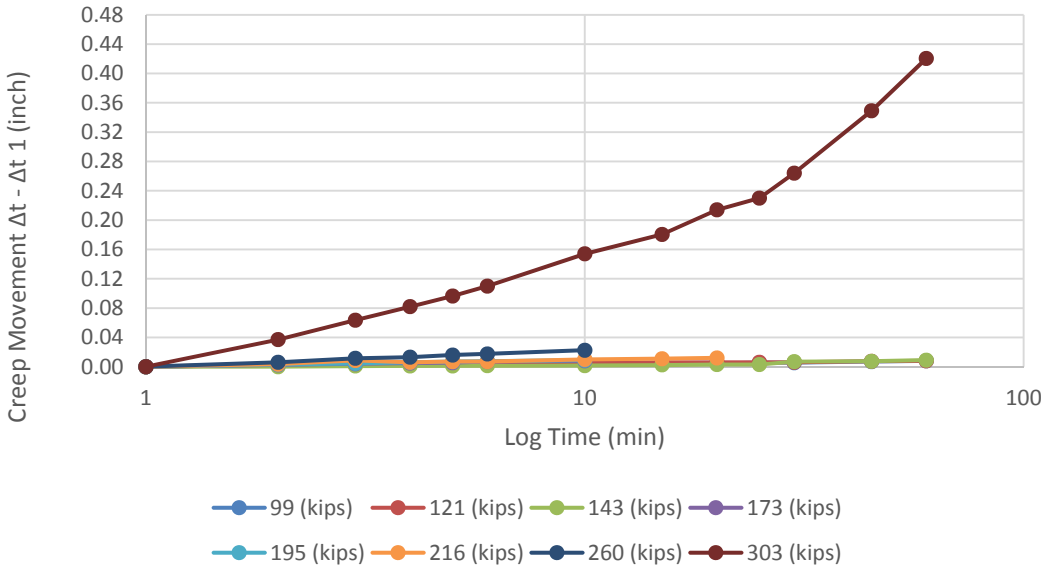

Figure 78. Creep Movement versus Time for Anchor 1 at Different Load Steps.

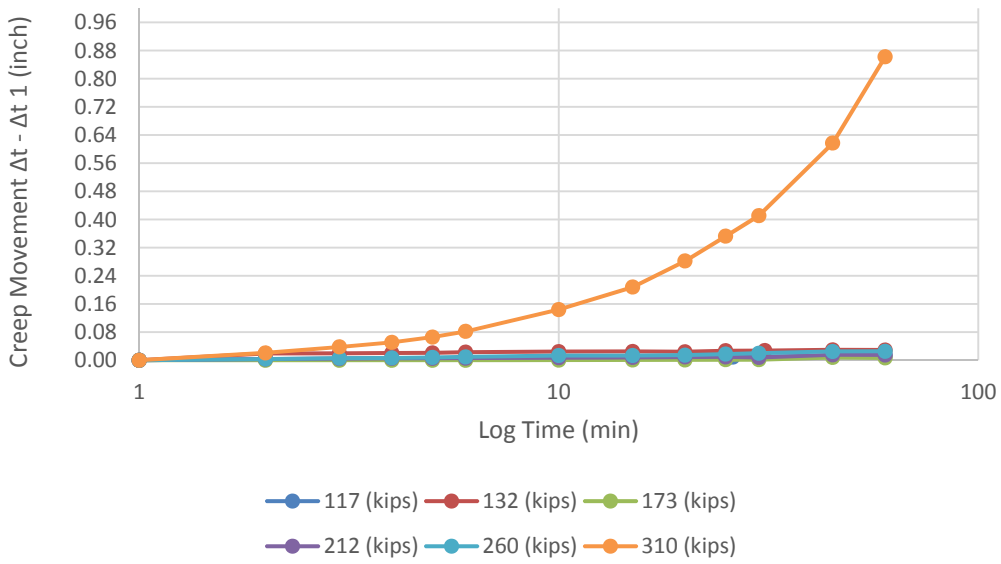

Figure 79. Creep Movement versus Time for Anchor 2 at Different Load Steps.

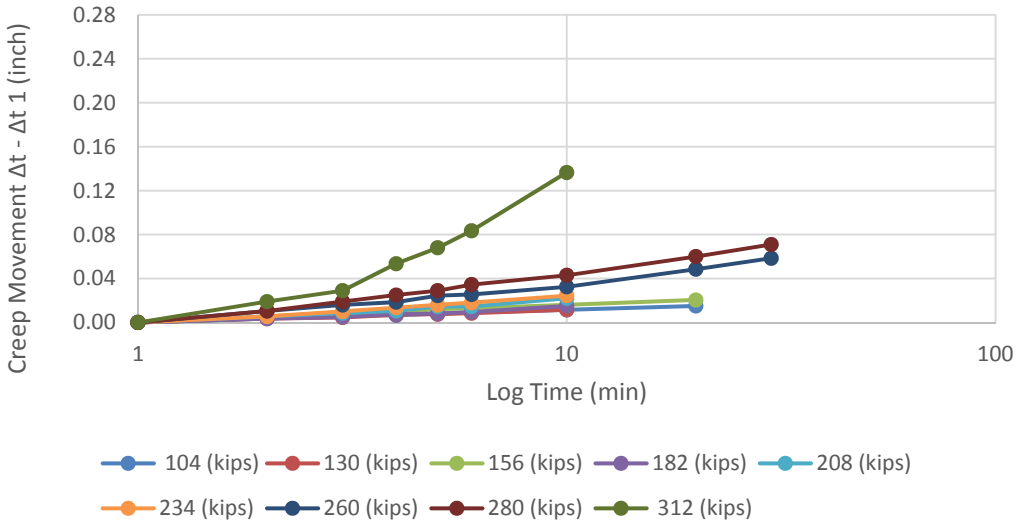

Figure 80. Creep Movement versus Time for Anchor 7 at Different Load Steps.

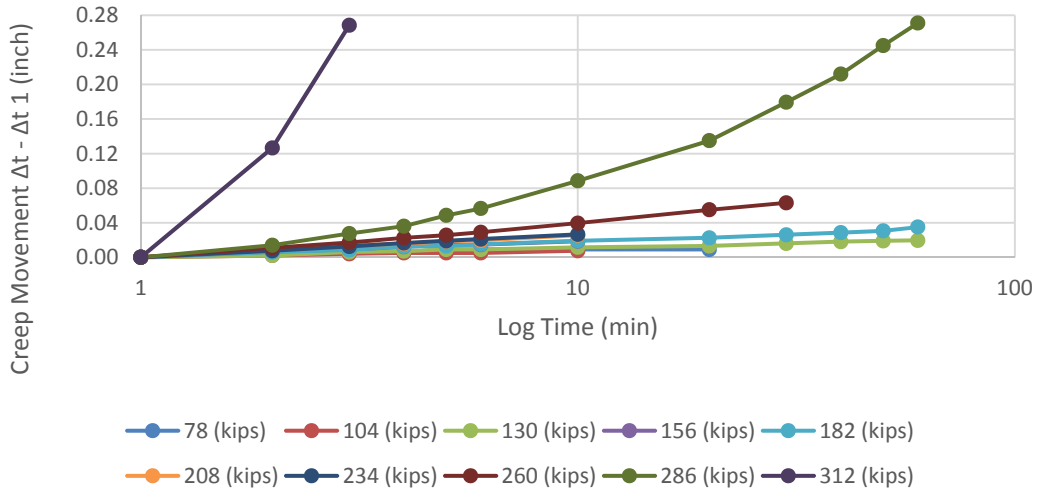

Figure 81. Creep Movement versus Time for Anchor 8 at Different Load Steps.

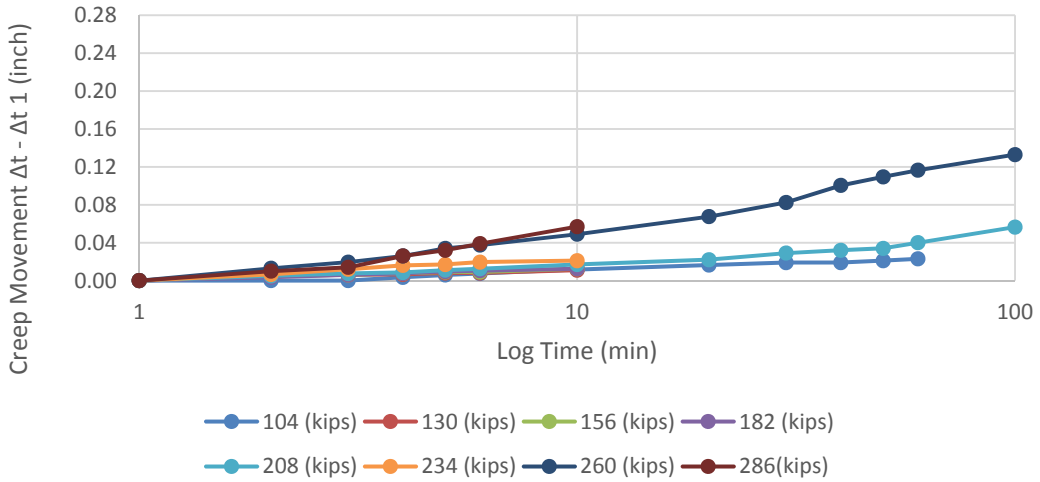

Figure 82. Creep Movement versus Time for Anchor 9 at Different Load Steps.

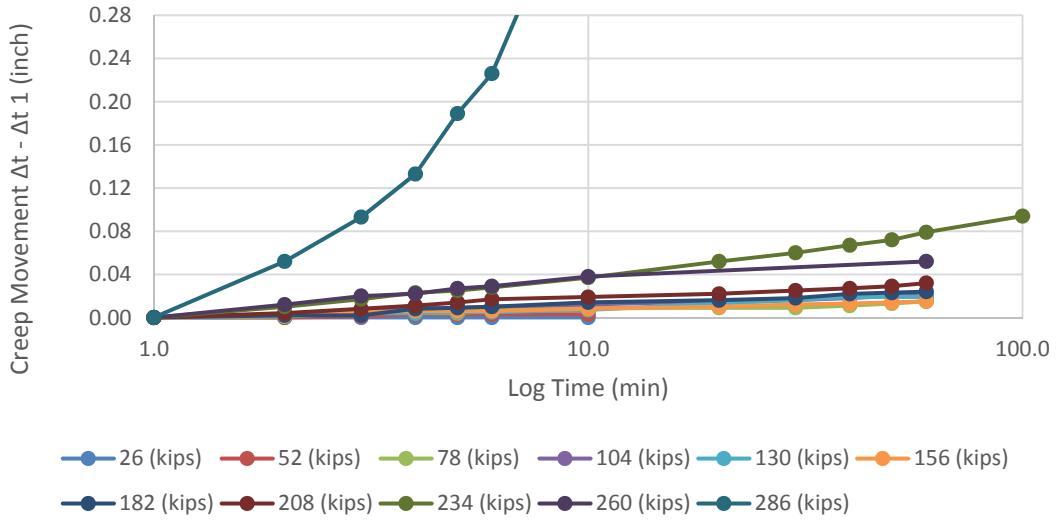

Figure 83. Creep Movement versus Time for Anchor 10 at Different Load Steps.

For anchors 1 and 2, no creep failure occurred until the ultimate pullout capacity of the anchors was reached. These two anchors showed creep failure at 100 percent of failure load. Anchor 7 showed creep movements higher than 0.04 in. for readings between 1 to 10 minutes at 280 kips load, while the ultimate pullout capacity for this anchor was 312 kips. Anchors 8, 9, and 10 showed creep movements at 100 percent of the pullout capacity, which was 286 kips. Table 15 shows the loads at which the creep failure occurred. Table 15 shows that the load threshold for creep failure is about 90 percent of the ultimate pullout capacity of the anchors.

Table 15. Percentage of Pullout Capacity that Creep Occurred.

Anchor No.	Pullout capacity (kips) (Failure load)	Creep failure load (kips)	Percentage of pullout capacity that creep occurred
1	303	303	100%
2	310	310	100%
7	312	280	89.7%
8	286	260	90.9%
9	286	260	90.9%
10	286	260	90.9%

Figure 84 presents the creep rate in unit of inch per log cycle of time at different load steps for anchors 1 and 2. Figure 85 presents the same parameter for anchors 7, 8, 9, and 10. The creep rate increased at a low rate until the load was around the 90 percent of the ultimate pullout

capacity. At this point, the slope of the creep rate changed rapidly, increasing significantly until the failure took place.

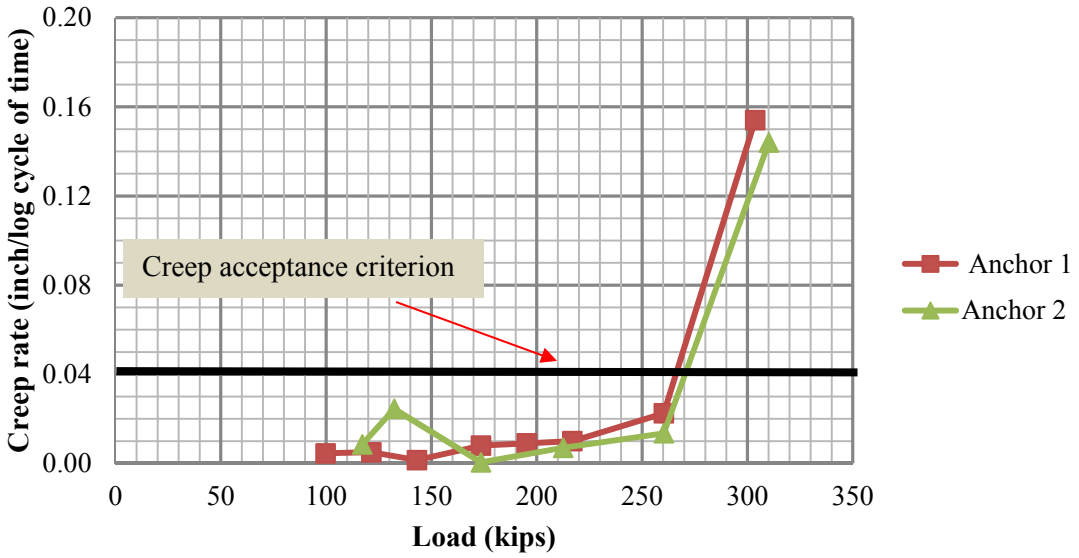

Figure 84. Creep Rate at Different Loads for Anchors 1 and 2 (1- to 10-Minute Readings).

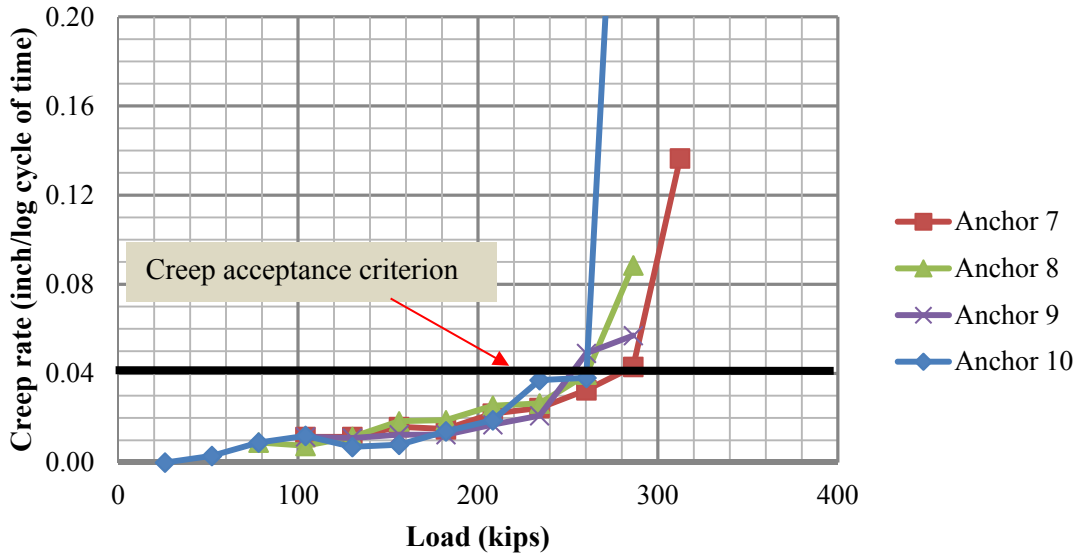

Figure 85. Creep Rate at Different Loads for Anchors 7, 8, 9, and 10 (1- to 10-Minute Readings).

n Value

The *n* value refers to the power law corresponding to Eq. 4 (Chapter 2). The exponent *n* corresponds to the slope of the line in the log–log space. In Eq. 4, the movement $s_{(t)}$ at a given

time is normalized by the movement at 1 minute after the application of the load step, $s_{(t1)}$. The time (t) is also normalized by time (t_1) equal to 1 minute. Figure 86 presents the viscous exponent *n* from the pullout tests on the anchors. The *n* value varies between 0.001 and 0.01 for loads lower than the 90 percent of the ultimate pullout capacity of the anchors. When the loads were higher than the 90 percent of the ultimate pullout capacity, the *n* values increased up to 0.04. To estimate the creep movements of the anchors in each load step using this power law, the log of movements are plotted versus the log of time, as shown in Figure 87 to Figure 92. From these results, Figure 86 was prepared.

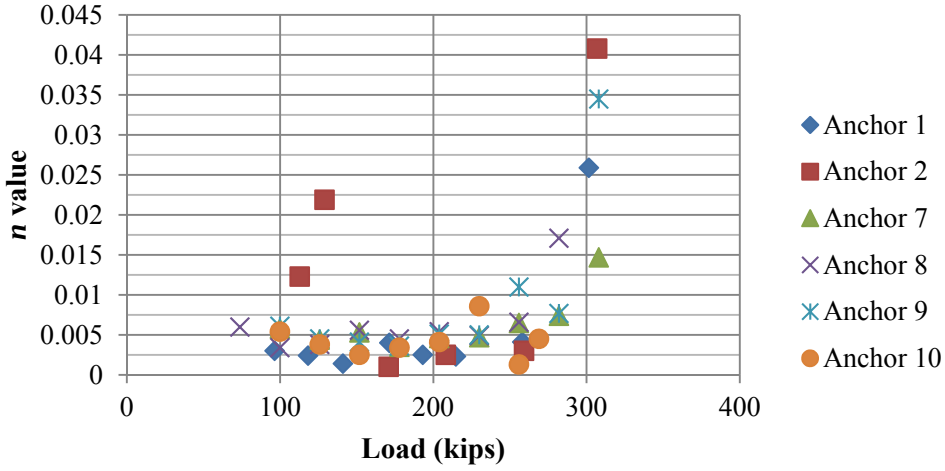

Figure 86. Viscous Exponent *n* for the Tested Anchors.

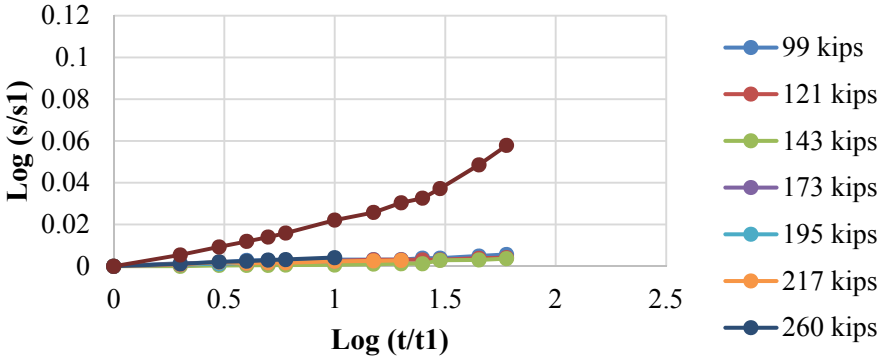

Figure 87. Normalized Creep Movement versus Normalized Time, Anchor 1.

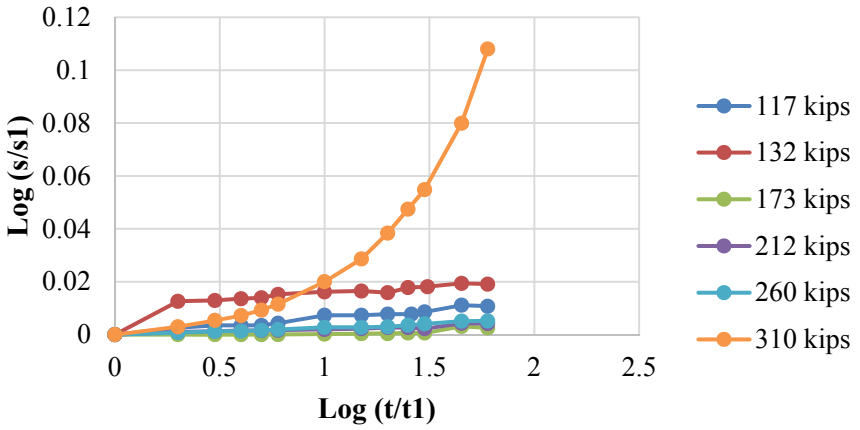

Figure 88. Normalized Creep Movement versus Normalized Time, Anchor 2.

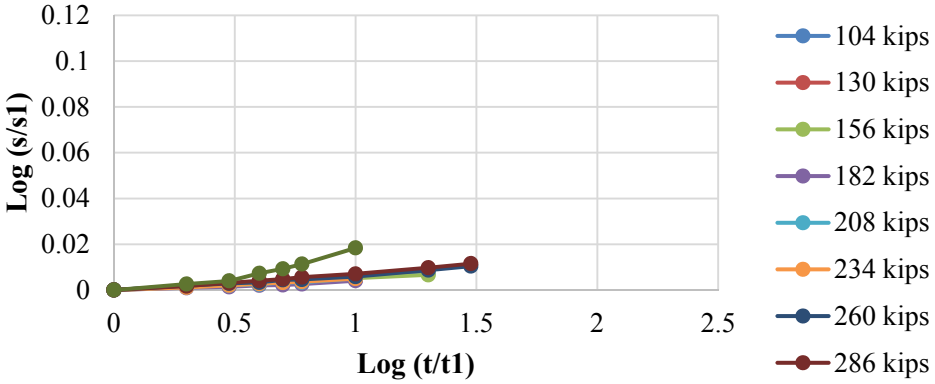

Figure 89. Normalized Creep Movement versus Normalized Time, Anchor 7.

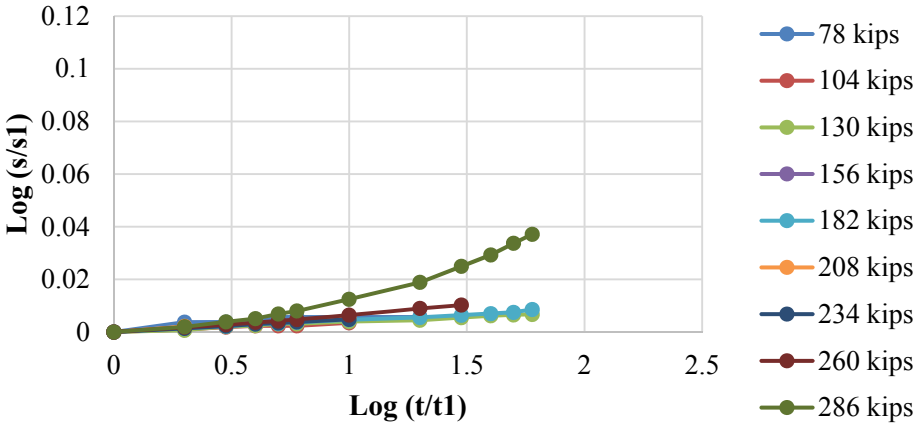

Figure 90. Normalized Creep Movement versus Normalized Time, Anchor 8.

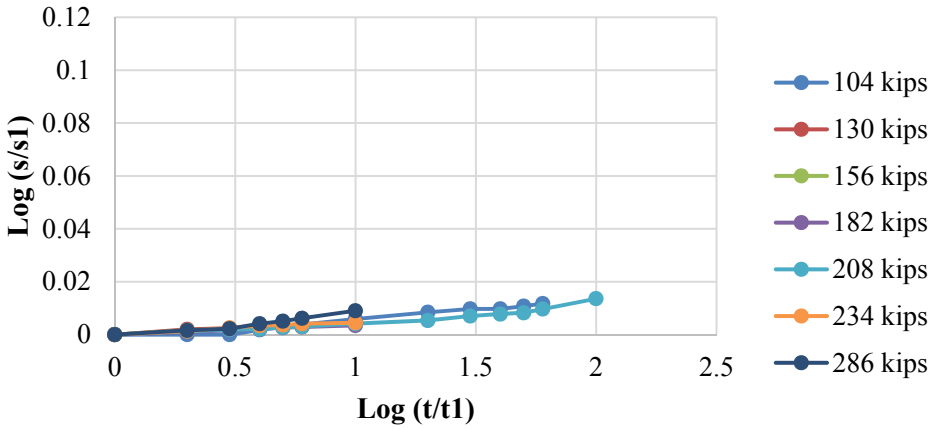

Figure 91. Normalized Creep Movement versus Normalized Time, Anchor 9.

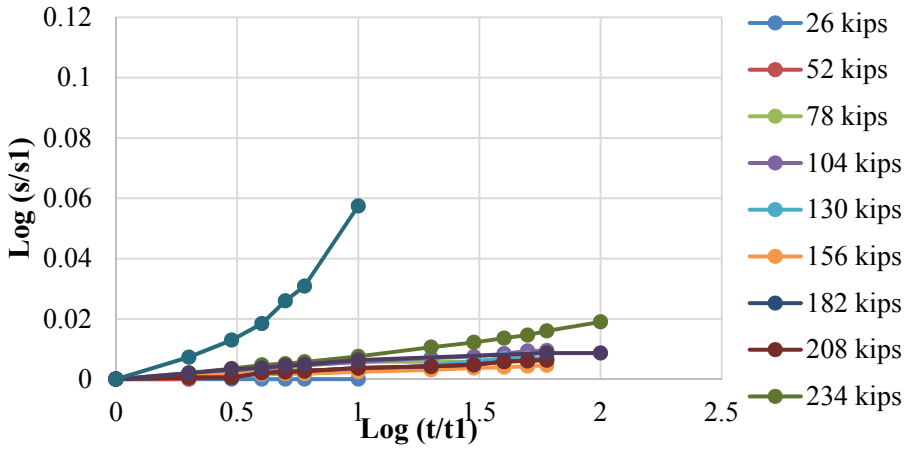

Figure 92. Normalized Creep Movement versus Normalized Time, Anchor 10.

NEW NAILS AT THE NGES-TAMU CLAY SITE

In the following sections, the researchers present the project activities including design of the new nails, instrumentation, soil nails installation at the NGES-TAMU clay site, setup, test protocols, and pullout test results.

Design of Test Load and Soil Nail Length

Some basic requirements regarding the design of the nails are (FHWA, 2003):

- The size of nail steel bar should be at least #8 (i.e., 1 in.). This recommendation is to prevent bending effects.
- The unbonded length should be at least 3 ft.

Ultimate Bond Strength for New Soil Nails

The ultimate bond strength may be estimated in the field during the site investigation stage of the project from the results of pressuremeter tests, using the following correlation (FHWA, 2003):

$$q_u(kPa) = 14P_L(MPa)[6 - P_L(MPa)] \text{ (SI Units)} \quad (9)$$

$$q_u(psi) = \frac{1}{214} P_L(ksf)[125 - P_L(ksf)] \text{ (Imperial Units)} \quad (10)$$

where PL is the limit pressure (i.e., as measured with the pressuremeter); and q_u is the ultimate bond strength. Based on the above equations, the ultimate bond strength at the NGES-TAMU clay site is shown in Table 16.

Table 16. Data for q_u for Two Layers of Clay.

Depth of Clay (ft)	PI	S_u (psf)	P_L* (psf)	q_u** (psf)
0 to 18	32.8	2297 (110 kN/m^2)	16708 (0.8 MPa)	1216 (58.24 kPa)
21 to 41	43.5	2924 (140 kN/m^2)	45948 (2.2 MPa)	2444 (117.04 kPa)

*q_u means ultimate bond strength per unit length.

**Pressuremeter data are from Briaud et al. (1998a).

Therefore, for this preliminary design, the bond strength was found to be 1216 psf.

Bonded Length

The bonded length for the verification testing has to be at least 3 m (FHWA, 2003):

$$L_{BVT} = \frac{C_{RT} \times A_t \times f_Y}{Q_{ALL} \times FS_{Tver}}; \quad Q_{ALL} = \frac{Q_u}{FS_P} \quad (11)$$

where C_{RT} is a reduction coefficient (C_{RT} = 0.9); A_t is the nail bar cross-sectional area; f_Y is the nail bar yield tensile strength; FS_{Tver} is the FS against tensile failure during the verification test (it is recommended to use 2.5 or 3); and Q_{ALL} is the allowable pullout resistance per unit length.

With the data and equations quoted above, the bonded length for designing new nails is shown in Table 17.

Table 17. Bonded Length.

Test Type	C_{RT}	A_t ($in.^2$)	f_Y (psi)	Q_u (lb/ft)	FS_P	FS_{Tver}	L_{BVT} (ft)
Verification	0.9	0.79	75000	2216	2	3	16

Note: The nail used in the table is #8 and the grade is 75.

Therefore, the bonded length should be between 10 and 16 ft, while the unbonded length is at least 3 ft (FHWA, 2003). The purchased nails were 20 ft long, in which 3.3 ft are necessary for performing the pullout test and remained above the ground level, and 16.7 ft were placed in the ground (i.e., 6.3-ft unbonded length and 13.4-ft bonded length).

Design Test Load and Maximum Load

Table 18 shows the DTL and maximum load for the new nails.

Table 18. DTL and Maximum Load.

L_{BVT} (ft)	Q_{ALL} (lb/ft)	Bonded length (ft)	DTL (kips)	Maximum load (kips)	
16	1114	14 (4.26 m)	15.6 (69.3 kN)	3.0 DTL	16

Note: The DTL = Q_{ALL} * bonded length.

Instrumentation Design

As mentioned in the previous section, the estimated maximum load is 46.8 kips, so a 110-kips jack was used for the pullout tests. To measure the strains and load distribution in the nails during the pullout tests, the strain gauge type UFCA-5-11 (manufactured by Tokyo Sokki Kenkyujo Co. Ltd.) was selected. The gauges were installed on nails at six different depths, as follows: 3.3, 3.9, 4.6, 7.8, 11.2, and 14.5 ft. Figure 93 illustrates the positions of the strain gauges.

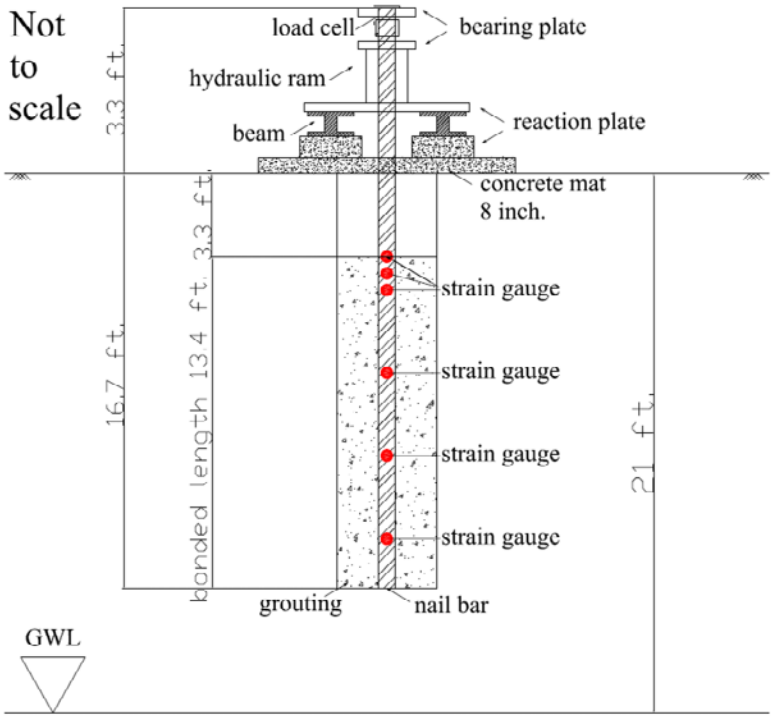

Figure 93. Drawing of Positions of Strain Gauges along the Soil Nail.

The step-by-step procedure necessary to properly attach the strain gauges to the metallic nails is briefly described below. The positions at which the strain gauges were attached to the nails were first marked (Figure 93). The primary steps contemplated in this procedure are as follows:

1. At each position, the nails were ground down with an electric grinder.
2. The nails' positions were carefully sanded with 200-grit sandpaper. The aim was to create a 4-in.-long smooth surface to mount the strain gauge.
3. Vishay Precision Group's CSM-2 degreaser was used to clean the smoothed surface.
4. A 400-grit extra-fine sandpaper was used along with Vishay's M-Prep Conditioner A to further smooth and clean the surface areas.
5. Vishay's M-Prep Neutralizer 5A was applied to neutralize the residual acid content from the M-Prep Conditioner A on the surface areas.
6. After the surface areas at the designated locations were clean, the strain gauges were glued to the nail bar using Vishay's M-Bond GA-2 adhesive. Teflon™ wires were used to

create two half-bridge connections and Vishay's TEC-1 Tetra-Etch® was applied on the end of the wires, serving as the treatment agent for the Teflon surface (Figure 94).

7. Each wired strain gauge (Figure 95) was then checked using Vishay's P3 Strain Indicator to ensure that the gauge was functional.
8. To extend the durability of the strain gauges, two layers of protective coatings (Figure 95) were applied to cover the wired gauges. Vishay's M-Bond GA-2 and M-Coat J were applied as the first and second coatings, respectively, covering around the perimeter of each 4-in.-long spot.

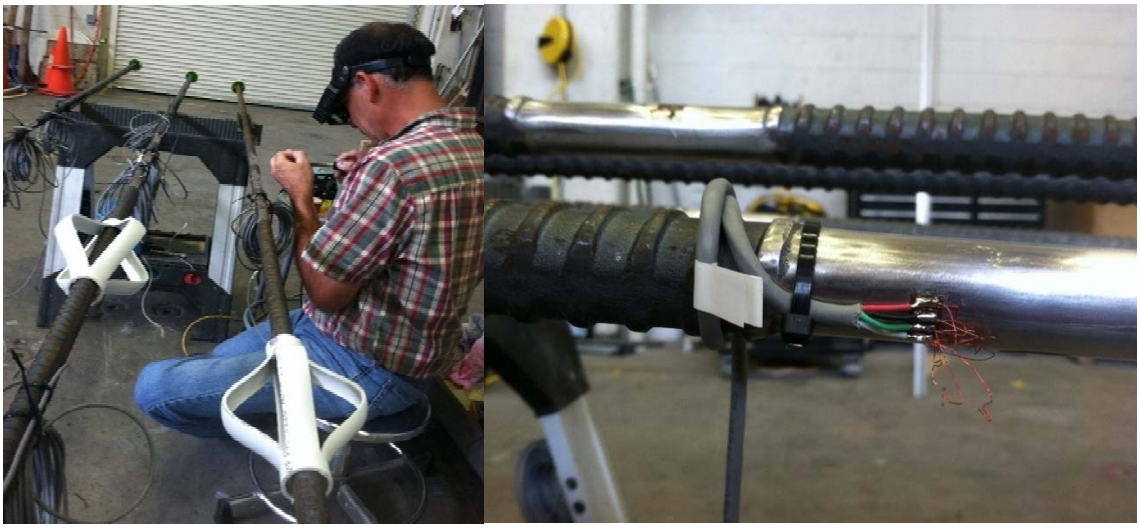

Figure 94. Gluing the Strain Gauges to the Threadbar.

Figure 95. Testing the Strain Gauges with Vishay's P3 Strain Indicator prior to Shipping to the NGES-TAMU Clay Site.

Nail Installation

The nails N1 to N6 were installed at the NGES-TAMU clay site in July 2013. As shown in Figure 93, a concrete slab was constructed and used as a reaction for these nails. Shorter nails (i.e., NS1 and NS2) were installed in the south side of the concrete in September 2013. Eight additional nails were installed in the north side of the concrete slab in November 2014. In the following sections, the concrete slab construction and nail installation are described in detail.

Concrete Slab Used for Reaction during the Pullout Tests on Nails N1 to N6

In order to perform the pullout tests on the new nails (i.e., N1 to N6), a concrete slab was designed to serve as a reaction for the pullout tests (i.e., to simulate the same behavior as an actual soil nail with a permanent concrete facing). The main following activities were performed to construct the concrete slab at the NGES-TAMU clay site: mow the site (Figure 96); lay the

plastic membrane (Figure 97a); mark the nail locations (Figure 97b); place the bottom of the reinforcement (Figure 98); place the top reinforcement (Figure 99); place the surrounding wood frame support (Figure 100); pour the concrete (Figure 101); and cure the concrete (Figure 102).

a)  b) 

Figure 96. NGES-TAMU Clay Site: a) before Mowing; b) after Mowing.

a)  b) 

Figure 97. a) Laying Plastic Membrane; b) Marking Nail Locations.

Figure 98. Placing the Bottom Layer Reinforcement.

Figure 99. Placing the Top Layer Reinforcement.

Figure 100. Placing the Wood Frame.

Figure 101. Pouring the Concrete.

Figure 102. Curing the Concrete.

Installation of Nails at the NGES-TAMU Clay Site

The nails identified as N1 to N6 were installed in July 2013 in collaboration with Schnabel Foundation Company and Terracon Consultants, Inc. The nails NS1 and NS2 were installed in September 2013. In November 2014, eight additional soil nails (i.e., NW1 to NW8) were installed at the NGES-TAMU clay site. During the installation of the soil nails, soil samples were gathered to conduct the laboratory tests by Terracon and Texas A&M University. The following activities were performed to install soil nails at the NGES-TAMU clay site: drill 7-in.-diameter holes (i.e., for nails N1 to N6 18-ft deep, for nails NS1 and NS2 10-ft deep, and for nails NW1 to NW8 15-ft deep; Figure 103); gather the soil samples (Figure 104); prepare the grout (Figure 105); and grout and install the nails (Figure 106).

Figure 103. Drilling the Holes.

Figure 104. Collecting the Soil Samples.

Figure 105. Grout Preparation.

Figure 106. Grouting and Nail Installation.

Figure 107. Final View of the Installed Soil Nails on Concrete Slab.

Load Test Setup

A center-hole jack was used to apply the load on the nails. For nails N1 to N6, the concrete slab was used for reaction during the pullout tests. It also simulates the behavior of an actual soil nail with permanent shotcrete facing. For the nails outside the concrete slab (i.e., NS1, NS2, and NW1 to NW8), eight wood posts (i.e., 8 × 8 × 9 in.) were used as reaction beams. The movements of the nail heads were measured with two dial gauges mounted on a tripod, which were independent of the jacking setup. A center-hole load cell (i.e., Geokon Model 3000) was used during the tests to monitor continuously the load applied during the tests. As mentioned in the GEC#7 (FHWA, 2003), the accuracy of the pressure gauge in the jack is not accurate enough to reflect possible loss in load; because of this, the center-hole load cell was very useful to check whether or not the target load was maintained constant during the extended periods of time corresponding to the creep tests. Figure 108 shows the load test setup for the nails on the concrete slab, while Figure 109 shows the setup for the nails outside the concrete slab.

Figure 108. Load Test Setup for the Nails on Concrete Slab (i.e., Nails N1 to N6).

Figure 109. Details of Load Test Setup for Nails outside the Concrete Slab (i.e., Nails NS1, NS2, and NW1 to NW8).

Load Test Protocols

In this section, the load test protocols adopted for the pullout tests of the nails at the NGES-TAMU clay site are presented. Also in this section, the predicted ultimate pullout capacity of the nails prior to their installation is described.

Ultimate Pullout Capacity Prediction

Based on the pullout tests on the existing anchors performed in 1991, Briaud found that the α value for the anchors at the NGES-TAMU clay site is around 0.52. Considering an undrained strength S_u = 2297 psf (FHWA, 1998b), the maximum shear strength at the interface between the soil and the grout is f_{max} = 1194 psf. Based on the site investigation performed in 1991, the research team decided that the maximum shear strength of the soil–grout interface is equal to f_{max} = 1216 psf (58.24 kPa). Table 19 presents the expected ultimate pullout capacity for the nails installed on the concrete slab.

Table 19. Specifications of the Nails Installed on the Concrete Slab in July 2013.

Nail No.	Drilled Length (ft)	Nail Bonded Length (ft)	Nail Unbonded Length (ft)	Diameter of the Hole (in.)	S_u (psf)	f_{max} (psf)	Q_u (kips)
1	17.30	14.30	6	7	2297	1216	38
2	19.16	16.16	6	7	2297	1216	42
3	19.00	16.00	6	7	2297	1216	42
4	19.33	16.33	6	7	2297	1216	43
5	19.25	16.25	6	7	2297	1216	43
6	19.50	16.50	6	7	2297	1216	43

Load Test Protocols

Verification tests were performed in July 2013 on nails coded N1, N2, N3, and N4. For each load step of the verification test, the load was held constant and the creep movements were recorded. These nails were incrementally loaded until failure. The total movements were recorded during the tests.

Table 19 presents the bonded and unbonded lengths of the nails. The loading protocols for the tests on nails N1, N2, N3, and N4 are shown in Figure 110 to Figure 113. For the pullout tests on N1, the test load was held constant at 24.5 kips (65 percent of the predicted failure load) for 30 minutes. A load increment of 4.3 kips load was adopted for the load steps lower than

24.5 kips, while for the loads higher than 24.5 kips the increment was 5 kips, and it was maintained until failure.

The nail N2 was loaded with load increments of 5 kips until 57 kips. Each load stage was held constant for 10 minutes and the creep movements were recorded. To study the effect of cyclic loading on nail behavior, the nail N2 was unloaded up to the contact load and was loaded again to 57 kips. This cycle was repeated several times. In each cycle, the load was held constant at 57 kips for 10 minutes and the creep movements were recorded.

The nail N3 was loaded with load increments of 5 kips until the load reached the predicted failure load at 37.5 kips. Then the nail was unloaded and reloaded up to 37.5 kips. The loading was continued with increments of 5 kips until 61 kips. Each load step was held constant for 10 minutes and the creep movements were recorded. At the loads of 52 kips, 57.8 kips, and 61.4 kips, the loads were held constant for 60, 100, and 100 minutes, respectively. The creep movements were recorded during these steps.

The load sequence on nail N4 was almost the same as for nail N3. For nail N4, the loads 56, 60, and 65 kips were held constant for 60 minutes and the creep movements were recorded during these steps.

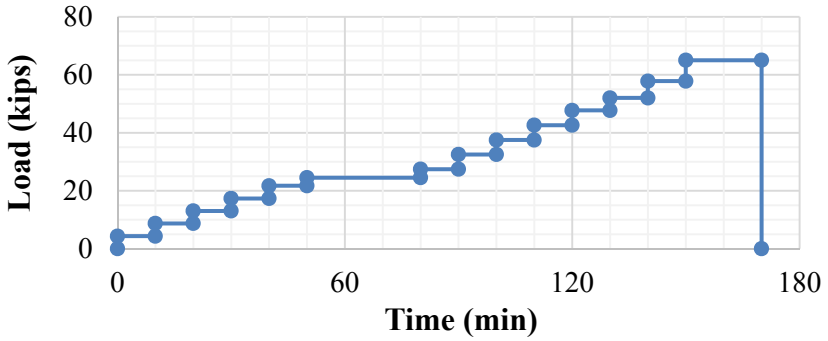

Figure 110. Loading Sequence for Pullout Test on Nail N1.

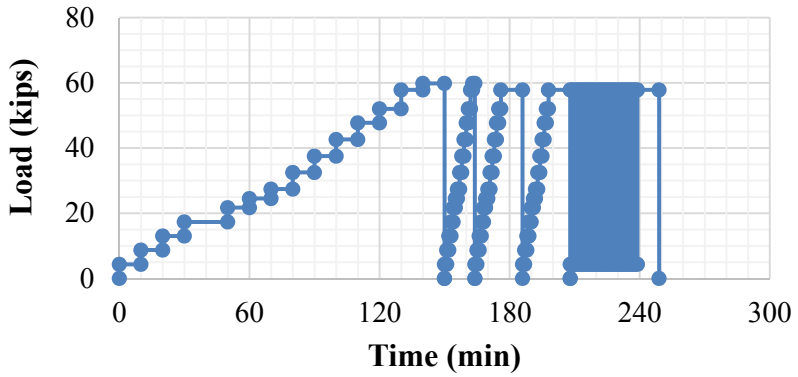

Figure 111. Loading Sequence for Pullout Test on Nail N2.

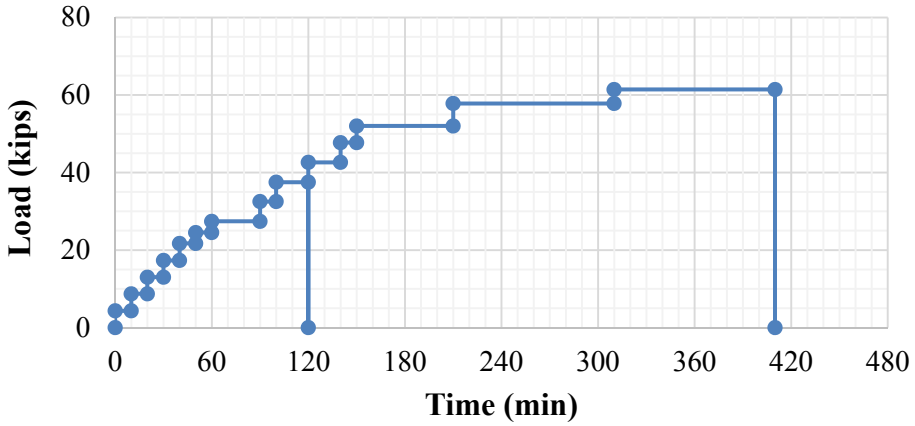

Figure 112. Loading Sequence for Pullout Test on Nail N3.

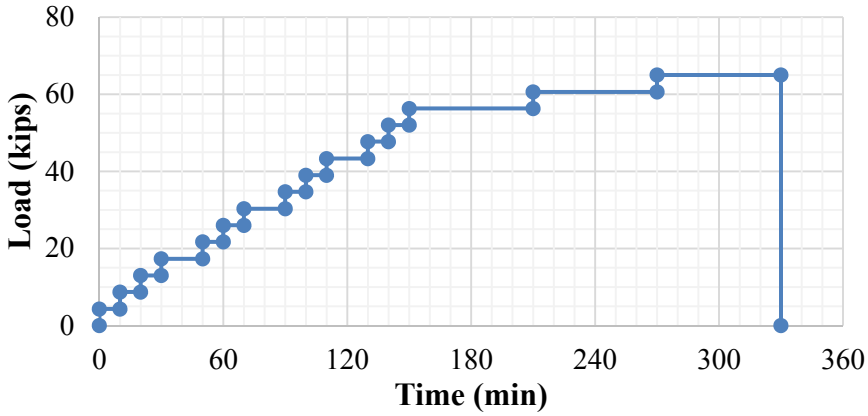

Figure 113. Loading Sequence for Pullout Test on Nail N4.

The nails N1 and N4 were retested in November 2013 and February 2014, respectively. The objective of these retests was to gain a better understanding of the preloading (load history) on the creep behavior, and also to determine the ultimate pullout capacity of these nails. The load

test protocols for retesting the nails N1 and N4 are presented in Figure 114 and Figure 115, respectively. The nail N1 was loaded up to 55 kips. Each load step was held for 10 minutes and the creep movements were recorded. The nail N4 was first loaded up to 33 kips. Each load step was held for 10 minutes and the creep movements were recorded. The load of 33 kips was held for 240 minutes and the creep movements were recorded. After 240 minutes, the nail was unloaded up to the contact load (2 kips) and then was reloaded up to 48 kips, with load increments of 4 kips. Each load step was held for 10 minutes and the creep movements were recorded.

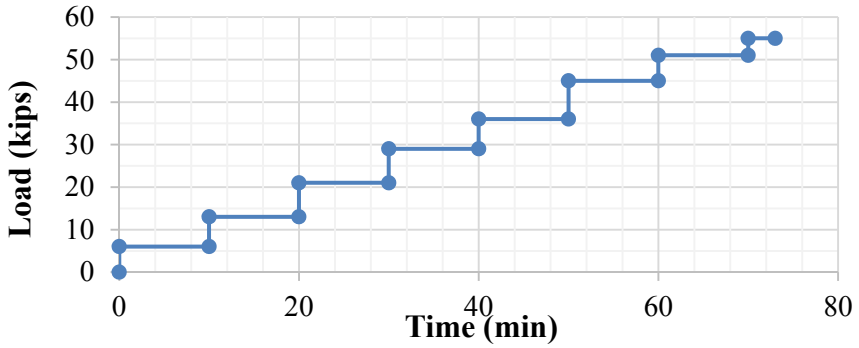

Figure 114. Loading Sequence for Retest on Nail N1 in November 2013.

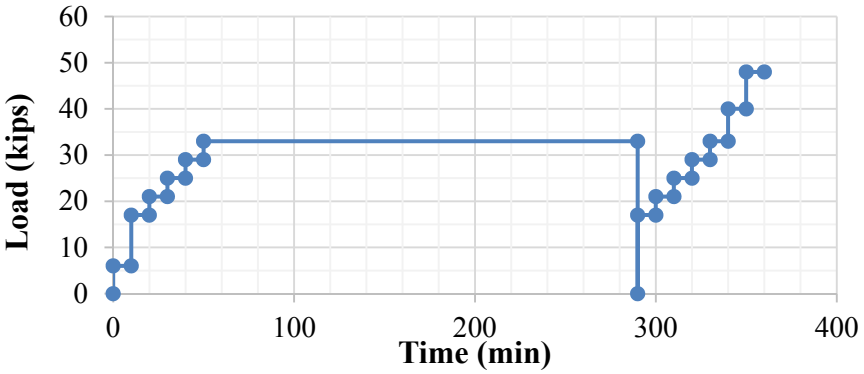

Figure 115. Loading Sequence for Retest on Nail N4 in February 2014.

The pullout test on nail NS1 was performed in September 2013. Nail NS1 was loaded with increments of 5 kips until failure. Each load was held for 10 minutes.

The pullout test on nail NW1 was carried out in November 2015. This nail was loaded with increments of 7 kips until the failure. In order to study the creep behavior, each load was held for 60 minutes and creep movement was recorded.

Test Results on New Nails

In this section, results of the pullout tests are presented. The results include total, elastic, and residual movement of the nail head. Furthermore, the water content measurements, results of the creep tests, and the corresponding *n* value for power model are discussed.

Total, Elastic, and Residual Movement

The total movements consisting of elastic and residual movements correspond to the measured displacements of the nail head during the test. The elastic movements are recoverable when the nail is unloaded (i.e., the nail load is reduced from a test load to an alignment load). The residual movements are non-recoverable when the nail is unloaded (FHWA, 1998a). The results of the tests on all the nails are presented as follows.

Tests on Nails N1 to N6, Performed in July 2013. Figure 116 to Figure 119 include the plots for the total, elastic, and residual movements for nails N1 to N4.

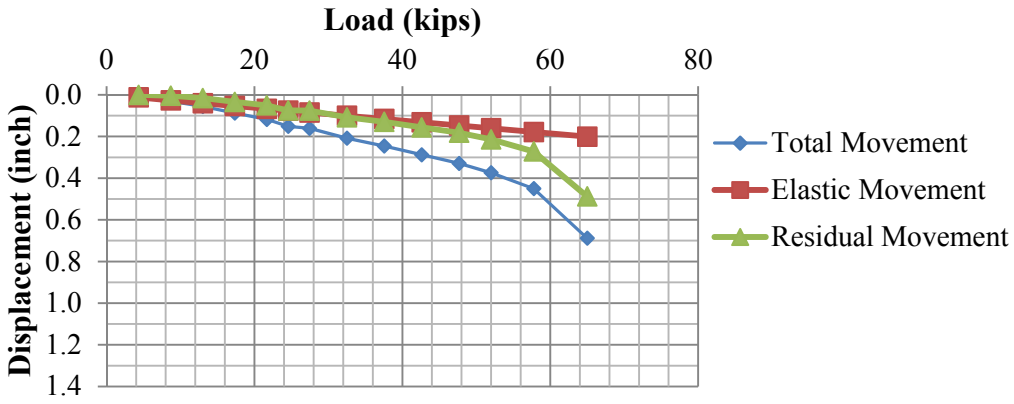

Figure 116. Load–Displacement Curve for Nail N1.

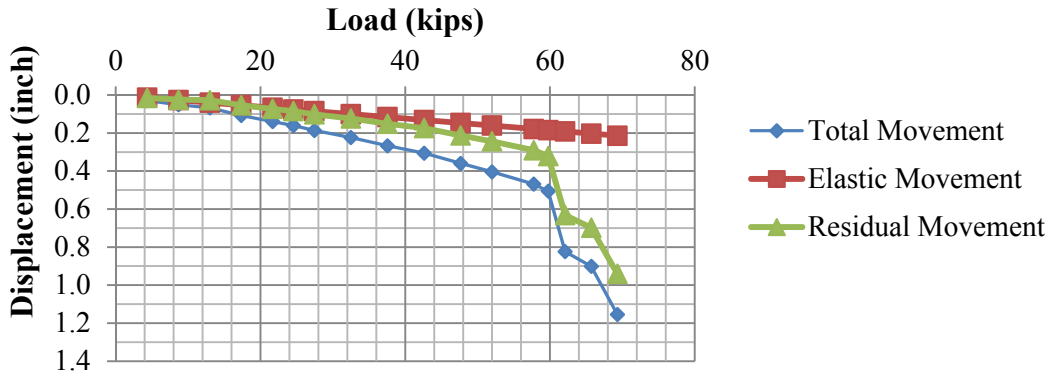

Figure 117. Load–Displacement Curve for Nail N2.

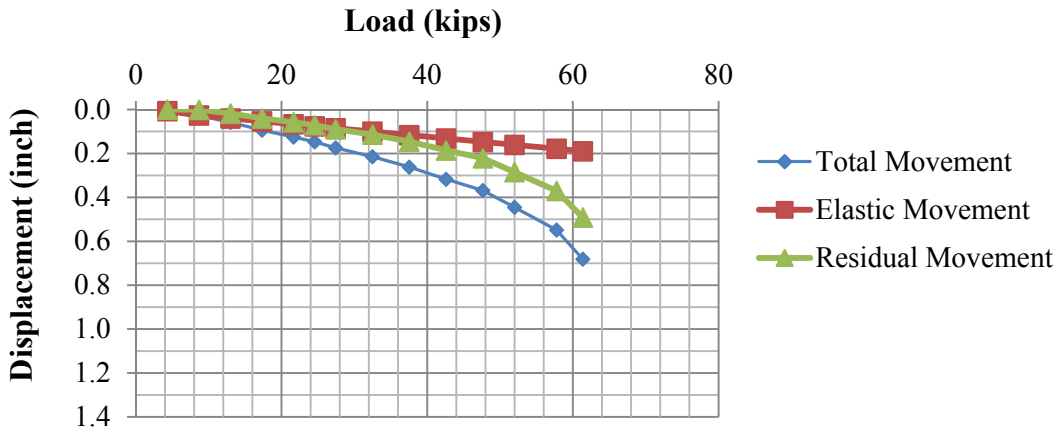

Figure 118. Load–Displacement Curve for Nail N3.

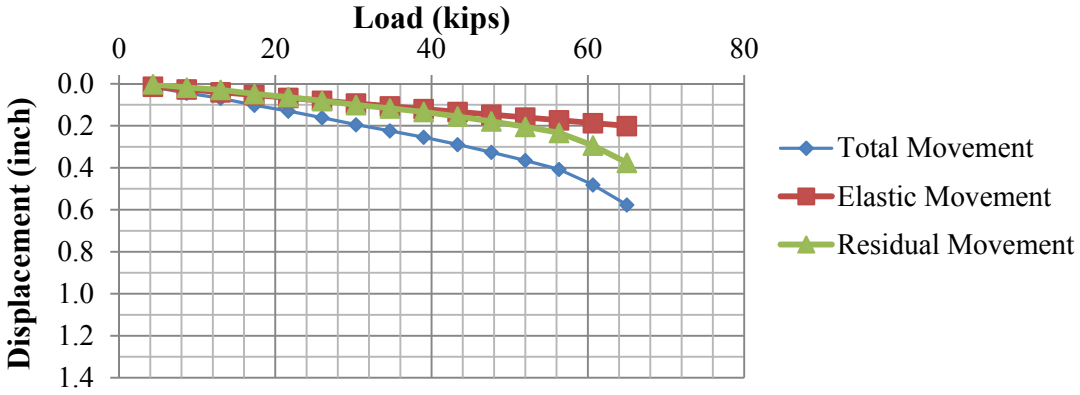

Figure 119. Load–Displacement Curve for Nail N4.

The yield strength for the threadbar used for the nails at NGES-TAMU is 59.3 kips (i.e., grade 75, size #8). Therefore, the measured movements of the nail head for the loads greater than

59.3 kips include the plastic movement of the threadbar. Figure 120 shows the residual movement of the nail for the load lower than the yield capacity of the threadbar.

The nails did not fail during the tests in July 2013. However, by extending the load–displacement curve to the failure criteria, the failure load could be estimated to be in the range of 70 to 80 kips. This means that the assumed value for maximum shear strength of the interface between the soil and grout ($f_{max} = \alpha * S_u$) was significantly underpredicted. The results of the laboratory tests for the soil samples taken in July 2013 show that the undrained shear strength (S_u) of the soil for the top 15 ft had increased noticeably. It is also possible that the changes in f_{max} could be because of the assumed α value. Table 20 presents the α values obtained from the tests performed in July 2013 for the undrained shear strength equal to 2880 psf (i.e., 138 kPa). Even considering that the friction of the interface between the soil and grout (f_{max}) was equal to 80 percent of the undrained shear strength of the soil (i.e., $\alpha = 0.8$), the nails did not reach the ultimate failure load.

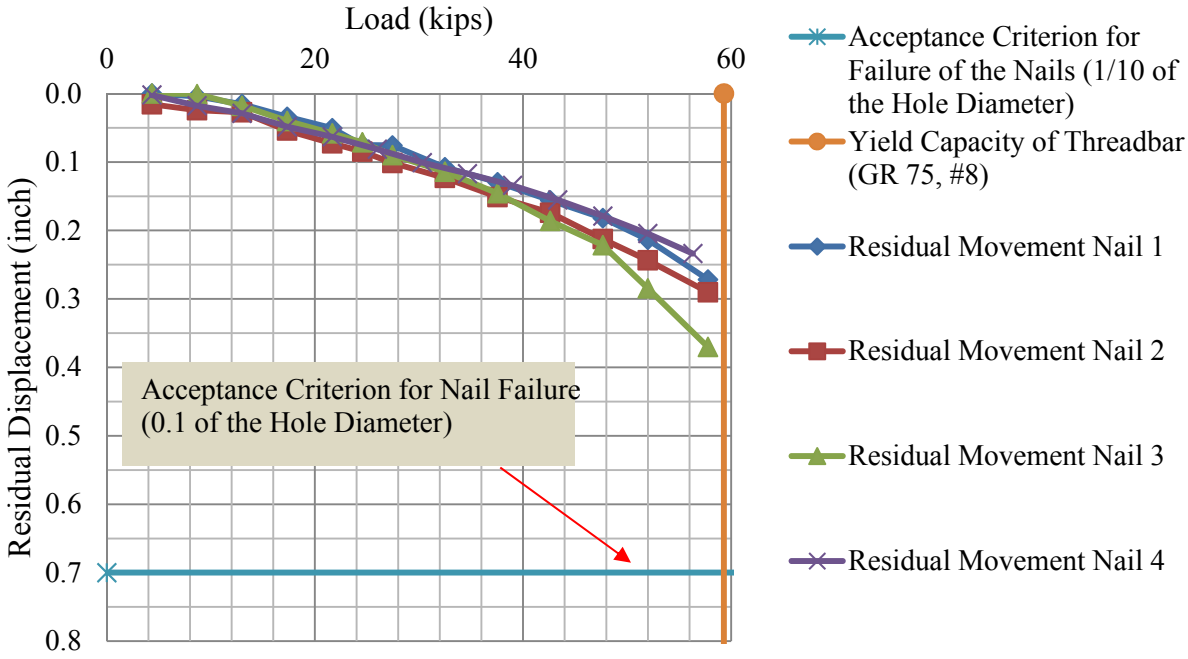

Figure 120. Residual Movement versus Load for Nails N1 to N4.

Table 20. The α Value Obtained from the Pullout Tests on Nails N1 to N4.

Nail Nº	Bond length (ft)	Hole diameter (in.)	Undrained shear strength, S_u (psf) (This research study, Chapter 6)	Maximum load applied (kips)	α value
1	14.30	7	2880	65	0.86
2	16.16	7	2880	69	0.81
3	16.00	7	2880	61	0.72
4	16.33	7	2880	65	0.75

Two more nails with shorter lengths (i.e., nails NS1 and NS2) were installed in September 2013 (next to the concrete slab) with the aim to find out the actual maximum shear strength of the interface between the soil and grout at failure (f_{max}). In addition, nails N1 and N4 were retested in November 2013 and February 2014. The locations of nails NS1 and NS2 are shown in Figure 49.

Test on Nail NS1 in September 2013. Figure 121 presents the total, elastic, and residual movements of the nail NS1.

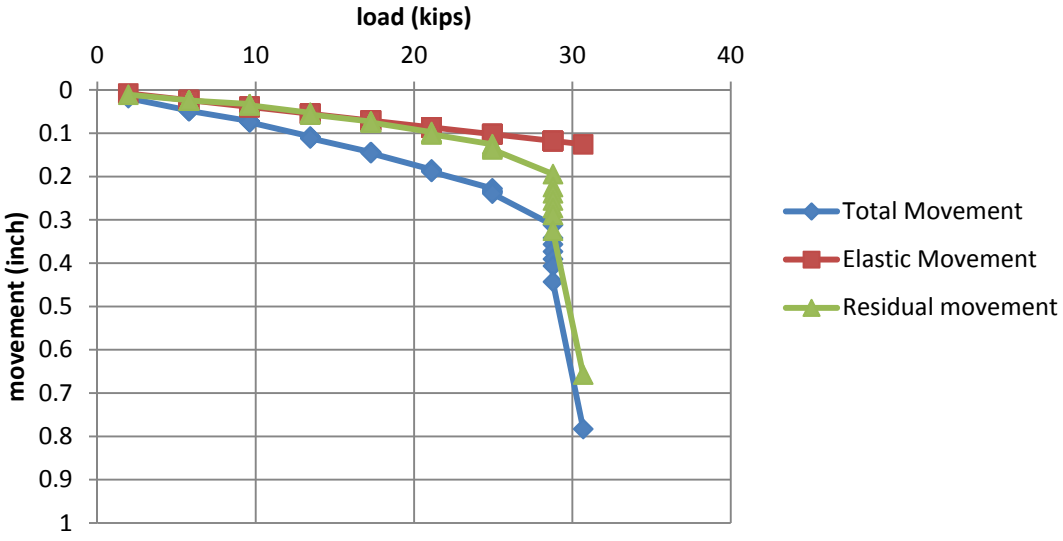

Figure 121. Load-Displacement Curve for Nail NS1 Test in September 2013.

The ultimate pullout capacity for nail NS1 was 29 kips. Once the ultimate pullout capacity was known, a back-calculated α value equal to 0.78 was obtained (i.e., $\propto = Q_u/\pi D L_a S_u$; see Table 21). With α equal to 0.78 and S_u equal to 2880 psf (i.e., 138 kPa), the ultimate pullout capacity of the nails on the concrete slab (i.e., nails N1 to N6) were recalculated based on the information obtained from nail NS4 (see Table 22).

Table 21. The α Value Back Calculated from the Pullout Test on NS1.

Nail No.	Drilled Length (ft)	Nail Bonded Length (ft)	Diameter of the Hole (in.)	S_u (psf)	Q_u (kips)	f_{max} (psf)	α
NS1	10	7	7	2880	29	2262	0.78

Table 22. Back Calculation of the Ultimate Pullout Capacity of the Nails on Concrete Slab (Nails N1 to N6) Based on the Test Performed on Shorter Nail (Nail NS1) in September 2013.

Nail Nº	Nail Bond Length (ft)	Nail Unbonded Length (ft)	Diameter of the Hole (in.)	S_u (psf)	α	f_{max} (psf)	Q_u Calculated from the Test on Shorter Nail (kips)
1	14.30	6	7	2880	0.78	2262	59
2	16.16	6	7	2880	0.78	2262	67
3	16.00	6	7	2880	0.78	2262	66
4	16.33	6	7	2880	0.78	2262	68
5	16.25	6	7	2880	0.78	2262	67
6	16.5	6	7	2880	0.78	2262	68

Retest of Nails N1 and N4 on the Concrete Slab. By comparing Table 21 and Table 19, the maximum load applied (Table 19) is higher than the Q_u calculated from the test on shorter nail (Table 21), which is somewhat unexpected. The nails on the concrete slab were tested during a very dry summer; therefore it was convenient to retest these nails in a different time of the year to evaluate any possible effect of the ground moisture on the pullout capacity of the nails. The total, elastic, and residual movements at different load steps on the nail N1 (test performed in November 2013) and nail N4 (test performed in February 2014, 2 cycles) are shown in Figure 122 to Figure 124.

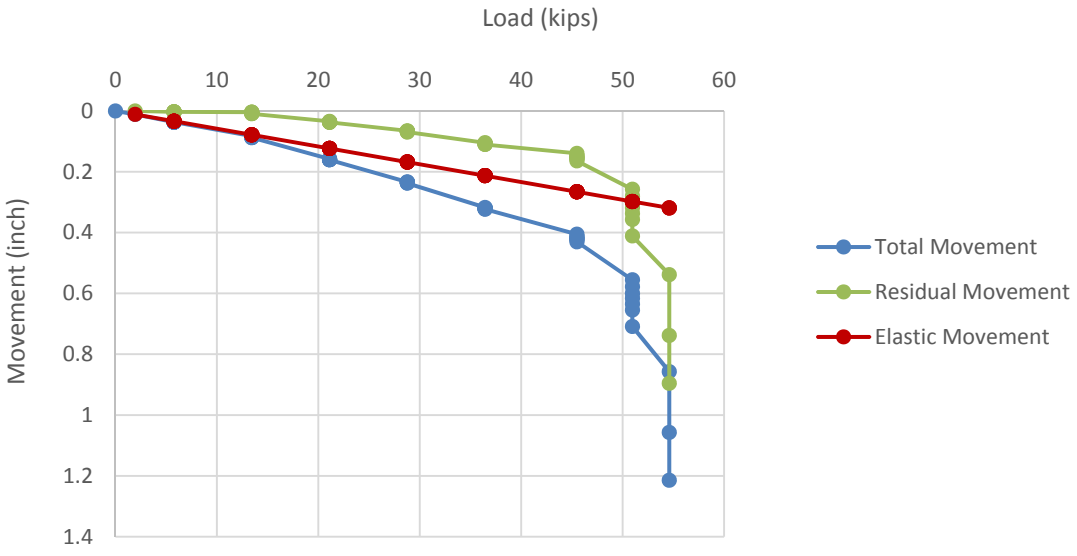

Figure 122. Total, Elastic, and Residual Movements for Retest on Nail N1 in November 2013.

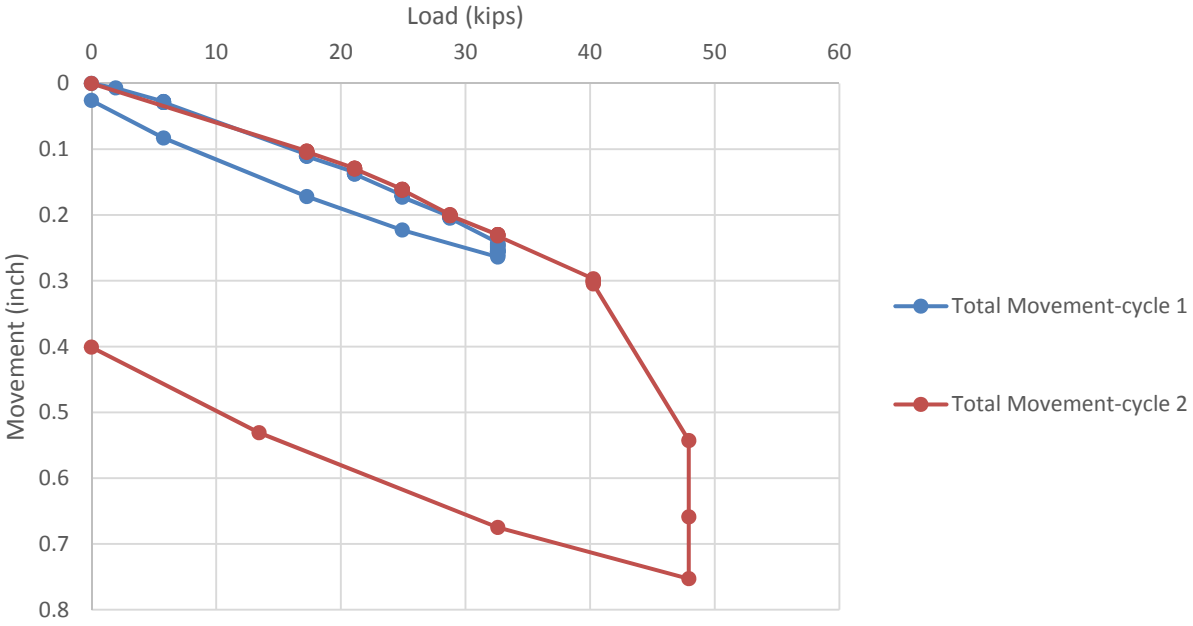

Figure 123. Total Movements for Two Cycles, Retest on Nail N4 in February 2014.

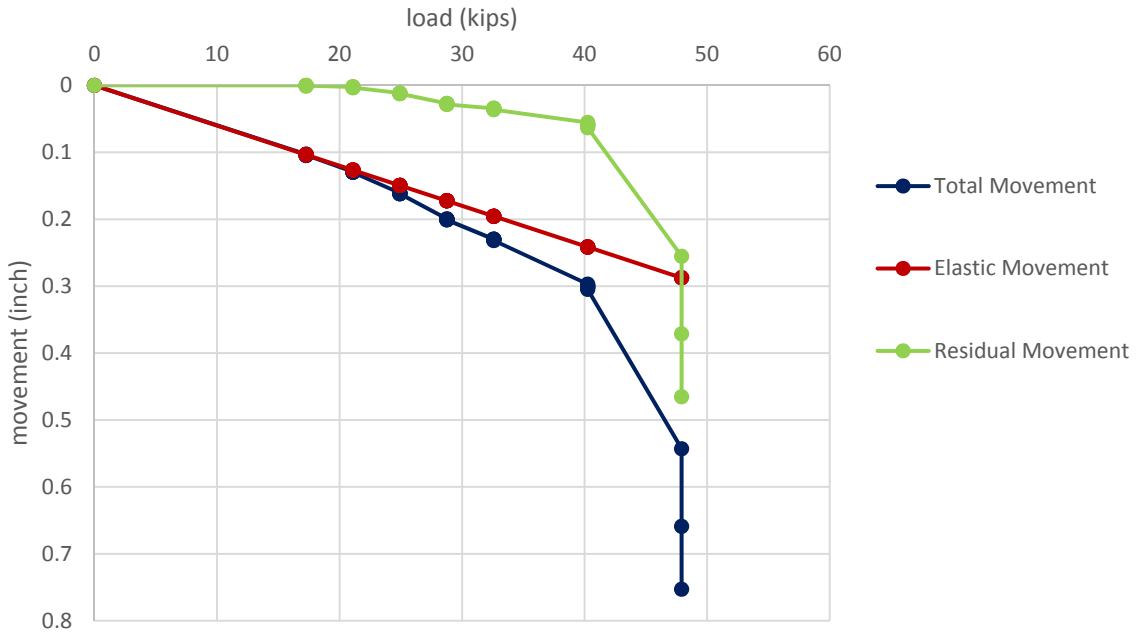

Figure 124. Total, Elastic, and Residual Movements for Retest on Nail N4 in February 2014 (Second Cycle).

In July 2013, the nail N1 was loaded up to 65 kips (i.e., close to the threadbar maximum load), and it did not fail. However, in November 2013 the same nail failed at 55 kips during the pullout test. A similar behavior was observed in nail N4, which failed at 48 kips during the pullout test in February 2014. This nail did not fail in the previous test carried out in July 2013 when a maximum load of 65 kips was applied. The main difference between these two tests was the time of year at which they were performed (i.e., the first test was carried out during the dry season and the second one during the wet season). Therefore, it could be assumed that the ultimate pullout capacity of the nails depends on the soil moisture. It is also well known that the undrained shear strength of the soil depends on the water content (or suction) of the soil, and this affects in turn, the ultimate pullout capacity of the nails. Table 23 presents data related to the comparison between the initial test in July 2013 and the retest performed on nails N1 and N4 in November 2013 and February 2014.

Table 23. Comparison of Tests Results on Nails N1 and N4 Performed in Different Seasons.

Nail N°	Nail Bond Length (ft)	Max load applied on July 2013 and the nail did not fail (kips)	α from the test on July 2013	Max load applied on Nov 2013 on N1 and Feb 2014 on N2, both nails failed (kips)	α from the tests in Nov and Feb
1	14.3	65	0.86	55	0.73
4	16.33	65	0.75	48	0.56

Test on Nail NW1 in November 2014. As discussed earlier, it is considered convenient to perform the pullout test in a different time of the year to evaluate any possible effect of the ground moisture on the pullout capacity of the nails. NW1 was tested in November 2014. Since there was a lot of rain between December 2014 and May 2015 and the ground condition was not appropriate to perform the pullout test, NW2 to NW8 were not tested. Tests on NW2 to NW8 will be performed in forthcoming months. Figure 49 shows the location of nails NW1 to NW8. Figure 125 shows the total, elastic, and residual movements at different load steps on the nail NW1.

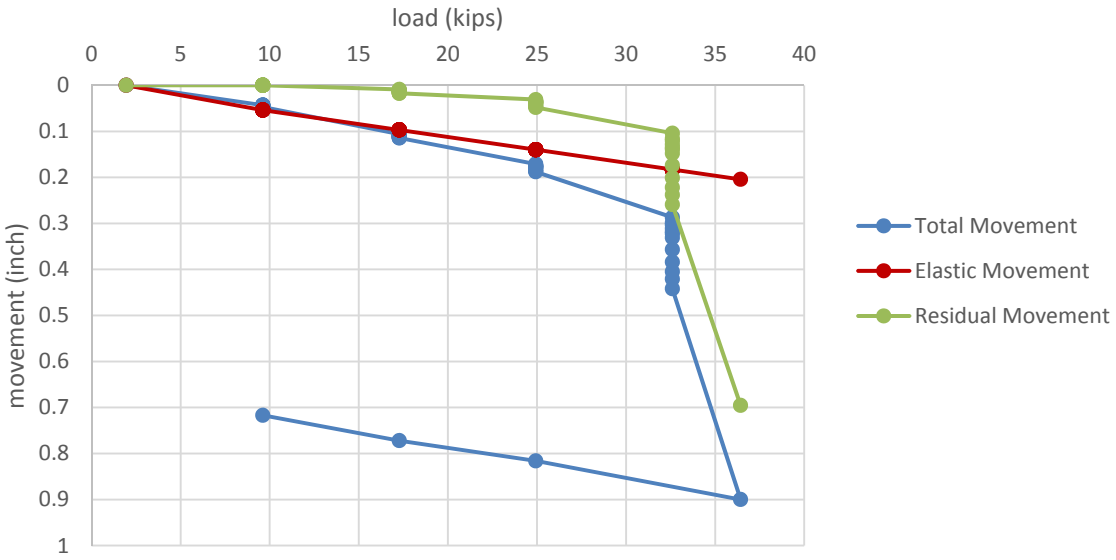

Figure 125. Total, Elastic, and Residual Movements for the Test on Nail NW1 in November 2014.

The ultimate pullout capacity of nail NW1 was 36 kips. Once the ultimate pullout capacity was known, a back-calculated α value equal to 0.455 was obtained (i. e. , $\propto = Q_u/\pi D L_a S_u$). As shown in Table 24, the f_{max} (i.e., maximum friction between grout and soil)

equal to 1310 (psf) was obtained. As discussed in the previous sections in this chapter, N1 was retested in November 2013. The ∝ value back calculated from the retest on N1 in November 2013 was 0.73, while the ∝ value back calculated from the test on N1 in November 2014 was 0.73.

Table 24. The α Value and f_{max} Back Calculated from the Pullout Test on NW1.

Nail No.	Drilled Length (ft)	Nail bonded Length (ft)	Diameter of the Hole (in.)	S_u (psf)	Q_u (kips)	f_{max} (psf)	α
NW1	18	15	7	2880	36	1310	0.45

Water Content Measurements

As mentioned previously, in order to study the change in the natural water content of the soil, four water content probes were installed at the NGES-TAMU clay site at depths of 3, 6, 9, and 10 ft. Figure 49 shows the location of the water content probes. Figure 126 shows the results of the water content evolution between October 27, 2014, and June 27, 2015. As shown, the natural water content at depth of 3 ft was significantly influenced by the weather condition (i.e., water content increased with rains and deceased quickly after the rain), while the water content at the other depths (i.e., 6, 9, and 13 ft) are less influenced by the weather conditions and remained almost constant.

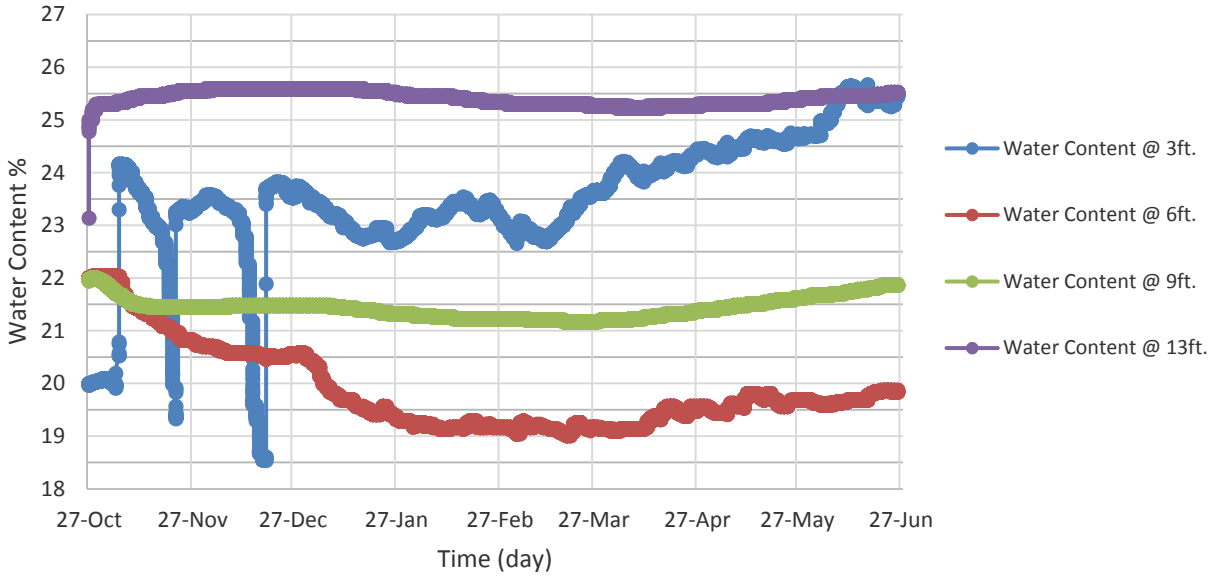

Figure 126. Variation of the Natural Water Content at the NGES-TAMU Clay Site at Different Depths.

Creep Tests

During the pullout tests, each load increment was held constant and the creep movements were recorded. Since some of the nails were loaded above the yield strength of the threadbar (i.e., 59 kips), the creep movements for those loads are not considered as the pure creep movement of the soil nails.

Tests on Nails N1 to N4 in July 2013. Figure 127 to Figure 131 present the creep rate for nails N1 to N2.

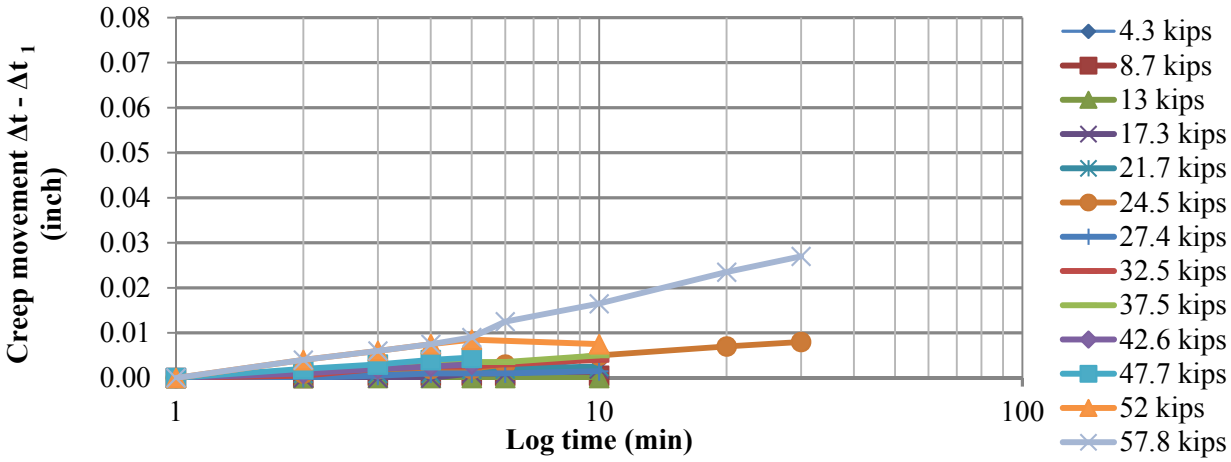

Figure 127. Creep Movement versus Time for Nail N1 at Different Load Steps.

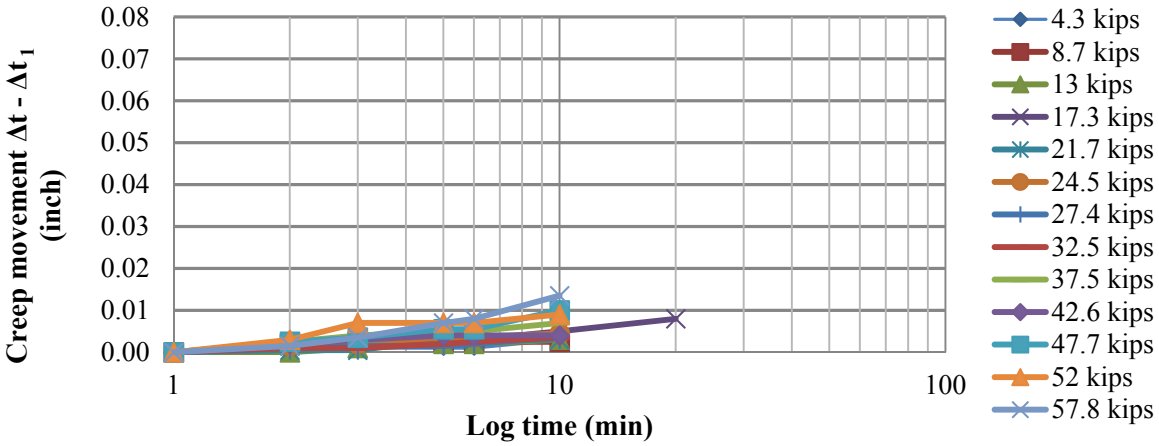

Figure 128. Creep Movement versus Time for Nail N2 at Different Load Steps for the First Cycle.

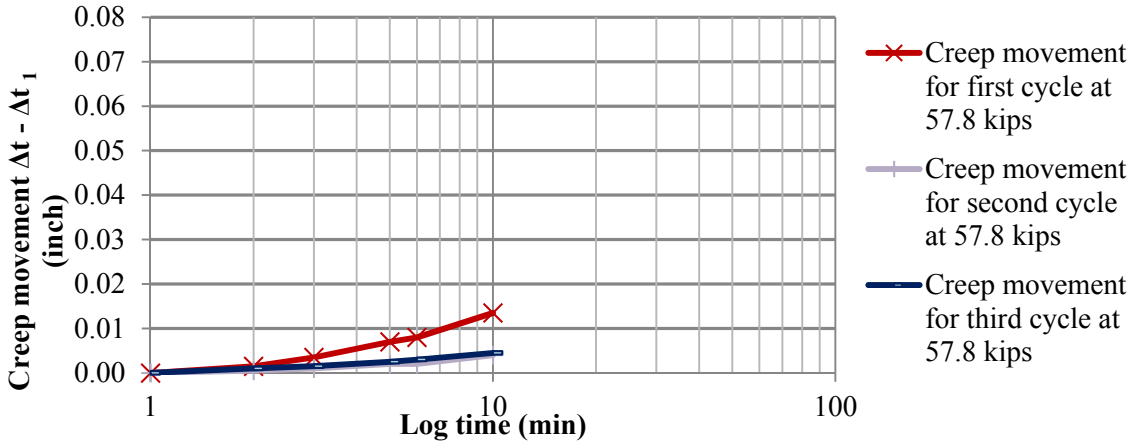

Figure 129. Creep Movement versus Time for Nail N2 at Different Load Steps for First, Second, and Third Cycles.

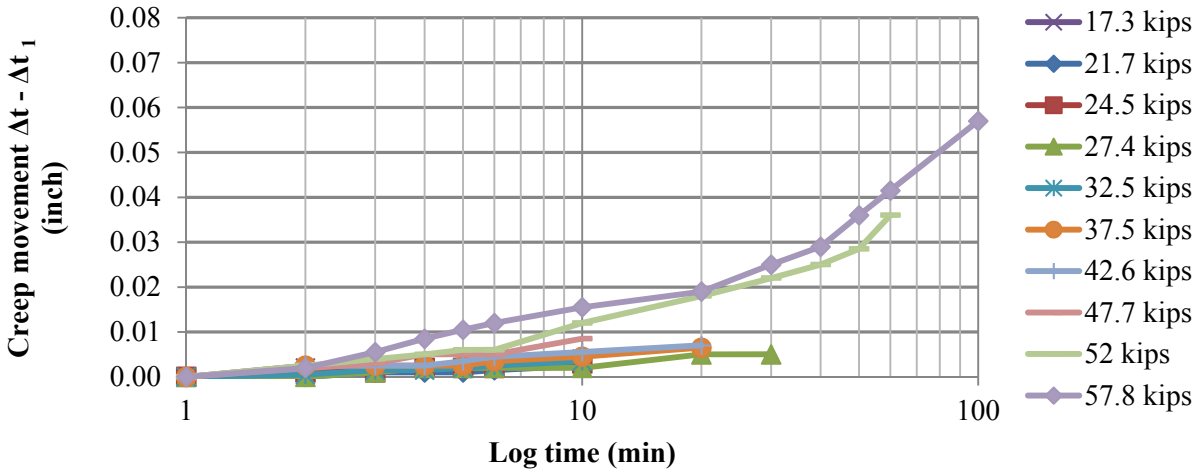

Figure 130. Creep Movement versus Time for Nail N3 at Different Load Steps.

The range of the creep movements for all the tested nails (i.e., N1, N2, N3, and N4) and all the load steps was lower than the acceptance criterion (i.e., the creep movements for the readings between 1 to 10 minutes was less than 0.04 in.).

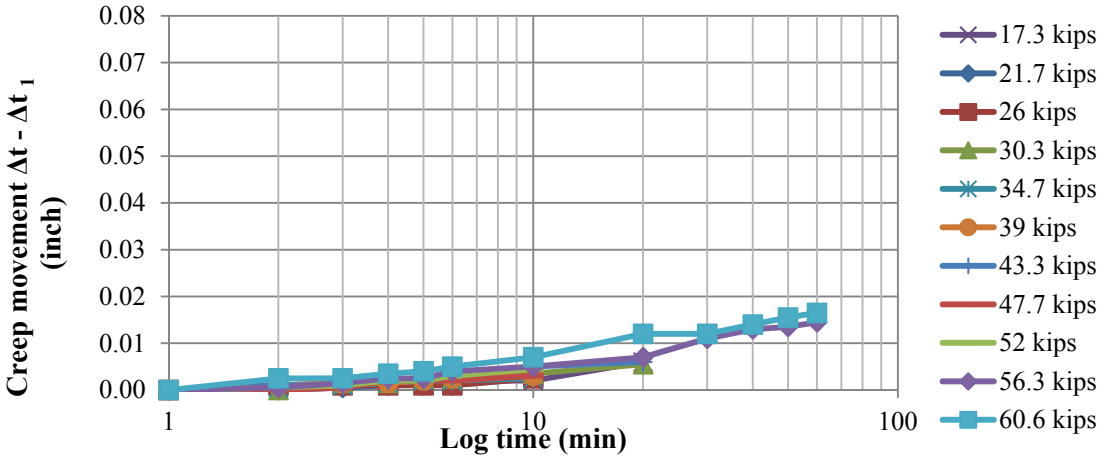

Figure 131. Creep Movement versus Time for Nail N4 at Different Load Steps.

As shown in Figure 129, the creep movement for the first cycle of loading is higher than the second and third cycles. This test clearly shows that preloading (i.e., load history) affects the creep behavior of soil nails. Figure 132 presents the creep rate in unit of inch per log cycle of time at different load steps for the nails N1, N2, N3, and N4. The creep rate for all the tested nails is well below the acceptance criterion.

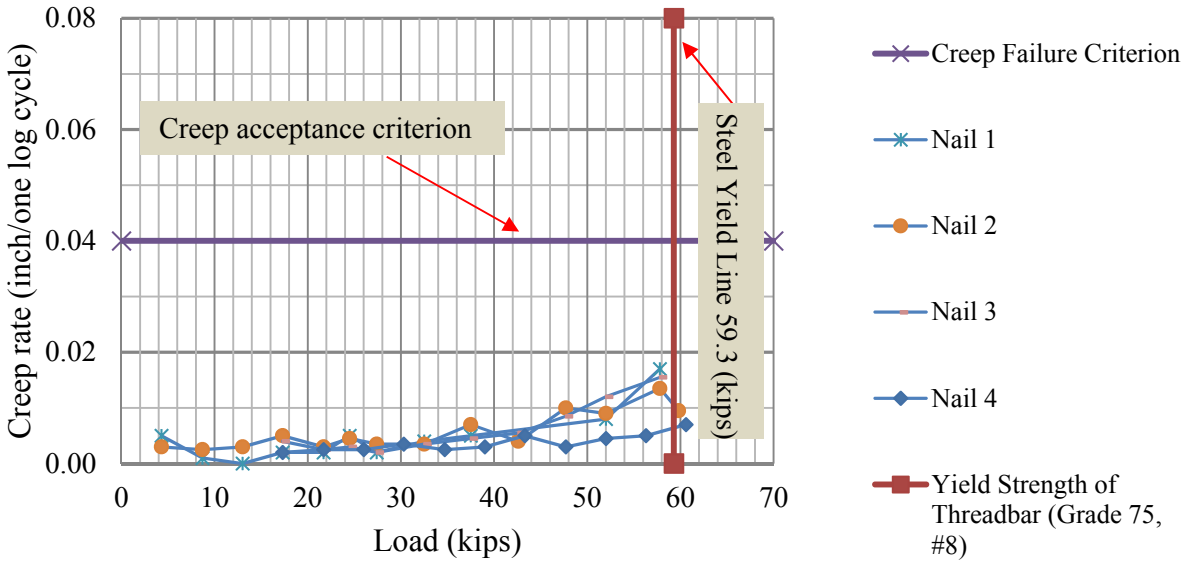

Figure 132. Creep Rate at Different Load Levels for Nails N1, N2, N3, and N4 (Readings between 1 and 10 Minutes).

Test on Nail NS1 in September 2013. During the pullout test on nail NS1, each load step was held constant for 10 minutes and the creep movements were recorded. Figure 133 and

Figure 134 show the creep movements and the creep rate (inch/log cycle of time) at different load steps for 1 to 10 minutes, respectively. The creep movements for loads below the failure load (i.e., 29 kips) were significantly lower than the creep acceptance criterion. For instance, at 86 percent of the failure load (i.e., one step before the failure load), the creep movement for 1 to 10 minutes was 0.012 in. At the failure load, the creep movements suddenly increased up to 0.131 in. This behavior is similar to that observed during the tests on the existing anchors and the new nails on the concrete slab. The creep movements above the acceptance criterion took place at the failure load, or at loads higher than 90 percent of the failure load.

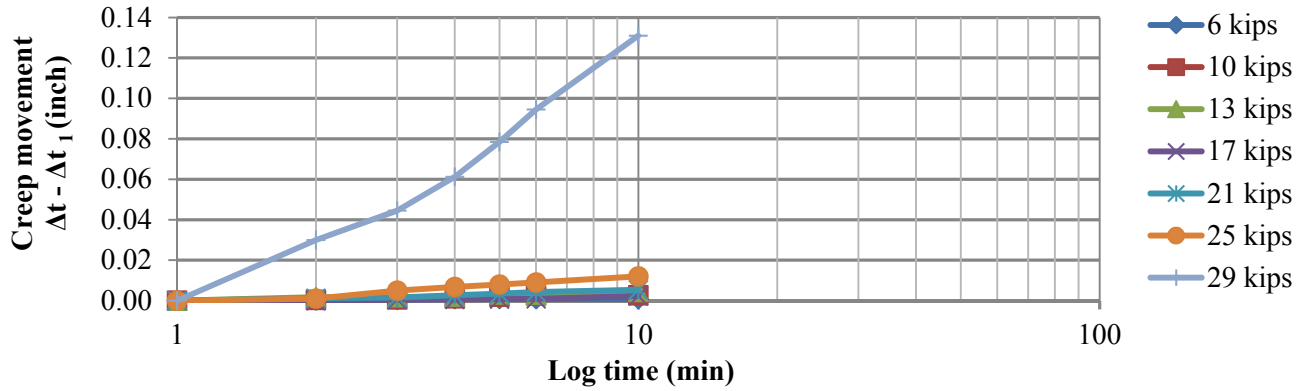

Figure 133. Creep Movements versus Time for Nail NS1 at Different Load Steps.

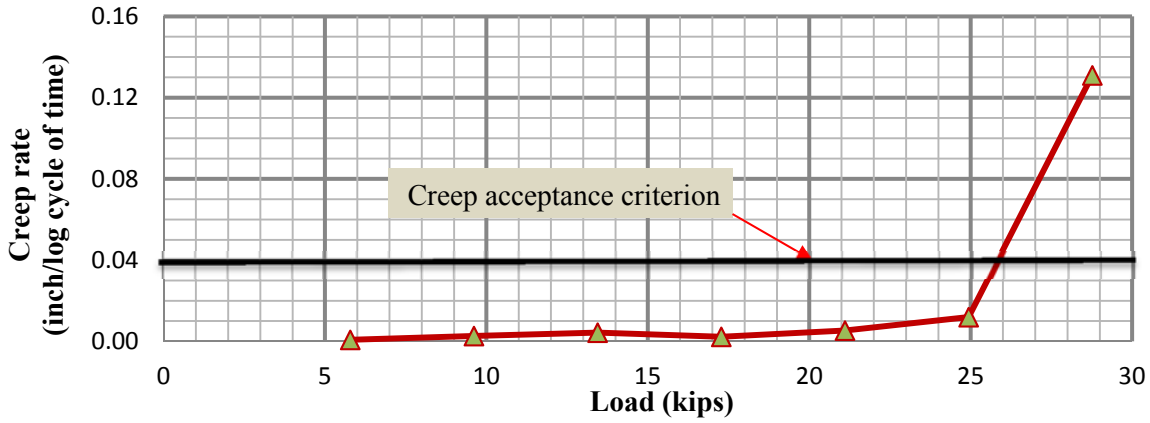

Figure 134. Creep Rate at Different Loads for Nail NS1 (Readings between 1 and 10 Minutes).

Retest of Nails N1 and N4 on Concrete Slab. Creep movements for each load step versus time for nails N1 and N4 are presented in Figure 135 and Figure 136, respectively. Figure 137 and Figure 138 present the creep rate at the loading steps.

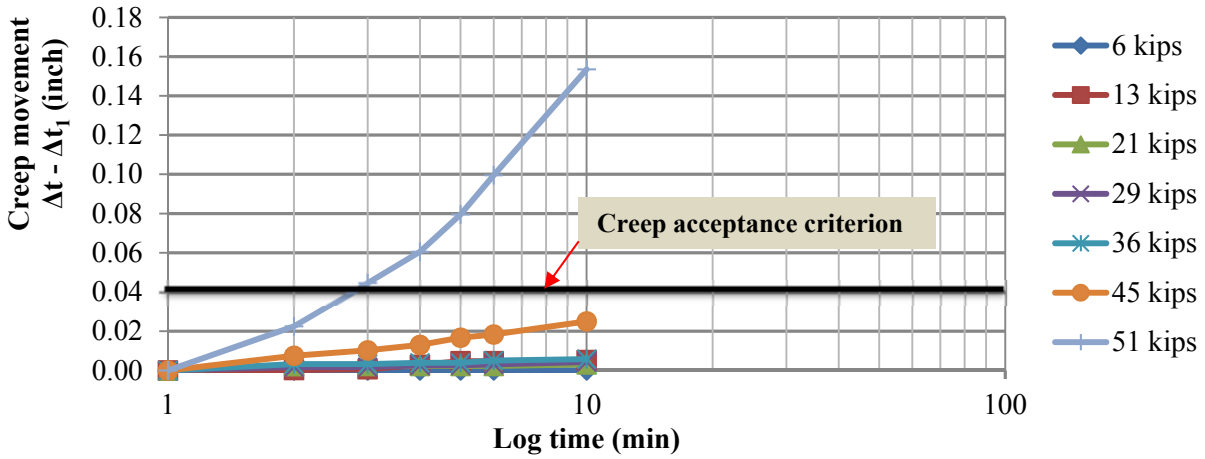

Figure 135. Creep Movements versus Time for the Retest on Nail N1 at Different Load Steps.

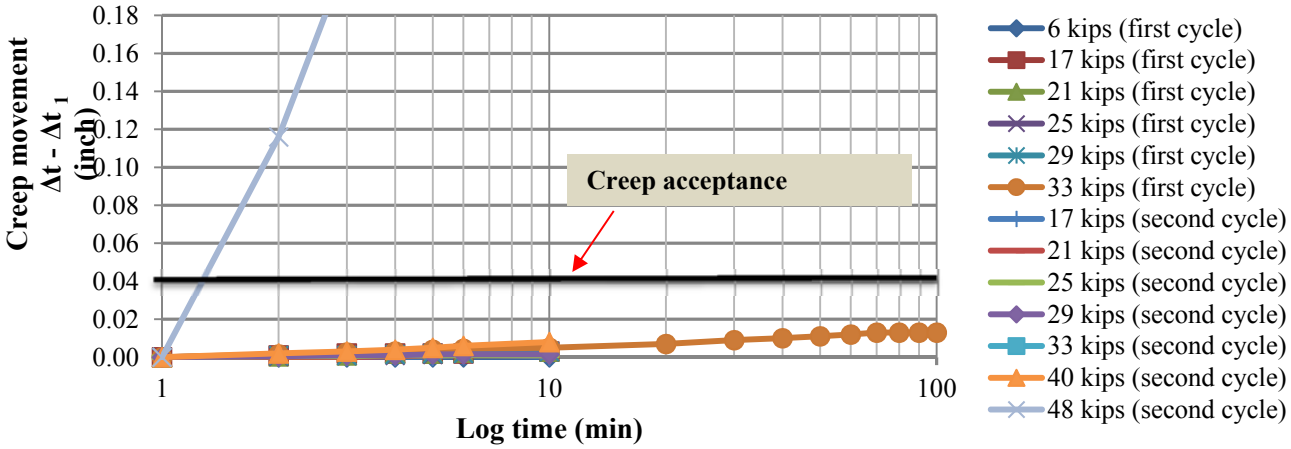

Figure 136. Creep Movements versus Time for the Retest on Nail N4 at Different Load Steps during the First and Second Load Cycles.

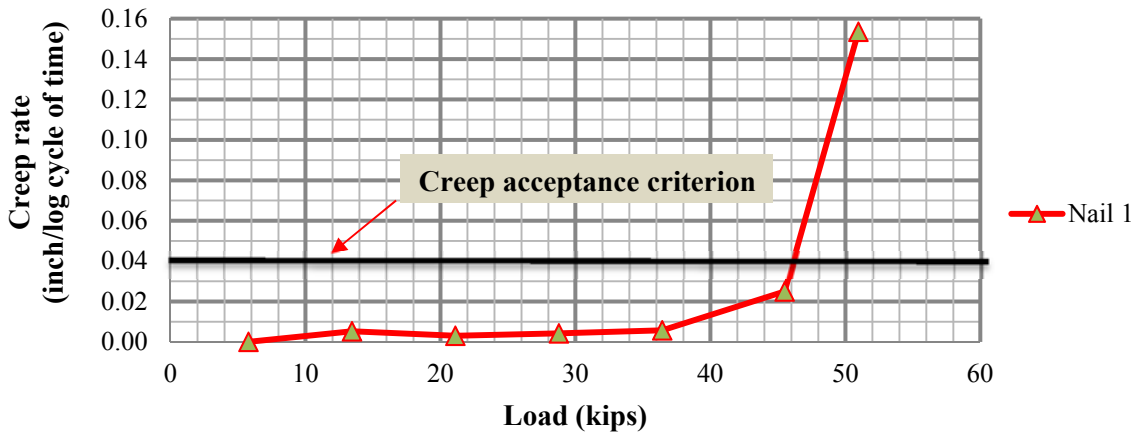

Figure 137. Creep Rate at Different Load Steps for 1- to 10-Minute Readings for the Retest on Nail N1.

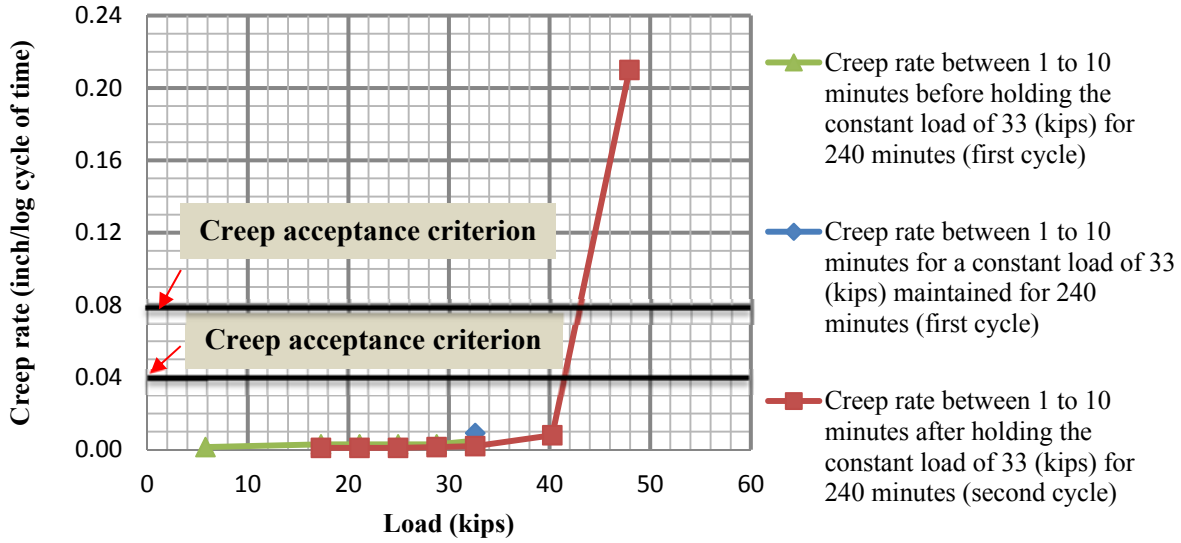

Figure 138. Creep Rate at Different Load Steps for 1- to 10-Minute Readings Related to the Retest on Nail N4.

The results of the creep tests show that the creep rates for loads below the nail capacity (i.e., 90 percent of the maximum load or lower) were very small compared with the acceptance criterion (i.e., creep movement for 1- to 10-minute readings should be smaller than 0.04 in.). The creep movements suddenly became higher than the acceptance criterion near the failure load. The results of the cyclic load tests on Nail N4 show that the creep movements are smaller in the second loading cycle than in the first cycle. Figure 139 shows the creep rates of the first and second cycles for loads in the range between 6 and 40 kips.

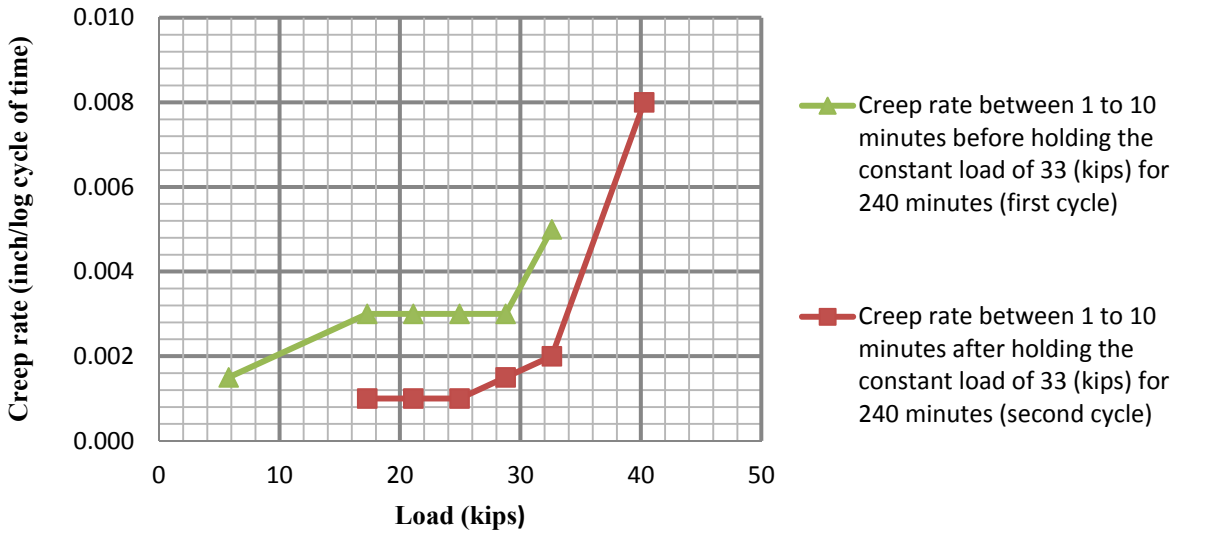

Figure 139. Creep Rates for the First and Second Cycles Related to the Retest on Nail N4.

Test on Nail NW1 in November 2014. Creep movements for each load step versus time for Nail NW1 are shown in Figure 140, while Figure 141 shows the creep rate (inch/log of time) for Nail NW1. The creep behavior of this nail is similar to the one observed in the previous tests. Creep movements for load levels below the failure load were very small (especially when compared with the acceptance criterion) and suddenly became relevant (and higher than the acceptance criterion) for loads near the nail capacity. The other nails (i.e., NW2 to NW8) could not be tested during the project, because of very adverse weather conditions. They will be tested in the future.

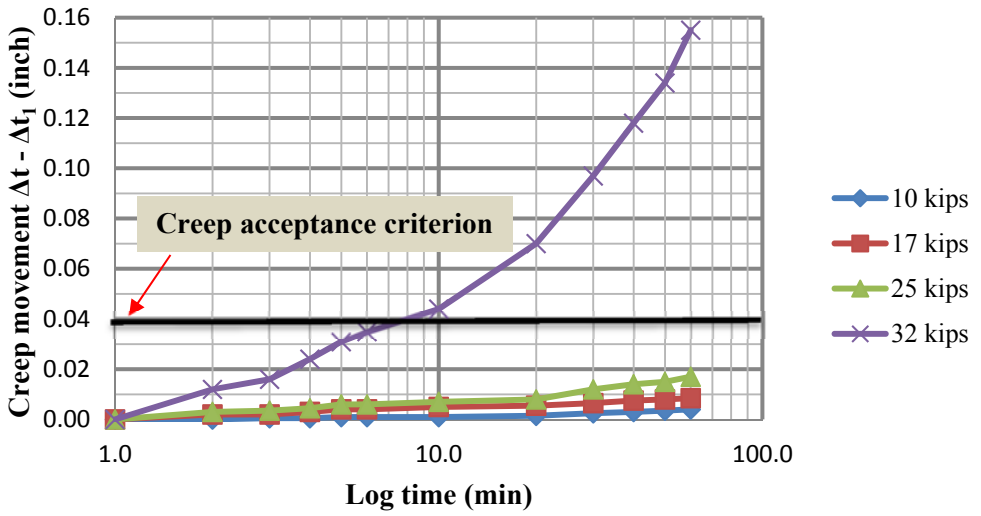

Figure 140. Creep Movements versus Time for the Test on Nail NW1 at Different Load Steps.

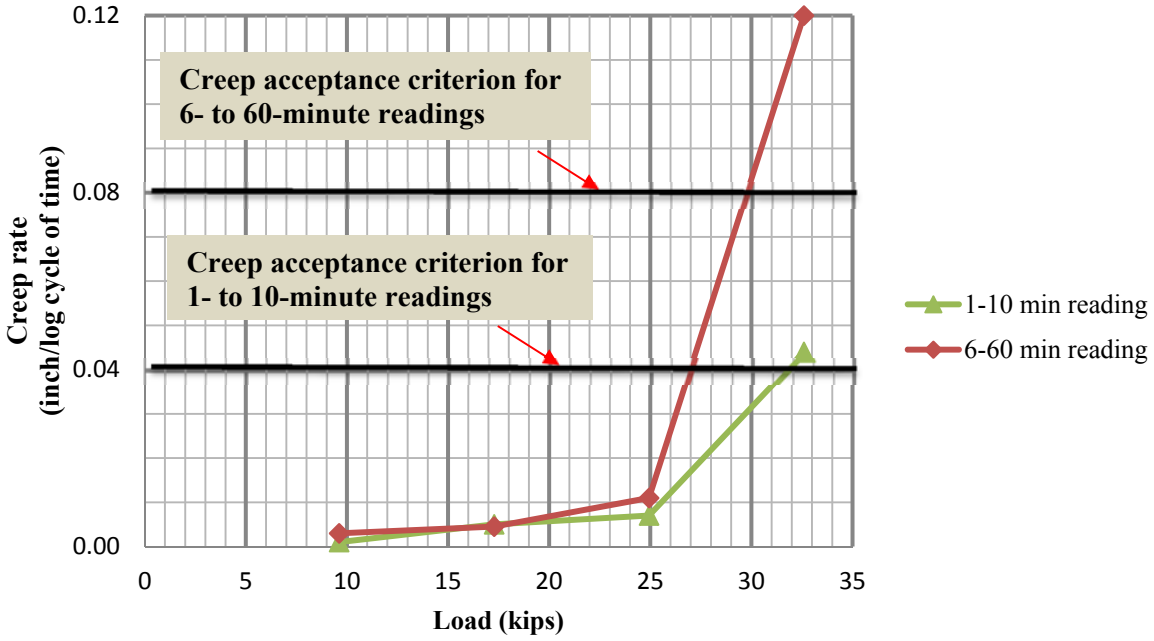

Figure 141. Creep Rate at Different Load Steps for the Test on Nail NW1.

n Value

The viscous exponent *n* obtained from the results of the pullout tests on the new nails at the NGES-TAMU clay site, for both the original tests on nails N1, N2, N3, and N4 and the retests of nails N1 and N4, are presented in Figure 142 and Figure 143, respectively.

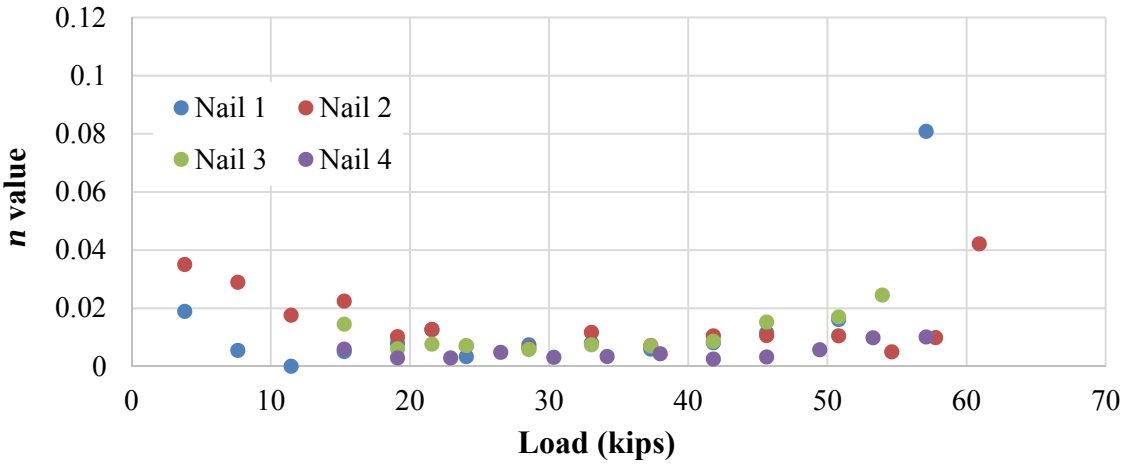

Figure 142. Viscous Exponent *n* for Nails N1 to N4.

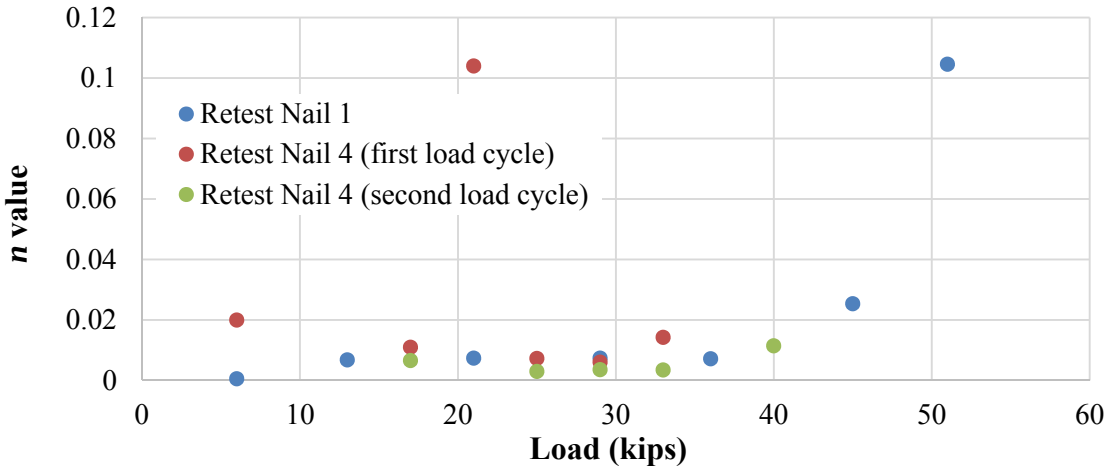

Figure 143. Viscous Exponent *n* for Retests of Nails N1 and N4.

Load Distribution in the Nails during Pullout Tests

The nails N3, N4, N5, and N6 were instrumented with strain gauges. The positions of the strain gauges along the nails are presented in the previous sections in this chapter. Considering that the cracking strain for the grout is around 100 με (100×10^{-6} in./in.) and that the measured strain exceeds the cracking strain in the grout, it has been assumed that load in the nails is related directly to the measured tensile strain of the threadbar (FHWA, 1998a).

The second strain gauge on nail N4 was broken during the nail installation. Figure 144 shows the load distribution on nail N4 during the pullout test. In this test, the 60 kips load was held constant for 60 minutes. As shown in Figure 145, the load distribution on the nail did not change when the load on the nail was held constant.

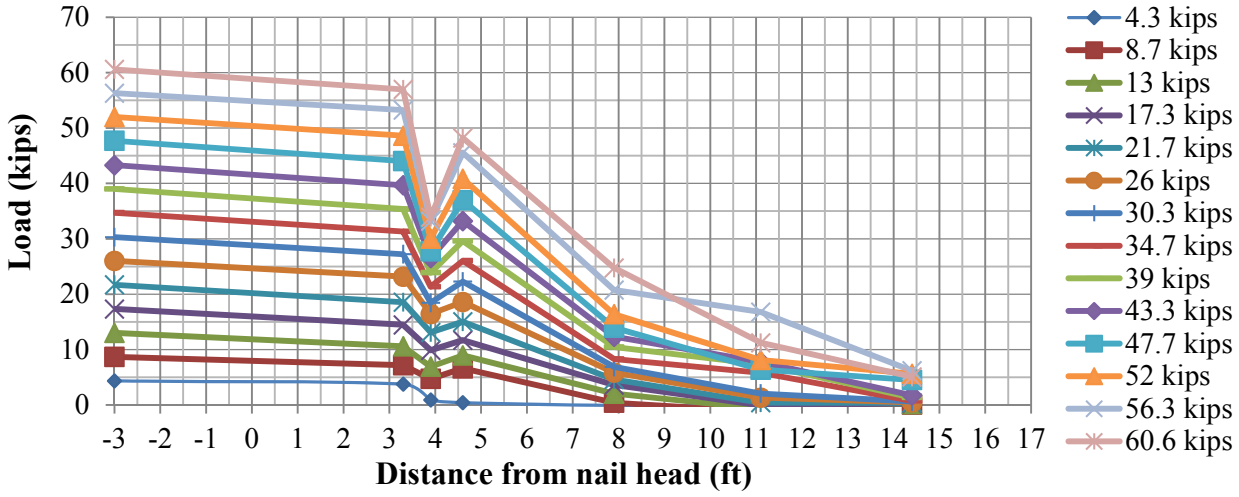

Figure 144. Load Distribution on Nail N4 during the Pullout Test in July 2013.

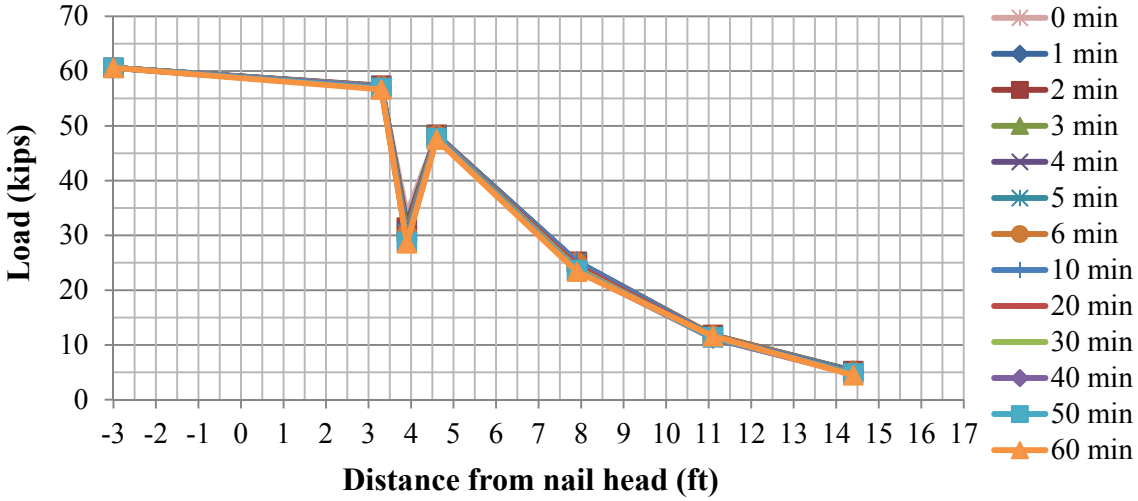

Figure 145. Load Distribution during the Creep Test for a Constant Load of 60.6 Kips Maintained for 60 Minutes on Nail N4.

SUMMARY AND CONCLUSIONS

Two types of pullout tests were conducted at the NGES-TAMU clay site: 1) experiments on existing anchors, and 2) tests on newly installed nails. The outcomes and conclusions obtained from those tests are detailed below. All of these conclusions, comments, and suggestions are based on and valid for the specific soil types and conditions studied in this research.

For tests of type 1 above, 10 anchors were installed and tested in 1991 and 1997 at the NGES-TAMU clay site. Anchors 1, 2, 3, 4. 7, 8, 9, and 10 were retested in July 2013 after 22

years of installation. The results of the tests on anchors performed in July 2013 can be summarized as follows:

- The ultimate pullout capacity of the anchors increased with time. For example, the comparison of the test results on anchors tested in 1991 and 1997 shows that there was a gain in strength of around 20 percent, and the increase in strength between 1997 and 2013 was almost 60 percent. This gain in strength could be attributed to long-term aging effects and past loading history.
- The load threshold for creep failure is around the 90 percent of the ultimate pullout capacity of the anchors. The results of the tests carried out in 2013 clearly showed that for loads below the 90 percent of the ultimate pullout capacity, the creep movements of the anchors were significantly lower than the acceptance criterion.
- The viscous exponent *n* varies between 0.001 and 0.01, for loads below the 90 percent of the ultimate pullout capacity. This value increased up to 0.04 for loads higher than the 90 percent of the pullout capacity.

For tests of type 2 above, to gain a better understanding of the creep behavior of soil nails in HP clays, 18 new vertical soil nails of different lengths were installed at the NGES-TAMU clay site. Four water content probes were installed to monitor the moisture content of the soil at the following depths: 3, 6, 9, and 13 ft. Verification tests with different creep steps were carried out on these nails. The results of these tests are summarized as follows:

- The maximum pullout capacity of the nails obtained in the tests performed in the dry season (i.e., low water contents) is significantly higher than the corresponding one obtained in the wet season (i.e., high water contents). This suggests that variations in the water content of the soil in different seasons affect the in situ undrained shear strength of the soil and consequently the grout–soil interface strength.
- The viscous exponent *n* obtained from the tests on the nails varies between 0.01 and 0.02 for loads below the 90 percent of the pullout capacity of the nails.
- The creep rate during pullout tests is well below the acceptance criterion for load levels lower than the 90 percent of the pullout capacity. Creep rates higher than the acceptance

criterion were observed for load levels near failure or above the 90 percent of the pullout capacity.

- Results of cyclic loading tests on the nails indicate that the creep behavior of the soil nails is influenced by the load history. The creep movements during the first cycle were higher than for the other cycles.
- The cracking strain for the grout is assumed to be 100 με (100×10^{-6} in./in.). The measured strains showed that most of the grout surrounding the threadbar was cracked. Since the measured strain exceeds the cracking strain in grout, the load on the nails is related directly to the measured tensile strain of the threadbar.

CHAPTER 5:
TESTING AND MONITORING AT TXDOT SITE

INTRODUCTION

This chapter presents the activities at the actual soil nail wall that was selected by TxDOT. The field investigations comprised two activities: 1) load tests on the sacrificial nails, and 2) long-term monitoring. In addition, undisturbed and disturbed soil samples from different positions and depths were gathered for examination in the laboratory.

It is suspected that the creep behavior of the soil nail walls in HP clays primarily depends on the load level (Recommendations Clouterre, 1991). Therefore, to gain a better understanding of the creep behavior of soil nails at different stresses, a number of pullout creep tests at different axial loads were performed on sacrificial nails installed in the wall selected by TxDOT. Since the ultimate pullout capacity and the service load of the permanent nails depend on the position of the nail, the sacrificial soil nails were installed at different heights in the wall and then tested to learn about the effect of the (nail) position on the pullout capacity.

The objective of the long-term monitoring was to study the creep behavior of the soil nail wall under operational conditions (i.e., to learn about the service load in the nails). The horizontal movements of the wall, load change in the nails during construction (i.e., excavation), load distribution in the nails, service load in the nails, soil creep during operation, head nail loads at the wall face, and change in the water content of the embankment were gathered during the monitoring, The study of most of these parameters are recommended by the *Geotechnical Engineering Circular No. 7: Soil Nail Walls* (FHWA, 2003) for those soil nail walls subjected to long-term monitoring.

This chapter includes four sections. The second section briefly presents the soil nail wall projects that were studied as possible candidates for this research, but were ultimately eliminated for different reasons. All the activities related to instrumentation and monitoring of the actual soil nail project are presented in that section. The third section includes the details of the load tests on the sacrificial soil nails at the selected TxDOT site in the Beaumont District. Section 4 provides a summary of the activities performed at the site and the conclusions associated with this chapter.

TENTATIVE MONITORING SITES SELECTED BY TXDOT

One of the major components of this project is the actual soil nail wall selected by TxDOT to test soil nails under real conditions and to perform long-term monitoring of the wall. This research project anticipated that TxDOT would suggest some possible new projects involving soil nail walls. The research team planned that TxDOT, in collaboration with Texas A&M University, would select the most convenient project for the scope and objectives of this research project. This appeared a simple task; however, many factors made this selection difficult. TxDOT proposed several tentative sites, but they were discarded for various reasons. To achieve the goals of this project, it was critical to find a proper site, with the right configuration, an appropriate construction schedule, and also the right soil conditions. For this project, the last item is particularly relevant, because the soil must be a HP clay (i.e., PI > 20).

A total of seven projects were considered during the first 16 months of the project, and none of them were selected. A brief explanation of each site and the reasons for each's rejection is presented below:

- **Site 1.** TTI was planning to build and instrument a scaled bridge at the Riverside Campus in the framework of another research project funded by TxDOT. Since the bridge was planned to be built in a flat area, an excavation would be needed to advance below the structure and to allow for proper monitoring of the bridge during the course of the research. A soil nail wall was one of the options considered to support the excavation. The research team studied the soil conditions at the site and they were acceptable. One of the problems associated with this project was the low height of the wall (7.5 ft only); in that height only two rows of soil nails could be installed. This was an issue because it did not truly represent the actual conditions for this kind of wall. Furthermore, in this proposal researchers intended to monitor soil nails in at least three different vertical positions. Finally, it was decided to study other types of solutions for the excavation (i.e., other than soil nails) and because of this the site was finally eliminated.
- **Site 2.** Denton County, SH 114 Ret Wall A; CSJ 0353-02-029. In this project, the soil nail walls were acting as retaining walls for the slopes on the sides of Highway 114. The largest problem related to this site was the start date of the project, which was planned to begin around May 2014, too late for the schedule of activities planned in this project.

- **Site 3.** Denton County, US 380 Ret Wall A; CSJ 0134-09-029. In this project, the soil nail wall was constructed as a retaining wall for the slopes on the sides of Highway 380. The problem with this site was that the soil nails were mostly in limestone (i.e., the ground conditions were not the proper ones for this research). In addition, at the time that the research team was notified about this site, the construction of the soil nail wall was about to start.
- **Site 4.** Denton County, US 380 at FM 156, CSJ 0134-09-063. The research team was informed about this project in April 2013. Dr. Sanchez and the graduate students visited the site on May 2, 2013, with TxDOT officers. To check the PI of the soil, soil samples were taken on May 15, 2013. The problem with this site was the facing of the soil nail wall. The facing of the soil nails was a concrete crash wall with a thickness of 2 ft-6 in. Because of this significant thickness of the concrete crash wall, it would not be possible to capture the true behavior of a soil nail wall in HP clays.
- **Site 5.** Collin County, SH 5 CSJ 0047-09-027. In this project, the soil nail wall was constructed as retaining walls for the slopes on the sides of SH 5. The research team had a meeting with a TxDOT officer and visited the site on May 14, 2013. According to the construction drawings and preliminary site investigations, the soil nail layout and soil profile in this site were appropriated for this research project. So, it seemed that this was the ideal site for this project. The research team decided to request of the contractor the delivery of the nine nails (rebar) to the Texas A&M campus to start with the installation of the strain gauges. The contractor delivered the nails to the Texas A&M High-Bay laboratory, and the works related to the grinding of the nails to attach the strain gauges were completed. Simultaneously, a more in-depth site investigation was carried out and soil samples were gathered from the site to verify whether all the local soils correspond to an HP clay or not. HVJ Associates, Inc. took the soil samples on July 23, 2013. The data from the new field tests revealed that limestone dominated the natural ground in this project. The profile obtained in this second and more detailed study was quite different from the information reported in the original report, in which it seemed quite clear that the whole wall was clay (at least at the selected positions). The new boreholes showed that the contact between limestone and clay layers was not horizontal but inclined, and because of this, only half of the height of wall was clay according to the new and detailed

site data. In light of this new site investigation, the research team and TxDOT felt that these conditions were not ideal for this research project, since moderate or limited creep can be expected in a soil nail wall installed under these conditions. The decision to discard this site was made in agreement with TxDOT officers.

- **Site 6.** Navasota, intersection of SH 6 and SH 105. The research team was notified about this project on September 2013, and the time expected to start the project was three to four months later. This project was not discarded definitively, but a more convenient site was proposed around the same time (see Site 8 below).
- **Site 7.** Huntsville, intersection of IH 45 and SH 75. The construction in this project was planned to start in December 2013. This team was notified about the project in September 2013. On October 3, 2013, Dr. Sanchez and the graduate students visited the site and had a meeting with the local TxDOT officers. To ensure that the soil was an HP clay, soil samples were taken on a subsequent visit on October 10, 2013. While studying this site, the research team was notified about a unique project in Beaumont, where the PI of the natural ground is around 50. TTI, in agreement with TxDOT, did not consider the site at Huntsville for the monitoring, and the Beaumont project (Site 8 below) was selected as the final site.

Finally, the eighth proposed project was selected. This site is described in detailed in the forthcoming sections; some preliminary information about it is presented as follows:

- **Site 8.** This site corresponds to an emergency slope repair in the Beaumont District. The PI of the embankment material was around 50, which made this project very unique for the field tests and monitoring. This project is the one that was finally selected to investigate the time-dependent behavior of the soil nail wall in an HP clay. A meeting with the constructor was organized at the Hayward Baker headquarters on October 31, 2013, to discuss the details of the instrumentation. Dr. Sanchez and the graduate students also met with TxDOT officers and Hayward Baker engineers at the site on December 17, 2013. In this meeting, several aspects were discussed including technical matters related to the soil nail installation, site investigation, schedule of activities, and details of monitoring and instrumentation of the wall. The nails (threadbars) were delivered to the

Texas A&M High-Bay laboratory on November 3, 2013, and the activities related to gluing the strain gauges to the nails and wiring were completed in January 2014.

EMERGENCY SLOPE REPAIR AT THE BEAUMONT DISTRICT

The field tests and monitoring activities were carried out at the emergency slope repair at the Beaumont District. The field investigations comprised two activities:

- Loading tests on sacrificial nails.
- Long-term monitoring of the soil nail wall.

These activities are presented and discussed in the following sections.

Project Information

An emergency slope repair at the Beaumont District was selected to study the time-dependent behavior of a soil nail wall in HP clay. This project started in late March 2014. The site is located at the ramp below US 69 overpassing Avenue A in the Beaumont District, Jefferson County. The coordinate of the project site is 30°1′54.61″ N, 94°5′22.77″ W. Figure 146 and Figure 147 show the location of the project site.

Figure 146. Map Location of the Project Site.

Figure 147. Aerial View of the Project Site.

Figure 148 and Figure 149 show the condition of the embankment soil before the project was started. The soil was unstable and failed at the section next to the bridge. The soil nailing technique was selected to construct a wall replacing the slope. Figure 150 presents a schematic representation of the adopted solution for this site.

Figure 148. Condition of the Embankment Soil before the Project Was Started.

Figure 149. View of the Embankment before the Project Was Started (the Soil Was Unstable and Failed at the Section Next to the Bridge).

As shown in Figure 151, the length of the soil nail wall is 453 ft (i.e., from station 0+00 to station 4+53). The maximum height of the wall is 25 ft at station 0+76 (i.e., next to the bridge) and the minimum height is 3.75 ft at station 4+53. The number of soil nail rows and length of the soil nails change with the position. Table 25 shows detailed information associated with the soil nails at different sections.

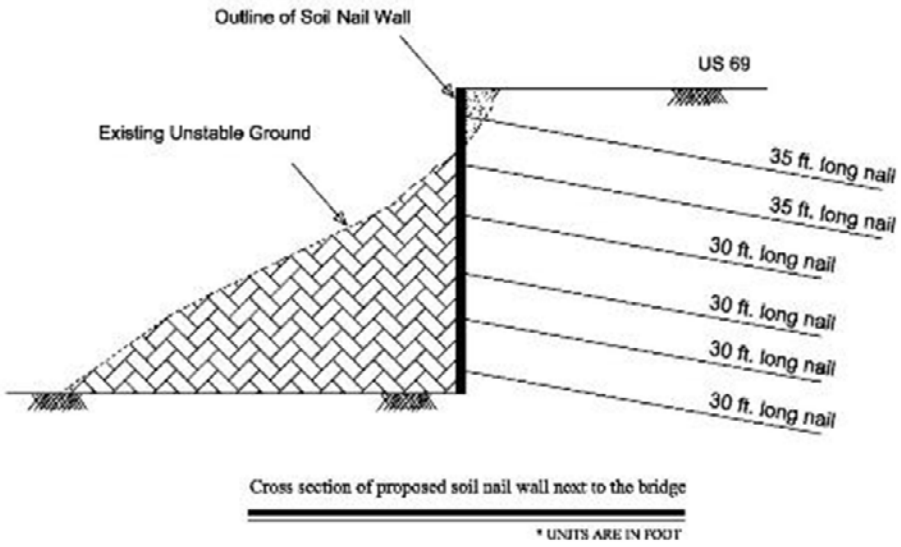

Figure 150. Proposed Soil Nail Wall to Stabilize the Unstable Section next to the Bridge.

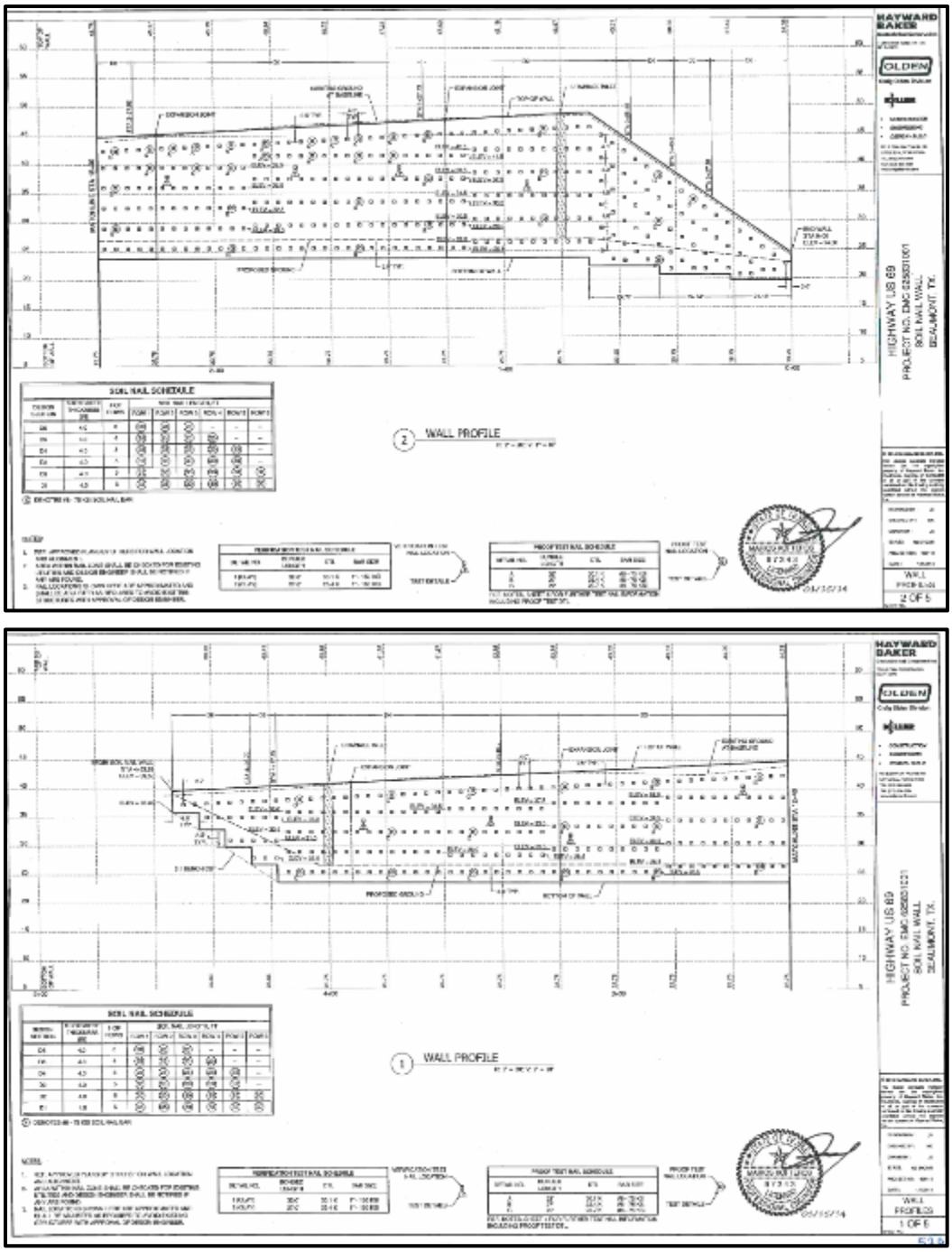

Figure 151. Soil Nail Wall Profile.

Table 25. Soil Nail Schedule.

DESIGN SECTION	SHOTCRETE THICKNESS (IN.)	# OF ROWS	LOCATIONS OF THE SECTION	SOIL NAIL LENGTH FT					
				ROW 1	ROW 2	ROW 3	ROW 4	ROW 5	ROW 6
D6	4	3	ST 0+00 to ST 0+27, ST 4+26 to ST 4+53	20	20	20	-	-	-
D5	4	4	ST 0+27 to ST 0+40, ST 4+17 to ST 4+26	25	25	20	20	-	-
D4	4	5	ST 0+40 to ST 0+55, ST 3+40 to ST 4+17	25	25	25	25	25	-
D3	4	5	ST 2+40 to ST 3+40	30	30	30	30	30	-
D2	4	6	ST 0+55 to ST 1+27, ST 2+27 to ST 2+40	30	30	30	30	30	30
D1	4	6	ST 1+27 to ST 2+27	35	35	30	30	30	30

This research project contemplated the following components to study the behavior of soil nail walls under actual construction and service conditions:

- **Sacrificial nails** (both instrumented and non-instrumented) to study the pullout capacity and the load distribution in nails located at different positions in the wall.
- **Instrumented service nails** to learn about the load distribution in the nails under operational conditions (i.e., service load monitoring).
- **Load cells** to track the load at the soil nail head during operation conditions.
- **Inclinometer casings** to learn about the wall movements during construction and operation through regularly scheduled inclinometer readings.
- **Tiltmeters** to provide additional information about the wall movement during service conditions.
- **Water content probes** to learn about the distribution of water content in the ground and its evolution in time.

The primary aspects related to these components of the field investigation are detailed in the following sections.

Sacrificial Nails

To perform the pullout and creep tests under actual nail installation conditions, it is critical to understand the behavior of soil nails at different load levels. These types of tests cannot be performed on production nails because their performance under service load will be jeopardized by the (previous) load and/or creep tests. Therefore, additional sacrificial nails were contemplated in this project to study the soil nail behavior under in situ conditions. This section presents the activities performed in this project related to the sacrificial soil nails installed in at the Beaumont project.

Background

Since the actual load acting on the soil nail depends on the nail position, the study of the nails' behavior at different heights was considered very relevant in this research. Therefore, a total of six sacrificial nails, at three different heights, were contemplated in this project. Two sacrificial nails were installed at each height: one with instrumentation and the other without it. The horizontal spacing between nails was 8 ft. A preliminary study investigating the effect of sacrificial nails on the service load of the production nail was performed using the geotechnical software Plaxis. All the instrumented soil nails (i.e., sacrificial and permanent nails) were shipped to the Beaumont site on March 25, 2014.

A total of six sacrificial nails were installed in this project. Three of those nails were instrumented at the Texas A&M University facilities. The researchers intended to use the other three (non-instrumented) nails for the first pullout tests to learn about the pullout capacity of the nails at different heights and then, based on this information, design the load protocol to be used in the subsequent tests on the instrumented soil nails. The activities related to the nail preparation, installation, and test procedures are presented in the following sections.

Preparation of the Instrumented Nails

To study the load distribution in the soil nails during the load tests, the nail bars were instrumented with foil strain gauges (i.e., Model EA-06-125VB-120). The strain gauges were glued to the nail bar in pairs and were mounted on the top and bottom of the already prepared

positions. The first pair of strain gauges was attached at 6.5 ft from the top of the nail (i.e., 6.5 ft of the nail bars were left for load test setup and as an unbonded length of the sacrificial nail). The other strain gauges were installed at 5-ft intervals. Figure 152 shows the distribution of the strain gauges. Skyline was the provider of the steel threadbars used as sacrificial nails. The adopted threadbars were #8 with a grade of 75. The minimum yield strength of these threadbars is 59.3 kips.

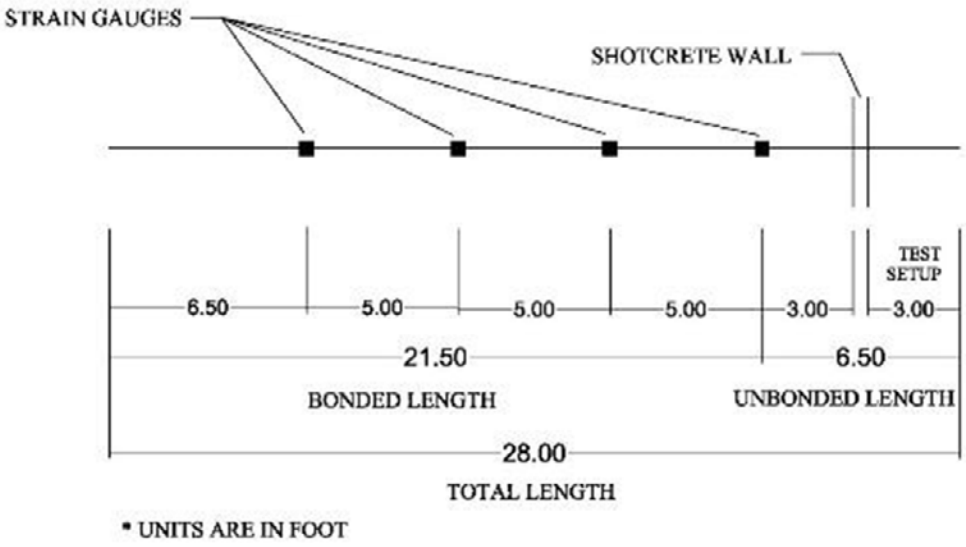

Figure 152. Positions of Strain Gauges in Sacrificial Nails.

The procedure adopted for attaching the strain gauges to the nail bars is presented as follows:

1. Grind down the ribs of the nail bars at the designated locations with an electric grinder (Figure 153a).
2. Sand the selected positions with 200-grit and 400-grit sandpaper to create a 4-in-long smooth surface.
3. Glue the strain gauges to the nail bars in pairs (i.e., top and bottom of the designated position; Figure 153b and c).
4. Wire the strain gauges (Figure 154).
5. Apply two layers of protective coating (i.e., Vishay's M-Coat J) to the strain gauges to protect them (Figure 155).

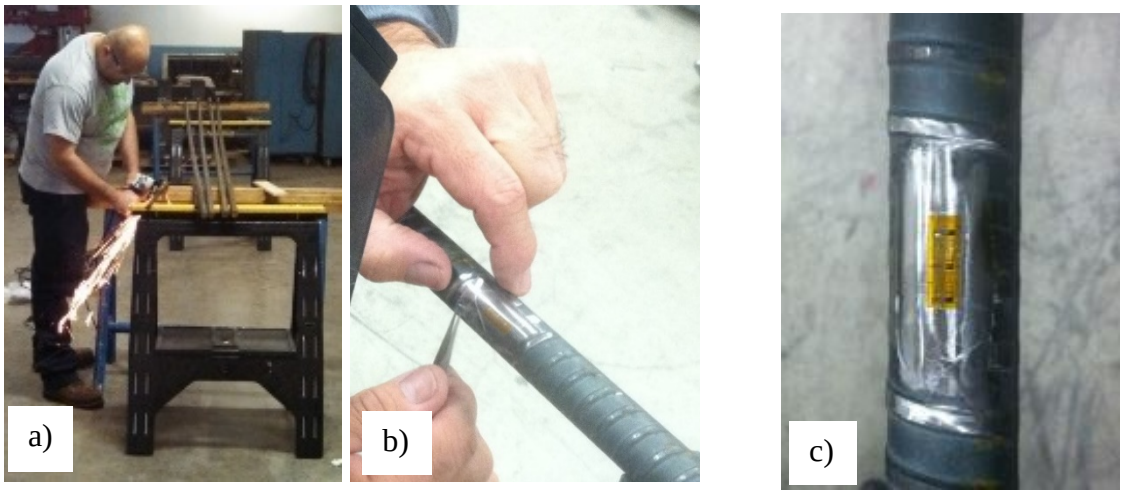

Figure 153. Stages for Attaching the Strain Gauges to the Soil Nail: a) Grinding the Nail Bars, b) Gluing the Strain Gauges to Nail Bar, and c) Detail of the Treated Position of the Bar and Glued Strain Gauge.

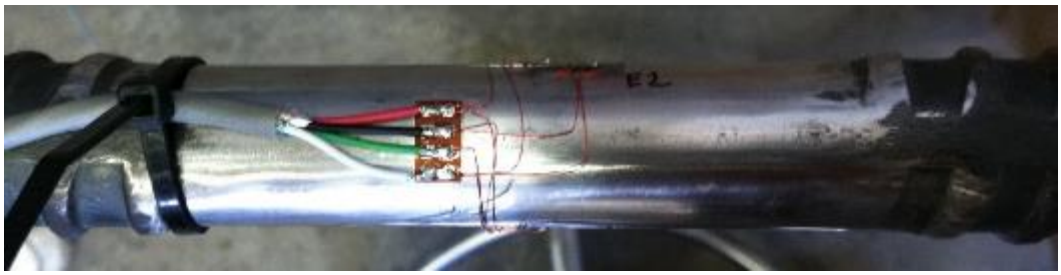

Figure 154. Wiring the Strain Gauges.

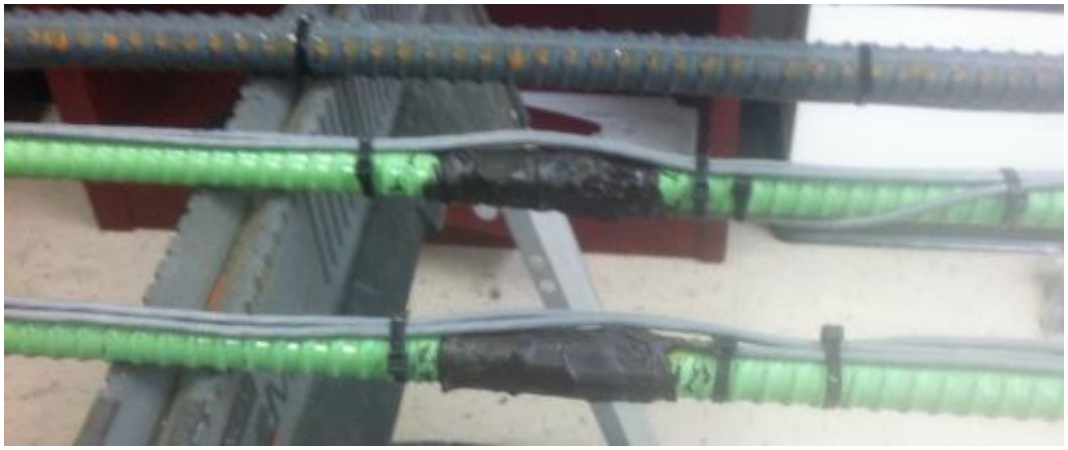

Figure 155. Double Coating to Protect the Strain Gauges and Wiring.

Prior to shipping the nail bars to the Beaumont site, axial tensile load tests were performed on all the instrumented threadbars to ensure that the strain gauges were working

properly. The nail bars were loaded up to 10 kips, and the strain was recorded with a data acquisition system during the tests.

Figure 156 shows the setup prepared for the load tests on the nails.

Figure 156. Adopted Setup for the Load Tests on Instrumented Nails Performed at TAMU prior to Shipping the Nail Bars to the Beaumont Site.

As shown in Figure 157, six soil nails were installed at three different heights of the wall (i.e., in three different rows). In each of these rows, a sacrificial nail with instrumentation and another without it were installed. The first row of sacrificial nails (i.e., position 1) was installed on April 22, 2014, between the second and third rows of production nails, at 7.4 ft from the top of the wall. The second and third rows of sacrificial nails were installed on May 14, 2014, between the fourth and fifth rows, and fifth and sixth rows of production nails, respectively. The second row of sacrificial nails (i.e., position 2) was installed at 14.4 ft from the top of the wall, while the third row (i.e., position 3) was installed at 17.9 ft from the top of the wall. Figure 158 shows the positions of the sacrificial nails at the soil nail wall profile.

Figure 157. Installation of the Sacrificial Nails at Different Heights of the Wall.

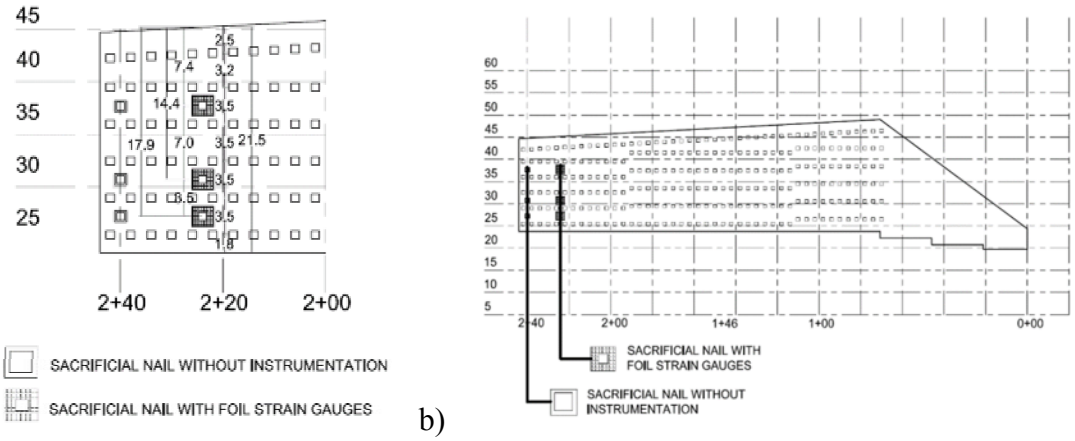

a) b)

Figure 158. Positions of the Sacrificial Nails at the Soil Nail Wall Profile at a) Section 2+20, and b) Front View of the Embankment.

Load Test Protocol

Verification and (modified) creep tests were carried out on the sacrificial nails. The first row of sacrificial nails (i.e., at 7.4 ft from the top of the wall) were tested on April 30, 2014. To evaluate the maximum shear strength between grout and soil (i.e., f_{max}) and the maximum pullout capacity of the nail in this row, verification tests according to the GEC#7 (FHWA, 2003) were

carried out on the sacrificial nails (i.e., with and without instrumentation). Verification testing is carried out to verify the bond strength used in the design. Verification tests should be performed to failure or to a test load that corresponds to the design allowable pullout capacity times the pullout FS (FHWA, 2003). Table 26 presents the incremental loading steps of the verification tests according to the GEC#7. The DTL adopted for the Beaumont soil nail wall project was 16 kips. Therefore, the load increment of 4 kips (0.25 DTL = 0.25*16 = 4) was adopted to perform the verification test on the sacrificial nails. Figure 159 presents the load test protocol adopted to test the sacrificial nails in the first row.

Table 26. Verification Test Loading Schedule.

Load	Hold Time (minutes)
0.05 DTL	1
0.25 DTL	10
0.5 DTL	10
0.75 DTL	10
1.00 DTL	10
1.25 DTL	10
1.50 DTL (Creep test)	60
1.75 DTL	10
2.00 DTL	10
2.50 DTL	10 max.
3.0 DTL or Failure	10 max.
0.05 DTL	1

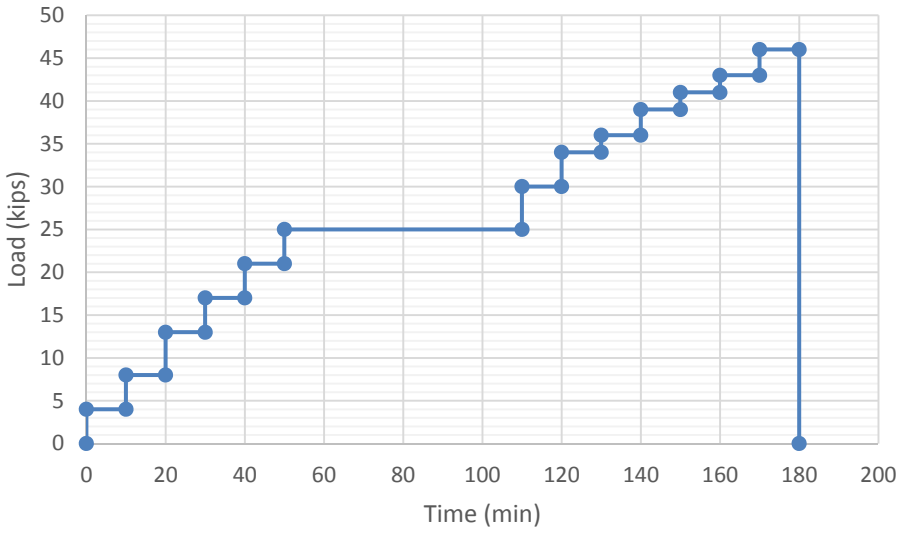

Figure 159. Pullout Load Protocol Related to the Test Performed on the First Row of Sacrificial Nails (i.e., at 7.4 Ft from Top of the Wall).

The second row of sacrificial nails (i.e., at 14.4 ft from the top of the wall) was tested on May 22, 2014. To evaluate the maximum shear strength between grout and soil (i.e., f_{max}) and the maximum pullout capacity of the nail in this row, verification tests according to the GEC#7 (FHWA, 2003) with the load increment of 4 kips (i.e., 0.25 times the DTL) were carried out on the sacrificial nail without instrumentation first. Once the maximum pullout capacity of the nail was known, and based on the pullout capacity, the creep test was conducted on the instrumented sacrificial nail (i.e., in the same row). Since the non-instrumented nail failed at 45 kips, the creep test on the instrumented nail was performed in 9 loadings steps (i.e., with a load increment of 5 kips), each load step was held for 60 minutes, and the creep movements were recorded. As shown in Figure 160, the test lasted for 540 minutes.

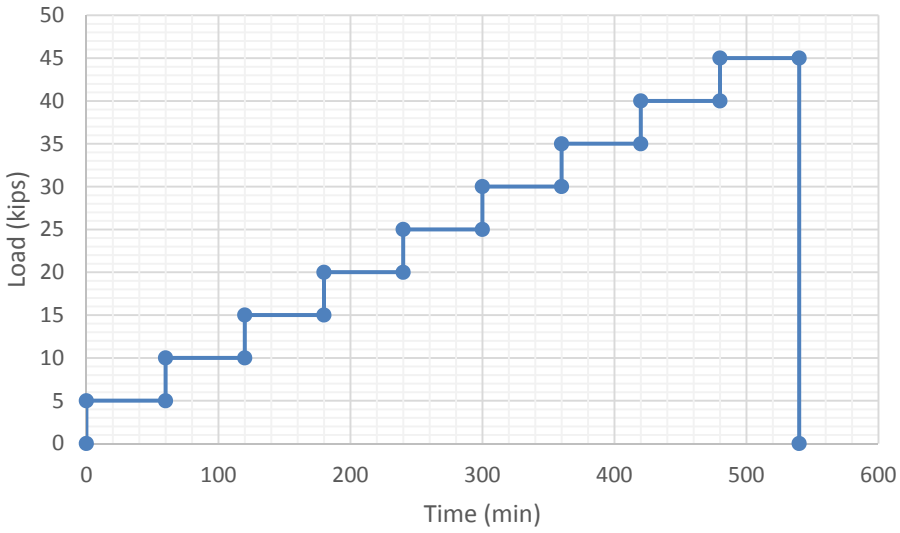

Figure 160. Pullout Load Protocol for the Second Row of Sacrificial Nails (i.e., at 14.4 Ft from Top of the Wall).

The third row of sacrificial nails (i.e., at 17.9 ft from the top of the wall) was tested on May 21, 2014. The load sequence for these sacrificial nails was the same as the sacrificial nails in the first row. The sacrificial nails at this row were loaded with increments of 4 kips until failure. At 1.5 times the design load, the load was held constant for 60 minutes and the creep movements were recorded.

Load Test Setup

A center-hole hydraulic jack and an electrical hydraulic pump were used to apply the axial load on the sacrificial nails. A reaction beam was placed between the hydraulic jack and the shotcrete facing to align the axis of the nail bar and the axis of the hydraulic jack. To ensure that a constant load was kept fixed during the creep test, a center-hole load cell was placed at the top of the nail. Figure 161 shows the load test setup. As shown in Figure 162, the wires of the strain gauges were connected to the data acquisition system during the load tests and the data gathered from the strain gauges were recorded.

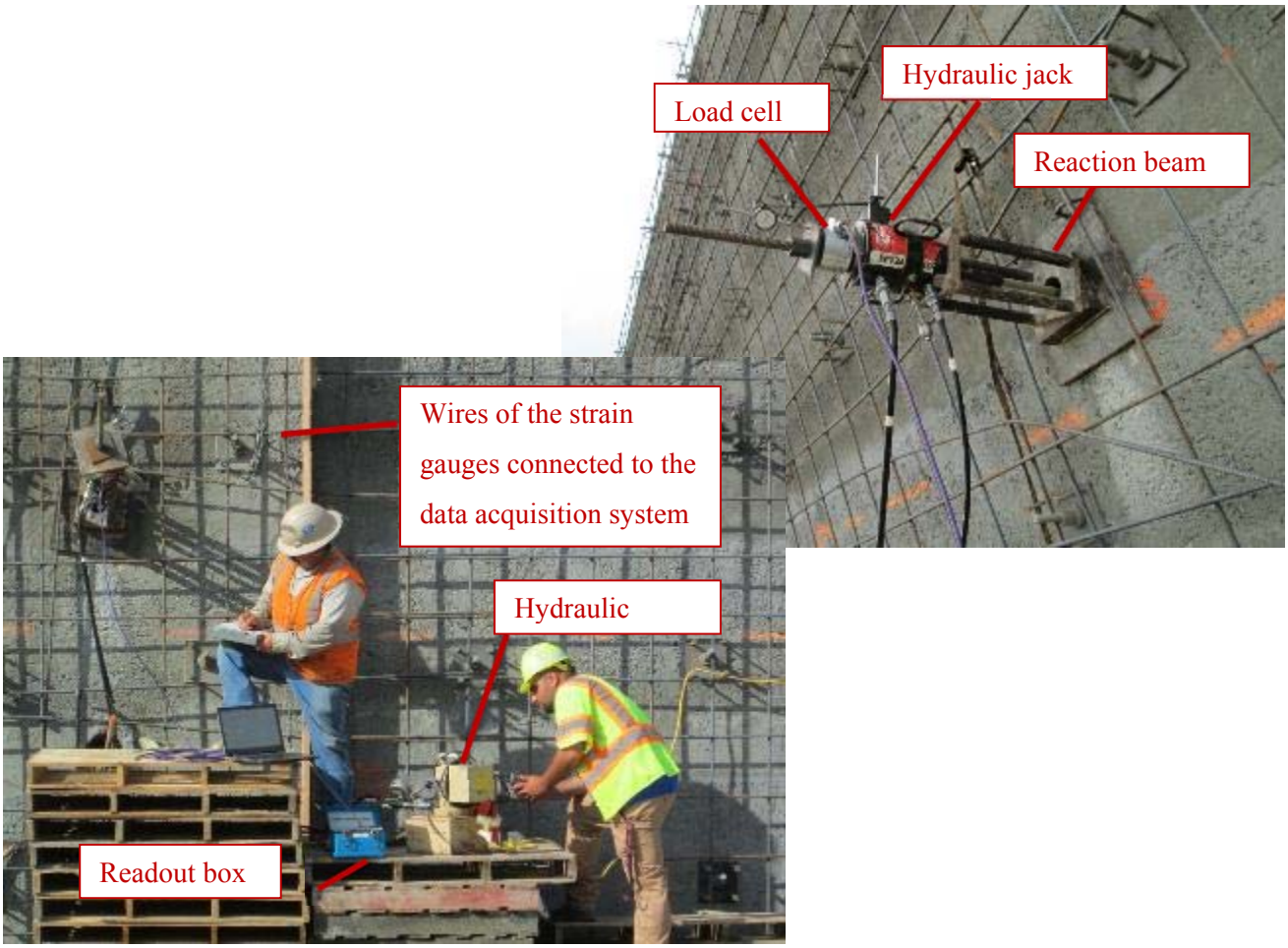

Figure 161. Adopted Setup for the Load Test on Nails.

Test Results

In this section, the outputs from the pullout tests on the sacrificial nails are discussed. The presentation of the test outputs is organized into three sections: 1) results involving total, elastic, and residual movements of the nail head; 2) information from the (modified) creep tests; and 3) load distribution along the nails during the tests.

Total, Elastic, and Residual Nail Movements. The sacrificial nails were incrementally loaded until their failure. The total movement is defined as the measured movement of the nail head during the test. The total movement consists of two components: 1) the elastic movement and 2) the residual movement. The elastic movements are recoverable when the load in the nail is released (i.e., the load in the nail is reduced from a test load to an alignment load).

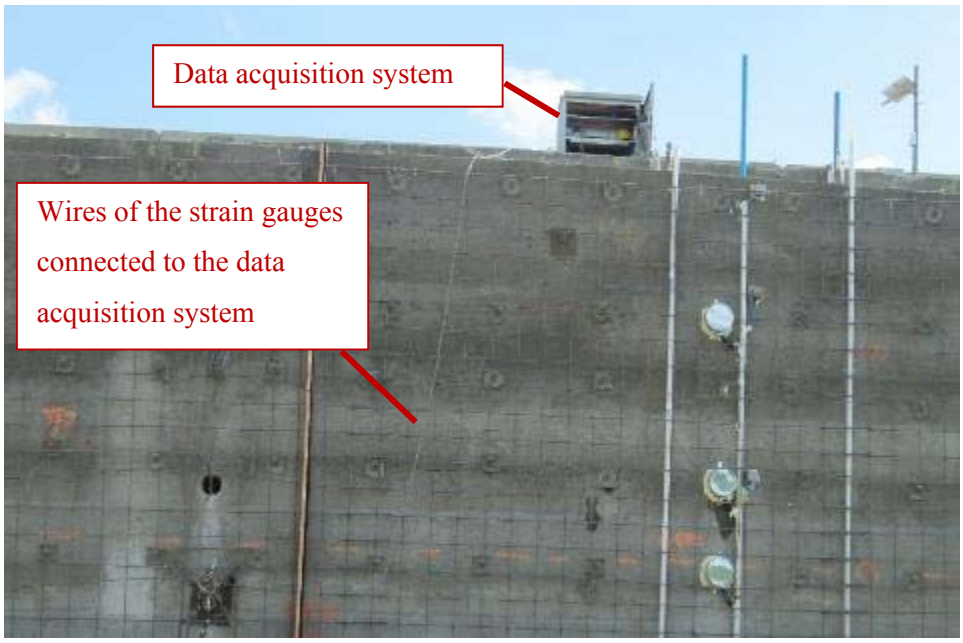

Figure 162. Data Acquisition System and Wires Used to Gather the Information during the Test.

The residual movements of the nail are the non-recoverable (permanent) movements observed once the nail is unloaded (FHWA, 1998a). The results of the pullout tests on the sacrificial nails are presented as follows:

- The test outputs on sacrificial nails at position 1 (i.e., at height = 7.4 ft) are shown in Figure 163 and Figure 164, for non-instrumented and instrumented nails, respectively.
- The test outputs on sacrificial nails at position 2 (i.e., at height = 14.4 ft) are shown in Figure 165 and Figure 166, for non-instrumented and instrumented nails, respectively.
- The test outputs on sacrificial nails at position 3 (i.e., at height = 17.9 ft) are shown in Figure 167 and Figure 168, for non-instrumented and instrumented nails, respectively.

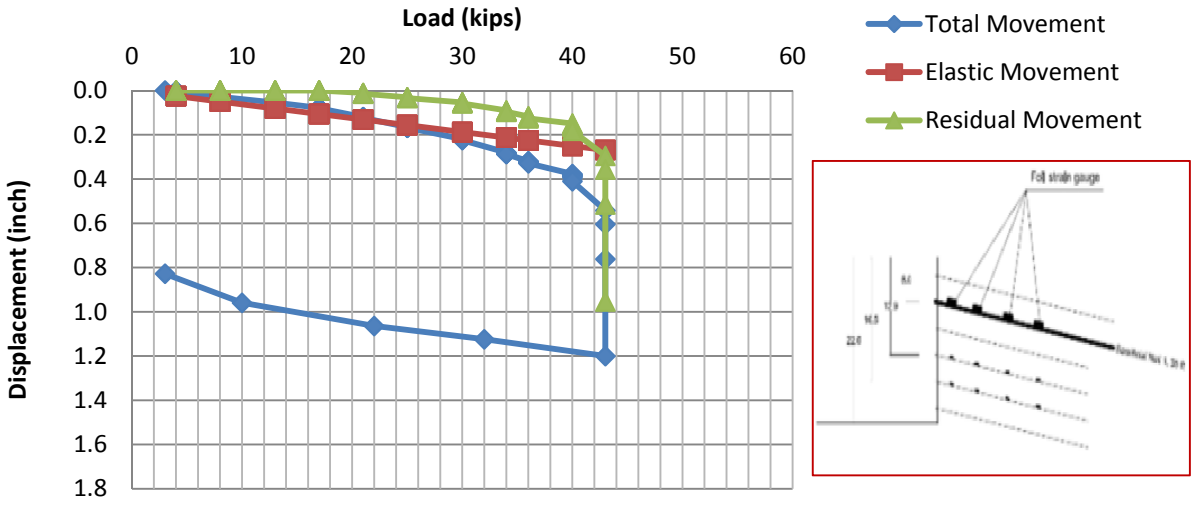

Figure 163. Total, Elastic, and Residual Nail Movements versus Load for the Non-Instrumented Sacrificial Nail at Position 1.

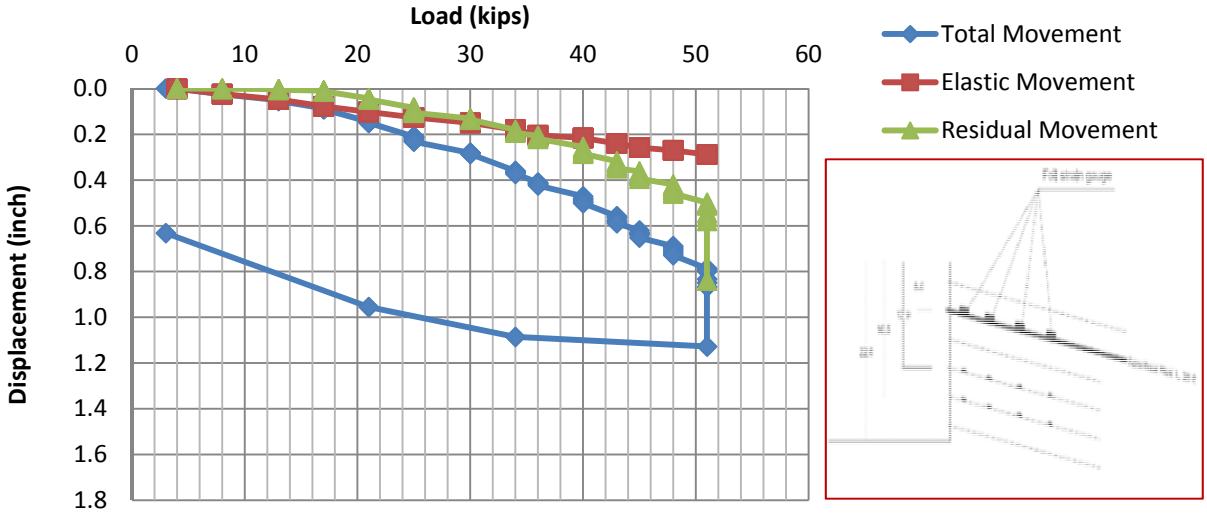

Figure 164. Total, Elastic, and Residual Nail Movements versus Load for the Instrumented Sacrificial Nail at Position 1.

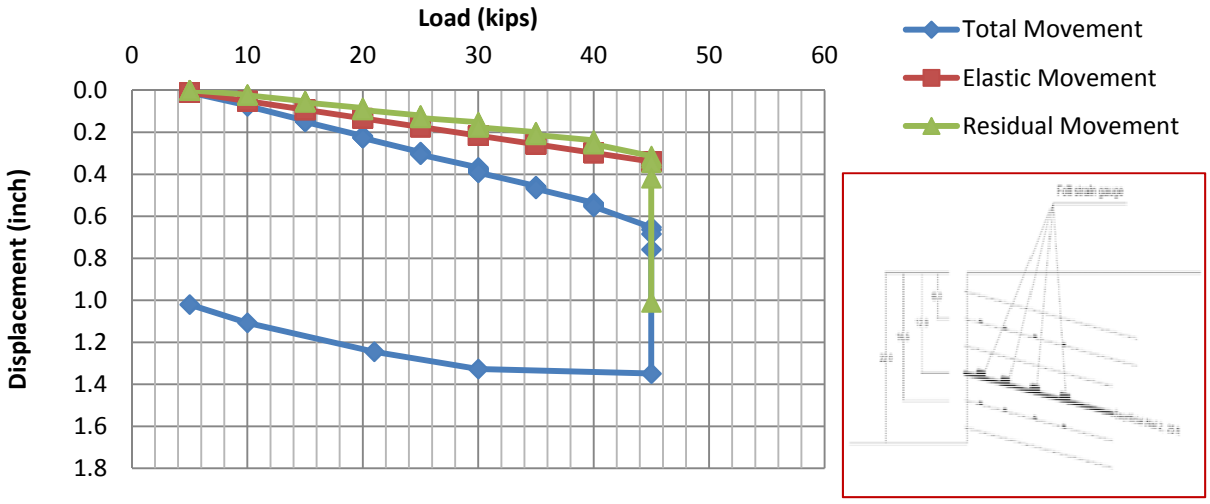

Figure 165. Total, Elastic, and Residual Nail Movements versus Load for the Non-Instrumented Sacrificial Nail at Position 2.

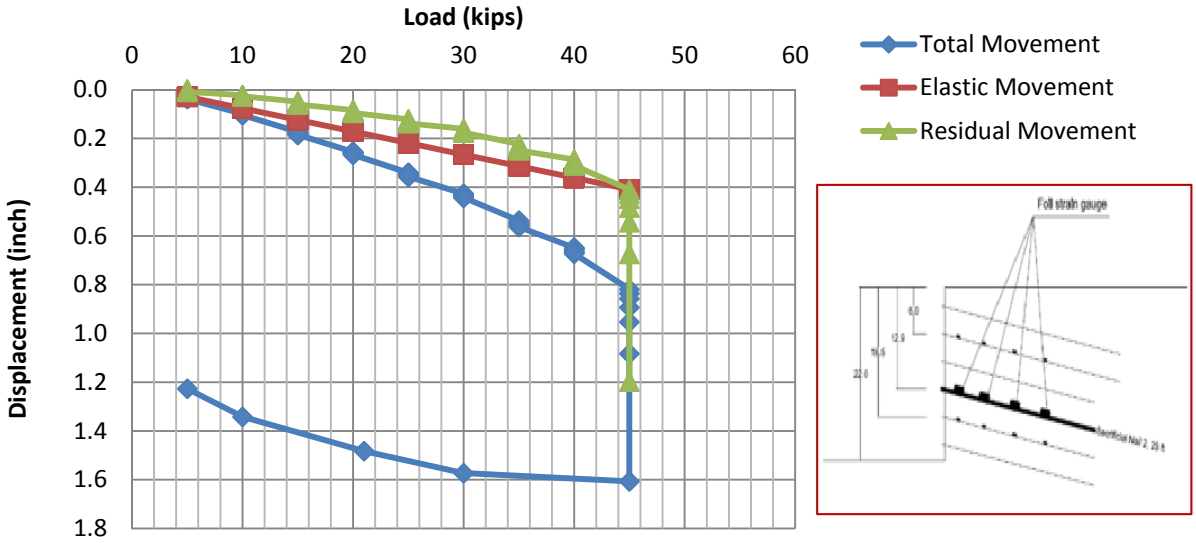

Figure 166. Total, Elastic, and Residual Nail Movements versus Load for the Instrumented Sacrificial Nail at Position 2.

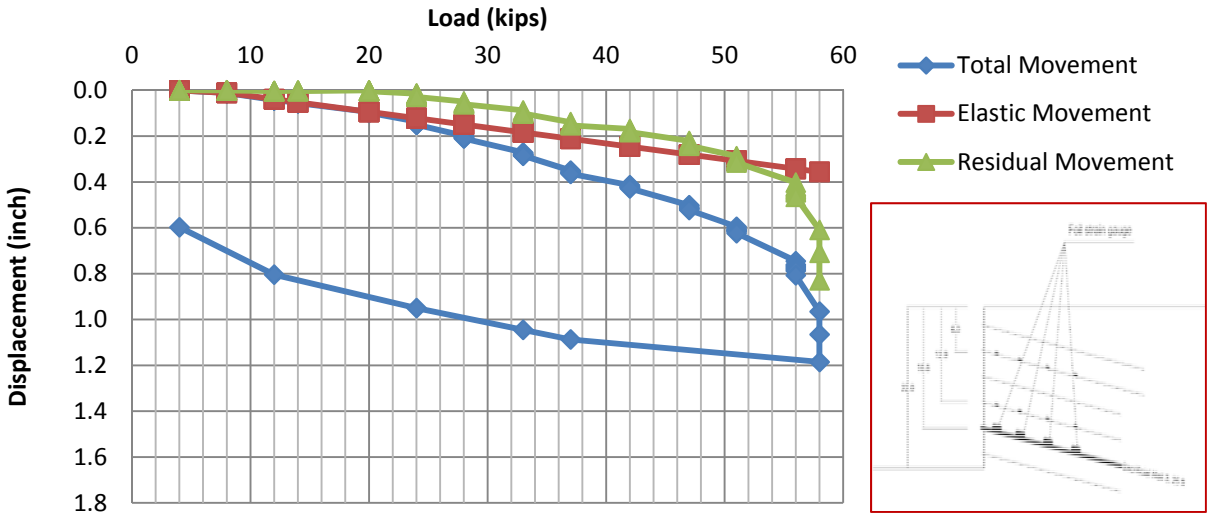

Figure 167. Total, Elastic, and Residual Nail Movements versus Load for the Non-Instrumented Sacrificial Nail at Position 3.

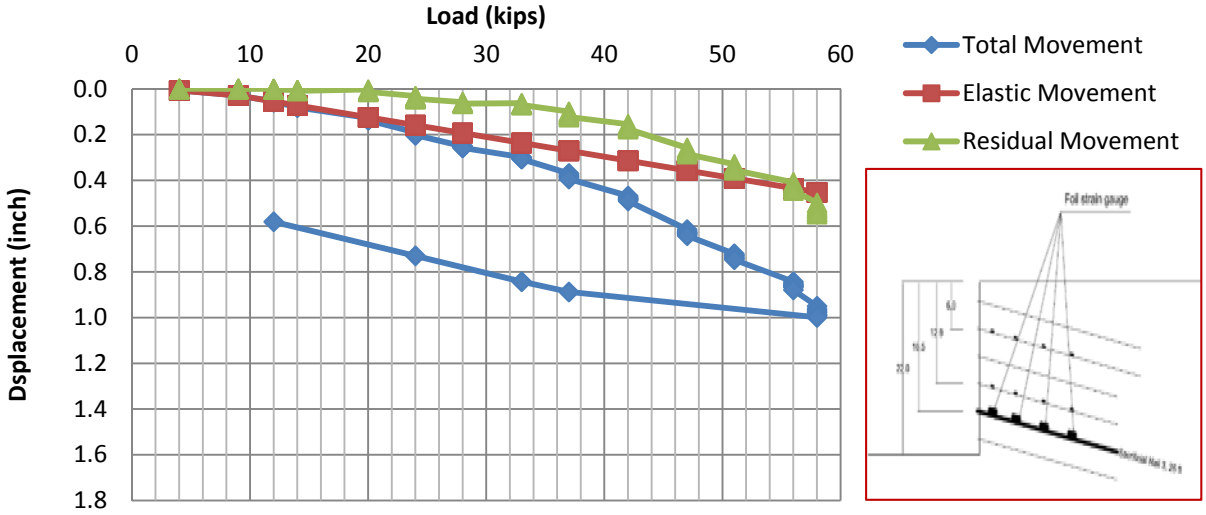

Figure 168. Total, Elastic, and Residual Nail Movements versus Load for the Instrumented Sacrificial Nail at Position 3.

For the three positions considered in these tests, there were some differences in the results obtained from non-instrumented and instrumented nails at the same height. These differences may be attributed to local variations in soil conditions, or slight variations on the soil–nail bond associated with installation issues, or a combination of both. Particularly noticeable is the difference in the results of the tests at position 1. In this case, there was a change in the load protocol, which could have an influence in the final response of the nails.

Table 27 presents a summary of the test results and sacrificial nails information. The bond length for sacrificial nail position 1 is 27 ft, while for sacrificial nail positions 2 and 3, the bond length is the same and equal to 23 ft. The design bond stress used in designing the nails in all the rows was the same and equal to 300 psf. The maximum bond stress at failure for the sacrificial nails at position 1 was 760 psf, while for the sacrificial nails position 3 (i.e., the bottom of the wall), it was 1204. Therefore, the FS for pullout for the nails in the upper rows of the nails was 2.5, while for the nails at the bottom of the wall it was 4.0.

Table 27. Summary of Tests on Sacrificial Nails.

Summary of Tests on Sacrificial Nails					
Nail No.	**Bond Length (ft)**	**Hole diameter (in.)**	**Failure load (kips)**	**Maximum bond stress at failure (psf)**	**Design bond stress (psf)**
Non-instrumented 1 (H=7.4 ft)	27	8	43	760	300
Instrumented 1 (H=7.4 ft)	27	8	51	902	300
Non-instrumented 2 (H=14.4 ft)	23	8	45	935	300
Instrumented 2 (H=14.4 ft)	23	8	45	935	300
Non-instrumented 3 (H=17.9 ft)	23	8	58	1204	300
Instrumented 3 (H=17.9 ft)	23	8	58	1204	300

Creep Tests. According to the GEC#7 (FHWA, 2003), the acceptance criterion for soil nails with respect to creep requires that the nail movement between minutes 1 and 10 of the creep test must be lower than 0.04 in. (i.e., 1 mm), or the creep movement between 6 and 60 minutes must be lower than 0.08 in. (i.e., 2 mm).

The test protocol introduced in Figure 159 was adopted for the verification tests on the non-instrumented nails. In these tests, each load increment was held constant for 10 minutes and the creep movements of the nail head were recorded. At 150 percent of the design load (i.e., for a design bond stress of 300 psf), the load was held for 60 minutes and the creep movements were recorded. Results of the movement versus time for each load are shown in Figure 169 to Figure 171 for the non-instrumented nails at positions 1, 2, and 3, respectively.

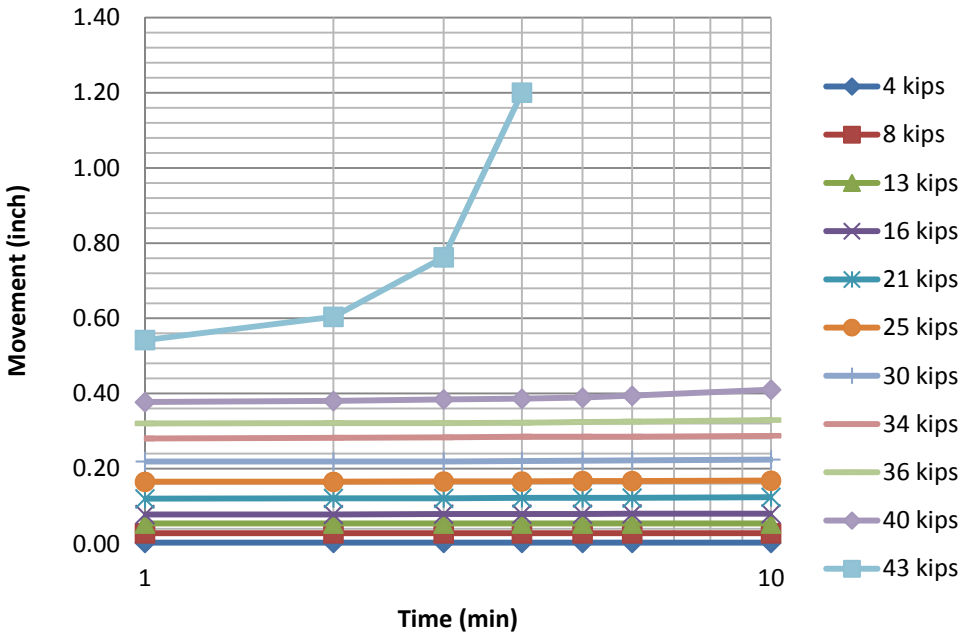

Figure 169. Creep Movement versus Time at Different Loads during the Verification Test on the Non-Instrumented Sacrificial Nail at Position 1.

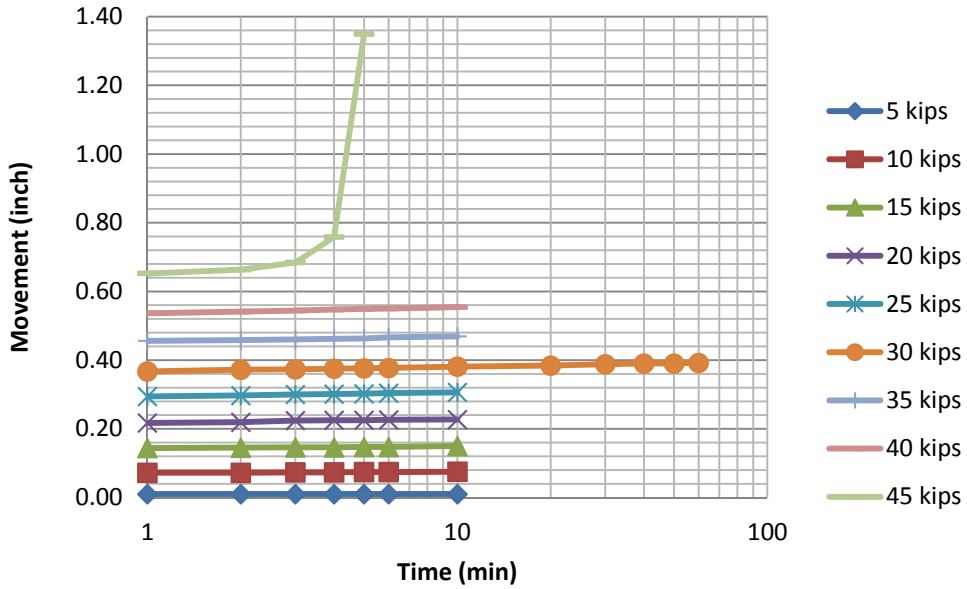

Figure 170. Creep Movement versus Time at Different Loads during the Verification Test on the Non-Instrumented Sacrificial Nail at Position 2.

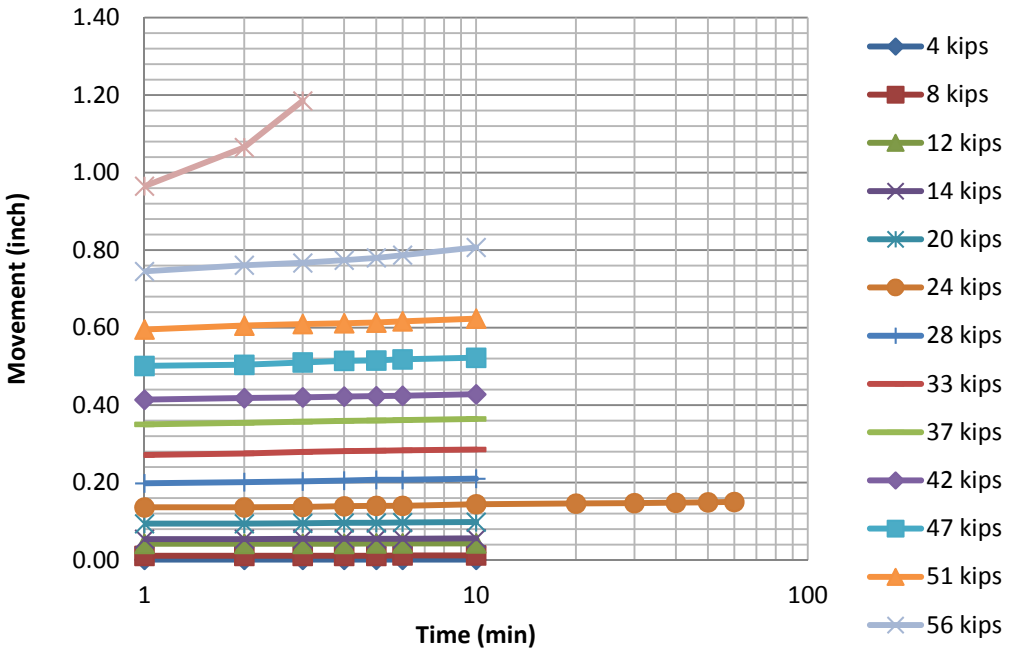

Figure 171. Creep Movement versus Time at Different Loads during the Verification Test on the Non-Instrumented Sacrificial Nail at Position 3.

The creep rate was calculated from these tests by relating the increments in the displacement of the nail head with time. The results of the creep tests are presented in Figure 172 to Figure 174 for the tests on non-instrumented nails at positions 1, 2, and 3, respectively.

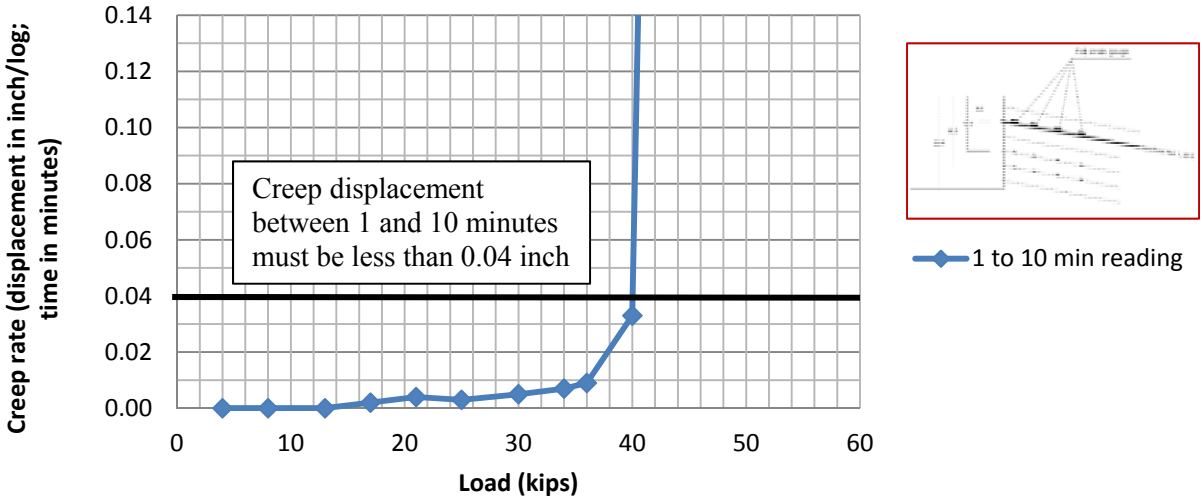

Figure 172. Creep Rate between 1- and 10-Min Readings at Different Loads during the Verification Test on the Non-Instrumented Sacrificial Nail at Position 1.

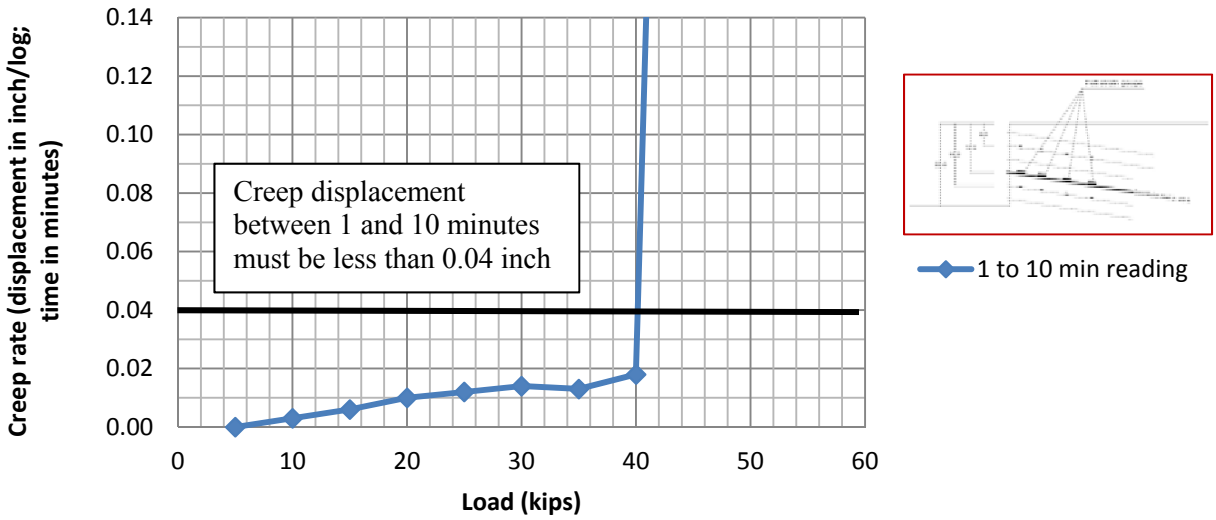

Figure 173. Creep Rate between 1- and 10-Min Readings at Different Loads during the Verification Test on the Non-Instrumented Sacrificial Nail at Position 2.

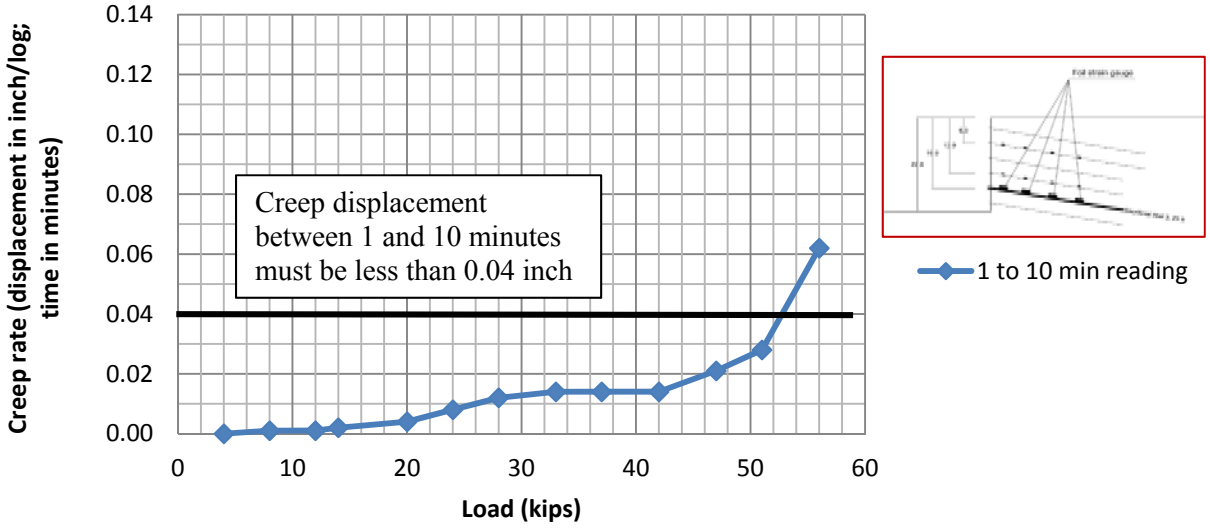

Figure 174. Creep Rate between 1- and 10-Min Readings at Different Loads during the Verification Test on the Non-Instrumented Sacrificial Nail at Position 3.

As illustrated in Figure 160, the load protocol adopted for the creep tests on instrumented nails was slightly modified; each load was held constant for 60 minutes and the creep movements of the nail head were recorded. Results of the movement versus time for each load are illustrated in Figure 175 to Figure 177 for the instrumented nails at positions 1, 2, and 3, respectively.

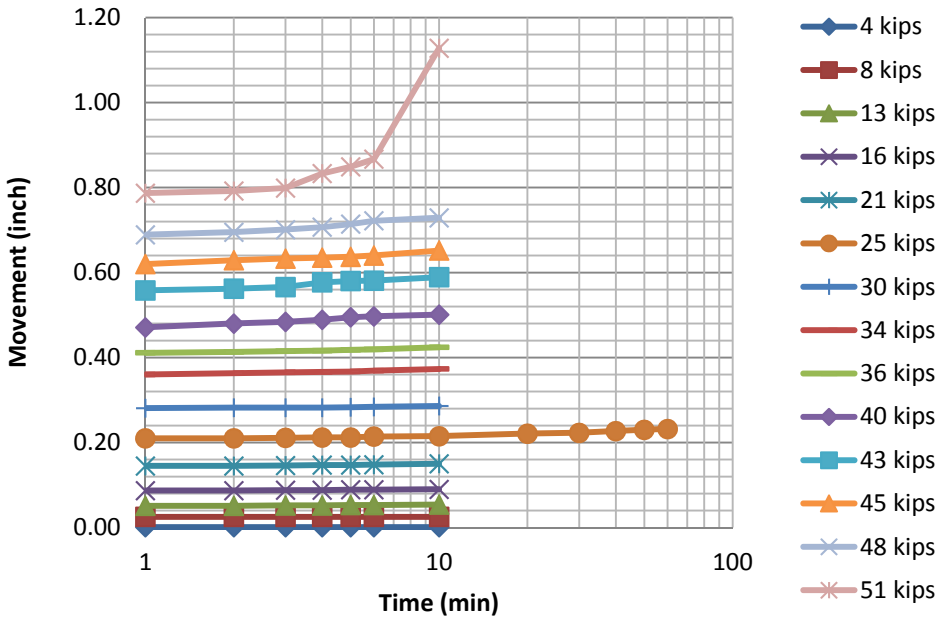

Figure 175. Creep Movement versus Time at Different Loads during the Verification Test on the Instrumented Sacrificial Nail at Position 1.

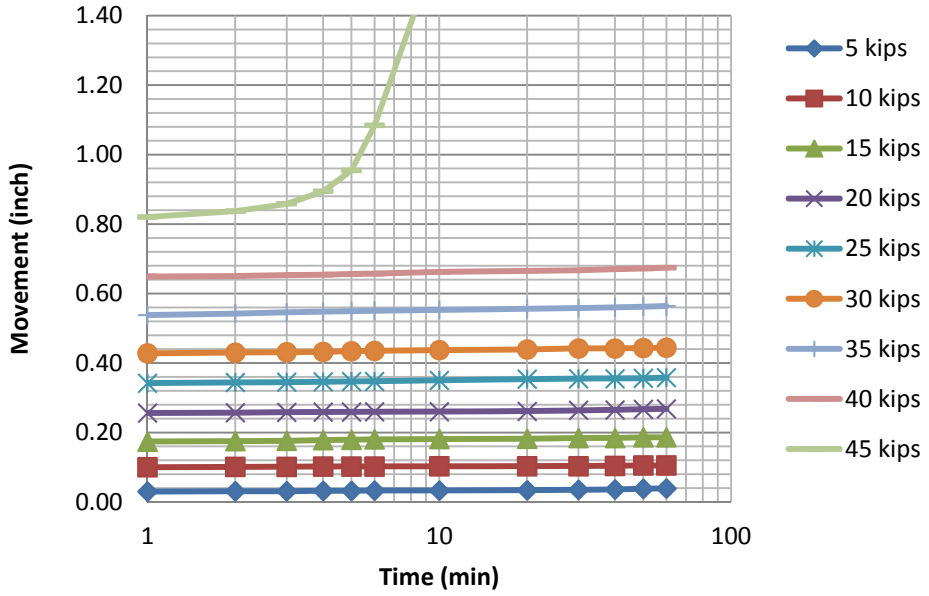

Figure 176. Creep Movement versus Time at Different Loads during the Verification Test on the Instrumented Sacrificial Nail at Position 2.

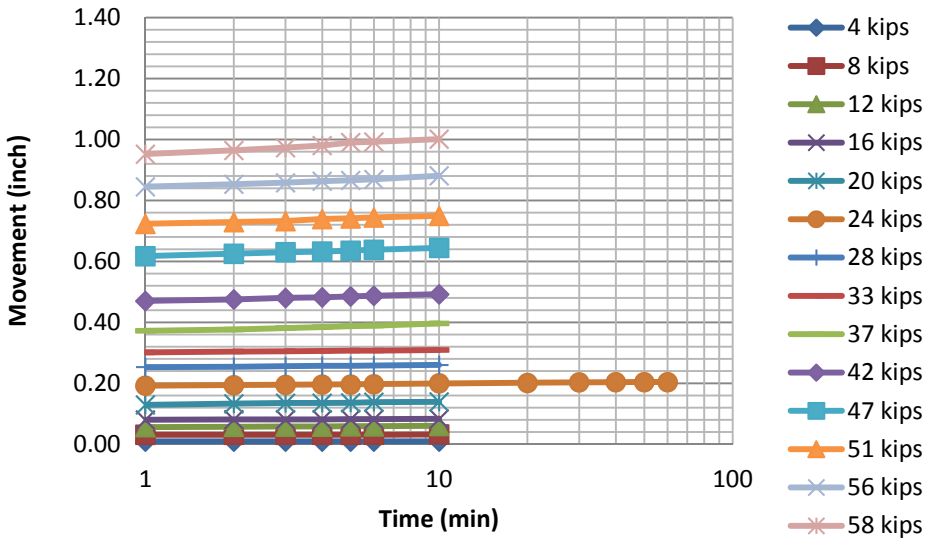

Figure 177. Creep Movement versus Time at Different Loads during the Verification Test on the Instrumented Sacrificial Nail at Position 3.

Figure 178 to Figure 180 clearly show that the creep rate of the soil nail depends on the load level. As the loads in the non-instrumented creep tests increased, the creep rate also increased. However, the creep rate was significantly lower than the acceptance criterion (i.e., a creep movement of 0.04 in. for readings between 1 and 10 minutes, plotted as a horizontal line in Figure 172 to Figure 174), particularly for those load levels that were below the 90 percent of the failure load. As expected, at the failure load the creep rate increased notably.

The creep displacements between minutes 1 and 10 of the tests are presented in Figure 178 to Figure 180, while Figure 181 presents the creep movements obtained between minutes 6 and 60 of the tests on the instrumented sacrificial nail at position 2.

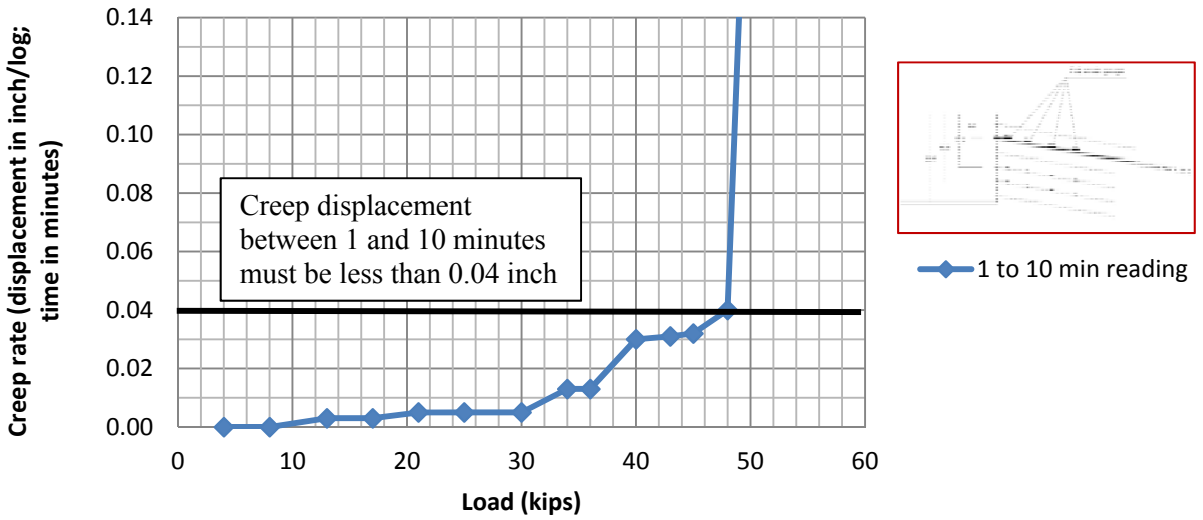

Figure 178. Creep Displacements Related to 1- and 10-Minute Readings at Different Load Levels during the Modified Creep Test on the Instrumented Sacrificial Nail at Position 1.

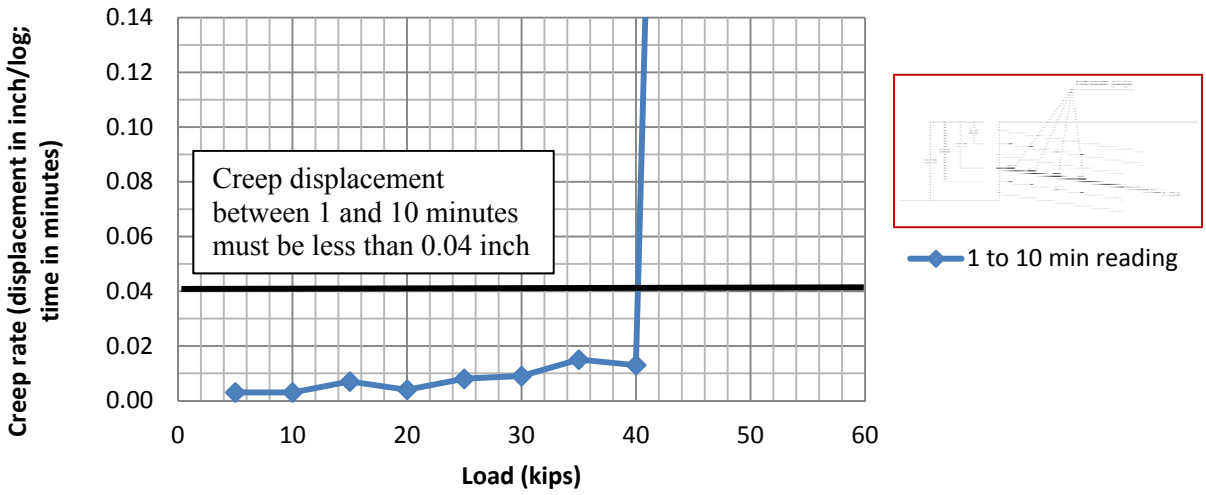

Figure 179. Creep Displacements Related to 1- and 10-Minute Readings at Different Load Levels during the Modified Creep Test on the Instrumented Sacrificial Nail at Position 2.

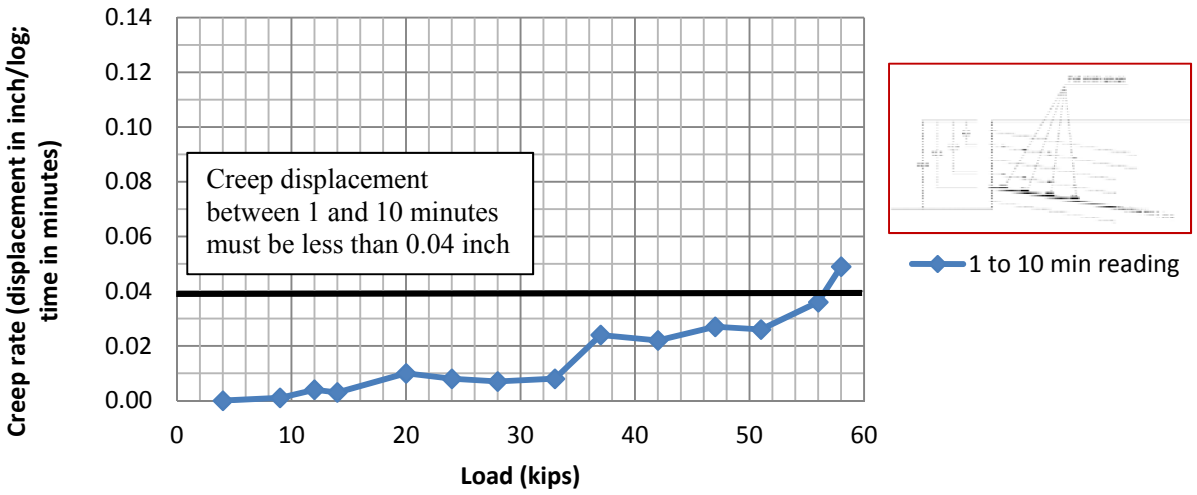

Figure 180. Creep Displacements Related to 1- and 10-Minute Readings at Different Load Levels during the Modified Creep Test on the Instrumented Sacrificial Nail at Position 3.

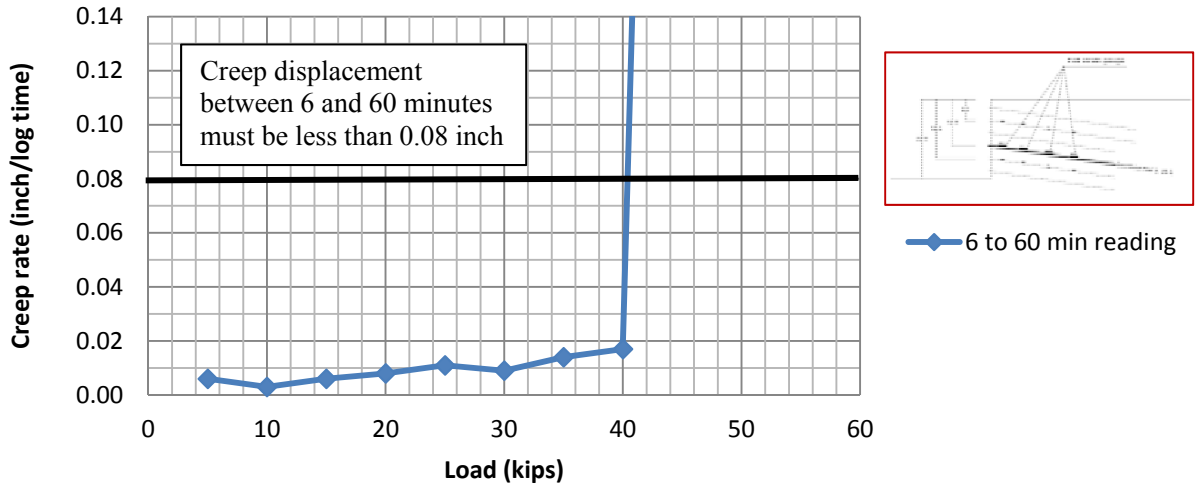

Figure 181. Creep Displacements Related to 6- to 60-Minute Readings at Different Load Levels during the Modified Creep Test on the Instrumented Sacrificial Nail at Position 2.

The response of instrumented sacrificial nails in terms of creep is quite similar to that of non-instrumented nails, at least in terms of general trends, that is, the creep rate increased with the increase of the load level. The creep rate was significantly below the acceptance criterion for loads lower than the failure load. As expected, at the failure load the creep rate increased dramatically and the nails failed. Table 28 presents a summary of the creep tests on the instrumented sacrificial nails. The creep failure occurred in practically all the tests at a load level that is around 94 percent (or above) of the pullout capacity of the nail.

Table 28. Summary of the Creep Tests on Instrumented Nails.

Instrumented nails						
Nail No.	**Failure load (kips)**	**Creep failure threshold (kips)**	**Maximum bond stress at failure (psf)**	**Design bond stress (psf)**	**Bond stress creep threshold (psf)**	**Percentage of pullout capacity where creep failure occurred**
1 Instrumented	51	48	902	300	849	94%
2 Instrumented	45	45	935	300	935	100%
3 Instrumented	58	56	1204	300	1162	96%

Load Distribution in the Nails during Pullout Tests. As mentioned in previous sections, three sacrificial nails were instrumented with foil strain gauges at four different positions. The cracking strain for the grout is assumed to be 100 με (100×10^{-6} in./in.). The measured strains showed that most of the grout surrounding the threadbar was cracked. Since the measured strain exceeds the cracking strain in grout, the load on the nails is related directly to the measured tensile strain of threadbar (FHWA, 1998a). During the pullout tests on these nails, strain gauges were connected to the data acquisition system (Figure 162) to gather the load distribution along the nails during the experiment. Figure 182 to Figure 184 illustrate the load distribution along the nails. As expected, the applied load decreases progressively from the top of the bonded length (i.e., where the load is applied) to the end of the nail where the tension in the nail must become zero. The grout–soil interface friction is not mobilized along the entire unbonded length. The decrease in the load along the unbonded length occurs at an almost constant rate. The smaller rate of load decrease was observed for lower load levels (i.e., less than 10 kips). For instance, in the instrumented sacrificial nail at position 1, at the load step equal to 25 kips, the load decreased to 2 kips at 15 ft, far from the top of the bonded length, while for the 34 kips load step, at 15 ft from the top of the bonded length, the load decreased to 18 kips.

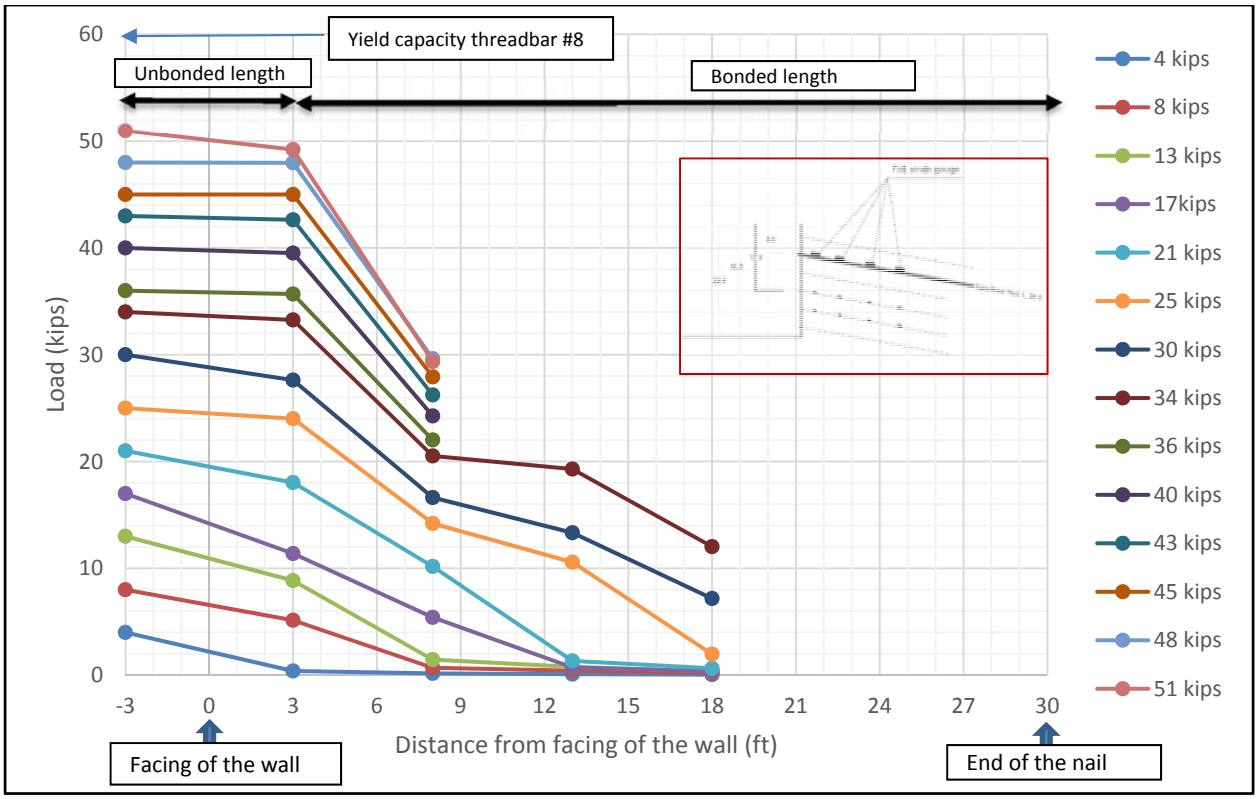

Figure 182. Load Distribution along the Instrumented Sacrificial Nail 1 (Height = 7.4 Ft).

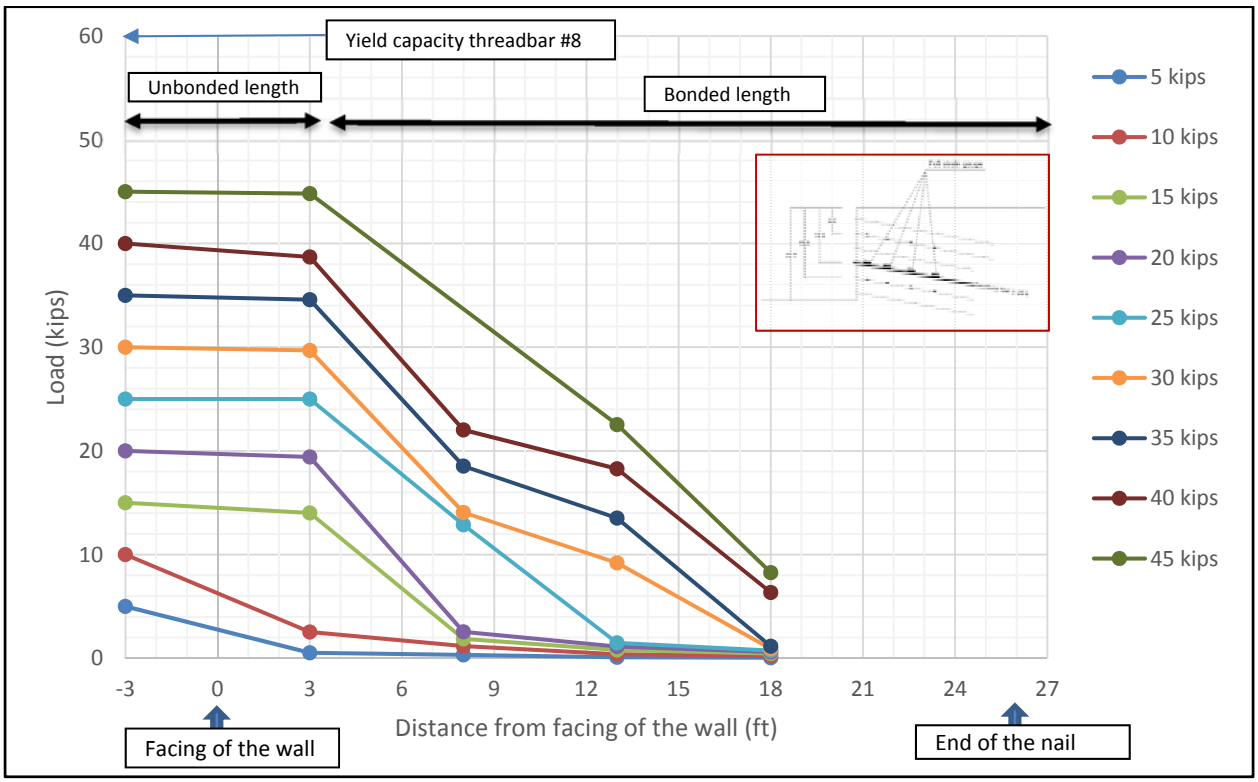

Figure 183. Load Distribution along the Instrumented Sacrificial Nail 2 (Height = 14.4 Ft).

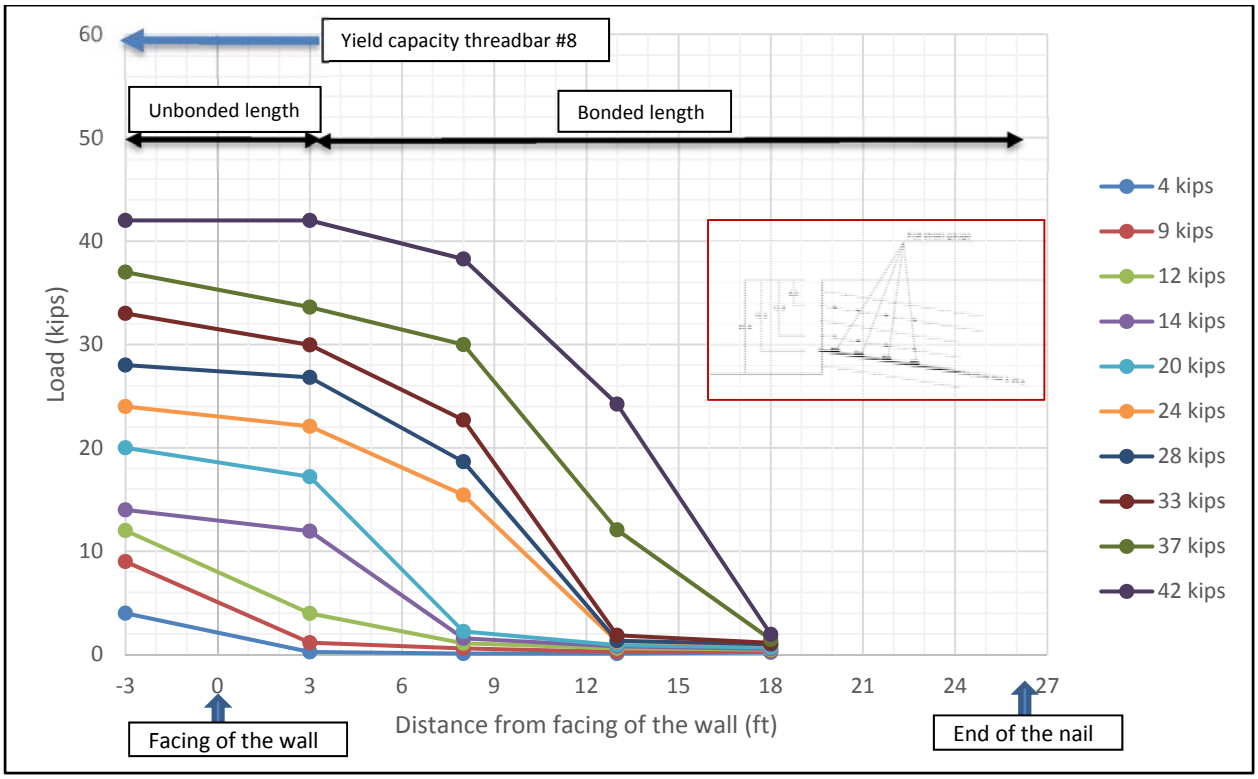

Figure 184. Load Distribution along the Instrumented Sacrificial Nail 3 (Height = 17.9 Ft).

During the test on the instrumented sacrificial nail at position 1, the third and fourth strain gauges (i.e., at a distance of 13 and 19.5 ft behind the shotcrete, respectively) broke at a load around 34 kips. Because of this, in Figure 182 there are not readings for these strain gauges for loads greater than 34 kips. As for the instrumented sacrificial nail at position 3 (Figure 184), the four strain gauges broke at a load around 42 kips.

Long-Term Monitoring

The objective of long-term monitoring of an actual soil nail wall is to study its performance under real conditions and in a site with HP clays. The collection of data from the field experiments and the monitoring of the soil nail wall behavior are two critical components of this research. This study will provide useful information on the soil nail behavior under real operational conditions that will allow a better understanding of soil nail walls in HP clays. The information obtained from the actual site will also be very useful for calibrating the numerical models proposed in the research.

The parameters to be monitored during the long-term monitoring are the following (FHWA, 2003):

- Horizontal movements of the wall due to the construction.
- Horizontal movements of the wall due to the creep of the soil mass.
- Service load of the nails at different depths.
- Load distribution in the nails.
- Load change in the nails as a function of time (due to the creep).
- Load at the nail head.
- Change in temperature of the soil mass.
- Change in water content of the soil mass.

In order to perform the above investigations, the following instrumentations were installed at the site project:

- Inclinometer casings to perform periodic inclinometer readings.
- Tiltmeters.
- Strain gauges in the production nail.
- Load cells at the nail head.
- Water content probes.

In the following sections, the information gathered from these different devices are discussed.

Inclinometer

Inclinometers provide valuable quantitative data associated with the deflection of the soil mass in depth. This information can be associated with the soil movements. Inclinometer casings need to be installed (in boreholes previously drilled) to allow the operation of the inclinometer torpedo. The inclinometer allows recording of the deflection of the entire profile (in depth) at given times. This technique requires the installation of the inclinometer casing in a borehole behind the shotcrete facing. This device is perhaps the more common one used to measure lateral movements of earthworks or structures. It also provides the pattern of deformations and the zones of potential failure.

On March 26, 2014, the first inclinometer casing was installed at station 2+00 (Figure 185). The casing was located 4 ft behind the facing of the soil nail wall. The inclinometer casing

was installed 23 ft below the soil embankment to ensure that the deformation of the soil is zero at that depth. The bottom of the casing is the reference value for calculating the deflections along the borehole and needs to be fixed with no deflection (i.e., the tangent to the deformed casing alignment needs to be vertical at all times). The total length of the inclinometer casing is 46 ft.

Figure 185. First Inclinometer Casing at Station 2+00.

Figure 186 shows the soil profiles obtained from inclinometer readings on April 2, 8, and 9, 2014 (i.e., the construction was at Stage 2 and the height of the excavation was at that time 7 ft). The deflections of the casing were huge on April 8 and 9, and localized at a depth around 12 ft from the top of the embankment. These movements were associated with a sliding of the soil mass at that depth, which could be possibly induced by an over-excavation during this stage accompanied by a bad soil condition. Because of these soil movements, the inclinometer casing was bent at this depth and the inclinometer probe could not go deeper than 12 ft. Therefore it was decided to replace this casing, and on April 14, two more inclinometer casings were installed at stations 1+46 and 2+00. The length of these two casings are 46 ft. Figure 187 and Figure 188, respectively, show the installation of the additional inclinometer casings at stations 2+00 and 1+46 on April 14, 2014. Figure 189 illustrates the locations of the two additional inclinometers in the wall profile.

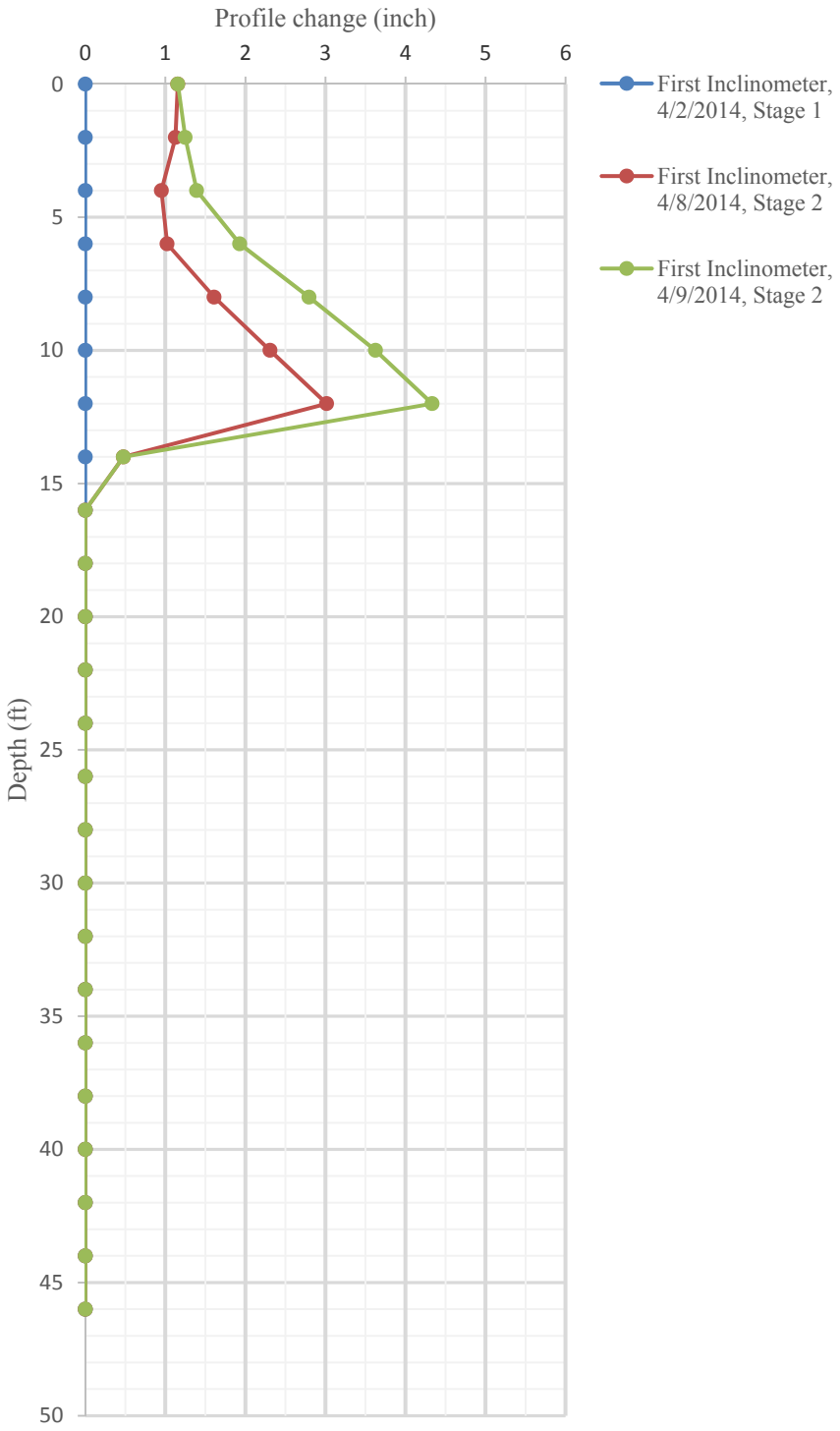

Figure 186. Soil Profile for Inclinometer Casing.

Figure 187. Installation of the Second Inclinometer Casing at Station 2+00 on April 14.

Figure 188. Installation of Second Inclinometer Casing at Station 1+46 on April 14.

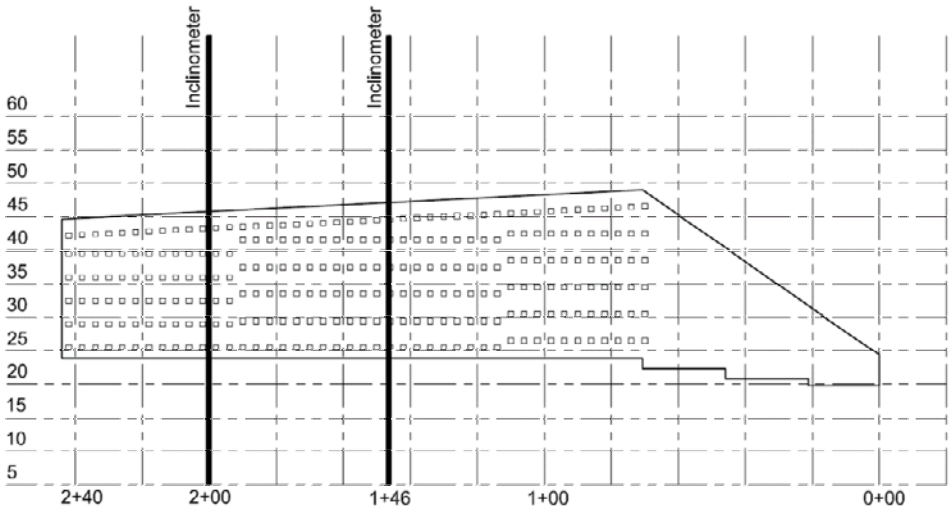

Figure 189. Location of the Second Set of Inclinometer Casings (at Stations 2+00 and 1+46).

Figure 190 shows the inclinometer casing after installation and the inclinometer probe. In each stage of construction, inclinometer readings for stations 2+00 and 1+46 were taken. Figure 191 and Figure 192 present the lateral deformation of the wall during the construction at stations 2+00 and 1+46, respectively.

Figure 190. Inclinometer Probe and Casing.

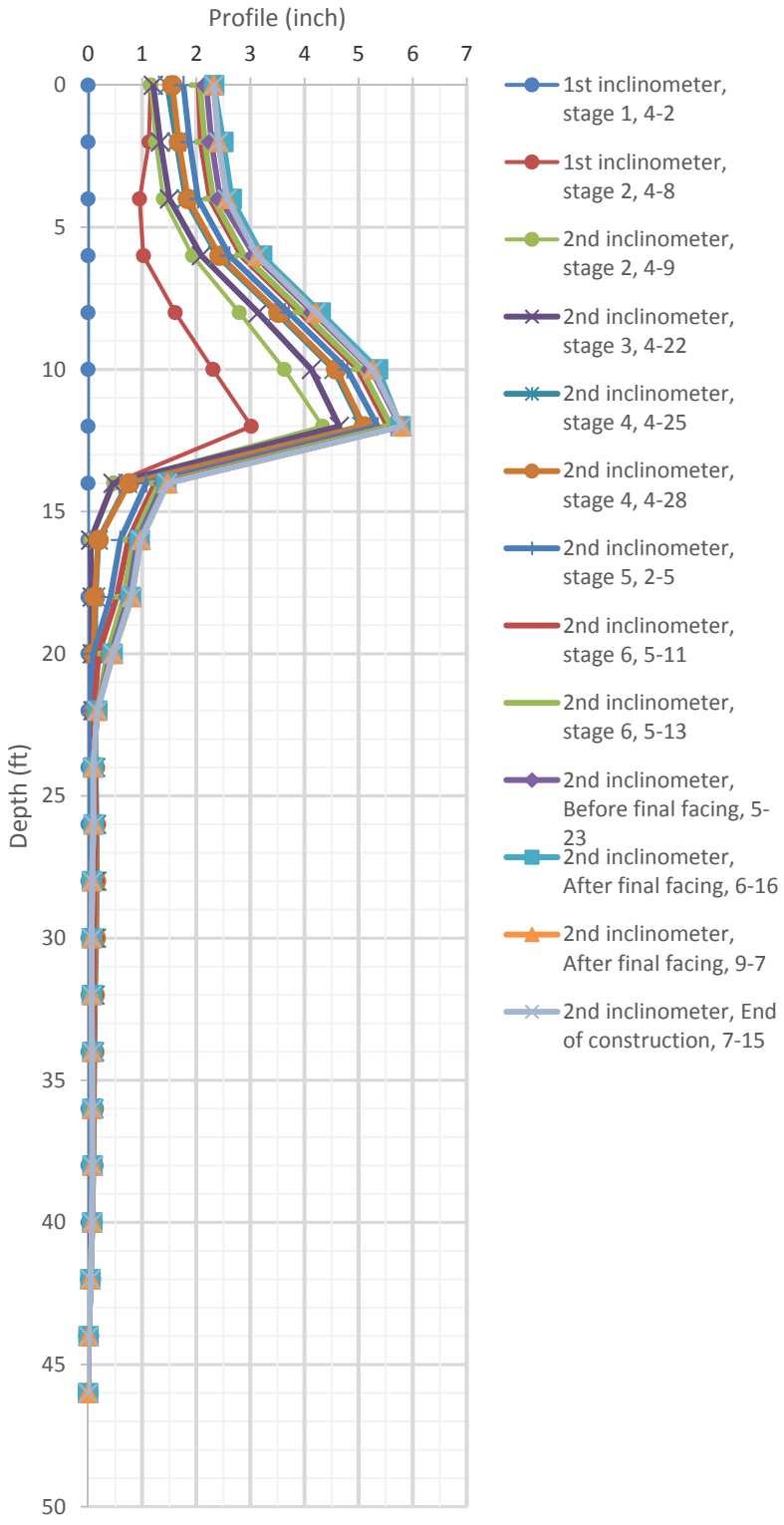

Figure 191. Lateral Displacement of the Soil Profile 3 Ft behind the Facing of the Wall at Station 2+00 during Construction (Each Line Presents the Lateral Displacement in a Different Stage of Construction).

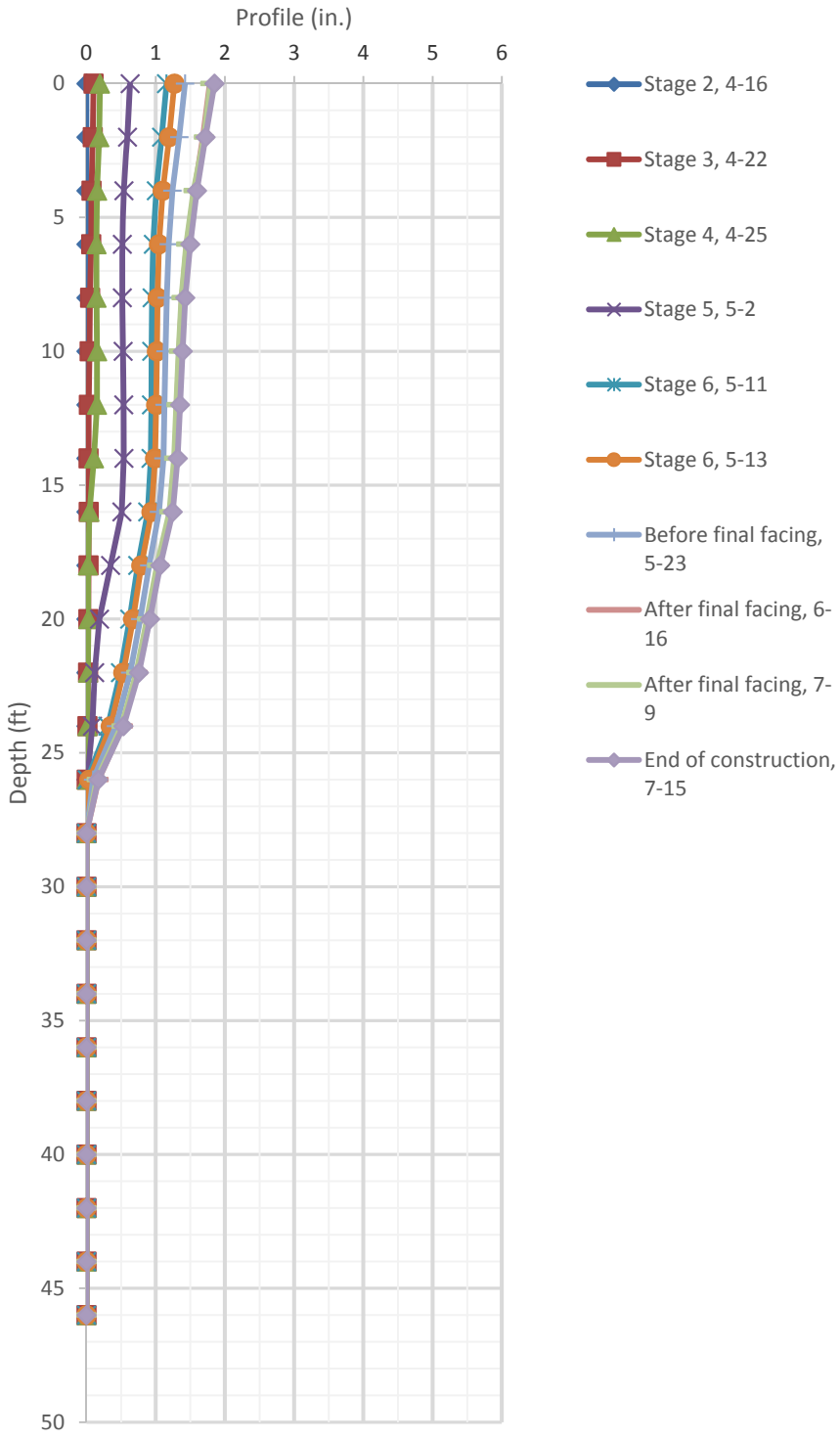

Figure 192. Lateral Displacement of the Soil Profile 3 Ft behind the Facing of the Wall at Station 1+46 during Construction (Each Line Presents the Lateral Displacement in a Different Stage of Construction).

The soil profile at station 2+00 showed the large deformations at a depth of 12 ft during the second stage of construction. Some modifications to the original design were considered, such as: 1) to reduce the height of the excavation in each stage; 2) to increase the diameter of the holes (e.g., from 6 in. to 8 in.); and 3) to add more pretensioned soil nails to the current soil nails in stage 2. Therefore, as illustrated in Figure 191, the very large lateral deformations observed during the initial stages were reduced for the remaining stages. At station 1+46, the maximum lateral displacement took place at the top of the wall and decreased toward the toe of the wall. The maximum horizontal displacement at the top of the wall is 1.85 in. at the sixth stage of construction, which is 0.006 times the height of the wall (i.e., 25 ft).

In order to monitor the horizontal displacements of the wall in depth after construction, inclinometer readings were taken every month for a period of 13 months after construction. As shown in Figure 193 and Figure 194, the deformation of the wall at station 2+00 for the post-construction monitoring is less than 0.08 in., while the deformation of the wall at station 1+46 is less than 0.2 in., which is around 10 percent of the deformation observed just after construction. Typically, the post-construction deformation increases up to 15 percent of that observed just after construction (FHWA, 2003).

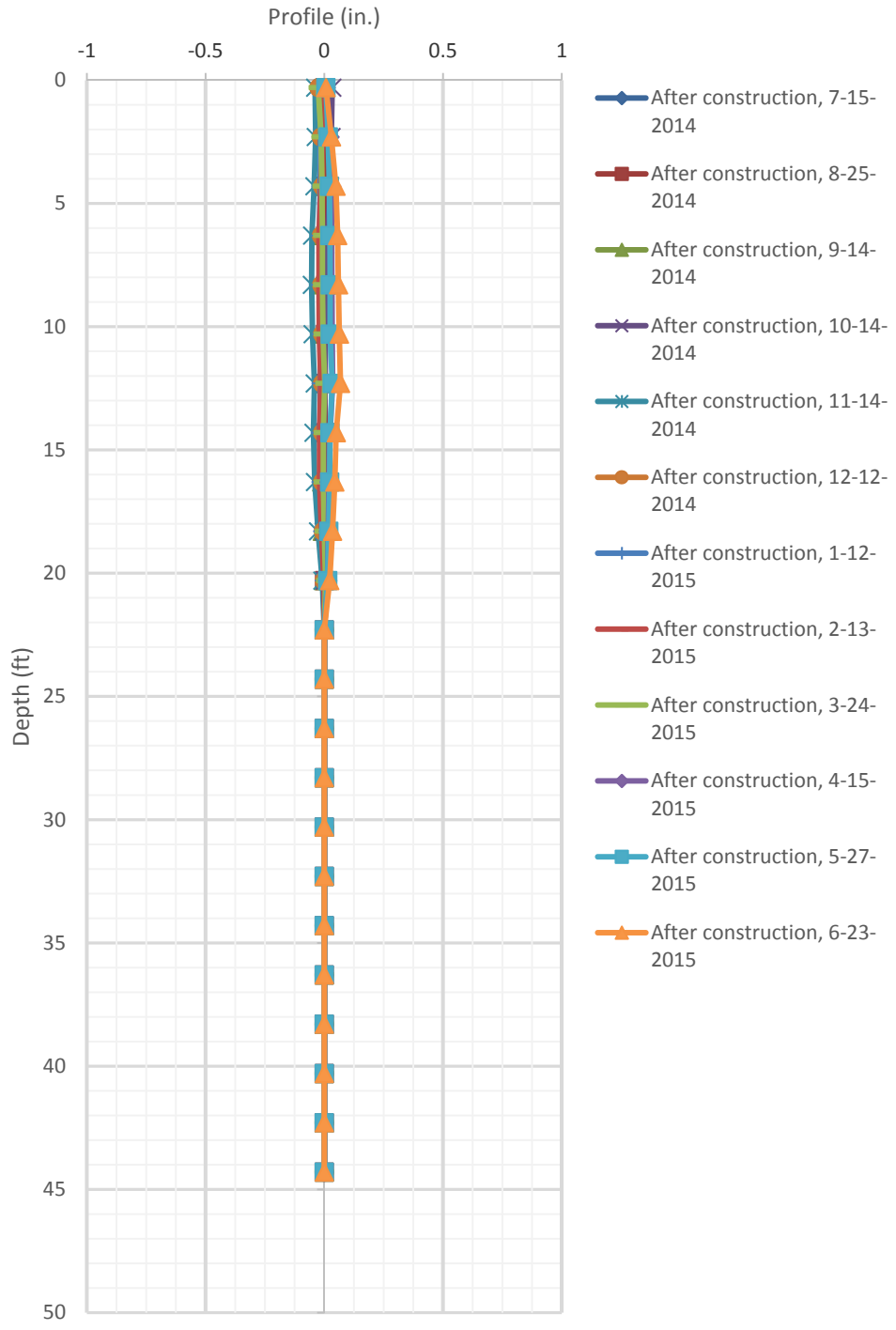

Figure 193. Lateral Displacements of the Soil Profile at 3 Ft behind the Facing of the Wall at Station 2+00 after Construction.

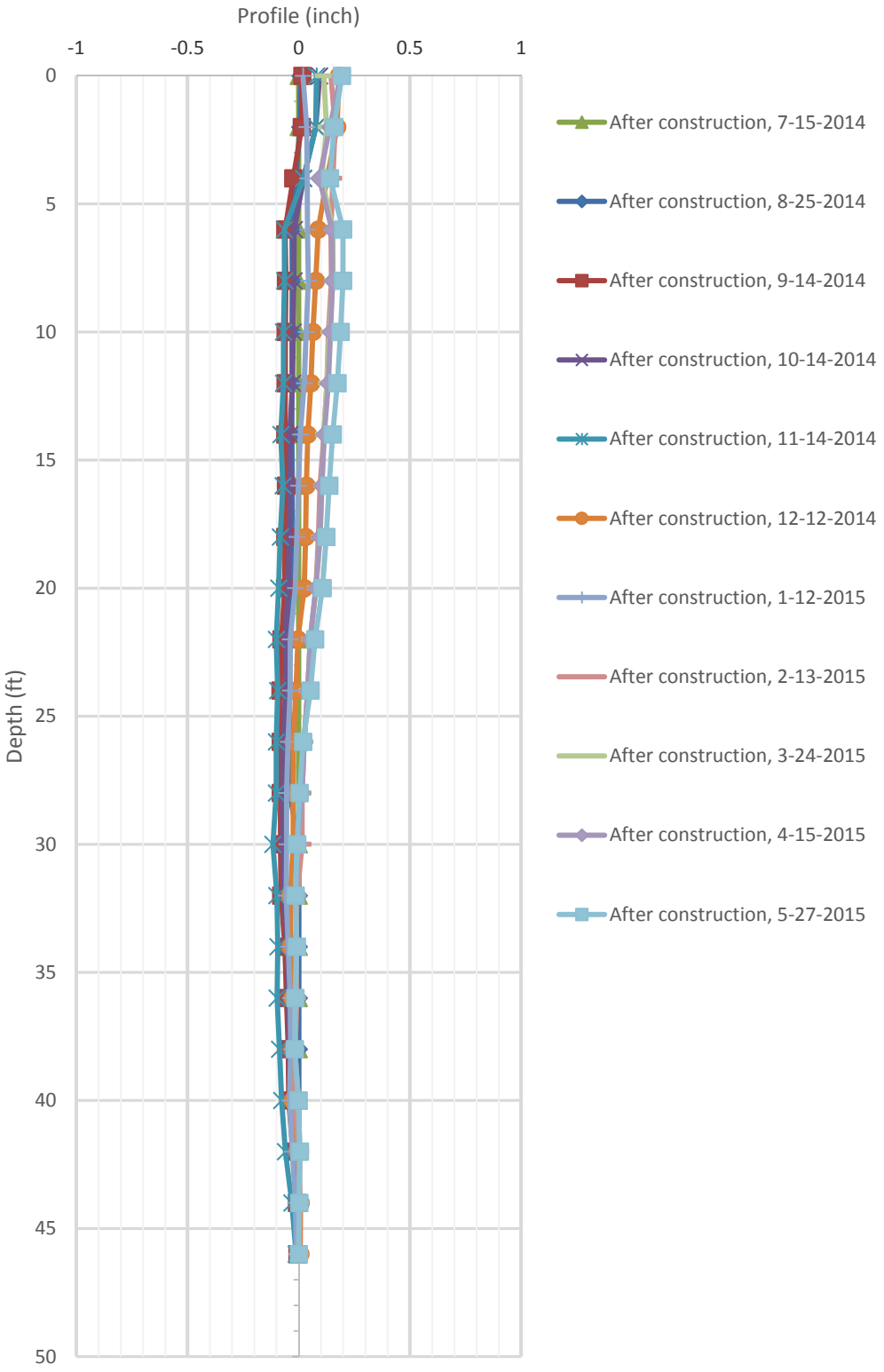

Figure 194. Lateral Displacements of the Soil Profile at 3 Ft behind the Facing of the Wall at Station 1+46 after Construction.

Figure 195 shows the maximum movements of the wall (12-ft height) at station 2+00 versus the construction time. Around 78 percent of the movements (i.e., 4.4 in.) happened during the second stage of construction, and 22 percent (i.e., 1.2 in.) of them took place during the third stage of construction, toward the end of construction. Figure 196 presents the lateral displacements at the top of the wall, at stations 2+00 and 1+46.

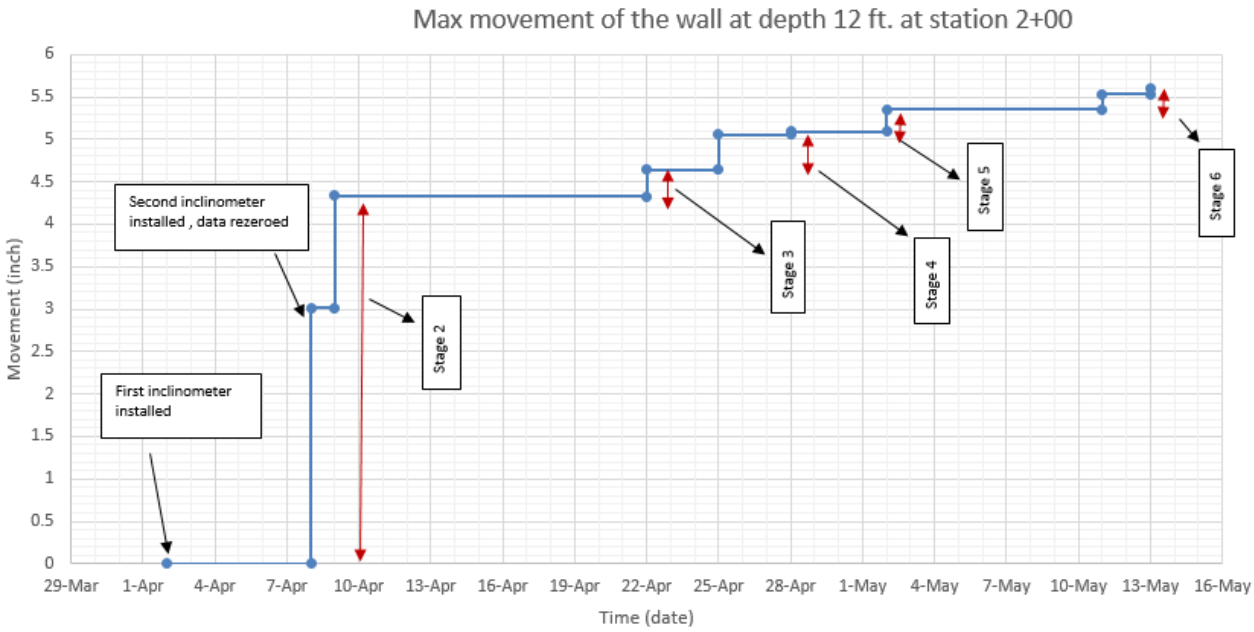

Figure 195. Movements of the Wall (12-Ft Height) at Station 2+00 during Construction.

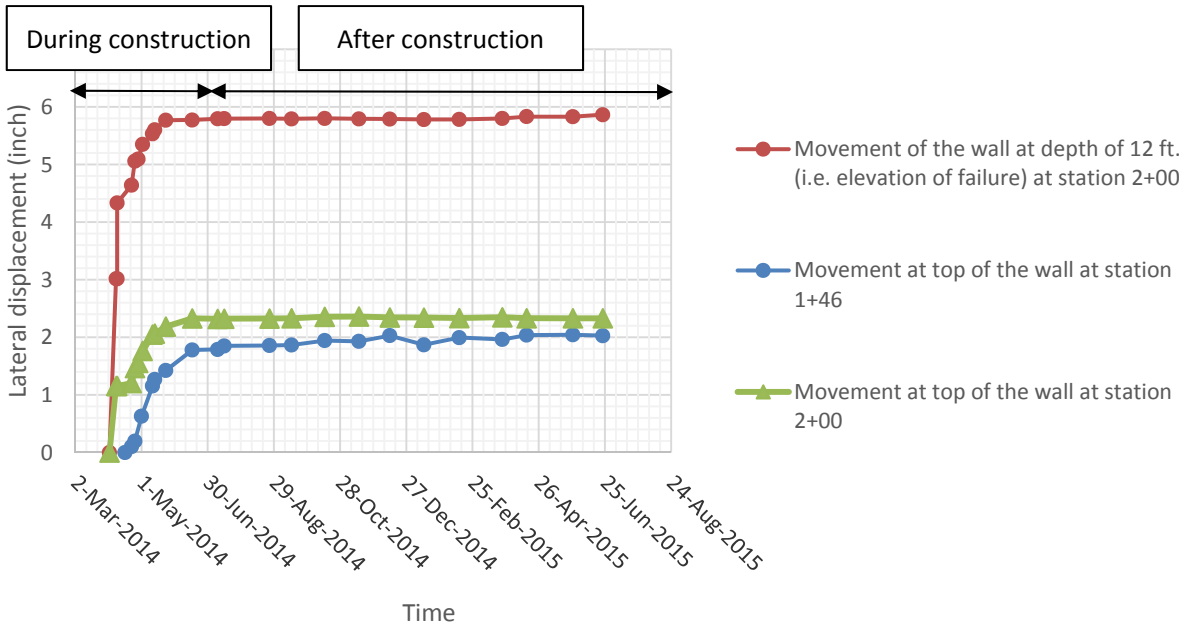

Figure 196. Movements of the Wall at Stations 2+00 and 1+46 from the Start of the Project up to 13 Months after Construction.

Tiltmeters

A tiltmeter allows the measurement of the inclination of an object. It responds to the local acceleration of gravity, *g*. The tiltmeter output is determined by the mass distribution of the earth. This instrument allows for tracking the (continuous) variation in time of the inclination at a fixed position. In this project, the tiltmeters were put inside aluminum boxes to protect them from the elements and vandalism, as shown in Figure 197.

Figure 197. Aluminum Box Used to Protect Tiltmeter.

A total of three tiltmeters were attached to the facing of the wall at station 2+00 (Figure 198) at depths of 1 ft, 5 ft, and 13 ft from the top of the wall. These tiltmeters were connected to the data acquisition system to record the change of the inclination of the wall during and after the construction. During the completion of the soil nail facing, the third tiltmeter was broken, possibly due to the pressure of the shooting shotcrete.

Figure 198. Three Tiltmeters Installed at Different Depths of the Wall.

Figure 199 and Figure 200 present the angle of inclination for the first (i.e., 1 ft from the top of the wall) and second (i.e., 5 ft from the top of the wall) tiltmeters, respectively. After the construction, the first tiltmeter showed significant variations in time, and the second inclinometer showed a significant jump at the beginning, and then stayed almost constant. This jump could be induced by the shooting of the concrete at the completion of the facing.

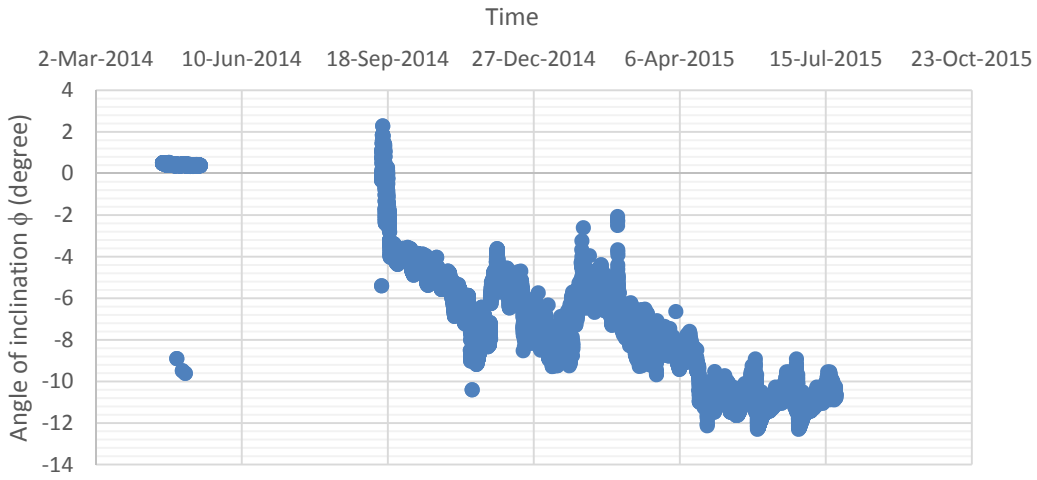

Figure 199. Inclination of the Wall versus Time for the First Tiltmeter at 1 Ft from Top of the Wall. The Tiltmeter Was Installed with an Initial Inclination of 0.490°.

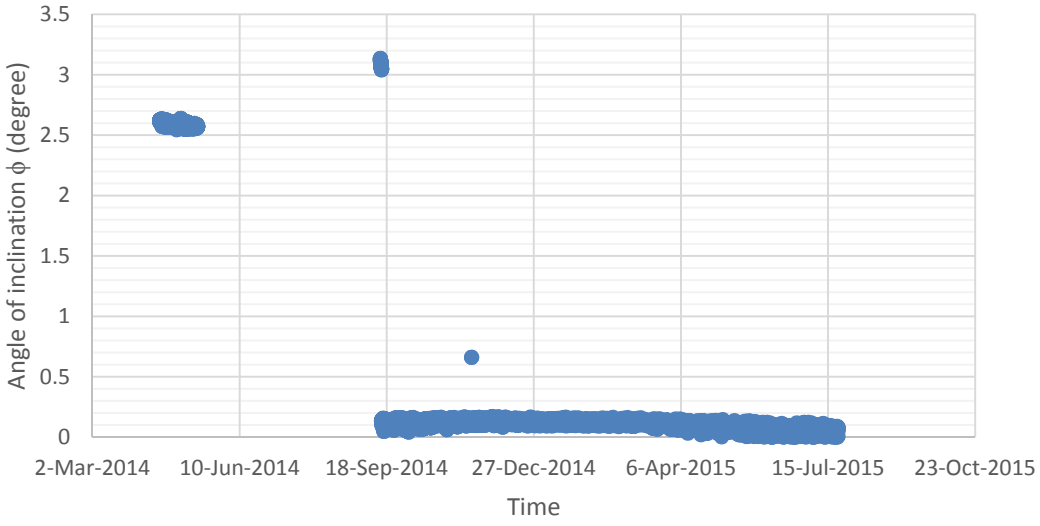

Figure 200. Inclination of the Wall versus Time for the Second Tiltmeter at 5 Ft from Top of the Wall. The Tiltmeter Was Installed with Initial Inclination of 2.615°.

Strain Gauges

The instrumented soil nails with strain gauges are used to assess the load distribution along the nails during construction (i.e., as the excavation progresses down) and wall operation. The strain gauges can provide useful information about the service load of the soil nails.

The original plan in this project was to instrument three production soil nails with foil strain gauges. After consulting with TxDOT officers and the contractor of the soil nail wall

project, the researchers concluded that it would be more convenient to install more instrumented production nails, in at least two different sections of the wall. The original plan was updated to include six additional instrumented production nails with two gauge-positions per nail. The additional instrumented nails would allow for the validation of the model results at more positions and would also introduce redundancy in the readings. The six new instrumented production nails were instrumented with VW strain gauges (i.e., Model 4150 Geokon), while the three production soil nails in the original plan were instrumented with micro-measurements foil strain gauges (i.e., Model EA-06-125VB-120).

A total of nine instrumented production nails were installed at two sections of the wall (i.e., stations 1+98 and 2+06). The preparation of the nails, their installation, and related instruments for VW and foil strain gauges are presented in the next sections.

Preparation of Instrumented Nails with Foil Strain Gauges. Three production nails were instrumented with foil strain gauges at Texas A&M University laboratories. The procedure followed to instrument these nails was the same as the one followed for the sacrificial nails, which is detailed in previous sections of this chapter. The first strain gauges were attached 2 ft behind the wall facing. The second strain gauges were attached at a distance of 5 ft from the first one. The third and fourth strain gauges were attached at equal intervals of 6 ft from the second strain gauges. Figure 201 shows the distribution of the strain gauges along the nail bars.

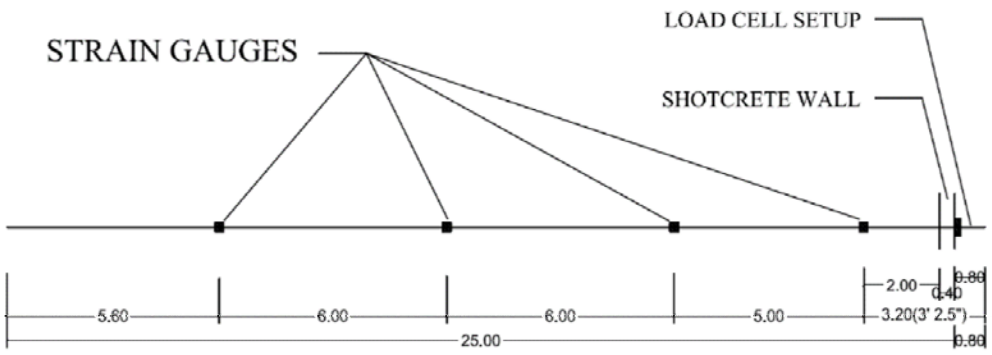

DISTRIBUTION OF STRAIN GAUGES IN PERMANENT NAILS

* UNITS ARE IN FOOT SC:Not to scale

Figure 201. Distribution of the Foil Strain Gauges along the Production Nails.

Data Acquisition System for Foil Strain Gauges. The data acquisition system was used to read and store the data gathered from the different instruments. To collect the data from the strain gauges during the construction, the data acquisition system was set up at a temporary location at the top of the wall (Figure 202) prior to the construction. After finishing the construction of the wall, the data acquisition system box was moved down to the bottom of the wall (i.e., on the ground surface). The solar panel was used to provide the power for the data acquisition system (Figure 203).

Figure 202. Temporary Location of the Data Acquisition System and Solar Panel.

Figure 203. Solar Panel for Providing Power for Data Acquisition System.

Installation of the Instrumented Nails with Foil Strain Gauges. The instrumented nails were installed at the second (i.e., 6 ft from the top of the wall), fourth (i.e., 13 ft from the top of the wall), and fifth (i.e., 16.5 ft from the top of the wall) row of the soil nails at station 2+06. Figure 204 and Figure 205 show the position of these instrumented nails on the wall profile. The height of the wall at this station is 22 ft.

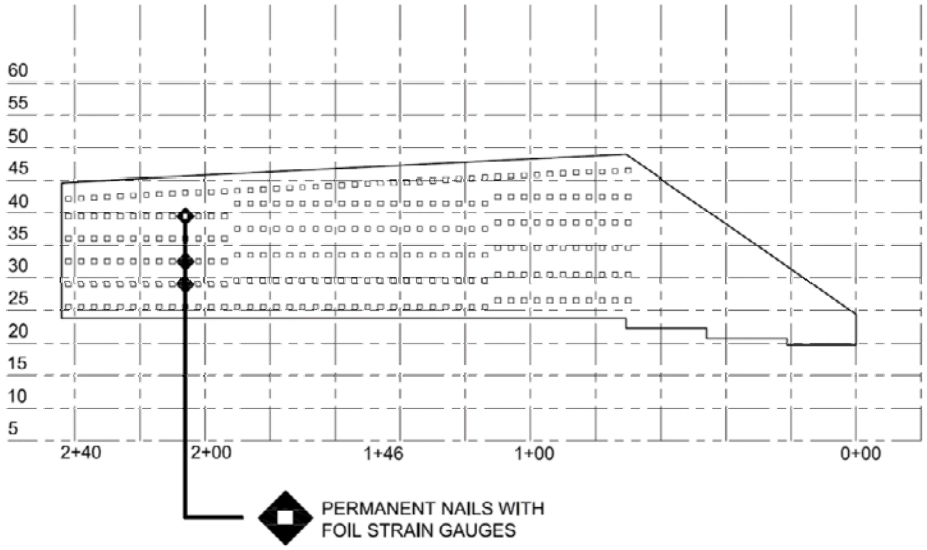

Figure 204. Positions of the Instrumented Production Nails with Foil Strain Gauges at Station 2+06.

Figure 205. Instrumented Production Nails with Foil Strain Gauges at Station 2+06.

The information provided by the strain gauges during the construction is very relevant for this research project. The following information can be obtained from the strain gauges during construction:

- Zero reading of the strain gauges (i.e., forthwith after installation while the grout is still liquid).
- Service load of the nails at different stages of construction.
- Load change in the nails due to the excavation at each stage of construction.
- Load change in the nails due to the creep during construction.
- Magnitude and location of the maximum load.

To take the readings during the construction, the strain gauge wires needed to be connected to the data acquisition system during that time. The most convenient way to conduct the wires to the temporary location of the data acquisition box was to pass them behind the shotcrete facing. Once the nails were installed, and prior to shooting the shotcrete, PVC tubes were placed in front of the excavated facing. The wires of the strain gauges were passed through the PVC pipe. Considering that at the first stage of excavation there were three instrumented nails, four PVC pipes were used, as follows: one PVC pipe was used per each set of wire gauges, and a fourth one was installed to bring all the wires from the temporary location of the data acquisition system (i.e., at the top of the wall) to the permanent location (i.e., at the bottom of the wall, on the ground surface). The PVC pipes were extended as the excavation progressed from top to bottom. Figure 206 to Figure 208 show the PVC pipes used to conduct the wires to the data acquisition system.

Figure 206. Location of the PVC Pipes to Conduct the Wires from the Strain Gauges to the Data Acquisition System, First Stage of Construction.

Figure 207. Extending the PVC Pipes to Conduct the Wires to the Data Acquisition System at the Second Stage of Construction.

Figure 208. Extending the PVC Pipes to Conduct the Wires to the Data Acquisition System at the Fourth Stage of Construction.

Monitoring Instrumented Nails with Foil Strain Gauges. The readings from the strain gauges during and after the construction were recorded continuously every 30 minutes. Figure 209 to Figure 211 shows the service load in the nails during the construction. The foil strain gauges at three production nails did not last for a long time and failed.

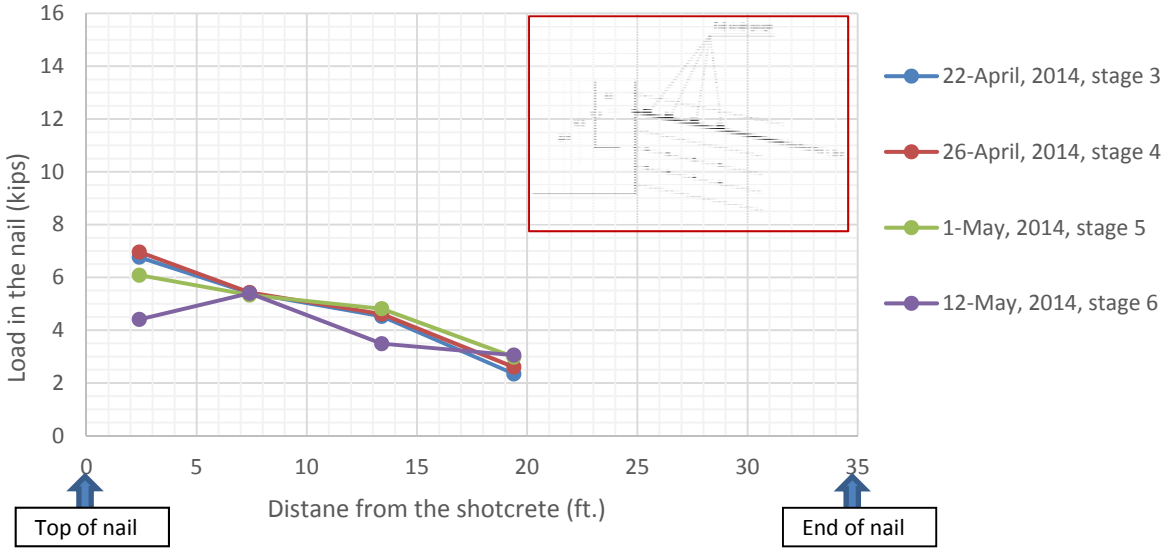

Figure 209. Load Distribution along the Instrumented Production Nail in Second Row of the Soil Nail Wall (Nail 35 Ft Long).

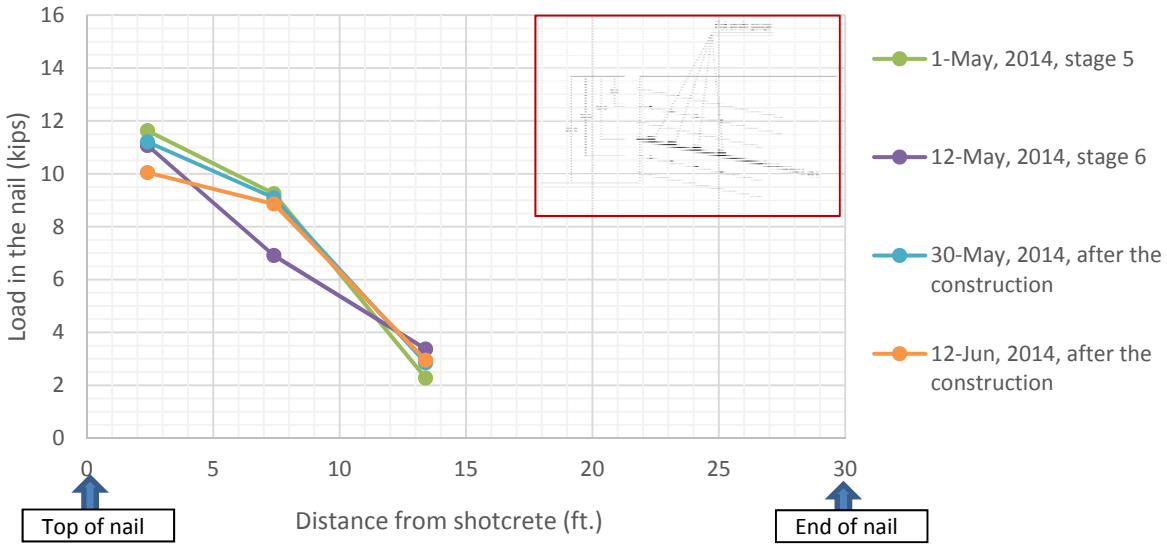

Figure 210. Load Distribution along the Instrumented Production Nail in Fourth Row of the Soil Nail Wall (Nail 30 Ft Long).

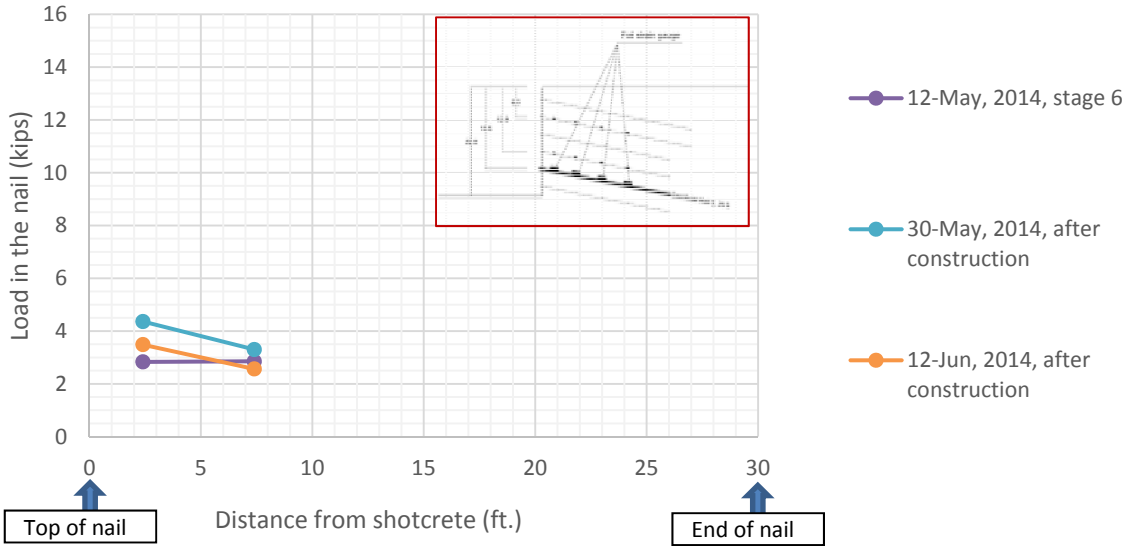

Figure 211. Load Distribution along the Instrumented Production Nail in Fifth Row of the Soil Nail Wall (Nail 30 Ft Long).

As shown in Figure 209, the first instrumented production nail was installed at the second stage of construction. The third and fourth strain gauges in the nail at the fifth row were broken during the nail installation. In Figure 209 to Figure 211, a significant portion of the nail load took place at the excavation stage performed just after the installation of the nail.

The instrumented production nails at the three planned positions were installed at the same height as the sacrificial nails. Table 29 presents the results of the pullout tests on the

sacrificial nails, along with the service load on the nails. The service load on the nails is always less than 60 percent of the design load and less than 22 percent of the maximum pullout capacity of the nails.

Table 29. Comparison of Service Load, Design Load, and Maximum Pullout Capacity.

Instrumented Nails with Foil Strain Gauges				
Nail No.	**Length of the nail (ft)**	**Maximum pullout capacity from load test (kips)**	**Design load (kips)**	**Maximum service load in the nail (kips)**
Nails in second row	35	63	21	7
Nails in fourth row	30	56	18	12
Nails in fifth row	30	72	18	5

The service load obtained from the strain gauge readings is used in Chapter 7 to validate the numerical model proposed in this research.

Preparation of the Instrumented Nails with VW Strain Gauges. Considering that the contractor had a prior successful experience at monitoring a soil nail wall in this type of soil (i.e., HP clay) and that none of the VW strain gauges (Model 4150 Geokon) failed during the monitoring in previous projects, the research team decided to attach two VW strain gauges (Model 4150 Geokon) to each nail bar. Figure 212 shows the distribution of the VW strain gauges along the nail bars. The first and second strain gauges were welded at 2.5 ft and 15 ft from the top of the nail bar, respectively.

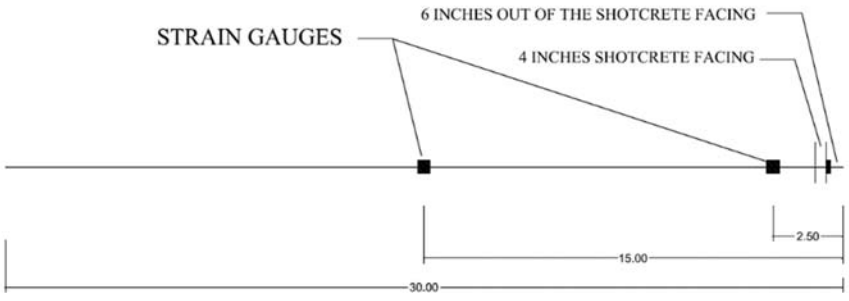

Figure 212. Distribution of the VW Strain Gauges along the Nail Bar.

The instruments and accessories related to the six additional production nails were purchased on March 12, 2014, as follows:

- VW strain gauge with plucking coil and cover plate (Geokon Model 4150).
- MICRO-800 Datalogger with integral multiplexer (16 VW + 16 thermistors).
- LoggerNet software and starter data logger program.
- Solar panel, 20 W.
- Rental spot welder.
- Rental VW readout (i.e., GK-404).

The VW strain gauges were welded to the nail bars on March 21, 2014, at the warehouse located at the Hayward Baker headquarters in Dallas. The step-by-step procedure for attaching the strain gauges is as follows:

- Grind down the ribs of the nail bar at the designated locations with an electric grinder (Figure 213).
- Weld the gauges to the nail bars with the spot welder (Figure 214).
- Test the gauges before installing the aluminum cover (Figure 215).
- Install the aluminum cover (Figure 216).

Figure 213. Grinding Nail Bars at Designated Position with Electric Grinder.

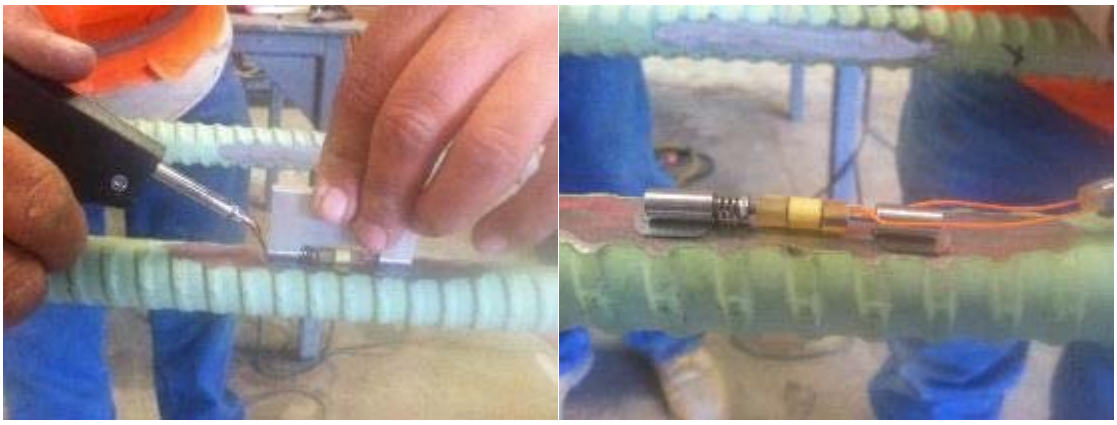

Figure 214. Welding the Gauges to the Nail Bars with Spot Welder.

Figure 215. Testing the Gauges before Installing the Aluminum Cover.

Figure 216. Installing the Aluminum Cover.

After shipping the instrumented nails to the site, and making sure that none of the strain gauges had failed during transportation or installation at the site, a plastic tube was placed around the bar. The gap between the tube and bar was filled with a grout. The cross section and final view of the instrumented nails are shown in Figure 217 and Figure 218, respectively.

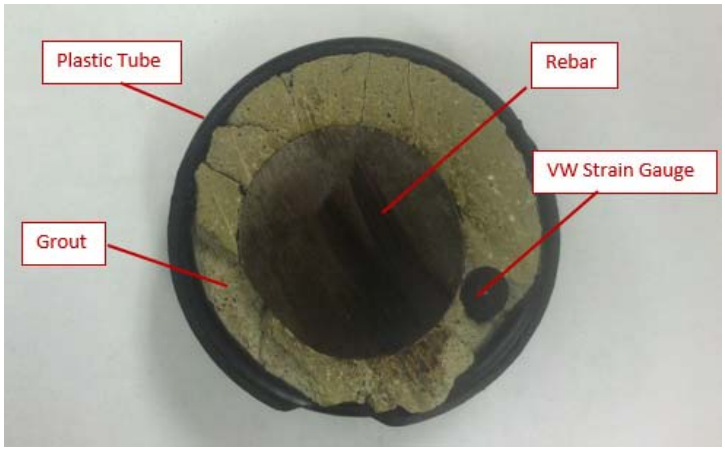

Figure 217. Cross Section of the Instrumented Nail.

Figure 218. Final View of the Instrumented Nails.

Data Logger for VW Strain Gauges. The MICRO-800 data logger was used to read the data from the instrumented nails with VW strain gauges. The data logger was programmed at Texas A&M University and installed at the temporary location at the top of the wall at station 2+00. After construction of the wall, the data logger was moved to the permanent location at the bottom of the wall at station 2+00. Figure 219 shows the temporary location of the data logger. To provide the power for the data logger, a 20 W solar panel was installed next to the data logger (Figure 220).

Figure 219. Data Logger Box at the Temporary Location Top of the Wall at Station 2+00.

Figure 220. Solar Panel Installed next to the Data Logger at the Temporary Location at Station 2+00.

Installation of the Instrumented Nails with VW Strain Gauges. The instrumented nails with VW strain gauges were installed at all the rows (i.e., rows 1, 2, 3, 4, 5, and 6) at station 1+98. Figure 221 and Figure 222 show the locations of these nails on the wall profile. The height of the wall at this station is 22 ft.

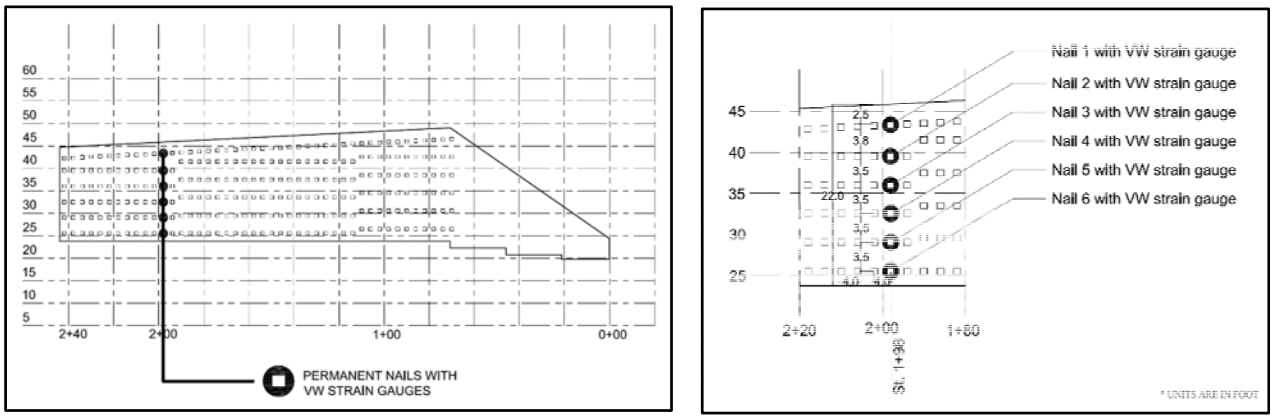

Figure 221. Location of the Instrumented Nails with VW Strain Gauges on Wall Profile at Station 1+98.

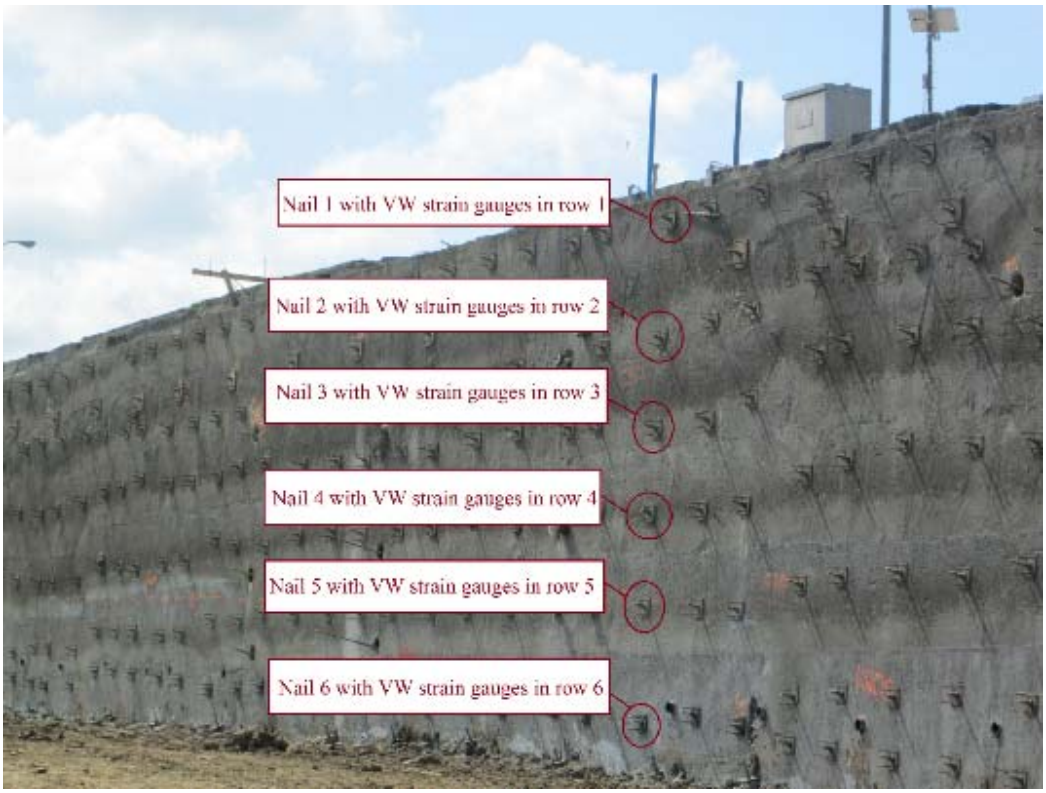

Figure 222. Location of the Instrumented Nails with VW Strain Gauges on Wall Profile at Station 1+98.

During the construction, the wires of each instrumented nail were connected to the data logger. The wires were passed through the PVC pipes behind the shotcrete facing in the same way as for the instrumented nails with foil strain gauges. Since there are six instrumented nails with VW strain gauges, seven PVC pipes were placed in front of the excavation facing at the first stage of the construction (Figure 223 and Figure 224). Six PVC pipes were used to conduct the

wires of the six instrumented nails to the temporary location of the data logger, while the seventh PVC pipe was used to conduct all the wires of the six instrumented nails from the temporary location of the data logger (i.e., the top of the wall at station 2+00) to the permanent location of the data logger (i.e., the bottom of the wall at station 2+00).

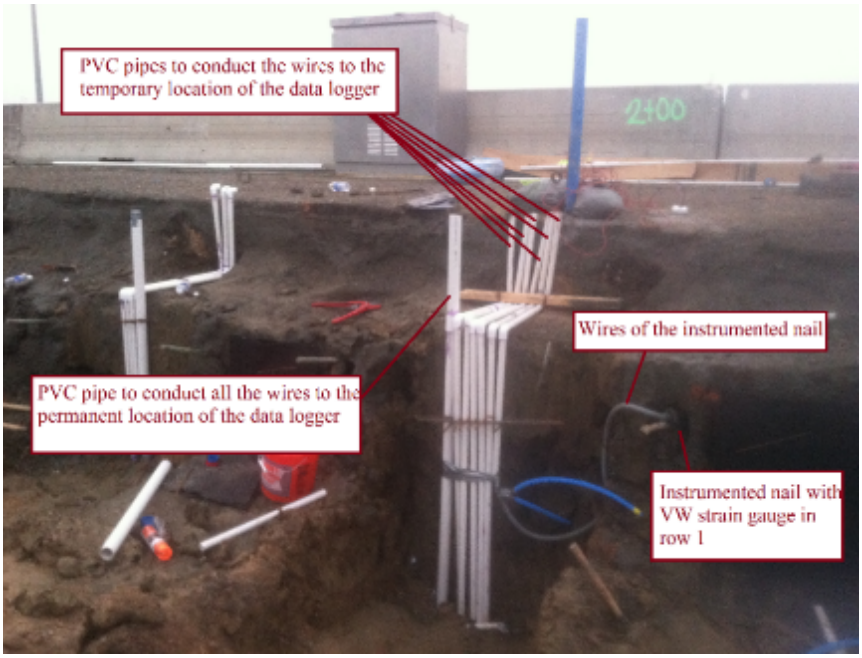

Figure 223. PVC Pipes to Conduct the Wires to the Data Logger at First Stage of Construction at Station 2+00.

Figure 224. PVC Pipes to Conduct the Wires to the Data Logger at Fourth Stage of Construction at Station 2+00.

Monitoring the Instrumented Nails with VW Strain Gauges. The reading intervals adopted for the VW strain gauges were the same as for the foil strain gauges. During the construction, the readings were recorded every 30 minutes. The zero readings were taken immediately after the installation of the nails. Figure 225 to Figure 230 show the load distribution along the nails in each stage of construction.

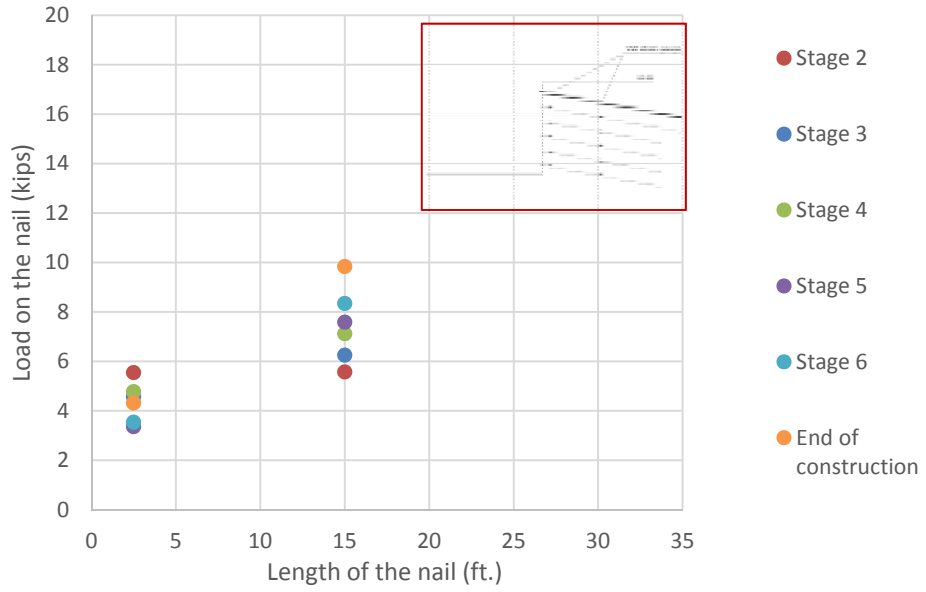

Figure 225. Load Distribution along the Instrumented Nail at First Row of Soil Nails from Top, VW Strain Gauge Readings.

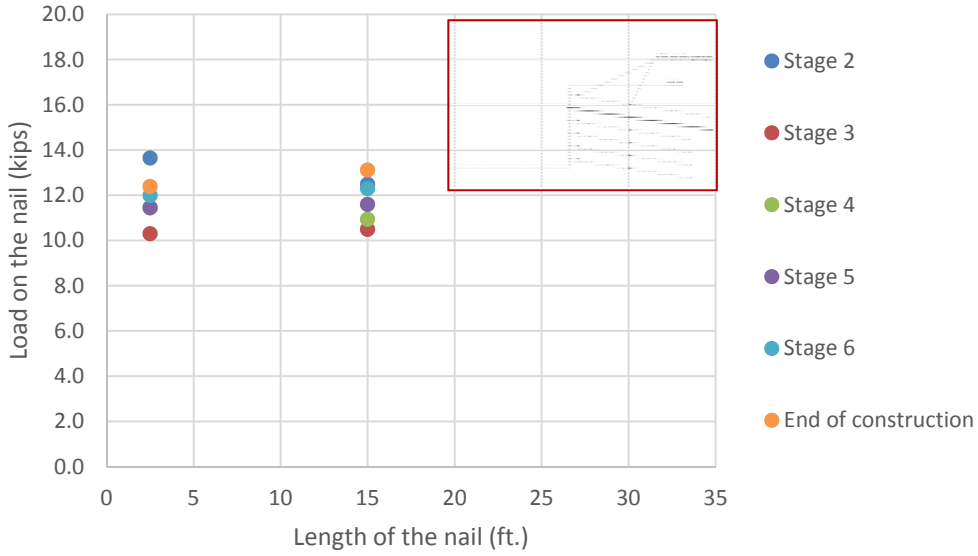

Figure 226. Load Distribution along the Instrumented Nail at Second Row of Soil Nails from Top, VW Strain Gauge Readings.

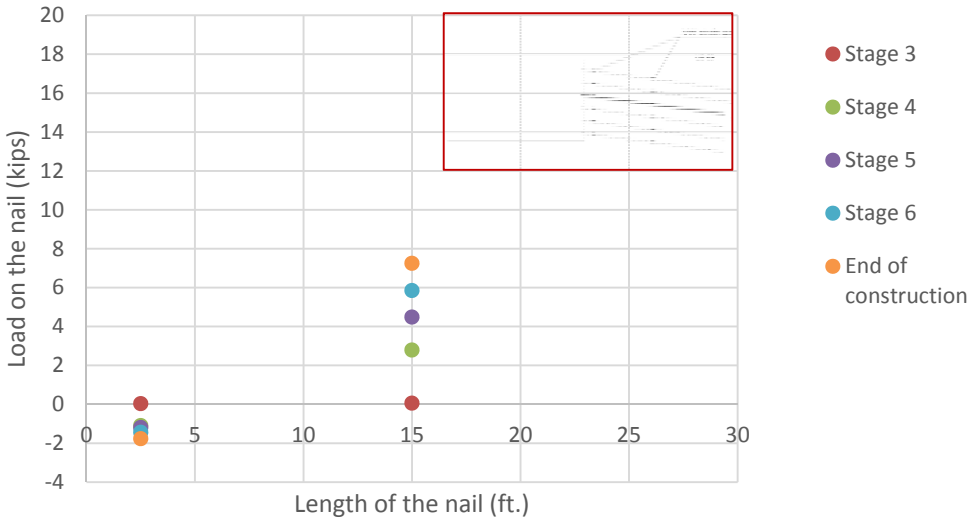

Figure 227. Load Distribution along the Instrumented Nail at Third Row of Soil Nails from Top, VW Strain Gauge Readings.

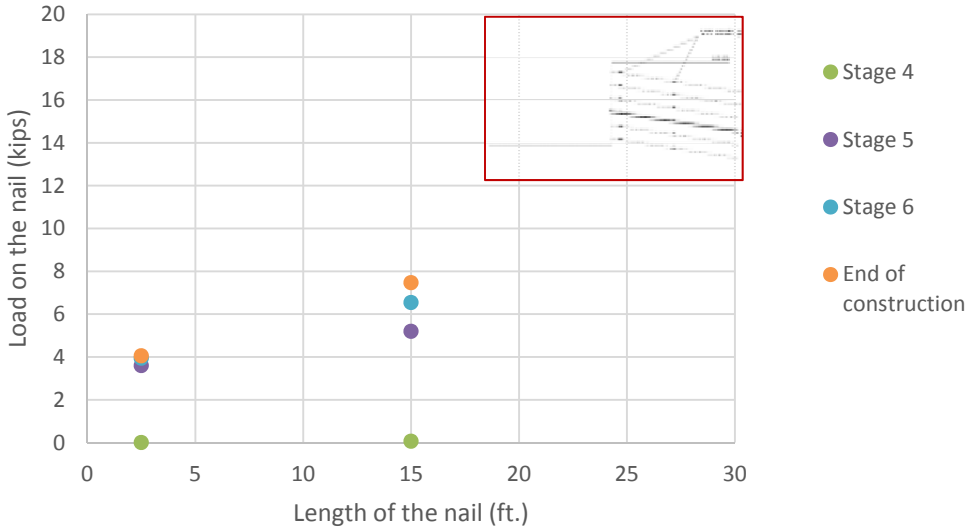

Figure 228. Load Distribution along the Instrumented Nail at Fourth Row of Soil Nails from Top, VW Strain Gauge Readings.

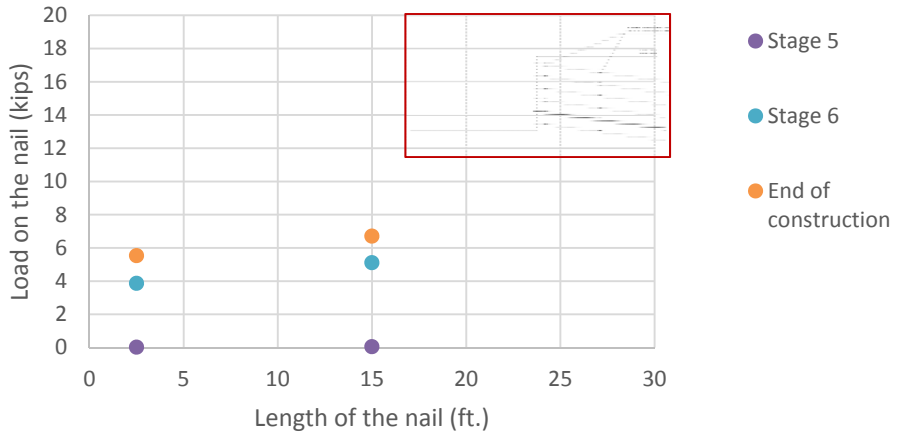

Figure 229. Load Distribution along the Instrumented Nail at Fifth Row of Soil Nails from Top, VW Strain Gauge Readings.

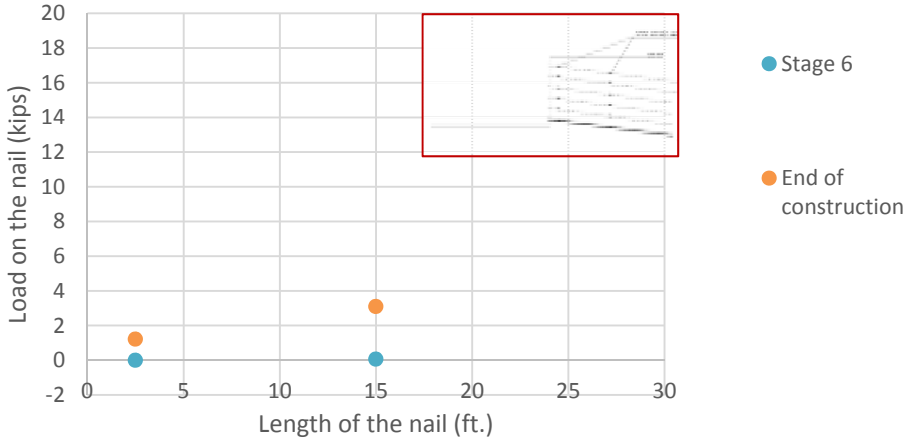

Figure 230. Load Distribution along the Instrumented Nail at Sixth Row of Soil Nails from Top, VW Strain Gauge Readings.

During the construction, only the first strain gauge (i.e., at 2.5 ft from the head of the nail) in the third row was broken. In each nail, a significant portion of the service load took place during the subsequent excavation. Considering that after the second stage of construction, one row of pretensioned nails was installed in the middle of the first and second rows, the load in the first strain gauges (i.e., at 2.5 ft from the head of the nail) in the first and second production nails decreased in each stage. For instance, in the first position of nail 1 (i.e., first row of the soil nails), at stage 2 the load was 5.5 kips, while after the installation of the pretensioned nails the service load dropped to 4.6 kips. Table 30 presents the summary of the service load in each stage of construction.

Table 30. Summary of the Service Load in the Nails at Each Stage of Construction.

Stage	Load in Nail 1 (kips)		Load in Nail 2 (kips)		Load in Nail 3 (kips)		Load in Nail 4 (kips)		Load in Nail 5 (kips)		Load in Nail 6 (kips)	
	2.5 ft from nail head	15 ft from nail head	2.5 ft from nail head	15 ft from nail head	2.5 ft from nail head	15 ft from nail head	2.5 ft from nail head	15 ft from nail head	2.5 ft from nail head	15 ft from nail head	2.5 ft from nail head	15 ft from nail head
2	5.5	5.6	13.6	12.5	-	-	-	-	-	-	-	-
3	4.6	6.2	10.3	10.5	0.0	0.1	-	-	-	-	-	-
4	4.8	7.1	11.4	10.9	−1.1	2.8	0.0	0.1	-	-	-	-
5	3.4	7.6	11.5	11.6	−1.2	4.5	3.6	5.2	0.0	0.1	-	-
6	3.5	8.3	12.0	12.3	−1.4	5.8	3.9	6.5	3.9	5.1	0.0	0.1
End of construction	4.3	9.8	12.4	13.1	−1.8	7.3	4.1	7.5	5.5	6.7	1.2	3.1

Broken strain gauges during construction

Following a similar strategy as during construction, the readings during wall operation were taken every 30 minutes. After the construction, only the second strain gauge in the sixth nail was broken. Figure 231 to Figure 236 present the service load in the nails just after construction and after one year of operation.

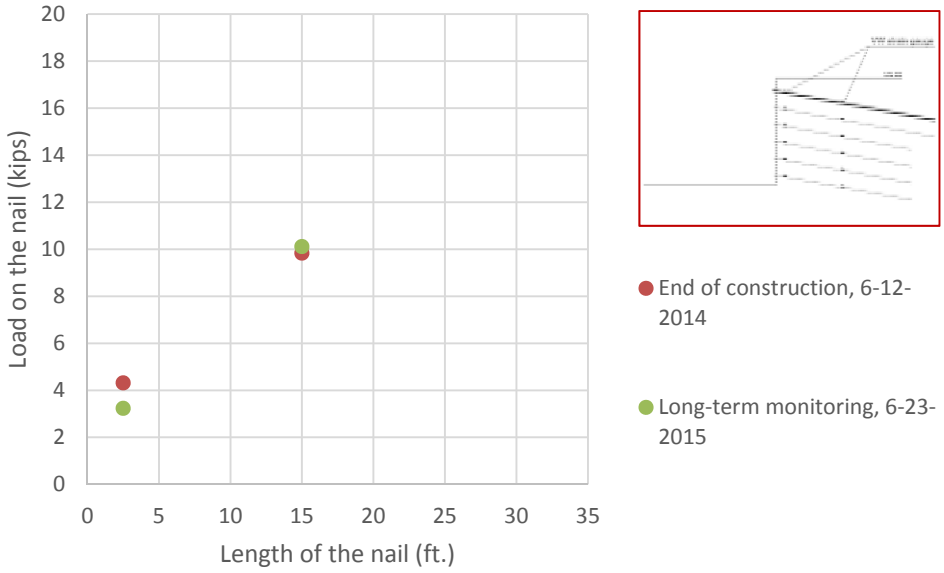

Figure 231. One Year Post-Construction Monitoring, Load Distribution along the Instrumented Nail at the First Row of the Soil Nails from the Top.

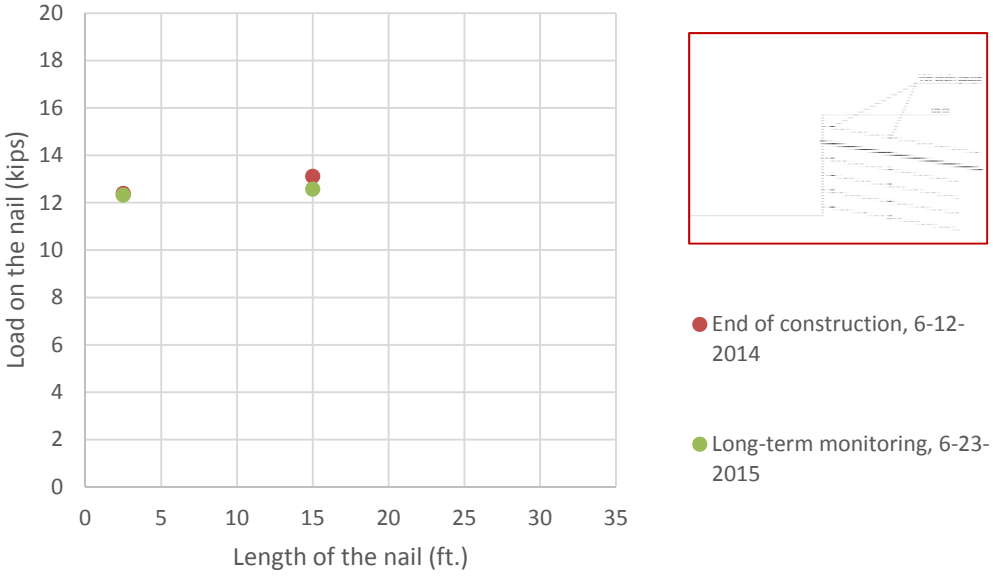

Figure 232. One Year Post-Construction Monitoring, Load Distribution along the Instrumented Nail at the Second Row of the Soil Nails from the Top.

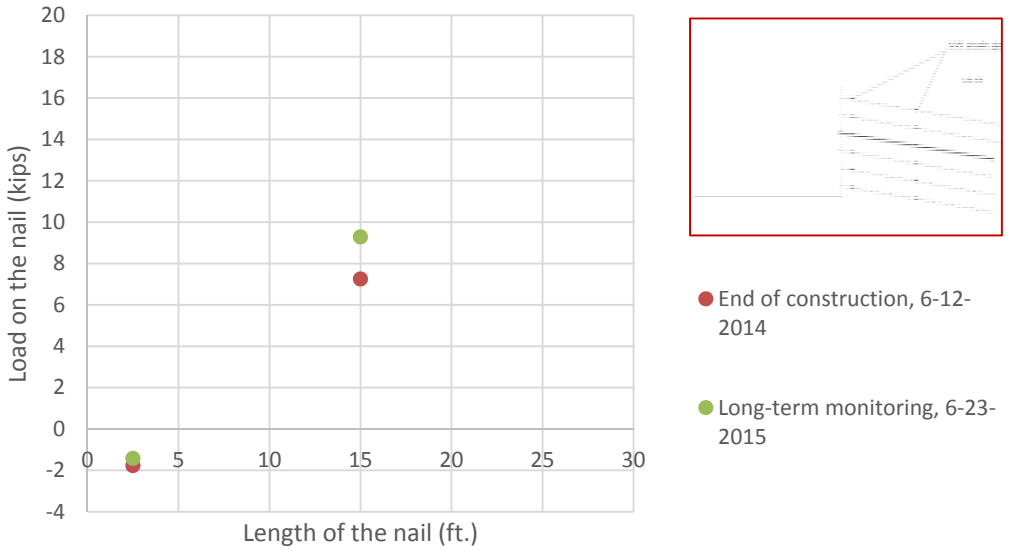

Figure 233. One Year Post-Construction Monitoring, Load Distribution along the Instrumented Nail at the Third Row of the Soil Nails from the Top.

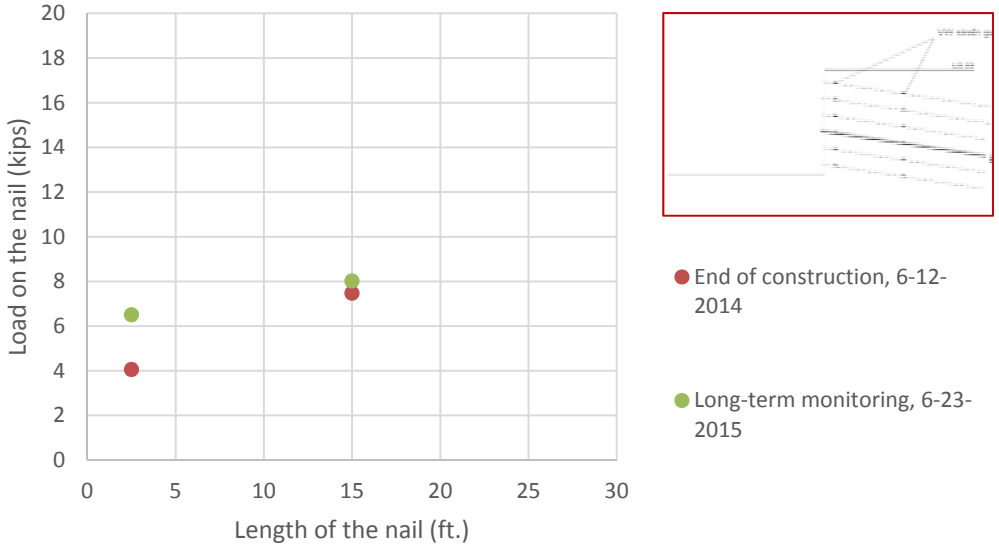

Figure 234. One Year Post-Construction Monitoring, Load Distribution along the Instrumented Nail at the Fourth Row of the Soil Nails from the Top.

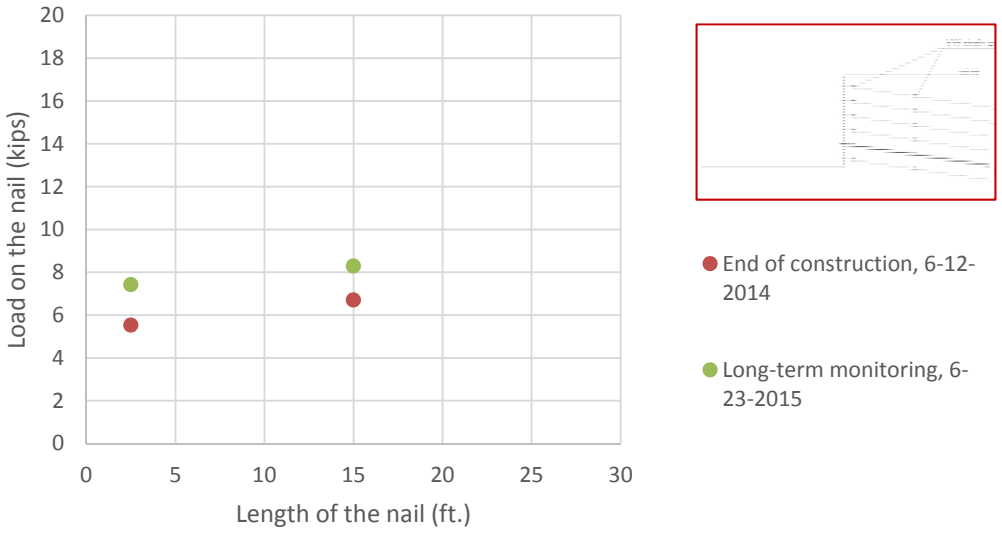

Figure 235. One Year Post-Construction Monitoring, Load Distribution along the Instrumented Nail at the Fifth Row of the Soil Nails from the Top.

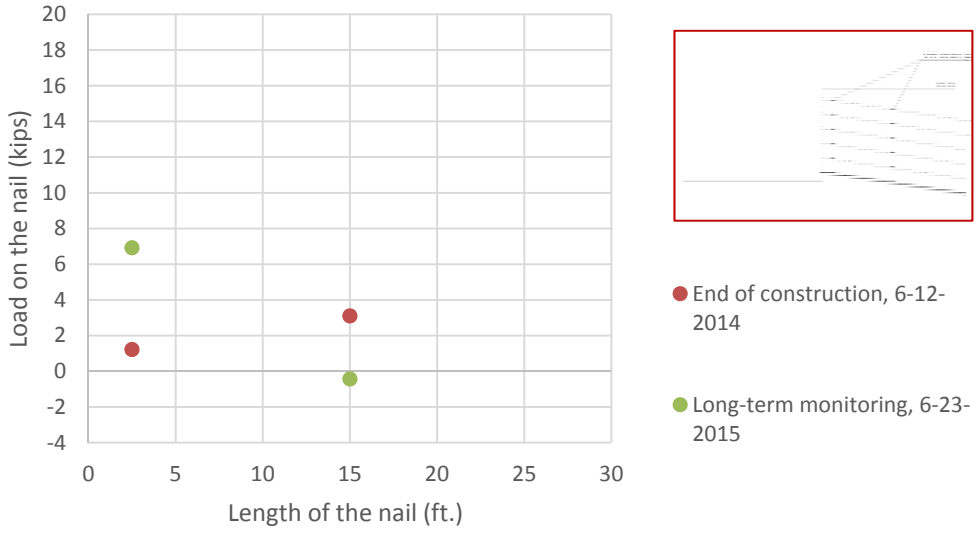

Figure 236. One Year Post-Construction Monitoring, Load Distribution along the Instrumented Nail at the Sixth Row of the Soil Nails from the Top.

As explained in previous sections, the soil nail wall showed additional lateral displacements after the construction induced by creep. As a consequence of these movements, additional stresses developed in the nails (FHWA, 2003). Since after the second stage of construction pretensioned nails were installed and the service load in the first two rows dropped by a minimum of 12 percent, these nails do not show additional load after one year of

monitoring. In other words, these nails were loaded to the higher load (i.e., due to the excessive deformation at the second stage of construction) and then reloaded (i.e., due to the installation of the pretensioned nails in between rows 1 and 2). In addition, the pretensioned nails took the additional load induced by the post-construction movement of the wall. In the other nails (i.e., rows 3 to 6), it is clear that the service load in the nails increased because of the creep movements of the wall during operation. Table 31 summarizes the additional load in the nails induced by the post-construction (creep) movements of the wall.

Table 31. Service Load in the Nails at End of Construction and One Year after End of Construction.

Instrumented Nails with VW Strain Gauges				
Nail No.	**Design load (kips)**	**Max. load at the end of construction (kips)**	**Max. service load one year after construction (kips)**	**Percentage of the additional load in the nails due to the creep (%)**
Nail in first row	21	9.8	10.11	3
Nail in second row	18	13.11	12.57	-
Nail in third row	18	7.25	9.28	28
Nail in fourth row	18	7.47	8.01	7
Nail in fifth row	18	6.7	8.3	24
Nail in sixth row	18	1.2	6.9	575

Considering that after the last stage of the construction (i.e., stage 6) there is no further excavation, the service load in these nails were almost zero at the end of the construction. The maximum additional load in the nails induced by creep movements of the soil nail wall was less than 30 percent of the service load. However, even with the additional load in the nails due to the creep behavior of the soil nail wall, the service load of the nails for a period of one year after the construction is less than 80 percent of the design load of the nails and less than 22 percent of the maximum pullout capacity.

The results of this instrumentation are used in Chapter 7 to validate the numerical model adopted in this research project and to perform the parametric study of the soil nail wall.

Load Cell at the Nail Head

Load Cell Setup. The load cells were used to learn about the load at the nail head during the monitoring period. Three load cells were installed at the top of the three instrumented nails with foil strain gauges. Figure 237 shows the setup of the load cell at the nail head (FHWA, 1998a).

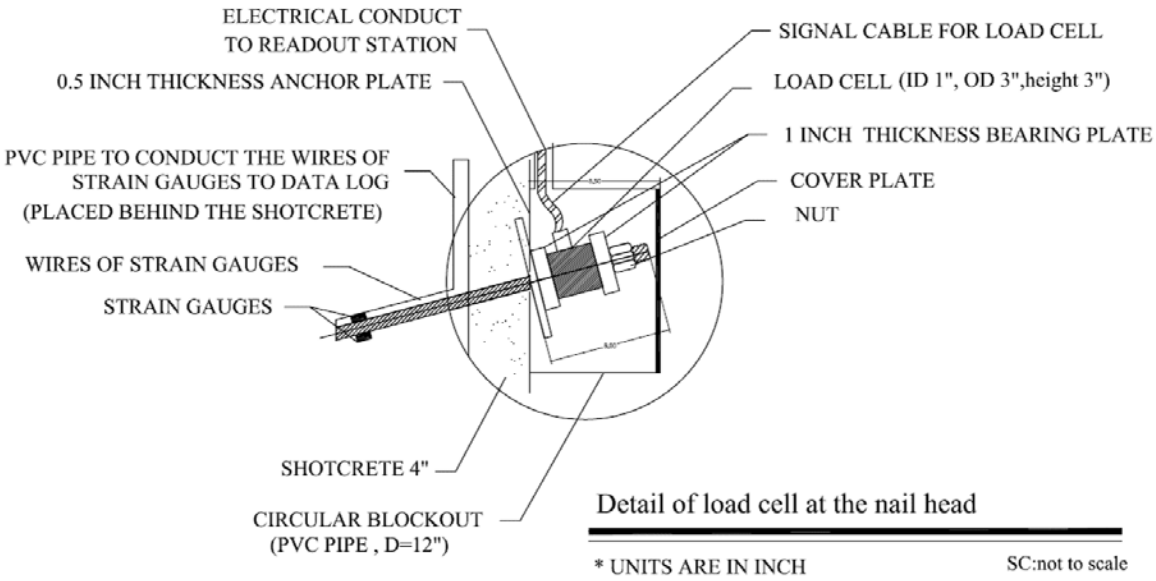

Figure 237. Details of the Load Cell at the Nail Head.

The step-by-step procedure to install the load cell at the nail head is as follows:

- Leave about 8 in. of the designated nail bar (instrumented nails with foil strain gauges) out of the shotcrete facing.
- Place an anchor plate (1 in.) bearing plate, load cell, and a (1 in.) bearing plate at the nail head (Figure 238).
- Cut a 12-in. diameter PVC pipe and place it at the top of the nail in a way that the load cell is located at the middle of the PVC pipe (Figure 239).
- Drill a hole at the bottom surface of the PVC pipe to conduct the load cell cable.
- Place a cover plate at the top of the PVC pipe (Figure 240a).

- Seal a gap between the PVC pipe and the shotcrete facing (Figure 240b).
- Install a PVC pipe at the instrumented section (i.e., station 2+06) to conduct the wires to the bottom of the wall (Figure 241).

Figure 238. Load Cell Setup at the Nail Head.

Figure 239. 12-In.-Diameter PVC Tube around the Load Cell Setup.

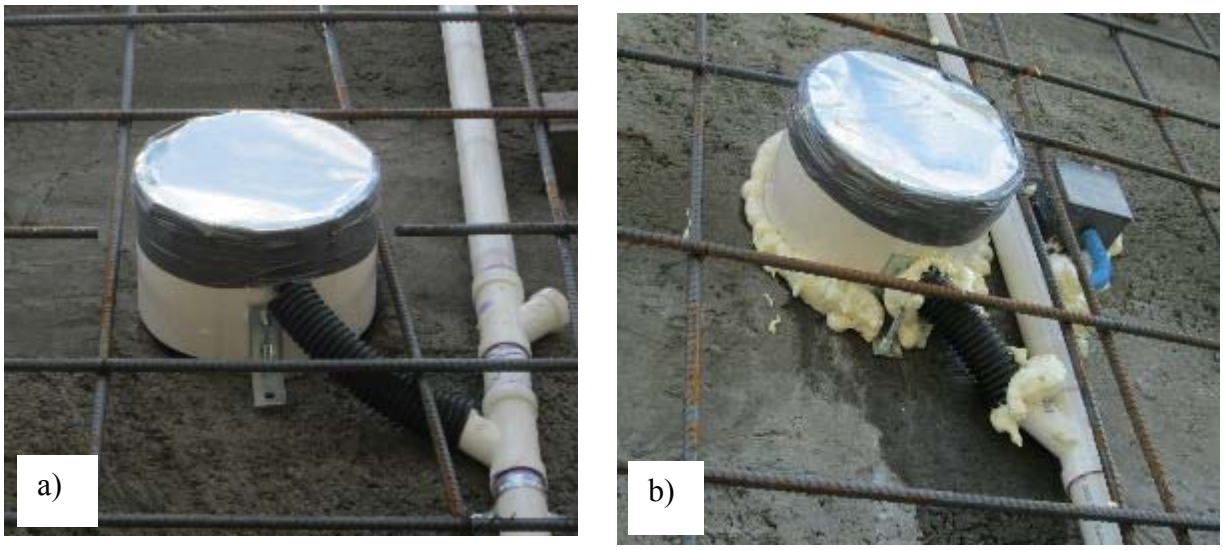

Figure 240. a) Cover Plate at Top of the PVC Tube; and b) Seal the PVC Pipe to the Shotcrete Facing.

Figure 241. Pipes Used to Conduct the Load Cell Cables to the Ground.

Monitoring the Load Cells. Since the load cell was placed in front of the shotcrete (i.e., at top of the nail), it was not possible to connect the load cells to the data acquisition system during the construction. The zero readings for each load cell were taken after the installation. After the construction, the load cells were connected to the data acquisition system and the data were recorded every 30 minutes. Figure 242 shows the service load at the nail head obtained from the load cells for a period of one year after the construction. From the results of the load cells, it is concluded that the load at the nail head remains constant even though the service load along the nail increased.

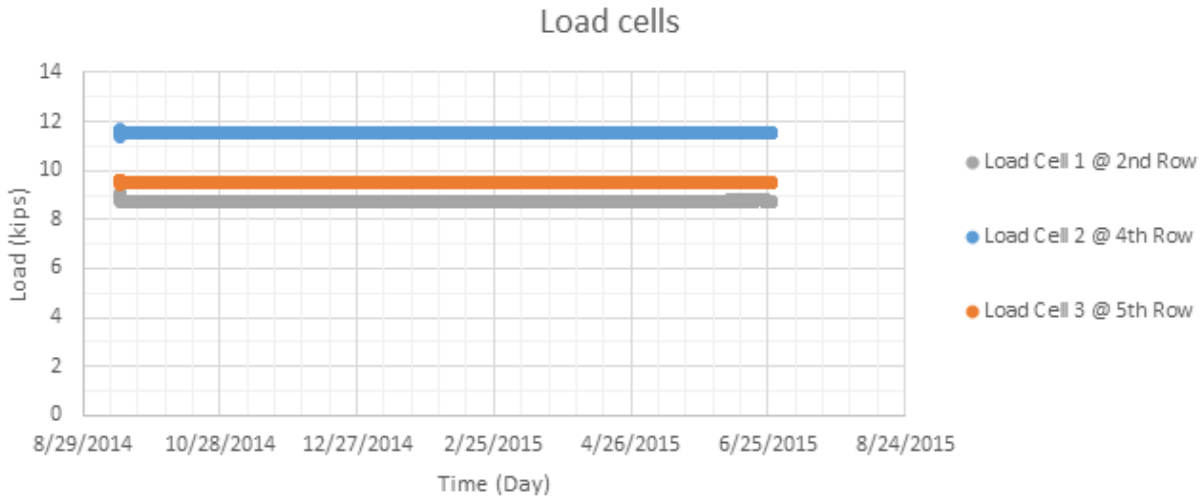

Figure 242. The Service Load at the Nail Head for Three Instrumented Nails in Second, Fourth, and Fifth Row of the Soil Nails.

Water Content Probes

To monitor the seasonal variation of water content of the embankment soil, five water content probes (i.e., Decagon 5TE VWC+Temp+EC) were installed at different heights of the wall at station 2+00. Figure 243 shows the location of the probes at station 2+00.

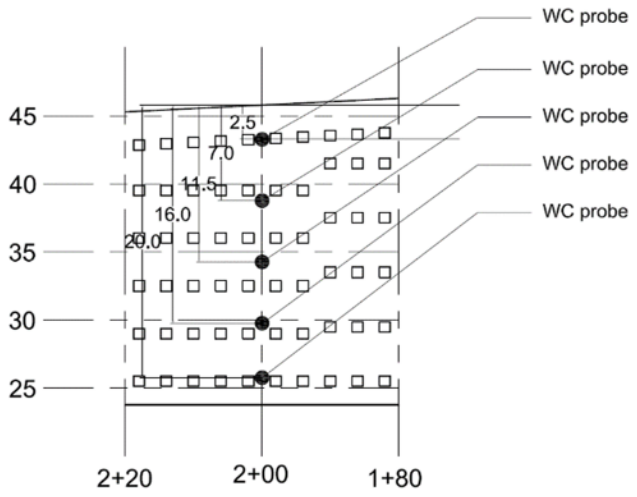

Figure 243. Distribution of the Water Content Probes on the Wall at Station 2+00.

The water content probes were installed at different stages of construction. The wires of these probes were passed through the PVC pipe together with the wires of VW strain gauges in each stage of construction. The wires related to the water probes were connected to the data logger. Data were recorded every 30 minutes during and after construction. Figure 244 shows the water content probe and the data logger (i.e., EM50 ECH$_2$O logger).

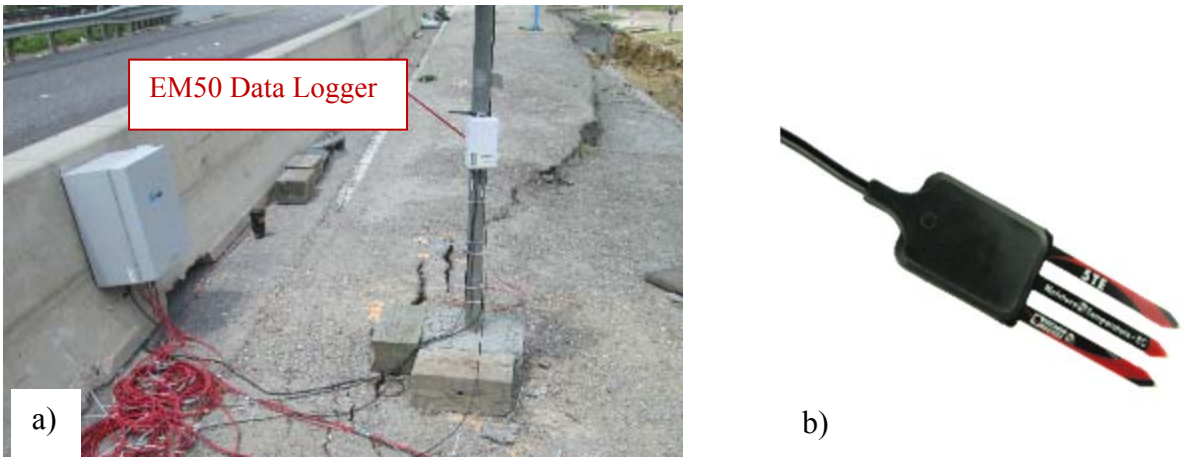

Figure 244. a) EM50 Data Logger; and b) Water Content Probe.

Figure 245 shows the variation of the water content of the embankment during construction and after one year of operation. During the construction (i.e., from April to June),

the water content of the embankment increased at depths of 4 and 12 ft by 5 percent and at the depth of 8 ft by almost 6 percent.

For the period of July and August 2014, the probes did not record any data, but by interpolating the data, it seems that the embankment soil started to dry out so the water content decreased by almost 4 percent. Again, the probes did not record any data for January 2015, but it is clear that the water content started to increase. The fluctuation of the moisture content of the embankment soil is around 4 percent to 5 percent during the wet season and dry season.

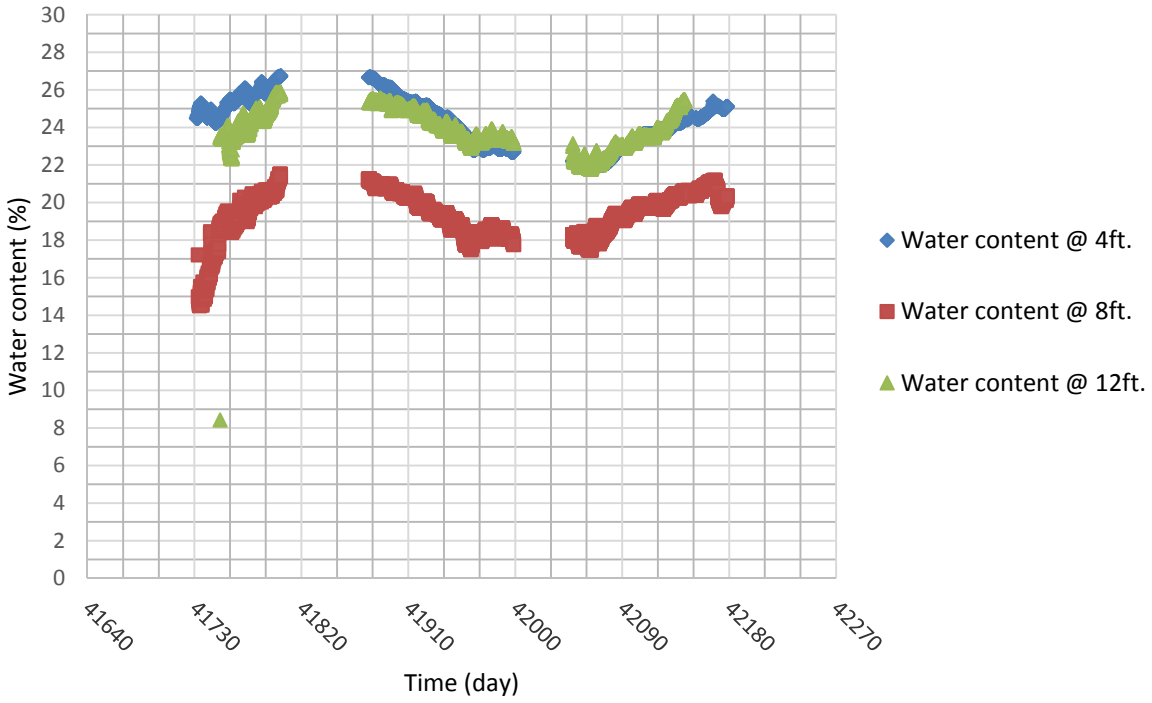

Figure 245. Variation of the Water Content of the Embankment during and One Year after the Construction.

SUMMARY AND CONCLUSIONS

The research team, in collaboration with TxDOT officials, selected an emergency slope repair in the Beaumont District to monitor the time-dependent behavior of the soil nail wall in HP clays. The PI of the embankment fill is around 50. This implies that this project is very well suited for the field tests and monitoring campaign planned in this project. Inclinometer casings and tiltmeters were installed to track the wall deflections over time. A total of nine production nails were instrumented and installed at two different sections. Three of those nails were

instrumented with load cells at the nail head. Water content probes were installed at different depths. Furthermore, six sacrificial nails were installed at three different depths. Three of them were instrumented with foil strain gauges. Verification and modified creep test protocols were adopted for testing the sacrificial nails.

The following conclusions can be obtained from the instrumentation of the soil nail wall at the Beaumont project:

- After studying the actual service loads measured in the field, the FS for the design of the bond stress at the top of the soil nail wall was 2.5 (i.e., maximum friction between the grout and the surrounding soil is 2.5 times the design friction between the grout and the surrounding soil), while for the nails at the bottom of the wall the FS was around 4.
- For the tested sacrificial nails at the Beaumont project, creep rate increased with the load level. The creep rate was significantly below the acceptance criteria for the load and less than failure load. At the failure load, creep rate increased and the tested nail failed.
- The maximum lateral displacement took place at the top of the wall and decreased toward the toe of the wall. The maximum horizontal displacement at the top of the wall at station 1+46 was 1.85 in. at the sixth stage of construction, which is 0.006 times the height of the wall (i.e., 25 ft).
- The deformation of the wall at station 2+00 for the post-construction monitoring (i.e., due to the creep of the soil nail wall) is less than 0.08 in., while the deformation of the wall at station 1+46 is less than 0.2 in., which is 10 percent of the deformation observed soon after construction.
- The service load in the nails is less than 60 percent of the design load and less than 22 percent of the maximum pullout capacity of the nails.
- In each nail, a significant portion of the service load took place just after the subsequent excavation.
- The soil nail wall exhibited extra lateral displacements after the construction (i.e., induced by creep). As a result of this movement, additional loads were developed in the nails.
- The maximum additional load in the nails due to the creep movements of the soil nail wall after one year was less than 30 percent of the service load. However, even

considering this additional creep load in the nail, the service load of the nails for a period of one year after the construction was around 80 percent of the design load of the nails, and less than 22 percent of the maximum pullout capacity.

- From the results of the water content probes, the variation of the moisture content of the embankment soil oscillated around 4 percent to 5 percent between the wet season and dry season.

CHAPTER 6:
LABORATORY TESTS

INTRODUCTION

This chapter presents the laboratory tests performed in the context of this research project. Two different HP clays with PI above 15 were studied in this research, as follows: 1) samples from the NGES-TAMU clay site, and 2) samples from the Beaumont TxDOT site. Two additional soils, adopted as reference materials, were also investigated: a low PI clay and sand from TTI.

The laboratory tests are organized into three groups: index soil properties, soil strength, and creep behavior. All the laboratory experiments were performed according to the test manuals available on the TxDOT website, http://onlinemanuals.txdot.gov/manuals/. For those tests not contemplated in the TxDOT manual, the ASTM standards were followed, and the corresponding source information can be found in the References.

This chapter includes five sections. The second section presents the laboratory tests performed on high PI clay from the Beaumont field site. The third section describes in detail the laboratory tests performed on high PI clay from the NGES-TAMU clay site. The fourth section focuses on the laboratory tests performed on the low PI clay and the dry sand. The final section presents the conclusions from this chapter.

LABORATORY TESTS ON HIGH PI CLAY FROM BEAUMONT FIELD SITE

In total, two boreholes were drilled at Beaumont field site to collect soil samples for laboratory tests (i.e., B1 and B2). Soil samples were collected from five different depths: 3 to 5 ft, 8 to 10 ft, 13 to 15 ft, 23 to 25 ft, and 33 to 35 ft. All the samples were collected using the Shelby tube sampling method. The dimensions of the samples were 7 in. long and 2.75-in. diameter.

The laboratory tests were organized into three groups:

- Soil properties.
- Soil strength.
- Creep behavior.

Because of limitation in the number of the soil samples, the soil samples primarily were used for triaxial unconsolidated undrained (UU) tests and direct shear tests. The leftovers of the soil samples from preparing the samples for the triaxial UU test and the direct shear test were used to perform Atterberg's limits and water content tests. Density and unit weight tests were obtained directly from the test samples.

Soil Properties

Water content (TxDOT Tex-103-E, 1999), unit weight (ASTM D7263, 2009), the determination of the degree of saturation, and Atterberg's limits (TxDOT Tex-104-E, 1999; TxDOT Tex-105-E, 1999) are included in this section. The tests results are presented separately in the sections that follow.

Water Content

Table 32 and Figure 246 show the water content values measured for the samples used in the triaxial UU tests. Table 33 and Figure 247 show the measured water content values of the samples used in the direct shear tests. Figure 248 shows the test data from both tests. All the samples were left in the oven to dry for 24 hours at 110°C. The soil profile at the field site consists of two different soils, backfill and natural soils. Since the boreholes were drilled through the bridge abutment, the first 20 ft was backfill (i.e., height of the abutment at the location of the boreholes is 20 ft) and below this position the soil samples correspond to the natural soil. Water content profile also shows the difference between these two soils. The water content of backfill is between 30 and 36 percent, while the water content for natural soil varies between 16 and 22 percent.

Table 32. Water Content of the Samples Used in the Triaxial UU Tests.

Time	Borehole	Depth (ft)	Before Test					After Test			
			Container (g)	Container + Sample (g)	Container + Dry Sample (g)	Water Content (%)	Avg. Water Content (%)	Container (g)	Container + Specimen (g)	Container + Dry Specimen (g)	Water Content (%)
01/22/2014	B1	3-5	0.99	4.68	3.71	35.7	35.0	0.82	1172.52	876.21	33.8
			0.99	5.65	4.46	34.3					
01/21/2014		8-10	0.99	26.00	19.44	35.6	35.7	1.64	1261.05	1020.61	23.6
			0.99	13.84	10.45	35.8					
01/21/2014		13-15	1.00	30.06	22.93	32.5	33.3	0.88	1180.40	940.68	25.5
			0.99	20.07	15.56	31.0					
			0.99	12.22	9.22	36.5					
01/22/2014		23-25	1.00	18.16	15.25	20.4	20.6	4.06	1086.25	892.86	21.8
			1.00	20.78	17.39	20.7					
01/23/2014		33-35	1.00	19.47	16.73	17.4	17.3	4.36	1129.77	981.24	15.2
			1.00	20.39	17.55	17.2					
01/17/2014	B2	23-25	1.00	37.10	29.50	26.7	27.6	1.93	1186.19	969.80	22.4
			1.00	34.13	26.96	27.6					
			0.98	23.56	18.57	28.4					

Table 33. Water Content Measured during Direct Shear Test.

			Before Test					After Test			
Time	Borehole	Depth (ft)	Container (g)	Container + Sample (g)	Container + Dry Sample (g)	Water Content (%)	Avg. Water Content (%)	Container (g)	Container + Specimen (g)	Container + Dry Specimen (g)	Water Content (%)
01/22/2014	B1	3-5	0.98	25.66	18.60	40.1	40.2	2.72	169.58	120.47	41.7
			1.02	24.95	18.08	40.3					
01/21/2014		8-10	1.00	25.71	19.67	32.4	31.8	3.53	188.28	143.82	31.7
			0.99	29.28	22.56	31.2					
01/21/2014		13-15	0.98	26.43	19.99	33.9	34.4	2.12	164.08	125.08	31.7
			1.01	28.22	21.17	35.0					
01/22/2014		23-25	0.99	30.72	26.03	18.7	19.0	1.67	179.60	152.71	17.8
			0.99	35.10	29.61	19.2					
01/23/2014		33-35	0.99	27.10	23.06	18.3	18.3	3.92	199.85	169.04	18.7
			0.99	25.69	21.87	18.3					

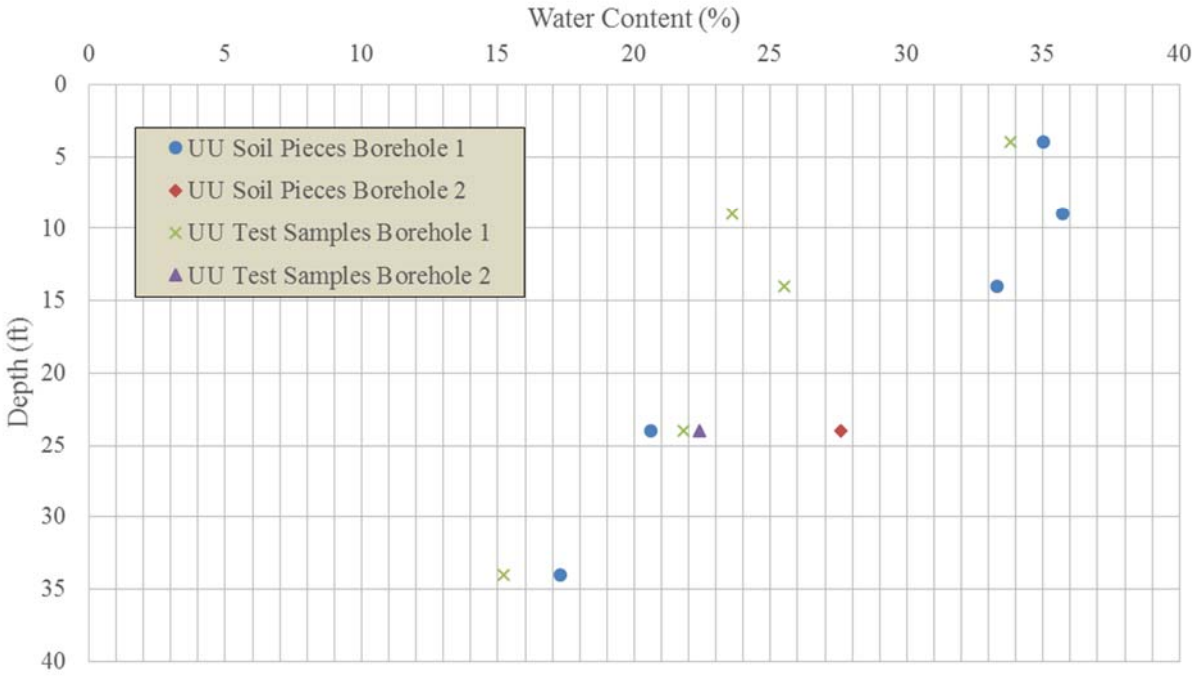

Figure 246. Variation in Depth of the Water Content.

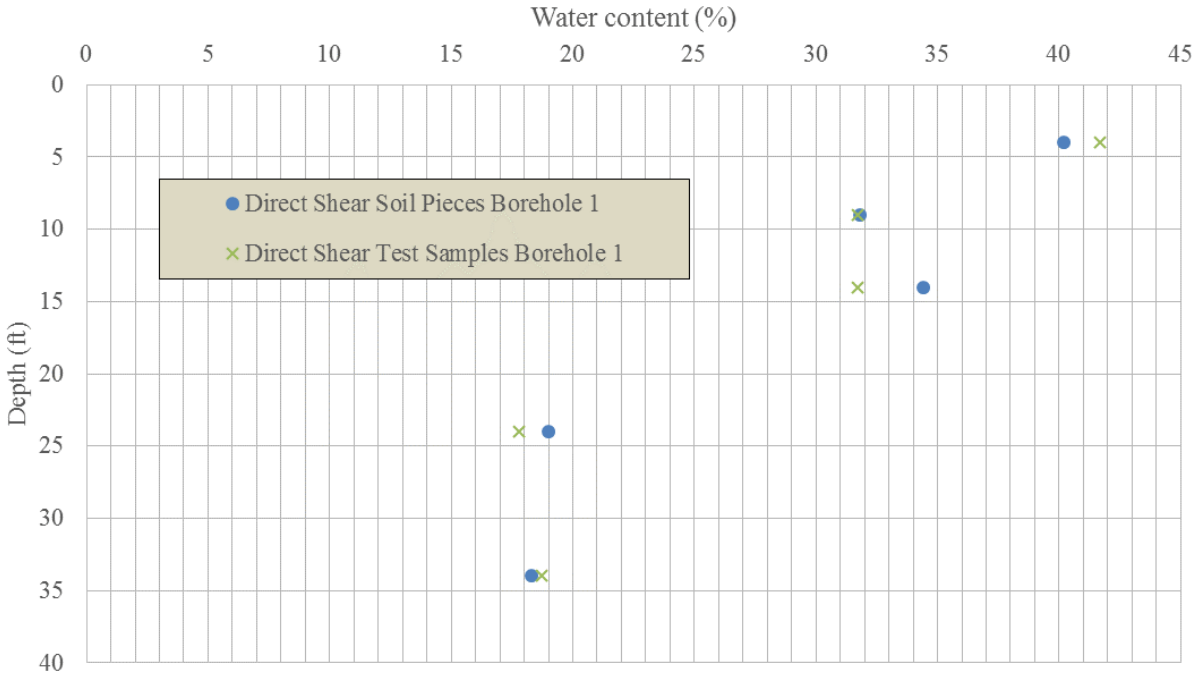

Figure 247. Water Content Measured during Direct Shear Test.

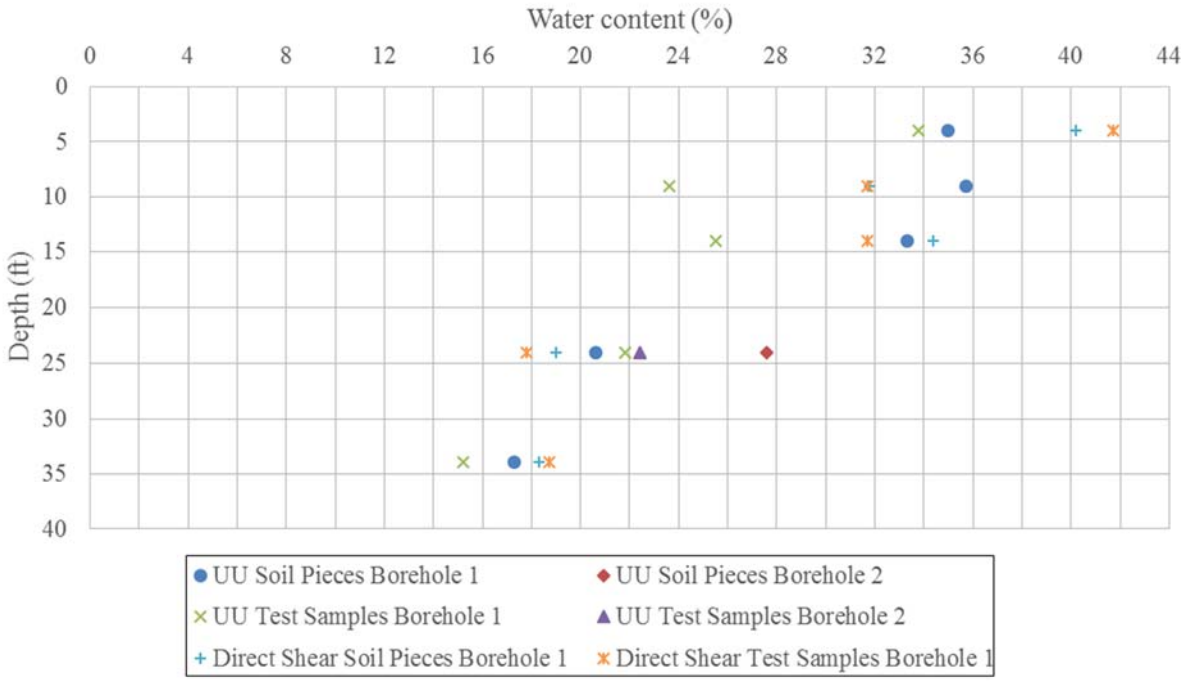

Figure 248. Water Content Profile with Depth on Samples from Beaumont Field Site.

Unit Weight

Table 34 and Figure 249 show the unit weight values determined for the samples used in the triaxial UU tests.

Table 34. Unit Weight Values Determined in Samples Used in Triaxial UU Tests.

Time	Borehole	Depth (ft)	Height (in)	Avg. Height (in)	Diameter (in)	Avg. Diameter (in)	Whole Specimen (g)	Density (g/cm^3)	Unit Weight (kN/m^3)	Unit Weight (pcf)
01/22/2014	B1	3-5	6.61	6.72	2.639	2.636	1172.10	1.95	19.10	121.6
			6.74		2.637					
			6.81		2.633					
01/21/2014		8-10	6.99	6.99	2.674	2.668	1260.11	1.97	19.28	122.7
			6.94		2.685					
			7.05		2.645					
01/21/2014		13-15	6.61	6.61	2.697	2.699	1177.25	1.90	18.62	118.5
			6.59		2.703					
			6.63		2.697					
01/22/2014		23-25	5.58	5.63	2.719	2.700	1082.58	2.05	20.09	127.9
			5.56		2.682					
			5.75		2.698					
01/23/2014		33-35	5.80	5.66	2.696	2.686	1125.53	2.14	20.97	133.5
			5.62		2.679					
			5.57		2.684					
01/17/2014	B2	23-25	6.23	6.22	2.724	2.709	1183.51	2.01	19.74	125.6
			6.23		2.716					
			6.20		2.687					

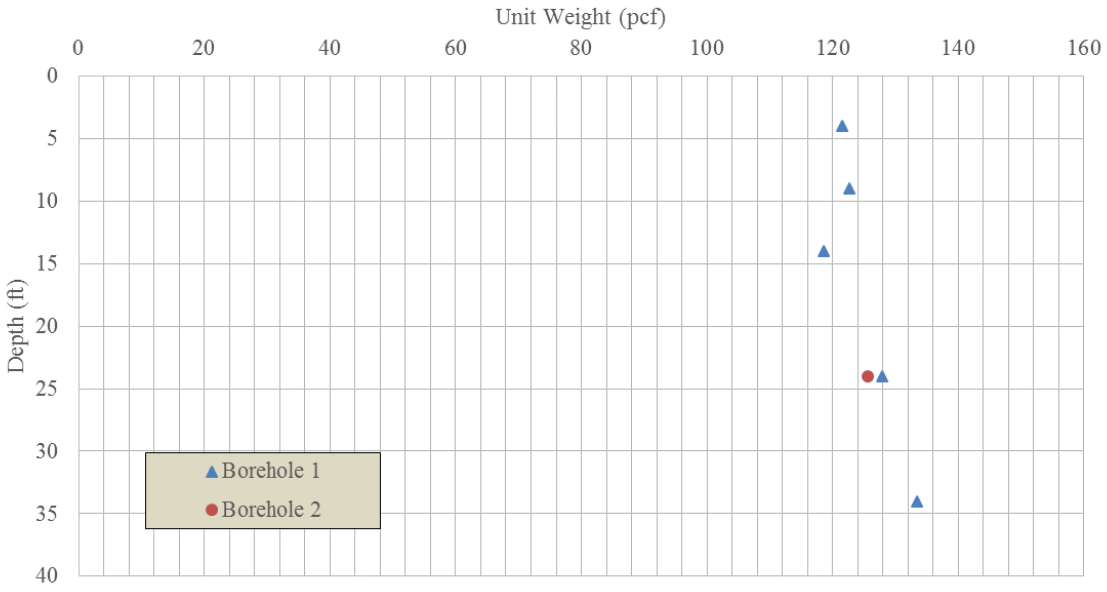

Figure 249. Unit Weight Measured in Samples Used in the Triaxial UU Tests.

Table 35 and Figure 250 show the measured unit weights (ASTM D7263, 2009) of the samples used in the direct shear tests. Figure 251 shows the test data from both tests. As shown in Figure 251, the unit weight is quite constant, around 120 pcf for backfill and around 130 pcf for the natural soils.

Table 35. Unit Weight Measured in Samples Used in Direct Shear Tests.

Time	Borehole	Depth (ft)	Height (in)	Avg. Height (in)	Diameter (in)	Avg. Diameter (in)	Whole Specimen (g)	Density (g/cm^3)	Unit Weight (kN/m^3)	Unit Weight (pcf)
01/22/2014	B1	3-5	1.245	1.26	2.368	2.356	167.03	1.86	18.25	116.2
			1.245		2.388					
			1.276		2.312					
01/21/2014		8-10	1.320	1.33	2.351	2.360	185.09	1.95	19.09	121.5
			1.351		2.451					
			1.306		2.277					
01/21/2014		13-15	1.192	1.19	2.407	2.374	162.20	1.87	18.36	116.9
			1.204		2.339					
			1.184		2.376					
01/22/2014		23-25	1.109	1.11	2.462	2.456	176.96	2.05	20.06	127.7
			1.130		2.482					
			1.102		2.424					
01/23/2014		33-35	1.249	1.25	2.375	2.370	196.12	2.17	21.25	135.3
			1.255		2.337					
			1.249		2.399					

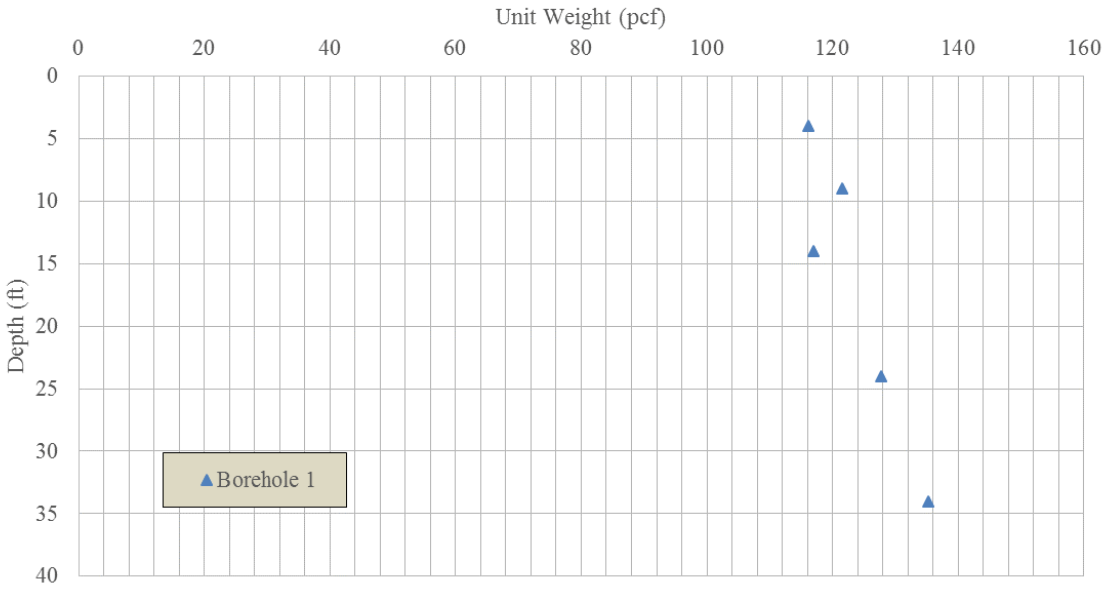

Figure 250. Unit Weight Measured in Samples Used in Direct Shear Tests.

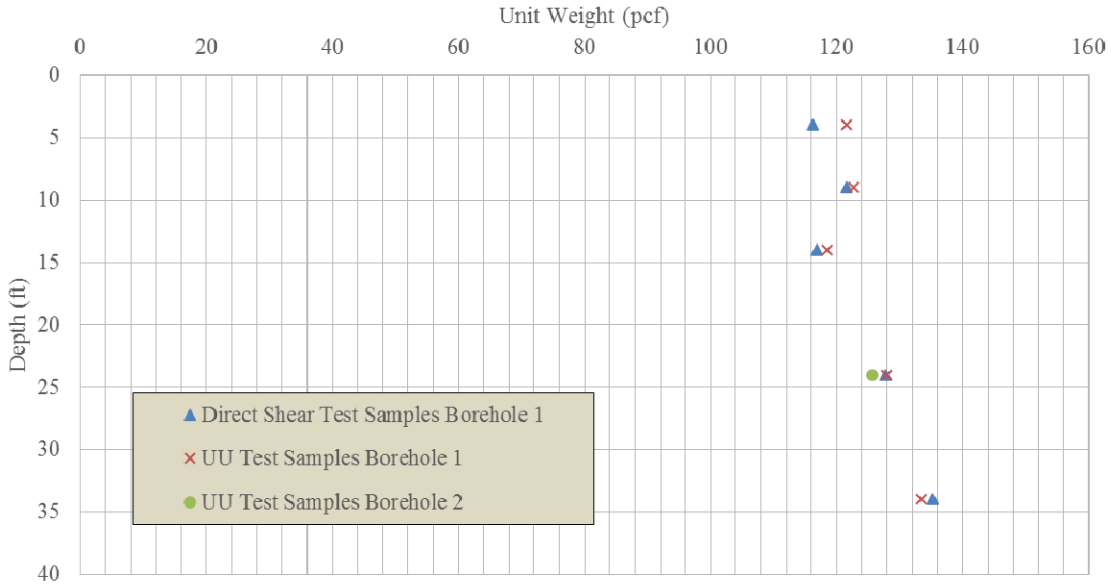

Figure 251. Variation of Unit Weight with Depth for Samples from Beaumont Field Site.

Degree of Saturation

The degree of saturation can be calculated from the following equation:

$$S_r = \frac{\omega \cdot G_s}{e} \tag{12}$$

where ω is the water content; e is the void ratio; and G_s is the specific gravity (adopted as 2.65 in this research). Table 36, Table 37, and Figure 252 show the experimental data.

Table 36. Degree of Saturation Calculated Based on Data from Triaxial UU Test.

Borehole	Unit Weight (pcf)	Depth (ft)	Water Content (%)	Void Ratio	Saturation (%)
B1	121.6	4	33.8	0.82	109
	122.7	9	23.6	0.66	94
	118.5	14	25.5	0.75	90
	127.9	24	21.8	0.57	101
	133.5	34	15.2	0.43	94
B2	125.7	24	22.4	0.61	97

Table 37. Degree of Saturation Calculated Based on Data from Direct Shear Test.

Borehole	Unit Weight (pcf)	Depth (ft)	Water Content (%)	Void Ratio	Saturation (%)
B1	116.2	4	41.7	1.02	109
	121.5	9	31.7	0.79	106
	116.9	14	31.7	0.86	97
	127.7	24	17.8	0.53	90
	135.3	34	18.7	0.45	110

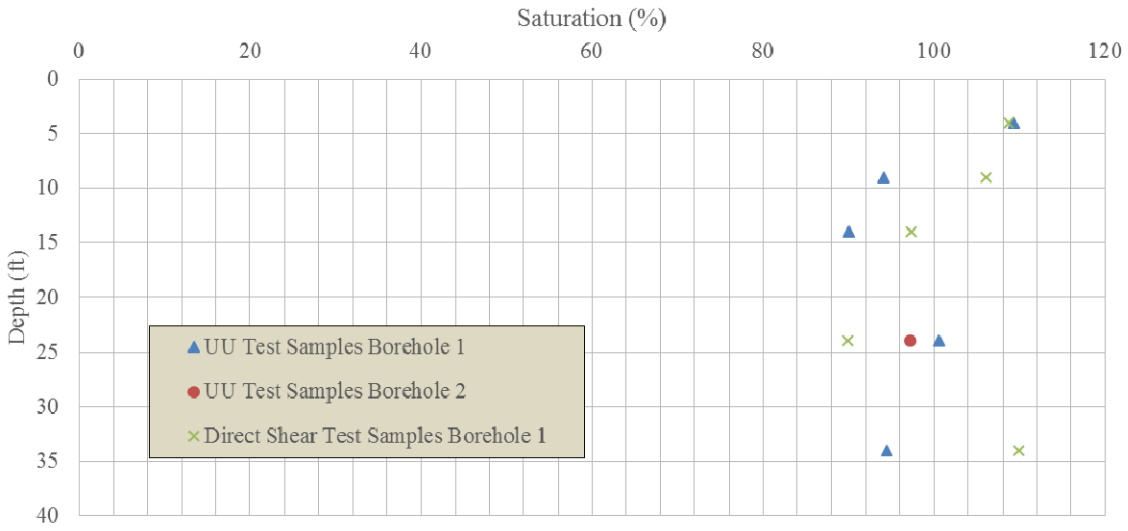

Figure 252. Degree of Saturation Profile with Depth on Samples from Beaumont Field Site.

Atterberg's Limits

The Atterberg's limits were performed on six samples at five different depths. The PI profile and the test data are presented in Figure 253 and Table 38, respectively. In Figure 253, this is a high PI clay. The PI varies between 45 and 55, and the average value of PI is around 50.

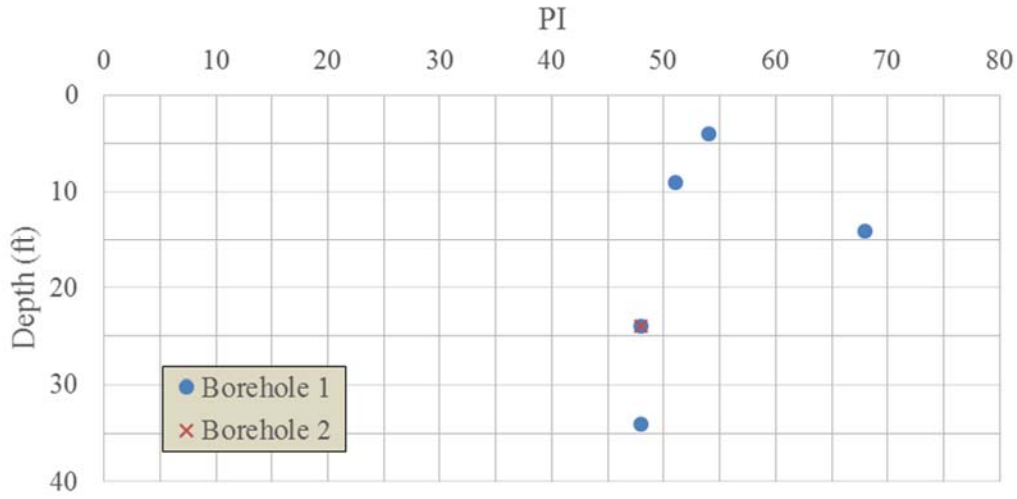

Figure 253. Variation of PI with Depth on Samples from Beaumont Field Site.

Table 38. Atterberg's Limits.

Borehole	Depth ft	Atterberg's Limits	Number	Container (g)	Container + Sample (g)	Container + Dry Sample (g)	Water Content (%)	Blows	Avg Water Content (%)	PI
B2	23-25	PL	#1	0.99	7.61	6.64	17.2	NA	17.4	48
			#2	0.98	7.84	6.81	17.7	NA		
		LL	#1	1	8.98	5.77	67.3	15	65.5	
			#2	0.98	9.43	6.23	61.0	16		
			#3	0.97	11.33	7.13	68.2	28		
B1	3-5	PL	#1	0.98	4.24	3.62	23.5	NA	23.7	54
			#2	1.01	5.22	4.41	23.8	NA		
		LL	#1	0.99	9.4	5.7	78.6	23	77.8	
			#2	0.98	8.48	5.29	74.0	19		
			#3	1.02	6.1	3.83	80.8	15		
B1	8-10	PL	#1	0.98	6.48	5.5	21.7	NA	21.3	51
			#2	0.99	5.86	5.02	20.8	NA		
		LL	#1	0.99	9.91	6.11	74.2	15	72.7	
			#2	0.98	9.42	5.88	72.2	18		
			#3	1	12	7.41	71.6	22		
B1	13-15	PL	#1	0.99	7.46	6.19	24.4	NA	24.3	68
			#2	0.99	6.64	5.54	24.2	NA		
		LL	#1	1.13	15.39	8.85	84.7	21	91.9	
			#2	0.99	8.56	4.88	94.6	20		
			#3	0.99	9.75	5.45	96.4	19		
B1	23-25	PL	#1	0.99	6.76	5.93	16.8	NA	16.8	48
			#2	0.99	9.8	8.53	16.8	NA		
		LL	#1	1.13	15.64	9.94	64.7	22	65.1	
			#2	0.99	8.5	5.53	65.4	19		
			#3	0.98	9.29	6.01	65.2	15		
B1	33-35	PL	#1	0.99	8.17	7.23	15.1	NA	14.8	48
			#2	0.98	10.75	9.51	14.5	NA		
		LL	#1	1.14	8.32	5.58	61.7	15	63.2	
			#2	1.02	8.28	5.41	65.4	18		
			#3	0.98	11.65	7.54	62.7	21		

Soil Strength

The results obtained from the direct shear test (ASTM D3080/D3080M, 2011), the triaxial UU test (ASTM D2850-03a, 2007), and the miniature vane test are reported in this section. The triaxial CU test (ASTM D4767, 2011) on one sample is also presented.

Direct Shear Test

The following equation was used to estimate the vertical stress at different depths and, based on these data, the normal stress to be applied in the direct shear test was selected:

$$\sigma_3\,[psi] = \frac{\gamma\,[pcf]\;\; h\,[ft]}{144} \tag{13}$$

where γ is the soil unit weight; and h is the position.

The in situ stress is assumed to be equal to the soil self-weight, though this is not always exactly true. Table 39 shows the magnitude of the applied normal/confining stress during direct shear and triaxial tests for the samples at different depths.

Table 39. Applied Normal/Confining Stress for Direct Shear Tests and Triaxial UU Tests.

Depth (ft)	Applied Normal/Confining Stress (psi)
4	3.5
9	8
14	12.4
24	21.2
34	30

The ratio of applied normal stress over stress by self-weight was equal to 1. The adopted strain rate was equal to 0.5 mm/min. Since the diameter of the shear box is 2.5 in., the strain rate was almost 1 percent/min.

Figure 254 presents the test results at five different depths from borehole 1. In all the curves, after reaching the peak strength, the stress drops to the residual strength. The peak strength is between 4 and 22 psi, while the residual strength is between 3 and 17 psi. The ratio of residual strength over peak strength is about 0.8. The peak and residual strengths increased with the depth of the sample. The shear strength profile and data are presented in Table 40 and Figure 255, respectively.

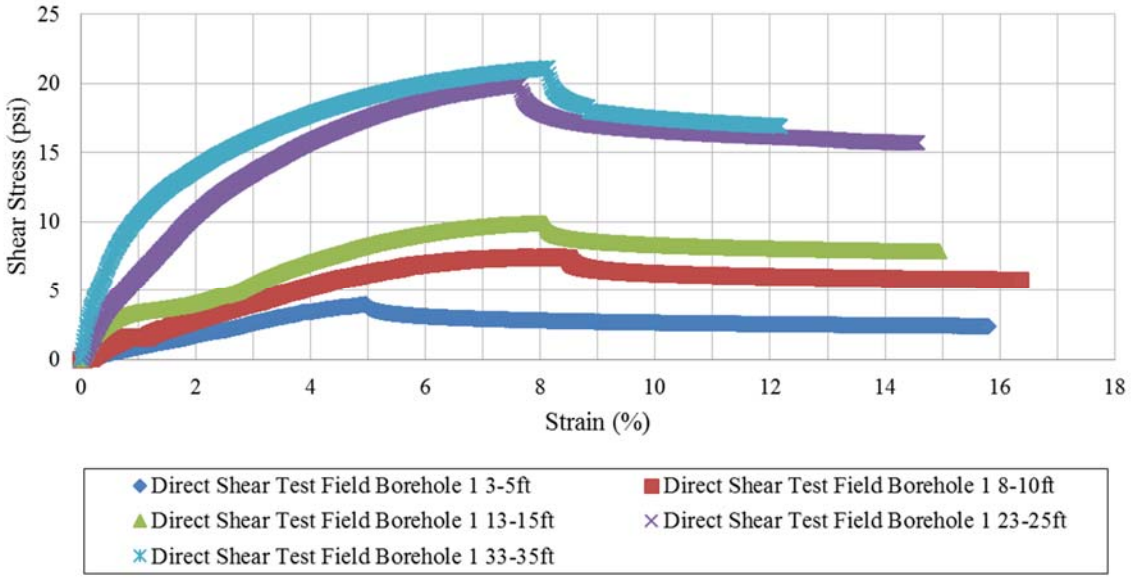

Figure 254. Direct Shear Test on Samples from Beaumont Field Site.

Table 40. Data of Samples from Beaumont Field Site at Failure.

Borehole	Depth (ft)	Shear Stress at Failure (psi)	Normal Stress (psi)	Strain at Failure (%)
B1	4	3.99	5.06	4.96
	9	7.48	7.56	8.2
	14	9.9	14.94	8.08
	24	19.92	20.94	7.64
	34	21.12	39.97	8.12

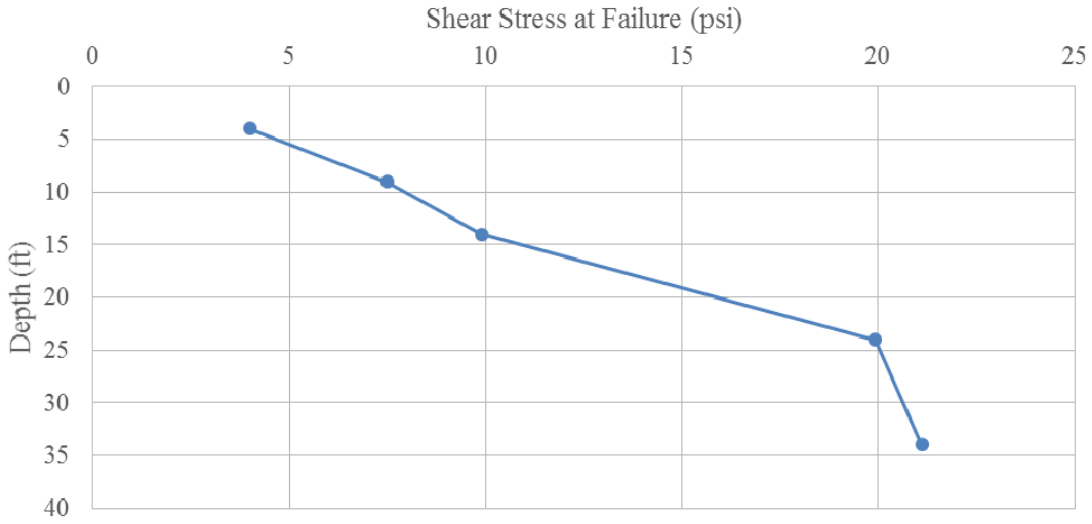

Figure 255. Direct Shear Test Strength Variation with Depth on Samples from Beaumont Field Site.

Triaxial UU Test

Table 39 shows the applied confining stress during the triaxial UU tests. The strain rate during these tests was 1 percent/min. The soil samples used for these tests are:

- Borehole 1, depth between 3 and 5 ft.
- Borehole 1, depth between 8 and 10 ft.
- Borehole 1, depth between 13 and 15 ft.
- Borehole 1, depth between 23 and 25 ft.
- Borehole 1, depth between 33 and 35 ft.
- Borehole 2, depth between 23 and 25 ft.

Figure 256 shows the triaxial UU test results. In almost all the curves, no hump (i.e., stress decrease after the peak strength) was observed. The soil strength at 15 percent strain (except the curve with peak strength) was selected as the shear strength, which is illustrated in Table 41 and Figure 257. The soil strength profile from the triaxial UU tests in Figure 257 is quite close to the soil strength profile from the direct shear tests in Figure 255.

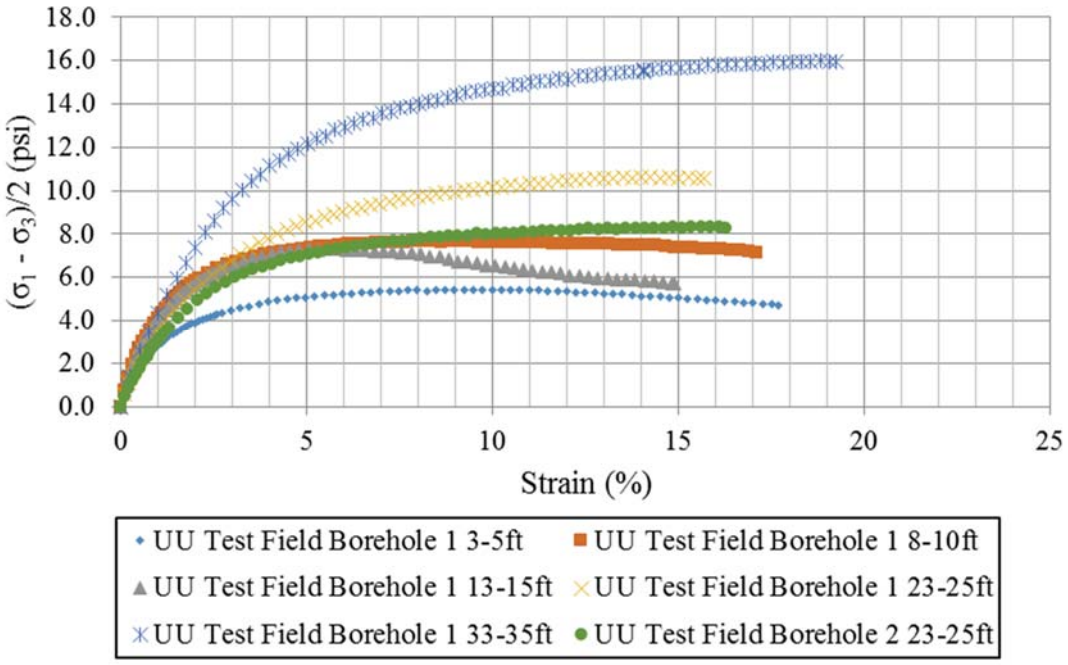

Figure 256. Triaxial UU Tests on Samples from the Beaumont Field Site.

Table 41. Data of Samples at Failure in Figure 256 Summary.

Borehole	Depth (ft)	Shear Stress at Failure (psi)	Confining Stress (psi)	Strain at Failure (%)
B1	4	5.44	3.5	10.48
	9	7.56	8	9.12
	14	7.31	12.4	5.81
	24	10.56	21.2	15
	34	15.66	30	15
B2	24	8.32	21.2	15

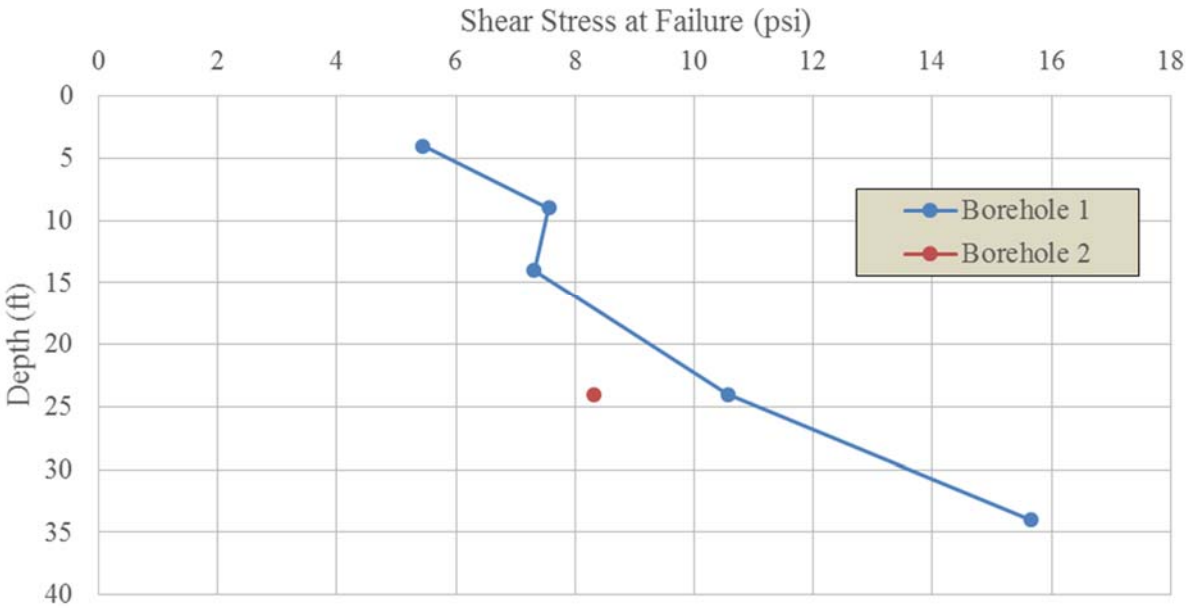

Figure 257. Triaxial UU Test Shear Strength Profile with Depth on Samples from the Beaumont Field Site.

In Figure 258 to Figure 263, the stress–strain curves presented in Figure 256 were replotted in the space "Strain/Stress versus Strain (%)," which is typically used to find the two parameters needed to define the hyperbola. The experimental curves fitted very well with the line defining the hyperbola in this space. Then, the curves were normalized by the stress at 15 percent (or peak stress) and 15 percent strain (or the strain corresponding to the peak stress), shown in Figure 264.

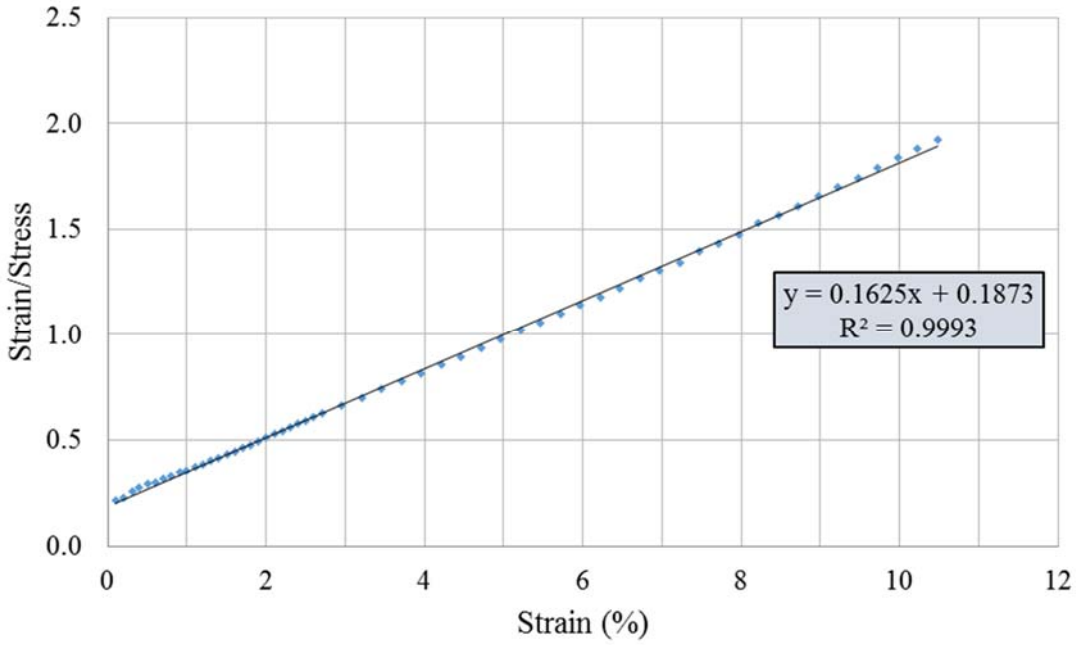

Figure 258. Sample at a Depth between 3 and 5 Ft from Borehole 1 (Hyperbola Fitting).

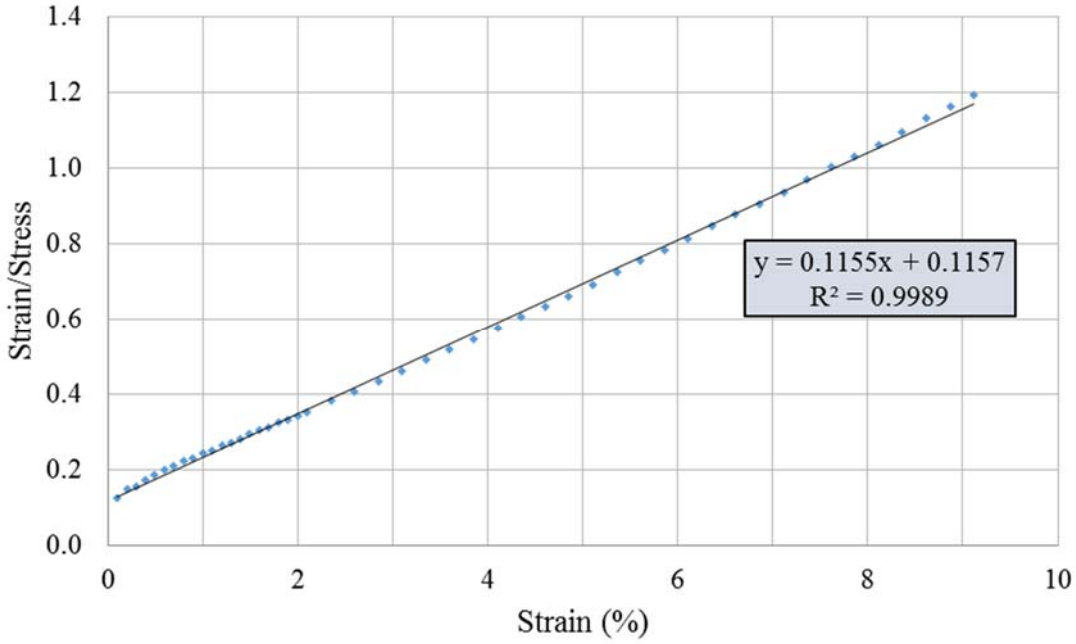

Figure 259. Sample at a Depth between 8 and 10 Ft from Borehole 1 (Hyperbola Fitting).

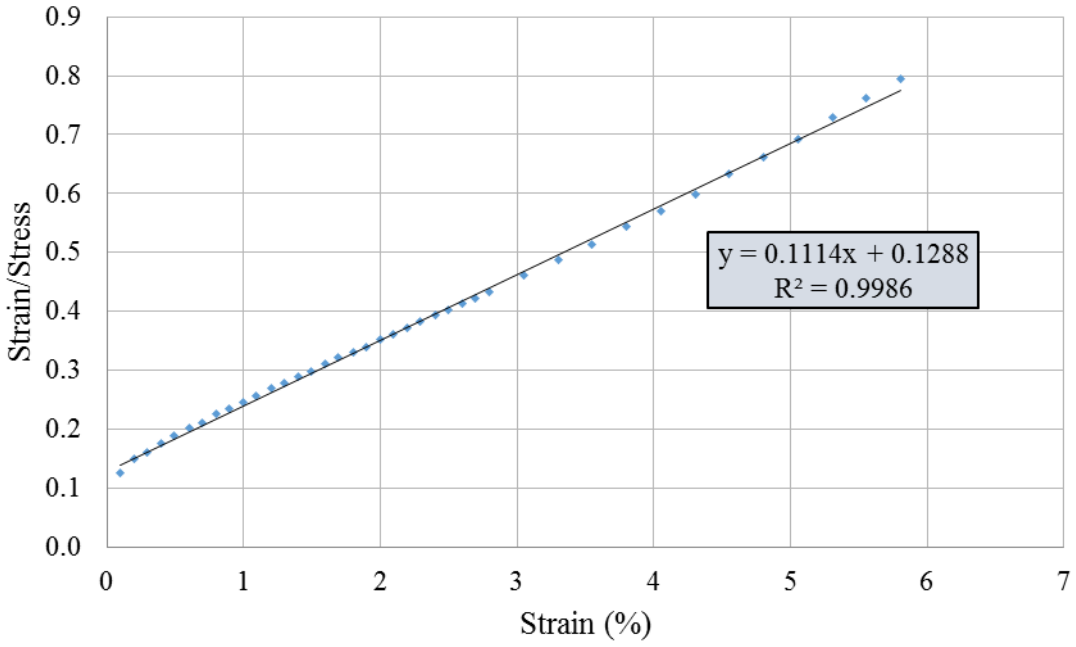

Figure 260. Sample at a Depth between 13 and 15 Ft from Borehole 1 (Hyperbola Fitting).

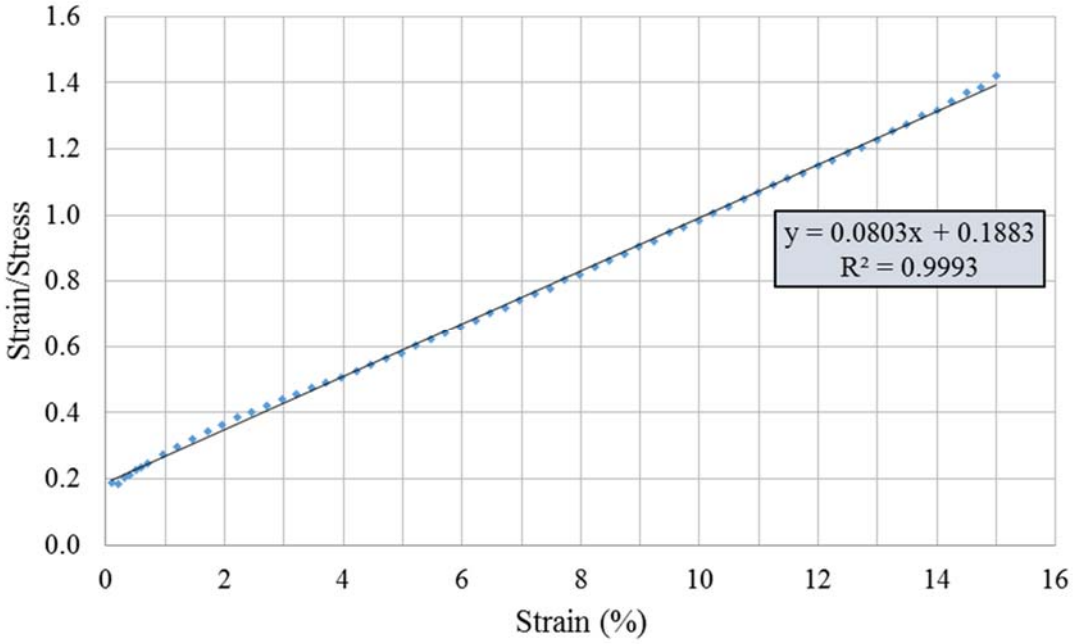

Figure 261. Sample at Depth between 23 and 25 Ft from Borehole 1 (Hyperbola Fitting).

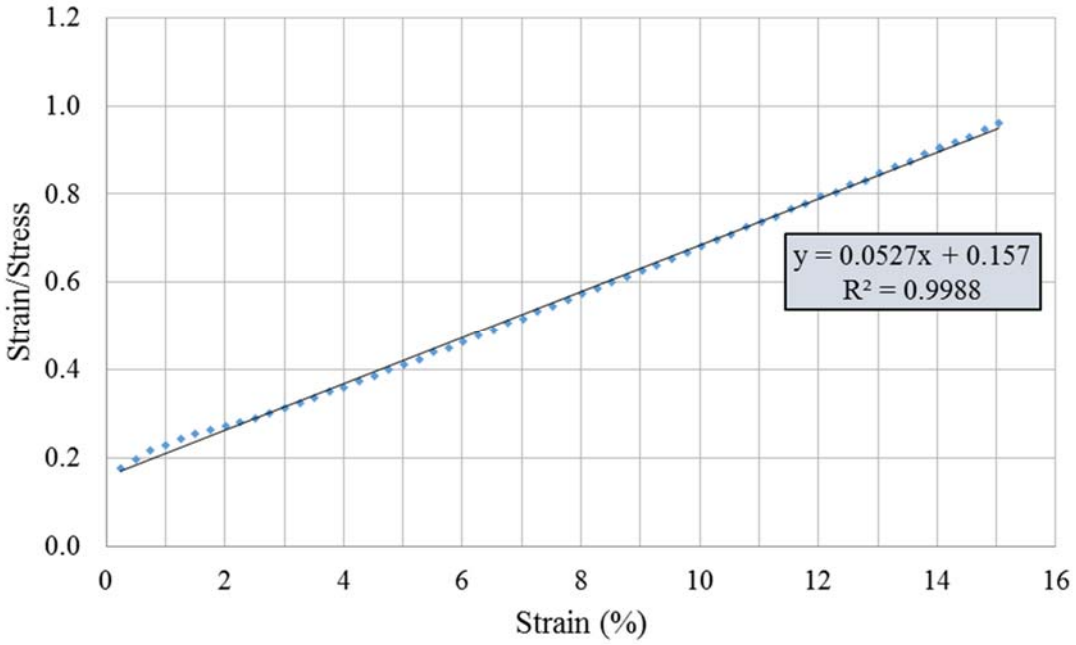

Figure 262. Sample at a Depth between 33 and 35 Ft from Borehole 1 (Hyperbola Fitting).

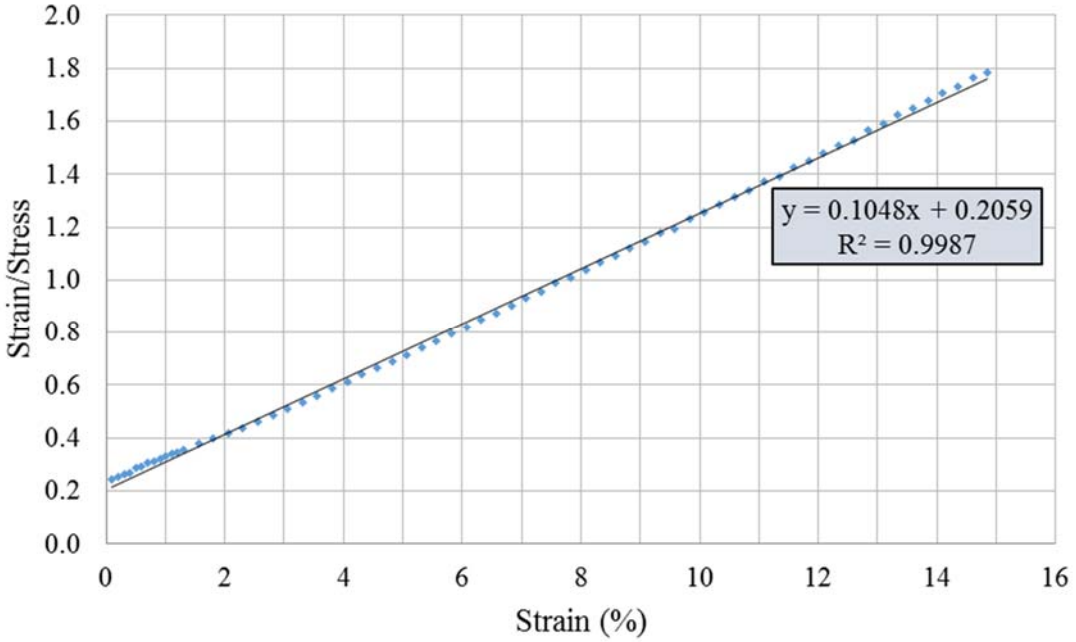

Figure 263. Sample at Depth between 23 and 25 Ft from Borehole 2 (Hyperbola Fitting).

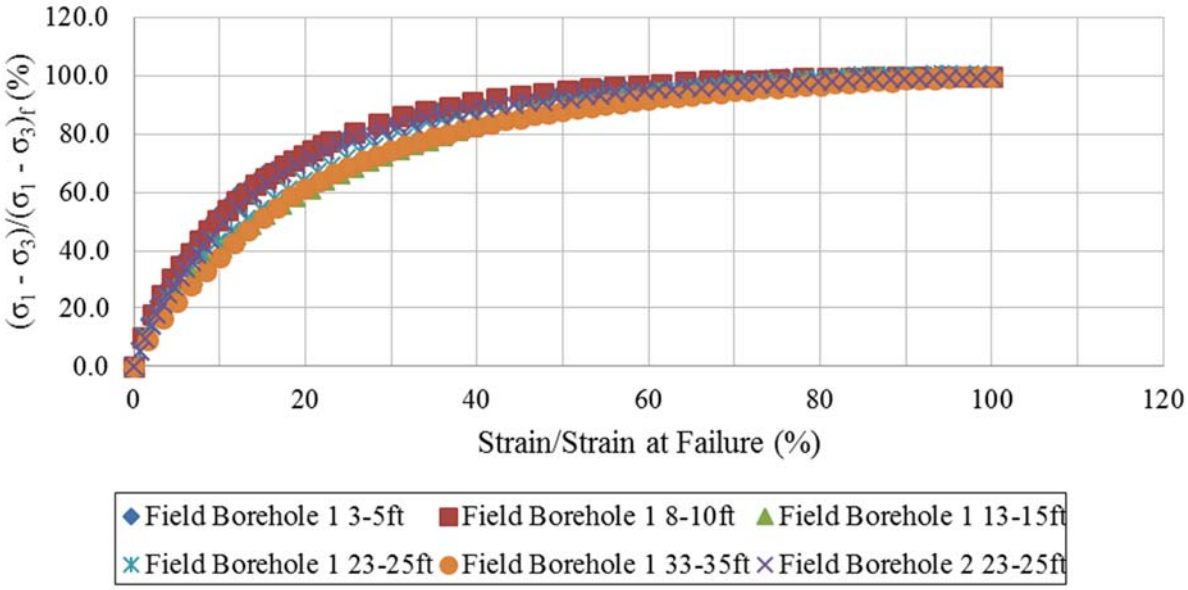

Figure 264. Normalized Strain–Stress Curves from Triaxial UU Test.

Miniature Vane Test

The mini vane test was performed to assess the undrained shear strength of the soil. The mini vane tests were carried out in five samples from different depths from borehole 1. The results of the mini vane tests are presented in Table 42, Figure 265, and Figure 266, respectively.

The undrained shear strength profiles from direct shear tests, triaxial UU tests, and mini vane tests are plotted together, as shown in Figure 267. Figure 267 shows the undrained shear strength in the backfill material (i.e., depth between 0 and 20 ft) is around 8 psi, then increases gradually to 16 psi at 30 ft depth (layer natural soil). The undrained shear strength gradually increases for the depth below 20 ft (natural soil).

Table 42. Data of Samples at Failure Summary.

Borehole	Depth (ft)	Strength (kPa)	Strength (psi)
B1	4	38	5.51
	9	47	6.82
	14	55.4	8.04
	24	48.5	7.03
	34	80	11.60

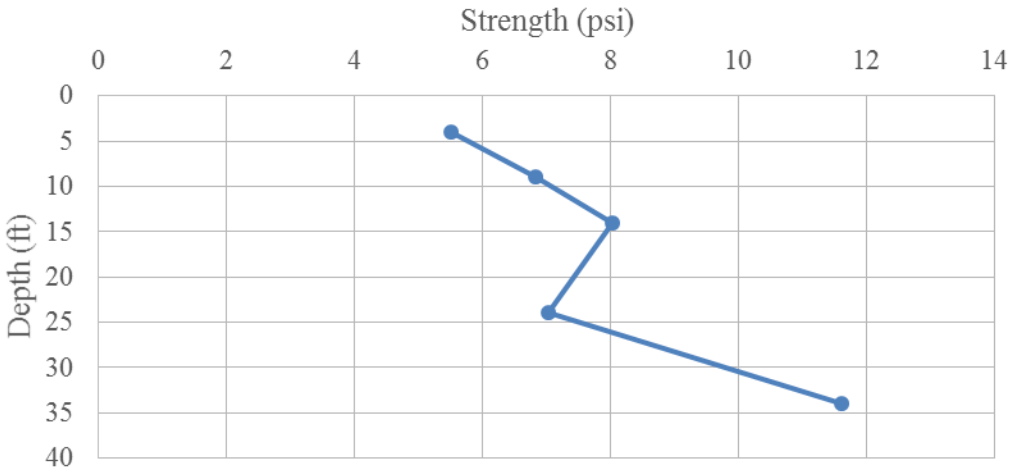

Figure 265. The Profile of Shear Strength with the Mini Vane Test Profile with Depth Test on Sample from Beaumont Field Site.

Figure 266. Photo of the Mini Vane Test on Sample from Beaumont Field Site.

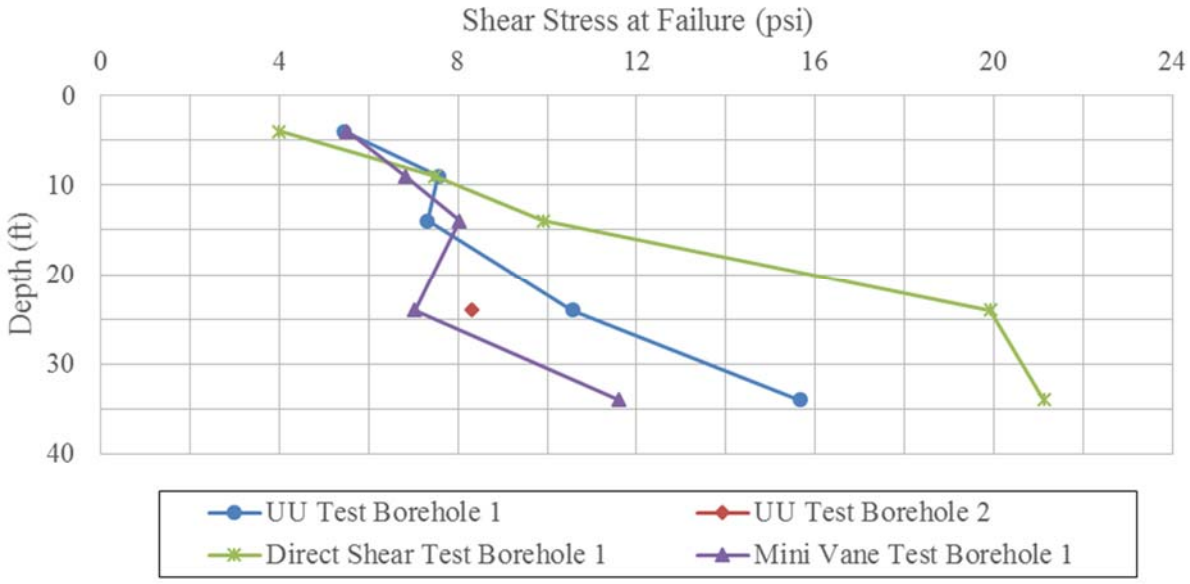

Figure 267. Variation of the Strength in Depth for the Four Soils Studied in This Project.

Triaxial CU Tests Performed on One Sample at Depth 33 from 35 from Borehole 1

To obtain the Mohr circle, triaxial CU tests were performed with three different confining stresses. The test procedure is as follows:

- Consolidate the sample first.
- With the first confining stress applied, load the sample until failure, pausing the test at peak stress.
- After dissipation of the excess of pore water pressure, apply the second confining stress (larger than the first confining stress), restart the test, pausing the test again at the next point of peak stress.
- After the pore water pressure is dissipated again, apply the third confining stress (larger than the second confining stress), restart the test, and perform it until the end.

To perform this test, in each stage it took more than one week to back saturate the sample, and one week until the excess pore water pressure was dissipated. The total time for this test was one month. The total stress, effective stress, and Mohr circle are shown in Figure 268, Figure 269, and Figure 270, respectively. The calculated cohesion and friction angle are included in Figure 270.

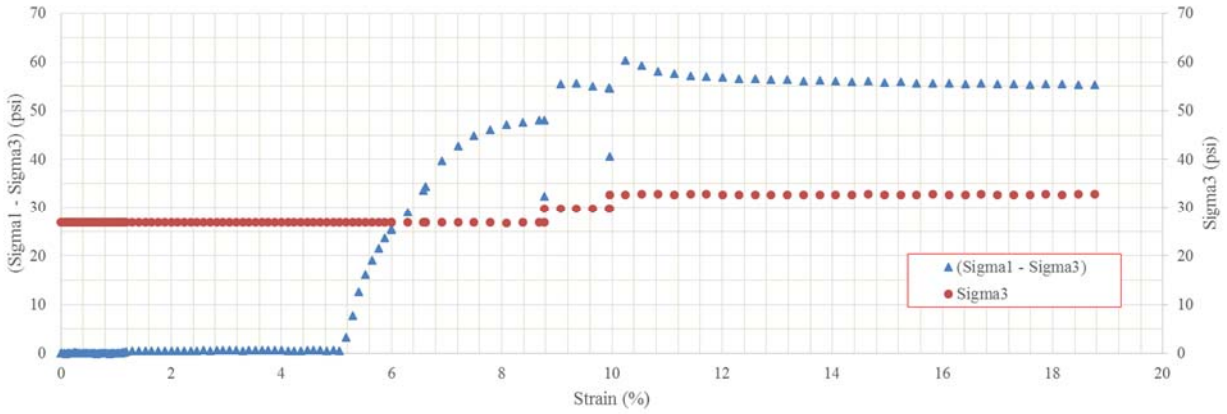

Figure 268. Stress–Strain Curve on Sample from Borehole 1 at Depth between 33 and 35 Ft.

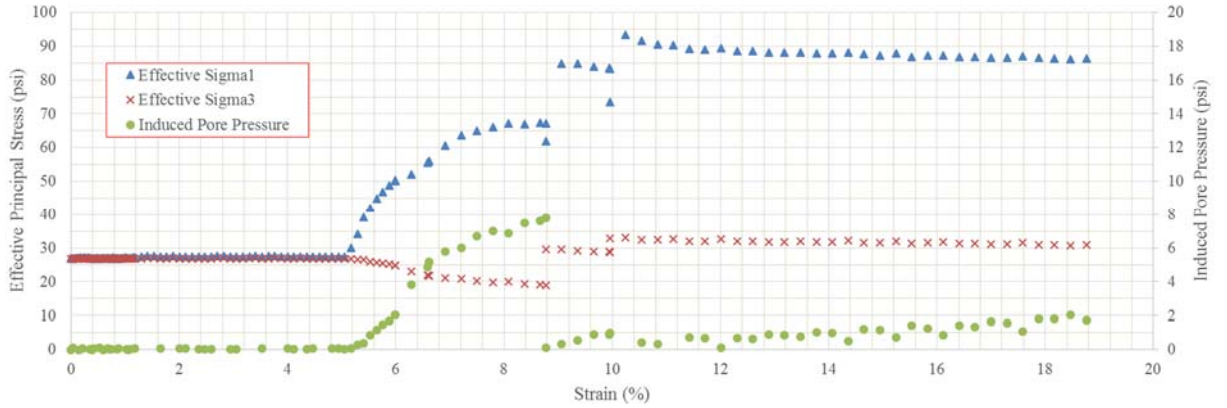

Figure 269. Effective Stress and Pore Pressure.

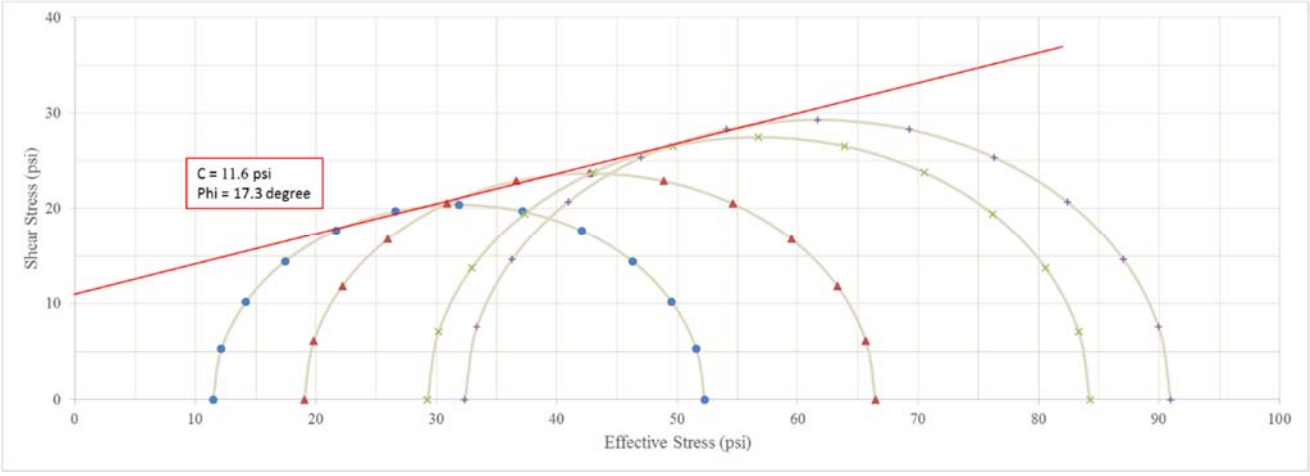

Figure 270. Mohr Circle.

Triaxial CD Tests

Triaxial CD tests were performed to obtain parameters to be used in the numerical simulations. The loading procedure is almost the same as that adopted for the triaxial CU test. The main difference was the loading rate, which is much smaller to ensure that the induced excess pore pressure could be dissipated. However, only two tests on different samples were conducted (Figure 271 and Figure 272).

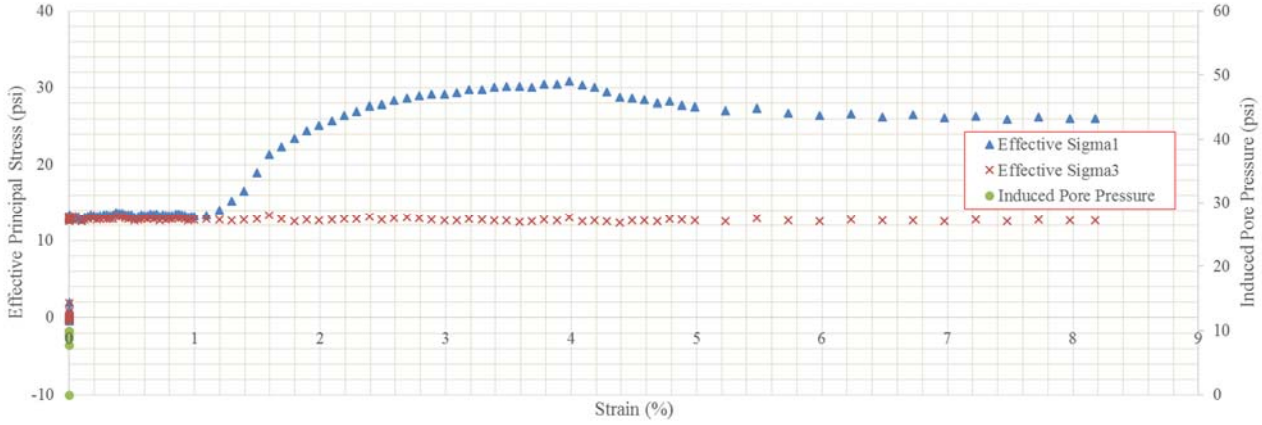

Figure 271. Triaxial CD Test, Sample B2 at a Depth between 13 and 15 Ft.

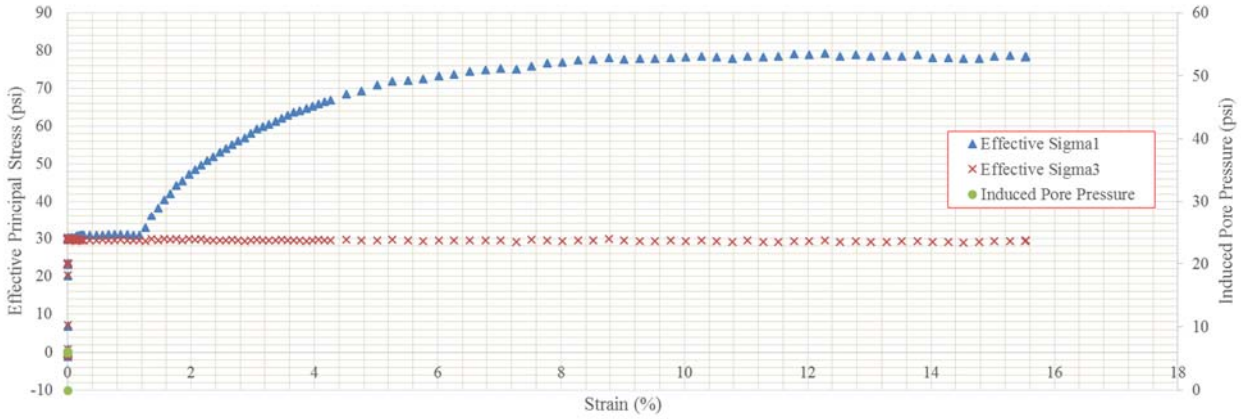

Figure 272. Triaxial CD Test, Sample B2 at a Depth between 33 and 35 Ft.

Triaxial UU Creep Tests

To investigate the creep behavior of the HP clay, triaxial UU creep tests were performed on the soil samples from the Beaumont project. The triaxial creep tests were performed by loading steps. The protocol consisted of an initial strain-control loading stage, until a predefined target load was achieved; at this point the triaxial device was switched to the stress-control mode

to allow the creep of the samples for 24 hours at this constant load. After this creep stage, the triaxial device was switched back to strain-control mode until the next predefined target stress level was achieved and a new creep stage was performed, as before. This loading-creep procedure by steps continued until the failure of the sample. The strain rate in the loading part is 1 percent/min. Specification of the sample (i.e., water content and dimension of the sample) is presented in Table 32 and Table 34.

To determine the effective stress acting on the soil samples, pore water pressure is measured during the test. Figure 273 shows the total stress, effective stress, and pore water pressure versus strain for the sample from a depth between 33 and 35 ft. As shown in Figure 273, during the holding loads effective, stress and total stress is constant.

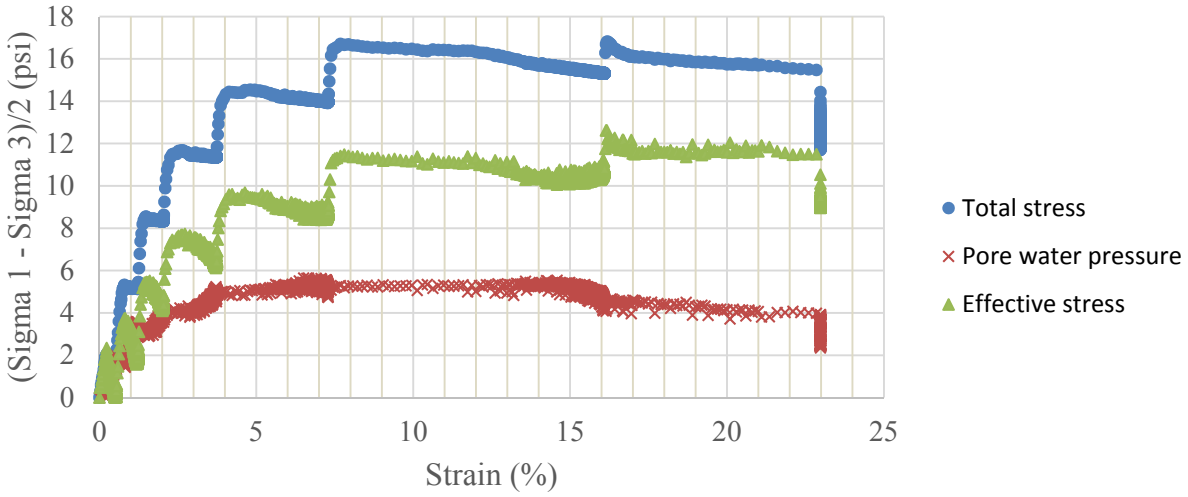

Figure 273. Total Stress, Effective Stress, and Pore Water Pressure versus Strain, Triaxial UU Test on the Soil Sample from the Beaumont Project, Depth between 33 and 35 Ft.

The creep deformations of the soil sample were measured at the axial loads equal to 30, 70, 110, 150, 190, and 230 lb. Figure 274 illustrates the strain versus time response for each load step. At the higher stress levels (i.e., 230 lb), the soil sample exhibits a larger creep deformation compared to the lower load levels (i.e., 70 lb).

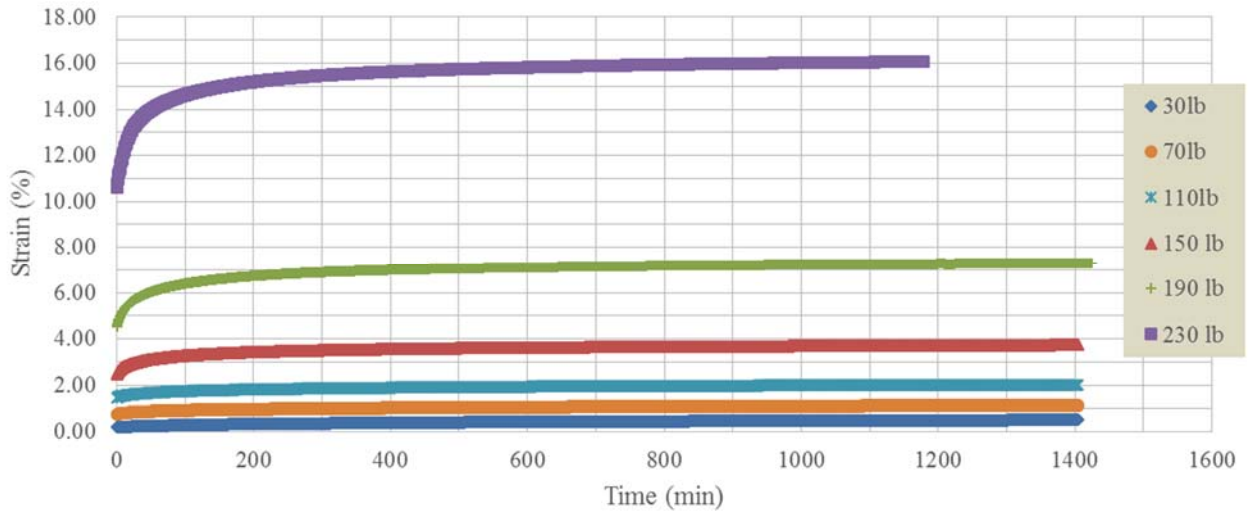

Figure 274. Strain–Time Curves from a Triaxial UU Creep Test Performed on the Sample from Beaumont Project at a Depth between 33 and 35 Ft.

As mentioned in Chapter 2, Briaud and Garland (1985) proposed a power model to account for the time-dependent behavior of soils. The model can be expressed as:

$$\frac{s}{s_1} = \left(\frac{t}{t_1}\right)^n \tag{14}$$

where t is time; s is the settlement; S_1 is the settlement observed after 1 minute of the constant load application; and n is the creep exponent (which is considered a soil property).

If the strain–time curve obtained from the triaxial creep tests is normalized with s_1 and t_1, respectively, and plotted in the log–log scale, the slope of this line defines the power n value. Figure 275 and Figure 276 present the strain–time curve for the creep tests performed on the soil sample from the Beaumont project from depth 33 to 35 ft.

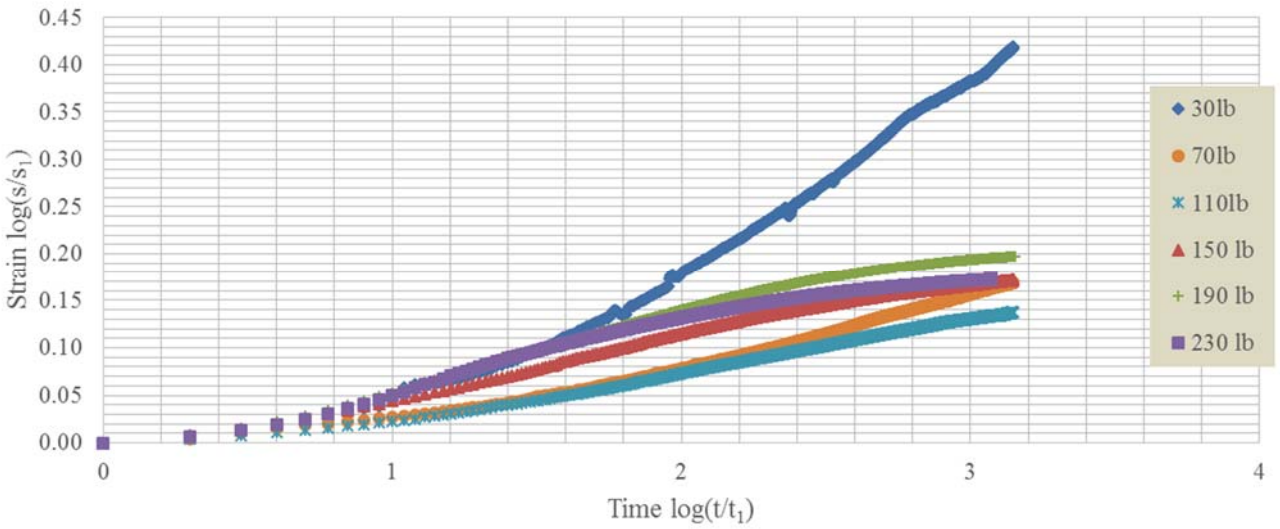

Figure 275. Strain–Time Curves for all the Holding Loads Plotted in Log–Log Scale on the Soil Sample from the Beaumont Project from a Depth between 33 and 35 Ft.

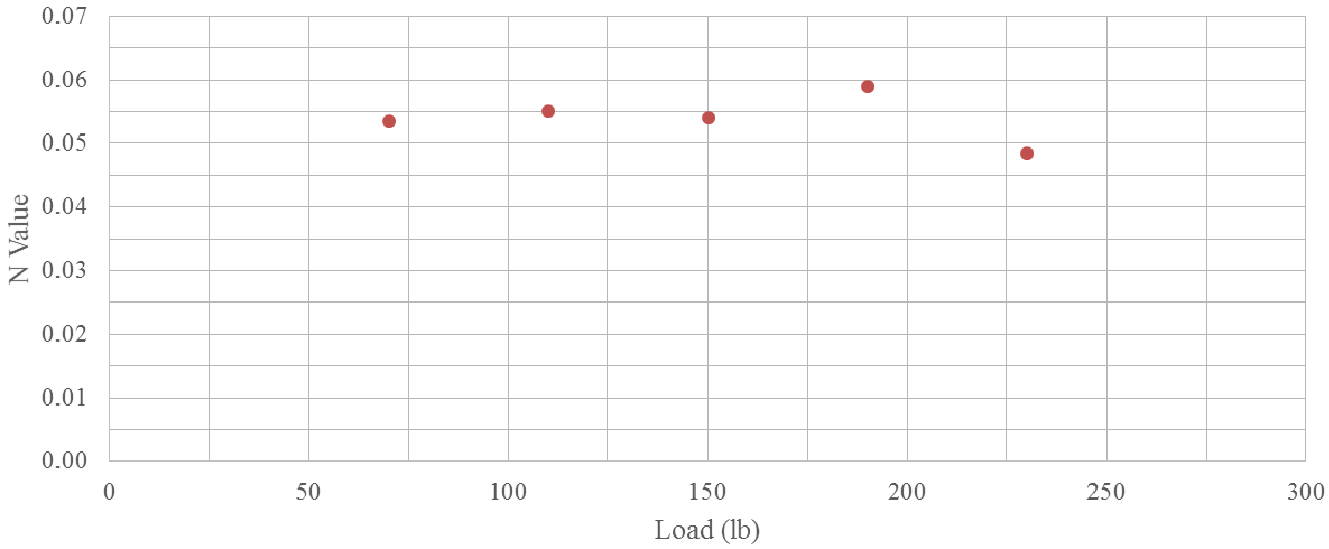

Figure 276. The *n* Value Obtained from the Triaxial Creep Tests on the Soil Sample from the Beaumont Project from a Depth between 33 and 35 Ft at Different Load Steps.

LABORATORY TESTS ON HIGH PI CLAY FROM THE NGES-TAMU CLAY SITE

The soil samples from the NGES were gathered on three different occasions, as follows:

- In November 2012, soil samples were recovered from two boreholes especially drilled to sample the natural soils to be used in the laboratory investigation. These samples are coded as BH1 and BH2 in Figure 277.
- In July 2013, soil samples were gathered during the installation of the soil nails from positions coded as N1 to N6 in Figure 277.
- In September 2013, soil samples were retrieved during an additional installation of soil nails. Four soil nails with shorter length were installed at the NGES, positions coded as N1s to N4s in Figure 277. The boreholes BH3 and BH4 (Figure 277) were drilled, and the soil samples were collected from them.

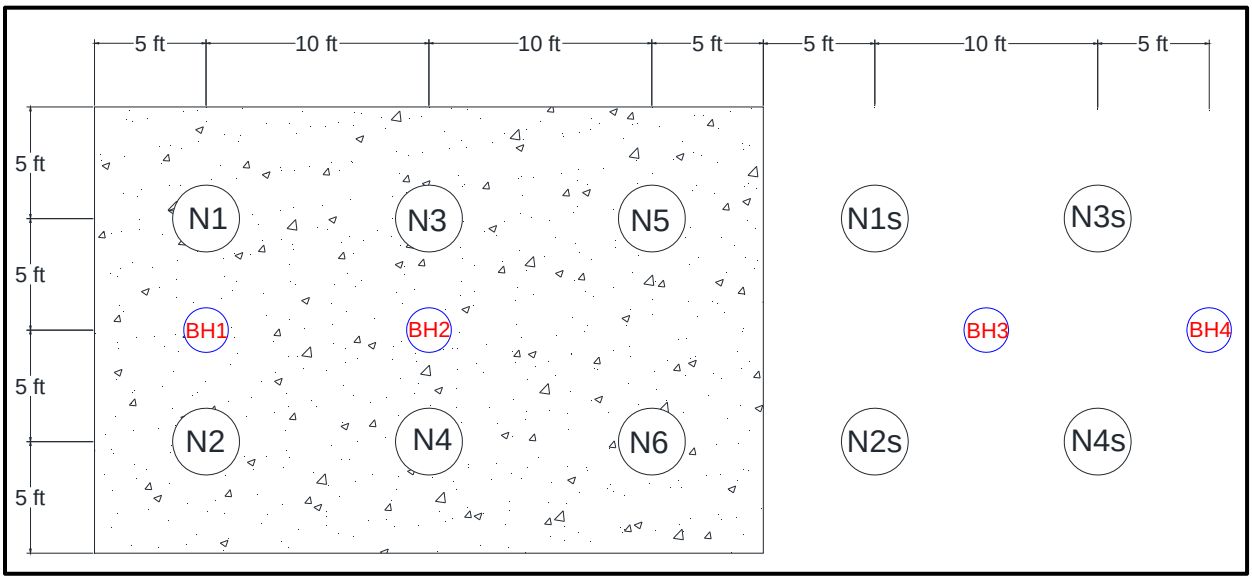

Figure 277. Drawing Showing the Locations of the Soils Nails and Boreholes at the NGES Clay Site.

All samples were gathered with the Shelby tube sampling method to minimize soil disturbance. The soil samples were around 7 in. long with 2.75-in. diameter. The soil samples were taken in the following order from the boreholes:

- BH1 and BH2, one sample every 2 ft until a depth of 18 ft.
- N1 to N6, one sample every 2 ft until a depth of 10 ft, then between 13 and 15 ft and finally between 16 and 18 ft.
- BH3 to BH4, one sample every 2 ft until a depth of 10 ft.

Table 43 summarizes all the laboratory tests performed and the particular soil samples used in the experimental campaign. As mentioned above, the laboratory tests are organized into three groups: index properties, soil strength, and creep behavior. These tests are described as follows.

Table 43. Summary of the Laboratory Tests Performed during This Project and the Corresponding Samples Used in the Experiments.

Depth (ft)	Water content	Unit weight	Atterberg's limits	Direct shear test	Triaxial UU test	Triaxial UU creep test
0–2	BH1	BH1				
2–4	BH4		BH2	BH4		
4–6	BH2, BH4	BH2		BH4		
6–8	BH1, BH4, N1, N2, N4, N6	BH1, N1, N2, N6	N1	BH4, N4	N2	N1, N6
8–10	BH4, N3	N3	N1	BH4		N3
10–12	BH1	BH1				BH1
12–14	BH1, BH2	BH1, BH2				BH1
14–16	BH1	BH1				BH1
13–15	N1, N4	N4	N2	N1	N4	
16–18	BH2, N1, N3, N5, N6	BH2, N1, N5, N6	N5	N3	N6	N5

Index Properties

This section is related to the following laboratory tests: water content (TxDOT Tex-103-E, 1999), unit weight (ASTM D7263, 2009), degree of saturation, and Atterberg's limits (TxDOT Tex-104-E, 1999; TxDOT Tex-105-E, 1999). The results of these tests are presented as follows.

Water Content

Several tests were performed to measure the water content of samples from positions BH1 and BH2. The data and corresponding information are shown in Figure 278, Table 44 (data series #1 and #2 in Figure 278), and Table 45 (data series #3 and #4 in Figure 278). The tables report the date of water content determination. In addition, the water content was measured during other laboratory tests such as direct shear test, triaxial UU test, and triaxial UU creep test. These data are shown in Table 46 to Table 48 separately (also data series #5 to #7 in Figure 278). Each sample was left 24 hours in the oven to dry.

As shown in Figure 278, water content is almost constant from the ground surface to a depth of 10 ft. It gradually increases below this level, and at 18 ft the ground water level was found. The driest sample in Figure 278, with a water content of 6 percent, contained a significant amount of sand, which was quite dry.

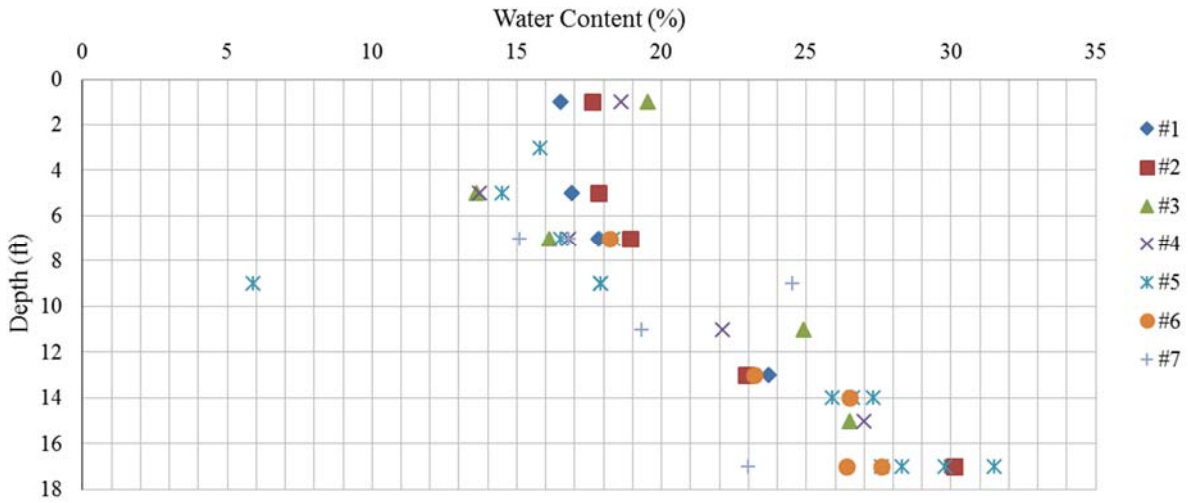

Figure 278. Water Content Variation with Depth.

Table 44. Water Content Measured on Jan. 15, 2013.

Borehole	BH2						BH1			
Depth (ft)	0-2		6-8		14-16		4-6		10-12	
Container (g)	1.00	0.99	0.96	0.98	1.00	0.98	0.97	0.96	0.98	0.98
Container + Sample (g)	20.84	30.09	7.82	8.08	13.78	12.78	22.50	4.78	6.59	5.84
Container + Dry Sample (g)	17.60	25.52	6.87	7.06	11.10	10.27	19.92	4.32	5.47	4.96
Water Content (%)	19.5	18.6	16.1	16.8	26.5	27.0	13.6	13.7	24.9	22.1

Table 45. Water Content Measured on Jan. 17, 2013.

Borehole	BH1						BH2			
Depth (ft)	0-2		6-8		12-14		4-6		16-18	
Container (g)	0.98	0.99	1.00	1.00	0.98	1.00	0.98	0.98	0.97	0.98
Container + Sample (g)	12.07	9.29	7.87	9.54	9.64	11.00	7.35	10.38	13.81	11.01
Container + Dry Sample (g)	10.50	8.05	6.83	8.18	7.98	9.14	6.43	8.96	10.85	8.69
Water Content (%)	16.5	17.6	17.8	18.9	23.7	22.9	16.9	17.8	30.0	30.1

Table 46. Water Content Measured during Direct Shear Test.

Time	Borehole	Depth (ft)	Container (g)	Container + Specimen (g)	Container + Dry Specimen (g)	Water Content (%)
08/19/2013	N4	6-8	0.96	211.83	179.50	18.1
08/20/2013	N3	16-18	0.97	173.76	132.40	31.5
08/21/2013	N3	16-18	1.00	170.36	131.48	29.8
08/21/2013	N3	16-18	0.98	172.42	135.37	27.6
08/29/2013	N4	6-8	0.98	174.98	148.12	18.3
08/29/2013	N3	16-18	0.99	170.74	133.34	28.3
08/29/2013	N1	13-15	0.97	171.45	134.84	27.3
08/29/2013	N1	13-15	0.98	175.36	138.76	26.6
08/29/2013	N1	13-15	1.00	184.03	146.33	25.9
09/06/2013	BH4	4-6	1.00	8.70	7.68	15.3
			1.00	124.98	109.26	14.5
09/07/2013	BH4	6-8	1.00	10.63	9.34	15.5
			1.00	124.73	107.24	16.5
09/07/2013	BH4	8-10	1.00	12.25	10.39	19.8
			1.00	116.60	95.50	22.3
09/11/2013	BH4	2-4	0.98	162.44	140.36	15.8
09/11/2013	BH4	8-10	0.96	162.48	153.46	5.9
09/11/2013	BH4	8-10	0.98	189.37	160.74	17.9
09/11/2013	BH4	8-10	0.99	149.48	126.93	17.9

Table 47. Water Content Measured during Triaxial UU Test.

Time	Borehole	Depth (ft)	Container (g)	Container + Sample (g)	Container + Dry Sample (g)	Water Content (%)	Avg. Water Content (%)
04/22/2013	BH2	12-14	0.99	5.92	5.17	17.9	17.5
			0.97	3.59	3.19	18.0	
			0.98	5.85	5.16	16.5	
07/31/2013	N1	16-18	0.99	5.87	5.09	19.0	18.6
			0.95	5.65	4.89	19.3	
			0.99	7.07	6.17	17.4	
08/01/2013	N2	6-8	0.99	3.87	3.53	13.4	14.2
			0.96	7.32	6.47	15.4	
			0.97	6.23	5.59	13.9	
08/06/2013	N4	13-15	0.98	4.11	3.54	22.3	22.5
			0.97	4.00	3.41	24.2	
			0.96	4.14	3.59	20.9	
08/07/2013	N6	16-18	0.98	3.04	2.74	17.0	17.7
			0.97	2.45	2.22	18.4	
			1.00	3.94	3.50	17.6	

Table 48. Water Content Measured during Triaxial UU Creep Test.

Time start	Time end	Borehole	Depth (ft)	Container + Sample (g)	Container g	Container + Dry Sample (g)	Water Content (%)
10/17/2013	10/21/2013	BH1	10-12	1408.49	13.11	1182.9	19.3
10/21/2013	10/24/2013	N5	16-18	1341.84	3.33	1091.26	23.0
10/24/2013	11/04/2013	N1	6-8	1074.20	2.40	933.21	15.1
11/04/2013	11/13/2013	N3	8-10	1379.34	4.04	1108.26	24.5
11/13/2013	01/06/2014	N6	6-8	209.10	1.00	179.21	16.8

Unit Weight

As in the case of the water content, the unit weight (ASTM D7263, 2009) was measured directly from the samples gathered from boreholes BH1 and BH2. These measurements are presented in Table 49 (data series #1 and #2, Figure 279). In addition, the unit weight was also measured while performing the direct shear tests, the triaxial UU tests, and the triaxial UU creep test. These data are shown separately in Table 51 to Table 53 (also see data series #3 to #5, in Figure 279).

As shown in Figure 279, the unit weight is quite constant, with values between 120 and 130 pcf. Also in this case, the soil sample used in the direct shear test (i.e., the one containing sand) presented the lower value (around 108 pcf).

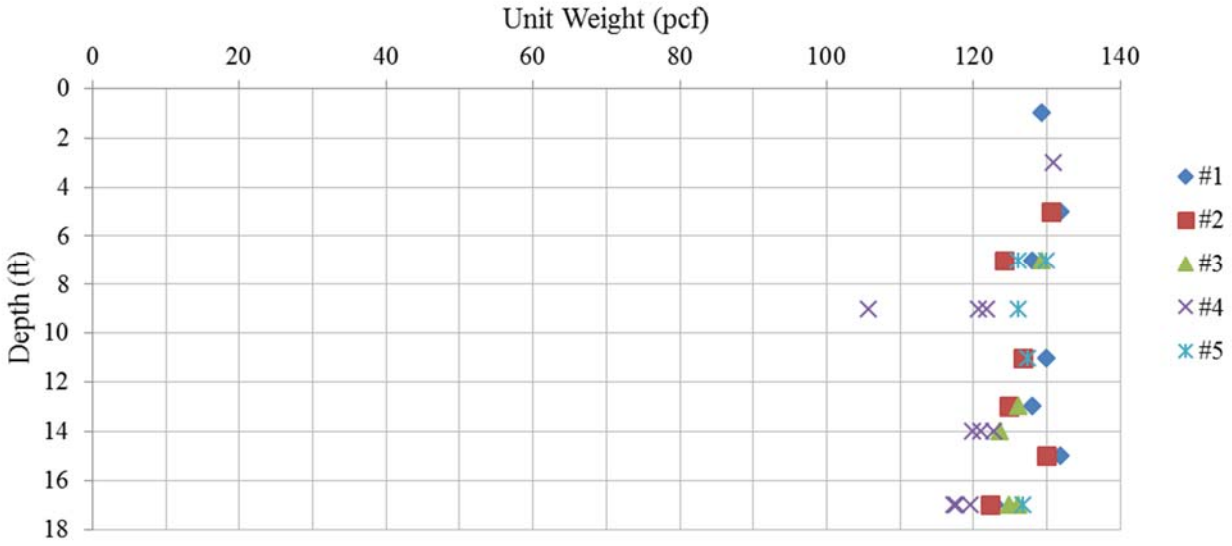

Figure 279. Unit Weight Profile with Depth.

Table 49 (I). Unit Weight Measured on January 22, 2013.

Borehole	BH1	BH2		BH1		BH1	
Depth (ft)	0-2	4-6		6-8		10-12	
Data series	#1	#1	#2	#1	#2	#1	#2
Height (cm)	18.20	17.92	11.45	16.60	13.80	14.80	19.06
	17.90	17.90	12.18	16.90	13.80	14.62	18.36
	18.16	18.30	11.84	16.30	14.40	14.72	18.78
	18.24	18.00	11.90	16.35	14.85	14.72	18.58
Average Height (cm)	18.13	18.03	11.84	16.54	14.21	14.72	18.70
Diameter (in)	2.797	2.886	2.816	2.812	2.812	2.796	2.788
	2.782	2.768	2.808	2.782	2.725	2.739	2.779
	2.768	2.776	2.784	2.806	2.746	2.765	2.777
Average Diameter (cm)	7.067	7.137	7.119	7.112	7.013	7.027	7.065
Mass (g)	1474.32	1520.50	987.79	1304.73	1126.52	1158.18	1523.91
Density (g/cm^3)	2.07	2.11	2.10	1.99	2.05	2.03	2.08
Unit Weight (kN/m^3)	20.3	20.7	20.5	19.5	20.1	19.9	20.4
Unit Weight (pcf)	129.4	131.5	130.7	123.9	128.0	126.6	129.7

Table 50 (II- continuation). Unit Weight Measured on January 22, 2013.

Borehole	BH1		BH2		BH2	
Depth (ft)	12-14		14-16		16-18	
Data series	#1	#2	#1	#2	#1	#2
Height (cm)	16.25	10.80	9.61	17.50	17.21	14.65
	16.32	10.81	8.57	16.80	16.02	15.62
	16.30	10.65	9.36	17.40	16.81	15.61
	16.26	11.05	8.26	16.80	15.68	15.05
Average Height (cm)	16.28	10.83	8.95	17.13	16.43	15.23
Diameter (in)	2.809	2.738	2.784	2.780	2.784	2.871
	2.782	2.755	2.773	2.792	2.745	2.826
	2.811	2.758	2.778	2.776	2.805	2.794
Average Diameter (cm)	7.114	6.986	7.057	7.068	7.056	7.189
Mass (g)	1329.97	829.55	729.26	1418.50	1261.38	1218.37
Density (g/cm^3)	2.06	2.00	2.08	2.11	1.96	1.97
Unit Weight (kN/m^3)	20.1	19.6	20.4	20.7	19.2	19.3
Unit Weight (pcf)	128.2	124.7	130.0	131.7	122.5	122.9

Table 51. Unit Weight Measured during Direct Shear Test.

Time	Borehole	Depth (ft)	Height (in)	Avg. Height (in)	Diameter (in)	Avg. Diameter (in)	Whole Specimen (g)	Density (g/cm^3)	Unit Weight (kN/m^3)	Unit Weight (pcf)
08/19/2013	N4	6-8	1.335	1.335	2.464	2.463	211.59	2.03	19.9	126.6
			1.330		2.481					
			1.339		2.445					
08/21/2013	N3	16-18	1.166	1.165	2.440	2.453	169.7	1.9	18.4	117.3
			1.165		2.450					
			1.163		2.470					
08/21/2013	N3	16-18	1.148	1.150	2.462	2.467	172.6	1.9	18.8	119.5
			1.148		2.474					
			1.154		2.464					
08/29/2013	N4	6-8	1.200	1.174	2.462	2.447	174.1	1.9	18.9	120.0
			1.164		2.428					
			1.158		2.452					
08/29/2013	N3	16-18	1.169	1.179	2.434	2.437	170.0	1.9	18.5	117.6
			1.181		2.430					
			1.187		2.448					
08/29/2013	N1	13-15	1.165	1.151	2.426	2.439	170.7	1.9	19.0	120.9
			1.144		2.450					
			1.144		2.440					
08/29/2013	N1	13-15	1.169	1.175	2.452	2.454	174.9	1.9	18.8	119.8
			1.180		2.459					
			1.176		2.450					
08/29/2013	N1	13-15	1.222	1.217	2.424	2.440	183.5	2.0	19.3	122.7
			1.209		2.475					
			1.220		2.422					
09/11/2013	BH4	2-4	1.014	1.017	2.419	2.428	161.6	2.1	20.5	130.8
			1.012		2.428					
			1.024		2.436					
09/11/2013	BH4	8-10	1.220	1.241	2.454	2.446	162.0	1.7	16.6	105.7
			1.235		2.408					
			1.269		2.476					
09/11/2013	BH4	8-10	1.275	1.288	2.468	2.425	188.5	1.9	18.9	120.6
			1.305		2.406					
			1.285		2.401					
09/11/2013	BH4	8-10	1.082	1.067	2.368	2.356	148.6	2.0	19.1	121.7
			1.055		2.339					
			1.063		2.360					

Table 52. Unit Weight Measured during Triaxial UU Test.

Time	Borehole	Depth (ft)	Height (in)	Avg. Height (in)	Diameter (in)	Avg. Diameter (in)	Whole Specimen (g)	Density (g/cm^3)	Unit Weight (kN/m^3)	Unit Weight (pcf)
07/31/2013	N1	16-18	6.90	6.99	2.736	2.736	1352.0	2.0	19.7	125.3
			7.00		2.742					
			7.06		2.730					
08/01/2013	N2	6-8	6.50	6.48	2.763	2.745	1298.5	2.1	20.2	128.9
			6.50		2.727					
			6.44		2.746					
08/06/2013	N4	13-15	5.77	5.76	2.712	2.749	1110.2	2.0	19.4	123.7
			5.75		2.755					
			5.75		2.780					
08/07/2013	N6	16-18	6.60	6.61	2.727	2.736	1275.6	2.0	19.6	124.9
			6.62		2.725					
			6.62		2.756					

Table 53. Unit Weight Measured during Triaxial UU Creep Test.

Time start	Time end	Borehole	Depth (ft)	Height (cm)	Height (in)	Avg. Height (in)	Diameter (in)	Avg. Diameter (in)	Specimen (g)	Unit Weight (kN/m^3)	Unit Weight (pcf)
10/09/2013	10/09/2013	BH1	12-14	16.25	6.398	6.427	2.723	2.759	1297.3	20.2	128.5
				16.3	6.417		2.768				
				16.42	6.465		2.786				
10/14/2013	10/17/2013	BH1	14-16	17	6.693	6.698	2.787	2.785	1300.3	19.1	121.3
				16.94	6.669		2.766				
				17.1	6.732		2.803				
10/17/2013	10/21/2013	BH1	10-12	17.5	6.890	6.854	2.760	2.773	1386.3	20.0	127.5
				17.37	6.839		2.801				
				17.36	6.835		2.757				
10/21/2013	10/24/2013	N5	16-18	17.58	6.921	6.923	2.700	2.715	1334.1	19.9	126.7
				17.71	6.972		2.743				
				17.46	6.874		2.703				
10/24/2013	11/04/2013	N1	6-8	13.51	5.319	5.280	2.759	2.741	1060.5	20.4	129.6
				13.38	5.268		2.726				
				13.34	5.252		2.739				
11/04/2013	11/13/2013	N3	8-10	18.10	7.125	7.063	2.747	2.734	1372.1	19.8	126.0
				17.94	7.063		2.722				
				17.78	7.000		2.733				
11/13/2013	01/06/2014	N6	6-8	13.25	5.217	5.220	2.752	2.738	1018.7	19.8	126.2
				13.03	5.130		2.756				
				13.5	5.315		2.706				

Degree of Saturation

As discussed previously, the degree of saturation can be calculated from Eq. 8. The data in Table 44, Table 45, and Table 49 were used here to calculate the degree of saturation. Note that at each depth two determinates of water content were performed (i.e., from Table 44 or Table 45), and only one of unit weight (Table 49). Therefore, four different saturations (i.e., data series #1 to #4, Figure 280) were calculated, as shown in Table 54. Though the depth of

groundwater level is 18 ft, samples from depths between 0 and 18 ft are still near full saturation ($S_r \geq 85\%$, Figure 280), which is quite typical of HP clays.

Table 54. Degree of Saturation Calculated Based on Table 44, Table 45, and Table 49.

Data Series	Unit Weight (pcf)	Depth (ft)	Water Content (%)	Void Ratio	Saturation (%)
1	129.2	1	16.5	0.49	89
	131.8	5	16.9	0.47	96
	128.0	7	17.8	0.52	90
	129.9	11	24.9	0.59	112
	128.0	13	23.7	0.60	105
	131.8	15	26.5	0.59	120
	122.9	17	30	0.75	106
2	129.2	1	17.6	0.50	92
	131.8	5	17.8	0.48	99
	128.0	7	18.9	0.54	93
	129.9	11	22.1	0.55	106
	128.0	13	22.9	0.59	103
	131.8	15	27	0.59	121
	122.9	17	30.1	0.75	106
3	129.2	1	16.5	0.49	89
	130.5	5	16.9	0.48	93
	124.1	7	17.8	0.57	83
	126.7	11	24.9	0.63	105
	124.8	13	23.7	0.64	98
	129.9	15	26.5	0.61	115
	122.2	17	30	0.76	105
4	129.2	1	17.6	0.50	92
	130.5	5	17.8	0.49	96
	124.1	7	18.9	0.58	86
	126.7	11	22.1	0.59	99
	124.8	13	22.9	0.63	97
	129.9	15	27	0.62	116
	122.2	17	30.1	0.76	105

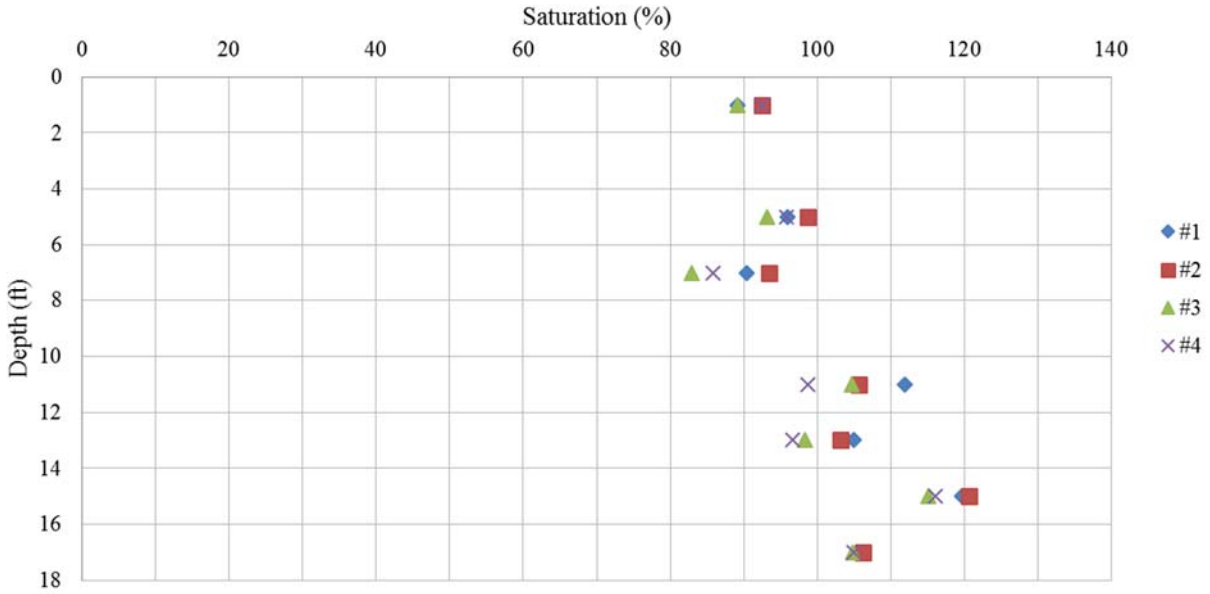

Figure 280. Variation of the Degree of Saturation with Depth.

Atterberg's Limits

The Atterberg's limits were carried out on soil samples at five different depths. The PI profile of the tested soil samples and the test data are shown in Figure 281 and Table 55, respectively. As shown in Figure 281, the PI varies between 35 and 50. Therefore, the soil at the NGES-TAMU clay site can be classified as is a HP clay, with an average PI of 40.

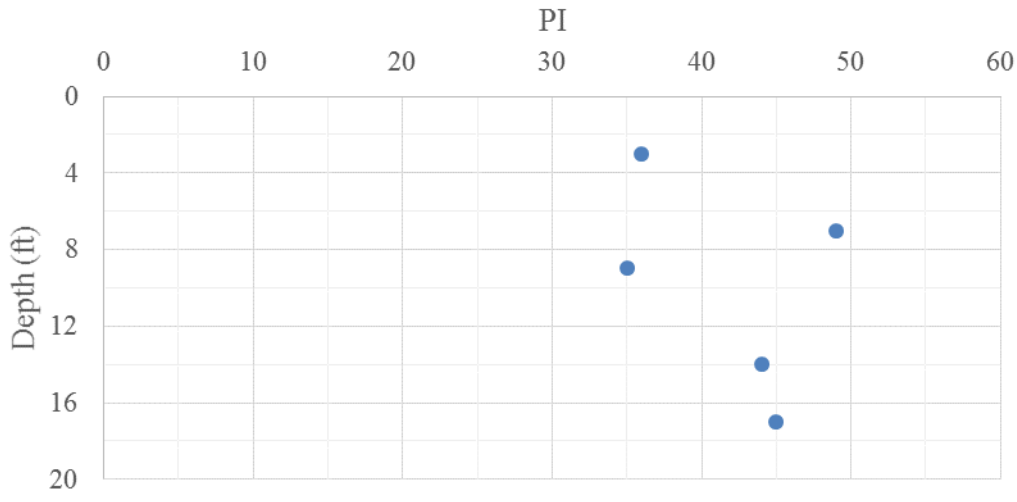

Figure 281. Variation of the PI with Depth.

Table 55. Atterberg's Limits Test Data.

Borehole	Depth (ft)	Atterberg's Limits	Number	Container (g)	Container + Sample (g)	Container + Dry Sample (g)	Water Content (%)	Blows	Avg. Water Content (%)	PI
N2	13-15	PL	#1	1.00	15.18	12.16	27.1	NA	27.0	44
			#2	1.00	21.11	16.85	26.9	NA		
		LL	#1	1.00	24.20	14.75	68.7	28	71.4	
			#2	1.00	21.70	13.10	71.1	16		
			#3	1.00	21.02	12.71	71.0	30		
			#4	1.00	22.36	13.22	74.8	23		
N1	8-10	PL	#1	0.98	6.86	5.95	18.3	NA	20.5	35
			#2	1.02	5.12	4.36	22.8	NA		
		LL	#1	0.99	9.50	6.48	55.0	17	55.6	
			#2	0.99	9.10	6.18	56.3	18		
			#3	1.02	8.35	5.73	55.6	22		
N1	6-8	PL	#1	0.99	3.12	2.78	19.0	NA	20.0	49
			#2	0.99	3.07	2.71	20.9	NA		
		LL	#1	1.00	11.66	7.28	69.7	17	69.1	
			#2	0.99	6.97	4.53	68.9	26		
			#3	0.98	6.83	4.45	68.6	18		
N5	16-18	PL	#1	0.98	2.80	2.53	17.4	NA	17.8	45
			#2	0.99	3.13	2.80	18.2	NA		
		LL	#1	1.00	9.36	6.18	61.4	36	62.7	
			#2	1.01	8.80	5.78	63.3	29		
			#3	0.99	8.75	5.74	63.4	33		
BH2	2-4	PL	#1	0.98	4.66	4.15	16.1	NA	16.3	36
			#2	1.02	3.13	2.83	16.6	NA		
		LL	#1	1.00	6.96	5.04	47.5	34	52.3	
			#2	1.00	4.01	2.93	56.0	19		
			#3	1.00	9.00	6.21	53.6	16		

Soil Strength

The results of the direct shear test (ASTM D3080/D3080M, 2011) and triaxial UU test (ASTM D2850-03a, 2007) are presented in this section. In addition to direct shear and triaxial tests, pocket penetrometer tests were performed on the soil samples. Most of the results indicated a strength of 4.5 ton/ft^2. Based on these data, this soil at the NGES-TAMU clay site can be categorized as a stiff clay.

Direct Shear Test

As mentioned in previous sections, Eq. 2 can be used to estimate the vertical stress at different depths. Table 56 shows the normal stress to be applied in the direct shear test.

Table 56. Estimation of the In Situ Stress (Self-Weight Only).

Depth (ft)	Depth (m)	σ_3 (kPa)	σ_3 (psi)
1	0.3	6	0.9
3	0.91	18	2.7
5	1.52	30	4.4
7	2.13	43	6.2
9	2.74	55	8
11	3.35	67	9.7
13	3.96	79	11.5
15	4.57	91	13.3
17	5.18	104	15

The ratios of the applied normal stress over the self-weight stress are 0.5, 1, 2, and 3 (Table 57).

Table 57. Summary of the Applied Normal Stress.

Borehole	Depth (ft)	Depth (ft)	Normal Stress Applied (psi)	Shear Stress at Failure (psi)	Note (Applied Normal Stress/Normal Stress by Gravity)
N3	16-18	17	6.92	22.22	0.5
B2	2-4	3	2.38	26.24	1
B2	4-6	5	4.21	27.95	1
N4	6-8	7	6.94	52.42	1
B2	6-8	7	6.28	37.89	1
B2	8-10	9	9.38	16.39	1
N1	13-15	14	11.8	14.83	1
N3	16-18	17	16.51	15.43	1
N4	6-8	7	11.72	37.54	2
B2	8-10	9	16.71	39.14	2
N1	13-15	14	23.31	22.38	2
N3	16-18	17	30.31	21.27	2
B2	8-10	9	25.29	31.83	3
N1	13-15	14	37.71	19.68	3
N3	16-18	17	44.89	21.95	3

The applied strain rate was 0.5 mm/min, considering that the diameter of the shear box is 2.5 in., the strain rate is around 1 percent/min. All the soil samples used to perform the direct shear tests are listed as follows (see also Table 57):

- Borehole N1, samples from a depth located between 13 and 15 ft, tests at three different applied normal stresses were performed.
- Borehole N3, samples from a depth located between 16 and 18 ft, tests at three different applied normal stresses were performed.
- Borehole N4, samples from a depth located between 6 and 8 ft, tests at two different applied normal stresses were performed.

- Borehole BH4, samples from four depths; for samples from depths between 8 and 10 ft tests at three different applied normal stresses were performed; for the other depths (i.e., between 2 and 4 ft, 4 and 6 ft, and 6 and 8 ft), only one applied normal stress was adopted.

The test results and photographs of the samples at depths 13 to 15 ft from borehole N1 are shown in Figure 282 and Figure 283, respectively. All curves reach the peak strength and then drop to the residual strength. The peak strength is between 15 and 23 psi, while the residual strength is between 9 and 12 psi. The ratio of the residual strength over the peak strength is about 0.55. However, by increasing the applied normal stress the peak stress does not increase, while the residual strength increases. The same behavior was observed in other samples.

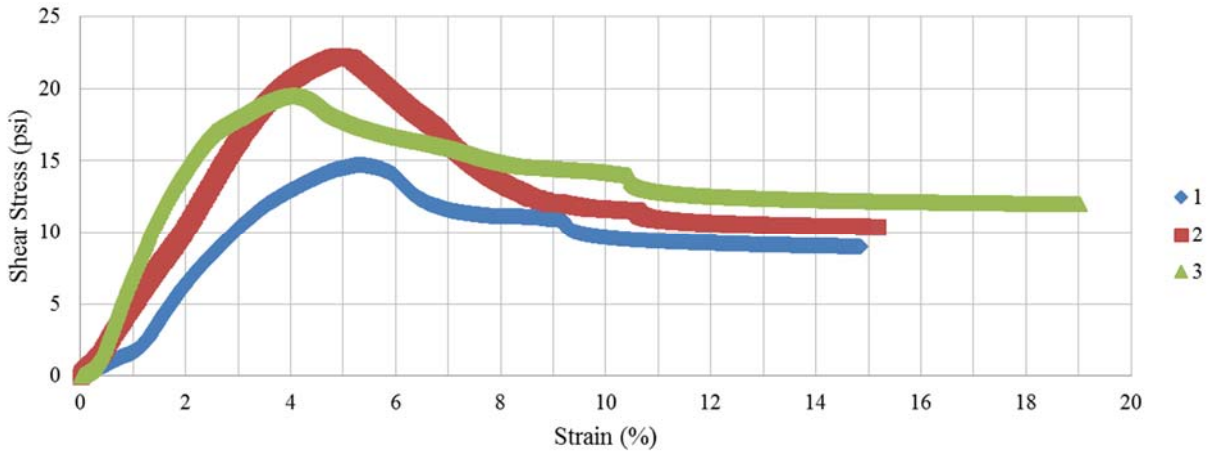

Figure 282. Direct Shear Tests on Samples, Depths 13 to 15 Ft, Borehole N1.

Figure 283. Photos of Samples (Depths 13 to 15 Ft Borehole N1) at Failure a) at Ratio of 1, b) at Ratio of 2, and c) at Ratio of 3.

The test results and photos of samples at depths between 16 and 18 ft from borehole N3 are shown in Figure 284 and Figure 285, respectively. All curves reach the peak strength then drop to the residual strength. All peak strengths are 22 psi, except for the ratio equal to 1 the

peak strength is 16 psi. The residual strengths are between 4 and 11 psi. The ratio of residual strength over peak strength is between 0.2 and 0.5.

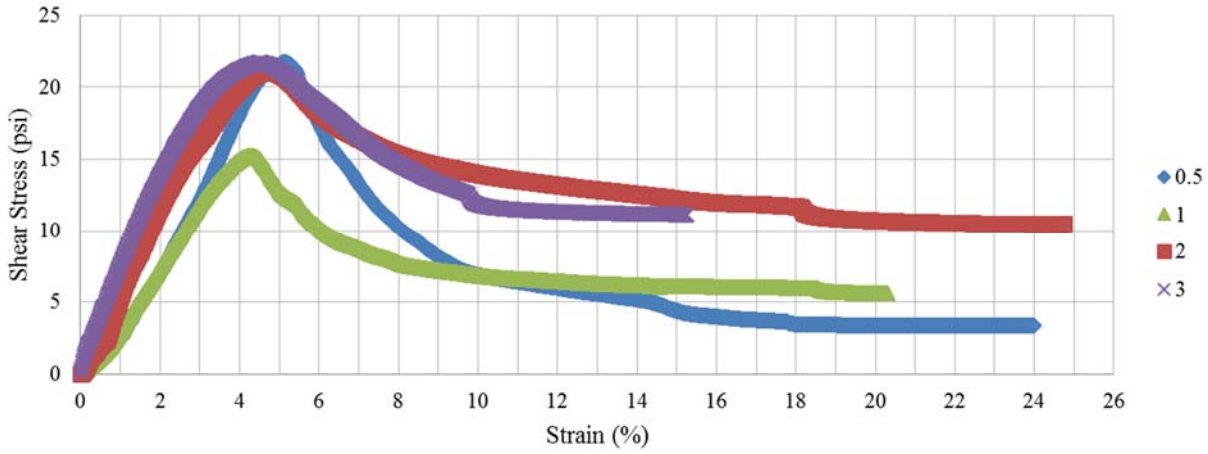

Figure 284. Results of Direct Shear Tests on Samples from Depths 16 to 18 Ft, Borehole N3. Tests at Different Applied Normal Stresses.

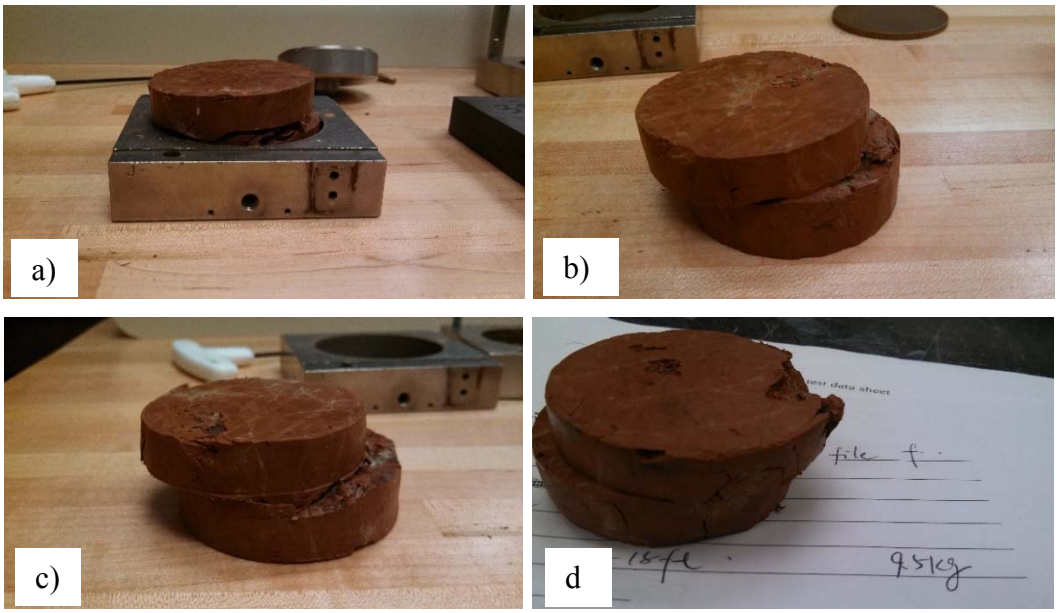

Figure 285. Photos of Samples after Failure, Depths between 16 and 18 Ft, Borehole N3 a) at Ratio of 0.5, b) at Ratio of 1, c) at Ratio of 2, and d) at Ratio of 3.

The test results and photos from samples at depths between 6 and 8 ft from borehole N4 are shown in Figure 286 and Figure 287, respectively. Two different normal stresses were applied. All curves reach the peak strength and then drop to the residual strength. This corresponds to a very stiff layer, and the peak strength is between 38 and 50 psi (i.e., these are

around twice the values obtained from samples at other depths). The residual strength is between 5 and 9 psi, which is close to the residual strength obtained from samples at other depths. In this case, the ratio of residual strength over peak strength is between 0.1 and 0.25, which is much lower than the results from samples at other depths and boreholes. Results from the triaxial UU test and the triaxial UU creep test also confirm that this is a very stiff clay.

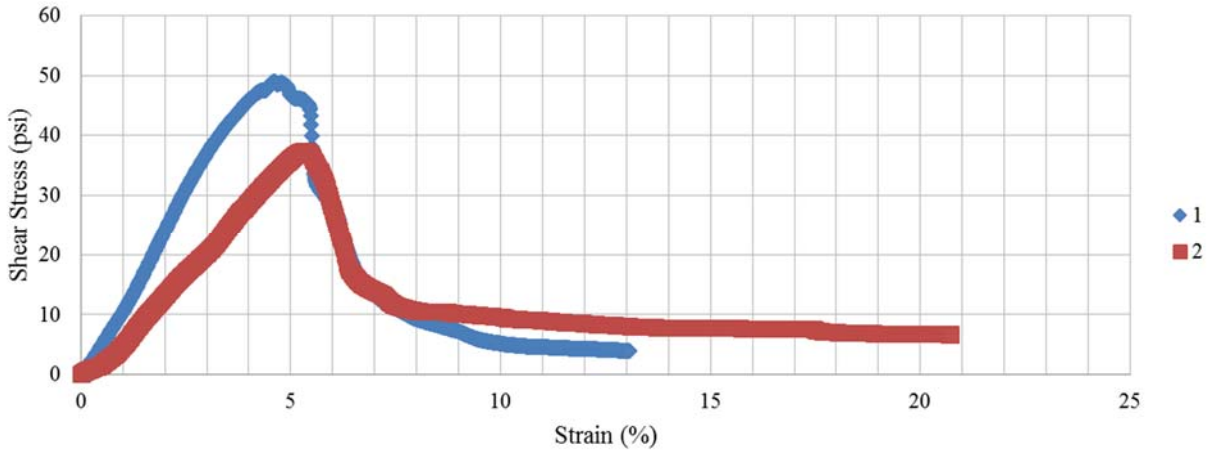

Figure 286. Direct Shear Test on Samples at Depths between 6 and 8 Ft, Borehole N4, Different Applied Normal Stresses.

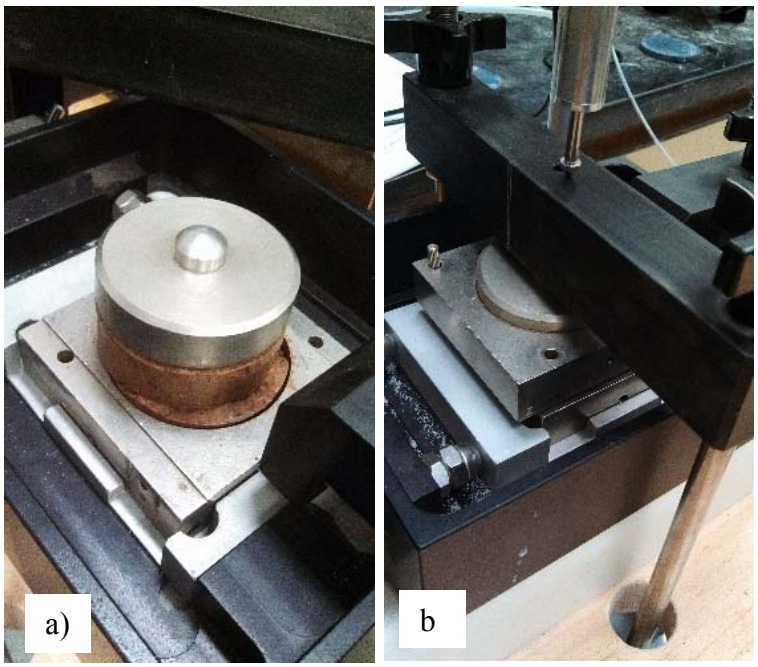

Figure 287. Photos of Samples (Depths between 6 and 8 Ft, Borehole N4) at Failure a) at Ratio of 1, and b) at Ratio of 2.

Figure 288 and Figure 289 show test results and photos of samples at depths between 8 and 10 ft from borehole BH4. All curves reach the peak strength then drop to the residual strength. The ratio of residual strength over peak strength is between 0.4 and 0.7. The sample with the ratio equal to 1 (Figure 289a) contains an important amount of dry sand. It was also observed that the color of this sample is quite different from the other samples. The peak strength and residual strength of this sample is much lower than those of the clay sample without dry sand taken from a similar depth.

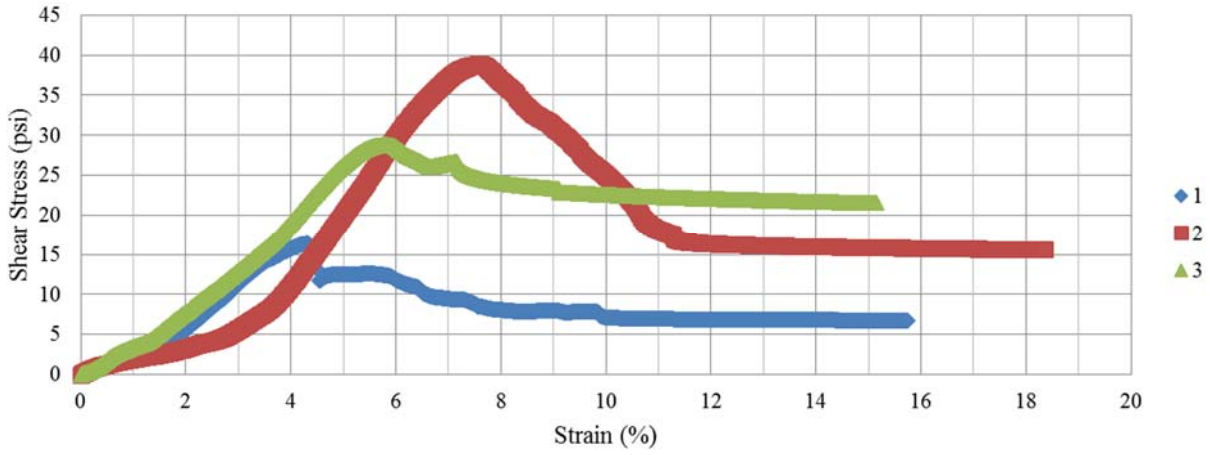

Figure 288. Direct Shear Test on Samples from a Depth between 8 and 10 Ft, Borehole BH4, Different Applied Normal Stress.

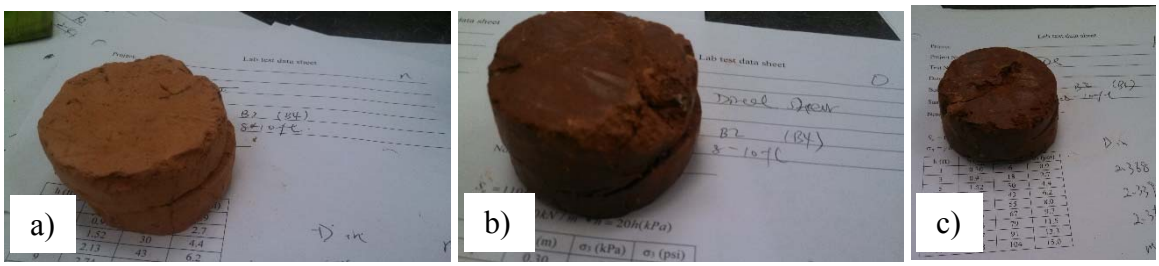

Figure 289. Photos of Samples (Depths 8~10 Ft, Borehole BH4) at Failure a) at Ratio of 1, b) at Ratio of 2, and c) at Ratio of 3.

Figure 290 shows test results of samples at different depths from the same borehole (BH4). The ratio of applied normal stress over stress by gravity is equal to 1 in all these tests. All curves reach the peak strength then drop to residual strength. The following observations can be drawn from Figure 290:

- The layer at a depth between 6 and 8 ft is very stiff, particularly when compared to the other layers at different depths.
- Shallow samples exhibited larger residual strengths, at least from a depth between 2 and 10 ft. In Figure 291, the strength decreases with depth, excluding the much stiffer layer between 6 and 10 ft. It seems this is caused by desiccation.
- The sample at a depth between 8 and 10 ft, which contains dry sand, exhibited a different behavior (see Figure 291).

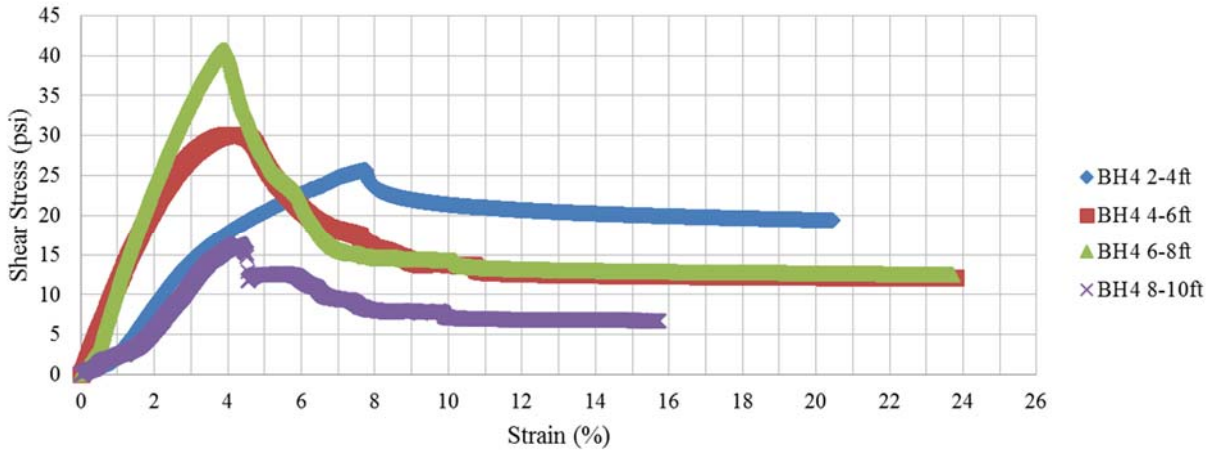

Figure 290. Direct Shear Test on Samples at Different Depths. Borehole BH4.

Figure 291. Direct Shear Test Shear Strength Profile with Depth.

Figure 291 shows the shear strengths of the soil at different depth obtained from direct shear tests. Excluding the much stiffer layer from 6 and 10 ft, the shear strength varies between 15 and 28 psi. The strength decreases with depth from 0 to 10 ft, then it becomes nearly constant at depths between 10 and 18 ft. This strength difference can be attributed to soil desiccation.

Triaxial UU Test

As with the direct shear test, the in situ stress is assumed to be equal to the soil self-weight, though it is not always in reality. Three samples at different depths from different boreholes were tested. The soil samples used in these tests were gathered from the borehole N2 at depths between 6 and 8 ft, from borehole N4 at depths between 13 and 15 ft, and from borehole N6 at depths between 16 and 18 ft. Only one confining stress was applied to each sample (i.e., ratio of applied confining stress over self-weight stress was equal to 1). The strain rate was 1 percent/min.

Test results and photos of the triaxial UU tests are shown in Figure 292 and Figure 293, respectively. The shear strength obtained from the triaxial UU test is similar to the shear strength obtained from direct shear tests, as shown in Figure 294. The peak strength varies considerably with a maximum value around 52 psi at depths between 6 and 8 ft. The residual strength is around 10 psi.

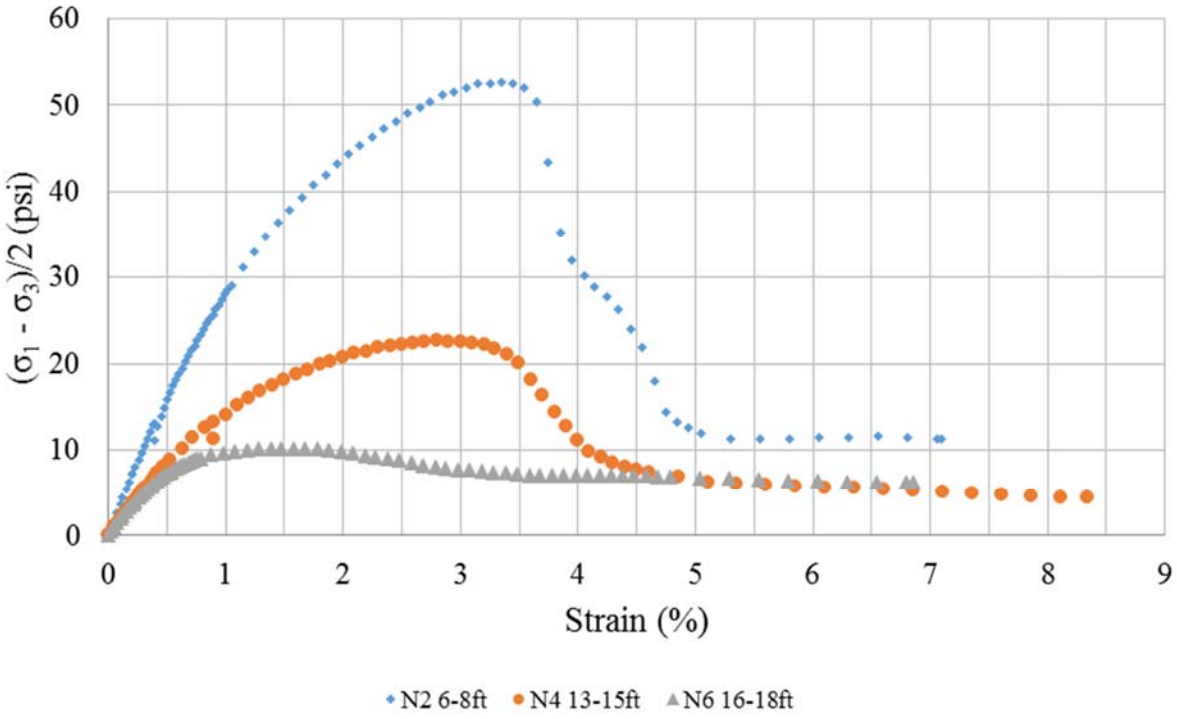

Figure 292. Triaxial UU Test.

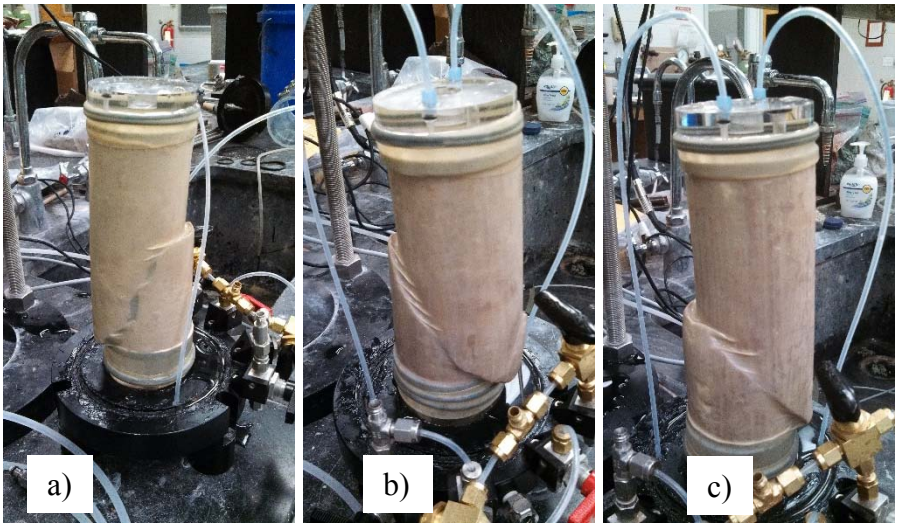

Figure 293. Photos of the Triaxial UU Test at a) N2, Depth between 6 and 8 Ft; b) N4, Depth between 13 and 15 Ft; and c) N6, Depth between 16 and 18 Ft.

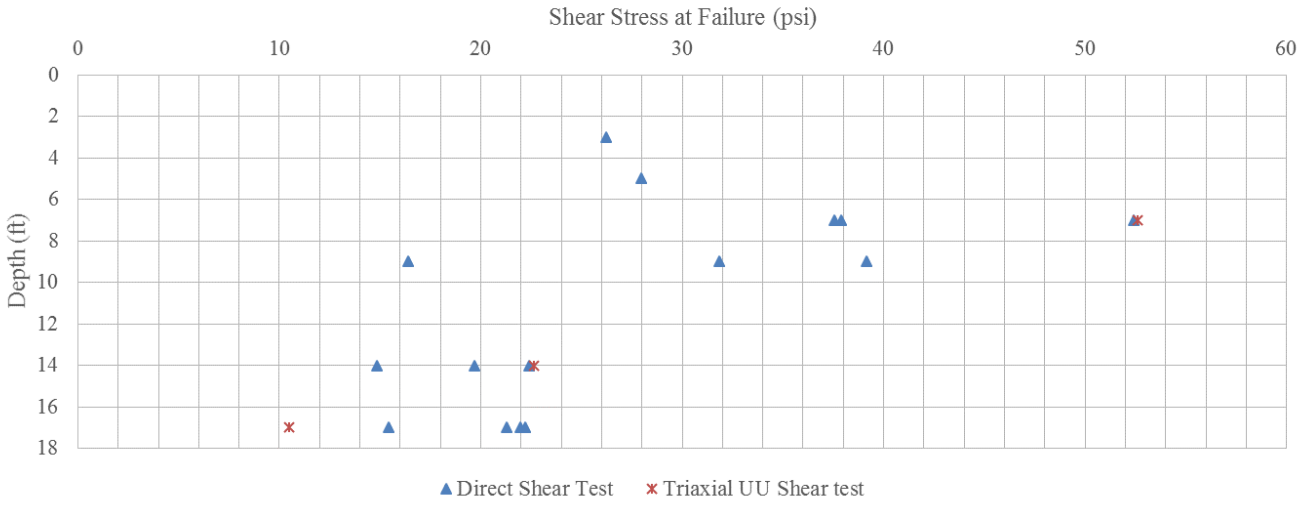

Figure 294. Soil Strength Profile with Depth.

The curves in Figure 292 were fitted using a hyperbolic model. In Figure 295 to Figure 297, the stress strain curves presented in Figure 292 were replotted in the space, "Strain/Stress versus Strain (%)," which is typically used to find the two parameters needed to define the hyperbola. The experimental curves fitted very well with the line defining the hyperbola in this space. The curves until failure were normalized in terms of the peak stress and the strain corresponding to peak stress (Figure 298).

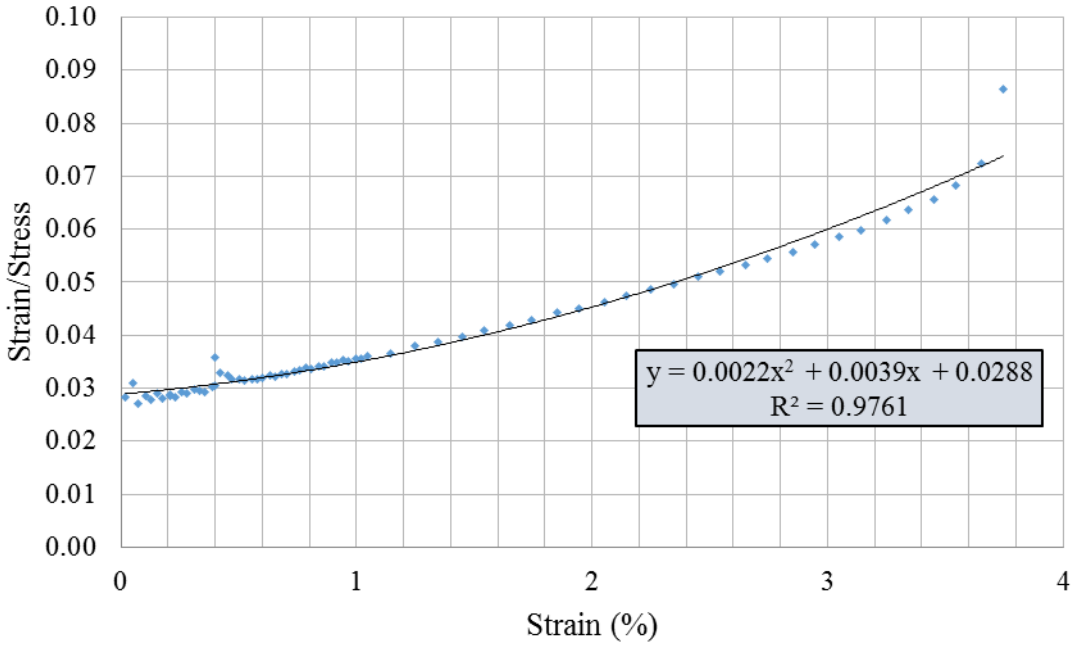

Figure 295. Sample at Depths between 6 and 8 Ft from Borehole N2 (Hyperbola Fitting).

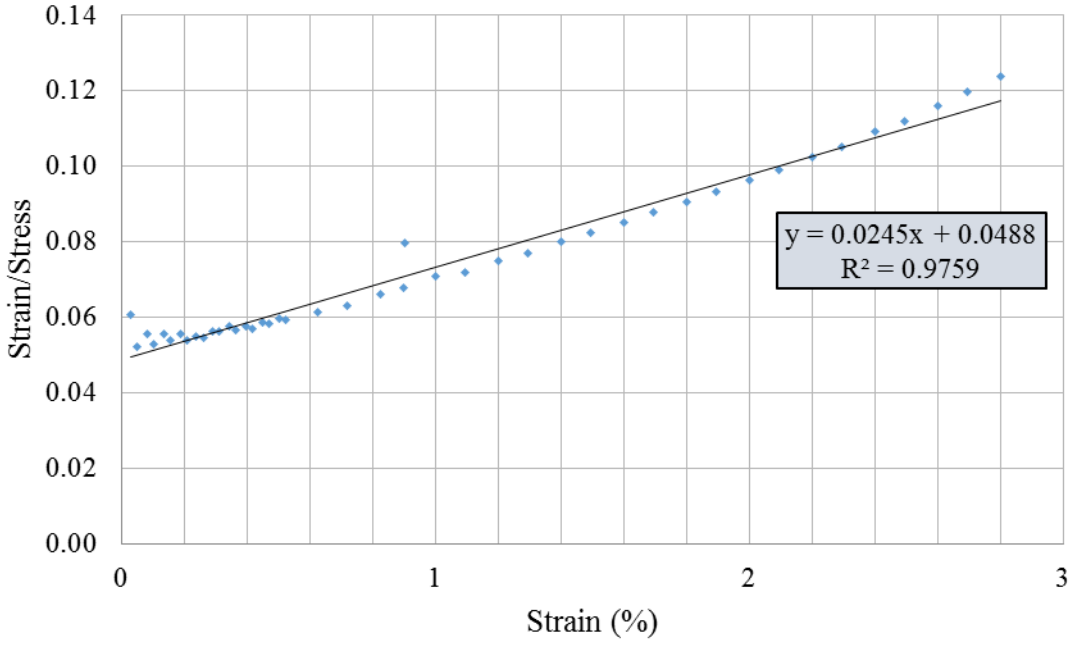

Figure 296. Sample at Depths between 13 and 15 Ft from Borehole N4 (Hyperbola Fitting).

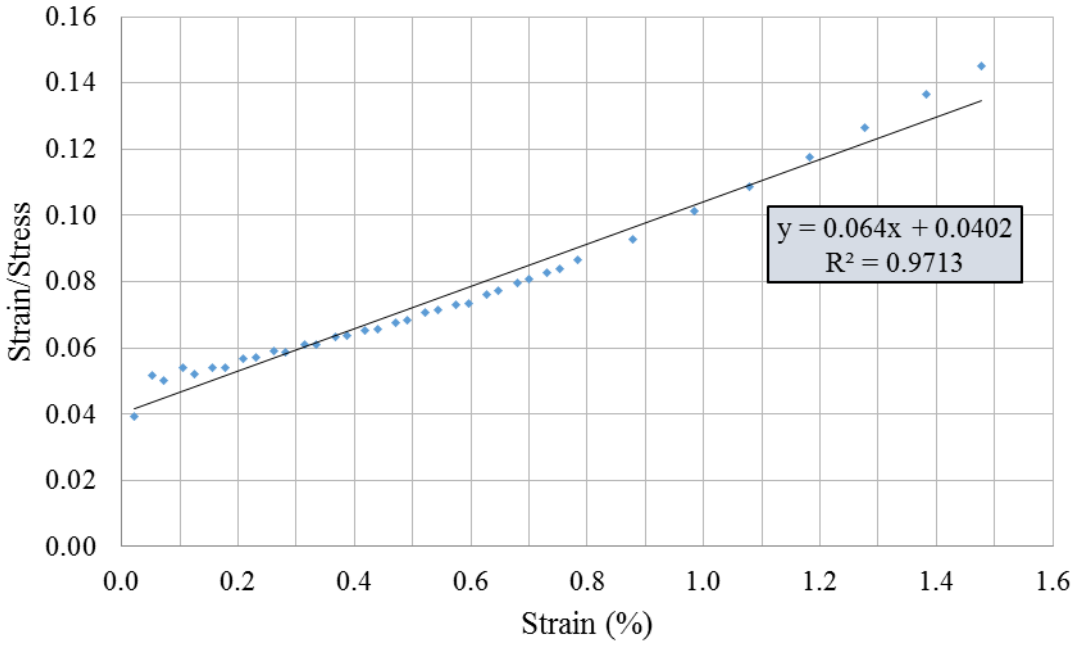

Figure 297. Sample at Depths between 16 and 18 Ft from Borehole N6 (Hyperbola Fitting).

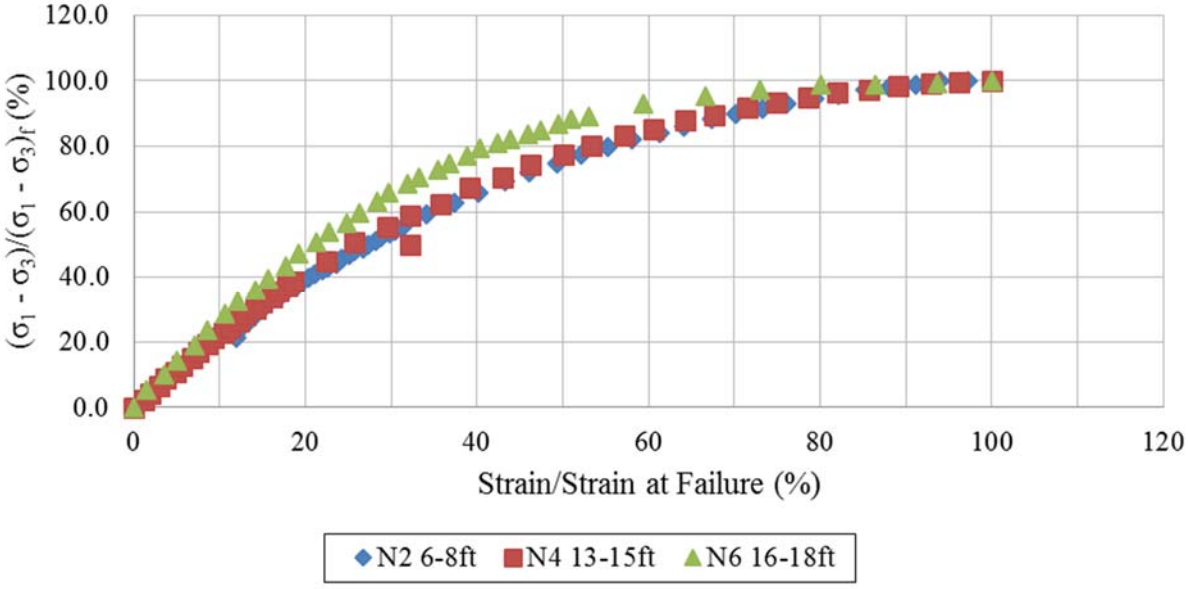

Figure 298. Normalization of Curves from Triaxial UU Tests.

Creep Behavior, Triaxial UU Creep Tests

The triaxial UU creep test is similar to the triaxial UU test except that creep is allowed at specific preselected loads. In this case, the applied confining stress is assumed to be related to the

self-weight of the soil. Table 45 reports the adopted values. In short, the general procedure adopted for the triaxial creep test is:

1. Prepare the samples in the usual way for triaxial tests.
2. Set the triaxial cell, the instruments, and the cell pressure following the typical practice for triaxial tests.
3. Apply the axial loading following a strain control procedure.
4. After reaching the first target load for the creep stage, switch the device to stress control to allow samples to creep.
5. Record the creep deformation for a predefined period of time. (Generally, the researchers used 24 hours, but in some tests up to several days.)
6. Once the creep stage is completed, switch the device back to strain control and increase the axial load until reaching the subsequent target load selected for the creep test; at this point, switch the machine again to stress control.
7. Repeat the procedure indicated from step 5 in subsequent creep stages until the failure of the sample.

Strain rate in the loading part was 1 percent/min. The selected holding loads were 30, 70, 110, 190, and then until failure. Both equal and unequal load increments were investigated in the laboratory. Based on the soil strength profile (i.e., Figure 294), for the samples with higher strength more steps would be applied. In total, four triaxial UU creep tests were performed on the following samples:

- From borehole N1, depth between 6 and 8 ft.
- From borehole N6, depth between 6 and 8 ft.
- From borehole N3, depth between 8 and 10 ft.
- From borehole BH1, depth between 10 and 12 ft.

Triaxial UU Creep Test on a Sample from Borehole N1, Depth between 6 and 8 Ft

The holding loads for this test were: 30, 70, 110, 390, and 430 lb. The sample failed at 430 lb after holding this load for 90 min. Each load was held for 24 hours.

Figure 299 shows the complete stress–strain curve. Creep was observed at low loads; as expected, the more noticeable creep was observed at higher holding loads.

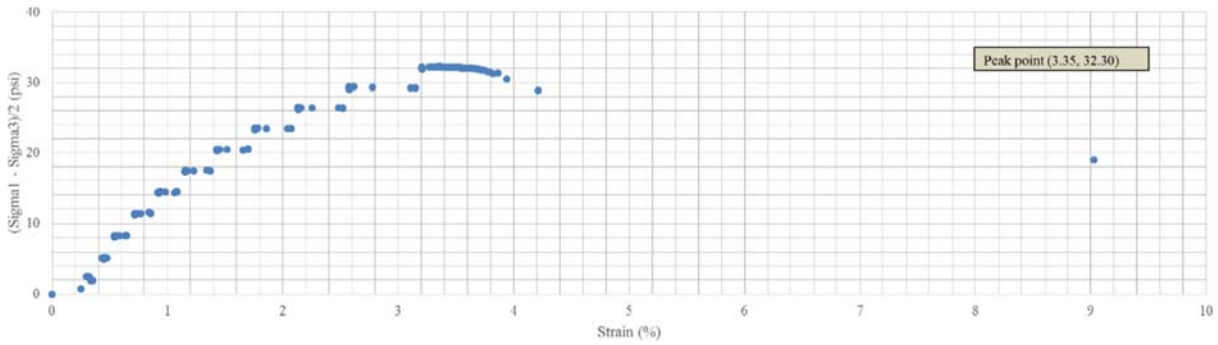

Figure 299. Stress–Strain Curve of a Triaxial UU Creep Test on a Sample from a Depth between 6 and 8 Ft from Borehole N1.

The strain–time curves for all the creep loads applied in this test are presented in Figure 300 and Figure 301 in linear scale and log–log scale, respectively. These figures clearly show that the sample deformations accelerate when approaching the failure load (around 430 lb).

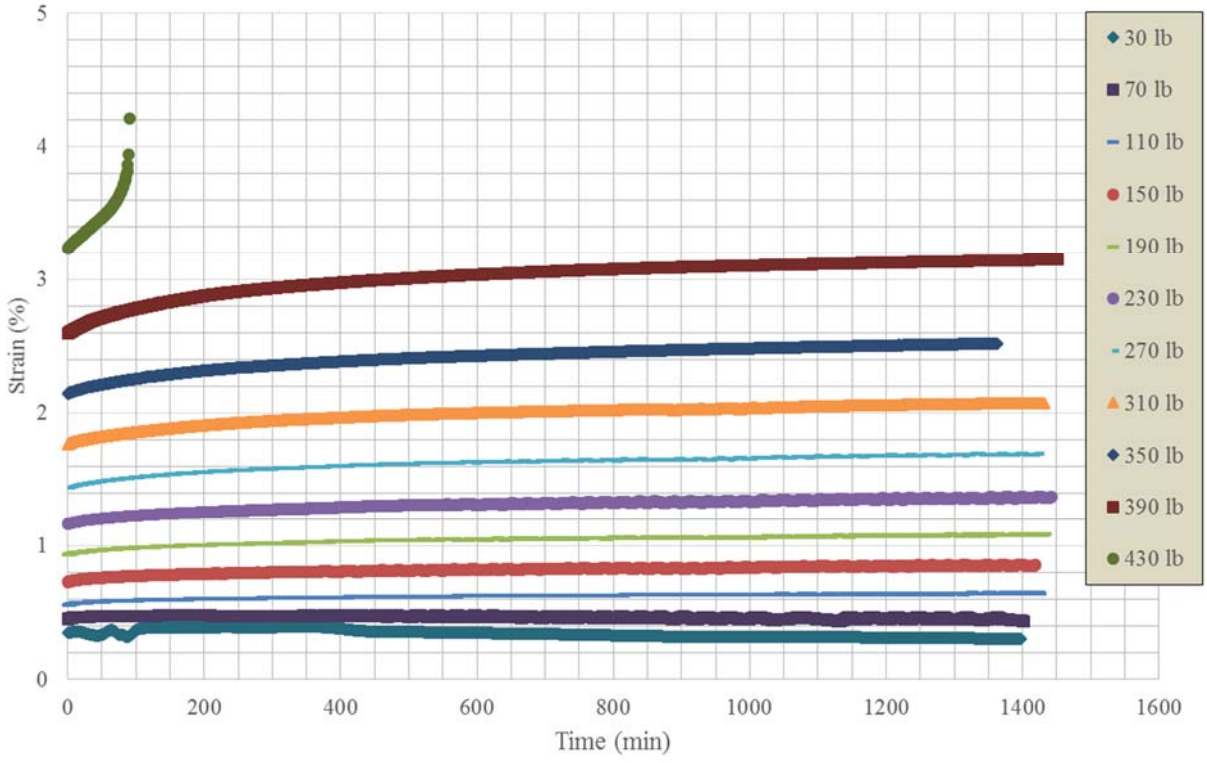

Figure 300. Strain Time Curves (Linear Scale) for All Loads of the Triaxial UU Creep Test from a Sample at a Depth between 6 and 8 Ft from Borehole N1.

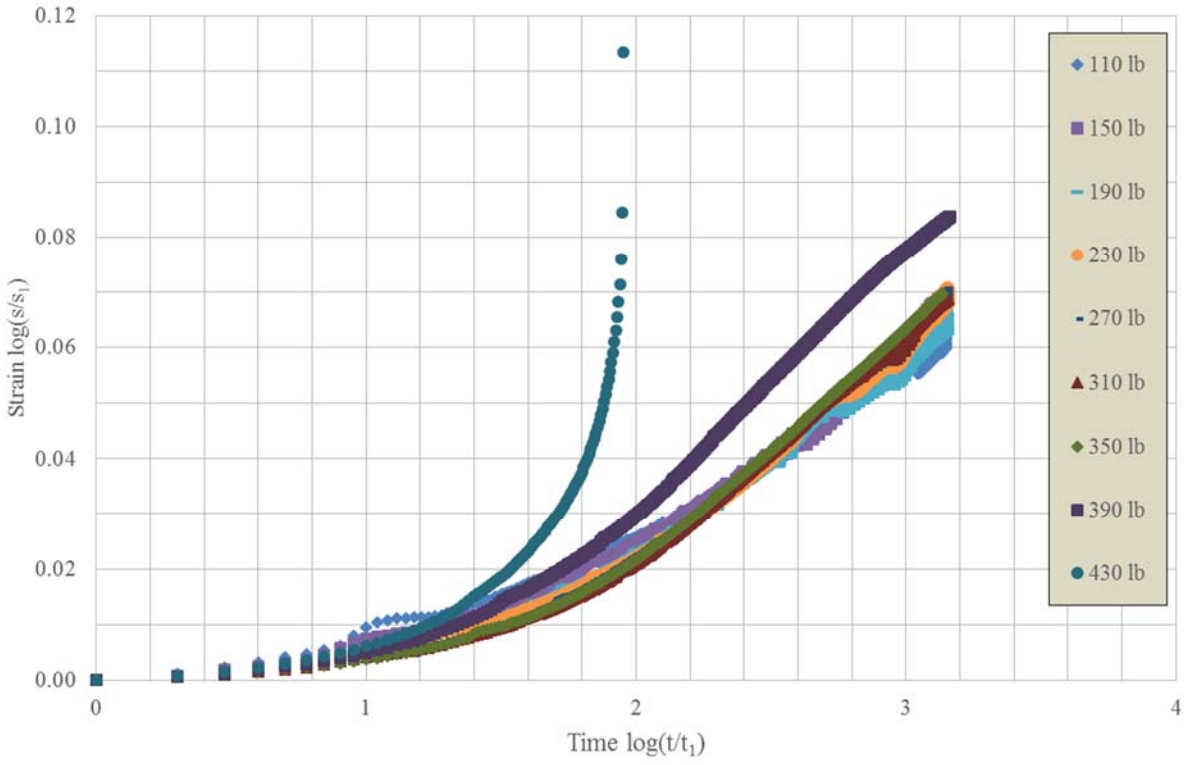

Figure 301. Strain Time Curves (Log–Log Scale) for All Loads excluding the Initial One, Triaxial UU Creep Test at a Depth between 6 and 8 Ft from Borehole N1.

Triaxial UU Creep Test on Sample from Borehole N6, Depth between 6 and 8 Ft

The holding loads for this test were: 190, 230, 270, 430, and 470 lb. Each load was held for a period of 24 hours. Based on the previous test results on samples from the same depth from borehole N1, 470 lb was adopted as the target failure load. Therefore, the stage at 470 lb was held for eight weeks. However, the sample did not fail and the sample was then loaded until failure. The sample failed at a load equal to 578 lb. Figure 302 shows the complete stress–strain curve. Strain–time curves are plotted in linear scale and log–log scale in Figure 303 and Figure 304, respectively.

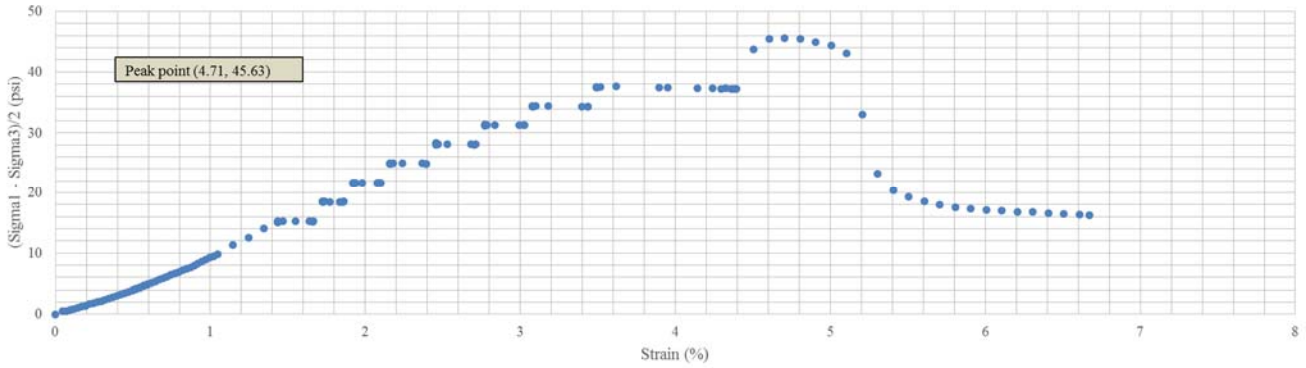

Figure 302. Stress–Strain Curve of the Triaxial UU Creep Test from the Sample at a Depth between 6 and 8 Ft from Borehole N6.

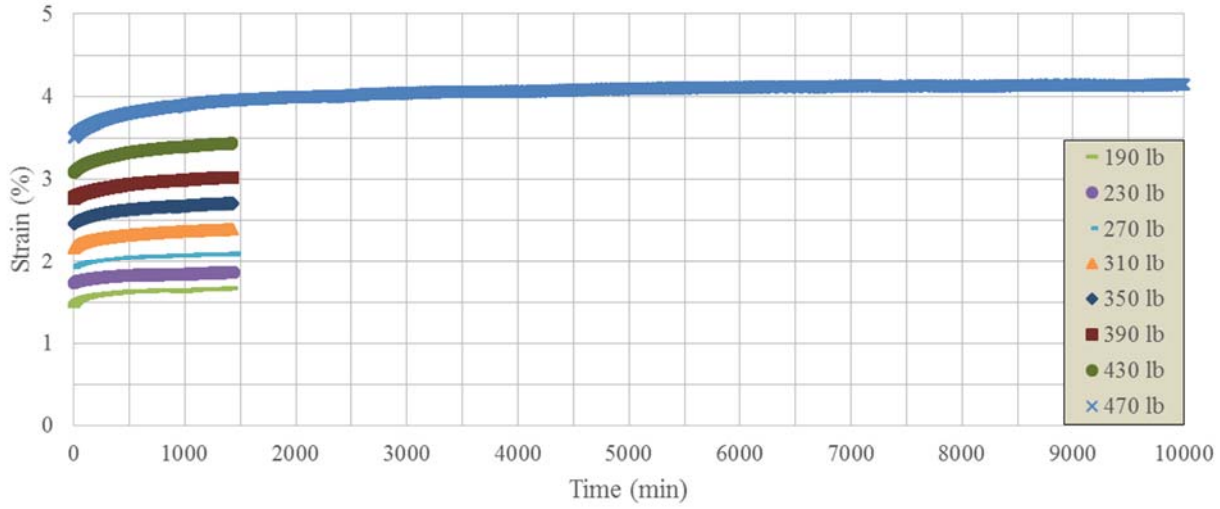

Figure 303. Strain–Time Curves (Linear Scale) at All Loads for the Triaxial UU Creep Test from the Sample at a Depth between 6 and 8 Ft from Borehole N6.

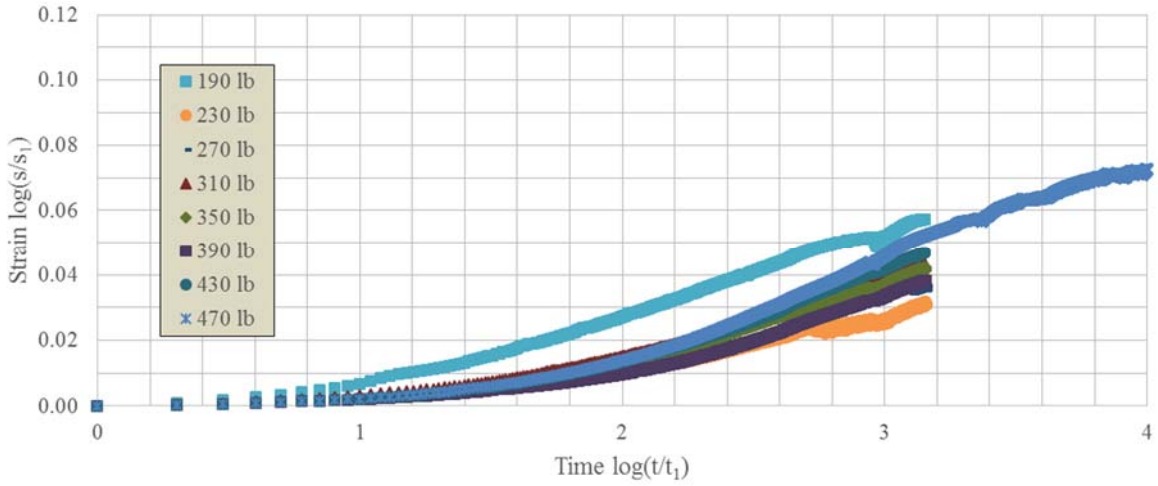

Figure 304. Strain–Time Curves (Log–Log Scale) at All Loads of the Triaxial UU Creep Test from a Sample at a Depth between 6 and 8 Ft from Borehole N6.

Triaxial UU Creep Test on a Sample from Borehole N3, Depth between 8 and 10 Ft

The holding loads for this test were: 30, 70, 110, 190, and 230 lb. Each load was held for 24 hours. The 230-lb load was held for three days. However, the sample did not fail at this load. It failed at the next step of 265 lb. Figure 305 shows the complete stress–strain curve. The strain–time curves for all loads considered in this test are plotted together in Figure 306 and in Figure 307 in linear and log–log scales, respectively. These plots clearly show that the sample failed at 265 lb.

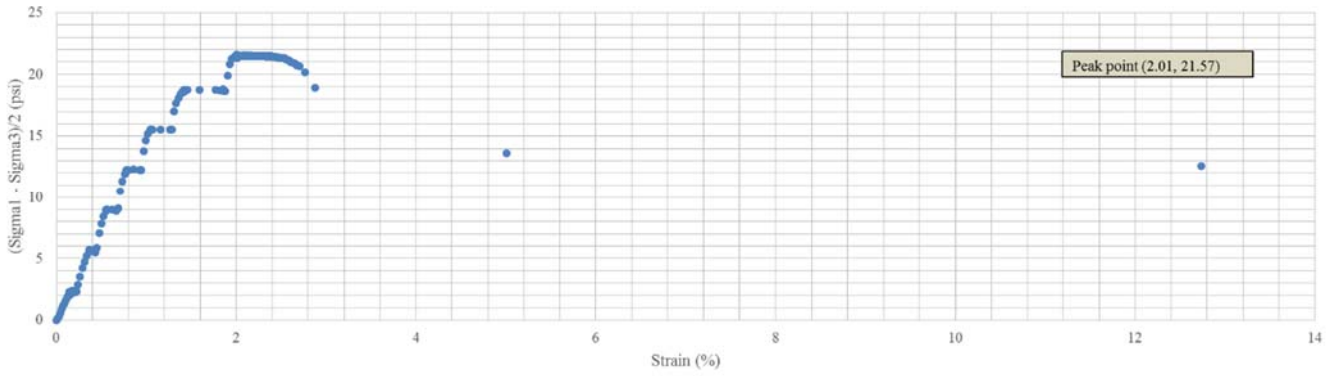

Figure 305. Stress–Strain Curve of the Triaxial UU Creep Test on Sample at a Depth between 8 and 10 Ft from Borehole N3.

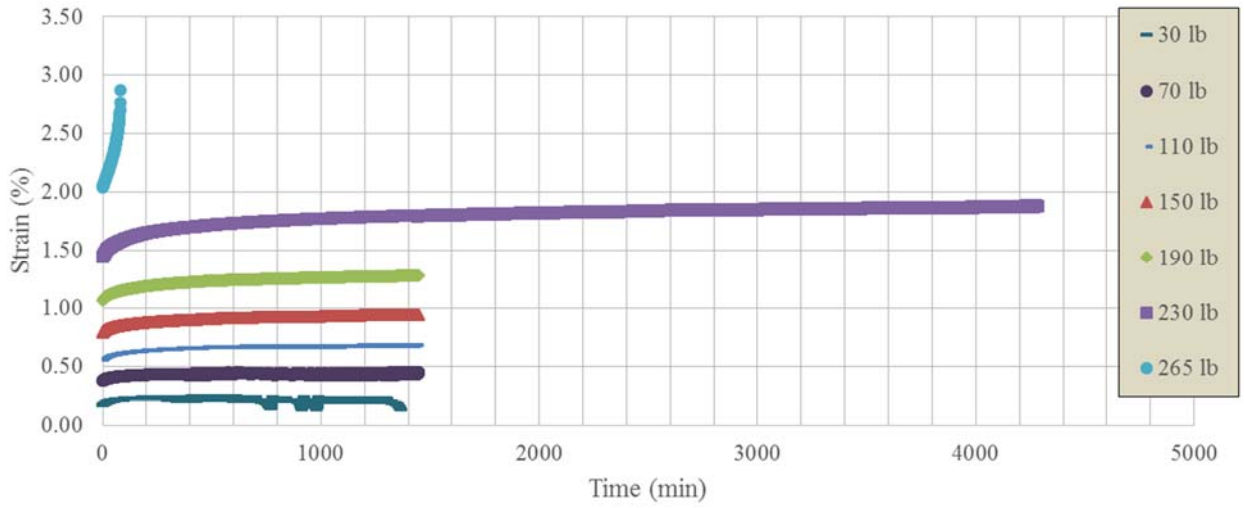

Figure 306. Strain–Time Curves (Linear Scale) for All Loads of Triaxial UU Creep Test on a Sample from a Depth between 8 and 10 Ft from Borehole N3.

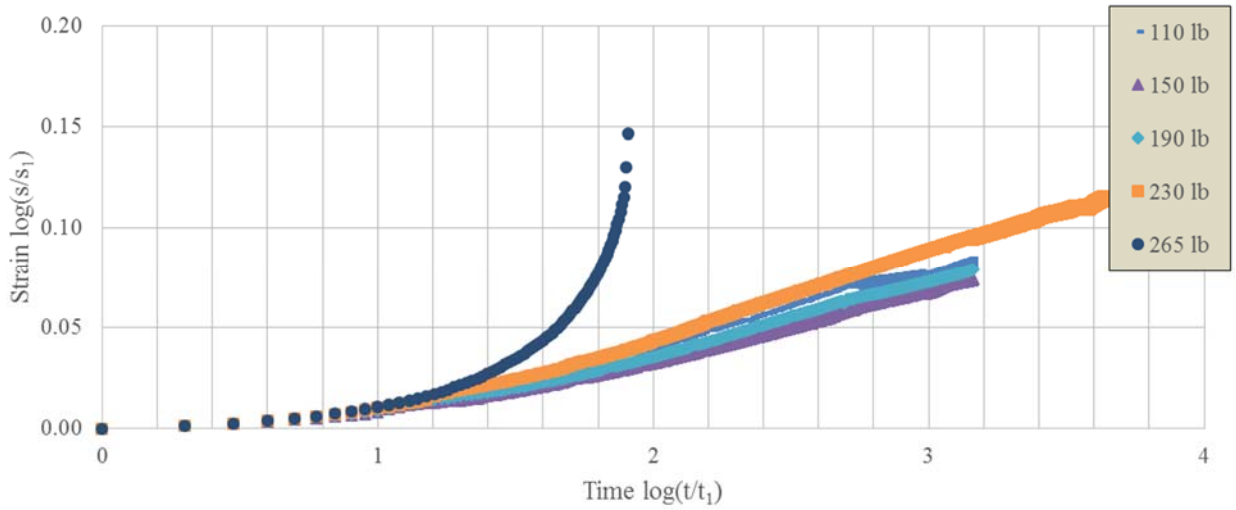

Figure 307. Strain–Time Curves (Log–Log Scale) for All Loads of the Triaxial UU Creep Test on a Sample from a Depth between 8 and 10 Ft from Borehole N3.

Triaxial UU Creep Test on a Sample from a Depth between 10 and 12 Ft from Borehole BH1

The holding loads for this test were: 150, 190, and 230 lb. Each load was held for 24 hours. The sample failed at 255 lb. Figure 308 shows the complete stress–strain curve.

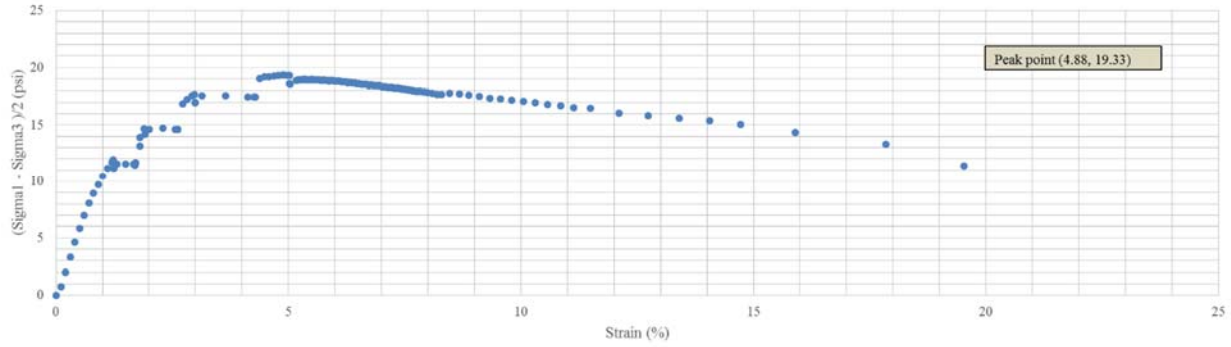

Figure 308. Stress–Strain Curve from the Triaxial UU Creep Test on a Sample from a Depth between 10 and 12 Ft from Borehole BH1.

Strain–time curves for all the loads of this test are plotted together in Figure 309 and Figure 310 in linear and log–log scales, respectively. They show that the sample failed at 255 lb.

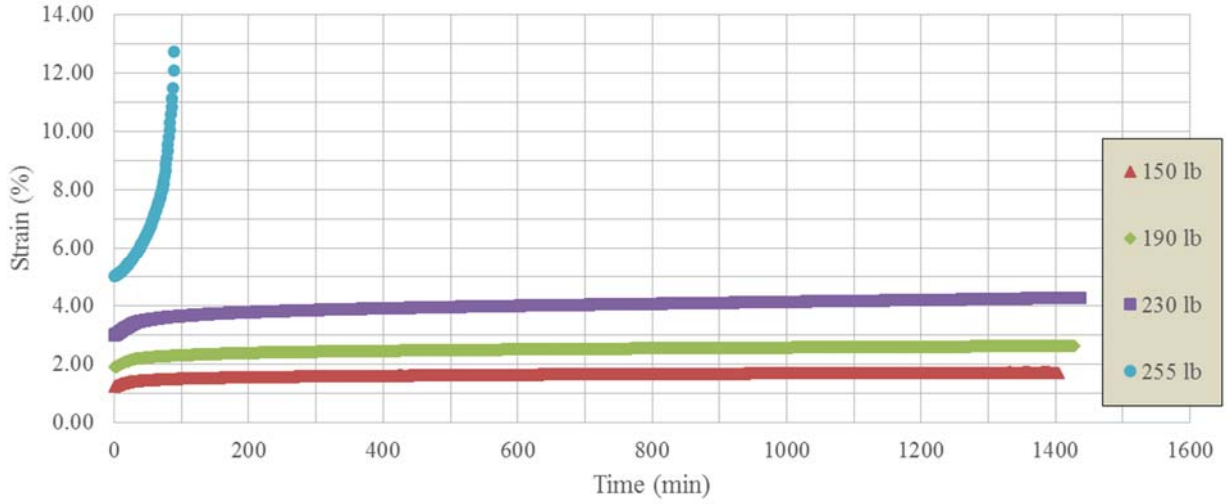

Figure 309. Strain–Time Curves (Linear Scale) for All Loads of Triaxial UU Creep Test on a Sample from a Depth between 10 and 12 Ft from Borehole BH1.

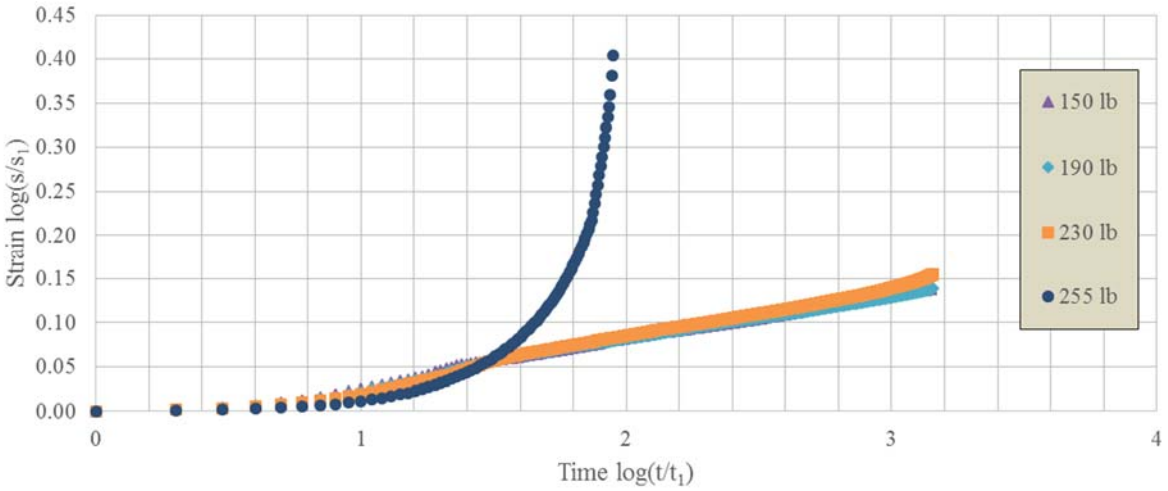

Figure 310. Strain Time Curves (Log–Log Scale) for the All Loads of Triaxial UU Creep Test on a Sample from a Depth between 10 and 12 Ft from Borehole BH1.

Creep Model Based on the *n* Value Concept

As mentioned earlier, Briaud and Garland (1985) proposed the rate effect model to predict the time-dependent behavior of soils (i.e., Eq. 14, Chapter 6). At each load stage, the strain–time curve can be plotted in the log–log scale and the *n* value can be obtained from the slope that fits the experimental data. The curve is generally not linear near the origin of the coordinate system due to lagging adjustment from strain control to stress control protocols.

The peak stress of the creep test could be estimated with the conventional triaxial test, then the holding stresses for the creep stages can be normalized by the peak stress, so that the *n* value from the tests on different samples could be compared. As an example, the *n* values versus stress level are plotted in Figure 311 for different soil samples. It is observed a tendency to a slight increase of the *n* value (and therefore of the creep deformations) with the stress level.

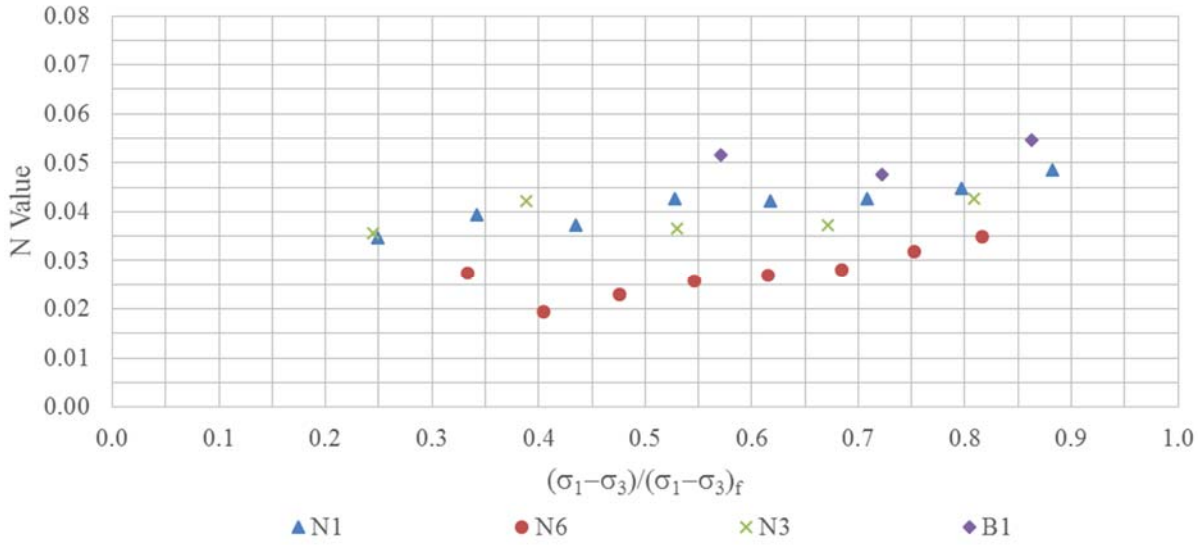

Figure 311. *n* Value–Stress Level Curve.

Oedometer Test

The aim of the oedometer tests was to learn about the creep behavior of the clays investigated in this project under 1D compression conditions. The soil samples were investigated under two different conditions: saturated (as in a typical oedometer consolidation test, identified here as "oedometer test") and at natural water content (called here "1D compression test"). In the first condition the samples are immersed in water during the test and in the second the samples are wrapped to avoid drying during the experiment (i.e., a constant water content test). For both types of tests the ASTM D2435/D2435M, 11 was followed. As is typical in these types of tests, at each loading step, the strain–time curve or modulus–time curve was plotted in a log–log scale. The slope of the curves would be the exponent *n* value in the power law model. Generally, two slopes are observed, one associated with the primary consolidation and the other associated with the secondary consolidation. Figure 312 presents a typical example. In fact, the first linear segment includes two parts: deformation associated with the dissipation of the excess of pore pressure and deformation associated with creep. These two parts of deformation need to be separated. As for the second linear segment (i.e., secondary compression) the deformation is entirely related to soil creep. If it is assumed that the creep mechanism is the same during the primary consolidation and the secondary compression, then the deformation associated with excess pore pressure dissipation could be separated.

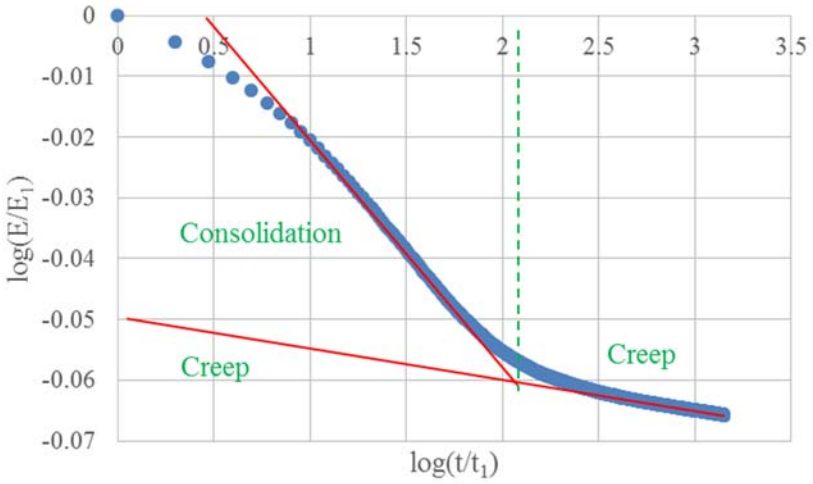

Figure 312. Modulus–Time Curve from Oedometer Test.

An example of the oedometer test and the associated *n* value are plotted in Figure 313 and Figure 314, while an example of a 1D compression test and its *n* value are plotted in Figure 315 and Figure 316, respectively. The following aspects can be mentioned for the soil investigated in this project:

- The *n* values associated with creep from both types of tests (i.e., saturated oedometer test and 1D compression test at constant water content) are quite similar.
- The *n* value corresponding to consolidation is much larger than the *n* value related to creep.
- The *n* value from the oedometer test or 1D compression test is much smaller than the *n* value from the triaxial tests. The difference may be caused by the different confining boundary between the triaxial tests and 1D tests. The deformations in triaxial tests are mostly related to deviatoric stresses, while in the oedometer test, the deformations are under highly confined conditions and in one direction only (generally vertical).

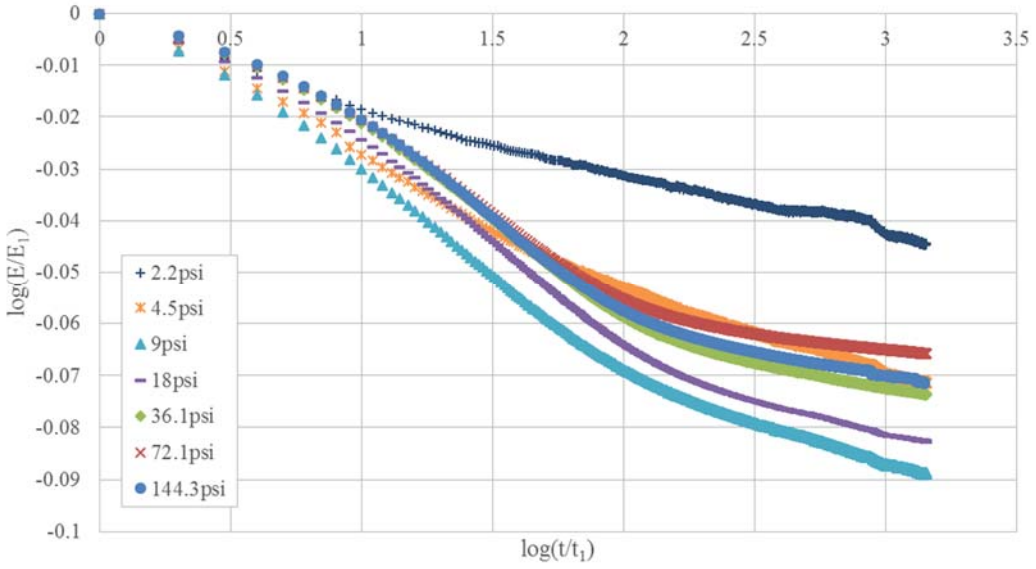

Figure 313. Oedometer Test on Sample N5 from a Depth between 13 and 15 Ft.

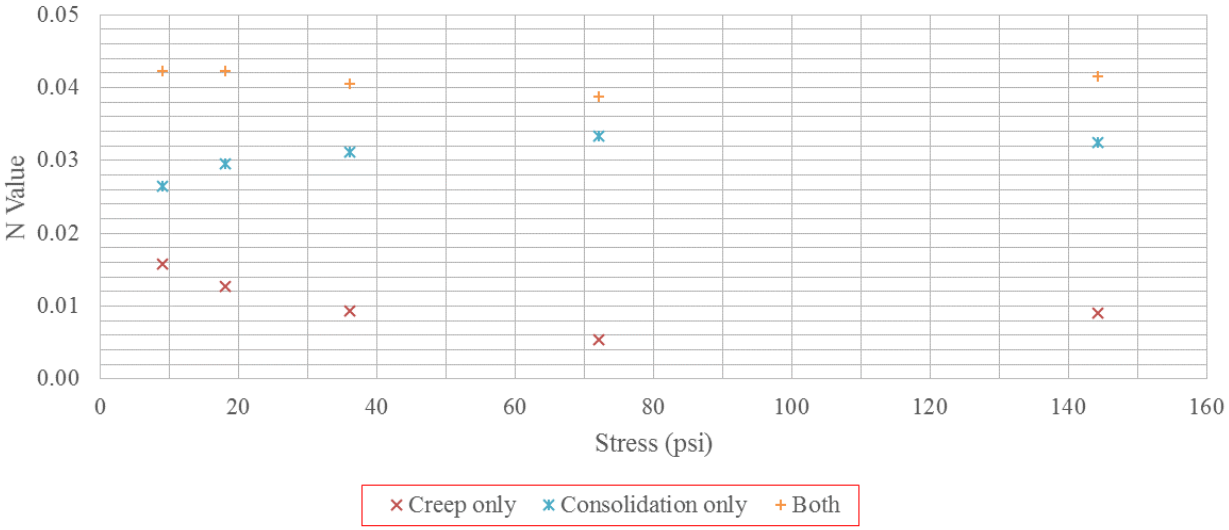

Figure 314. *n* Value Obtained from the Oedometer Test on Sample N5 from a Depth between 13 and 15 Ft.

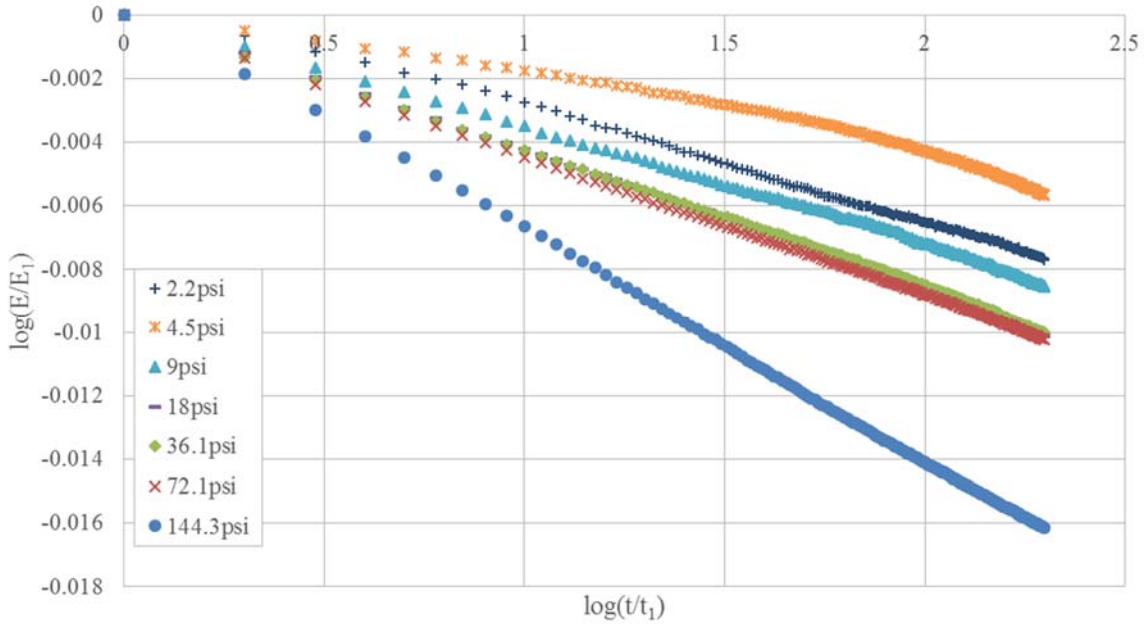

Figure 315. 1D Compression Test on Sample N4 from a Depth between 16 and 18 Ft.

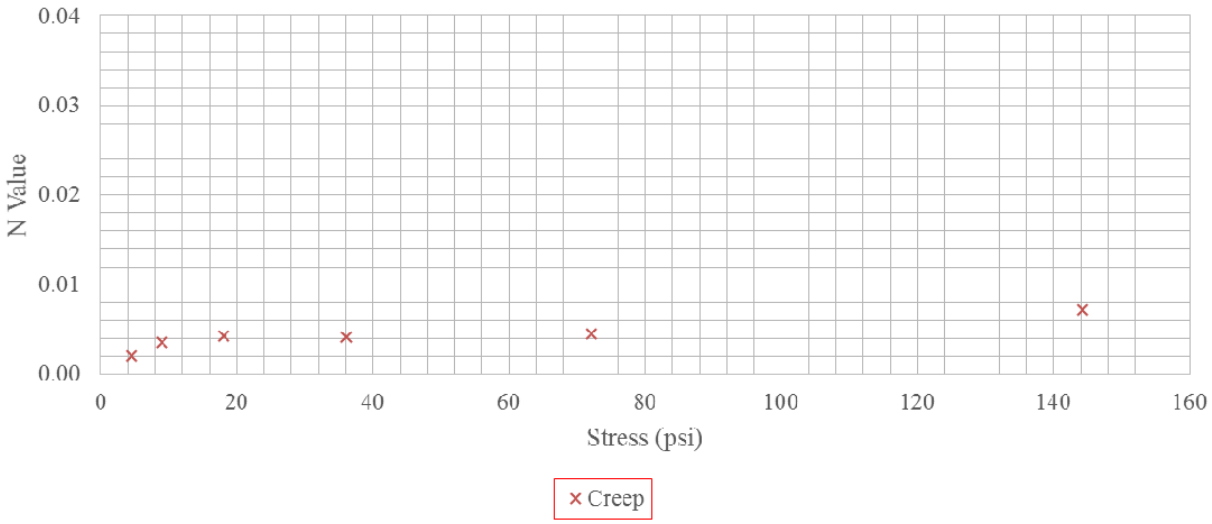

Figure 316. *n* Values Obtained from 1D Compression Test on Sample N4 from a Depth between 16 and 18 Ft.

LABORATORY TESTS ON LOW PI CLAY AND DRY SAND

Creep tests were carried out on a low PI clay and in a sand. The aim was to compare the creep behavior of HP plastic clays with that of low-plasticity clay and a non-plastic soil.

Creep Behavior of Low PI Clay

The low PI soil was a porcelain clay, purchased from Armadillo Clay & Supply, Inc. The water content of this clay was around 20 percent. The strength from the mini vane shear test was between 46.3 kPa and 54 kPa (the average of six measurements was 49.7 kPa). The PI was 13.8, and it was classified as low PI clay according to GEC#7.

Triaxial UU Creep Test

The loading procedure is the same one adopted for the Beaumont clay. Figure 317 plots the stress–strain curve of the triaxial UU creep test on low PI clay specimen. Figure 318 and Figure 319 plot the strain–time curves for all the holding stresses.

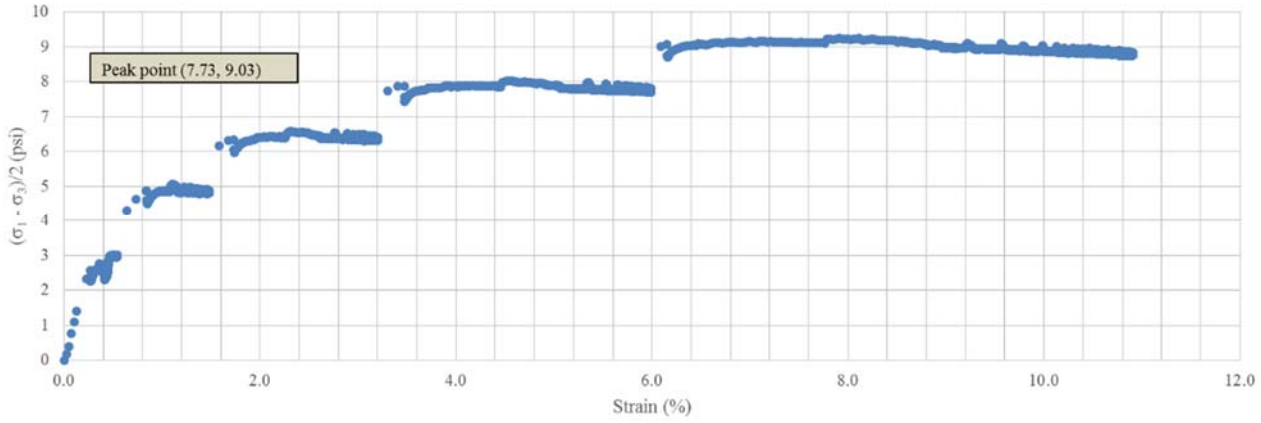

Figure 317. Stress–Strain Curve of Triaxial UU Creep Test on Low PI Clay.

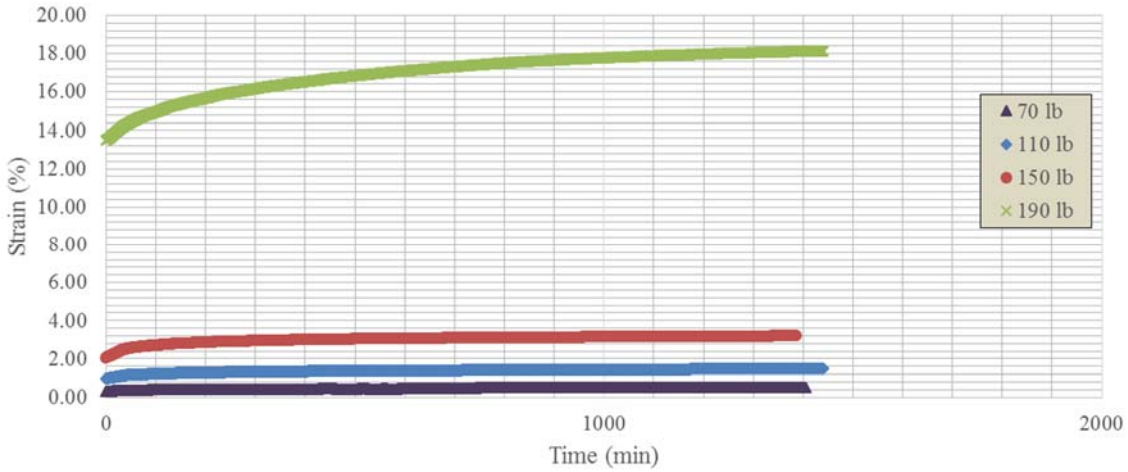

Figure 318. Strain–Time Curves (Linear Scale) of Triaxial Creep Test on Low PI Clay.

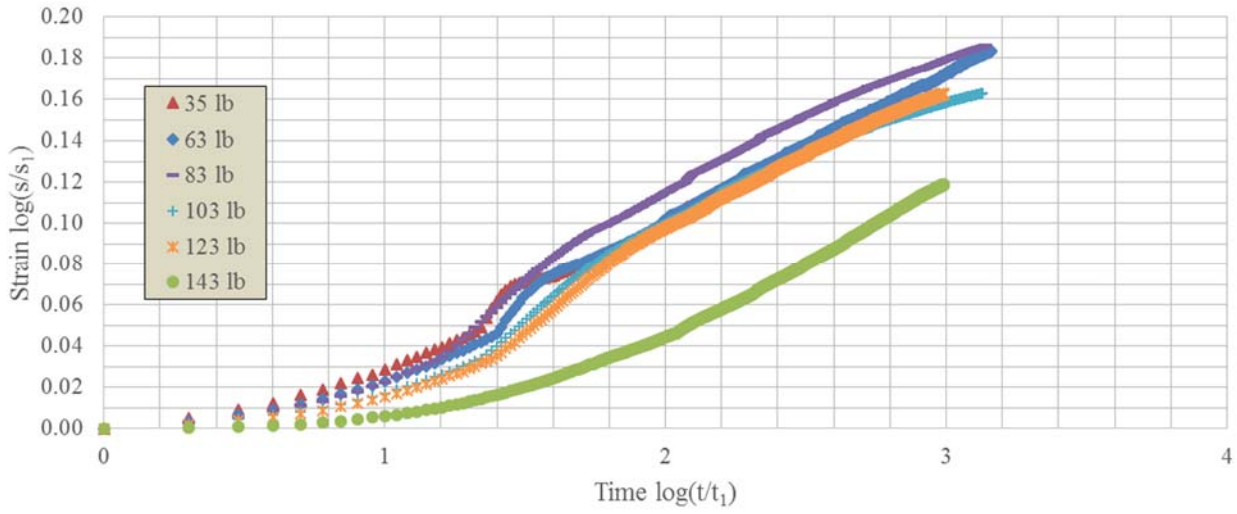

Figure 319. Strain–Time Curves (Log–Log Scale) of Triaxial Creep Test on Low PI Clay.

n Value–Stress Level Curve

As before, the *n* value was obtained by plotting the test results in a log–log scale (Figure 319). The slope of the straight line is the *n* value. Figure 320 plots the curve relating the *n* value and the stress level. The *n* value is practically independent of the stress level.

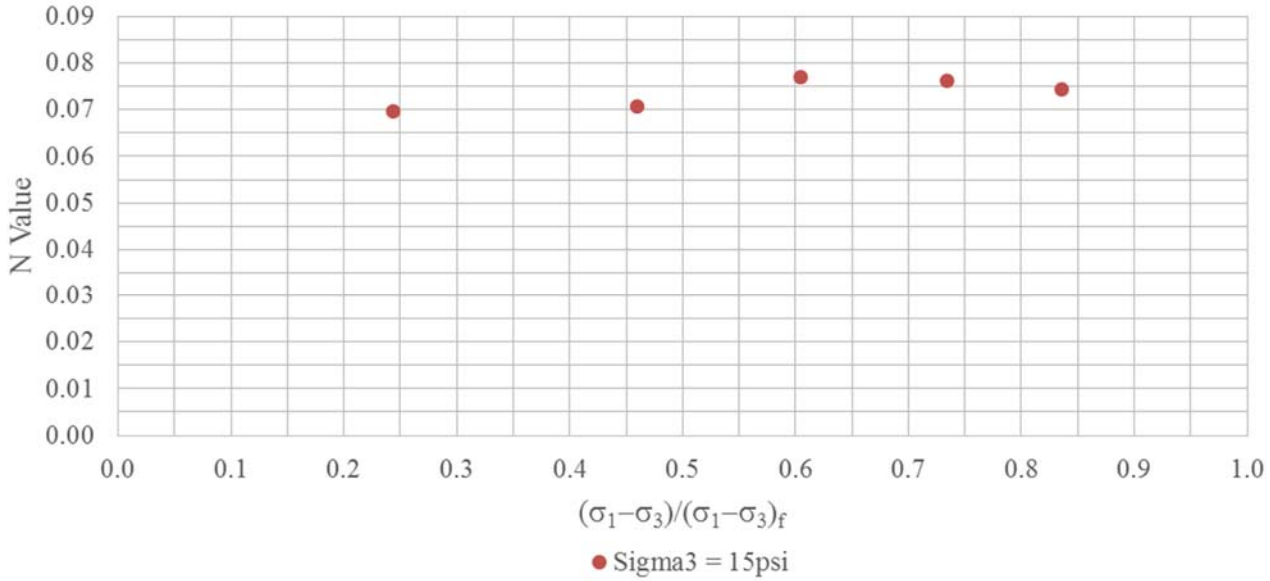

Figure 320. *n* Value–Stress Level Curve of Triaxial Creep Test on Low PI Clay.

Creep Behavior of Sand

A fine sand supplied by Humboldt Mfg. Co was used in this research. It was a clean, dry, free-flowing uncemented sand with less than 1 percent variation in bulk density. The protocol followed for the triaxial UU creep test on dry sand was similar to the one used for the triaxial UU creep test on high PI clays. Soil samples were allowed to creep at constant selected loads. The only difference in creep test on dry sand was the load increment. In the creep test on the clay sample from NGES, the load increment was constant, while in the test on dry sand it was not constant. The applied confining stresses were 8, 12, 16, and 24 psi, which are equal to self-weight for samples at depths of 9, 13.5, 18, and 27 ft. The general test procedure was described in previous sections of this chapter.

Triaxial UU Creep Test on Dry Sand with Confining Stress 8 psi

The holding loads for this test were: 70, 110, 150, and 190 lb. Each load was held for 24 hours. The sample failed at 202 lb. Figure 321 shows the complete stress–strain curve. Even at low loads, dry sand also creeps. As expected, more creep is observed at higher holding loads.

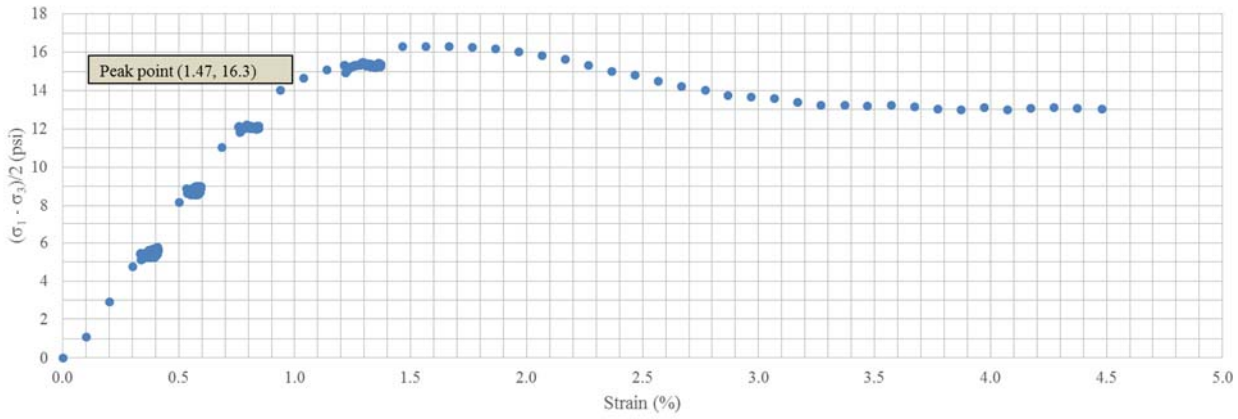

Figure 321. Stress–Strain Curve of Triaxial UU Creep Test on Dry Sand Sample with Confining Stress 8 Psi.

The strain–time curves for all loads studied are plotted together in Figure 322 and Figure 323, linear scale and log–log scale, respectively.

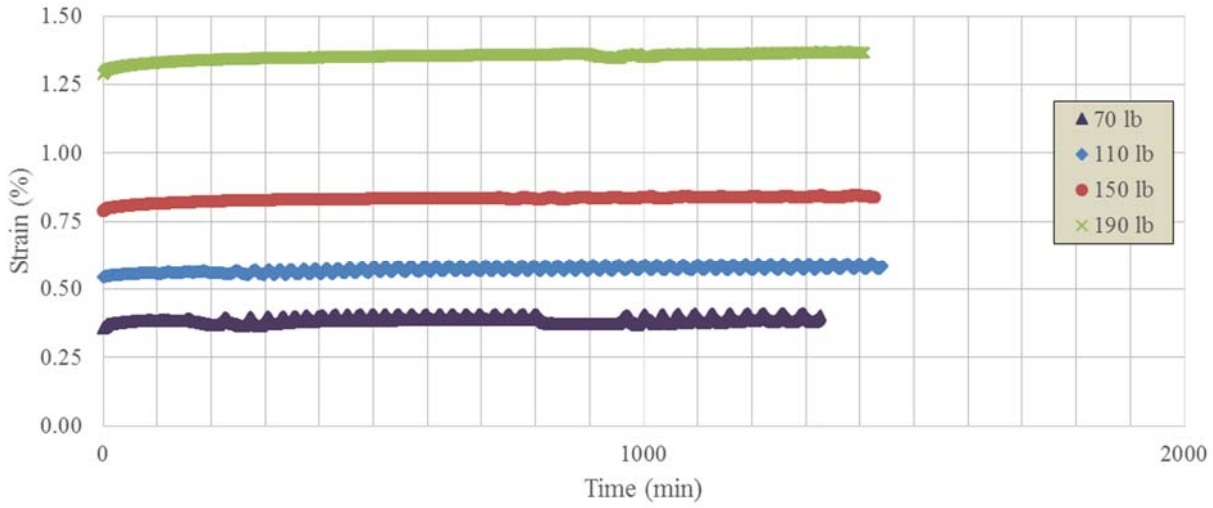

Figure 322. Strain–Time Curves (Linear Scale) at All Loads of Triaxial UU Creep Test on Dry Sand Sample with Confining Stress 8 Psi.

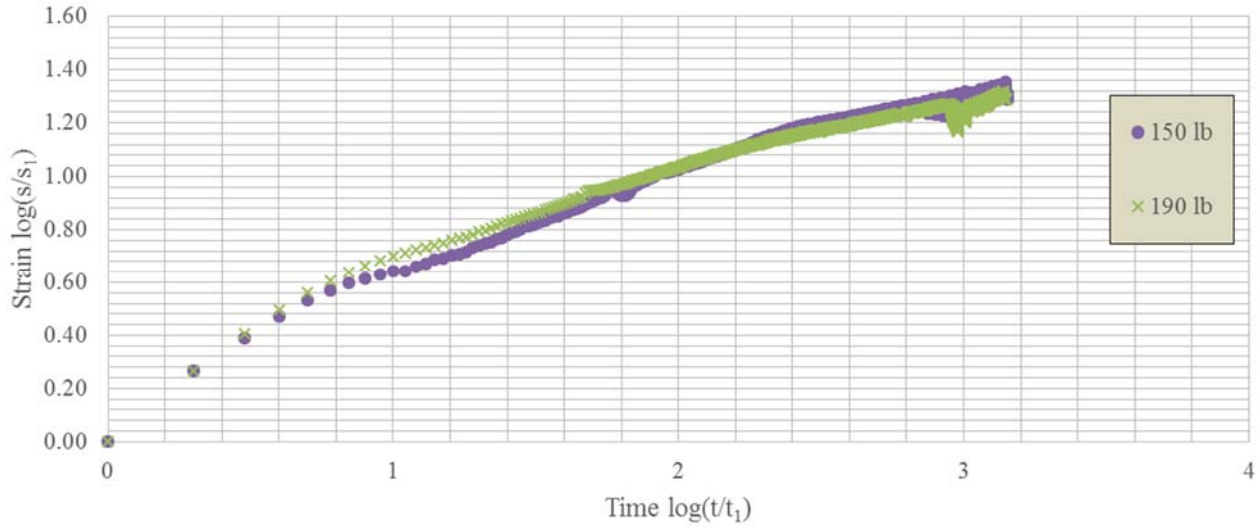

Figure 323. Strain Time Curves (Log–Log Scale) at All Loads Excluding Seating Range of Triaxial UU Creep Test on Dry Sand Sample with Confining Stress 8 Psi.

Triaxial UU Creep Test on Dry Sand with Confining Stress 12 psi

The holding loads for this test were: 250, 280, 310, and 340 lb. Each load was held for 24 hours except the 340-lb load, which was maintained for 5 days. It was held for 5 days to see whether the sample failed due to the creep or not. Figure 324 shows the stress–strain curve.

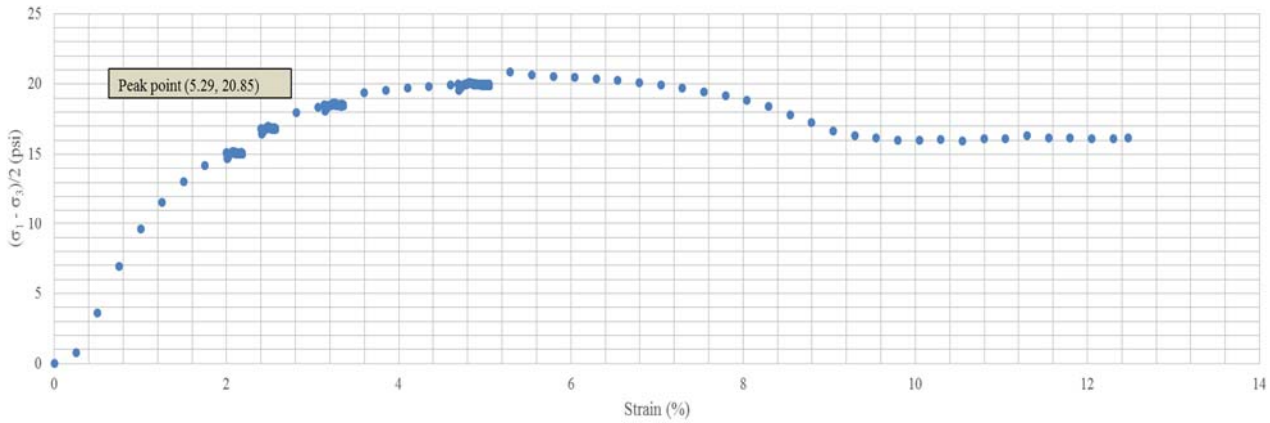

Figure 324. Stress–Strain Curve of a Triaxial UU Creep Test on Dry Sand Sample with Confining Stress 12 Psi.

The strain–time curves at all load steps adopted in this test are plotted together in Figure 325 and Figure 326 in linear scale and log–log scale, respectively. In Figure 326, all the curves cluster together, with a nearly constant *n* value-.

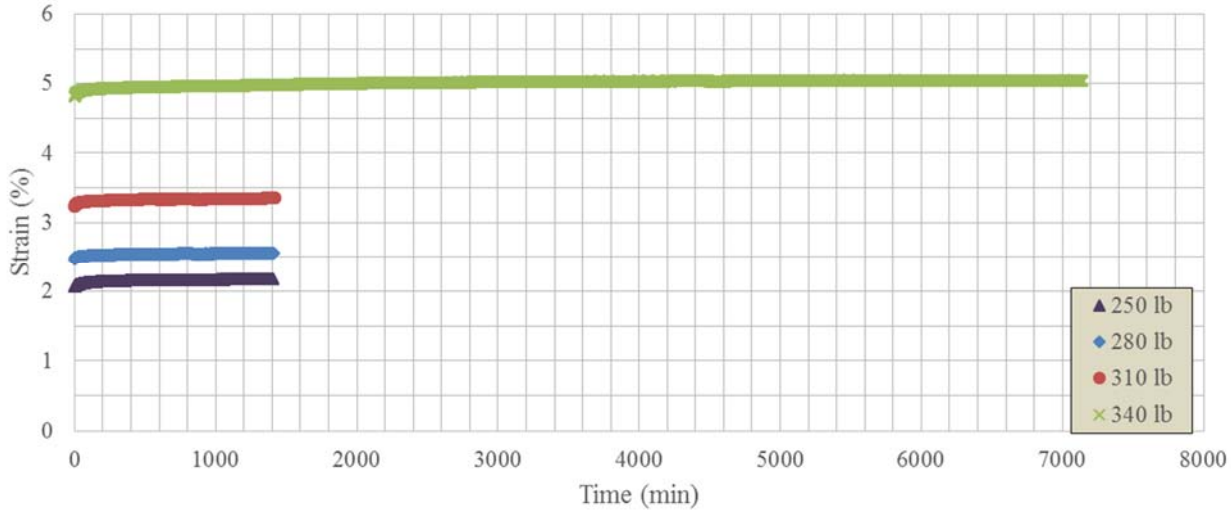

Figure 325. Strain–Time Curves (Linear Scale) at All Loads of Triaxial UU Creep Test on Dry Sand Sample with Confining Stress 12 Psi.

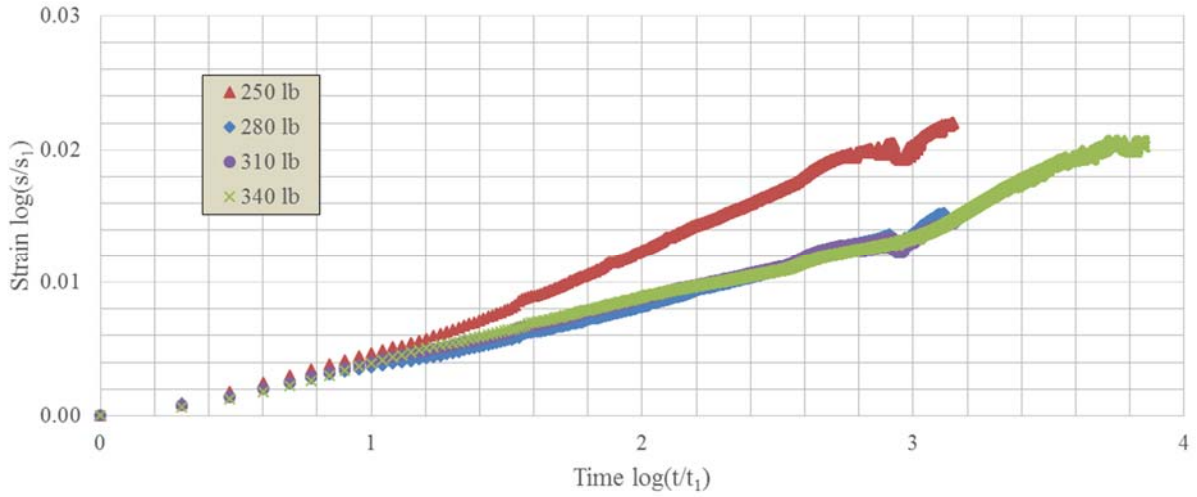

Figure 326. Strain–Time Curves (Log–Log Scale) at All Loads of Triaxial UU Creep Test on Dry Sand Sample with Confining Stress 12 Psi.

Triaxial UU Creep Test on Dry Sand with Confining Stress 16 Psi

The holding loads for this test were: 70, 110, 150, 190, 230, 260, 290, and 330 lb. Up to 230 lb, each load was held for 24 hours, while the loads from 260 lb to 330 lb were held for 48 hours (2 days). The sample failed at 352 lb. Figure 327 shows the complete stress–strain curve. Note that during the load increment from 260 to 290 lb, the strain suddenly increased from 2 percent to 4.8 percent in less than 1 minute, while the test machine recorded data each minute. This increase significantly reduced the creep on the next two holding loads (i.e., 290 and 330 lb).

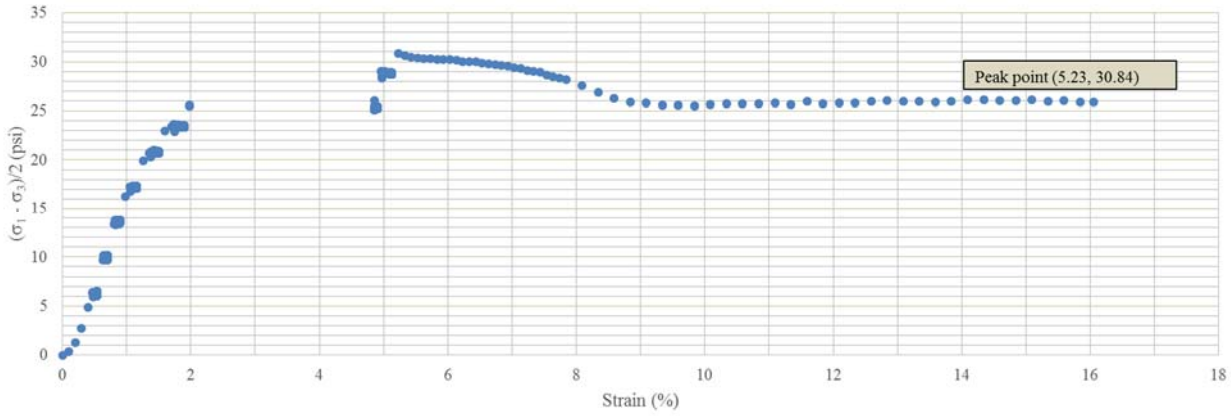

Figure 327. Stress–Strain Curve of Triaxial UU Creep Test on Dry Sand Sample with Confining Stress 16 Psi.

Strain–time curves for all the loads of this test are plotted together in Figure 328 and Figure 329 in linear scale and log–log scale, respectively.

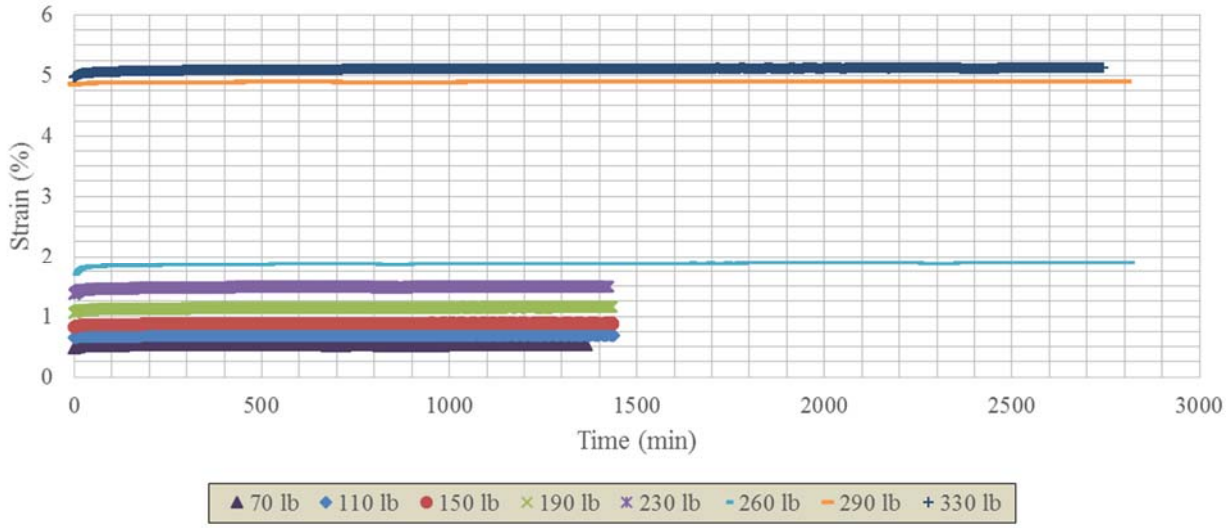

Figure 328. Strain Time Curves (Linear Scale) for All Loads of Triaxial UU Creep Test on Dry Sand Sample with Confining Stress 16 Psi.

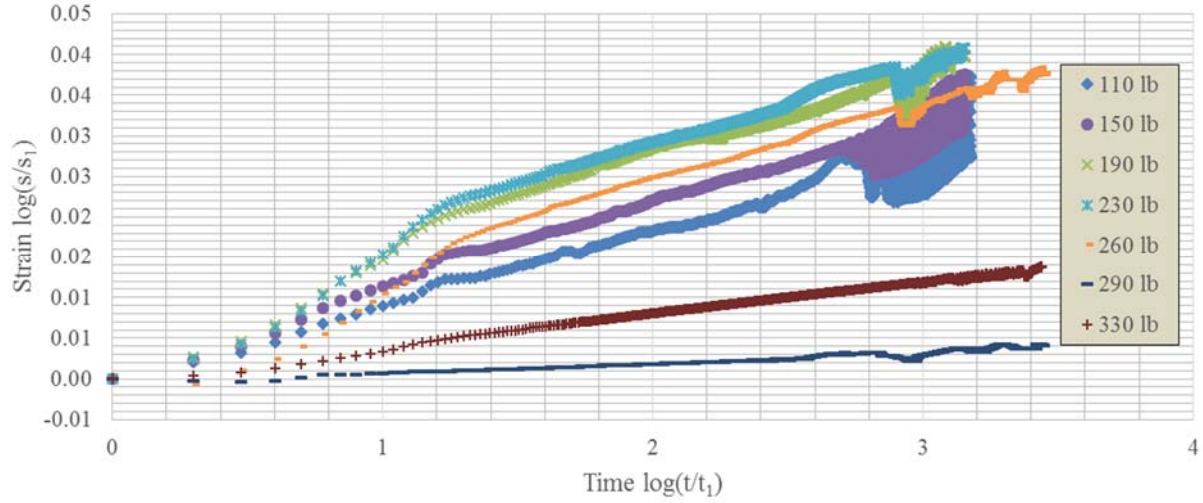

Figure 329. Strain Time Curves (Log–Log Scale) at All Loads of Triaxial UU Creep Test on Dry Sand Sample with Confining Stress 16 Psi.

Triaxial UU Creep Test on Dry Sand with a Confining Stress of 24 Psi

The holding loads for this test were: 70, 110, 150, 190, 230, 270, and 350 lb. Each load was held for 24 hours. After 350 lb, the sample was loaded until failure. The sample failed at

503 lb. Figure 330 shows the complete stress–strain curve. Even the residual strength is higher than the stress at 350 lb.

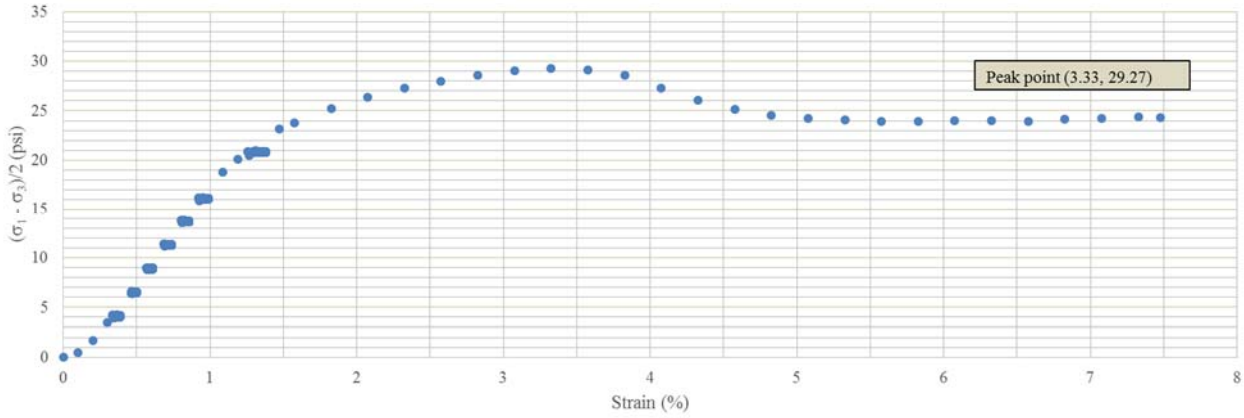

Figure 330. Stress–Strain Curve of Triaxial UU Creep Test on Dry Sand Sample with Confining Stress 24 Psi.

The strain–time curves for all the loads adopted in this test are plotted together in Figure 331 (linear scale) presents in log–log scale the results for loads from 150 to 350.

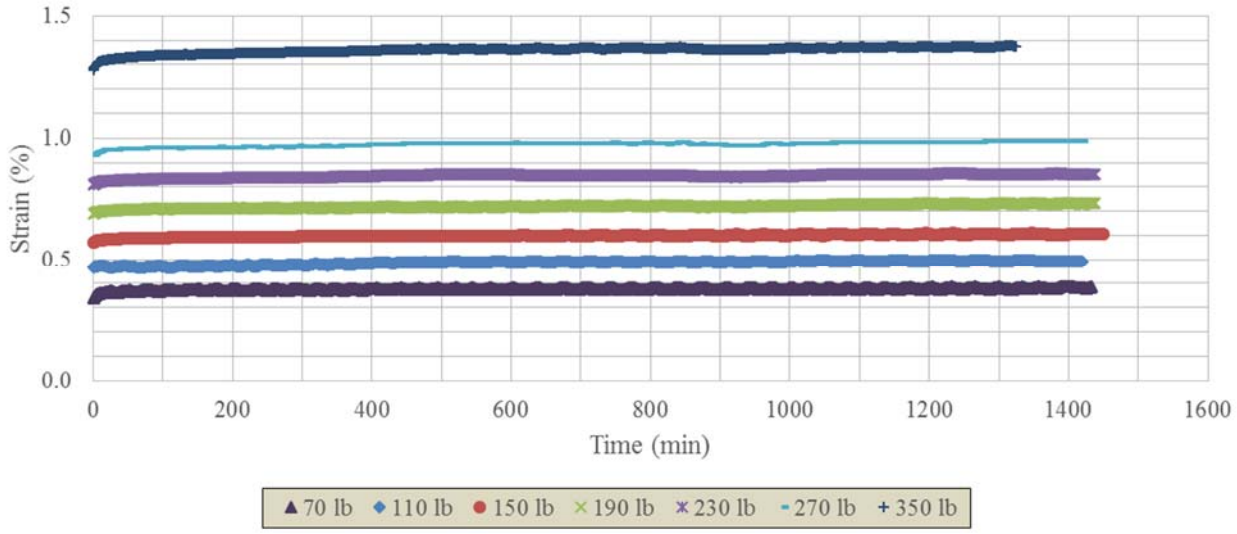

Figure 331. Strain–Time Curves (Linear Scale) at All Loads of Triaxial UU Creep Test on Dry Sand Sample with Confining Stress 24 Psi.

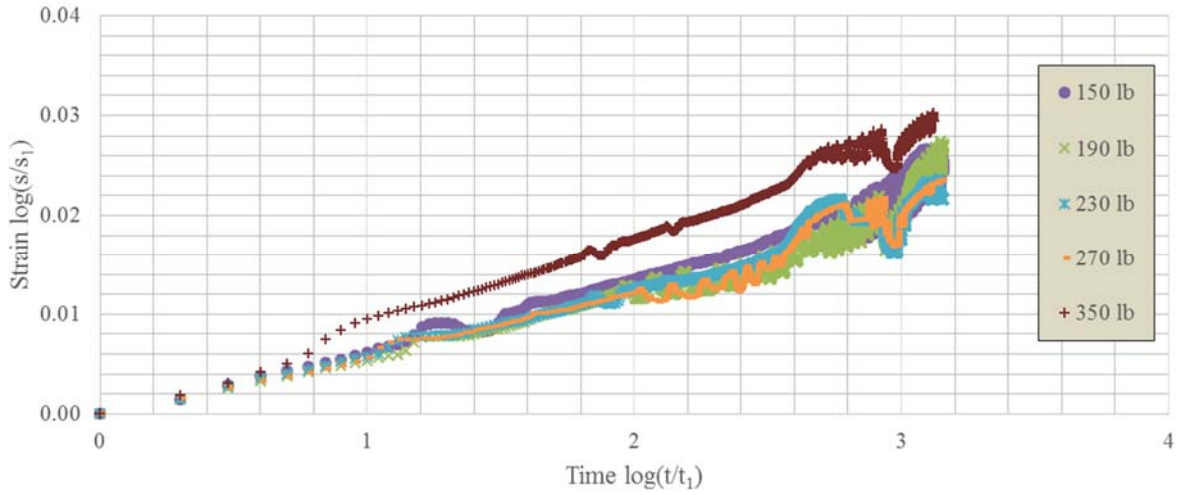

Figure 332. Strain–Time Curves (Log–Log Scale) at All Loads Excluding Seating Range of Triaxial UU Creep Test on Dry Sand Sample with Confining Stress 24 Psi.

n Value–Stress Level Curve

The *n* value calculated from the triaxial creep tests on sand was obtained from the plots. Figure 333 plots the *n* value–stress level curve. Practically no dependence of the *n* value on load level was observed.

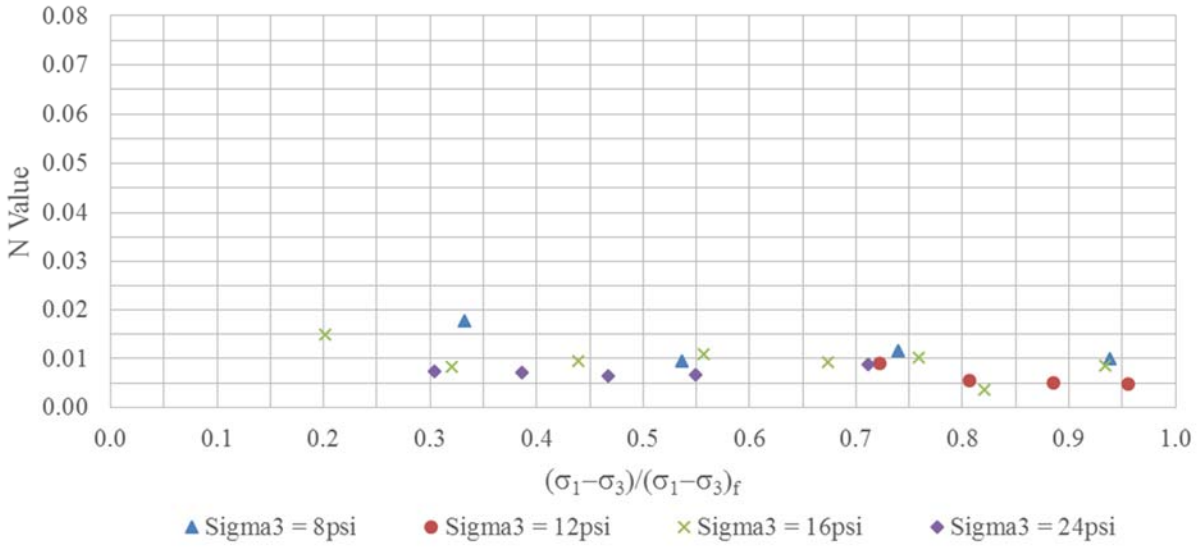

Figure 333. *n* Value–Stress Level Curve of Triaxial Creep Test on Sand.

SUMMARY AND CONCLUSIONS

In this chapter, the results of the laboratory campaign performed at Texas A&M laboratories, which aimed at gaining a better understanding of the creep behavior of HP clays, were presented. Four different materials were studied: 1) a high PI clay from the NGES-TAMU clay site, 2) a high PI clay from the Beaumont field site, 3) a low PI clay (used as a reference clay material of low plasticity), and 4) a fine sand available at TTI (also used as a reference non-plastic material).

A full characterization of the four soils studied in this research was performed. The PI of the clay samples from the NGES and Beaumont field sites was very high (i.e., PI > 15). This implies that the two clays are very suitable for studying the creep behavior in high PI clays. The degree of saturation of these two clays was also very high (i.e., $S_r \geq 85\%$). Index properties experiments, direct shear tests, consolidation tests, and triaxial and triaxial creep tests were carried out.

The power law, based on the *n* exponent, was adopted to characterize the viscous and creep behaviors of the different soils. It was observed that there is a slight effect of the stress level on the creep behavior, particularly at low stress levels. Large creep deformations were observed near failure (i.e., in general terms when the applied load was higher than 85 percent of the failure stress). This behavior is quite similar to that observed in the pullout tests at the NGES-TAMU clay site (i.e., Chapter 4) and Beaumont site (i.e., Chapter 5).

The laboratory experiments presented in this chapter were used in different components of the numerical modeling. They were instrumental for the numerical simulations performed in this project.

CHAPTER 7:
NUMERICAL MODELING

INTRODUCTION

This chapter presents the activities related to the numerical modeling performed in the framework of this project. The goal is to achieve a better understanding about the creep behavior of the soil nail walls in HP clays. A number of computational tools are used to investigate the performance of soil nail walls in HP clays. The commercial code, FLAC3D, version 4.0 (Itasca, 2006), was used to simulate the mechanical behavior of the walls studied in this project during construction, as well as the time-dependent (creep) behavior of the soil nail walls after their construction. The advantages of using FLAC3D in this research project are multiple, including: it is a well-known and validated code for geotechnical problems involving excavations; it allows the modeling of soil nails via existing anchors elements; and it has a very complete library of mechanical constitutive equations with a large variety of creep soil models (e.g., more than eight creep soil models). The numerical code was used in the various steps of this research, particularly the following:

- Wall design and verification.
- Simulation of pullout tests and model calibration against the experimental data gathered in the field from both the NGES-TAMU and TxDOT sites.
- Modeling of triaxial tests.
- Parametric study of soil nail walls to cover different wall conditions and soil properties.

Two soil nail wall geometries were studied in this project. The first corresponds to the actual soil nail wall selected in collaboration with TxDOT at the Beaumont test site. As explained in Chapter 5, this soil nail wall is related to an emergency slope repair project that was instrumented and monitored during construction and under operational conditions for a period of around 13 months after construction. A section of the wall was simulated using a FLAC3D model. The modeling activities involve the different construction steps of the soil nail wall and its subsequent operational stage. The proposed numerical model of the soil wall was validated against the information gathered during the wall construction (i.e., basically wall movements and

load in the nails). A creep soil model was adopted to simulate the post-construction operational stage, and it was validated against the data obtained from the wall monitoring.

The model adopted for simulating the nail behavior (and the associated parameters) was independently proposed and validated against the information gathered from the pullout experiments presented in Chapter 5. A similar comment can be made with respect to the mechanical and creep models adopted for reproducing the soil behavior; they were independently proposed and validated against the laboratory tests presented in Chapter 6. These aspects (i.e., the independent validation of the constitutive and soil nail models) provide an additional strength to the framework proposed in this research project to study the creep behavior of soil nail walls in HP clays. In the following sections, the procedures used to calibrate the constitutive and nail models are presented in detail.

The second soil nail wall studied in this project corresponds to a soil nail wall typically adopted in the design of the Texas turnaround. This alternative soil nail wall was studied because the wall at Beaumont does not correspond to the typical soil nail wall used in practice because of its height and length. Therefore, for the parametric studies envisaged in this project a more representative soil nail wall was provided by TxDOT and adopted in this research as the base case for the parametric study. The aim of this parametric study was to investigate the sensitivity of the soil nail wall behavior when key design parameters are changed with respect to those in the base case. Particular attention was given to the influence of different parameters on the long-term performance of the soil nail wall. The experience gained during the calibration of the Beaumont soil nail wall was instrumental for developing the base case and the subsequent parametric study.

The geotechnical program Plaxis (Babu and Singh, 2009) was also used in this research to study the mechanical behavior of the soil nail wall. The 2D plane deformation analyses performed with this software were oriented to learn about the influence of the additional sacrificial nails (planned for the TxDOT soil nail wall) on the service load. The idea was to design the location of the sacrificial nails in a way that they do not affect the service load of the nails in the section under study. The analyses discussed above, solved as boundary value problems, were complemented with limit equilibrium analyses of the soil nail walls performed with the stability program SNAILZ (www.dot.ca.gov).

This chapter includes seven sections. The second section discusses the results of the numerical simulation of the pullout tests on the sacrificial nails installed at the Beaumont project. The results of this simulation were used to verify the nail-grout interface parameter adopted for the cable model used in the numerical modeling of the soil nail wall. The third section presents the model calibration and results of the numerical simulations of the soil nail wall at the end of the construction. The fourth section presents some background information about the rheological behavior of the soils and the models adopted in this research. In this section, the results of the modeling of the triaxial creep tests are presented and the adopted parameters of the soil constitutive model adopted to simulate the creep behavior. The fifth section focuses on the modeling of the long-term behavior of the soil nail wall. This section also covers all the activities related to the simulation of the long-term behavior (i.e., for one year post-construction monitoring) of the soil nail wall at the Beaumont project. The details of the adopted model and model calibration are also discussed in this section. The sixth section presents the results of the parametric study on the typical Texas turnaround soil nail wall suggested by TxDOT. The influence of the various factors on the long-term behavior of the soil nail wall is discussed in this section, as well. The seventh section summarizes all the activities performed in the numerical modeling and presents the conclusions of this chapter.

MODELING OF PULLOUT TESTS

This section focuses on the numerical modeling of the pullout tests performed at Beaumont TxDOT site.

Introduction

To study the behavior of the nails and to estimate the soil–grout interface resistance at different heights, a total of six sacrificial nails were installed at three different heights (i.e., 7.4 ft, 14.4 ft, and 17.9 ft from the top of the wall) at the emergency slope repair at the Beaumont District. At each height, two sacrificial nails were installed, one with instrumentation (i.e., strain gauges) and the other without. The non-instrumented nails were primarily used to learn about the pullout capacity of the soil nails at different heights and to plan (based on this information) the loading protocols to be used in the instrumented ones. The nails were installed with a horizontal spacing of 8 ft. Figure 334 shows these sacrificial nails. The results of the pullout tests on the sacrificial nails are presented in detail in Chapter 5.

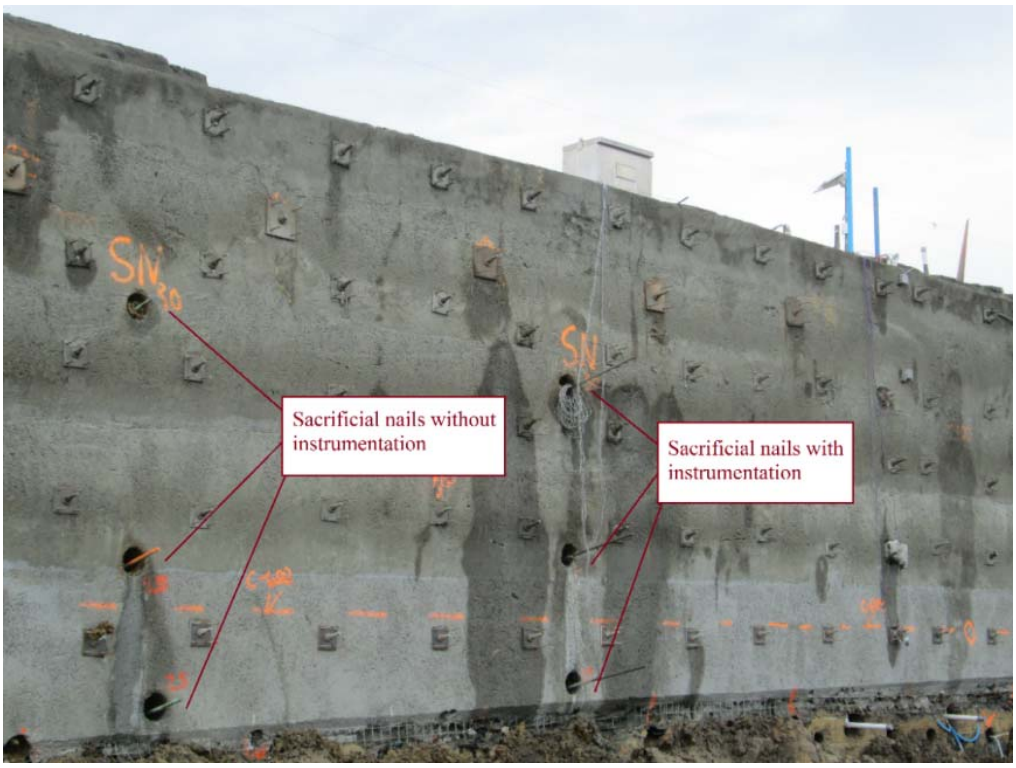

Figure 334. Sacrificial Nails Installed at Beaumont Project at Three Different Heights.

Table 58 presents a summary of the results of the pullout tests and key information about the sacrificial nails. The bond length for sacrificial nails identified as 1 (i.e., installed at the height h = 7.4 ft) is 27 ft, while the bond length for the sacrificial nails identified as 2 and 3 (i.e., installed at heights h = 14.4 ft and 17.9 ft, respectively) is 23 ft.

Table 58. Summary of the Results of Pullout Tests on Sacrificial Nails at Beaumont Project.

Test Summary on Sacrificial Nails				
Nail No.	**Bond length (ft)**	**Hole diameter (in.)**	**Failure load (kips)**	**Maximum bond stress at failure (psf)**
Non-instrumented 1 (h=7.4 ft)	27	8	43	760
Instrumented 1 (h=7.4 ft)	27	8	51	902
Non-instrumented 2 (h=14.4 ft)	23	8	45	935
Instrumented 2 (h=14.4 ft)	23	8	45	935
Non-instrumented 3 (h=17.9 ft)	23	8	58	1204
Instrumented 3 (h=17.9 ft)	23	8	58	1204

Simulation of the Pullout Tests

The goal of this section is to use the information gathered from the pullout tests on sacrificial nails to calibrate the constitutive model adopted to simulate the nails' behavior and their interactions with the surrounding soil. As mentioned in the introduction, the numerical code FLAC3D was adopted to simulate the creep behavior of soil nail walls in HP clays. The structural element identified as cable element in FLAC3D was adopted to simulate the soil nail behavior in this research. These elements provide a shearing resistance (by defining the grout properties) along the nail length (Itasca, 2006). The grout behaves as an elastic, perfectly plastic material, with a dependence of its peak strength on the confining stress. The bending effects are not considered in the formulation of cable element. To consider the effect of bending in the analysis, it will be necessary to adopt a different type of element, like the pile structural element (Itasca, 2006). In this research, bending effects in the nail were disregarded.

The shear behavior of the cable–soil interface is assumed to be cohesive and frictional. Figure 335a shows the idealized system of grout–soil interface. This system (i.e., grout–soil interface) is modeled using a spring (with the grout shear stiffness, Kg, as the associated parameter) and a slider (with the grout cohesive stiffness, Cg, as the associated parameter) located at the nodal points along the cable axis as shown in Figure 335b.

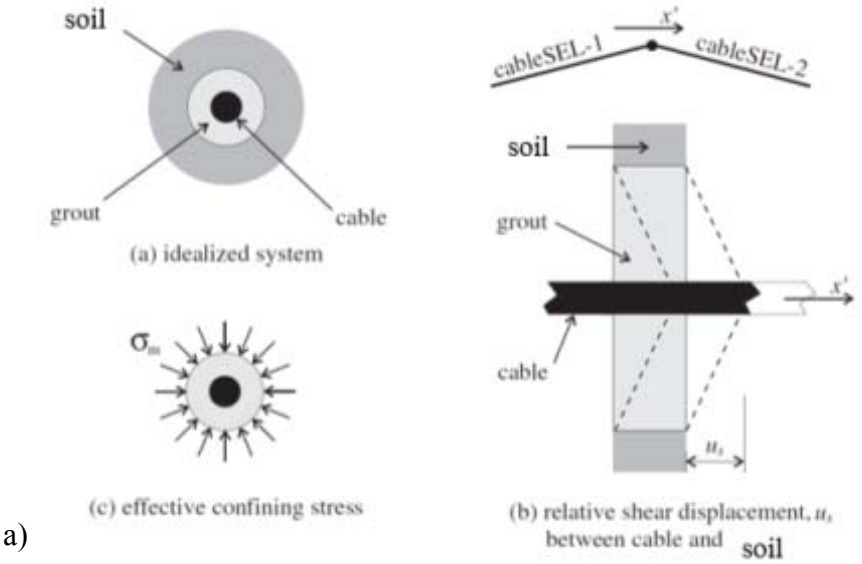

a)

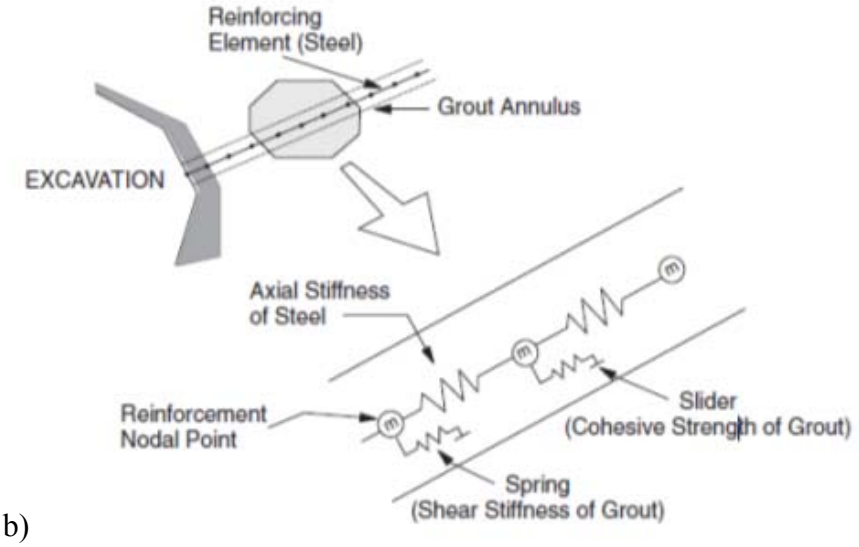

b)

Figure 335. Cable Structural Elements: a) Idealization of Grouted-Cable System, and b) Mechanical Representation of Fully Bonded Reinforcement (Itasca, 2006).

In order to learn about the soil–grout interface behavior (i.e., grout cohesive strength, Cg, and grout shear stiffness, Kg), pullout tests on sacrificial nails installed at the Beaumont project were modeled using FLAC3D. Figure 336 shows the geometry and the mesh adopted to model the pullout tests. The cable element is located at the center of the square cross section (50 ft × 50 ft) of the adopted geometry. A displacement rate in the axial direction was applied at the head of the cable element and the axial force in the cable element was measured. Table 59 presents the parameters adopted in this modeling.

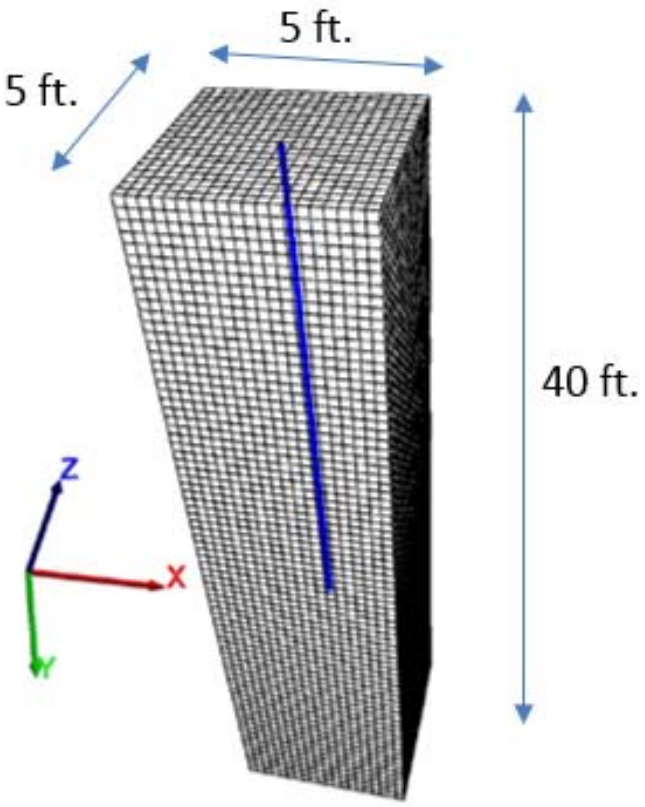

Figure 336. Geometry and Mesh Adopted for Modeling the Pullout Tests.

Table 59. Parameters Used in Simulation of the Pullout Test.

Pullout Tests		
Material	**Constitutive Model**	**Properties**
Soil	MC	E=2.9e5 psf (14 MPa), υ=0.3, γ=125 pcf, c=0, ϕ=26°
Nail (cable element)	Elastic-perfectly plastic	E steel=4.17e9 psf (200 GPa), c_grout=1e3 psf, ϕ_grout=20°

Figure 337 to Figure 339 show the results associated with the numerical modeling of the sacrificial nails. The model captures very satisfactorily the tendencies observed in the pullout experiments.

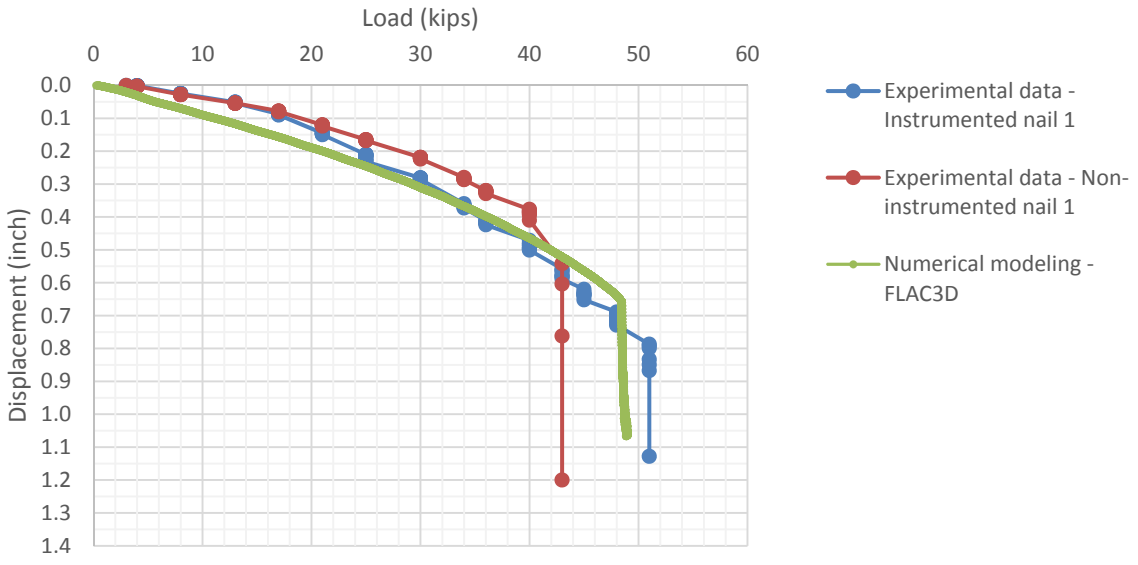

Figure 337. Comparison of the Experimental Results against the Numerical Modeling for the Sacrificial Nail Installed at Depth of 7.4 Ft from Top of Wall.

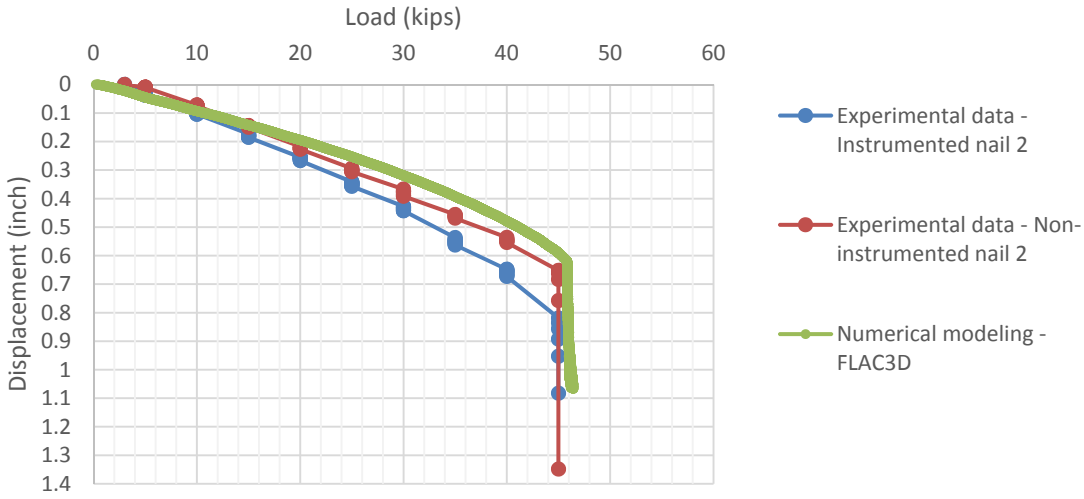

Figure 338. Comparison of the Experimental Results against the Numerical Modeling for the Sacrificial Nail Installed at Depth of 14.4 Ft from Top of Wall.

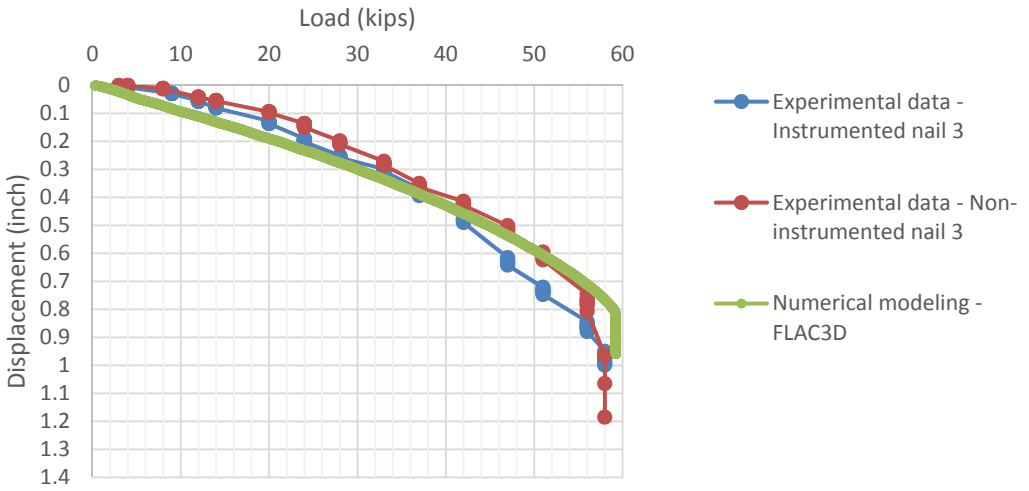

Figure 339. Comparison of the Experimental Results against the Numerical Modeling for the Sacrificial Nail Installed at Depth of 17.4 Ft from Top of Wall.

Figure 340 to Figure 342 show the shear stress at the soil–grout interface. A high level of agreement between experimental data and model results was obtained. The soil–grout interface parameters (i.e., grout cohesive strength, Cg, and grout shear stiffness, Kg) obtained from this modeling will be used later on to simulate the nail elements in the modeling of the soil nail walls.

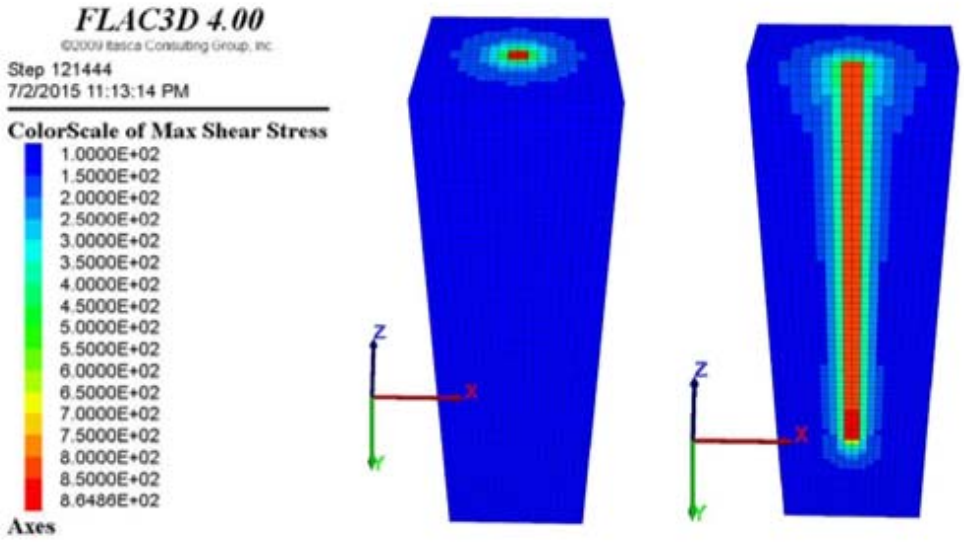

Figure 340. Shear Stress at the Soil–Grout Interface for the Modeling of the Sacrificial Nail at 7.4 Ft from Top of Wall (Shear Stress Obtained from Numerical Is 864 Psf).

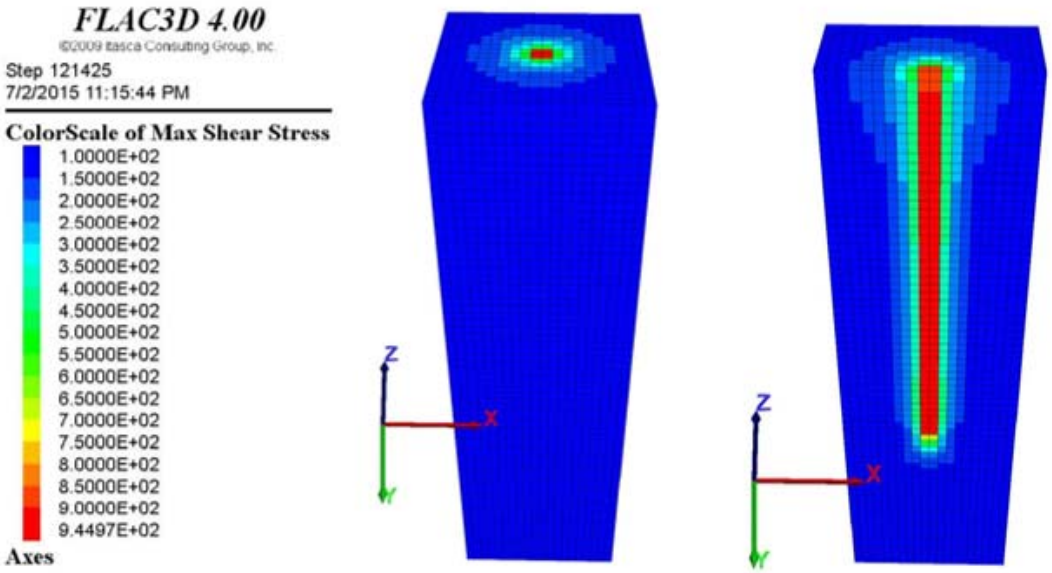

Figure 341. Shear Stress at the Soil–Grout Interface for the Modeling of the Sacrificial Nail at 14.4 Ft from Top of Wall (Shear Stress Obtained from Numerical Is 950 Psf).

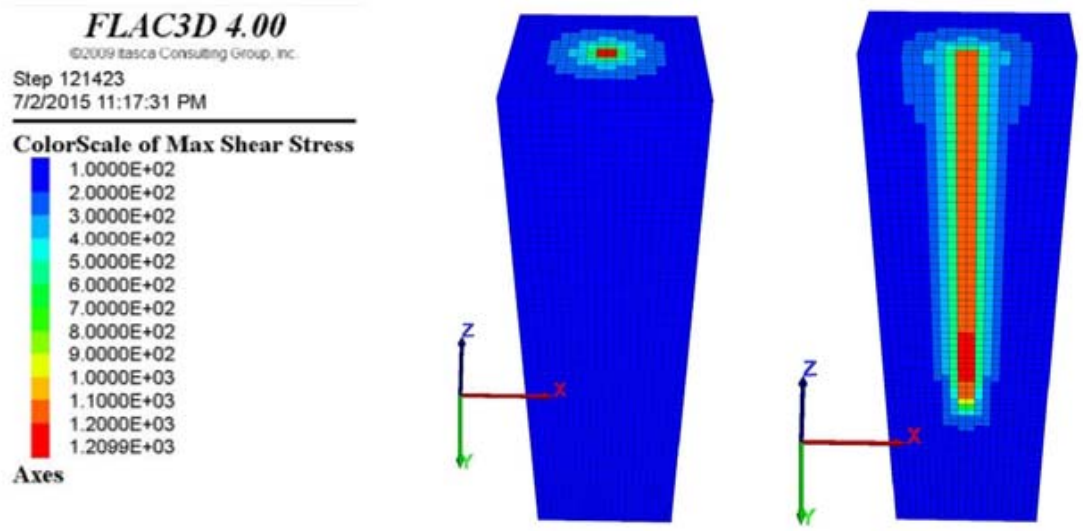

Figure 342. Shear Stress at the Soil–Grout Interface for the Modeling of the Sacrificial Nail at 17.9 Ft from Top of the Wall (Shear Stress Obtained from Numerical Is 1200 Psf).

MODELING THE SOIL NAIL WALL DURING CONSTRUCTION

The focus of this section is on the modeling of the soil nail behavior during excavation and wall construction.

Introduction

The numerical modeling of the soil nail wall construction was performed to: 1) gain a better understanding of how the different components of the retaining structure work, 2) study the changes in stress and displacement fields, and 3) evaluate the performance and stability of the soil nail wall. The global stability of the soil nail wall can be determined by using the limit equilibrium codes specifically developed for the design of the soil nail walls, such as SNAILZ and GOLDNAIL. However, this type of program is not capable of accounting for composite failure surfaces, which might be applicable when multiple soil layers with dissimilar strengths exist (FHWA, 2003). Performance of the soil nail walls depends on many parameters, including nail inclination, soil type, soil–grout behavior, and construction stages. Advanced geotechnical software such as Plaxis has been used by researchers to assess the performance of soil nail walls (e.g., Shiu, and Cha, 2006; Fan and Luo, 2008; Sivakumar and Singh, 2010). FLAC has also been used to solve problems involving soil nails (e.g., Briaud, 1997), as well as Abaqus (e.g., Barrows, 1994). These programs are very useful for the design and verification of soil nail walls, as they can predict the horizontal and vertical deformations of the wall along with the distribution of the loads in the nails.

The objective of this research project is to investigate the long-term behavior of soil nail walls. The MC and HS models are the most popular constitutive equations used for reproducing the soil behavior when modeling excavations and retaining structures (Sivakumar and Singh, 2010). However, these constitutive models cannot simulate the time-dependent behavior of soils. Plaxis has a specific creep model that is called the soft soil creep model, but it is not recommended for its use in excavation problems because its performance under shear has not been fully checked yet (PLAXIS 2D Manual, 2014). In FLAC3D, there are at least eight constitutive models available to simulate the creep behavior of soils, including the classical viscoelastic (Maxwell) model, the Burger's substance viscoelastic model, and two-component power law models. Based on that background information, the program FLAC3D was selected in this research to simulate the long-term behavior of the soil nail walls in HP clays.

The numerical modeling of the soil nail walls was carried out in two phases: 1) construction (up to its completion) and 2) post-construction (including creep behavior). The numerical modeling for phase 1 was validated against the lateral displacements of the wall and the load distribution along the nails at the end of the construction (i.e., the computed service

load). The procedure the researchers followed to model the soil nail wall construction is presented in the following section; the results of the modeling of the wall and the model calibration for the post-construction phase will be discussed in the next sections.

Modeling the Construction of the Soil Nail Wall Using FLAC3D

The components and factors associated with the behavior of a soil nail wall are: embankment fill; nail elements (i.e., the reinforcement elements); soil–grout interaction; and facing of the wall. Some key aspects related to the modeling of these components are presented as follows.

The drained shear strength of the soil is defined as (Terzaghi, 1942):

$$\tau=\sigma' \tan\phi'+c' \quad (15)$$

where σ' is the effective stress; ϕ' is the drained friction angle; and c' is the drained cohesion.

The MC constitutive model was adopted to simulate the soil behavior during the construction. In fine-grained soils, the drained strength should be considered when analyzing the long-term stability of the soil nail walls under a steady static loading condition (FHWA, 2003). The drained shear strength of the soil is defined by means of the effective friction angle. Mitchell (1993) proposed the correlation between drained angle of friction of fine-grained soils and PI (Figure 343). This correlation can be used to estimate the drained friction angle (FHWA, 2003). In this project, both drained and undrained numerical analyses were performed.

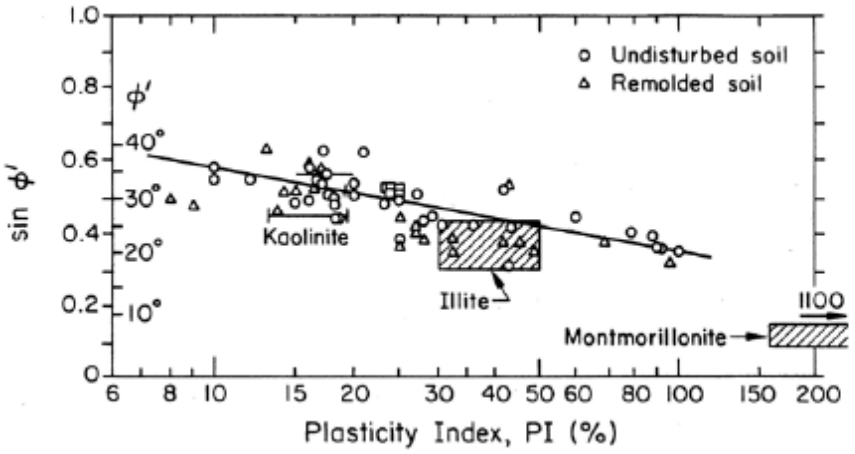

Figure 343. Correlation between Drained Angle of Friction of Fine-Grained Soils and PI (Mitchell, 1993).

As already mentioned, the reinforcement elements (i.e., nails) were modeled as cable elements. The shear behavior of the grout–soil interface is cohesive and frictional. The idealized system of grout–soil interface is shown in Figure 335a. This system was modeled as a spring (i.e., with associated shear stiffness of the grout, Kg) and a slider (i.e., the grout cohesive stiffness, Cg) located at the nodal points along the cable axis (Figure 335b). These parameters were obtained from the modeling of the pullout test on sacrificial nails as explained in the previous section.

Figure 344 shows the geometry and mesh adopted to simulate the soil nail wall at the Beaumont project. A relatively coarse mesh is adopted globally, which is refined to fine density in the vicinity of the soil nail wall (Singh and Babu, 2010). The mesh boundaries were adopted to minimize the effect of the boundaries on the results of the numerical modeling (Briaud, 1997).

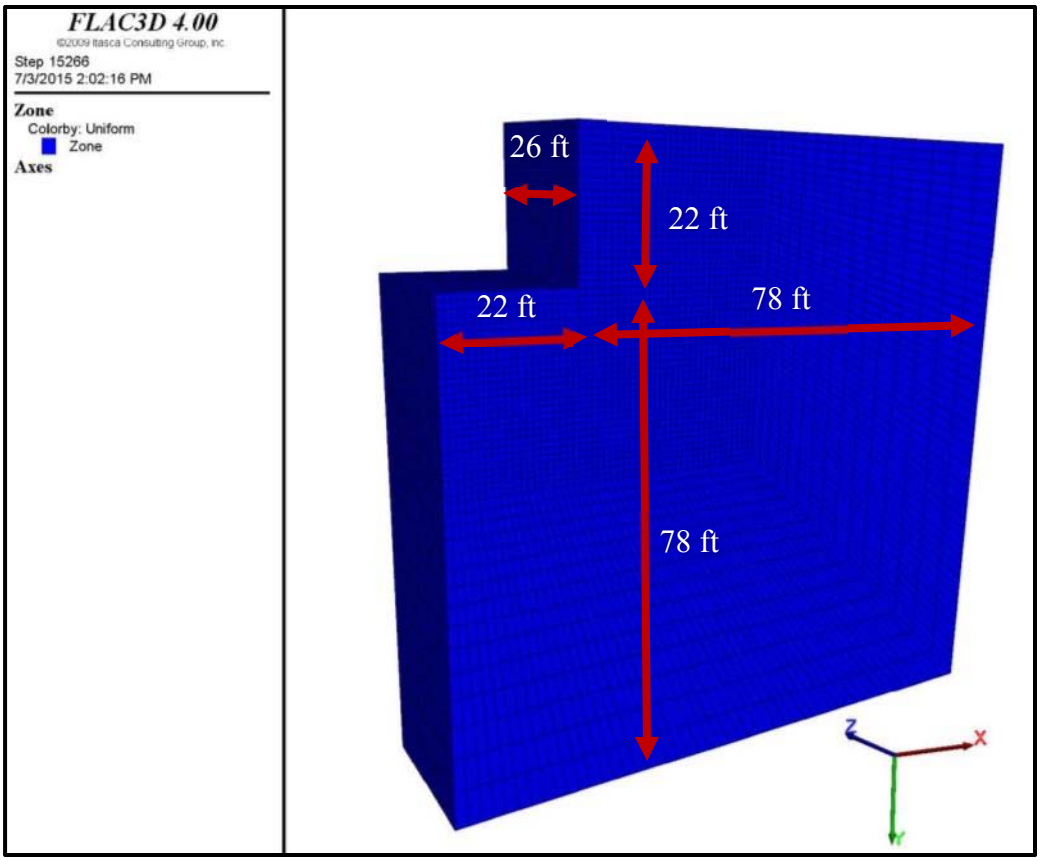

Figure 344. Geometry of the Soil Nail Wall Model.

The modeling of the wall was performed in successive steps. First, the geometry and mesh of the embankment was generated. The soil parameters were obtained from the information gathered in the tests performed in the laboratory. This step was followed by imposing the initial and boundary conditions of the problem to the adopted mesh. To reach the initial condition (i.e., in situ stresses), FLAC3D was run from the initial non-equilibrium conditions until an equilibrium state was obtained (Itasca, 2006). Once the equilibrium state was achieved, excavation stages were used to simulate the construction process of the soil nail wall (Singh and Babu, 2010). In each stage of construction, an excavation depth of 4 ft was simulated by assigning the null model to the zone of excavation. This step was followed by the simulation of the soil nail installation and shotcrete emplacement. The simulation of each stage continued until an equilibrium state was achieved. Six stages of construction were carried out to simulate the completion of the soil nail wall (i.e., up to the bottom of the excavation). Figure 345 illustrates the six stages of the construction defined in this modeling.

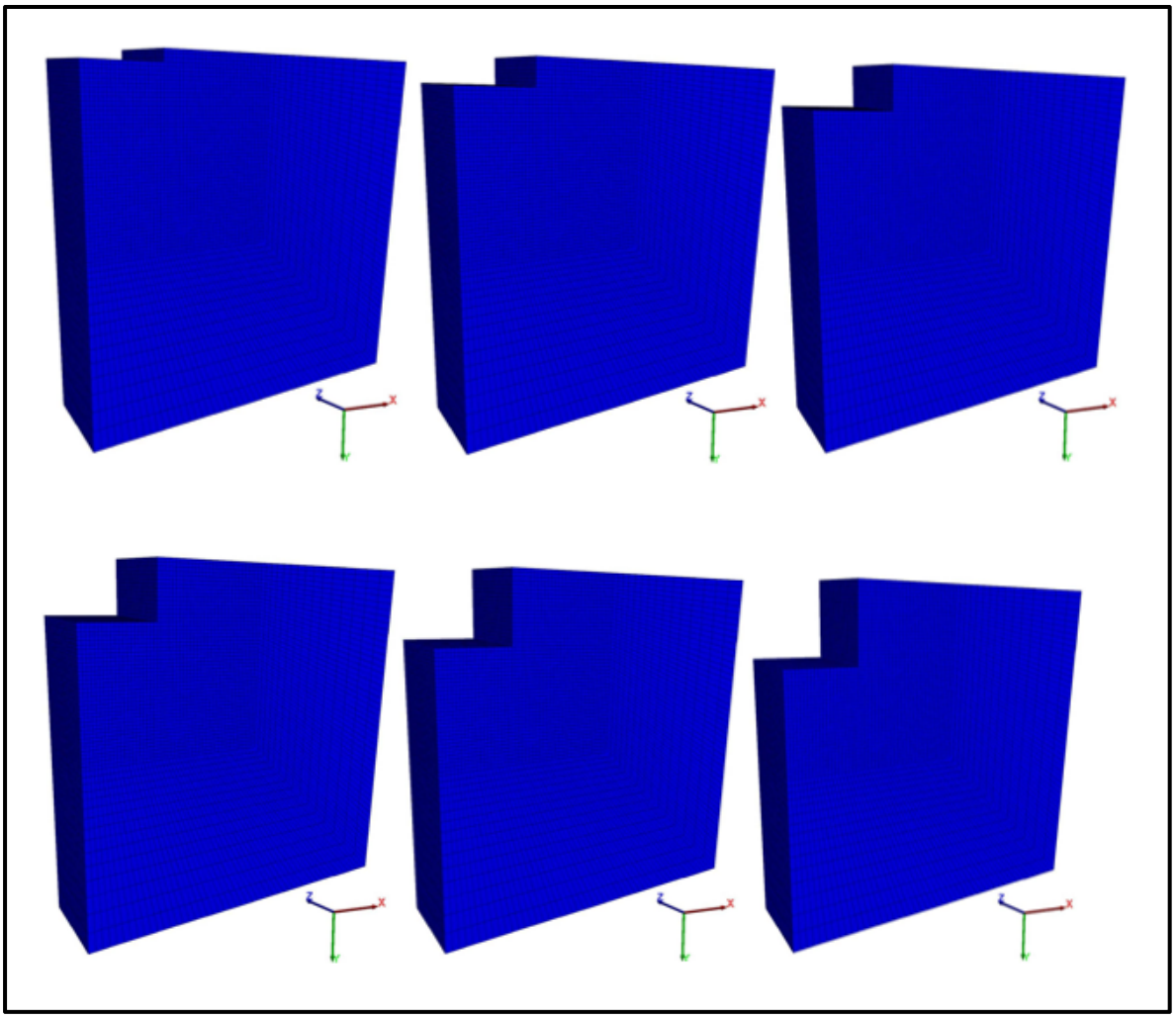

Figure 345. Simulation of the Soil Nail Wall at the Beaumont Project in Six Stages of Construction.

Table 60 summarizes the parameters adopted for the numerical simulation of the soil nail wall at the Beaumont project. Figure 346 presents the contours of the horizontal deformations predicted by the model at the end of construction (i.e., Stage 6). The horizontal movements obtained from the simulation are compared against the results of the inclinometer readings at station 1+46 in Figure 347. The model slightly underpredicts the horizontal movement of the wall for the first 5 ft, but for the remaining height of the wall, the numerical results are comparable with the actual data obtained from wall monitoring. This provides support to the model assumptions considered in this analysis.

Table 60. Parameters Adopted for Numerical Simulation of the Wall at Beaumont Project.

Material	Constitutive Model	Properties
Embankment soil	MC	ϕ′=26, c′=0, γ =125 pcf, E=2.9e5 psf, υ=0.3
Soil nails (cable element)	Elastic-perfectly plastic	E steel=4.17e9 psf (200 GPa), c_grout=1e3 psf, ϕ_grout=20°
Shotcrete (shell element)	Elastic (isotropic)	E shot=2.2e8 psf, υ=0.25, thickness=4 in.

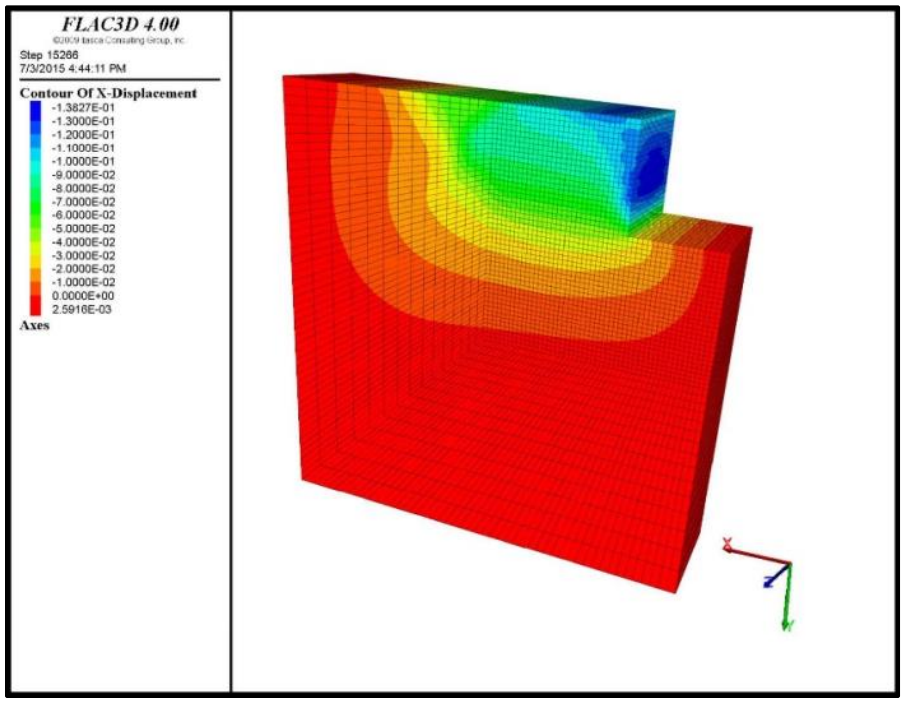

Figure 346. Soil Nail Wall Lateral Displacements Contours Predicted by the Model at the End of the Construction.

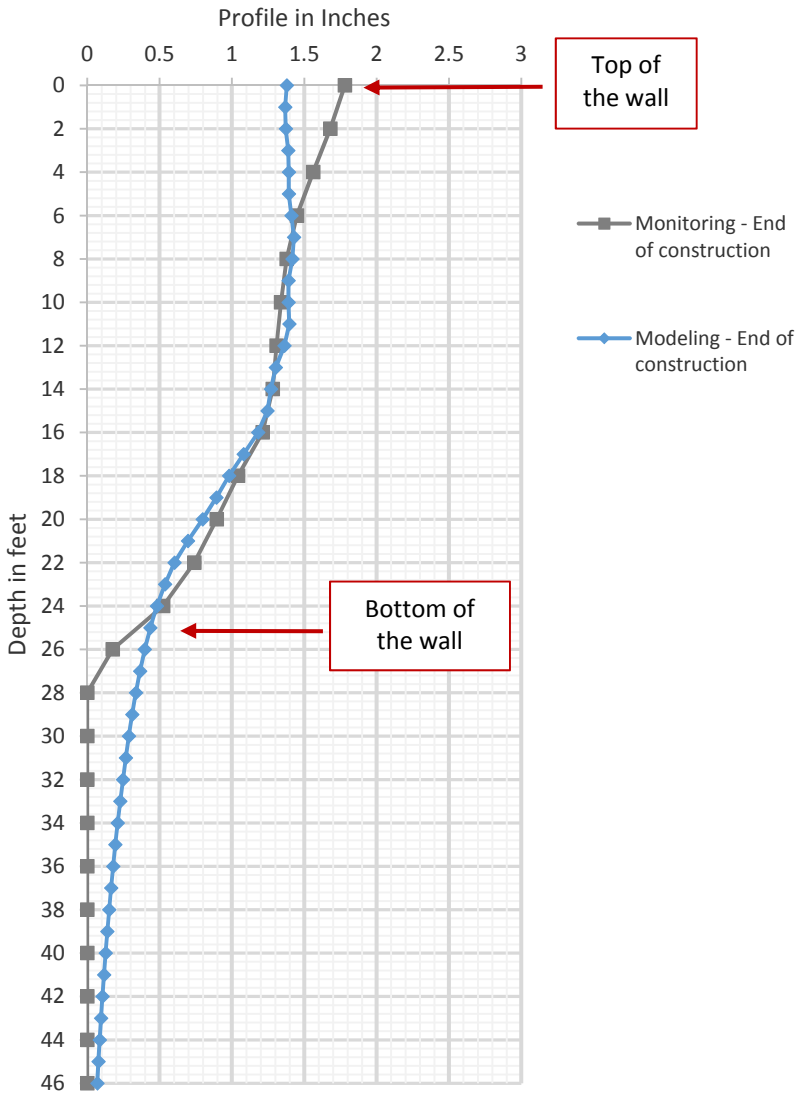

Figure 347. Comparison of the Results of the Lateral Displacements of the Soil Nails Obtained from Numerical Modeling against the Actual Lateral Displacement of the Wall Obtained from Inclinometer Readings at Station 1+46.

In Figure 348 to Figure 353, the service load in the nails obtained from the numerical modeling at the end of the construction is compared with the service load obtained from the instrumentation of the soil nail wall at the Beaumont project. Considering that the numerical model slightly underpredicted the horizontal deformations of the wall for the first 5 ft, it is anticipated that the service load developed in these two first rows of soil nails would also be smaller than the actual measured service load. However, for the other rows of soil nails, the results of modeling are very satisfactory when compared with the field data.

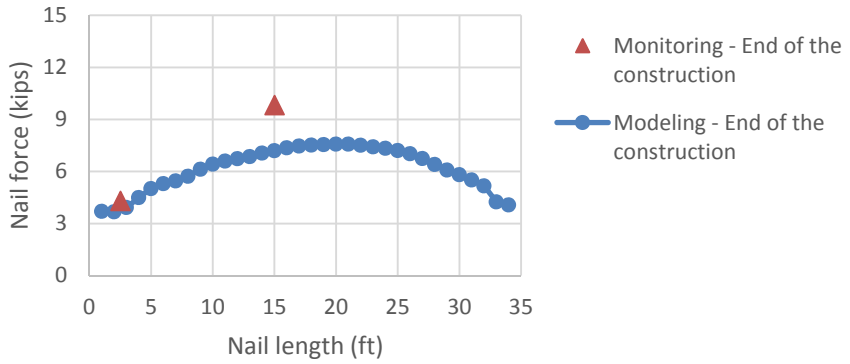

Figure 348. Comparison of the Service Load in the Nails in First Row of the Soil Nails from Both Numerical Modeling and Instrumentation of the Soil Nail Wall at Beaumont.

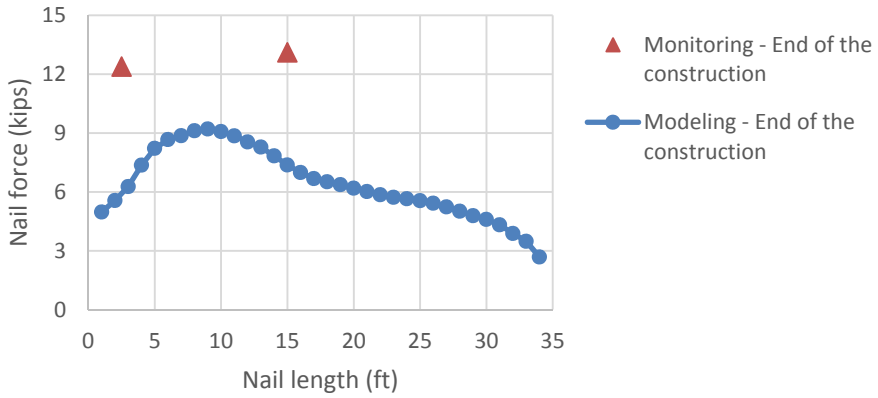

Figure 349. Comparison of the Service Load in the Nails in Second Row of the Soil Nails from Both Numerical Modeling and Instrumentation of the Soil Nail Wall at Beaumont.

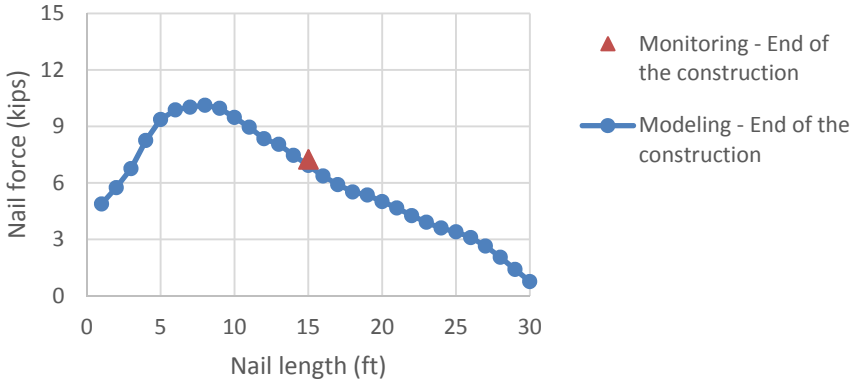

Figure 350. Comparison of the Service Load in the Nails in Third Row of the Soil Nails from Both Numerical Modeling and Instrumentation of the Soil Nail Wall at Beaumont.

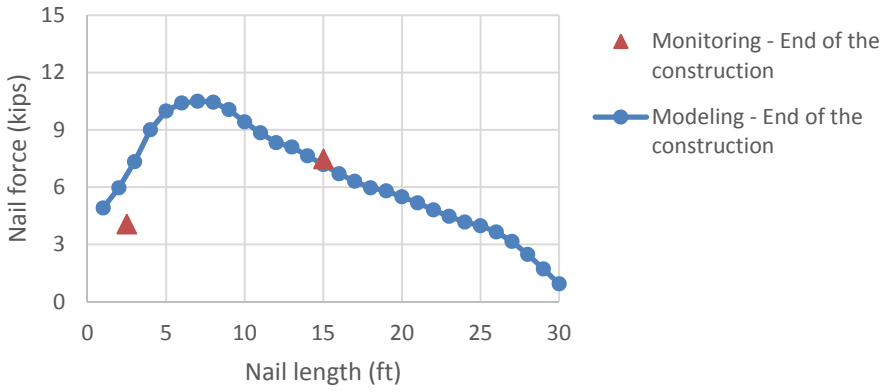

Figure 351. Comparison of the Service Load in the Nails in Fourth Row of the Soil Nails from Both Numerical Modeling and Instrumentation of the Soil Nail Wall at Beaumont.

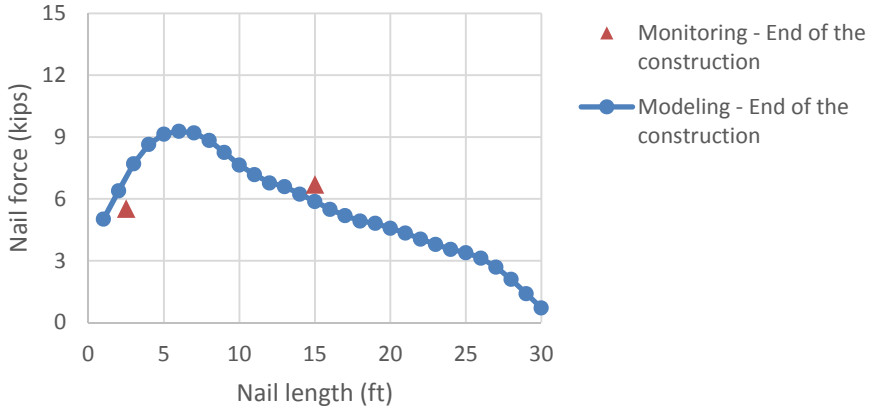

Figure 352. Comparison of the Service Load in the Nails in Fifth Row of the Soil Nails from Both Numerical Modeling and Instrumentation of the Soil Nail Wall at Beaumont.

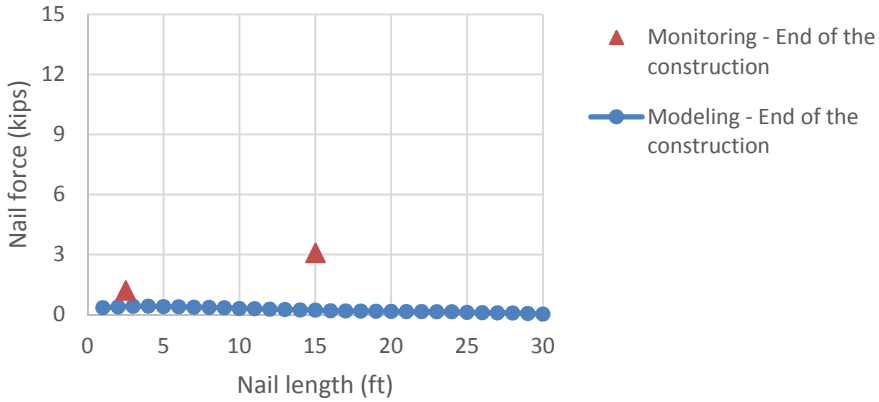

Figure 353. Comparison of the Service Load in the Nails in Sixth Row of the Soil Nails from Both Numerical Modeling and Instrumentation of the Soil Nail Wall at Beaumont.

RHEOLOGICAL BEHAVIOR OF HP CLAYS

Any material subjected to constant stress will deform in the course of time. The magnitude of the time-dependent deformations depends on the particular material properties. The rheology of materials investigates the relations between stress, strain, and time (Feda, 1992). Creep is a long-term deformation of the material under a constant applied load.

This section presents some key aspects about the rheological behavior of soils. Some previous research related to the creep in soils is discussed, as well as investigations looking at the estimation of the soil viscosity. The viscous response of HP clays and some available mechanical models to simulate their behavior are discussed, as well.

To gain a better understanding of the creep behavior of soils, triaxial creep tests were carried out on the soil samples. Detailed description of these tests was presented in Chapter 6. These tests were modeled with FLAC3D. Results of this simulation were used to obtain the viscous parameters of the soil at the Beaumont tests used for modeling the soil nail wall.

Rheological Behavior of the Soil

The rheological behavior (or time-dependent) behavior of soils can be described, in a very general form, like as a viscous fluid (Whitman, 1957). In 1687, Newton studied the flow behavior of liquids. He observed that some fluids have a constant viscosity (i.e., slope of the shear stress vs. strain rate line). These kinds of fluids are generally called Newtonian fluids. In the case of non-Newtonian fluids, the viscosity depends on the applied force (or stress conditions). Bingham (1917) stated that a viscoplastic material behaves as a rigid body at low stresses, but it flows as a viscous fluid at high stresses. This implies that in the Bingham model when the shear stress is less than the critical value $'\tau_0'$ the material is considered a rigid body; but once the shear stresses exceed this critical value (i.e., yield stress), the material flows and the viscous behavior is controlled by a constant viscosity. Figure 354 presents different fluid models.

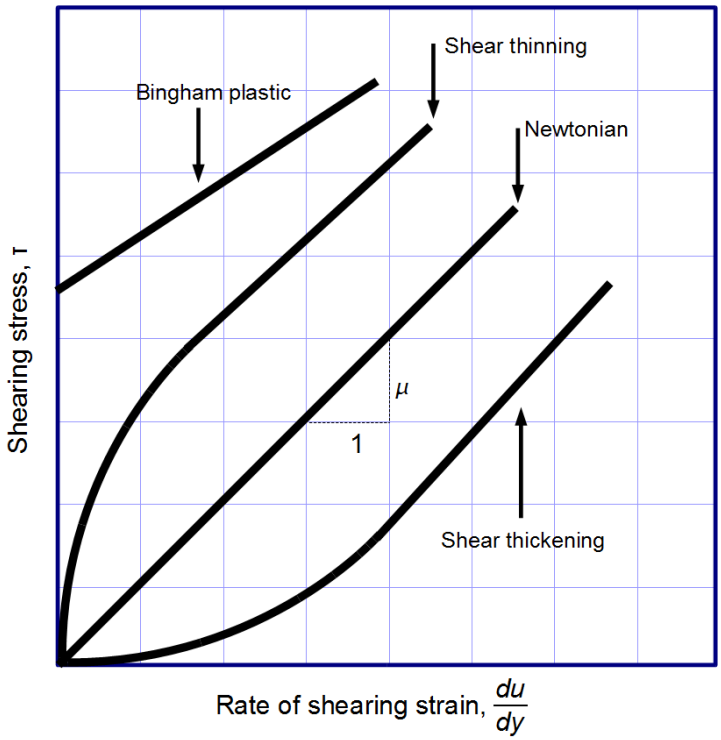

Figure 354. Fluid Models (Viscosity Is the Slope of Each Line).

O'Donovan and Tanner (1984) proposed the bi-viscosity model (which is a modified Bingham model) to represent the behavior of those materials that exhibit two different viscosity values, as follows: a low viscosity when the shear stress is less than a yield shear stress, and another viscosity when the shear stress exceeds the yield shear stress. In this model, the viscosity parameter is generally around 1000 times lower than the viscosity parameter for the shear stresses below the yield stress (O'Donovan and Tanner, 1984; Mitsoulis, 2007). The general form of a bi-viscosity model is:

$$\tau = \eta_{pN}\dot{\gamma}\ for\ \dot{\gamma} \leq \dot{\gamma}_c \tag{15}$$

$$\tau = [\eta_p + \frac{\tau_y}{\dot{\gamma}}]\dot{\gamma}\ for\ \dot{\gamma} > \dot{\gamma}_c \tag{16}$$

where, η_{pN} is the pseudo-Newtonian viscosity in the unyielded zone; η_p is the Bingham viscosity; and $\dot{\gamma}_c$ is the critical shear rate (Jeong, 2013). Figure 355 illustrates the shear stress versus shear strain rate for the modified Bingham model.

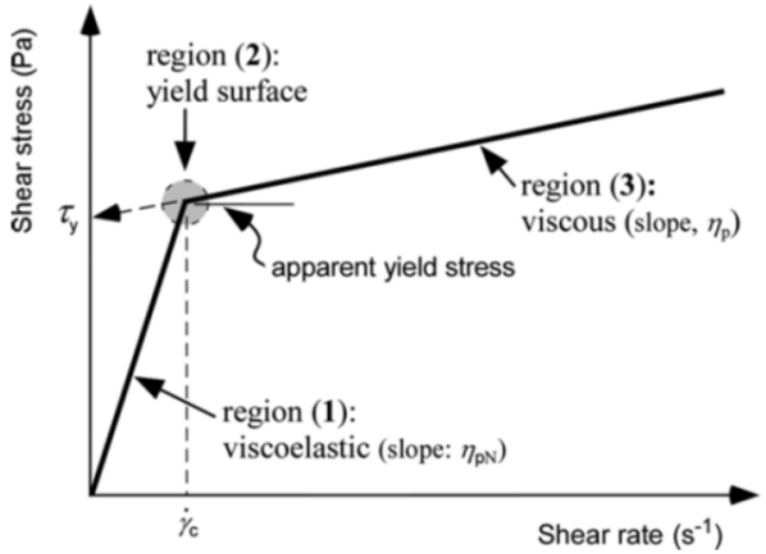

Figure 355. Scheme of a Bi-Viscosity Model, Shear Stress vs. Shear Strain Rate for the Modified Bingham Fluids Model $\dot{\gamma}$ = Critical Shear Strain Rate (after Jeong, 2013).

Viscoelastic materials exhibit both viscous and elastic behaviors (Itasca, 2006). Elastic behavior is defined by a spring with elastic constant, G. According to Hooke's law, the shear behavior is defined as:

$$\tau = G\gamma \tag{17}$$

where, τ is the shear stress; G is the elastic constant (i.e., shear modulus); and γ is the shear strain.

The viscous behavior in rheological models is defined with a dashpot. According to Newton's law, the viscous behavior can be written as:

$$\tau = \mu\dot{\gamma} \tag{18}$$

where, μ is the shear viscosity of the material; and $\dot{\gamma}$ is the shear strain rate. Figure 356 illustrates the basic viscoelastic elements in mechanical rheological models. The mechanical rheological models are typically obtained by combining, in different ways, some of these basic elements. They are adapted to study different features related to the time-dependent behavior of soils. The Maxwell model is the combination in series of an elastic spring and a dashpot (Figure 357a), while the Kelvin-Voigt model consists of a dashpot and an elastic spring combined in parallel. Burger's model consists of the Maxwell and Kelvin models in series (Figure 357b).

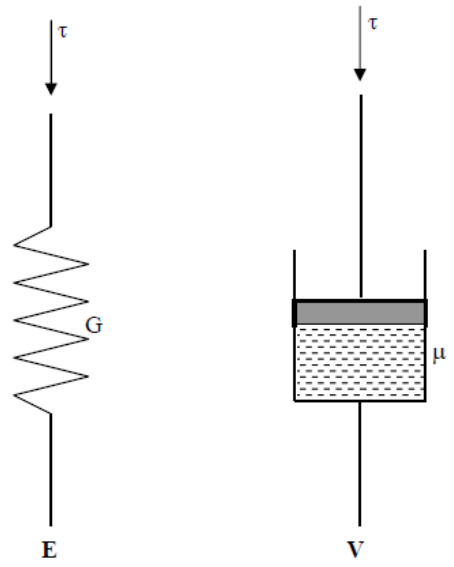

Figure 356. Elastic (E) and Viscous (V) Element Used in Mechanical Rheological Models (after Mahajan and Budhu, 2006).

In FLAC3D, there are eight rheological mechanical models available to simulate the creep behavior of soils, including the classical viscoelastic (Maxwell) model, and the Burger substance viscoelastic model. As already mentioned, in these models, the creep deformations are simulated by a displacement of dashpot.

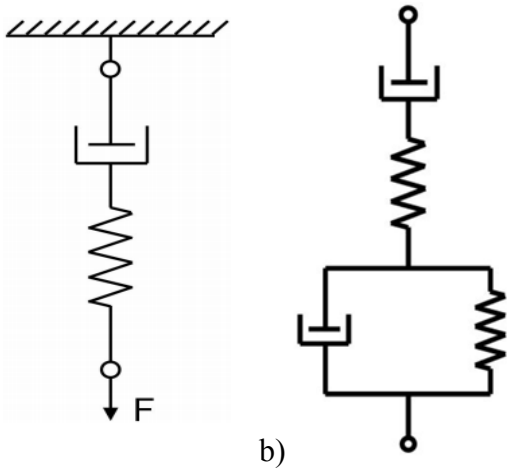

Figure 357. Typical Rheological Models: a) Maxwell's Model, and b) Burger's Model.

In rheological models the total strain of the body can be written as:

$$\gamma = \gamma_0 + \gamma(t) \tag{19}$$

where, γ_0 is the elastic instantaneous deformation (i.e., the one developed immediately after loading); and $\gamma(t)$is the strain developed in time because of the viscous behavior of the material. The Maxwell model (i.e., a dashpot and a spring in series) exhibits constant strain rate ($\dot{\gamma} = \frac{d\gamma}{dt}$) under an applied constant shear (Figure 358a). In the Burger model (i.e., a combination of the Kelvin and Maxwell models), under a constant shear, elastic deformations, γ_0, are predicted immediately after the loading and then the rate of the strain decreases in time until reaching a constant value (Figure 358b).

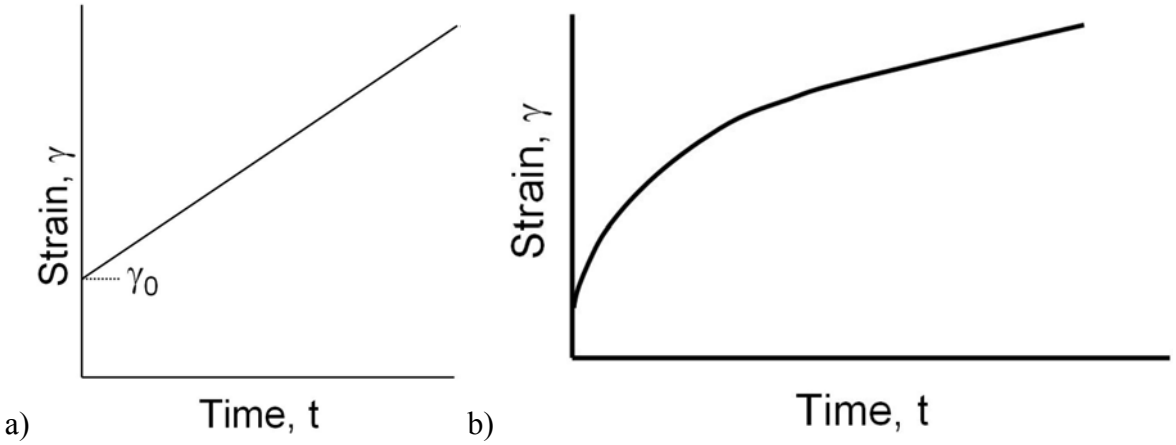

Figure 358. Strain vs. Time for a) Maxwell's Model, and b) Burger's Model.

Many researchers have studied the rheological behavior of soils (Gersevanov, 1937; Whitman, 1957; Keedwell, 1984; Vyalov, 1986; Feda, 1992). There is a consensus that the creep behavior of the majority of soils is nonlinear, therefore linear types of rheological models (e.g., the Maxwell model) usually correspond to quite simplified assumptions of rheological behavior of soils.

Segalini et al. (2009) performed several UU triaxial tests with creep steps and used the FLAC code to study the creep behavior of a landslide in Italy. The Burger model was adopted in this research to study the creep behavior of the soil. Figure 359 presents the strains normalized with confining pressures versus time for the laboratory tests and numerical modeling obtained in that study. This simplified model was able to capture quite well the tendencies observed in the experiments.

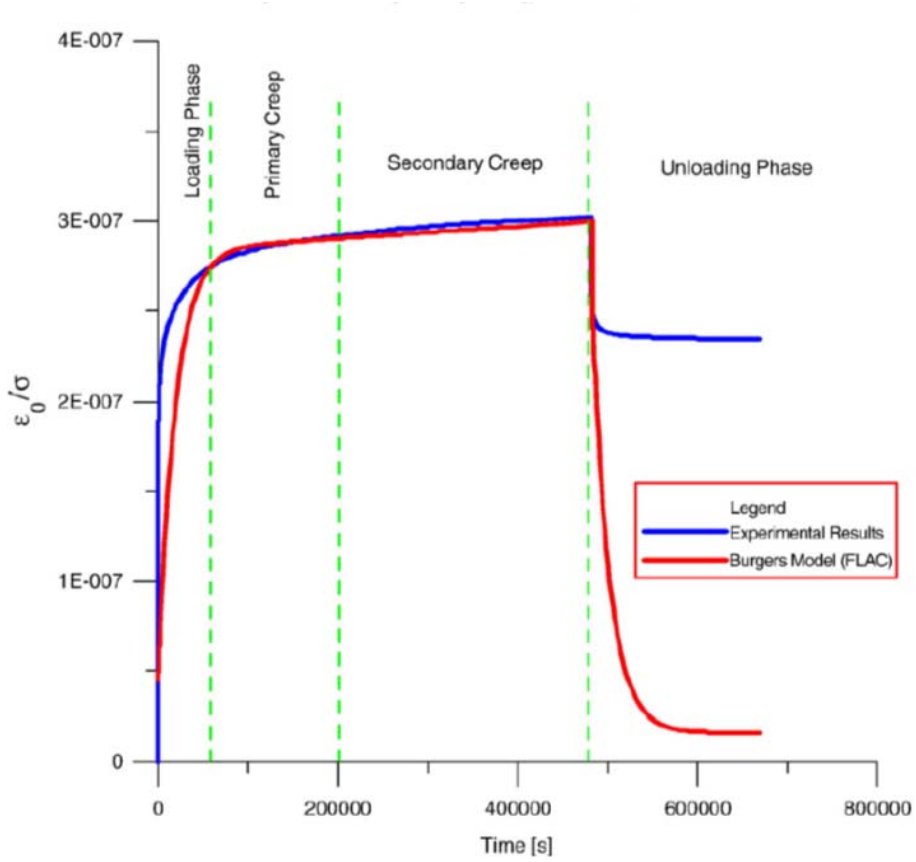

Figure 359. Results of the Triaxial UU Creep Test along with Numerical Modeling Using Burger Model (Segalini et al., 2009).

The general case of creep in soils is characterized by three steps (Figure 360), as follows:

- Step I is related to a primary creep (δ^{I}); characterized by an attenuated deformation with a decreasing rate of deformation ($d\delta/dt$). The duration of this stage is generally very short.
- Step II is known as secondary creep (δ^{II}) and takes place at a constant deformation rate.
- Step III is associated with a tertiary creep (δ^{III}) and is characterized by a non-attenuated deformation, with an increasing rate of deformation.

The actual configuration of this curve will depend on, among others, soil type, stress level, water content, and temperature. The load level (Q) has a predominant effect on creep behavior. Figure 360 shows the effect of different load levels (i.e., Q1, Q2, and Q3) on creep behavior. At higher loads, the soil exhibits the excess deformation and the creep rate significantly increases.

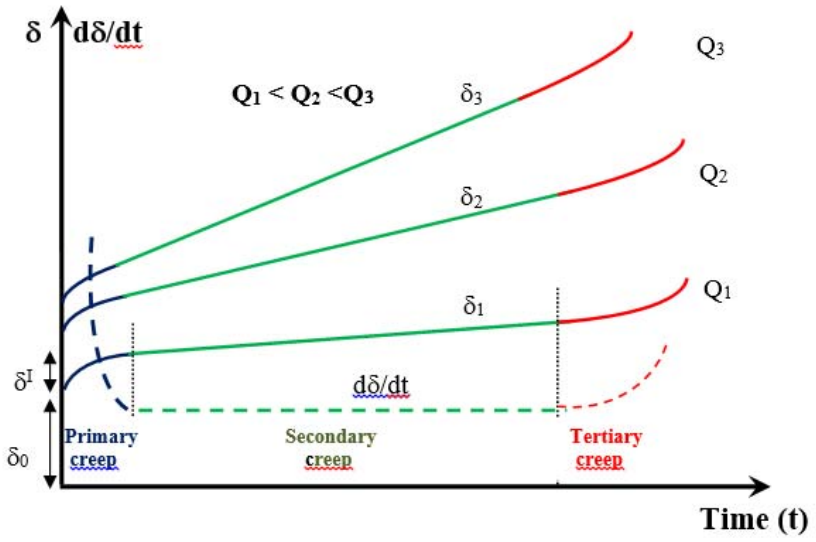

Figure 360. Three Steps Associated with Creep in Soils.

There are several works that discuss the creep behavior mentioned above; for example, Vyalov (1986) developed the series of creep curves shown in Figure 361 for tests performed at different load levels.

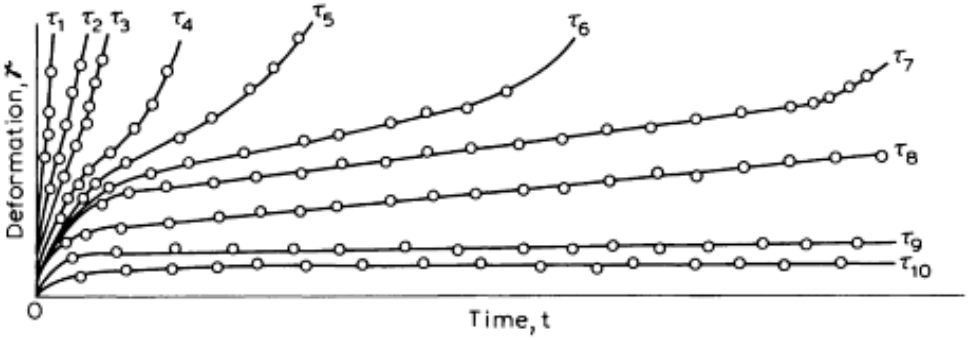

Figure 361. Curves of Creep in Soil for Various Constant Loading (Vyalov, 1986).

Shear Viscosity in HP Clays

The key parameter to determine the rheological behavior of HP clays is the soil shear viscosity. Most of the available literature related to soil viscosity focuses on soil flow, such as landslides, mudslides, or earth flow (Mahajan and Budhu, 2006). Soils in such conditions are characterized by a high water content (i.e., higher than the LL), and with LI less than 1.5. The LI

indicates the consistency of the soil in its natural states. The soil is very soft when the LI is near one, and very stiff when it is close to zero (Keedwell, 1984).

The LI is defined as:

$$LI = (w - w_p)/(w_l - w_p) \tag{20}$$

where w is the natural moisture content; w_l is the LL; and w_p is the plastic limit of the soil. The LI of the soil at the NGES-TAMU clay site and the Beaumont site are presented in Table 61 and Table 62, respectively. As observed in Table 61 and Table 62, the LI for both sites is less than 0.1, except for the soil sample from the Beaumont site at a depth of 3–5 ft.

Table 61. LI of the Samples from the NGES-TAMU Clay Site.

NGES-TAMU Clay Site						
Borehole	**Depth (ft)**	**Plastic Limit (PL)**	**LL**	**PI**	**Water Content %**	**LI**
N2	13–15	23	71.4	48	22	<0
N1	8–10	20.5	55.6	35	24	0.10
N1	6–8	20	69.1	49	16	<0
N5	16–18	17.8	62.7	45	22	0.09

Table 62. LI of the Samples from the Beaumont Site.

Beaumont Site						
Borehole	**Depth (ft)**	**Plastic Limit (PL)**	**LL**	**PI**	**Water Content %**	**LI**
B1	3–5	23.7	77.8	54	33.8	0.19
B1	8–10	21.3	72.7	51	23.6	0.04
B1	13–15	24.3	91.9	68	25.5	0.02
B1	23–25	16.8	65.1	48	21.8	0.10
B1	33–35	14.8	63.2	48	15.2	0.01
B2	23–25	17.4	65.5	48	22.4	0.10

The viscous parameter for the soil with high water content is generally determined with the viscometer. However, HP clays exhibit viscous behavior for water contents below the LL. The shear viscosity of a HP clay for such conditions should not be determined using the

viscometer. Furthermore, there is no standard method to measure the viscous parameter of the clay with low water content (Mahajan and Budhu, 2006).

Locat and Demers (1988) investigated the viscosity of sensitive clays with LI between 1.5 and 6 with a rotational viscometer. Based on field and experimental observations, they proposed the relationship between viscosity and LI presented in Figure 362.

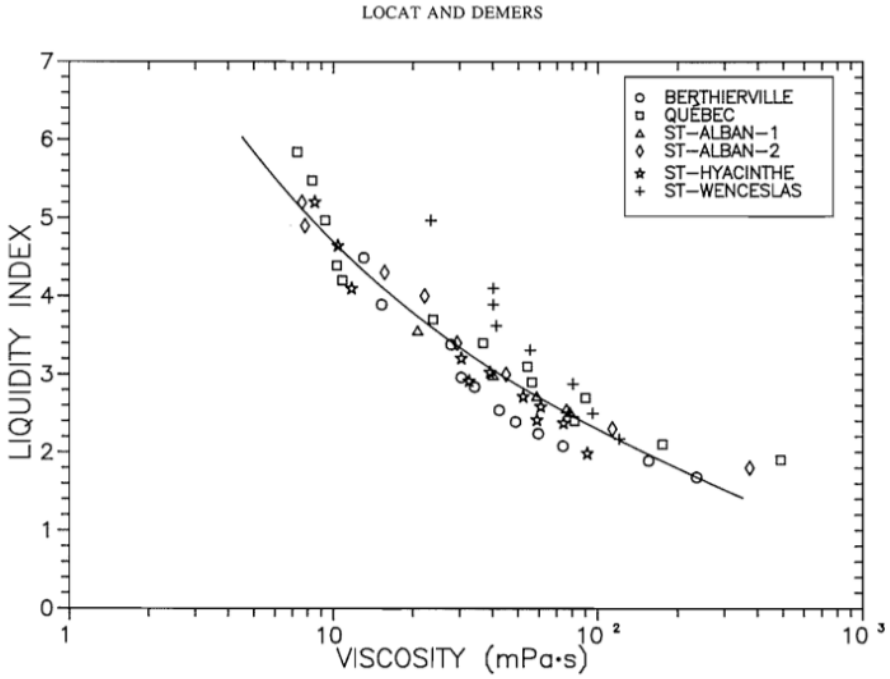

Figure 362. Relation between LI and Viscosity (Locat and Demers, 1988).

For the soil with low water content (i.e., less than the LL), rotary viscometer cannot be used to measure the viscosity (Fakher et al., 1999). Mahajan and Budhu (2006) investigated the viscous behavior of the clay during penetration of a rigid shaft. He investigated the shear viscous behavior of the plasticity clay based on the results of the fall cone test. He proposed the experimental equation presented in Figure 363 to determine the viscosity of the clay with low water content (i.e., for low LI). No information was provided for the viscosity of the soil with liquidity limit less than 0.5.

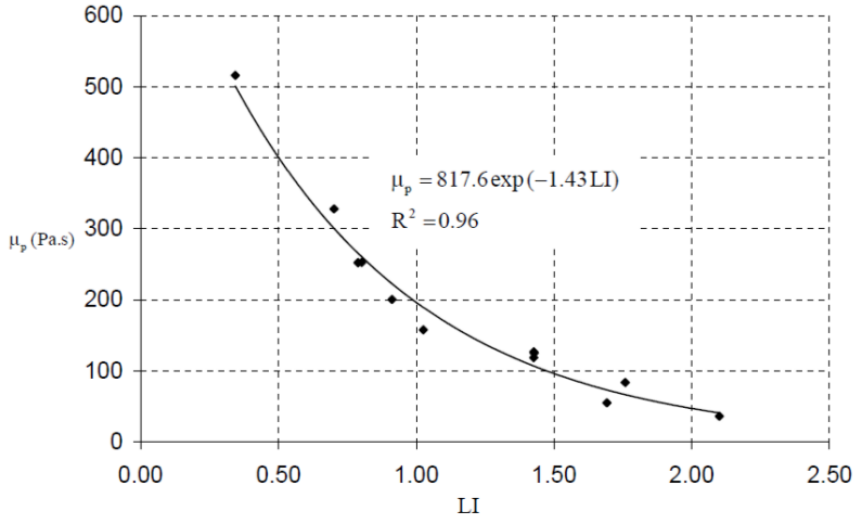

Figure 363. Relation between Shear Viscosity and LI Based on the Results of the Fall Cone Test on Kaolin (Mahajan and Budhu, 2006).

Segalini et al. (2009) investigated the rheological behavior of the clay under a constant active stress by performing the UU triaxial test with creep stages. The viscous parameters of the soil were obtained from the results of the creep tests. Furthermore, the creep test was modeled using the software FLAC for the calibration of the viscous parameters.

As discussed earlier (i.e., Chapter 6, Eq. 14), Briaud and Garland (1985) proposed a power law to model the time-dependent behavior of soils. Typical n values range from 0.005 to 0.03 for sands and 0.02 to 0.08 for clays.

Triaxial Creep Tests

Triaxial UU creep tests (some of them with pore pressure measurement) were carried out on the soil samples from the NGES-TAMU clay site and the Beaumont project in order to investigate the rheological behavior and the viscous parameters of the clays involved in this research. Furthermore, these tests were modeled using FLAC3D, and the viscous parameters were obtained from this modeling. The results of the triaxial creep tests and the related numerical modeling are briefly presented in this section.

Test Results

The triaxial creep tests were performed by loading steps. The protocol consisted of an initial strain-control loading stage, until a predefined target load was achieved. At this point, the triaxial device was switched to the stress-control mode to allow the creep of the samples for

24 hours (or any other defined time interval) at this constant load. After this creep stage, the triaxial device was switched back to strain-control mode until the next predefined target stress level was achieved and a new creep stage was performed, as explained previously. This loading-creep procedure by steps continues until the failure of the sample (more details are presented in Chapter 6). In some tests, the pore pressure was measured.

Some of the tests performed in this chapter are detailed as follows. For the NGES-TAMU clay site sample between 8 and 10 ft, the creep steps (duration of 24 hours) were performed at axial loads equal to: 30, 70, 110, 150, 190, 230, and 265 lb. Figure 364 presents the strain–time response for each load step. The test stopped at the failure load of 265 lb. Regarding the sample gathered from the NGES-TAMU clay site from a depth between 10 and 12 ft, the creep steps (duration of 24 hours) were performed at axial loads equal to: 70, 110, and 140 lb.

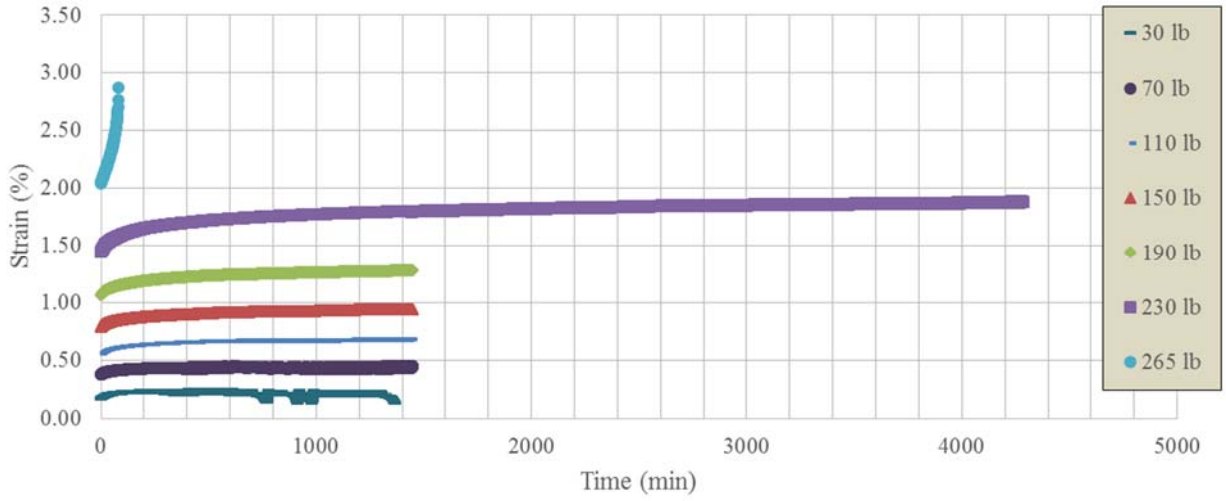

Figure 364. Strain-Time Curves Triaxial UU Creep Tests Conducted on Samples from NGES-TAMU Clay Site, Depth of 8-10 Ft (Holding Loads Were 30, 70, 110, 150, 190, 230, and 265 Lb).

As for the sample from the NGES-TAMU clay site between 16 and 18 ft, the creep steps (duration of 24 hours) were performed at axial loads equal to: 150, 190, 230, and 255 lb. Figure 365 and Figure 366 present the strain–time curves for each load step. Finally, for the sample from the Beaumont project corresponding to a depth between 33 and 35 ft, the creep steps (duration of 24 hours) were performed at axial loads equal to: 30, 70, 110, 150, 190, and 230 lb. Figure 367 presents the results of the tests on samples gathered from the Beaumont project.

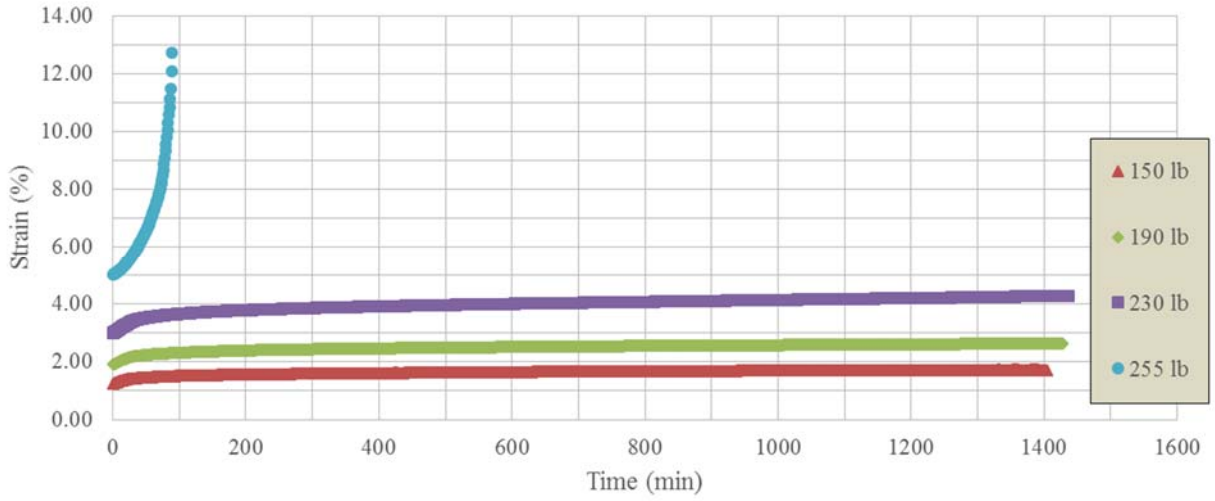

Figure 365. Strain-Time Curves Triaxial UU Creep Tests Conducted on Samples from NGES-TAMU Clay Site at the Depth of 10–12 Ft (Holding Loads Were 150, 190, 230, and 255 Lb).

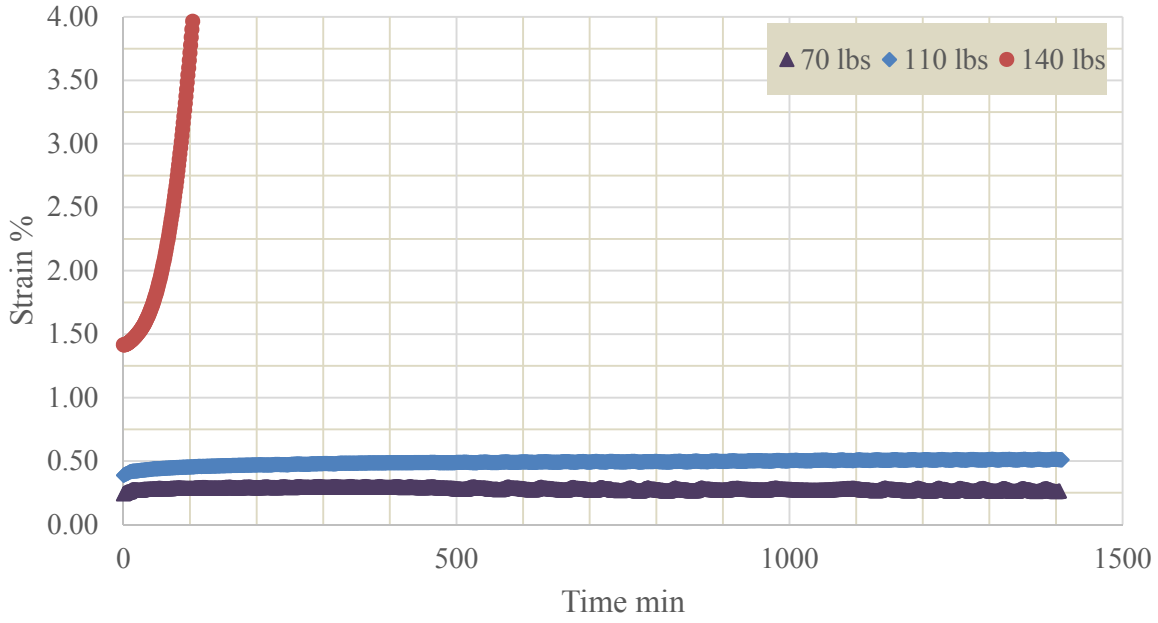

Figure 366. Strain–Time Curves Triaxial UU Creep Test Conducted on Samples from NGES-TAMU Clay Site at Depth of 16–18 Ft (Holding Loads Were 70, 110, and 140 Lb).

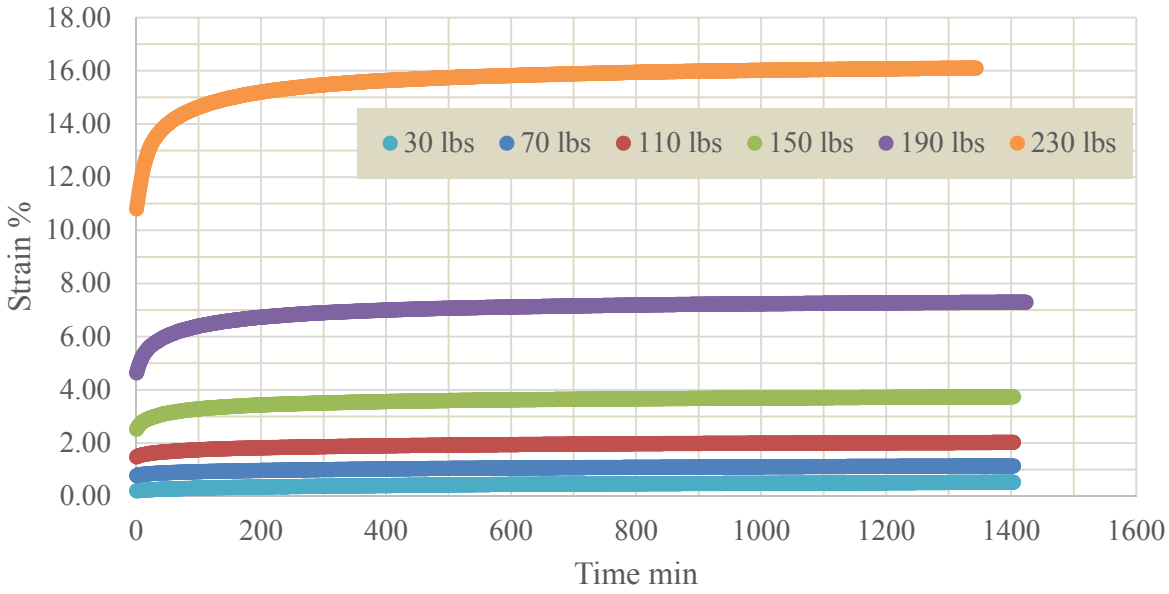

Figure 367. Strain-Time Curves Triaxial UU Creep Tests Conducted on Samples from Beaumont Project at the Depth of 33–35 Ft (Holding Loads Were 30, 70, 110, 150, 190, and 230 Lb).

Figure 364 to Figure 367 show the series of creep curves obtained from the triaxial creep tests. A similar behavior to that represented in Figure 361 (i.e., from Vyalov, 1986) can be observed in nearly all the performed tests. At the higher stress levels, the soil exhibits an excess of deformation and the creep rate increases remarkably. For instance, for the sample between 10 and 12 ft (i.e., Figure 365) at a load equal to 230 lb (i.e., one step before failure), the soil shows the same behavior as τ_8 in Figure 361. In the next loading step, the soil failed at 265 lb. From the information gathered from these tests, it appears that the creep behavior is practically the same and does not strongly depend on the stress level when the applied loads are lower than the 90 percent of the shear stress at failure. However, when the shear stress is above the 90 percent of the shear strength, the soil tends to fail during creep. This behavior has been considered in the modeling presented in the next section.

As discussed in Chapter 2, Briaud and Garland (1985) proposed a power model to account for the time-dependent behavior of soils. If the strain–time curve obtained from triaxial creep tests is normalized with s_1 and t_1, respectively, and plotted in the log–log scale, the slope of this line defines the power n (see Eq. 5, Chapter 2). Figure 368 to Figure 370 present the

strain–time curves in log–log scale for the triaxial creep tests performed at the NGES-TAMU clay site.

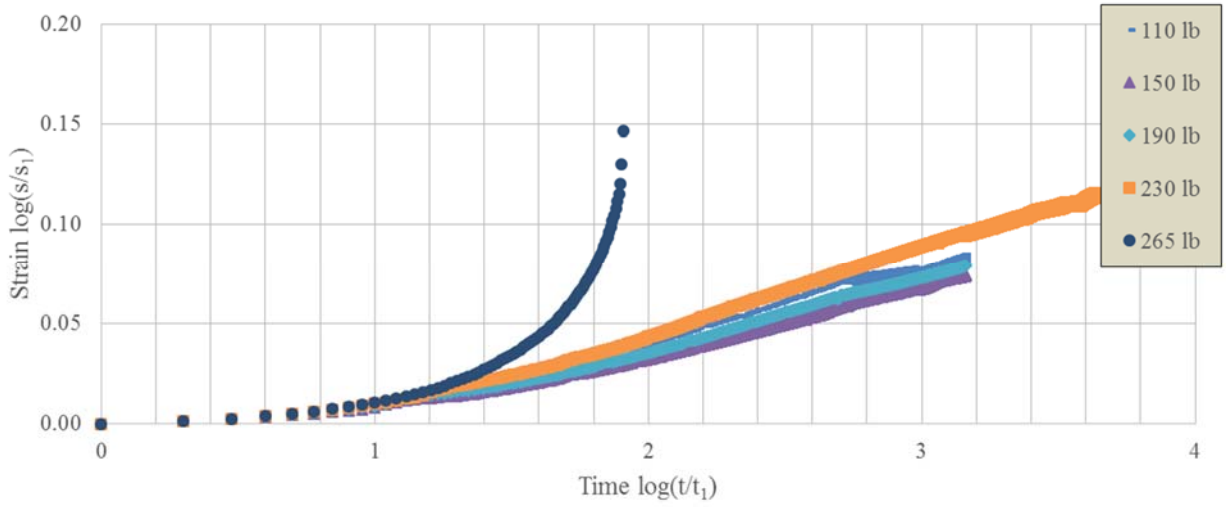

Figure 368. Strain–Time Curves (Log–Log Scale) for All the Holding Loads Plotted in Log–Log Scale. Samples from NGES-TAMU Clay Site Depth 8–10 Ft.

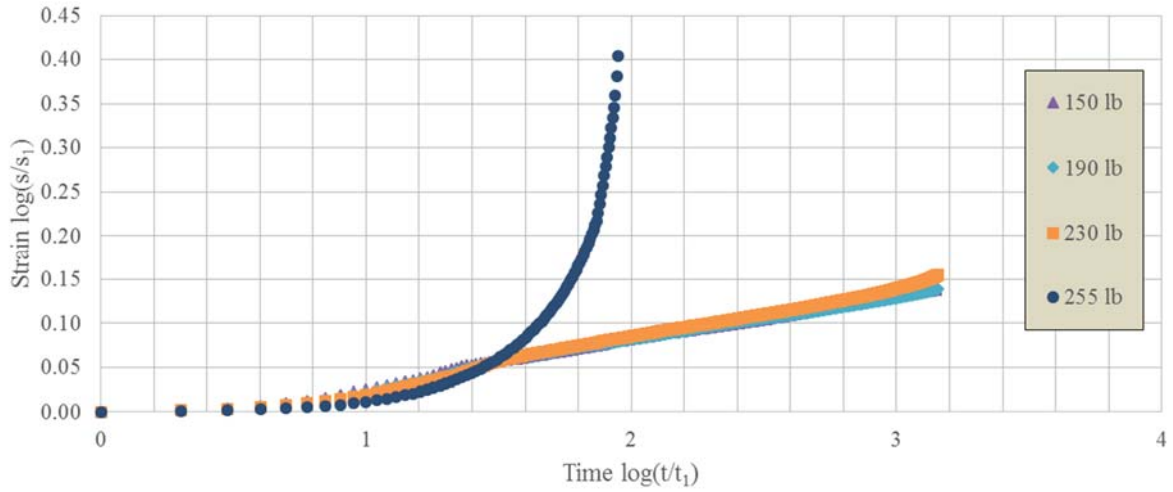

Figure 369. Strain–Time Curves (Log–Log Scale) for All the Holding Loads Plotted in Log–Log Scale. Samples from NGES-TAMU Clay Site Depth 10–12 Ft.

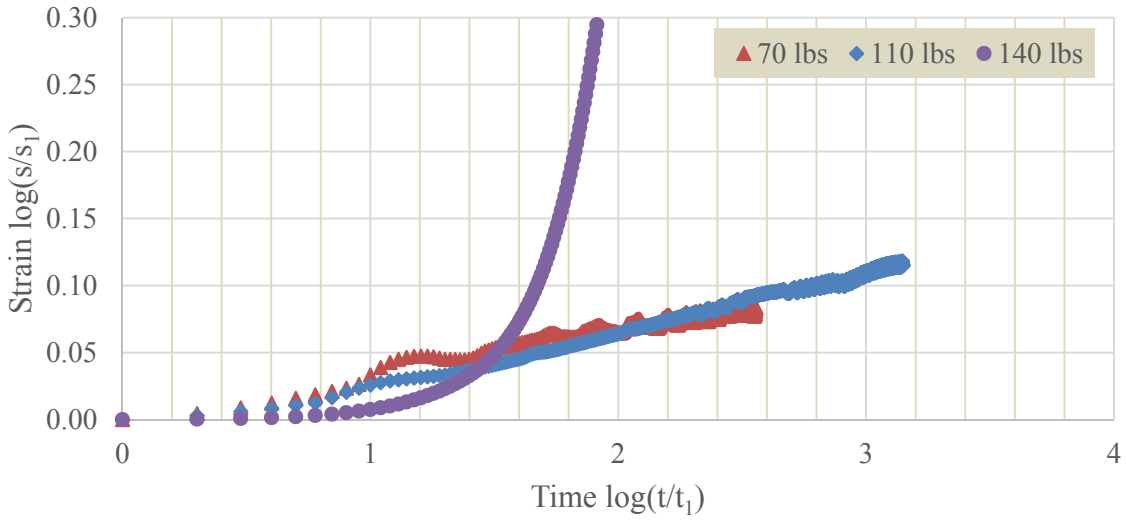

Figure 370. Strain–Time Curves for All the Holding Loads Plotted in Log–Log Scale. Samples from NGES-TAMU Clay Site Depth 16–18 Ft.

As shown in Figure 368 to Figure 370, the strain rate for the load less than the 90 percent of the failure load (approx.) is practically the same. A significant increase in the strain rate is observed for the loads higher than the 90 percent of the failure load. Figure 371 presents the n value obtained from the triaxial creep tests on the soil samples from the NGES-TAMU clay site at different depths. The n value varies between 0.02 and 0.04.

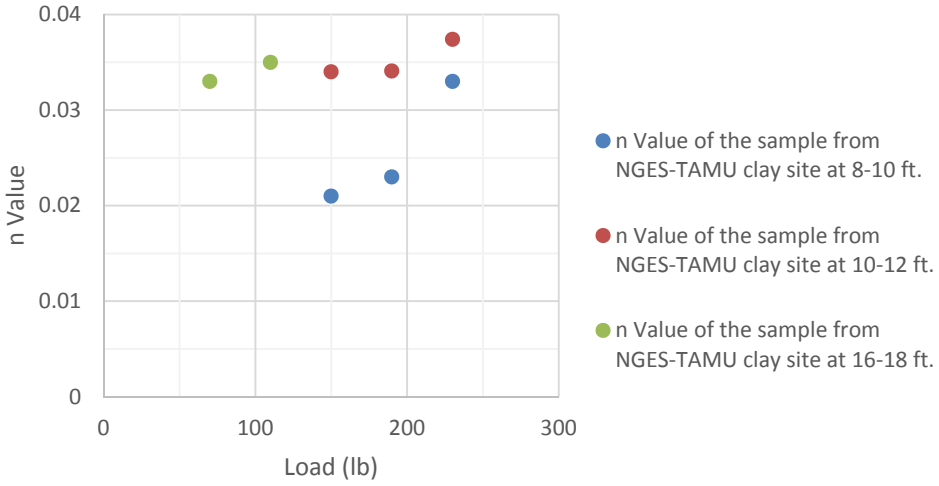

Figure 371. n Value Obtained from Triaxial Creep Tests on Samples from NGES-TAMU Clay Site at Different Depths.

The strain–time curve in the log–log scale at different holding loads, and the n values for the triaxial creep tests performed at the Beaumont site are presented in Figure 372 and Figure 373, respectively. The n value varies between 0.04 and 0.065.

The n values obtained from the tests on the sample from the Beaumont site are higher than the ones gathered from the NGES-TAMU clay site. As the n value increases, it means that strain rate will be higher for a given constant load. In other words, the viscosity parameters associated with soil samples from the Beaumont site are higher than those related to the samples from the NGES-TAMU clay site.

Based on the experimental information gathered from the triaxial creep tests performed in this project (plus some additional data from other published works), a linear strain–time curve (in the log–log space) can be assumed as a good approximation to describe the creep behavior of the HP clays. From these curves, the n values of the model (Eq. 4, Chapter 2) proposed by Briaud and Garland (1985) can be obtained and used to predict the creep behavior of the soil at different constant stresses. In the next section, the triaxial creep tests will be simulated using FLAC3D and the viscous parameters of the Burger model, and the n value will be obtained from this calibration. The calibrated mechanical model will be used subsequently to simulate the actual soil nail wall at the Beaumont project.

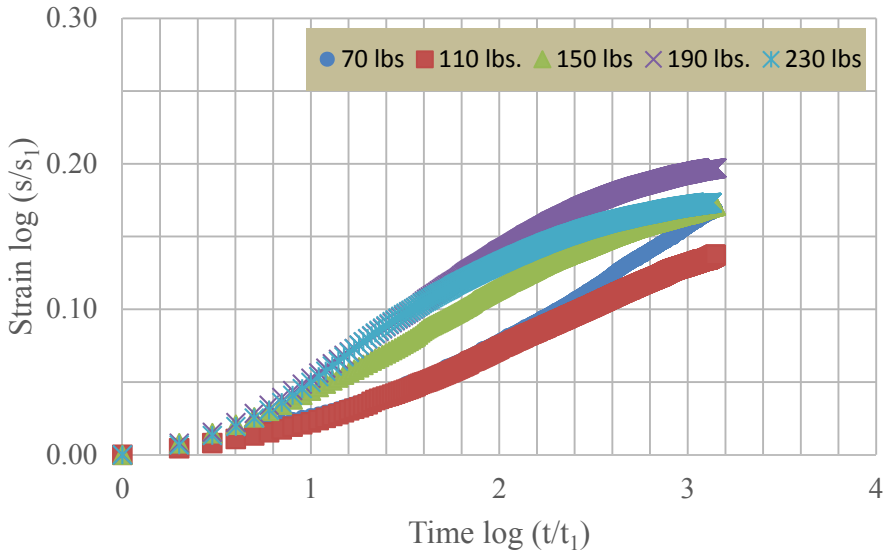

Figure 372. Strain–Time Curves for All the Holding Loads Plotted in Log-Log Scale on the Samples from the Beaumont Site.

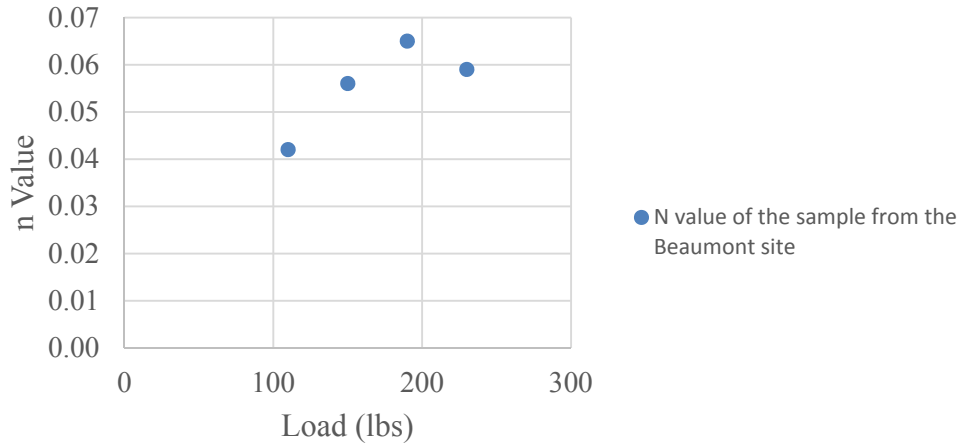

Figure 373. The n Value Obtained from the Triaxial Creep Tests on the Samples from the Beaumont Site.

Modeling the Triaxial Creep Test

To investigate the relationship between the n value and the viscosity parameters, the triaxial creep tests were simulated using FLAC3D. The viscoelastic model known as the Burger model was adopted to describe the time-dependent behavior of the clays involved in this research. The numerical model was calibrated against the laboratory triaxial creep tests data. Table 63 summarizes the adopted viscous parameters for each test and for the different n values.

Table 63. Adopted Viscosity in the Modeling for the Different n Values.

Soil Sample	Load (lb)	n value	m vis (lb*s/ft^2)	m shear (lb/ft^2)	k shear (lb/ft^2)	k vis (lb*s/ft^2)
NGES-TAMU 8–10 ft	150	0.021	9.00E+10	1.00E+06	6.00E+05	4.50E+09
NGES-TAMU 8–10 ft	190	0.023	1.12E+11	1.00E+06	4.50E+05	4.50E+09
NGES-TAMU 8–10 ft	230	0.033	1.45E+11	1.00E+06	3.10E+05	4.50E+09
NGES-TAMU 10–12 ft	150	0.034	3.34E+10	1.00E+06	2.08E+05	1.15E+09
NGES-TAMU 10–12 ft	190	0.0341	3.34E+10	1.00E+06	2.08E+05	1.15E+09
NGES-TAMU 10–12 ft	230	0.0374	1.45E+10	1.00E+06	1.50E+05	1.15E+09
NGES-TAMU 16–18 ft	110	0.035	6.80E+10	1.00E+06	5.00E+05	1.60E+09
Beaumont site 33–35 ft	110	0.042	2.20E+10	1.00E+06	1.00E+05	7.00E+08
Beaumont site 33–35 ft	150	0.056	2.00E+10	1.00E+06	5.50E+04	3.00E+08
Beaumont site 33–35 ft	190	0.0658	2.00E+10	1.00E+06	2.80E+04	2.00E+08
Beaumont site 33–35 ft	230	0.059	1.70E+10	1.00E+06	1.60E+04	8.00E+07

Figure 374 to Figure 376 plot the relationship between the n value and the viscous parameters adopted in the numerical modeling. The viscous parameters in the Burger model include the spring and the dashpot for the Maxwell element, identified as m shear and m vis, respectively. It also includes the spring and dashpot for the Kelvin element, identified as k shear and k vis, respectively.

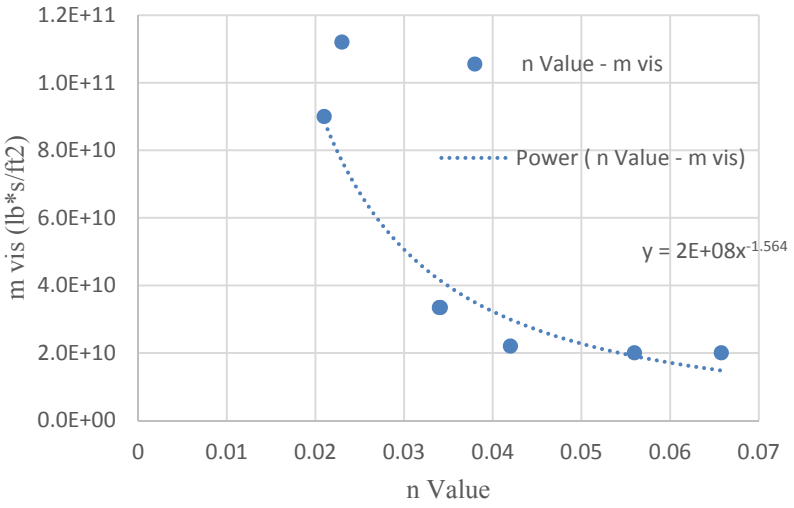

Figure 374. Relation between the n Value and m_vis (i.e., the Viscosity of the Maxwell Element in the Burger Model).

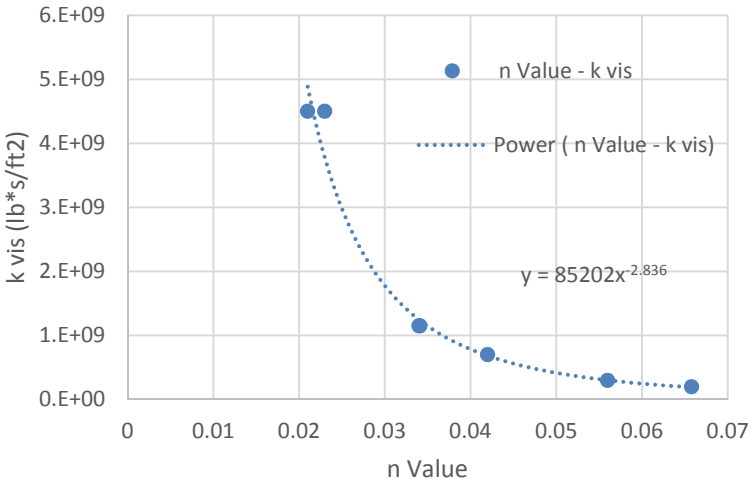

Figure 375. Relation between n Value and k_vis (i.e., Viscosity of the Kelvin Element in the Burger Model).

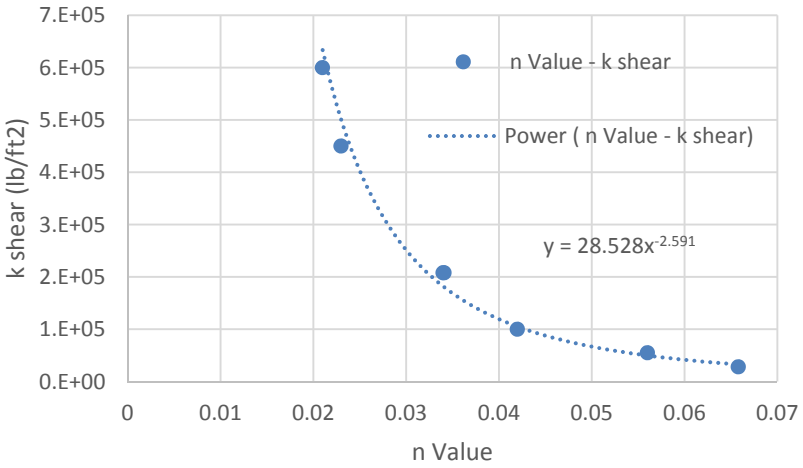

Figure 376. Relation between *n* Value and k Shear (i.e., Stiffness of the Kelvin Element in the Burger Model).

Figure 377 to Figure 380 present the strain–time curves obtained from the numerical modeling and compare them with the results obtained from the triaxial creep tests. The results of the numerical modeling of the triaxial creep tests show that the model results obtained with FLAC3D are quite satisfactory. Therefore, they could be used with confidence to study the time-dependent behavior of this HP clay. The viscous parameters obtained from modeling of the triaxial creep tests will be used in the modeling of the soil nail wall after the construction.

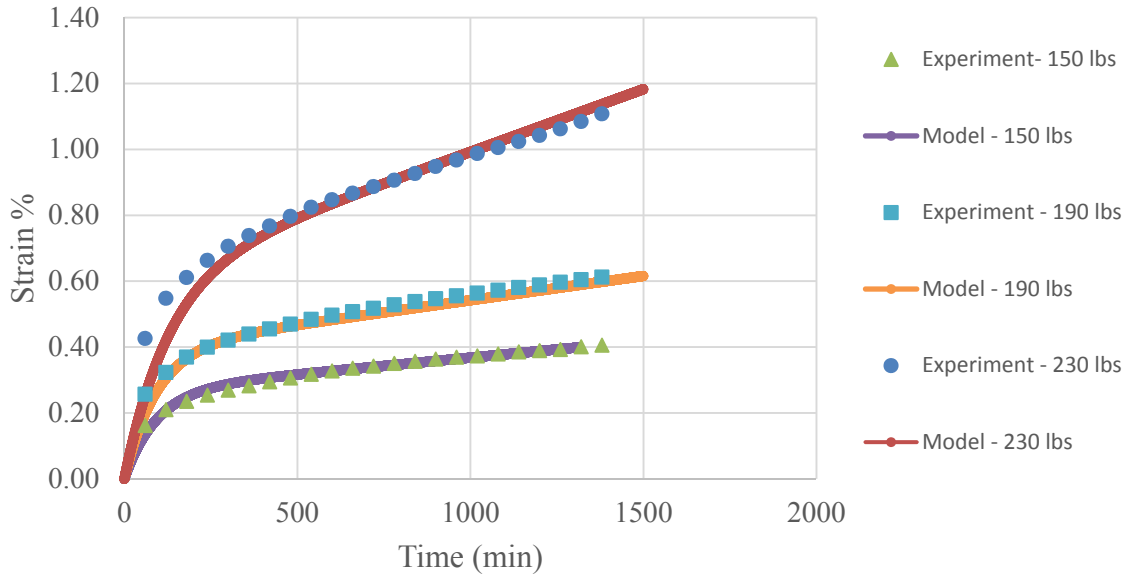

Figure 377. Strain–Time Curve for Both Numerical Modeling and Experimental Results, Triaxial Creep Tests on the Sample from the NGES-TAMU Clay Site at Depth of 10–12 Ft.

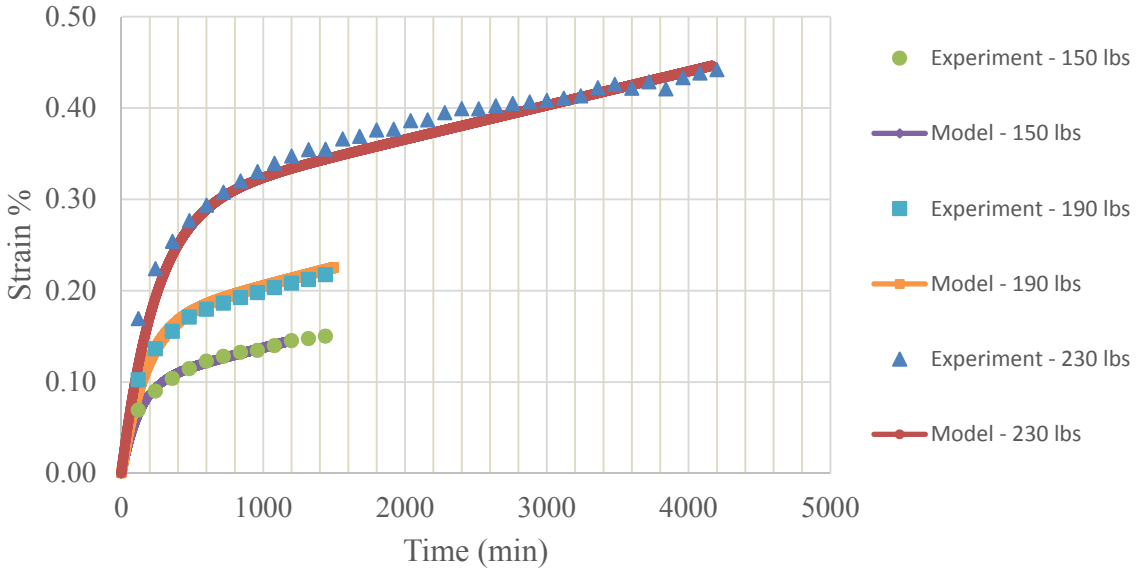

Figure 378. Strain–Time Curve for Both Numerical Modeling and Experimental Results, Tiaxial Creep Tests on the Sample from the NGES-TAMU Clay Site at Depth of 8–10 Ft.

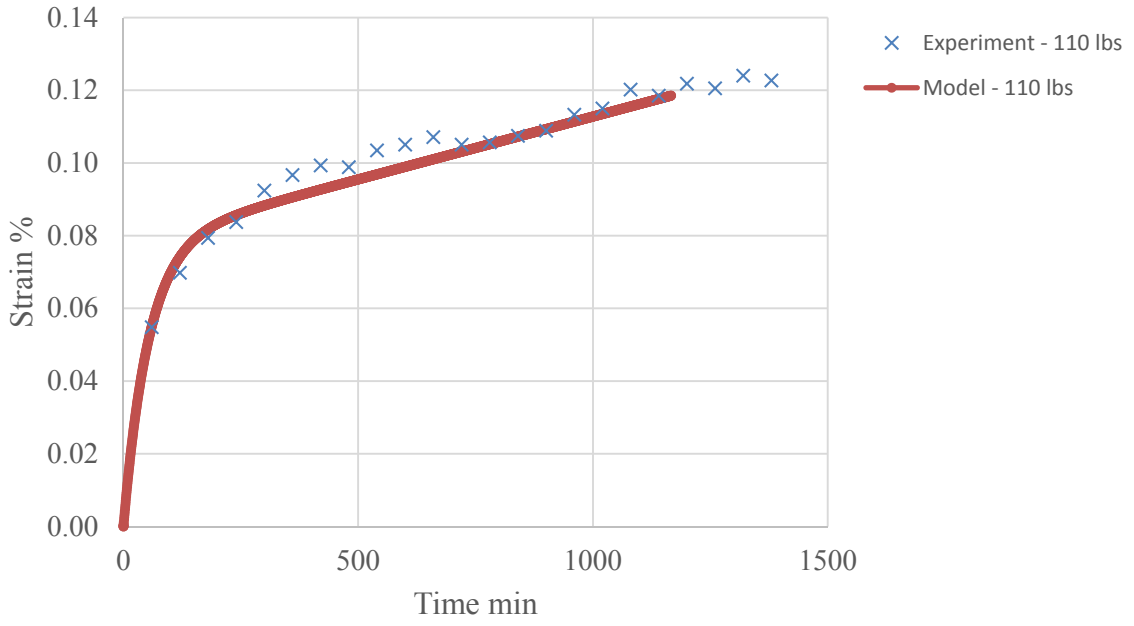

Figure 379. Strain–Time Curve for Both Numerical Modeling and Experimental Results, Triaxial Creep Tests on the Sample from the NGES-TAMU Clay Site at Depth of 16–18 Ft.

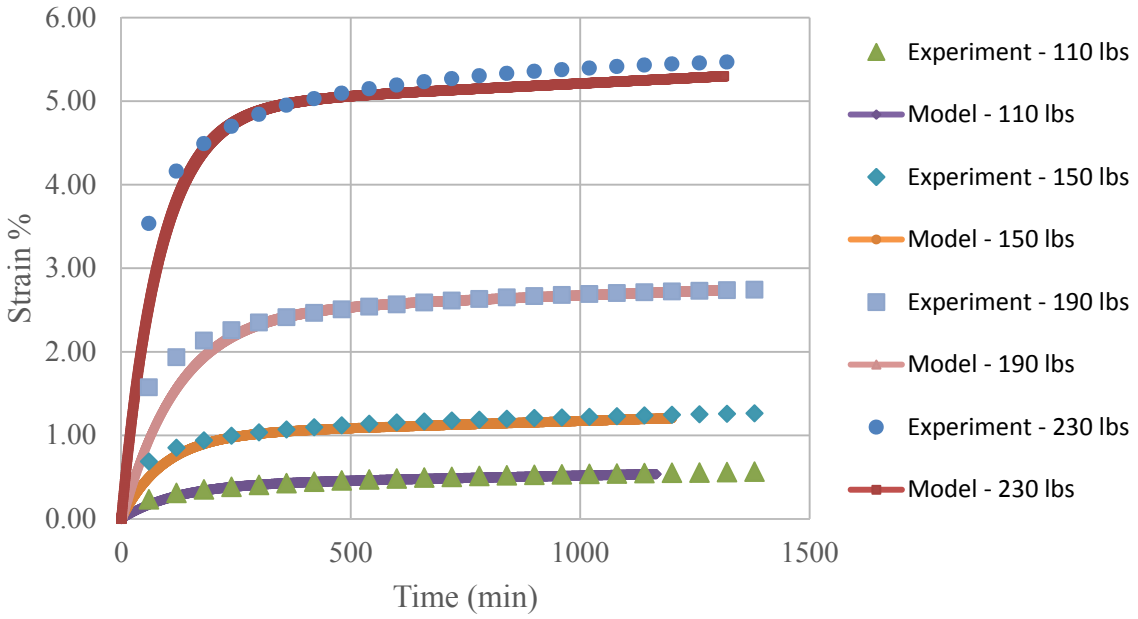

Figure 380. Strain–Time Curve for Both Numerical Modeling and Experimental Results, Triaxial Creep Tests on the Sample from the Beaumont Site at Depth of 33–35 Ft.

MODELING OF THE SOIL NAIL WALL AFTER CONSTRUCTION

In this section, the activities related to the numerical modeling of the time-dependent behavior of the soil nail wall during the operational stage are presented.

Introduction

After construction, the soil nail wall and the fill behind it tend to deform outward (FHWA, 2003). For the soil nail wall project at Beaumont, at station 1+46, the maximum lateral displacement at the end of the construction took place at the top of the wall and decreased toward the toe of it. The maximum horizontal displacement at the top of the wall is 1.85 in. at the end of the construction. This value is equivalent to 0.006 times the height of the wall (i.e., 25 ft). The deformation of the wall for a period of one year after the construction at the top of the wall was 0.2 in., which is around 10 percent of the deformation observed just after construction.

As mentioned in the previous sections, the creep behavior of the soil nail wall at Beaumont is simulated with the Burger creep model available in FLAC3D. The model predictions are compared against the experimental readings obtained during the post-construction monitoring of the wall.

FLAC3D Model for the Post-Construction Analysis

The in situ stresses and displacements of the soil nail wall at the end of the construction obtained from the numerical modeling presented in previous sections of this chapter were adopted as the initial condition for the post-construction modeling of the Beaumont wall. The MC mechanical model of the soil used during the simulation of the wall construction was substituted by the Burger model to simulate the time-dependent behavior of the soil behind the wall. The viscous behavior of the soil was adopted from the modeling of the triaxial creep tests on the soil samples from the Beaumont project. The modeling of one year of the post-construction creep behavior of the wall takes approximately one day of computer time.

Figure 381 presents the horizontal deformation at the top of the soil nail wall for both: results from the creep modeling, and data gathered from the monitoring one year after construction. As discussed, the lateral displacements measured at station 1+46 after one year of operation was 0.18 in., which is 9.73 percent of the deformation observed just after the end of the construction.

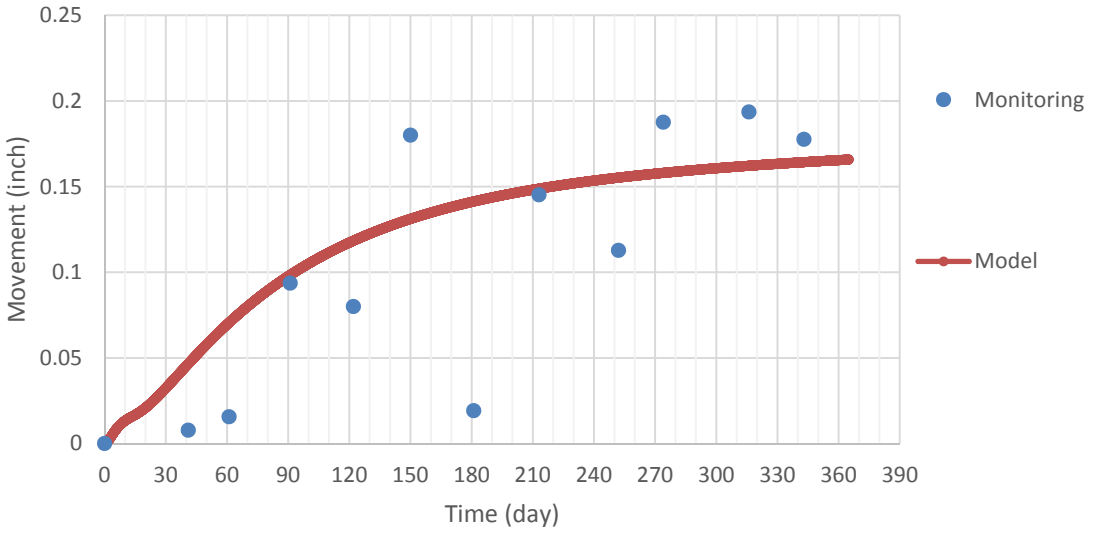

Figure 381. Horizontal Deformation, Top of the Wall, One Year Post-Monitoring: Wall and Model (Deformation of the Wall at the End of the Construction Reset to Zero).

Figure 382 presents the contours of creep deformation for one year after the end of the construction.

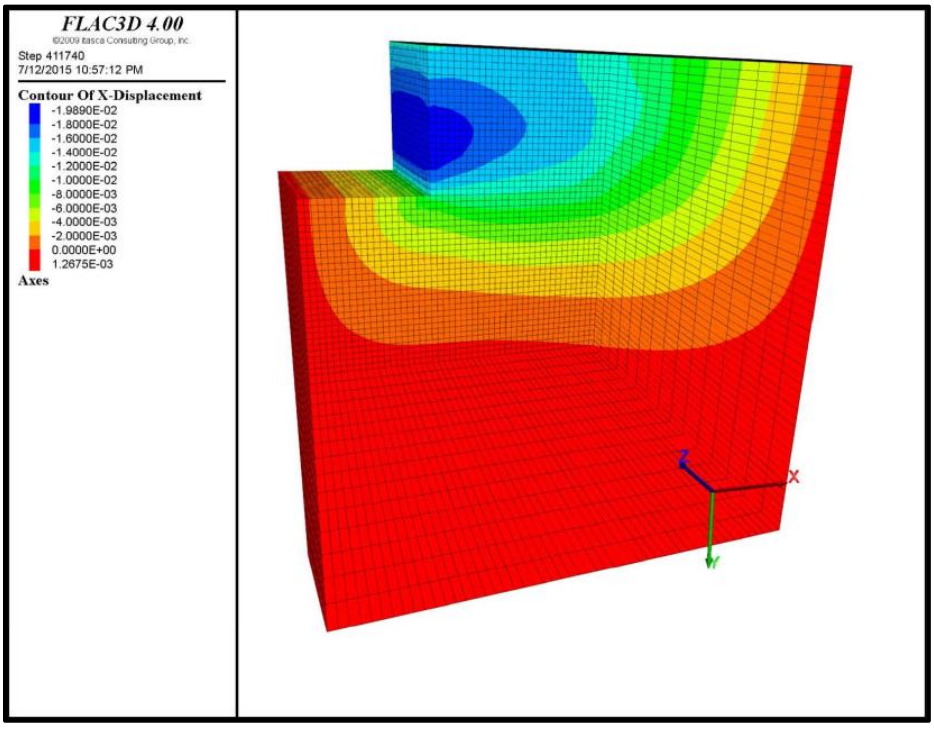

Figure 382. Contours of Creep Deformation of the Beaumont Project for a Period of One Year after Construction.

As discussed in previous sections of this chapter, the structural elements identified as cable in FLAC3D were used to simulate the soil nails. This type of element allows the computation of the axial load in the nails. Figure 383 shows the loads predicted in the nails at one year after the wall construction. Figure 384 to Figure 389 present the increase in the load because of the creep movements of the soil behind the wall for both: the modeling results and the strain gauge readings. There is very good agreement between the results of the monitoring and those corresponding to the numerical modeling.

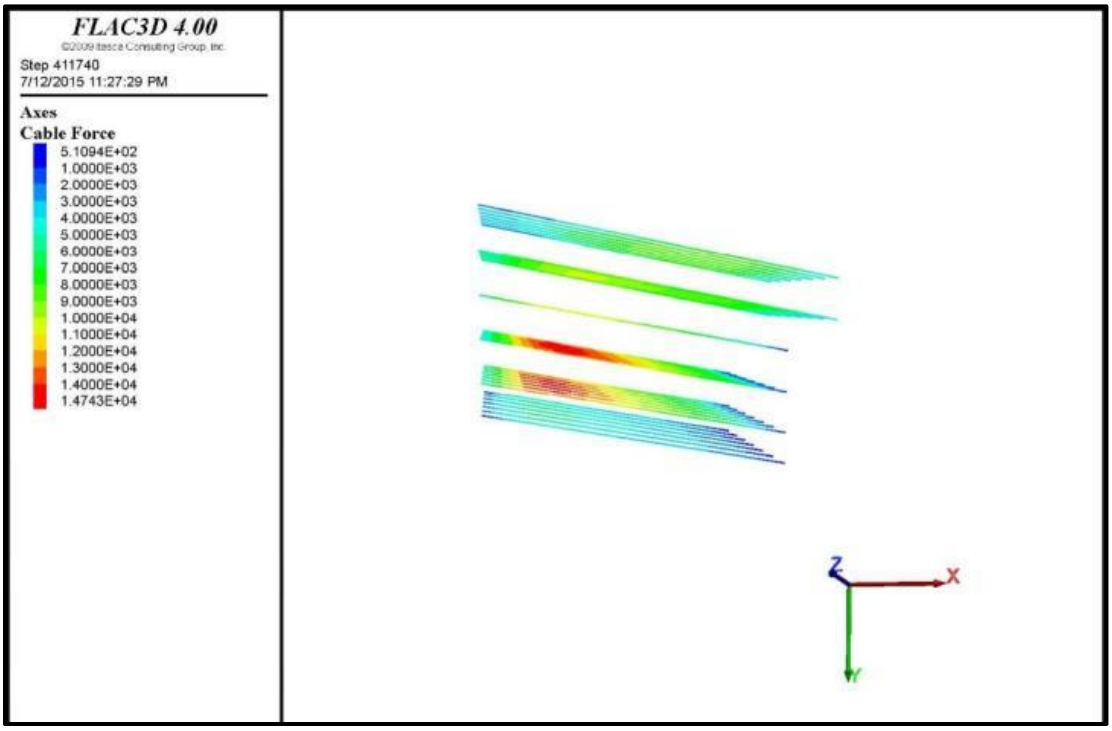

Figure 383. Axial Load in the Nails for One Year after the Construction.

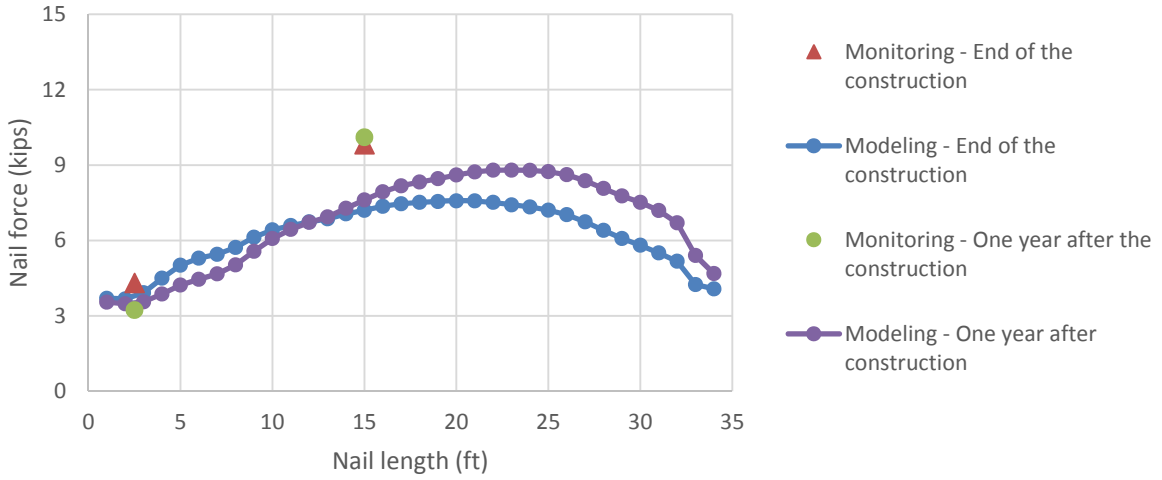

Figure 384. Axial Load, First Row of Nails, at the End of Construction and after One Year of Operation, Both Numerical Modeling and Inclinometer Results, Beaumont Project.

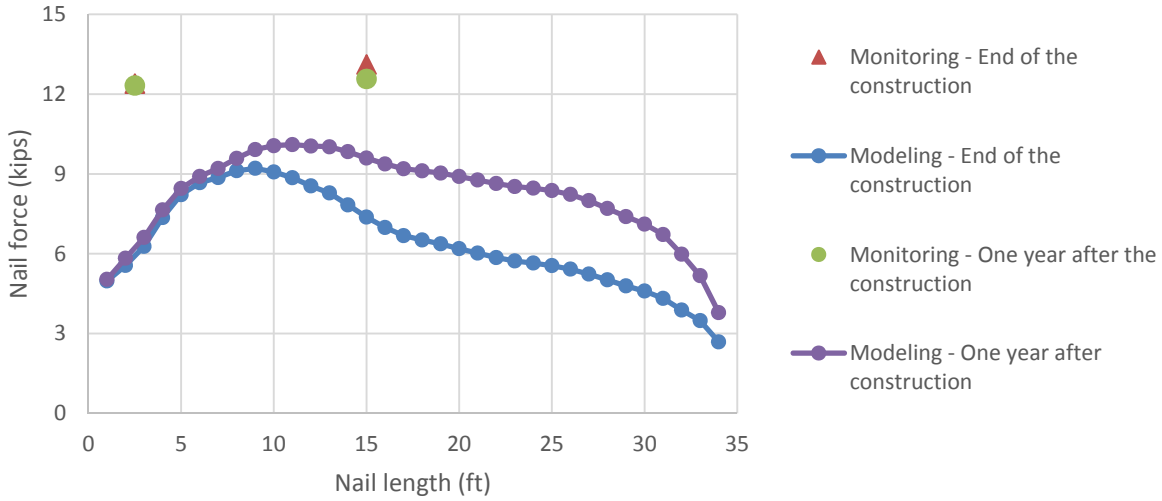

Figure 385. Axial Load, Second Row of Nails, at the End of Construction and after One Year of Operation, Both Numerical Modeling and Inclinometer Results, Beaumont Project.

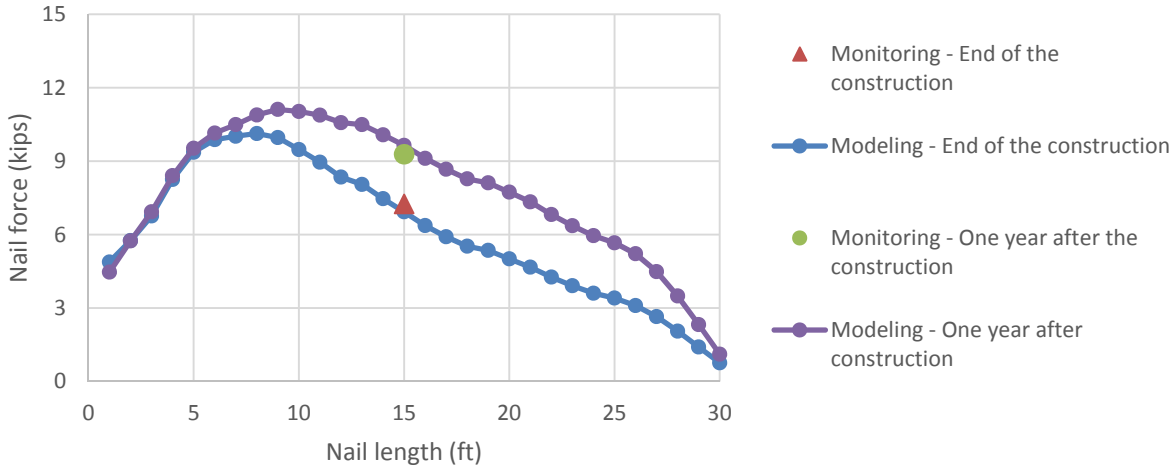

Figure 386. Axial Load, Third Row of Nails, at the End of Construction and after One Year of Operation, Both Numerical Modeling and Inclinometer Results, Beaumont Project.

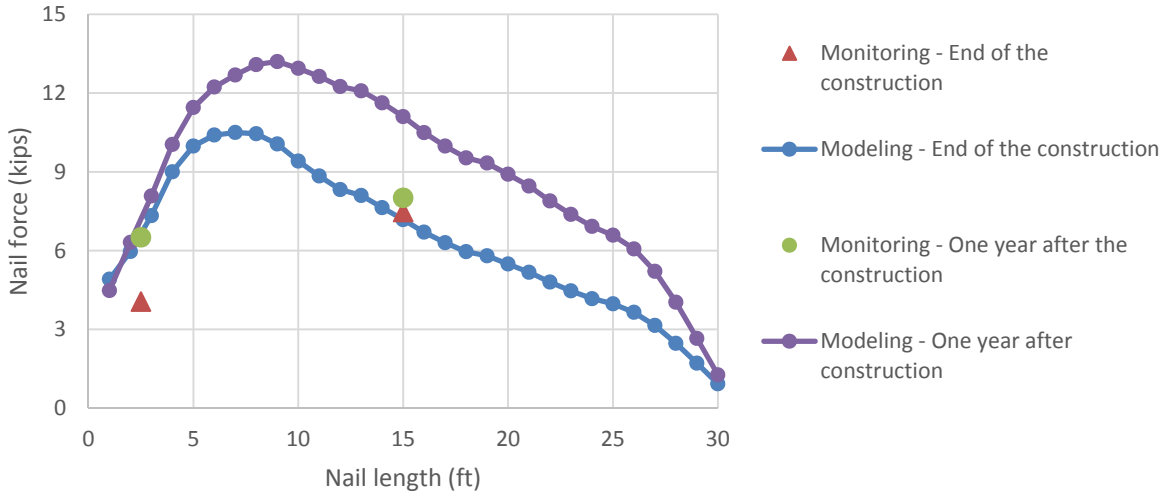

Figure 387. Axial Load, Fourth Row of Nails, at the End of Construction and after One Year of Operation, Both Numerical Modeling and Inclinometer Results, Beaumont Project.

After inspecting the results of the modeling and their comparisons against the experimental data gathered from the monitoring, the model was able to capture very satisfactorily the tendencies observed in this project, for both the construction stage and the post-construction creep behavior of the soil nail wall. This implies that FLAC3D, the adopted models, and assumptions can be considered as valid to study the behavior of soil nail walls in HP clays. Of the available models in FLAC3D, the Burger model appears to be the most appropriate one to study the creep behavior of the wall after construction.

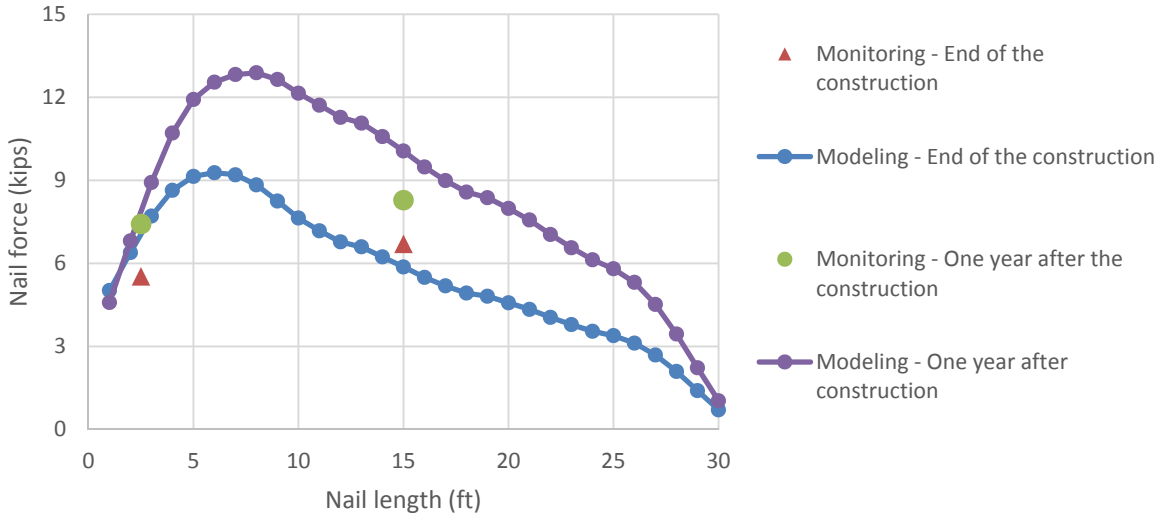

Figure 388. Axial Load, Fifth Row of Nails, at the End of Construction and after One Year of Operation, Both Numerical Modeling and Inclinometer Results, Beaumont Project.

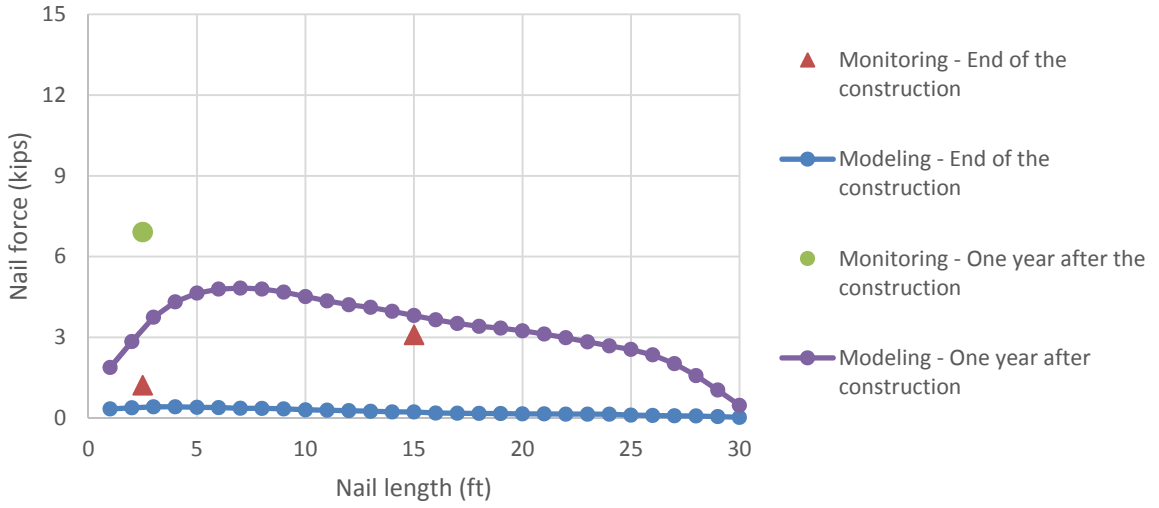

Figure 389. Axial Load, Sixth Row of Nails, at the End of Construction and after One Year of Operation, Both Numerical Modeling and Inclinometer Results, Beaumont Project.

Once the numerical framework adopted for the numerical modeling has been validated, the proposed approach can be used to simulate different wall geometries, model parameters, and other factors affecting the behavior of soil nail walls. The next section presents the parametric study performed in this project to learn about the influence of the different factors affecting the long-term behavior of a soil nail wall.

PARAMETRIC STUDY

The modeling results presented in the previous section focus on a particular soil type (Beaumont clay), a given geometry, and a specific design of the soil nail wall components. In this section, the effects of different wall conditions and soil parameters on soil nail wall performance are investigated numerically.

Introduction

The adopted numerical approach based on FLAC3D was calibrated and validated in the previous section for the construction and operational behaviors of a soil nail wall in a HP clay. This framework is adopted in this section to perform a parametric study of a typical Texas turnaround soil nail wall. The goal of the parametric study was to study the effect of different factors (e.g., soil properties and geometry) on the behavior of the soil nail wall. Considering that the soil nail wall at the Beaumont project does not correspond to a typical soil nail wall in Texas (especially because of its unusual height and extent), the parametric study was performed based on a typical Texas turnaround soil nail wall case provided by TxDOT. Figure 390 illustrates a typical soil nail wall used in Texas for turnarounds. The soil nail wall provided by TxDOT was adopted as the base case for the parametric study. Subsequent cases were analyzed, in which one parameter at a time was changed with respect to the base case, and the influence of this particular parameter on the long-term performance of the soil nail wall was investigated.

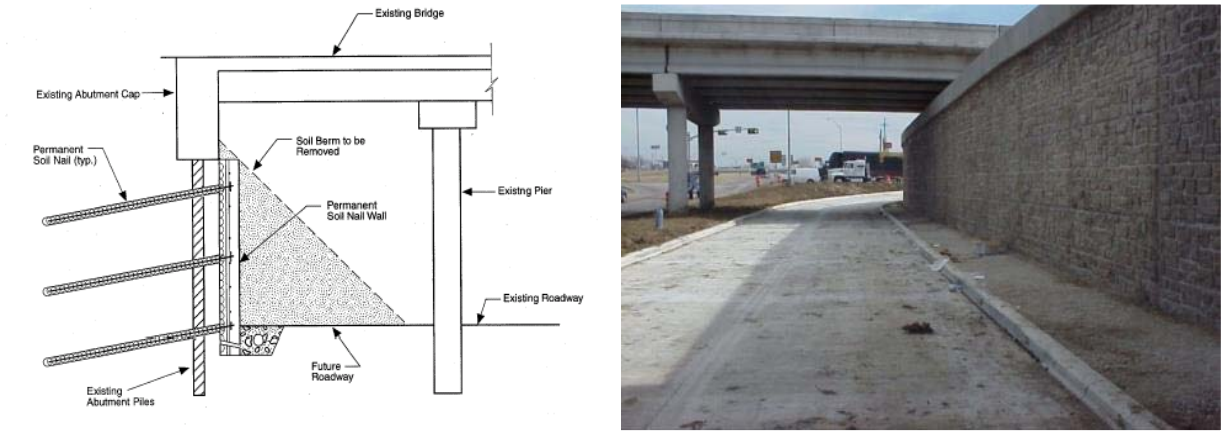

Figure 390. Typical Soil Nail Wall Texas Turnaround.

Texas Turnaround – Base Case

This section presents general information about the wall adopted for the parametric study and information about the related numerical analyses.

Geometric Configuration of the Base Case

The soil nail wall located at IH40 corresponding to Project 0275-01-168 was selected as the baseline case for this research. Figure 391 and Figure 392 present the layout of the soil nail wall. The soil nail wall consists of five rows of 22-ft-long nails. Table 64 summarizes the geometry and other design details related to the adopted wall. Since the aim of this modeling is to evaluate the long-term behavior of the soil nail wall, drained conditions were considered.

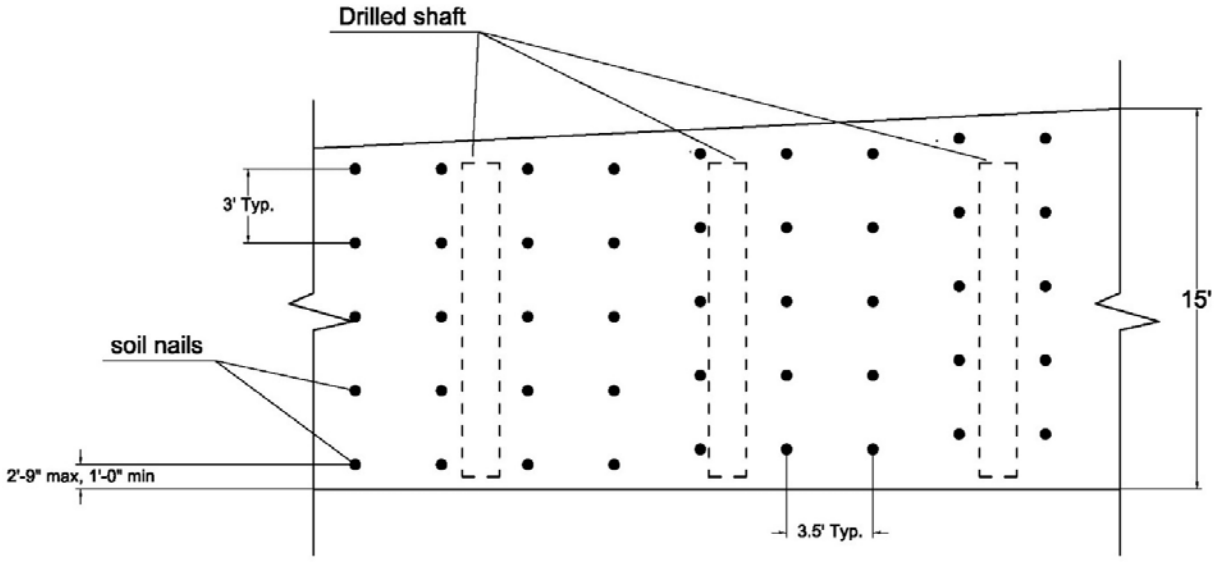

Figure 391. Soil Nail Pattern on the Wall Face.

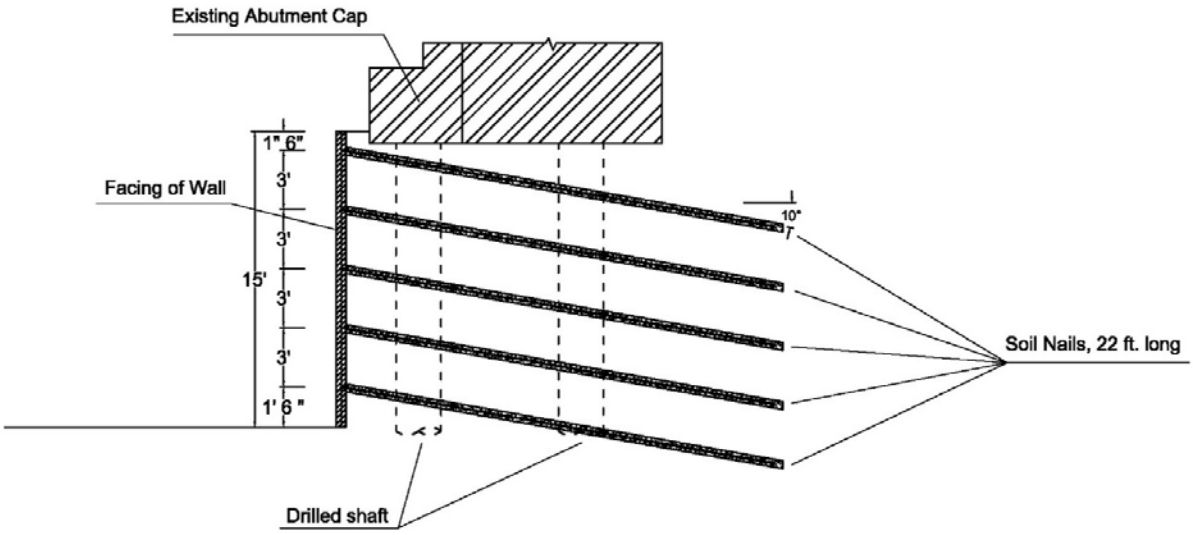

Figure 392. Soil Nail Wall Cross Section and Details.

Table 64. Soil Nail Wall Geometry and Other Parameters.

Parameter	Value
Vertical height of the wall, H (ft)	15
Face batter α (degree)	0
Backslope angle β (degree)	0
Yield strength of the reinforcement fy (ksi)	75
Diameter of the reinforcement d (in.)	0.86
Drill hole diameter (in.)	6
Spacing $S_h \times S_v$ (ft)	3.5 × 3.0
Length of the nails (ft)	22
Inclination of the nails (degree)	10
Number of rows of the nail	5
Drained cohesion c′ (psf)	0
Drained fiction angle Φ′ (degree)	26
Unit weight (pcf)	125
Bond stress (psf)	900
Surcharge (psf)	250

Modeling the Base Case at the End of Construction

Prior to simulating the soil nail wall in FLAC3D as a boundary value problem, the soil nail wall was modeled using SNAILZ, an allowable stress design (ASD) based limit equilibrium slope stability computer program. Table 65 presents the input parameters for the analysis.

Figure 393 presents the results of the modeling of the wall with SNAILZ. The ultimate pullout capacity of the nails obtained from the pullout tests on the sacrificial nail was around 900 psf (i.e., 6.3 psi), while the design bond stress is equal to 300 psf. The traffic load was assumed equal to 250 psf (i.e., equivalent to 2 ft of embankment soil) and applied at the top of

the wall. The FS and the maximum load in the nails are shown in Figure 393 and Table 65, respectively.

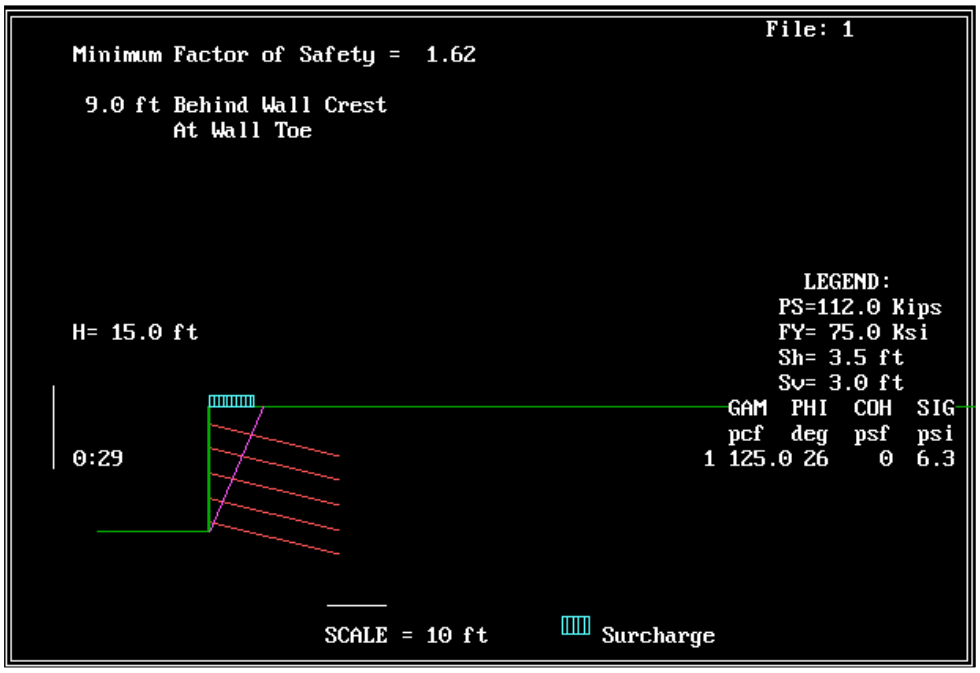

Figure 393. Safety Factor Obtained from SNAILZ.

Table 65. Maximum Tensile Load Obtained from SNAILZ along the Nails.

Nail #	Nail force (kips)
Nail #1 (first row)	4.8
Nail #2 (second row)	5.3
Nail #3 (third row)	5.8
Nail #4 (fourth row)	6.4
Nail #5 (fifth row)	6.9

Once the stability analyses were completed, the base case was modeled using FLAC3D. The step-by-step procedures for modeling the soil nail wall with FLAC3D were presented in previous sections of this chapter. Table 66 presents the parameters adopted for the numerical modeling with FLAC3D. The same geometry described in Table 64 was adopted in this analysis.

Table 66. Parameters Adopted for the Numerical Simulation of the Wall Baseline Case.

Material	Constitutive model	Material properties
Embankment soil	MC	ϕ′=26°, c′=0, γ=125 pcf, E=2.9e5 psf, υ=0.3
Soil nails (cable element)	Elastic-perfectly plastic	E steel=4.17e9 psf (200 GPa), c_grout=1e3 psf, ϕ_grout=20°
Shotcrete (shell element)	Elastic (isotropic)	E shot=2.2e8 psf, ν=0.25, Thickness=4 in.

Figure 394 and Figure 395 present the contours of horizontal movement of the top of the wall and load distribution along the nails at the end of the construction.

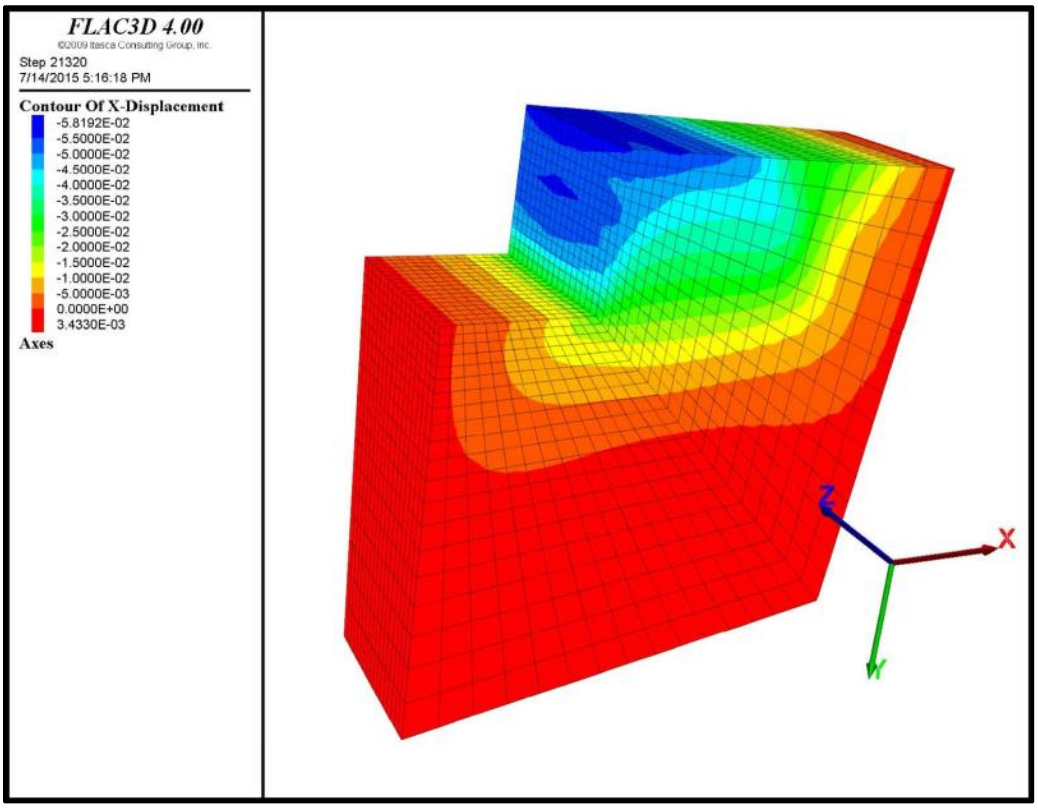

Figure 394. Horizontal Deformation of the Baseline Case at the End of the Construction (Note: Unit for the x-Displacement = Ft).

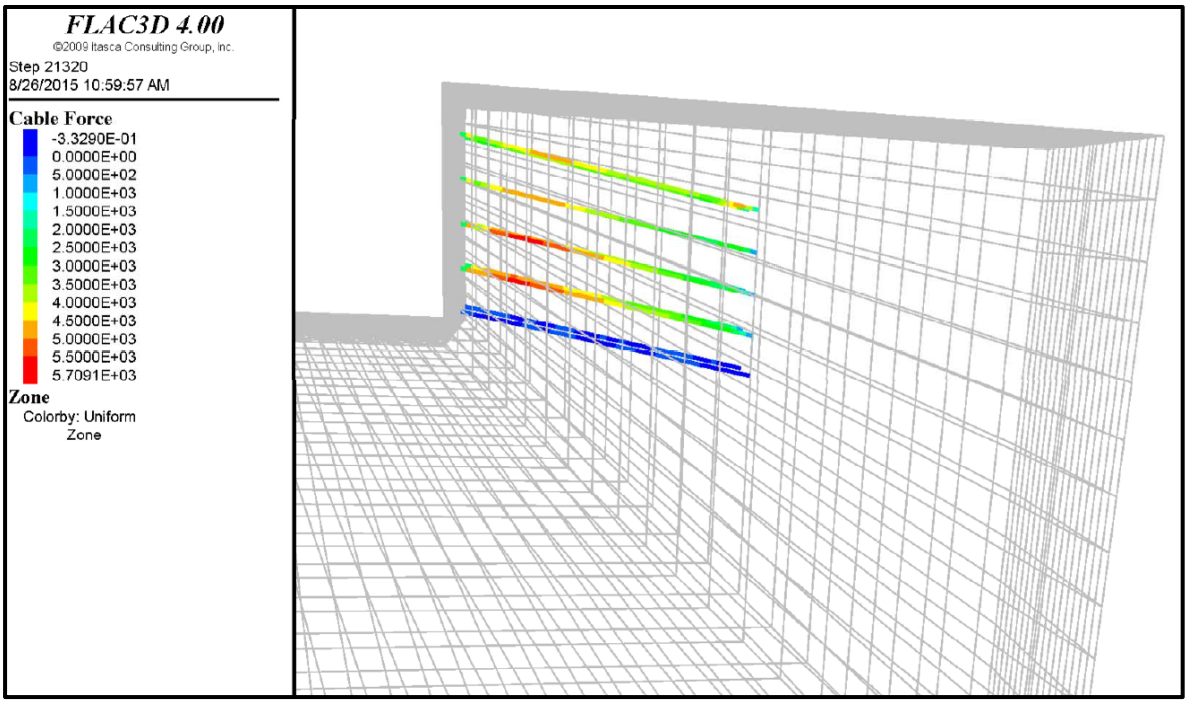

Figure 395. Force in the Nails for the Base Case at the End of Construction (Note: Unit for the Cable Force = Lb).

A very good agreement between the results of the modeling with SNAILZ and FLAC3D was obtained (Table 67). Perhaps the main difference is in the axial load in the nails of the bottom row. The monitoring of the soil nail wall at the Beaumont project showed that a significant portion of the axial load in the nails was induced by the excavation (i.e., as the excavation progressed, a gradual increase in the load taken by the nails was observed). Considering that after installing the last row of nails there is no additional excavation, the axial load in the nails in this row will not develop until the soil nail wall experiences some movements after construction.

Table 67. Comparison of the Axial Load in the Nail at the End of Construction Obtained with SNAILZ and FLAC3D.

Nail #	Nail force obtained from SNAILZ (kips)	Nail force obtained from FLAC3D (kips)
Nail #1 (first row)	4.8	4.7
Nail #2 (second row)	5.3	4.9
Nail #3 (third row)	5.8	5.7
Nail #4 (fourth row)	6.4	5.6
Nail #5 (fifth row)	6.9	0

Modeling the Base Case during the Operation Stage

The in situ stresses and displacements of the soil nail wall obtained from the modeling at the end of the construction (i.e., in the previous sections of this chapter) were adopted as the initial condition for modeling the post-construction behavior of the wall. To account for the creep behavior, the MC mechanical model (used to simulate the construction of the wall) was replaced by the Burger model to simulate the long-term behavior. The viscous parameters adopted in the numerical modeling are presented in Table 68. These parameters were obtained from the simulation of the soil nail wall at the Beaumont project and the calibration of the model with field data (i.e., inclinometer readings).

Table 68. Parameters Adopted in Numerical Modeling of the Base Case after Construction.

Material	Constitutive model	Properties
Embankment soil	Viscoelastic Burger model	m shear=1.04e9 lb /ft^2, m vis=2e14 lb*s/ft^2, k shear=5e5 lb /ft^2, k vis=3.5e12 lb*s/ft^2

The horizontal displacements at the top of the wall and the additional service load in the nails due to the creep behavior of the soil nail wall for one year after the construction obtained from numerical modeling are shown in Figure 396 and Figure 397, respectively. After construction, there was an additional displacement at the top of the soil nail wall induced by creep of 0.095 in., which is around 13 percent of the movement of the wall at the end of the construction (Figure 398). As a result of this additional movement, additional axial load developed in the nails. The maximum axial load in the fourth nail at the end of the construction

is 5.6 kips, while one year after construction the axial load in this nail was 8.4 kips, which implies an increase of around 50 percent in the axial load after one year of operation. Figure 400 to Figure 404 present the axial loads in the nails at the end of the construction and one year after the construction.

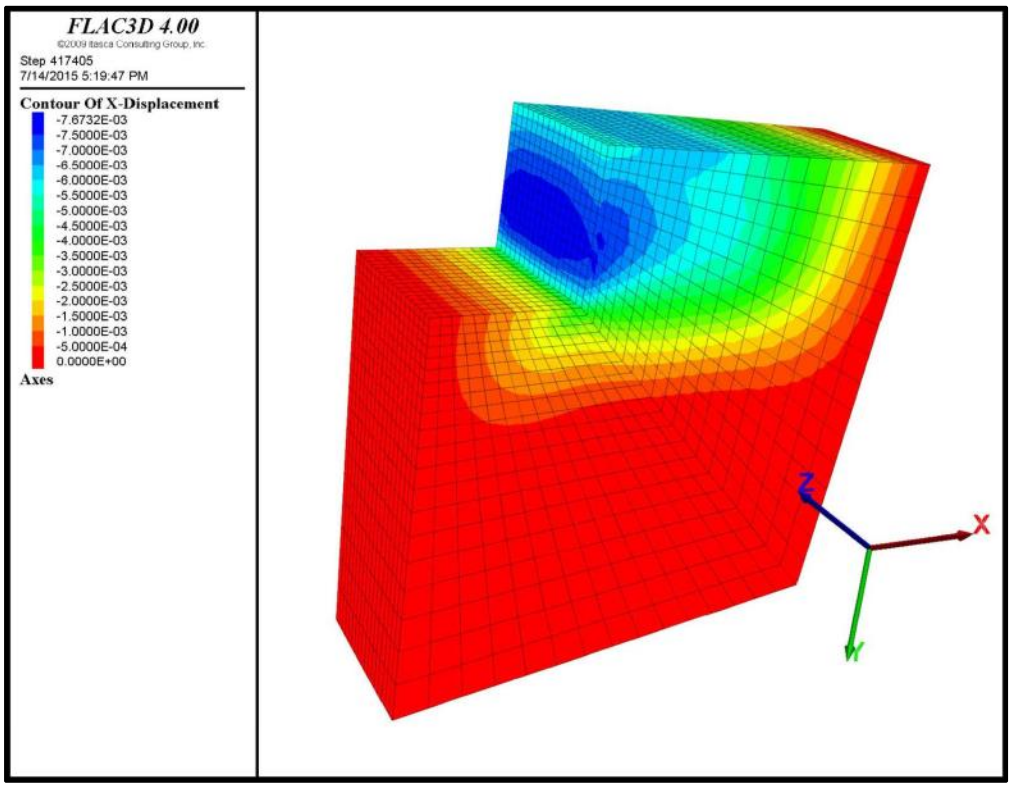

Figure 396. Horizontal Deformation of the Top of the Wall for One Year after the Construction. The Horizontal Deformations of the Wall at the End of the Construction Were Reset to Zero (Units in Ft).

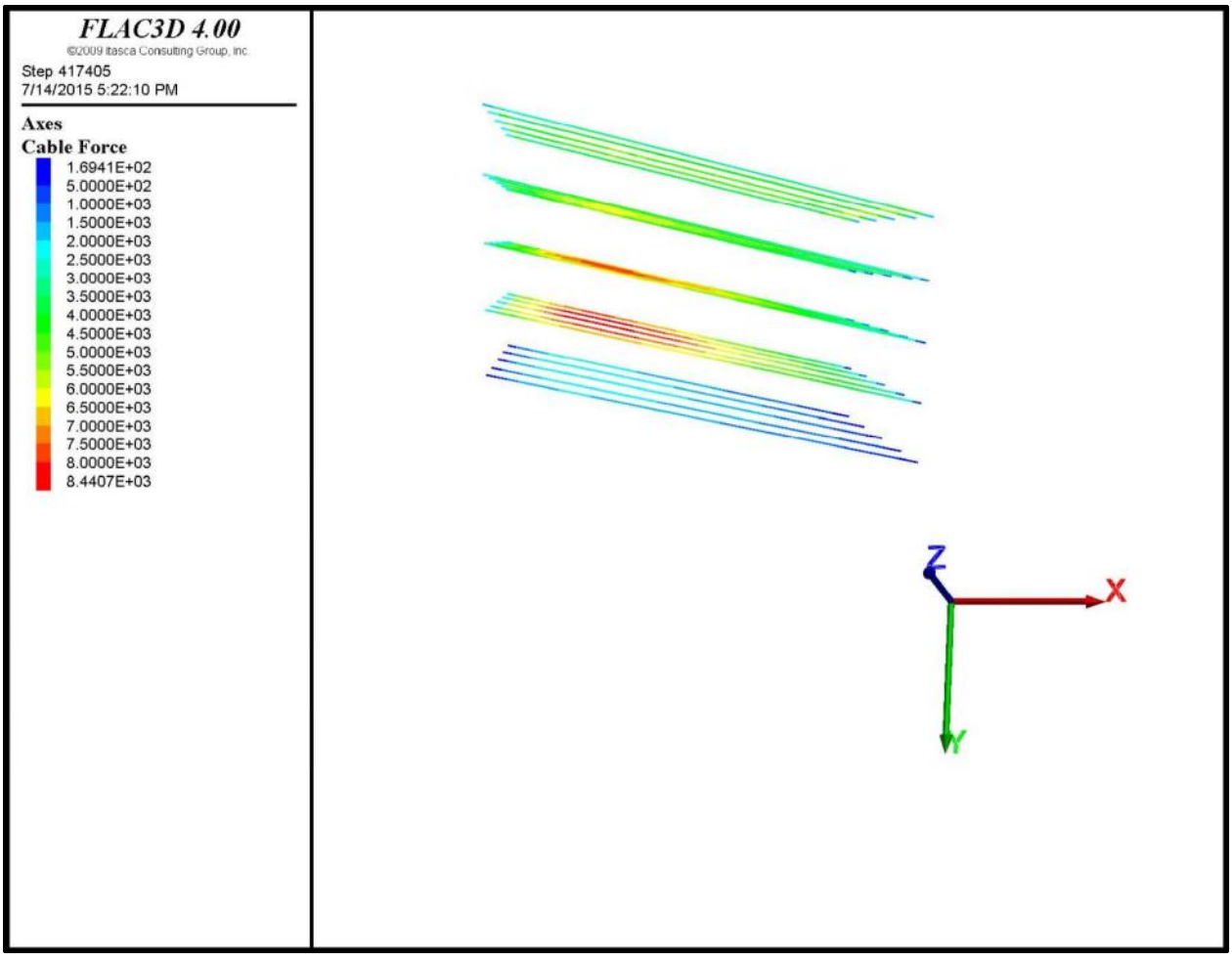

Figure 397. Additional Axial Load in the Nails due to the Extra Horizontal Displacement of the Wall One Year after Construction Obtained from Modeling (Units in Lb).

Figure 398 shows the profile of the horizontal movements of the wall at the end of the construction together with those corresponding to one year after construction. Figure 399 shows the movements of the top of the wall for a period of one year after construction. The rate of movements increases very rapidly at the beginning and then tends to reach a sort of constant rate, which is much smaller than the initial one.

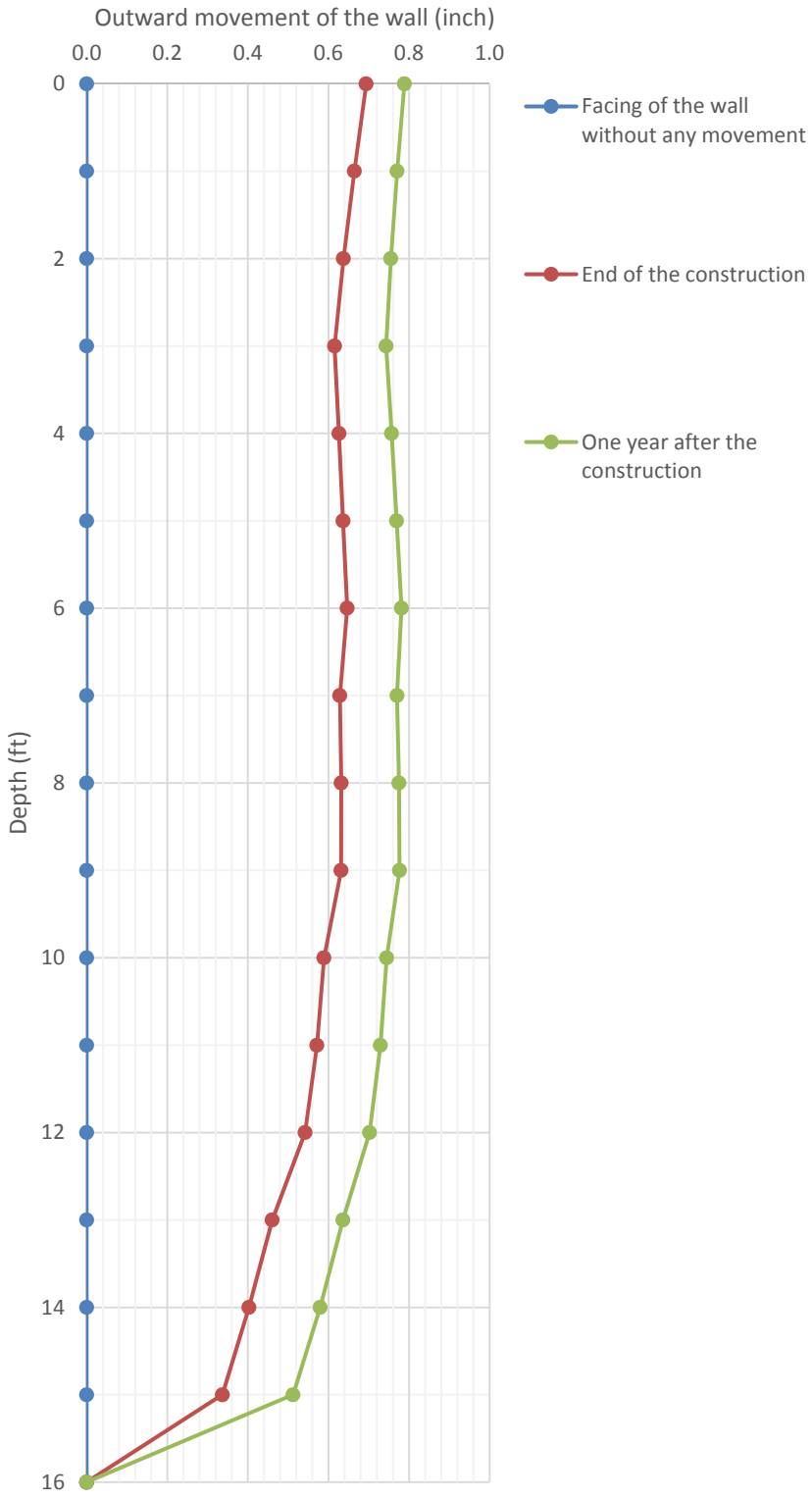

Figure 398. Profile of the Horizontal Movements of the Soil Nail Wall at the End and One Year after the Construction.

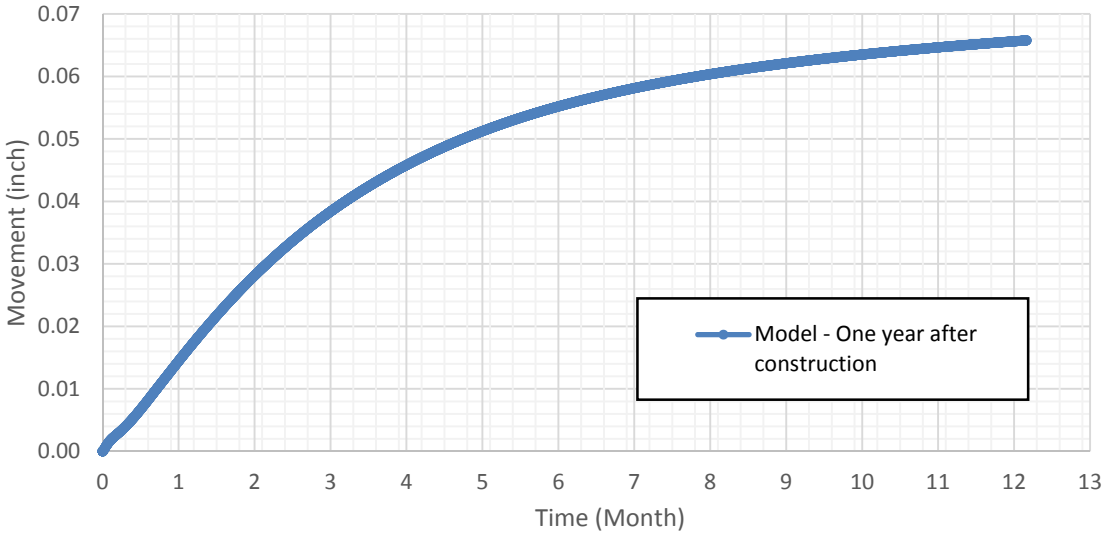

Figure 399. Horizontal Movements Top of the Wall Calculated for One Year after Construction (Movements Induced by Creep Only, Movements Related to Construction Were Removed).

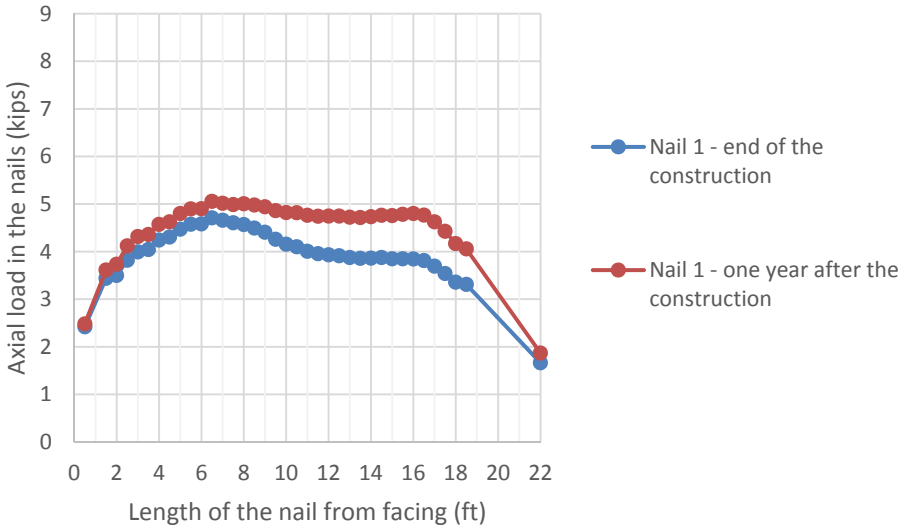

Figure 400. Axial Load in the First Nail of the Base Case for Both End of the Construction and One Year after the Construction.

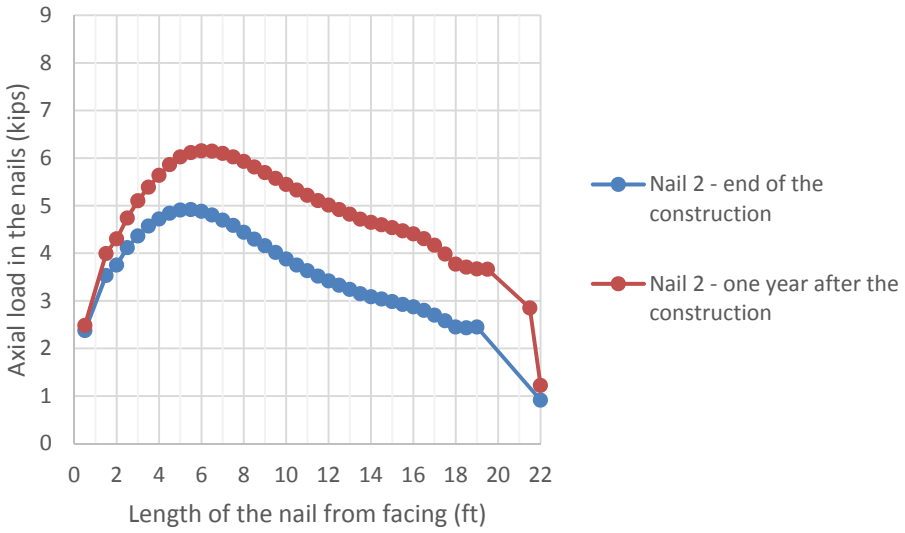

Figure 401. Axial Load in the Second Nail of the Base Case for Both End of the Construction and One Year after the Construction.

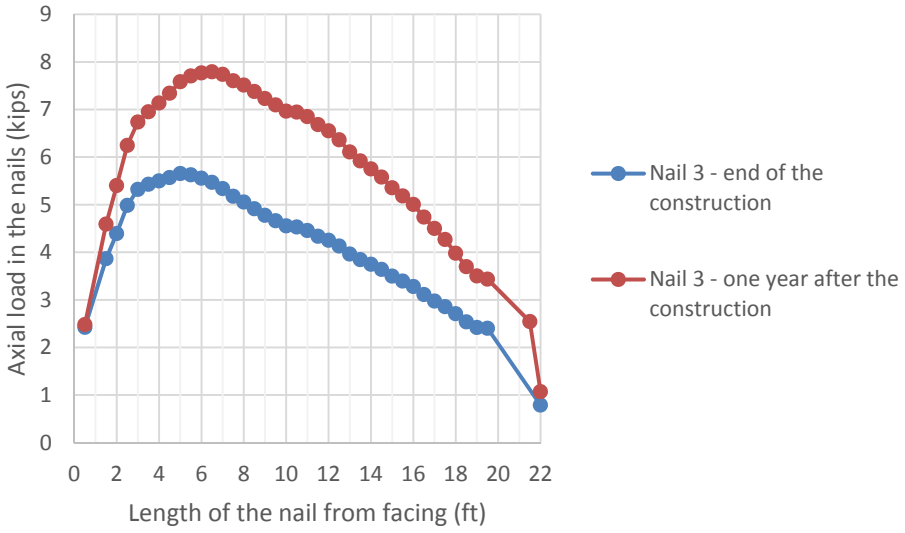

Figure 402. Axial Load in the Third Nail of the Base Case for Both End of the Construction and One Year after the Construction.

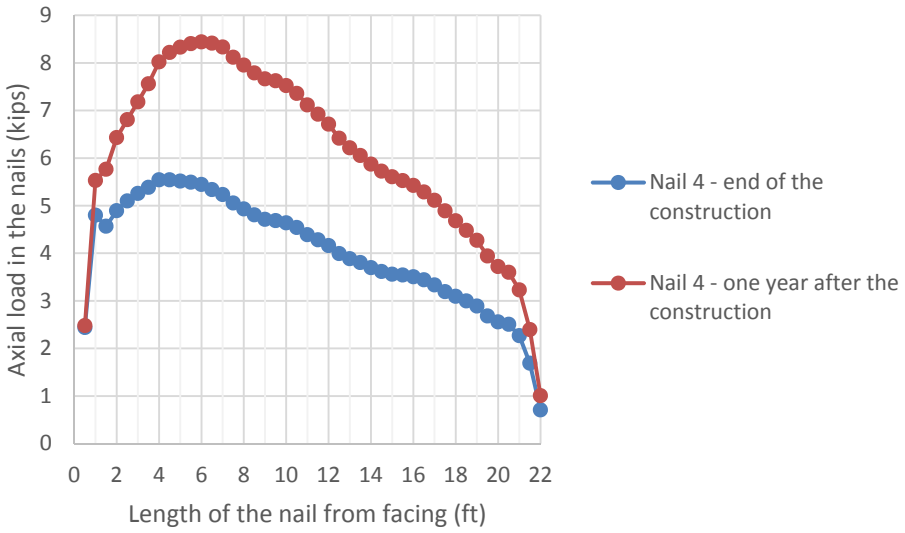

Figure 403. Axial Load in the Fourth Nail of the Base Case for Both End of the Construction and One Year after the Construction.

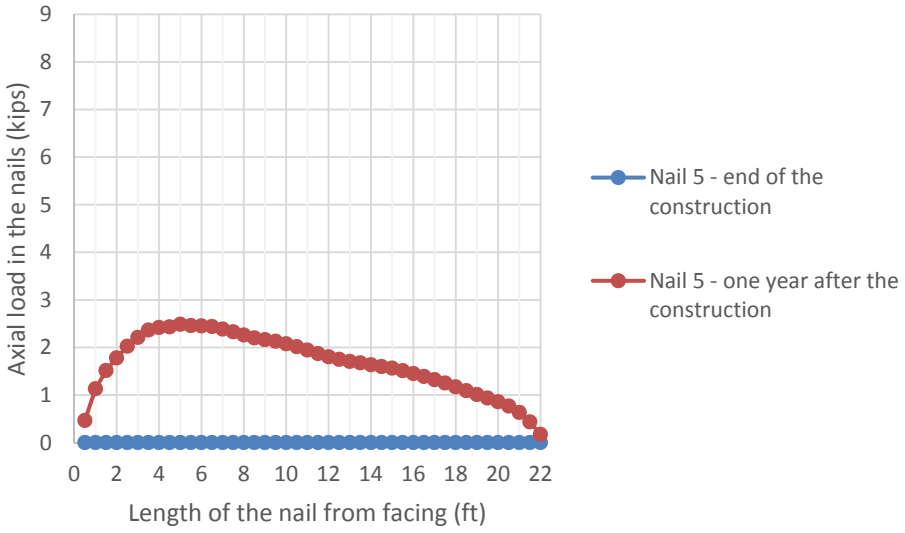

Figure 404. Axial Load in the Fifth Nail of the Base Case for Both End of the Construction and One Year after the Construction.

Outline of the Parametric Study

Table 69 presents all the cases related to the parametric study. The height of the wall in the baseline case is 15-ft uniform 22-ft, the longer nails were adopted for the analysis. The pattern for nail installation was given by 3.5 ft of horizontal spacing (S_h) and 3 ft of vertical

spacing (S_v). The effects of the different parameters on the long-term behavior of the soil nail wall in HP clays are presented as follows.

Table 69. Parametric Study Cases.

Material	Properties
Embankment soil	E=2.9e^5 psf*, Drained friction angle ϕ'=22°, 26°*, 30°, 36°
Soil nail wall height (ft)	12, 15*, 21
Soil nail length (ft)	15, 22*, 30
Viscosity	$0.02 < n < 0.04$, $0.05 < n < 0.07$*, $0.07 < n < 0.09$

Note: * indicates the base case parameters.

Embankment Soil

In this parametric study, it is assumed that the drained cohesion of the fill is zero (i.e., long-term analysis). Figure 405 shows horizontal deformation of the soil nail wall at the end of the construction for four drained friction angles (i.e., 22°, 26°, 30°, and 36°).

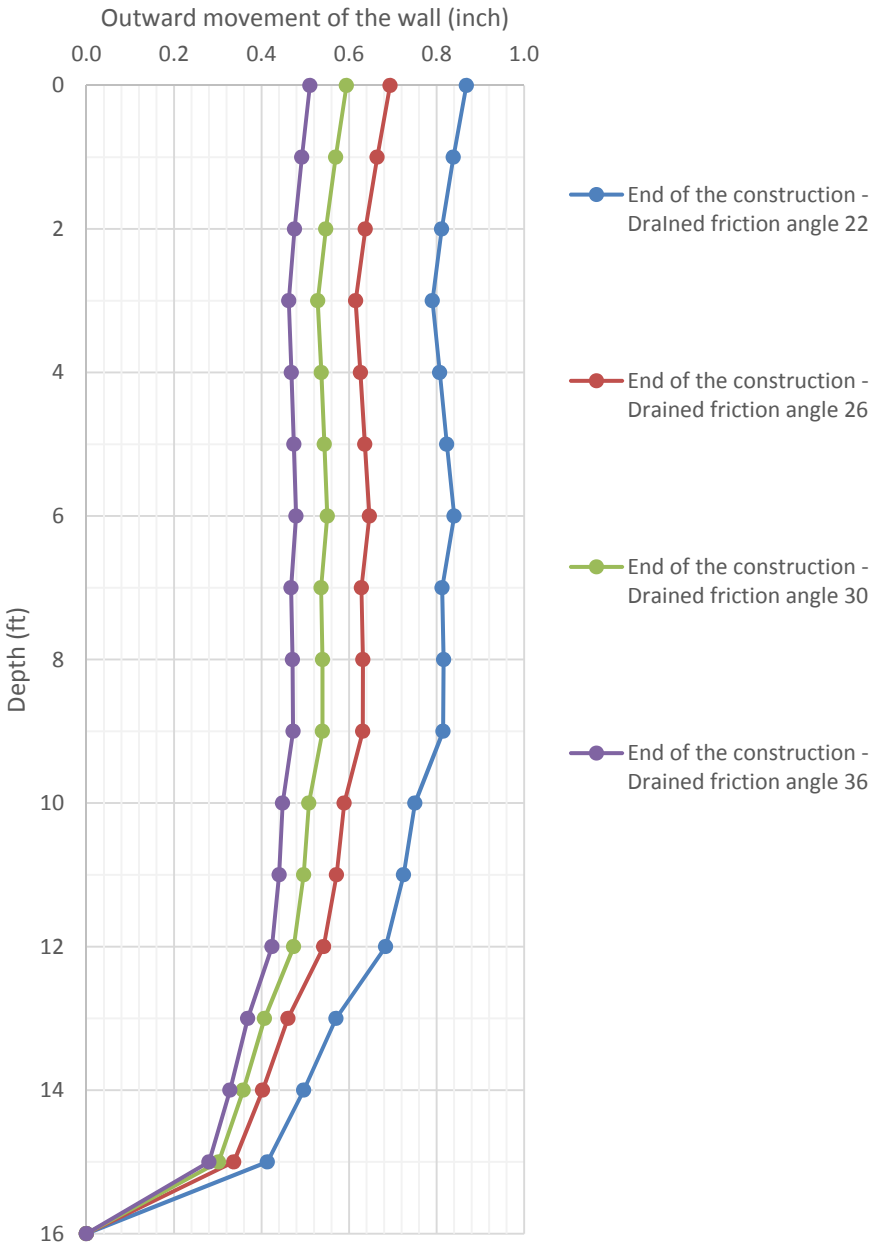

Figure 405. Horizontal Deformation of the Wall at the End of the Construction for Four Different Drained Friction Angles (22°, 26°, 30°, and 36°).

Drained friction angle has a huge impact on the movements of the soil nail wall at the end of the construction. As anticipated, the soils with higher drained friction angles exhibit less deformation at the end of the construction. Therefore, the maximum axial load that develops in the nails at the end of the construction for the soil with higher drained friction angle is less than that for the soil with lower drained friction angle (Table 70). Figure 406 presents the creep

movement of the wall for a period of one year after construction for the four drained friction angles. As expected, the creep behavior of the soil nail wall does not depend on the soil strength parameters, such as drained friction angle (i.e., these parameters are not included in the Burger model adopted for simulating the creep behavior of the embankment fill).

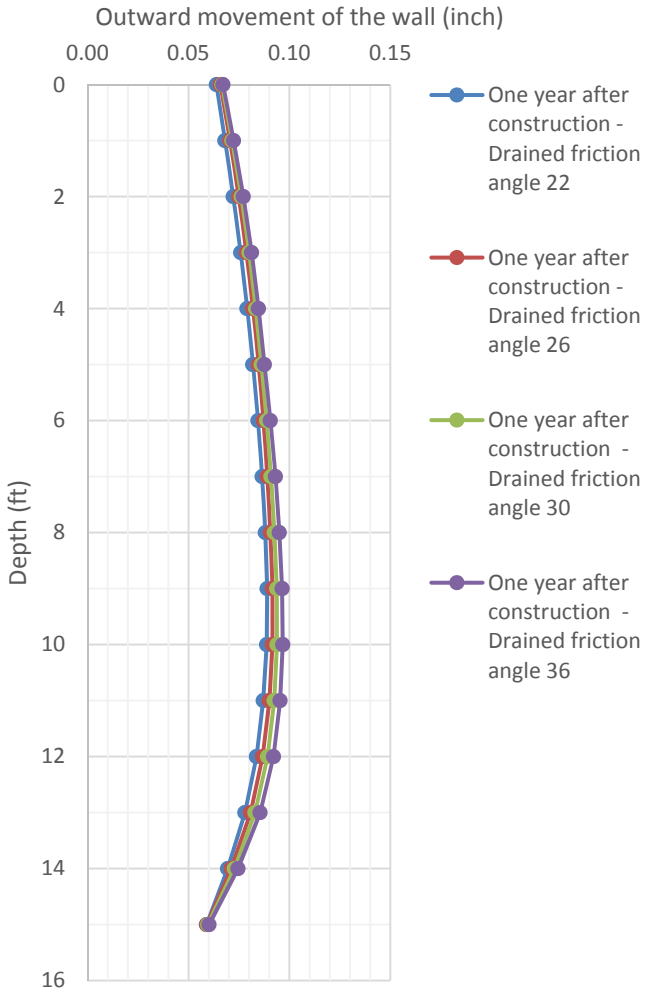

Figure 406. Horizontal Movements of the Soil Nail Wall for One Year after Construction for Drained Friction Angles 22°, 26°, 30°, and 36° (Movements Induced by Creep Only; Movements Related to the Construction Were Removed).

Table 70 shows the maximum axial load in the nails for soil nail walls with different drained friction angles (i.e., 22°, 26°, 30°, and 36°). As discussed previously, horizontal deformations of the soil nail wall in soils with higher drained friction angle are lower than that calculated for soils with lower drained friction angle. As a result, the maximum axial load at end of the construction for the stronger soil is lower than for the soil with lower strength parameters.

For a period of one year after construction, the creep movement of the wall with lower drained friction angle (i.e., 22°) is 8 percent of the movement at the end of the construction, while the creep movement for the higher drained friction angle (i.e., 36°) is 13 percent of the movement at the end of the construction.

Table 70. Maximum Axial Load in the Nails at the End of Construction and One Year after Construction.

Drained friction angle (°)	Additional horizontal deformation of the wall with respect to the horizontal deformation at the end of construction (%)	Maximum load at the end of the construction (kips)	Maximum load one year after the construction (kips)	Increase in the axial load due to the creep (%)
22	8	6.3	8.6	37
26	10	5.7	8.4	47
30	11	5.1	8.2	61
36	13	4.7	8	70

Soil Nail Wall Height

Generally, the height of the soil nail wall for the Texas turnaround varies between 10 and 20 ft. In this parametric study, three heights for the soil nail wall were considered, as follows: 12, 15, and 21 ft. Note that the same soil nails pattern (i.e., same S_h and S_v) was adopted for the soil nail wall with different heights. Furthermore, the same ratio of the length of the soil nail with respect to the height of the wall was adopted for the walls with different heights. Table 71 presents the basic information adopted in these analyses.

Table 71. Soil Nail Wall Parameters for Different Heights.

Height of the soil nail wall (ft)	L/H (ratio of length of the nails to the height of the wall)	Number of rows of soil nails	Length of the nails (ft)	Spacing ($S_h \times S_v$) (ft × ft)
21	1.47	7	31	3.5 × 3
15	1.47	5	22	3.5 × 3
12	1.47	4	17	3.5 × 3

In Figure 407, as the height of the soil nail wall increases, the deformation of the wall increases as well. Figure 408 presents the horizontal deformation for the three walls (i.e., 12, 15, and 21 ft) at both end of construction and after one year of operation.

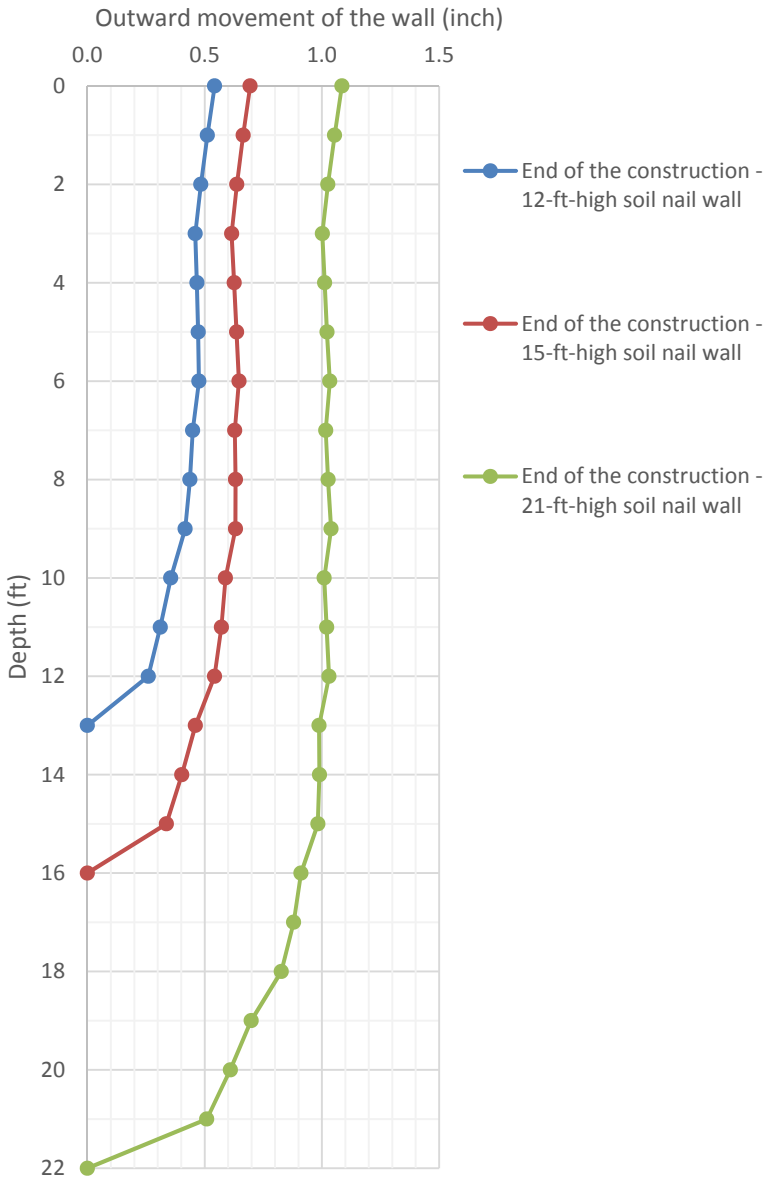

Figure 407. Horizontal Deformation at the End of the Construction, Wall Heights: 12, 15, and 21 Ft.

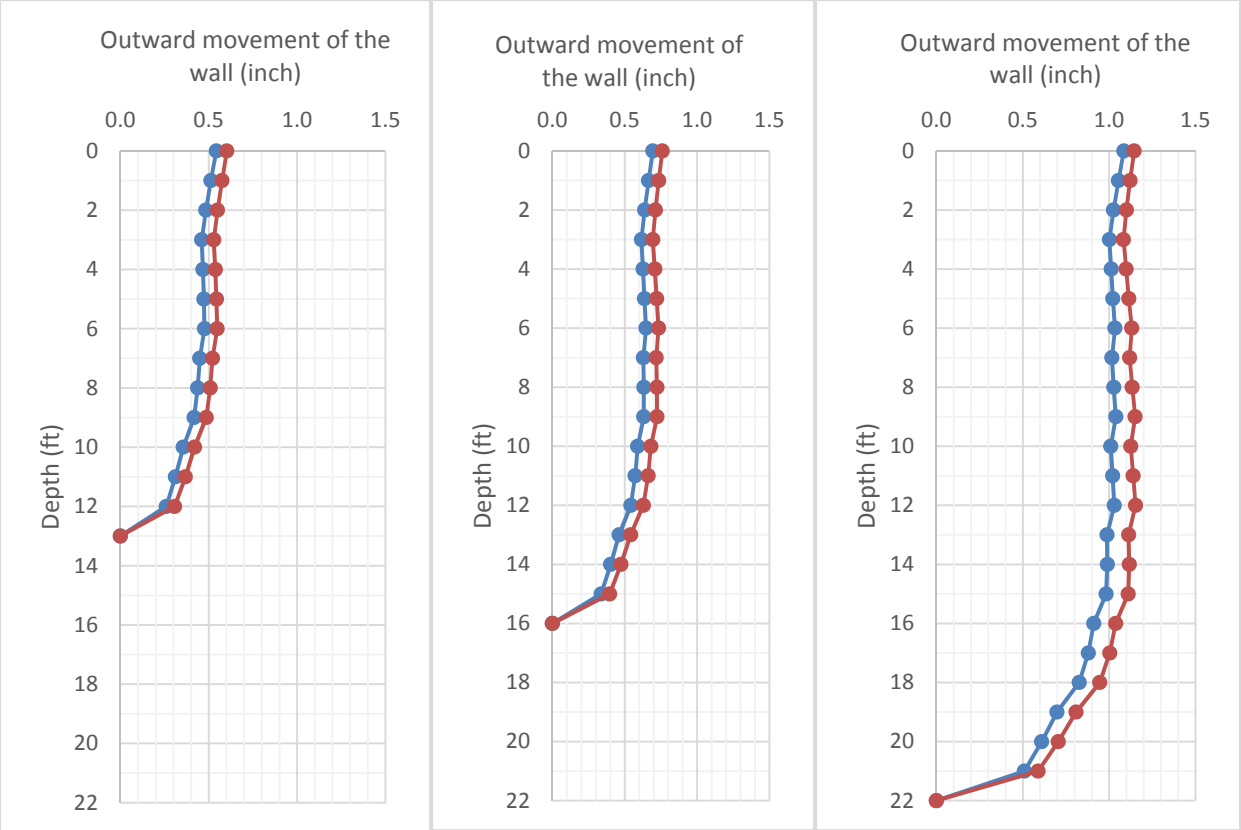

Figure 408. Horizontal Deformation One Year after Construction, Wall Heights: 12, 15, and 21 Ft.

The creep behavior of the soil nail wall is similar for the three cases. The same ratio of nail-length to wall-height was considered in all the analyses. The higher soil nail wall exhibits the larger creep deformation. Table 72 summarizes the ratio of the creep movement with respect to the height of the soil nail wall. For all the cases analyzed, the maximum creep movement calculated one year after construction was 5.0E−4 times the height of the wall, and took place at the bottom half of the soil nail wall.

Table 72. Normalized Creep Movement of the Wall with Respect to the Height of the Wall.

Depth (ft)	21-ft wall	15-ft wall	12-ft wall
	Creep movement/ height of the wall	Creep movement/ height of the wall	Creep movement/ height of the wall
0	2.36E−04	3.65E−04	4.14E−04
1	2.66E−04	3.92E−04	4.38E−04
2	2.95E−04	4.16E−04	4.59E−04
3	3.21E−04	4.37E−04	4.75E−04
4	3.44E−04	4.55E−04	4.87E−04
5	3.65E−04	4.70E−04	4.95E−04
6	3.86E−04	4.84E−04	5.01E−04
7	4.06E−04	4.95E−04	5.00E−04
8	4.25E−04	5.03E−04	4.93E−04
9	4.43E−04	5.09E−04	4.77E−04
10	4.58E−04	5.09E−04	4.45E−04
11	4.73E−04	5.01E−04	3.93E−04
12	4.87E−04	4.82E−04	3.27E−04
13	4.97E−04	4.49E−04	-
14	5.04E−04	3.96E−04	-
15	5.07E−04	3.28E−04	-
16	5.05E−04	-	-
17	4.94E−04	-	-
18	4.72E−04	-	-
19	4.37E−04	-	-
20	3.83E−04	-	-
21	3.15E−04	-	-

Table 73 presents the axial load at the end of construction and at one year after construction. In the three cases, the maximum load increased around 50 percent of the load at the end of the construction.

Table 73. Axial Load in the Nails at the End and after the Construction.

Soil nail wall height (ft)	Max load in the nails at end of the construction (kips)	Max load in the nails one year after the construction (kips)	Increase in the axial load due to the creep (kips)	Increase in the axial load due to the creep (%)
12	4.52	6.5	1.98	43.81
15	5.7	8.44	2.74	48.07
21	8.52	12.5	3.98	46.71

Soil Nails Length

The next parameter investigated in this project was the length of the soil nail. Figure 409 presents the horizontal movements of the wall at the end of the construction for nails 15-, 22-, and 30-ft long. As expected, by increasing the length of the soil nail, the horizontal movement of the wall at the end of the construction is smaller.

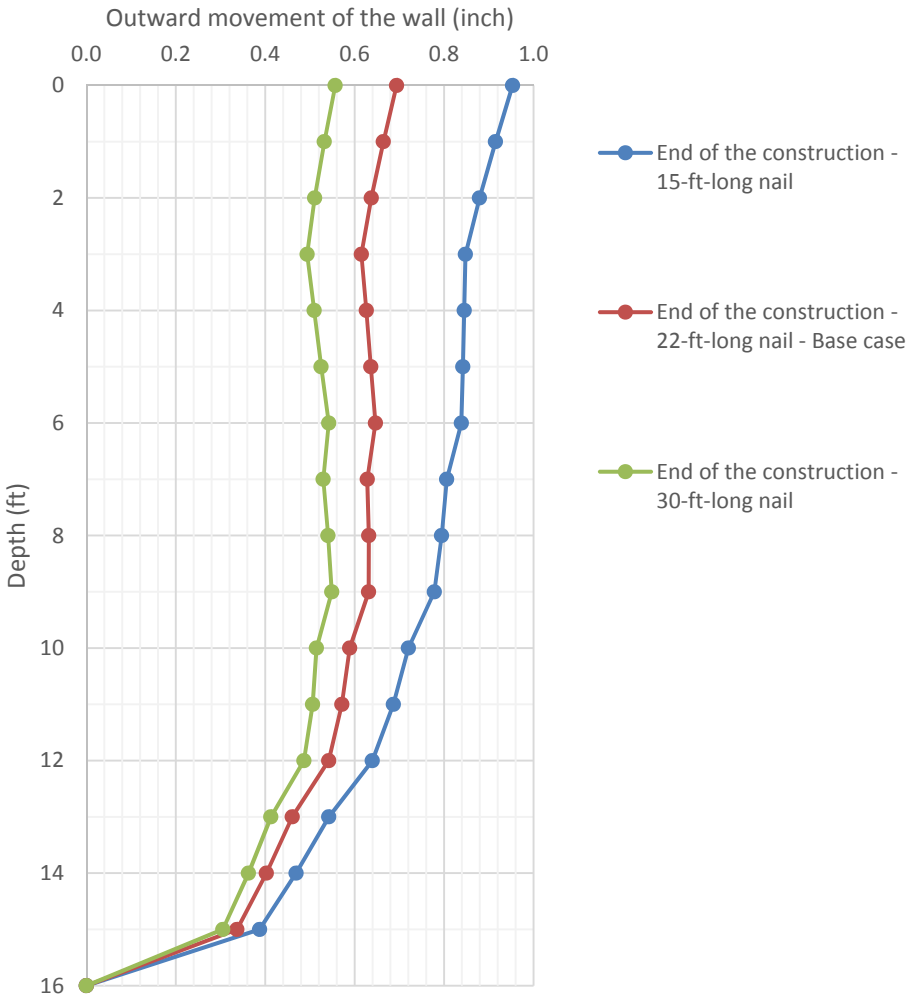

Figure 409. Horizontal Movement of the Wall at the End of Construction, Nails 15, 22, and 30 Ft Long.

The modeling of the creep behavior was performed on the soil nail wall with different nail lengths, as well. Figure 410 shows the horizontal deformation of the wall for one year after the construction for the three nail lengths studied in this project. To show the creep deformation after one year, the deformation at the end of the construction was removed.

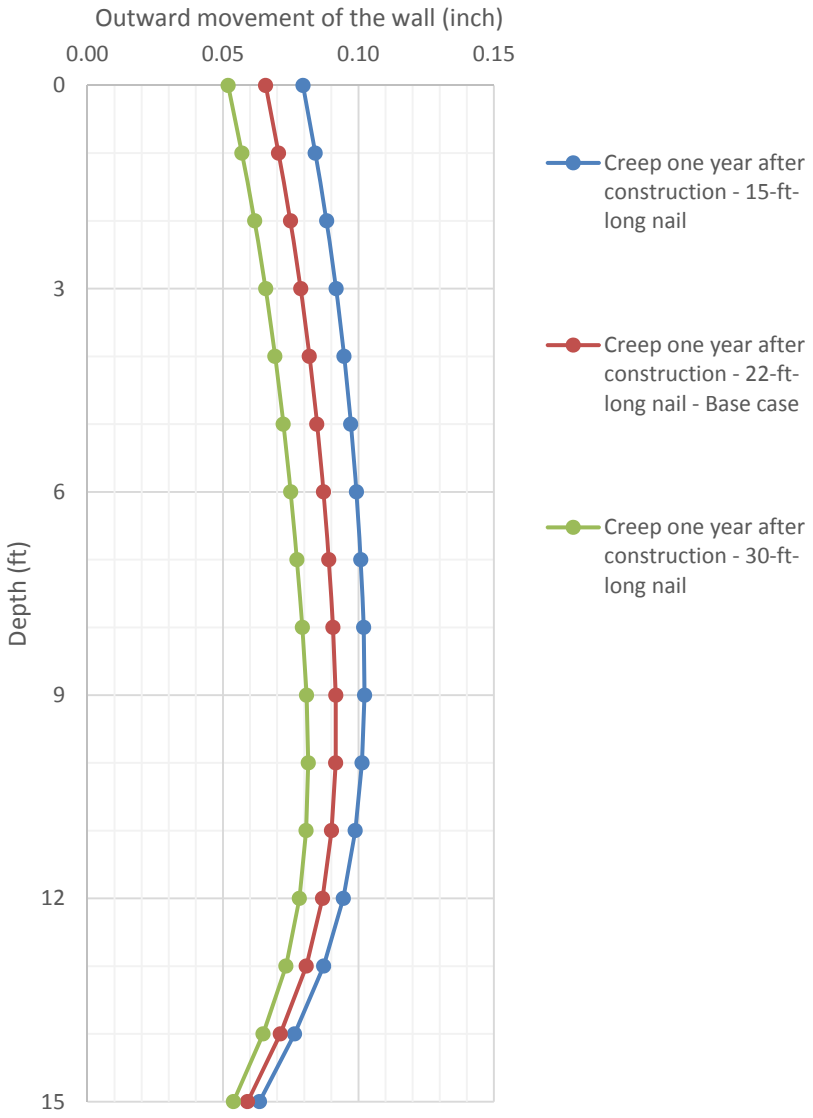

Figure 410. Creep Deformation of the Wall for a Period of One Year after Construction.

From Figure 410, the creep movement of the soil nail wall with longer nails is smaller than that with the shorter nails. However, in all the cases the creep movement one year after the construction was less than 10 percent of the horizontal movement calculated just after construction. Table 74 through Table 76 present the axial load in the nails at the end of construction and after one year of operation due to the creep for the nails 15, 22, and 30 ft long.

The maximum load at the end of the construction is practically of the same order of magnitude for the three cases analyzed. As for the creep period after construction, according to

this model, the maximum axial load after one year of operation on the nails 15, 22, and 30 ft long increased to around 50 percent with respect to loads on the nails at the end of construction.

Table 74. Axial Load in the Nails at the End and after Construction for 15-Ft-Long Nail.

Nail #	Max load in the nails at end of the construction (kips)	Max load in the nails one year after the construction (kips)	Increase in the axial load due to the creep (kips)	Increase in the axial load due to the creep (%)
	15-ft-long nail	15-ft-long nail	15-ft-long nail	15-ft-long nail
1	3.9	4.18	0.28	7.18
2	4.6	6.2	1.6	34.78
3	5.4	7.3	1.9	35.19
4	5.5	8.3	2.8	50.91
5	0	2.8	2.8	-

Table 75. Axial Load in the Nails at the End and after Construction for 22-Ft-Long Nail.

Nail #	Max load in the nails at end of the construction (kips)	Max load in the nails one year after the construction (kips)	Increase in the axial load due to the creep (kips)	Increase in the axial load due to the creep (%)
	22-ft-long nail	22-ft-long nail	22-ft-long nail	22-ft-long nail
1	4.6	5	0.4	8.70
2	4.9	6.2	1.3	26.53
3	5.6	7.8	2.2	39.29
4	5.5	8.3	2.8	50.91
5	0	2.4	2.4	-

Table 76. Axial Load in the Nails at the End and after Construction for 30-Ft-Long Nail.

Nail #1	Max load in the nails at end of the construction (kips)	Max load in the nails one year after the construction (kips)	Increase in the axial load due to the creep (kips)	Increase in the axial load due to the creep (%)
	30-ft-long nail	30-ft-long nail	30-ft-long nail	30-ft-long nail
1	4.7	5	0.3	6.38
2	5.1	6.4	1.3	25.49
3	5.7	8	2.3	40.35
4	5.5	8.3	2.8	50.91
5	0	2.4	2.4	-

Regardless of the length of the soil nails, the maximum loads in the nails increase by around 50 percent because of creep after 1 year. In the cases studied, the service load in the

fourth nail (for all three cases) at the end of the construction was 5.5 kips, while the maximum load one year after the construction was 8.3 kips.

Viscosity

The key parameter that affects the long-term behavior of the soil nail wall is the viscosity of the soil. The soils with HP index have the potential to creep more. The creep behavior of the HP clay depends strongly on water content of the soil. LI of the soil at the NGES-TAMU clay site and the Beaumont site are less than 0.2 (Table 61 and Table 62).

To determine/estimate the viscosity of the soil under fill conditions is not an easy task. In this research project, triaxial creep tests were performed on the soil samples from the NGES-TAMU clay site and the Beaumont site. The experimental results obtained from these tests were adjusted using the well-known creep model proposed by Briaud and Garland (1985; Chapter 2, Eq. 5) and the n value for the different stress levels were determined for these soils. Then, these triaxial creep tests were modeled using FLAC3D, and the viscosity parameters associated with the Burger model were obtained. This procedure also led to a correlation between *n* values and viscosity parameters (see Figure 374 to Figure 376).

In this section, the effect of different n values (and so different viscosity parameters) on the creep behavior of a reference soil nail wall is investigated. Table 77 presents the different *n* value and viscous parameters adopted in this parametric study. The numerical model was calibrated against the result of the triaxial creep test on the soil sample from the Beaumont project and also againt the data gathered from the instrumentation and post-construction monitoring the soil nail wall.

Table 77. Viscous Parameters Adopted in This Parametric Study.

***n* Value**	**Viscous Parameters for the Burger Model**
$0.02 < n < 0.04$	m shear=1.04e9 lb/ft^2, m vis=5.91e14 lb*s/ft^2, k shear=3e6 lb/ft^2, k vis=2.5e13 lb*s/ft^2
$0.05 < n < 0.07$*	m shear=1.04e9 lb/ft^2, m vis=2e14 lb*s/ft^2, k shear=5e5 lb/ft^2, k vis=3.5e12 lb*s/ft^2
$0.07 < n < 0.09$	m shear=1.04e9 lb/ft^2, m vis=1.28e14 lb*s/ft^2, k shear=2.37e5 lb/ft^2, k vis=1.55e12 lb*s/ft^2

*Indicates the behavior of the soil at the Beaumont project.

Figure 411 shows the creep deformation of the soil nail wall for one year after construction for three different cases. Figure 412 presents the creep movements at the top of the wall for one year after construction.

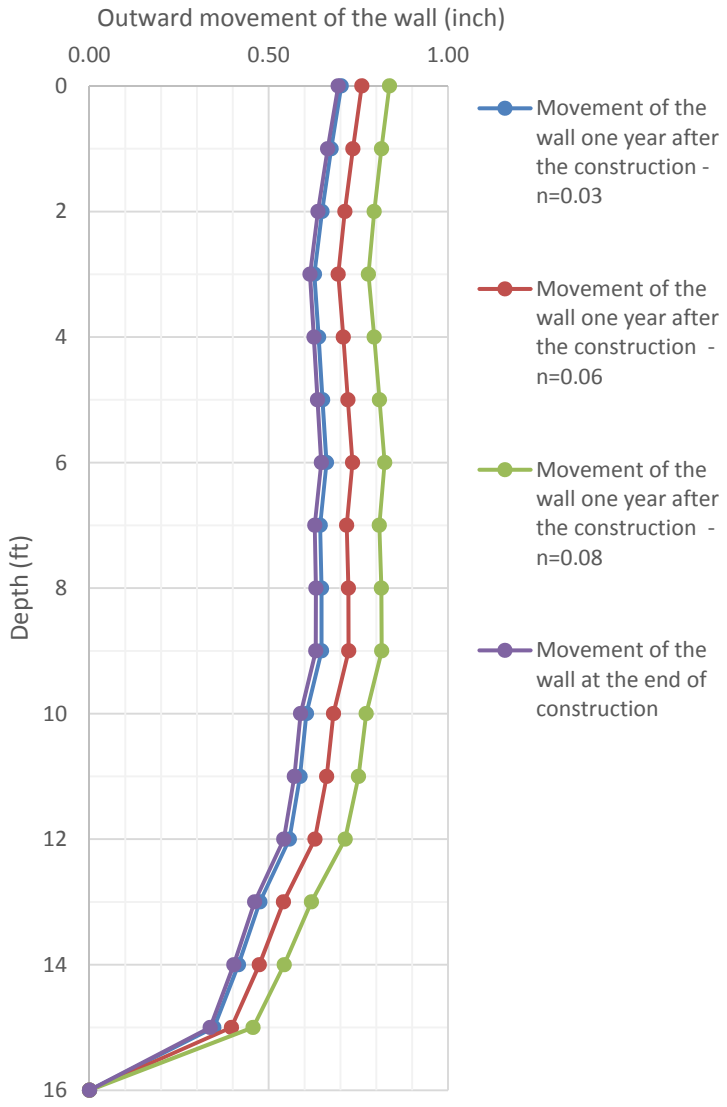

Figure 411. Creep Deformation at Top of the Wall for Different Soil Viscosity Values.

Table 78 to Table 80 present the axial load in the nails at the end of the construction and one year after the construction for $n = 0.03, 0.06$, and 0.08, respectively. The maximum axial load increases up to 16 percent of the load at the end of the construction for $n = 0.03$, while for $n = 0.06$ and 0.08 the maximum axial load increases up to 51 percent and 75 percent of the axial load at the end of the construction, respectively.

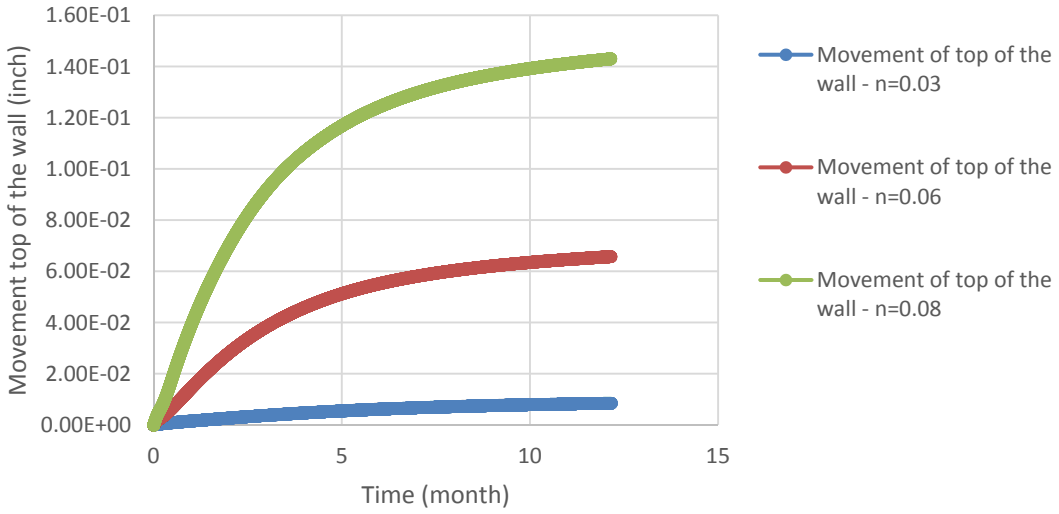

Figure 412. Horizontal Movements Top of the Wall Calculated for One Year after Construction for *n* = 0.03, 0.06, and 0.08 (Movements Induced by Creep Only, Movements Related to the Construction Were Removed).

Table 78. Axial Load in the Nails at the End and after Construction for *n* = 0.03.

Nail #	Max load in the nails at end of the construction (kips)	Max load in the nails one year after the construction (kips)	Increase in the axial load due to the creep (kips)	Increase in the axial load due to the creep (%)
	n = 0.03	n = 0.03	n = 0.03	n = 0.03
1	4.6	4.7	0.1	2.17
2	4.9	5.2	0.3	6.12
3	5.6	6.3	0.7	12.50
4	5.5	6.4	0.9	16.36
5	0	0	0	-

Table 79. Axial Load in the Nails at the End and after Construction for *n* = 0.06.

Nail #	Max load in the nails at end of the construction (kips)	Max load in the nails one year after the construction (kips)	Increase in the axial load due to the creep (kips)	Increase in the axial load due to the creep (%)
	n = 0.06	n = 0.06	n = 0.06	n = 0.06
1	4.6	5	0.4	8.70
2	4.9	6.2	1.3	26.53
3	5.6	7.8	2.2	39.29
4	5.5	8.3	2.8	50.91
5	0	2.4	2.4	-

Table 80. Axial Load in the Nails at the End and after Construction for n = 0.08.

Nail #	Max load in the nails at end of the construction (kips)	Max load in the nails one year after the construction (kips)	Increase in the axial load due to the creep (kips)	Increase in the axial load due to the creep (%)
	n = 0.08	n = 0.08	n = 0.08	n = 0.08
1	4.6	5.4	0.8	17.39
2	4.9	6.7	1.8	36.73
3	5.6	8.6	3	53.57
4	5.5	9.6	4.1	74.55
5	0	3.9	3.9	-

The n value (i.e., viscosity of the soil) plays a significant role in the long-term behavior of the soil nail wall. The soil nail walls involving soils with higher n value exhibit a more notorious creep behavior. The n value for the soil at the NGES-TAMU clay site is between 0.02 and 0.04, while the n value from the Beaumont project varies between 0.05 and 0.07. The typical range of n value for clays varies between 0.02 and 0.08 (Briaud and Garland, 1985).

SUMMARY AND CONCLUSIONS

This chapter presented the activities related to the numerical analyses performed in the framework of this research project involving various numerical tools. The analyses are related to an emergency slope repair project at the Beaumont District. The FLAC3D software was used to simulate the time-dependent (creep) behavior of the soil nail wall during construction and after it. The soil nail wall constructed at Beaumont was instrumented and monitored, and key information was gathered during wall construction and afterward, during post-construction service. The monitoring of the wall during operational conditions lasted for 13 months after construction and allowed the researchers to learn about the wall movements during wall operation and about the service load in the nails. The calibration of the numerical model was based on pullout tests on sacrificial nails, laboratory tests on soil samples from the Beaumont site, and the monitoring of the actual soil nail wall at the Beaumont project. The following key information was gathered from the numerical model of the soil nail wall: horizontal deformation of the wall at the end of the construction and during operational conditions, service load along the nails after the construction, and an extra load on the nails induced by creep after the construction.

The experience gained from the modeling of the Beaumont wall was used to develop the numerical model for the typical Texas turnaround wall provided by TxDOT. This model was then used to perform a parametric study aimed at learning about the influence of different soil parameters and wall factors on the short- and long-term behavior of a soil nail wall. The parameters of the rheological model used in the sensitivity study were obtained from the calibration of the triaxial creep tests. Correlations between the triaxial creep tests performed in this project, the *n* value of a well-known creep model for soils, and the viscous parameters of the Burger model used in FLAC3D to model creep behavior was obtained. From this parametric study, researchers found that it is key to have good information about the viscous parameters of the soil. Both wall movements and the load on the soil nail increase considerably during wall operation because of creep. The results of this parametric study were used to suggest tentative modification of the design method to account for creep behavior in soil nail walls. These activities are presented in Chapter 8.

Quite simple constitutive models to describe the soil behavior were adopted in this study. The aim was to use models already implemented in FLAC3D. To model the behavior of the soil during wall construction, the well-known MC was adopted. For modeling the creep behavior of soils, the viscoelastic Burger model was selected.

The numerical results revealed that for the specific soils considered in these analyses, the particular geometry and conditions of the studied walls, and for the adopted numerical models, the load on the nail could increase considerably during wall operation. The experimental studies presented in previous chapters (i.e., nail pullout tests and single element tests) showed that creep rates in HP clays were very low when the stress level was low (e.g., when the acting nail load is below the 90 percent of the pullout capacity), but increased considerably when the load level was high and close to the ultimate capacity of the nail. Therefore, this differed increment in the soil nail load may pose a problem for the long-term performance of soil nail walls in HP clays if it is not considered in the design.

CHAPTER 8:
ANTICIPATED DESIGN METHOD

INTRODUCTION

To thoroughly investigate the creep behavior of soil nail walls in HP clays, this research project combines experimental and numerical studies. A number of computational tools were used to investigate the performance of soil nail walls in HP clays. The computer software FLAC3D was adopted to simulate the mechanical and the time-dependent (creep) behavior of a soil nail wall during construction and after it, respectively (these activities are related in Chapter 7).

The filed data gathered from the monitoring of the emergency slope repair at the Beaumont District were used to validate the proposed numerical model. The goal of this chapter is to study the effect of the long-term behavior of the soil nail walls in HP clays. The numerical model was validated based on the results of the pullout tests on the nails at the NGES-TAMU clay site (Chapter 4) and sacrificial nails at the actual soil nail wall project (Chapter 5), instrumentation and monitoring the actual soil nail wall for one year post-construction (Chapter 5), and numerical models that were calibrated using the filed data (Chapter 7).

This chapter includes five sections. The second section presents the step-by-step design method based on the current soil nail wall design manual (i.e., GEC#7). The third section focuses on the tentative design method for soil nail walls in HP clays accounting for soil creep suggested in this project. A case study for designing a soil nail wall in a HP clay using the suggested procedure is illustrated in section four. The fifth section is related to the summary and conclusions of this report.

CURRENT METHODOLOGY TO DESIGN SOIL NAIL WALLS

Before explaining the tentative modification suggested in this project for accounting for creep effects in the design of soil nail walls, a brief explanation of the current design guideline is introduced in this section.

Introduction

In this section, the steps related to the design of soil nail walls in HP clays according to the GEC#7 are briefly discussed. The overview of the design procedure is listed in Table 81 and Table 82 (FHWA, 2015).

Table 81. Initial Design Considerations (FHWA, 2015).

Step No.	Description
Step 1	**Project Requirements**
a	Establish project requirements, standards and constraints
b	Establish project performance
c	Assemble preliminary geotechnical information
Step 2	**Subsurface Exploration and Development of Parameters for Design**
a	Plan and conduct subsurface exploration
b	Conduct soil laboratory testing program
c	Establish soil corrosion potential and level of corrosion protection
d	Develop subsurface profiles for analysis
e	Develop soil parameters for design
f	Obtain seismic parameters
g	Conduct a risk analysis
Step 3	**Load Definition**
a	Define unfactored, service loads
b	Select load combinations and load factors

Table 82. Steps for Designing a Soil Nail Wall (FHWA, 2015).

Step No.	Description
Step 4	**Soil-Nail Configuration and Material Selection**
a	Develop wall layout
b	Develop soil nail cross sections
c	Select soil nail pattern on wall face
d	Evaluate soil nail horizontal splaying
e	Detail corrosion protection
f	Select soil nail type and material properties
Step 5	**Selection of Resistance Factors**
Step 6	**Overall Stability Analyses**
a	Evaluate internal stability
b	Evaluate global stability
c	Evaluate basal heave (if applicable)
d	Evaluate sliding stability (if applicable)
Step 7	**Strength Limit States (Geotechnical and Structural)**
a	Verify pullout resistance
b	Verify sliding stability (if applicable)
c	Verify nail tensile resistance
d	Verify facing bending/flexural resistance
e	Verify facing punching shear resistance
f	Verify facing headed stud resistance
g	Other facing design considerations
Step 8	**Service Limit States (Deformations)**
a	Evaluate wall lateral and vertical displacements
b	Evaluate lateral squeeze (if applicable)
Step 9	**Seismic Design**
a	Select design seismic parameters
b	Adjustment of design seismic coefficients
c	Evaluate overall stability with seismic loads
Step 10	**Drainage and Drainage Details**
a	Evaluate internal drainage
b	Evaluate surface water runoff
c	Develop drainage details
d	Specialty items (if present)
Step 11	**Other Design Considerations**
a	Develop final constructability evaluation
b	Prepare plan for load-testing program
c	Prepare plan for geotechnical monitoring program
Step 12	**Preparation of Construction Drawings and Specifications**

Soil Parameters Used in the Design (Step 2, Table 81)

One of the starting points in the design of a soil nail wall is to learn about the soil properties. To that end appropriate laboratory tests need to be conducted to gather the soil parameters to be used in the design. The drained strength must be considered when evaluating the long-term performance of the soil nail wall in fine-grained soil (FHWA, 2015). Results from CU tests with measurement of pore water pressure need to be used to evaluate the long-term drained strength of fine-grained soils (FHWA, 2015). The effective friction angle could be also determined from the correlation between the PI and the friction angle of fine-grained soils presented in Chapter 7, Figure 343.

Soil-Nail Configuration (Step 4, Table 82)

Once the mechanical parameters of the soil are determined, the geometry (i.e., the height of the soil nail wall, and wall batter) and the cross section of the soil nail wall can be defined (e.g., number of nails, vertical and horizontal spacing between nails, nail inclination, and nail length). Uniform soil nail length is usually adopted by TxDOT to prevent placing nails in wrong positions and for the sake of simplicity. It is also quite common in Texas that horizontal and vertical spacing between nails (i.e., S_h and S_v, respectively) are set equal to 4 ft.

Stability Analysis (Step 6, Table 82)

The soil nail wall needs to be analyzed for internal and global stabilities using the 2D limit equilibrium ASD–based slope stability procedure (i.e., via SNAILZ, GOLDNAIL, or SNAP-2 programs [FHWA, 2015]). The ASD-based slope stability analysis calculates the safety factors for the overall stability of the wall. It also computes the maximum loads along the nails, which should not be higher than the pullout capacity of the nails. The input soil parameters for the ASD-based limit equilibrium program include the soil unit weight, effective strength parameters (i.e., effective cohesion and friction angle), and bond stress. For the case of non-critical structures (see FHWA, 2015) and for static conditions, the minimum FS for overall stability of the soil nail wall is 1.35.

Verification of Geotechnical and Structural Resistances (Step 7, Table 82)

In this step, the geotechnical (pullout) and structural (nail tensile) resistances of the nails are evaluated. From the results of the stability analysis (i.e., Step 6), the maximum load in the

nails (T_{max}) is obtained. T_{max} must be taken as the largest value for all the nails under study. The maximum load needs to be multiplied by a load factor ($\gamma = \gamma_{EV} = 1.35$), which is selected for the load and resistance factor design verification from the soil nail wall manual (FHWA, 2015).

The nail pullout resistance is related to the resistance of the nail mobilized behind the slip surface. The length of nail behind the slip surface (L_p, Figure 413) can be estimated from the graphical outputs of soil nail wall design programs. This length of the nail corresponds to portion of the nail can develop the pullout resistance (FHWA, 2015). According to the GEC#7 (FHWA, 2015), the ultimate pullout resistance of the nails is defined as:

$$R_{po} = \pi \, q_u \, D_{DH} \, L_p \tag{21}$$

where R_{po} is the nominal pullout resistance; q_u is bond stress of the nail-grout interface; and D_{DH} is the diameter of the drill hole. The pullout resistance is evaluated as follows:

$$CDR = \frac{\phi_{PO} \, R_{PO}}{\gamma \, T_{max}} \geq 1 \tag{22}$$

where γ is the load factor (equal to 1.35); T_{max} is the maximum tensile force; and ϕ_{PO} is the resistance factor for pullout resistance, which is equal to 0.65.

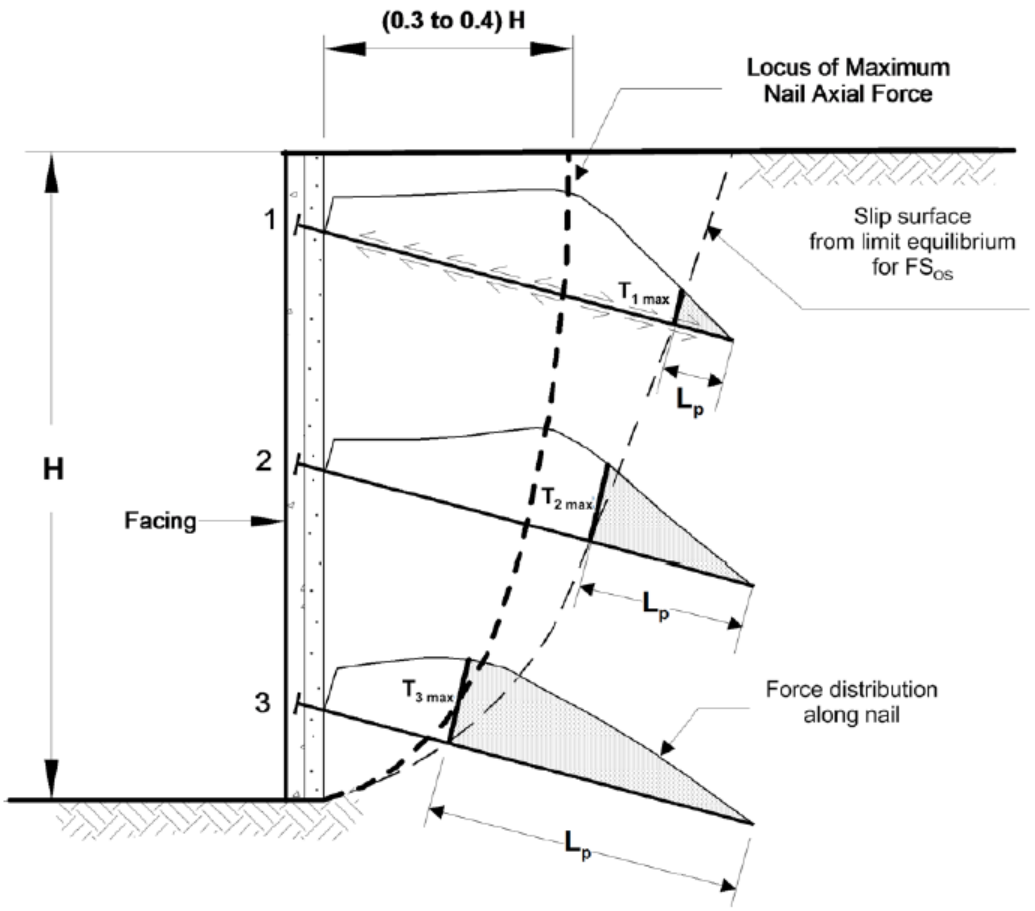

Figure 413. Force Distribution along the Nails and Length of Nail behind the Slip Surface, *Lp* (FHWA, 2015).

The tensile resistance of the tendon is defined as:

$$CDR = \frac{\phi_T \, R_T}{\gamma \, T_{max}} \geq 1 \tag{23}$$

where ϕ_T is the resistance factor for tensile resistance of the tendon (under static conditions for tendon grades 60/75 is 0.75 and for tendon grades 95/150 is 0.65); R_T is the nominal tensile resistance of the tendon; γ is the load factor selected for verification; and T_{max} is the maximum tensile force.

The nominal resistance of the tendon is:

$$R_T = A_t \, f_y \tag{24}$$

where A_t is the cross section area of the tendon; and f_y is the nominal yield strength of the tendon.

According to the GEC#7, the maximum nail tensile force can also be estimated from the plot prepared by Byrne (1998), which is based on experiments performed on full-scale instrumented soil nail walls (Figure 414).

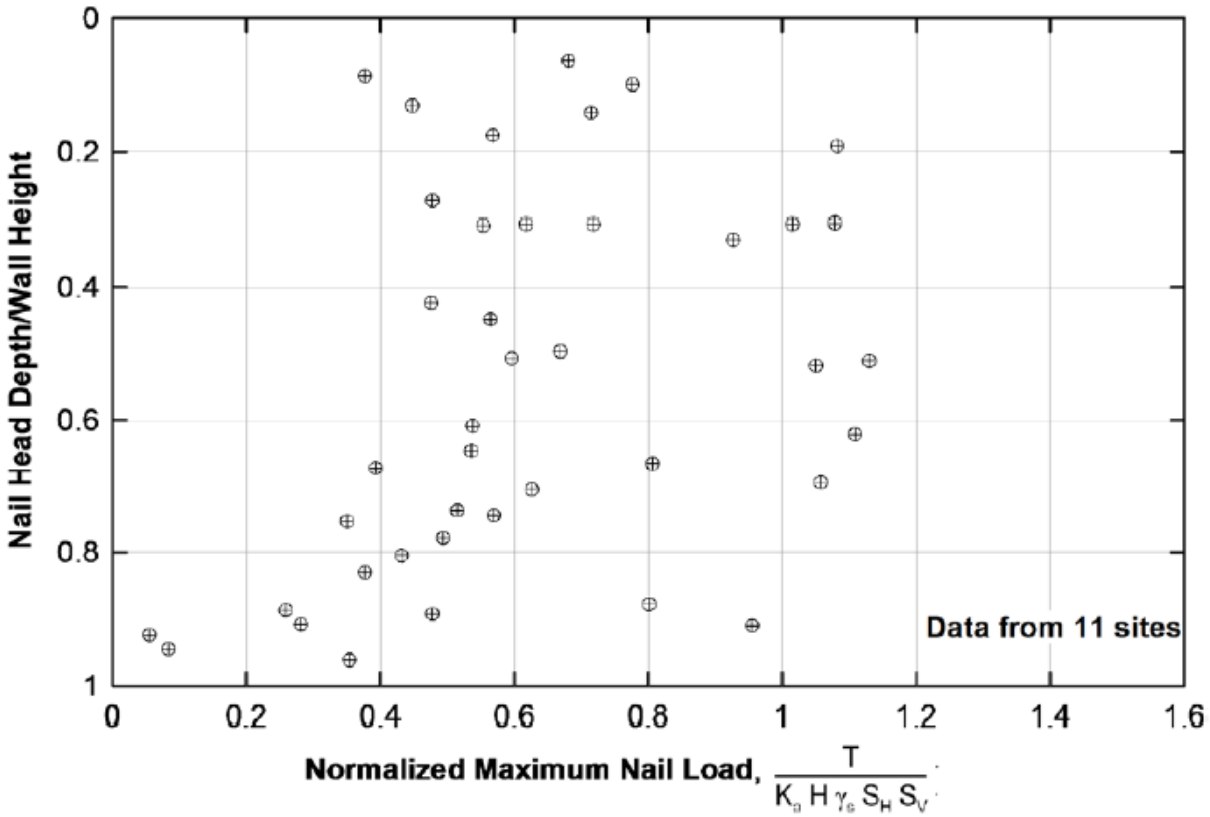

Figure 414. Maximum Tensile Force Measured from 11 Instrumented Full-Scale Soil Nail Walls (Byrne, 1998).

Briaud and Lim (1997) suggested that the average maximum load for the top row of the soil nails can be calculated according to Eq. 25, and half of this value should be used for the lower nails:

$$T_{max} = 0.65\, K_a\, \gamma_s\, H\, S_V\, S_H \tag{25}$$

where $K_a$is the active earth pressure coefficient; γ_s is the soil unit weight; H is the height of the wall; and S_V and S_H are the vertical and horizontal spacing values, respectively. The tensile force

at the wall facing (T_0) varies between $T_0 = 0.5\ K_a\ \gamma_s\ H\ S_V\ S_H$ and $T_0 = 0.6\ K_a\ \gamma_s\ H\ S_V\ S_H$ (FHWA, 2015).

Verification of the Facing Resistance (Step 7, Table 82)

Once the T_{max} and T_0 are known, the resistance of the facing (e.g., facing punching shear resistance, facing bending resistance) can be evaluated. The steps related to the verification of the facing resistance are not discussed in this report. The detailed step-by-step procedures for verifying the facing resistance are presented in GEC#7 (FHWA, 2015).

Evaluation of the Wall Lateral Displacement (Step 8, Table 82)

According to the GEC#7, numerical methods should be used to evaluate the vertical and horizontal movements of the wall for the case of critical structures. The most common numerical techniques are the 2D FEM and the finite difference method (FHWA, 2015). The maximum lateral movement should be limited to 0.3 percent H, where H is height of the soil nail wall.

TENTATIVE DESIGN METHOD ACCOUNTING FOR SOIL CREEP

This section presents a tentative modification of the design method for soil nail walls designed in HP clays aimed at accounting for soil-creep effects. The suggested modification to the traditional design method introduced in the previous section is explained hereafter. It is based on the experimental information gathered in this project, namely: the pullout tests at the NGES-TAMU clay site (Chapter 4), instrumentation and monitoring of the emergency slope repair project at the Beaumont District (Chapter 5), laboratory tests (Chapter 6), and numerical modeling (Chapter 7). The design method modifications presented in this chapter are based on the assumption that the permanent soil nail wall has a 75-year design life. This wall lifetime was adopted according to Lazarte et al. (2003).

Typical Texas Turnaround Soil Nail Wall

Soil nail walls tend to deform after construction, leading to the development of additional axial loads in the nails induced by these movements. The complex long-term behavior of the soil nail walls constructed in HP clays was modeled in this project using the commercial geotechnical finite difference code FLAC3D. The model was calibrated with the results of the instrumentation and monitoring of the slope repair project at the Beaumont District. Since the soil nail wall at the

Beaumont project is not the soil nail wall typically adopted in the design in Texas, the parametric study was performed on a typical Texas turnaround soil nail wall provided by TxDOT. The wall geometry and configuration of the Texas turnaround is shown in Figure 391 and Figure 392 (Chapter 7). A detailed description of the parametric study of the typical Texas turnaround was presented in Chapter 7.

The modeling of the wall was performed in successive steps. First, the geometry and mesh of the embankment was generated. The soil parameters were obtained from the information gathered in the tests performed in the laboratory. This step was followed by imposing the initial and boundary conditions of the problem to the mesh to reach the initial condition (i.e., in situ stresses). FLAC3D was run from the initial non-equilibrium conditions until an equilibrium state was obtained (Itasca, 2006). Once the equilibrium state was achieved, excavation stages were used to simulate the construction process of the soil nail wall (Singh and Babu, 2010). In each stage of construction an excavation depth of 3 ft was simulated by assigning the null model to the zone of excavation. This step was followed by the simulation of the soil nail installation and shotcrete emplacement. The simulation of each stage continued until an equilibrium state was achieved. Five stages of construction were carried out to simulate the completion of the soil nail wall (i.e., up to the bottom of the excavation). Figure 415 shows the geometry adopted to simulate the turnaround soil nail wall.

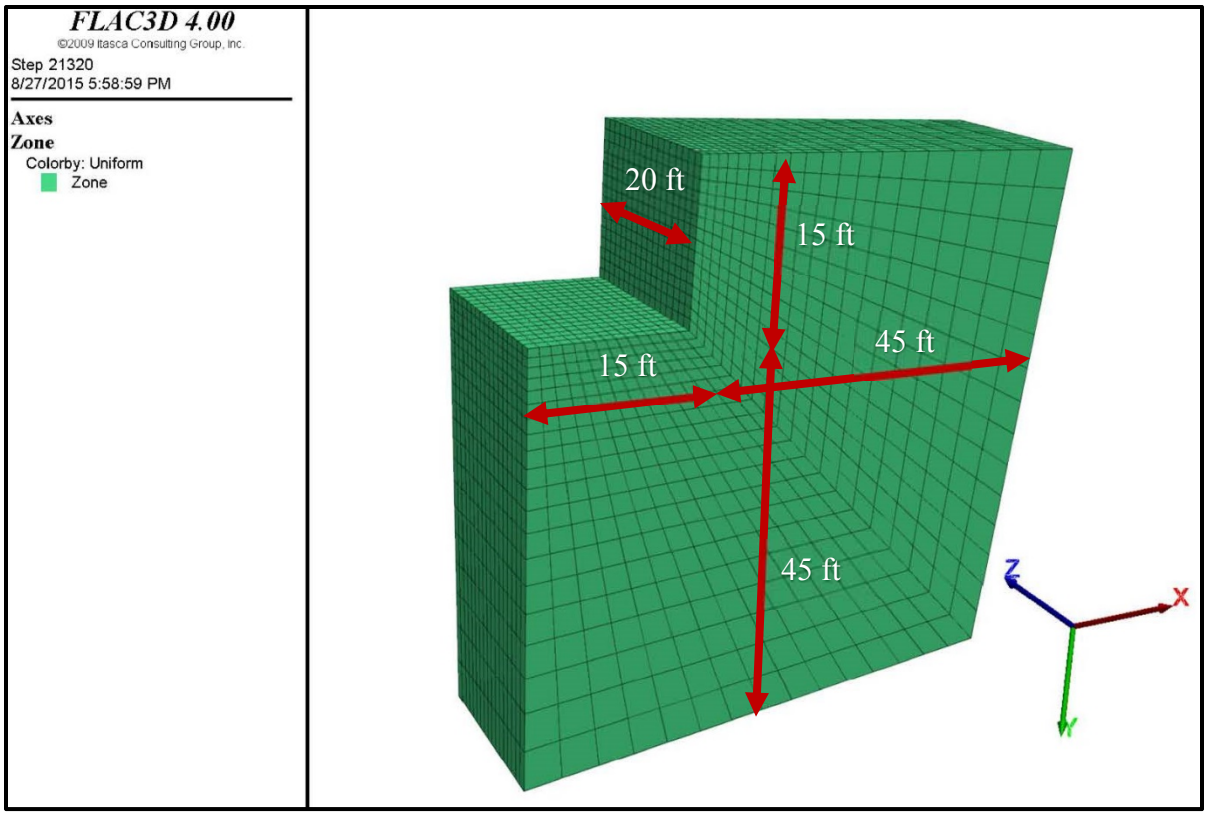

Figure 415. Geometry and Boundary Condition of the Turnaround Soil Nail Wall.

For the modeling the base case during the operation stage (i.e. post-construction), the in situ stresses and displacements of the soil nail wall obtained from the modeling at the end of the construction (i.e., Chapter 7) were adopted as the initial condition. To account for the creep behavior, the MC mechanical model (used to simulate the construction of the wall) was replaced by the Burger model to simulate the long-term behavior. The model described above ran for a period of 75 years. Figure 416 shows the horizontal deformation of the turnaround soil nail wall. The deformation at the top of the wall just after the construction is 0.694 in. and increases afterward up to 0.789 and 1.14 in. for a period of 1 and 75 years after construction, respectively.

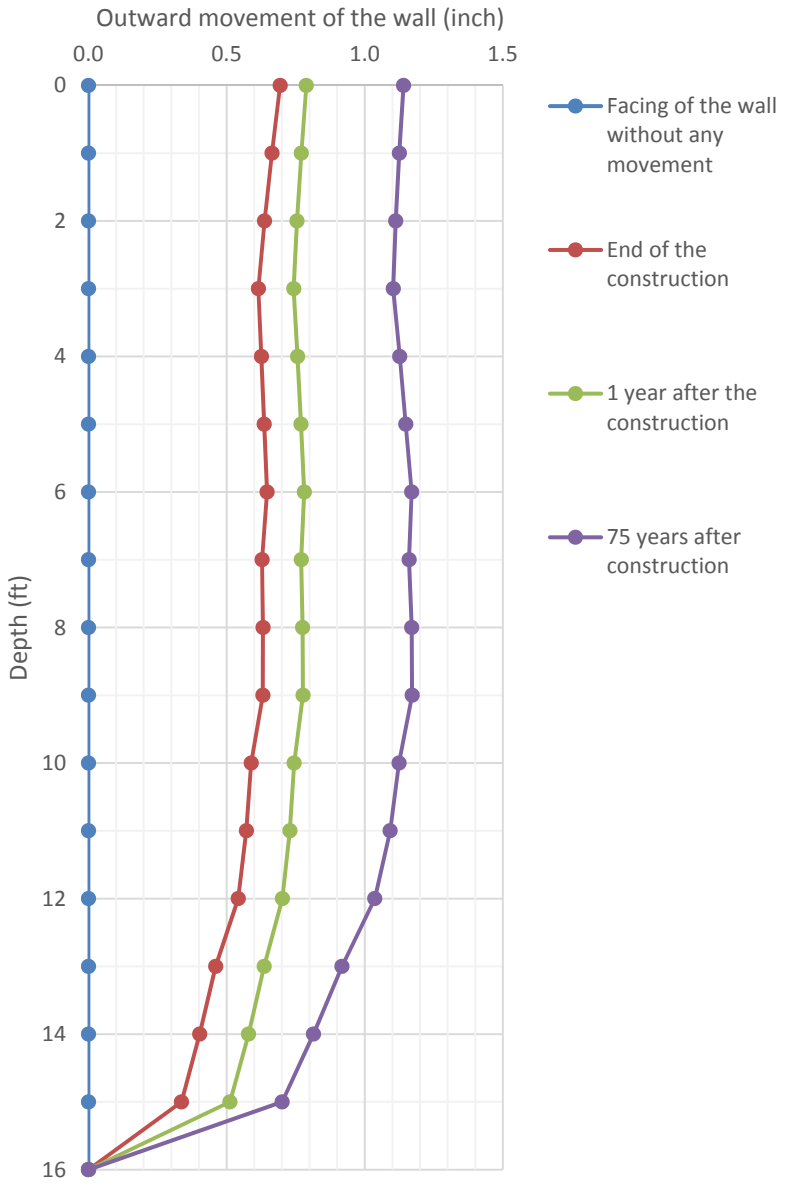

Figure 416. Horizontal Deformation of the Wall at the End of the Construction, and after 1 and 75 Years Post-Construction.

After construction, the additional deformations coming from the creeping soil mass induce movements of the soil nail wall, which in turn will lead to an increase in the axial loads in the nails. Table 83 presents the load developed in the nails at three different times: end of the construction, one year after construction, and 75 years after construction.

Table 83. Maximum Axial Load in the Nails for the Typical Texas Turnaround.

Nail #	Max load in the nails at end of the construction (kips)	Max load in the nails 1 year after the construction (kips)	Max load in the nails 75 years after the construction (kips)
1	4.6	5	5.9
2	4.9	6.2	7.8
3	5.6	7.8	9.91
4	5.5	8.3	11
5	0	2.4	7.6

During the construction of a soil nail wall, a significant portion of the axial loads on the nails develops during the subsequent stages of excavation. Considering that after installing the last row of nails (i.e., Nail 5 in this case) there are no further excavations, this nail will have (practically) no load at the end of construction. However, the wall movements induced by soil creep will load the nail later on. The calculated axial load in the nail one year after construction is 2.4 kips and increases up to 7.6 kips after 75 years. In the nail that is just above (i.e., Nail #4), the maximum load at the end of construction is 5.5 kips, which increases up to 8.3 kips (i.e., around 50 percent increase) after one year and 11 kips (i.e., 100 percent increase) for 75 years after construction. Figure 417 presents the distribution of the maximum axial load in the fourth nail for the following times: just after the construction, one year, 10 years, and 75 years after construction.

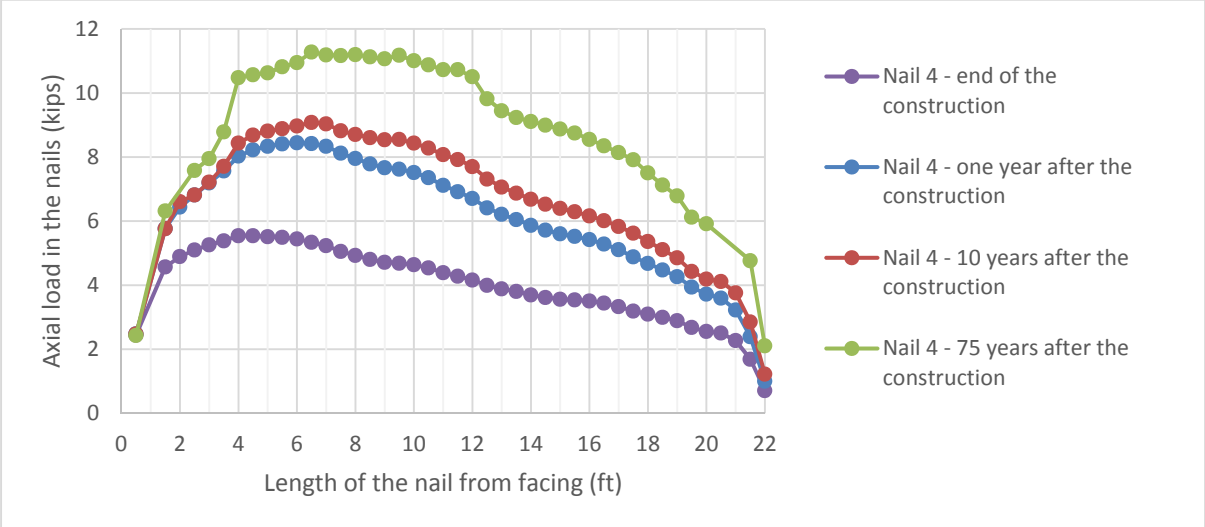

Figure 417. Maximum Axial Load in Nail #4 at the End of the Construction, 1 Year, 10 Years, and 75 Years after Construction.

Design Consideration

One of the possible failure mechanisms associated with soil nail walls is the nail pullout failure. This mechanism is related to the failure along the soil–grout interface. During the design of soil nail walls in HP clays, the additional axial load in the nail after construction induced by soil creep should be taken into account. The key parameter that affects the long-term behavior of the soil nail wall is the viscosity of the soil. Soil with higher viscosity exhibits more deformation after construction, and subsequently more additional axial load develops in the nails. Results of the parametric study on the base case show that the increase in the maximum axial load one year after the construction, for *n* equal to 0.03, 0.06, and 0.08, is 16 percent, 50 percent, and 75 percent of the axial load in the nails at the end of the construction, respectively. In all the cases, the maximum axial load increases to 100 percent for 75 years after the construction. In the soil with higher viscosity, more axial load develops in the other nails (i.e., nails in the last row located at bottom of the wall) compared to the soil with lower viscosity. In this section, a tentative approach to consider this additional load in the design of soil nail walls in HP clays is discussed. The viscous properties of the Beaumont clay are adopted for this discussion (i.e., n = 0.06 and LI = 0.01).

Maximum Axial Load in the Nails

Chapter 7 discussed that the maximum axial load in the nails in the long-term analysis may increase by around 100 percent with respect to the maximum nail load that develops just after construction. This increase in the axial load should be taken into consideration in the design.

The maximum axial load in the nails (T_{max}) is obtained from the stability analysis using the limit equilibrium slope stability program. In order to consider the creep behavior of the soil nail wall in HP clays, the maximum axial load in the nails during the service life of the soil nail wall should be taken as twice the maximum axial load obtained from the stability analysis. Therefore, the maximum axial load in the nails can be defined as:

$$T_{max-creep} = T_{max} \times 2 \tag{26}$$

where T_{max} is the maximum axial load obtained from the slope stability analysis for the end of the construction; and $T_{max-creep}$ is the maximum long-term axial load in the nails.

To verify the pullout capacity of the nails, the pullout resistance of the nails (Eq. 22) can be defined as:

$$CDR = \frac{\phi_{PO}\, R_{PO}}{\gamma\, T_{max-creep}} \geq 1 \tag{27}$$

where γ is the load factor (equal to 1.35); and ϕ_{PO} is the resistance factor for pullout resistance, which is equal to 0.65. If the pullout resistance of the nails is not sufficient, the design of the soil nail wall needs to be modified. Possible solutions to overcome this problem are to: 1) increase the nail length, 2) increase the diameter of the nail hole, or 3) reduce the nail spacing. All of these changes will reduce the maximum axial load at the end of the construction, or will increase the pullout resistance of the nail (FHWA, 2015).

Horizontal Deformation of the Soil Nail Wall

Based on the one-year post-monitoring of the soil nail wall at the Beaumont project (Chapter 5), and the numerical modeling of the typical Texas turnaround soil nail wall for the service life of the soil nail wall (i.e., 75 years), the estimated horizontal deformation of the wall one year after the construction is almost 13 percent of the deformation calculated just after the construction. This deformation increases up to 64 percent of the deformation calculated just after construction for a period of 75 years after the construction (Figure 416). Details are presented in Chapter 7.

GEC#7 recommends including some of the following modifications in the design of critical soil nail walls to prevent significant horizontal movements in these critical designs:

- Use a higher safety factor in the limit equilibrium slope stability program.
- Install longer nails in the top portion of the wall.
- Use ground anchors in conjunction with the soil nails.
- Use pretensioned nails at the top portion of the wall.

DESIGN EXAMPLE

In this section, a design example of a soil nail wall in HP clay incorporating soil creep effects is illustrated.

Texas Turnaround Soil Nail Wall

The typical Texas turnaround soil nail wall (i.e., Chapter 7) was adopted to assess whether or not the original wall design was able to account for the long-term effects of creep in HP clays. Chapter 7 summarizes the geometry and other design details of the soil nail wall studied in this section.

The results of the stability analysis with the limit equilibrium slope stability program SNAILZ were presented in Chapter 7 (i.e., Figure 393 and Table 65). The global safety factor of the wall is 1.62. The maximum axial load obtained from the program is 6.4 kips. The length of the nails behind the slip surface (i.e., *Lp*) for the nail with maximum axial load is 19.8 ft.

Verification of the Pullout Resistance

As discussed previously in this report, the maximum axial load in the nails in the long term can be defined as:

$$T_{max-creep} = T_{max} \times 2 = 6.4 \times 2 = 12.8\ kips \tag{28}$$

The ultimate pullout resistance of the nail is defined as:

$$R_{po} = \pi\ q_u\ D_{DH}\ L_p = 3.14 \times 900 \times 0.5 \times 19.8 \times .001 = 28\ kips \tag{29}$$

The pullout resistance can be evaluated as:

$$CDR = \frac{\phi_{PO}\ R_{PO}}{\gamma\ T_{max-c}} = \frac{0.65 \times 28}{1.35 \times 12.8} = 1.05 \geq 1 \tag{30}$$

In this analysis, the initial soil nail wall design proposed by TxDOT was verified to account for the increase in the soil nail load induced by the soil creep. The safety factor at the end of service life (considered as 75 years in this research) is still above one. So, there should be no need to modify the initial TxDOT design for including creep behavior, unless a higher FS for the long-term conditions is desired.

The tentative modification of the design method to include soil creep effect in the analyses discussed in this report does not consider the effect of the unsaturated condition, which

may be very relevant in some cases. The unsaturated condition will increase the strength of the soils and so the pullout capacity, so this effect is on the safe side. The suggested tentative method does not consider either the effect of soil aging, observed in the creep tests on riverside anchors. This is also a beneficial effect that will tend to increase the safety factor for the long-term analysis.

SUMMARY AND CONCLUSIONS

The current design method of the soil nail wall (according to GEC#7) does not consider the effect of the creep behavior of the soil retained by the soil nail wall. This chapter presented a tentative procedure to include the soil creep effects in the design of soil nail walls constructed in HP clays. This possible modification is based on the following studies: pullout tests at the NGES-TAMU clay site, instrumentation and monitoring of the emergency slope repair project at the Beaumont District, laboratory tests, and numerical models that were calibrated using the field data.

The tentative design method presented in this report is based on the assumption that the permanent soil nail wall has a 75-year design life. From the numerical analyses, wall movements induced by the creeping soil mass lead to an increase in the nail load that should be considered in the design. Taking as an example the Beaumont soil, with an n value around 0.06 and LI less than 0.1, it was estimated that for the wall design corresponding to the typical Texas turnaround case the increase in the nail load was around 100 percent with respect to the maximum load developed just after construction.

The original design of the typical Texas turnaround wall was rechecked to include the effect of soil creep behavior. The current design method adopted by TxDOT provides a safety factor just above 1 for the long-term analysis (i.e., 75 years) including creep effects. Some soil conditions and features of soil behavior, as for example, unsaturated condition and soil aging, were not considered in these analyses. These phenomena may provide additional strength to the system, reducing the nail load and wall movements, and also increasing the FS.

Before proposing a definitive guideline for the design of soil nail walls in HP clays incorporating creep effects, it will be recommendable to expand the field and experimental information gathered from this research with more data. The current research was based on the information gathered from only one actual case study (i.e., the Beaumont project), plus

numerical lab tests and numerical modeling. The inclusion of a larger number of case studies would allow development of a more reliable, robust, and general design methodology for the design of soil nail walls in HP clays incorporating creep effects. It will be also desirable to study in more detail the impact of environmental conditions (i.e., rain, drying, and freezing) on the creep behavior of soil nail walls.

CHAPTER 9:
CONCLUSIONS AND PROPOSAL FOR FUTURE WORKS

SUMMARY AND CONCLUSIONS

An aspect of particular concern in the *Geotechnical Engineering Circular No. 7: Soil Nail Walls* (i.e., the soil nail wall manual and construction guideline) is the creep behavior of soil nail systems in HP clays. Since there was not enough information on the creep behavior of soil nail walls in HP clays, this matter was addressed in GEC#7 based on some practices in fine-grained soil with PI higher than 20, which exhibited unfavorable creep behavior. This research project was aimed at gaining a better understanding of the long-term behavior of the soil nail walls in fine-grained soils with PI > 0. To achieve this objective this research project combined: 1) in situ pullout tests on nails at two different sites (i.e., the NGES-TAMU clay site and the Beaumont TxDOT project); 2) monitoring of an actual soil nail wall in HP clays, from construction to operation (i.e., Beaumont TxDOT site); 3) laboratory tests on samples from the two investigated sites; and 4) numerical modeling.

Two different kinds of tests were performed at the NGES-TAMU clay site. Tests on existing anchors installed more than 20 years ago (with a very well-known load history), and tests on new soil nails constructed in the context of this research project. These tests focused on studying the effect of the load level on the creep behavior of soil nails in HP clays.

An emergency slope repair at the Beaumont District was selected to monitor the time-dependent behavior of the soil nail wall in HP clay. The PI of the embankment material is around 50, which made this project well-suited for the field tests and monitoring activities planned in this research. Inclinometer casings and tiltmeters were installed to track the wall deformations across time. A total of nine production nails were instrumented and installed at two different sections and at different depths to learn about the distribution of loads in different positions of the wall. Three of the nails were instrumented with load cells at the nail head. Water content probes were installed at different depths. Furthermore, six sacrificial nails were installed at three different depths. Three of those were instrumented with foil strain gauges. Verification and modified creep tests were performed on the sacrificial nails.

A comprehensive laboratory campaign was undertaken at TAMU facilities to study the mechanical and creep behavior of the clays investigated in the project. Among others, soil index properties, direct shear, consolidation, triaxial, and triaxial-creep tests were carried out. The

power law, based on the *n* exponent, was adopted to characterize the viscous and creep behaviors of the different soils. The results from these tests were instrumental in the numerical modeling activities planned in this project.

Numerical models were used in different stages of this research. Several commercial codes were adopted, based on the limit stability theory (SNAILZ), the FEM (Plaxis), and the finite difference method (FLAC3D). FLAC3D was adopted to determine the performance of soil walls in HP clays. This software was adopted because it has special elements to represent the behavior of the soil nail (i.e., the cable elements) and it also has a variety of rheological constitutive models for soils (e.g., the Burger model). The pullout tests at the Beaumont project were used to calibrate the cable model simulating the soil nails. The parameters of the mechanical model were obtained from the experimental investigation presented in Chapter 6. In particular, the triaxial creep tests were modeled to obtain the parameters of the Burger model, which was adopted to represent the behavior of the creeping soils. Afterward this information was incorporated into the modeling of the actual TxDOT soil nail wall at Beaumont. Both wall constructions and operation (up to 13 months) were modeled and the numerical results were compared with the field observations.

A parametric study based on an actual Texas turnaround project provided by TxDOT was performed to investigate the effect of different factors and conditions on the creep behavior of soil nail walls in HP clays. Different factors were investigated, related to the wall geometry (e.g., wall height, nail length), soil properties (e.g., cohesion, friction angle), and viscous properties of the soil. Soils with *n* value between 0.02 and 0.06 were studied in this research, which correspond to *n* values of clays typically found in Texas. Based on this parametric study, a tentative modification of the design guideline for soil nail walls was proposed to account for creep effects in HP clays.

Specific and detailed conclusions about the different activities quoted above can be found at the end of the chapters dedicated to those activities. Those conclusions are not repeated here; only the most relevant findings are briefly discussed below.

From the pullout tests performed at the NGES-TAMU clay site and Beaumont TxDOT project, it could be concluded that the creep rate during those tests was well below the acceptance criterion (i.e., 0.04 in. between 1 and 10 minutes or 0.08 in. between 6 and 60 minutes) for load levels lower than the 90 percent of the nail pullout capacity. A moderate

dependence of the creep rate on stress level was observed during these conditions. The creep rate increased significantly for load levels above the 90 percent of the pullout capacity, up to values much higher than the acceptance criterion. A similar tendency was observed in the triaxial creep tests performed on samples from these two sites as follows: for stresses below the failure (i.e., deviatoric stress below the 90 percent of the peak stress) the creep rates of these HP clays were quite low and slightly dependent on load level; however, at higher stresses (i.e., above the 90 percent of the peak stress), the creep rate increased dramatically.

The load protocols adopted for the pullout creep tests did not limit to that suggested in the GEC#7, but were modified/designed to explore other relevant aspects that may help gain a better understanding of the behavior of soil nails subjected to constant loads. For example, the duration of creep tests was extended longer than 60 ft (i.e., the time suggested in the GEC#7), up to 100 ft and 240 ft; no major changes in the creep rate were observed in creep stages of longer duration. The load protocols were also modified to explore the influence of having more creep stages (i.e., more creep steps of 60 ft each) during the pullout tests and to investigate the effect of previous loading on (i.e., by loading, unloading, and performing creep tests at lower load levels); from these tests, it was observed that previous creep stages and loading have a noticeable effect on creep rates (e.g., creep rates are much smaller if a higher load was acting in the past).

The monitoring of the Beaumont wall and the numerical modeling revealed that the maximum horizontal deformation of the wall due to the creep one year after the construction is around 10 percent of the horizontal deformation of the wall soon after the construction. According to GEC#7, the horizontal deformation of the wall after construction usually increases up to 15 percent compared to the deformation observed just after construction. This movement is already considered in the safety factors used in the design of soil nail walls. As a result of this movement (i.e., because of the post-construction movements of the wall), an increase in load develops in the nails. According to the monitoring at the Beaumont wall and the numerical modeling, the maximum additional axial load developed in the nail row before the last nail row. The maximum additional load was around 50 percent of the axial load in the nails at the end of the construction. The service load in the nail after one year of operation (including this 50 percent of load increase induced by creep) is lower than the 30 percent of the maximum pullout capacity of the nails. This result confirms that the soil nails in actual projects are

operating at relatively low load level, so low creep rates are expected under these loading conditions.

The numerical results revealed that for the specific soils considered in these analyses, the particular geometry and conditions of the studied walls, and for the adopted numerical models, the load in the nail could increase considerably during wall operation (up to 100 percent in the long-term). As expected, the key parameters influencing the long-term behavior of the soil nail wall are related to the rheological behavior of the clay. The experimental studies presented in previous chapters (i.e., nail pullout tests and single element tests) showed that creep rates in HP clays were very low when the stress level was low (e.g., when the acting nail load is below the 90 percent of the pullout capacity), but increased considerably when the load level was high and close to the ultimate capacity of the nail. Therefore, this delayed increment in the soil nail load may pose a problem for the long-term performance of soil nail walls in HP clays if it is not considered in the design. From the U-turn wall project study, it was confirmed that the nails designed according to the current TxDOT design method for soil nail walls were able to take the additional load induced by the soil creep for a period of 75 years while keeping a long-term safety factor above 1.

As far as this research team knows, this is the first study attempting to include the influence of creep effects on the long-term performance of soil nail walls in HP clays. The procedure proposed here provides an insight into: the long-term creep wall movements, the delayed increment in the nail load, and the changes in the long-term safety factor of the wall. The following section presents some suggestions and ideas to expand and improve the research performed in this project.

PROPOSAL FOR FUTURE WORKS

Some aspects that can be studied in future research projects are briefly noted as follows:

- **Effect of environmental actions on soil nail wall behavior.** In the pullout tests at the NGES-TAMU clay site (i.e., Chapter 4), the maximum pullout capacity of the nails (or bond stress at the soil–grout interface) changed during different times of the year (which are associated with different ground moisture conditions). For example, the strength of the soil–grout interface per unit of the length in the dry season was around twice that measured in the wet season. The creep behavior of soils depends on their water content

(or suction). Further studies are needed to gain a better understanding of the effect of environmental actions on the long-term performance of soil nail walls.

- **Effect of test conditions on creep behavior.** The laboratory investigation in this research focused on the study of the creep behavior of soils via UU triaxial creep tests. Creep in clays should be investigated under other tests conditions as well. The tests were performed on undisturbed samples and under natural water content conditions. Other water content conditions (from fully saturated to fully dry soils) should be investigated to understand the impact of water content on rheological properties of HP clays and to support the research mentioned in the item above.
- **Extension to additional HP clays.** Only two HP clays were investigated in this research, namely: NGES-TAMU Riverside Campus clay and Beaumont clay. The research should be extended to other HP clays to expand the current database.
- **Extension to other soil nail walls.** Only one soil nail wall was studied in this research and for 13 months only. It would be beneficial to include information from the monitoring of other soil nail walls in HP clays and to extend the monitoring for a longer period of time as well.
- **Development of elasto-visco-plastic models.** Quite simple mechanical constitutive models were adopted in this research. Further research should be done to develop more refined elasto-visco-plastic models that are able to capture better the complex long-term behavior of HP clays. The effect of soil moisture or soil suction has not been considered in this study and should be incorporated in future research, ideally through coupled hydro-mechanical analyses.
- **Revision of the current proposed guideline modification based on additional data.** The proposed tentative modification of the guideline for the design of soil nail walls in HP clay incorporating creep effect should be revised when more laboratory information or monitoring data become available.

REFERENCES

Akhavan, M., Ghareh, S., and Naeini, M. B. (2011). "Comparing the Results of Numerical Analysis and Monitoring about the Behavior of Cracks Occurred Nearby Soil-Nailing Walls." *Electronic Journal of Geotechnical Engineering*, 16.

ASTM Standard D2850-03a (2007). "Standard Test Method for Unconsolidated-Undrained Triaxial Compression Test on Cohesive Soils." ASTM International, West Conshohocken, Pennsylvania.

ASTM Standard D7263 (2009). "Standard Test Methods for Laboratory Determination of Density (Unit Weight) of Soil Specimens." ASTM International, West Conshohocken, Pennsylvania.

ASTM Standard D4767. (2011). "Standard Test Method for Consolidated Undrained Triaxial Compression Test for Cohesive Soils." ASTM International, West Conshohocken, Pennsylvania.

ASTM Standard D3080/D3080M. (2011). "Standard Test Method for Direct Shear Test of Soils under Consolidated Drained Conditions." ASTM International, West Conshohocken, Pennsylvania.

Babu, G. S., and Singh, V. P. (2009). *Simulation of Soil Nail Structures Using PLAXIS 2D*. Plaxis Bulletin. Plaxis.

Banerjee, S., Finney, A., Wentworth, T., and Bahiradhan, M. (1998). *Evaluation of Design Methodologies for Soil-Nailed Walls, Volume 1*. Report No. WA-RD 371.1. Washington State Department of Transportation.

Barrows, R. J. (1994). *Two Dimensional Finite Element Modeling of Swift Delta Soil Nail Wall by ABAQUS*. Doctoral Dissertation, Portland State University, Oregon.

Bingham, E. C. (1917). *An Investigation of the Laws of Plastic Flow.* 13(2): Govt. Print. Off.

Briaud, J. L. (1997). *The National Geotechnical Experimentation Sites at Texas A&M University: Clay and Sand*. Report No. NGEC-TAMU-007, September, 1997.

Briaud, J. L., and Garland, E. (1985). "Loading Rate Method for Pile Response in Clay." *J. Geotech. Eng.*, 111(3), 319–335.

Briaud, J. L., and Gibbens, R. (1999). "Behavior of Five Large Spread Footings in Sand." *J. Geotech. Geoenviron. Eng*., 125(9), 787–796.

Briaud, J. L., Griffin, R., Yeung, A., Soto, A., Suroor, A., and Park, H. (1998a). *Long-Term Behavior of Ground Anchors and Tieback Walls*. Report No. FHWA/TX-99/1391-1. August, 1998.

Briaud, J. L., and Lim, Y. (1997). "Soil Nailed Wall under Piled Bridge Abutment: Simulation and Guidelines." *Journal of Geotechnical and Geoenvironmental Engineering*, 123(11), 1043–1050.

Briaud, J. L., Powers, W. F., and Weatherby, D. E. (1998b). "Should Grouted Anchors Have Short Tendon Bond Length?" *J. Geotech.Geoenviron. Eng*., 124(2), 110–119.

Byrne, R. J. (1998). *Manual for Design & Construction Monitoring of Soil Nail Walls*. US Department of Transportation, Federal Highway Administration.

Chu, L. -M., and Yin, J. H. (2005). "A Laboratory Device to Test the Pullout Behavior of Soil Nails." *Geotech*. Test. J., 28(5), 1–15.

Dornfest, E. M., Nelson, J. D., and Overton, D. D. (2007). "Case History and Causes of a Progressive Block Failure in Gently Dipping Bedrock." Proceedings of the First North American Landslide Conference, Colorado.

Eckardt, H. (1982). "Creep Tests with Frozen Soils under Uniaxial Tension and Uniaxial Compression." Proceedings of the 4th Canadian Permafrost Conference, Calgary, Alberta, National Research Council of Canada, 365–373.

Fakher, A., Jones, C. J., and Clarke, B. G. (1999). "Yield Stress of Super Soft Clays." *Journal of Geotechnical and Geoenvironmental Engineering*, 125(6), 499–509.

Fan, C. C., and Luo, J. H. (2008). "Numerical Study on the Optimum Layout of Soil Nailed Slopes." *ComputGeotech* 35(4):585–599.

Feda, J. (1992). *Creep of Soils and Related Phenomena*. Elsevier.

FHWA. (1998a). *Manual for Design and Construction Monitoring of Soil Nail Walls*. Publication No. FHWA-SA-96-069R. Revised October 1998. pp. 35. US Department of Transportation.

FHWA. (1998b). *Summary Report of Research on Permanent Ground Anchor Walls, Volume II: Model-Scale Wall Tests and Ground Anchors Tests.* Report No. FHWA-RD-98-067, US Department of Transportation.

FHWA. (2003). *Geotechnical Engineering Circular No. 7: Soil Nail Walls, GEC#7*. Report No. FHWA0-IF-03-017, US Department of Transportation.

FHWA. (2015). *GEC#7, Soil Nail Wall Reference Manual*. Report No. FHWA-NHI-14-007, US Department of Transportation.

Galvan (2012). "TxDOT Bridge Division, Proposal Meeting RMC5 - 0-6784." Unpublished.

Geoguide 7 (2008). *Guide to Soil Nail Design and Construction – Geoguide 7*. Geotechnical Engineering Office; Civil Engineering and Development Dept., Government of Hong Kong Special Administrative Region, Hong Kong.

Gersevanov, N. M. (1937). *The Foundations of dynamics of soils*. Stroiizdat: Moscow-Leningrad.

Havel, F. (2004). *Creep in Soft Soils*. PhD Thesis, Norwegian University of Science and Technology.

Hunter, G., and Khalili, N. (2000). "A Simple Criterion for Creep Induced Failure of Over-Consolidated Clays." Pro.GeoEng 2000 Conference, Melbourne.

Itasca. (2006). FLAC3D v.4.0 Manual, "Fast Lagrangian Analysis of Continua in 3D Dimension Version 4.0, Online Manual."

Jeong, S. W. (2013). “Determining the Viscosity and Yield Surface of Marine Sediments Using Modified Bingham Models.” *Geosciences Journal.* 17(3), 241–247.

Keedwell, M. J. (1984). *Rheology and Soil Mechanics*. London: Elsevier Applied Science.

Lazarte, C. A., Baecher, G. B., and Withiam, J. L. (2003, June). “New Directions in LRFD for Soil Nailing Design and Specifications.” In Proceedings of the International Workshop on Limit State Design in Geotechnical Engineering Practice (LSD 2003), Cambridge, Massachusetts (Vol. 26).

Li, J., Tham, L. G., Junaideen, S. M., Yue, Z. Q., and Lee, C. F. (2008). “Loose Fill Slope Stabilization with Soil Nails: Full-Scale Test.” *J Geotech Geoenviron Eng* 134(3):277–288.

Locat, J., and Demers, D. (1988). “Viscosity, Yield Stress, Remolded Strength, and Liquidity Index Relationships for Sensitive Clays.” *Canadian Geotechnical Journal*, 25(4), 799–806.

Ludwig, H. (1984). “Short-Term and Long-Term Behavior of Tiebacks Anchored in Clay.” PhD Thesis, McGill University.

Ludwig, H., Weatherby, D. E., and Schnabel, H. (1985). “Research on Tiebacks Anchored in Cohesive Soils.” Proceedings of the 11th International Conference on Soil Mechanics and Foundation Engineering, San Francisco, 1721–1724.

Mahajan, S. P., and Budhu, M. (2006). “Viscous Effects on Penetrating Shafts in Clays.” *Acta Geotechnica*, 1(3), 157–165.

Maric, B., Kvasnička, P., Radaljac, D., and Mavar, R. (2001). “An Example of a High Soil Nailed Wall in Plastic Clayey Soil.” International Symposium on Earth Reinforcement.

Martinez-Vasques, J. J., and Diaz-Rodriguez, J. A. (2009). “Creep Behavior of an Undisturbed Lightly Overconsolidated Clay.” Proceedings of the 17th International Conference on Soil Mechanics and Geotechnical Engineering: The Academia and Practice of Geotechnical Engineering, Egypt, Volume 1, 229–232.

Menkiti, C. O., and Long, M. M. (2008). "Performance of Soil Nails in Dublin Glacial Till." *Canadian Geotechnical Journal*, 45(12), 1685–1698.

Mitchell, J. K. (1993). *Fundamentals of Soil Behavior.* Second Edition, Wiley, New York.

Mitsoulis, E. (2007). "Flows of Viscoplastic Materials: Models and Computations." *Rheology Reviews*, 135–178.

NYSDOT (2008a). "Design Procedure for Launched Soil Nail Shallow Slough Treatment." New York State Department of Transportation.

NYSDOT (2008b). "Design and Construction Guidelines for a Soil Nail Wall System, Geotechnical Engineering Manual GEM#21, Revision #2." New York State Department of Transportation.

O'Donovan, E. J., and Tanner, R. I. (1984). "Numerical Study of the Bingham Squeeze Film Problem." *Journal of Non-Newtonian Fluid Mechanics*, 15(1), 75–83.

ODOT (1991). *Soil Nailing of a Bridge Fill Embankment.* Oregon Department of Transportation.

ODOT (1993). *A Numerical Investigation into the Performance of the Soil Nail Wall and Pile Foundation at the Swift Delta I-5 Interchange*. Oregon Department of Transportation.

ODOT (1995). *Soil Nailing of a Bridge Fill Embankment*. Oregon Department of Transportation.

ODOT (1999). *Monitoring of Soil Nailed Walls at the Highway 217 and Highway 26 Interchange Final Report.* Oregon Department of Transportation.

Ohtsuki, H., Nishi, K., Okamoto, Z., and Tanaka, S. (1981). "Time Dependent Characteristics of Strength and Deformation of a Mudstone." Proceedings of the Symposium on Weak Rock, Tokyo, 1, 119–124.

Olia, A., and Liu, J. (2011). "Numerical Investigation of Soil Nail Wall during Construction." 2011 Pan-Am CGS Geotechnical Conference, Oct. 2–6, 2011, Toronto, Canada.

Oral, T., and Sheahan, T. C. (1998). “The Use of Soil Nails in Soft Clays.” In Design and Construction of Earth Retaining Systems, ASCE, 26–40.

Ostermayer, H. (1975). “Construction, Carrying Behavior and Creep Characteristics of Ground Anchors.” Proc. Diaphragm Walls and Anchorages Conference, Institute of Civil Engineers, London, 141–151.

Pestana, J. M., and Whittle, A. J. (1995). “Compression Model for Cohesionless Soils.” *Geotechnique*, 45(4), 611–631.

Pestana, J. M., and Whittle, A. J. (1998). “Time Effects in the Compression of Sands.” *Geotechnique*, 48(5), 695–701.

PLAXIS 2D Manual (2014). “Material Models Manual.” Plaxis 2014.

Plumelle, C., Schlosser, F., Delage, P., and Knochenmus, G. (1990). “French National Research Project on Soil Nailing: Clouterre.” Design and Performance of Earth Retaining Structures, P. C. Lambe & L. A. Hansen, eds., Geotechnical Special Publication No. 25, ASCE, Reston, Virginia, 660–675.

Powers, W. F. (1993). “Behavior of 10 Full-scale Ground Anchors Installed in Stiff Clay.” MS Thesis, Texas A&M University.

Pradhan, B., Yue, Q. Z. Q., Tham, L. G., and Lee, C. F. (2003). “Laboratory Study of Soil Nail Pullout Strength in Loosely Compacted Silty and Gravelly Sand Fills.” 12th Panamerican Conf. on Soil Mechanics and Geotechnical Engineering, 39th U.S. Rock Mechanics Symp., Verlag Gluckauf Essen, Germany, 2139–2146.

Recommendations Clouterre (1991). English Translation of: “French Soil Nailing Recommendation 1991. For Designing, Calculating, Constructing and Inspecting Earth Support System Using Soil Nailing” (by Plumelle, Schlosser et al., 1990). Federal Highway Administration. FHWA-SA-93-026.

Sakr, C. T., and Kimmerling, R. (1995). *Soil Nailing of a Bridge Fill Embankment*. Report No. OR 89-07. Oregon Department of Transportation.

Sanzeni, A., Whittle, A., Germaine, J., and Colleselli, F. (2012). "Compression and Creep of Venice Lagoon Sands." *J. Geotech. Geoenviron. Eng*., 138(10), 1266–1276.

Schlosser, F., Plumelle, C., Unterreiner, P. and Benoît, J., (1992). "Failure of a Full Scale Experimental Soil Nailed Wall by Reducing the Nails Lengths (French Research Project CLOUTERRE)," Proceedings of the International Symposium on Earth Reinforcement Practice, Ochiai, Hayashi and Otani, Editors, IS Kyushi '92, Fukuoka, Japan, November 1992

Segalini, A., Giani, G. P., and Ferrero, A. M. (2009). "Geomechanical Studies on Slow Slope Movements in Parma Apennine." *Engineering Geology*, 109(1), 31–44.

Shiu, Y. K., and Chang, G. W. K. (2006). "Effects of Inclination, Length Pattern and Bending Stiffness of Soil Nails on Behaviour of Nailed Structures." Geotechnical Engineering Office, Civil Engineering and Development Department.

Singh, V. P., and Babu, G. L. S. (2010). "2D Numerical Simulations of Soil Nail Walls." *Geotech Geology Engineering*, 28, 299–309.

Sivakumar, B., and Singh, V. P. (2010). "*Reliability analyses of a prototype soil nail wall using regression models*." Geomechanics and Engineering, 2(2), 71–88.

Smith, T. D. (1993). *A Numerical Investigation into the Performance of the Soil Nail Wall and Pile Foundation at the Swift Delta I-5 Interchange*. Report No. FHWA-OR-RD-95-15. Oregon Department of Transportation.

Su, L. J. (2006). "Laboratory Pullout Testing Study on Soil Nails in Compacted Completely Decomposed Granite Fill." Ph.D. Thesis, Hong Kong Polytechnic Univ., Hong Kong.

Su, L. J., Chan, T. C. F., Shiu, Y. K., Cheung, T., and Yin, J. H. (2007). "Influence of Degree of Saturation on Soil Nail Pullout Resistance in Compacted Completely Decomposed Granite Fill." *Can. Geotech. J.*, 44(11), 1314–1428.

Su, L., Chan, T., Yin, J., Shiu, Y., and Chiu, S. (2008). "Influence of Overburden Pressure on Soil–Nail Pullout Resistance in a Compacted Fill." *J. Geotech. Geoenviron. Eng*., 134(9), 1339–1347.

Taib, S. N. L., and Craig, W. H. (2006). "Modeling Construction and Failure of Soil Nailed Structures in Clay." *Physical Modelling in Geotechnics*. Proceedings of the Sixth International Conference on Physical Modelling in Geotechnics, 6th ICPMG '06, Hong Kong, 577–583.

Tavenas, F., and Leroueil, S. (1981). "Creep and Failure of Slopes in Clays." *Canadian Geotechnical Journal*, 18(1): 106–120.

TDOT (2012). "Tennessee Department of Transportation Earth Retaining Structures Manual." Tennessee Department of Transportation.

Terzaghi, K. (1943). *Theoretical soil mechanics*. New York : J. Wiley & Sons, inc.; London : Chapman and Hall, limited, [1943].

Tian, T. (2011). *Numerical Study of Different Creep Models Used for Soft Soils*. MS Thesis, Chalmers University of Technology.

Tuozzolo, T. (2003). "Soil Nailing: Where, When and Why. A Practical Guide." 20th Central Pennsylvania Geotechnical Conference Hershey, Pennsylvania.

Turner, J. P., and Jensen, W. G. (2005). "Landslide Stabilization Using Soil Nail and Mechanically Stabilized Earth walls: Case Study." *J. Geotech. Geoenviron. Eng.*, 131(2), 141–150.

Turner, L. L., and Parnell, J. (2006). "CalNail – A Design Tool for Soil Nail Projects Using Field Case Histories." Report No. F/CA/IR-2006/05. California Department of Transportation.

TxDOT Tex-103-E. (1999). "Determining Moisture Content in Soil Materials." Tex-103-E, August 1999. Texas Department of Transportation, Texas.

TxDOT Tex-104-E. (1999). “Determining Liquid Limit of Soils.” Tex-104-E, August 1999. Texas Department of Transportation, Texas.

TxDOT Tex-105-E. (1999). “Determining Plastic Limit of Soils.” Tex-105-E, August 1999. Texas Department of Transportation, Texas.

TxDOT. (2012). “Geotechnical Manual.” Texas Department of Transportation, Texas.

Vermeer, P. A., and Neher, H. P. (1999). “A Soft Soil Model that Accounts for Creep.” In Proceedings of the International Symposium: Beyond 2000 in Computational Geotechnics, 249–261.

Vyalov, S. (1986). “Rheological Fundaments of Soil Mechanics.” *Developments in Geotechnical Engineering*, Vol. 36. Elsevier.

Weatherby, D. E. (1982). “Tiebacks.” Report No. FHWA/RD-32/047, US Department of Transportation, Washington, DC.

Weatherby, D. E. (1998). “Design Manual for Permanent Ground Anchor Walls.” Report No. FHWA/RD-97/130, US Department of Transportation, Washington, DC.

Whitman, R. V. (1957). “The Behavior of Soils under Transient Loadings.” In Proc. 4th International Conference on Soil Mechanics and Foundation Engineering, Vol. 1, 207.

WSDOT (1998). “Evaluation of Design Methodologies for Soil-Nailed Walls.” Volume 1. Washington State Department of Transportation.

WSDOT (2010). “Geotechnical Engineering Services Wall 18–SR 522 at US 2 Overcrossing.” Washington State Department of Transportation.

Yin, J. H., and Su, L. J. (2006). “Innovative Laboratory Pull-Out Boxes for Study of Soil Nail Pull-Out Shear Resistance.” *Geotech. Test. J.*, 29(6), 451–461.

Yin, J. -H., Su, L. -J., Cheung, R. W. M., Shiu, Y. -K., and Tang, C. (2009). “The Influence of Grouting Pressure on the Pullout Resistance of Soil Nails in Compacted Completely Decomposed Granite Fill.” *Geotechnique*, 59(2), 103–113.